

TMS2007

136th Annual Meeting & Exhibition

Linking Science and Technology for Global Solutions

Technical Program

Program-at-a-Glance	2
Session Listing	8
Monday AM	16
Monday PM.....	63
Tuesday AM.....	117
Tuesday PM.....	164
Wednesday AM	223
Wednesday PM	274
Thursday AM.....	327
General Posters	359
Index	363



ROOM	Monday		Tuesday		Wednesday		Thursday
	AM	PM	AM	PM	AM	PM	AM
America's Seminar	Materials Processing under the Influence of External Fields: Session I	Materials Processing under the Influence of External Fields: Session II	Intellectual Property in Materials Science: Patents, Tech Transfer and Licensing: Patents	Intellectual Property in Materials Science: Patents, Tech Transfer and Licensing: Commercialization	Materials Processing under the Influence of External Fields: Session III	Materials Processing under the Influence of External Fields: Session IV	Materials Processing under the Influence of External Fields: Session V
Asia 1	Bulk Metallic Glasses IV: Glass Science and Technology	Bulk Metallic Glasses IV: Mechanical Properties I	Bulk Metallic Glasses IV: Alloy Development and Glass-Forming Ability	Bulk Metallic Glasses IV: Mechanical Properties II	Bulk Metallic Glasses IV: Supercooled Liquids and Crystallization	Bulk Metallic Glasses IV: Mechanical Properties III	Bulk Metallic Glasses IV: Mechanical Properties IV
Asia 2	Materials in Clean Power Systems II: Fuel Cells, Solar, and Hydrogen-Based Technologies: Plenary Session	Materials in Clean Power Systems II: Fuel Cells, Solar, and Hydrogen-Based Technologies: PEMFCs	Materials in Clean Power Systems II: Fuel Cells, Solar, and Hydrogen-Based Technologies: SOFCs I	Materials in Clean Power Systems II: Fuel Cells, Solar, and Hydrogen-Based Technologies: SOFCs II	Materials in Clean Power Systems II: Fuel Cells, Solar, and Hydrogen-Based Technologies: Materials Oxidation/Corrosion and Protection	Materials in Clean Power Systems II: Fuel Cells, Solar, and Hydrogen-Based Technologies: Materials for Clean Coal Power Generation and Gas Separation	Materials in Clean Power Systems II: Fuel Cells, Solar, and Hydrogen-Based Technologies: Materials for Solar Cells and Photovoltaic Systems
Asia 3	Innovations in Titanium Technology Symposium: Low Cost Materials and Processing	Innovations in Titanium Technology Symposium: Novel Materials and Processes I	Innovations in Titanium Technology Symposium: Novel Materials and Processes II	Innovations in Titanium Technology Symposium: Advances in Materials Processing	Innovations in Titanium Technology Symposium: Advances in Alloy Development	Innovations in Titanium Technology Symposium: Microstructure and Properties I	Innovations in Titanium Technology Symposium: Microstructure and Properties II
Asia 4	Properties and Performance of High Temperature Alloys and Coatings: Single Crystal Alloys I	Properties and Performance of High Temperature Alloys and Coatings: Polycrystalline Alloys	Properties and Performance of High Temperature Alloys and Coatings: Single Crystal Alloys II and Oxidation	Properties and Performance of High Temperature Alloys and Coatings: Coatings and Oxidation I	Properties and Performance of High Temperature Alloys and Coatings: Coatings and Oxidation II	Properties and Performance of High Temperature Alloys and Coatings: Intermetallics and Multidiscipline	
Asia 5	SMD Symposium: Mechanical Behavior of Nanostructured Materials, in Honor of Carl Koch: Fatigue, and Strengthening Mechanisms at Small Length Scale	SMD Symposium: Mechanical Behavior of Nanostructured Materials, in Honor of Carl Koch: Processing and Characterization of Materials Subjected to Severe Plastic Deformation	SMD Symposium: Mechanical Behavior of Nanostructured Materials, in Honor of Carl Koch: Plasticity and Deformation Mechanisms at Small Length Scale I	SMD Symposium: Mechanical Behavior of Nanostructured Materials, in Honor of Carl Koch: Stability, Strain and Stress - and - Poster Session: Mechanical Properties of Nanostructured Materials	SMD Symposium: Mechanical Behavior of Nanostructured Materials, in Honor of Carl Koch: Plasticity and Deformation Mechanisms at Small Length Scale II	SMD Symposium: Mechanical Behavior of Nanostructured Materials, in Honor of Carl Koch: Plasticity and Deformation Mechanisms at Small Length Scale III	SMD Symposium: Mechanical Behavior of Nanostructured Materials, in Honor of Carl Koch: Microstructure and Mechanical Properties of Nanostructured Materials
Australia 2	Recycling and Waste Processing: Materials Recovery from Wastes	Recycling and Waste Processing: Batteries and Co/Ni	Recycling and Waste Processing: Automotive Recycling, Global Challenges and Opportunities	Recycling and Waste Processing: Precious Metals Recovery	Recycling and Waste Processing: Aluminum	Recycling and Waste Processing: Other Nonferrous	



Monday		Tuesday		Wednesday		Thursday	ROOM
AM	PM	AM	PM	AM	PM	AM	
Innovations in Measurement Science to Assess the Performance of New Materials in the Real-World: Fundamental Measurement Methods	8th Global Innovations Symposium: Trends in Materials and Manufacturing Technologies for Energy Production: Plenary	Innovations in Measurement Science to Assess the Performance of New Materials in the Real-World: High Strain Rate Deformation	8th Global Innovations Symposium: Trends in Materials and Manufacturing Technologies for Energy Production: Session I	Innovations in Measurement Science to Assess the Performance of New Materials in the Real-World: Characterization of Advanced Materials	Innovations in Measurement Science to Assess the Performance of New Materials in the Real-World: Advanced Measurement Techniques		Australia 3
Advances in Microstructure-Based Modeling and Characterization of Deformation Microstructures: Characterization of Deformed Structures I	Advances in Microstructure-Based Modeling and Characterization of Deformation Microstructures: Modeling of Deformed Structures I	Advances in Microstructure-Based Modeling and Characterization of Deformation Microstructures: Characterization of Deformed Structures II	Advances in Microstructure-Based Modeling and Characterization of Deformation Microstructures: Modeling of Deformed Structures II	Advances in Microstructure-Based Modeling and Characterization of Deformation Microstructures: Modeling of Deformed Structures III	Advances in Microstructure-Based Modeling and Characterization of Deformation Microstructures: Characterization of Deformed Structures III		Europe 1
Diffusion in Advanced Materials and Processing: Atomistic and Multiscale Simulations	Diffusion in Advanced Materials and Processing: Interfaces, Surfaces and Nanostructures	Diffusion in Advanced Materials and Processing: Energy Technology	Diffusion in Advanced Materials and Processing: Materials Processing	Diffusion in Advanced Materials and Processing: Phenomenology and Experiments	Diffusion in Advanced Materials and Processing: Intermetallics and Glasses		Europe 2
Dynamic Behavior of Materials: Deformation I	Dynamic Behavior of Materials: Deformation II	Dynamic Behavior of Materials: Deformation III	Dynamic Behavior of Materials: Deformation IV	Dynamic Behavior of Materials: Mechanical Properties I	Dynamic Behavior of Materials: Mechanical Properties II	Dynamic Behavior of Materials: Fracture	Europe 3
Biological Materials Science: Bioinspired Materials	Biological Materials Science: Mechanical Behavior of Biomaterials	Biological Materials Science: Biological Materials I	Biological Materials Science: Biological Materials/ Bio-Medical - and - Poster Session	Biological Materials Science: Implant Biomaterials	Biological Materials Science: Functional Biomaterials and Devices	Biological Materials Science: Biological Materials II	Europe 4
Materials Issues for Advanced Nuclear Systems: Energy Generation and Waste Issues	Materials Issues for Advanced Nuclear Systems: Material Characterization Issues	General Abstracts: SMD: Advances in Steel I	General Abstracts: SMD: Advances in Steel II	General Abstracts: SMD: Microstructure and Properties of Materials	General Abstracts: SMD: Nickel Alloys and High Temperature Materials I		Europe 5
Refractory Metals 2007: Processing and Mechanical Deformation	Refractory Metals 2007: Oxidation and Thin Films	Fundamentals of Shape Memory and Related Transitions: Electronic Structure and Phonons	Fundamentals of Shape Memory and Related Transitions: Atomistic and Microstructural Mechanisms	Fundamentals of Shape Memory and Related Transitions: Mechanical Behavior	Fundamentals of Shape Memory and Related Transitions: Multiscale Modeling and Applications	General Abstracts: SMD: Processing and Properties of Light Metals	Europe 6
Advances in Computational Materials Science and Engineering Methods: Methods at the Atom Scale I	Advances in Computational Materials Science and Engineering Methods: Methods at the Atom Scale II	Advances in Computational Materials Science and Engineering Methods: Phase Field Methods I	Advances in Computational Materials Science and Engineering Methods: Phase Field Methods II	Advances in Computational Materials Science and Engineering Methods: Finite Element Method I	Advances in Computational Materials Science and Engineering Methods: Finite Element Method II	Advances in Computational Materials Science and Engineering Methods: Dedicated Computational Methods	Europe 7

ROOM	Monday		Tuesday		Wednesday		Thursday	
	AM	PM	AM	PM	AM	PM	AM	
Europe 8	Microstructural Processes in Irradiated Materials: Dislocation - Obstacle Interactions and Radiation Induced Segregation	Microstructural Processes in Irradiated Materials: Irradiation Effects in Ceramics	Microstructural Processes in Irradiated Materials: Modeling, Microstructure and Embrittlement in Fe-Cr Alloys	Microstructural Processes in Irradiated Materials: Modeling - and - Poster Session I	Microstructural Processes in Irradiated Materials: Reactor Pressure Vessel Steels	Microstructural Processes in Irradiated Materials: He Effects, Deformation and Fracture - and - Poster Session II	Microstructural Processes in Irradiated Materials: Defect Clusters and Fundamental Radiation Effects	
Europe 9	Plasticity from the Atomic Scale to Constitutive Laws: Dislocation Core Structure and Solute-Dislocation Interactions	Plasticity from the Atomic Scale to Constitutive Laws: Dislocation Solute, Precipitate and Grain Boundary Interactions	Plasticity from the Atomic Scale to Constitutive Laws: Atomistic Simulations of Dynamic Processes and Nano-Scale Plasticity	Plasticity from the Atomic Scale to Constitutive Laws: Dislocation Ensembles	Plasticity from the Atomic Scale to Constitutive Laws: Meso-Scale Plasticity	Plasticity from the Atomic Scale to Constitutive Laws: Rate Limiting Behavior and Informed Constitutive Laws		
Europe 10	Advanced Metallic Composites and Alloys for High Performance Applications: Advanced Metallics	Advanced Metallic Composites and Alloys for High Performance Applications: Fe and Ni Alloys and Composites	Advanced Metallic Composites and Alloys for High Performance Applications: Refractory Alloys and Composites	Advanced Metallic Composites and Alloys for High Performance Applications: Al Alloys and Composites	Advanced Metallic Composites and Alloys for High Performance Applications: Ti Alloys and Composites	Advanced Metallic Composites and Alloys for High Performance Applications: Metallic Composites	Computational Thermodynamics and Phase Transformations: Nanomaterials and Confined Systems II	
Europe 11	Computational Thermodynamics and Phase Transformations: First Principles and Atomistic Calculations of Phase and Alloy Thermodynamics I	Computational Thermodynamics and Phase Transformations: First Principles and Atomistic Calculations of Phase and Alloy Thermodynamics II	Computational Thermodynamics and Phase Transformations: Microstructure Properties and Evolution I	Computational Thermodynamics and Phase Transformations: Microstructure Properties and Evolution II	Computational Thermodynamics and Phase Transformations: Modeling of Phase Transformations I	Computational Thermodynamics and Phase Transformations: Nanomaterials and Confined Systems I	Computational Thermodynamics and Phase Transformations: Modeling of Phase Transformations II	
N. H. Foyer	General Poster Session							
Northern A1	MPMD Symposium: Mechanics and Materials Modeling and Materials Design Methodologies, in the Honor of Dr. Craig Hartley's 40 Years of Contributions to the Field of Mechanics and Materials Science: Microstructure Analysis and Representation I	MPMD Symposium: Mechanics and Materials Modeling and Materials Design Methodologies, in the Honor of Dr. Craig Hartley's 40 Years of Contributions to the Field of Mechanics and Materials Science: Homogenization/ Constitutive Behavior I	MPMD Symposium: Mechanics and Materials Modeling and Materials Design Methodologies, in the Honor of Dr. Craig Hartley's 40 Years of Contributions to the Field of Mechanics and Materials Science: Homogenization/ Constitutive Behavior II	MPMD Symposium: Mechanics and Materials Modeling and Materials Design Methodologies, in the Honor of Dr. Craig Hartley's 40 Years of Contributions to the Field of Mechanics and Materials Science: Materials Design	MPMD Symposium: Mechanics and Materials Modeling and Materials Design Methodologies, in the Honor of Dr. Craig Hartley's 40 Years of Contributions to the Field of Mechanics and Materials Science: Nanostructure, Defects and Properties	MPMD Symposium: Mechanics and Materials Modeling and Materials Design Methodologies, in the Honor of Dr. Craig Hartley's 40 Years of Contributions to the Field of Mechanics and Materials Science: Microstructure Analysis and Representation II	General Abstracts: MPMD: Structure/ Processing/ Properties Relationships	
Northern A2	Materials Processing Fundamentals: Solidification and Deformation Processing	Materials Processing Fundamentals: Process Modeling	Materials Processing Fundamentals: Smelting and Refining	Materials Processing Fundamentals: Powders, Composites, Coatings and Measurements	General Abstracts: MPMD: In Situ Synthesis and Rapid Prototyping	General Abstracts: MPMD: Modeling and Simulation of Materials and Processes	General Abstracts: MPMD: Processing and Microstructural Development	



Monday		Tuesday		Wednesday		Thursday	ROOM
AM	PM	AM	PM	AM	PM	AM	
Frontiers in Solidification Science: Nucleation and Crystal Structure	Frontiers in Solidification Science: Atomic Scale - and - Poster Session	Frontiers in Solidification Science: Microstructures I	Frontiers in Solidification Science: Microstructures II	Degradation of Light Weight Alloys: Session I	Degradation of Light Weight Alloys: Session II		Northern A3
General Abstracts: MPMD: Forming of Materials and Processes	Aluminum Alloys for Transportation, Packaging, Aerospace and Other Applications: Aluminum Applications	Aluminum Alloys for Transportation, Packaging, Aerospace and Other Applications: Aluminum Products	Aluminum Alloys for Transportation, Packaging, Aerospace and Other Applications: Alloy Development	Aluminum Alloys for Transportation, Packaging, Aerospace and Other Applications: Alloy Processing	Aluminum Alloys for Transportation, Packaging, Aerospace and Other Applications: Alloy Characterization	Aluminum Alloys for Transportation, Packaging, Aerospace and Other Applications: Alloy Mechanical Behavior	Northern A4
General Abstracts: EPD: Hydrometallurgy, Wastewater Treatment	Cast Shop Technology: Cast House Operations and Melting	Cast Shop Technology: Metal Treatment	Cast Shop Technology: Quality Measurements and Grain Refining	Cast Shop Technology: Casting	Cast Shop Technology: Solidification and Microstructure	Cast Shop Technology: Cast Shop Safety	Northern E1
	Shape Casting: The 2nd International Symposium: Liquid Metal/Solidification	Shape Casting: The 2nd International Symposium: Process Design/Analysis	Shape Casting: The 2nd International Symposium: Structure/Property	Shape Casting: The 2nd International Symposium: Modeling	Shape Casting: The 2nd International Symposium: Applications/ Novel Processes		Northern E2
General Abstracts: EPD: Pyrometallurgy, Base Metals	Friction Stir Welding and Processing IV: Session I	Friction Stir Welding and Processing IV: Session II	Friction Stir Welding and Processing IV: Session III	Friction Stir Welding and Processing IV: Session IV	Friction Stir Welding and Processing IV: Session V	Friction Stir Welding and Processing IV: Session VI	Northern E3
		Alumina and Bauxite: Alumina Refinery Safety and Integrity	Alumina and Bauxite: Alumina Refinery Design and Development	Alumina and Bauxite: Bauxite, Digestion, Red Mud, Byproducts	Alumina and Bauxite: Role of Surface Chemistry in Enhancing Refinery Performances		Northern E4
Pb-Free Electronic Solders: Alloy Design, Characterization and Service Reliability: Interfacial Effects	Pb-Free Electronic Solders: Alloy Design, Characterization and Service Reliability: Microstructure and Characterization	Pb-Free Electronic Solders: Alloy Design, Characterization and Service Reliability: Electromigration and Void Formation	Pb-Free Electronic Solders: Alloy Design, Characterization and Service Reliability: Whisker Growth, Design, and Modeling	Pb-Free Electronic Solders: Alloy Design, Characterization and Service Reliability: Processing and Reliability Issues	Pb-Free Electronic Solders: Alloy Design, Characterization and Service Reliability: Mechanical Characterization		Oceanic 1
Internet and Other Electronic Resources	Phase Stability, Phase Transformations, and Reactive Phase Formation in Electronic Materials VI: Session I	Phase Stability, Phase Transformations, and Reactive Phase Formation in Electronic Materials VI: Session II	Phase Stability, Phase Transformations, and Reactive Phase Formation in Electronic Materials VI: Session III	Phase Stability, Phase Transformations, and Reactive Phase Formation in Electronic Materials VI: Session IV	Phase Stability, Phase Transformations, and Reactive Phase Formation in Electronic Materials VI: Session V		Oceanic 2

ROOM	Monday		Tuesday		Wednesday		Thursday
	AM	PM	AM	PM	AM	PM	AM
Oceanic 3	2007 Nanomaterials: Fabrication, Properties and Applications: Session I	2007 Nanomaterials: Fabrication, Properties and Applications: Session II	2007 Nanomaterials: Fabrication, Properties and Applications: Session III	2007 Nanomaterials: Fabrication, Properties and Applications: Session IV	2007 Nanomaterials: Fabrication, Properties and Applications: Session V	2007 Nanomaterials: Fabrication, Properties and Applications: Session VI	
Oceanic 4	Wide Band-Gap Semiconductor Nanostructures: Session I	Wide Band-Gap Semiconductor Nanostructures: Session II	Wide Band-Gap Semiconductor Nanostructures: Session III	Wide Band-Gap Semiconductor Nanostructures: Session IV	Integrated Computational Materials Engineering: Lessons from Many Fields: ICME in Materials Science - and - NSF Workshop: CyberInfrastructure to CyberDiscovery for Materials Science	Integrated Computational Materials Engineering: Lessons from Many Fields: ICME in Other Fields - and - National Academies ICME Study Community Town Hall Meeting	General Abstracts: EMPMD: ZnO Thin Films and Liquid Crystals
Oceanic 5	Towards Functional Nanomaterials: Synthesis, Characterization, and Applications: Directed Nano Fabrication	Towards Functional Nanomaterials: Synthesis, Characterization, and Applications: Nano Magnetism, Ferroelectric, Mechanics, and Other Properties	Towards Functional Nanomaterials: Synthesis, Characterization, and Applications: Nanoscale Superstructures, Metallic Nanoparticles and Plasmon	Towards Functional Nanomaterials: Synthesis, Characterization, and Applications: Nanowires and Nanotubes	Towards Functional Nanomaterials: Synthesis, Characterization, and Applications: Quantum Dots	Innovations in Electrometallurgy: Session I	Innovations in Electrometallurgy: Session II
Oceanic 6	Recent Developments in Semiconductor, Electro Optic and Radio Frequency Materials: Recent Advances in Semiconductor Technologies	Recent Developments in Semiconductor, Electro Optic and Radio Frequency Materials: Progress in Semiconductor Optoelectronics and Beyond	Metrologies for Advanced Materials and Devices: Characterization, Measurement and Testing Science: Metrology for Micro and Nano Structures	Materials in Clean Power Systems II: Fuel Cells, Solar, and Hydrogen-Based Technologies: Hydrogen Storage Materials in Conjunction with the 8th Global Innovations Symposium: Metal Powders for Energy Production and Storage Applications	8th Global Innovations Symposium: Metal Powders for Energy Production and Storage Applications: Session I in Conjunction with the Symposium on Materials for Clean Power Systems II - Hydrogen Storage	8th Global Innovations Symposium: Metal Powders for Energy Production and Storage Applications: Session II	
Oceanic 7	General Abstracts: EMPMD: GaN and Interconnects	Hume-Rothery Symposium: Scattering Studies and the Fundamental Properties of Materials: Session I	Hume-Rothery Symposium: Scattering Studies and the Fundamental Properties of Materials: Session II	Hume-Rothery Symposium: Scattering Studies and the Fundamental Properties of Materials: Session III	Hume-Rothery Symposium: Scattering Studies and the Fundamental Properties of Materials: Session IV	Hume-Rothery Symposium: Scattering Studies and the Fundamental Properties of Materials: Session V	General Abstracts: EMPMD: Magnetic and Ferroelectric Materials
Oceanic 8	Characterization of Minerals, Metals, and Materials: Characterization of Structure across Length Scales I	Characterization of Minerals, Metals, and Materials: Characterization of Structure across Length Scales II	Characterization of Minerals, Metals, and Materials: Characterization of Mechanical and Physical Properties of Materials I	Characterization of Minerals, Metals, and Materials: Characterization of Mechanical and Physical Properties of Materials II	Characterization of Minerals, Metals, and Materials: Characterization of Processing and Properties of Materials	Characterization of Minerals, Metals, and Materials: Characterization of Processing of Materials I	Characterization of Minerals, Metals, and Materials: Characterization of Processing of Materials II



Monday		Tuesday		Wednesday		Thursday	ROOM
AM	PM	AM	PM	AM	PM	AM	
Outreach Programs in Materials Science and Engineering: Outreach Programs at Universities	Outreach Programs in Materials Science and Engineering: Outreach Programs in Industry and Government Laboratories						Pacific Hall A
General Abstracts: LMD: Session I	General Abstracts: LMD: Session II			EMPMD Symposium: Advanced Metallizations and Interconnect Technologies, in Honor of Prof. K. N. Tu's 70th Birthday: Advanced Metallizations and Interconnect Technology I	EMPMD Symposium: Advanced Metallizations and Interconnect Technologies, in Honor of Prof. K. N. Tu's 70th Birthday: Advanced Metallizations and Interconnect Technology II		Pacific Hall B
The Material Recycling Industry: Global Challenges and Opportunities: Plenary Session	General Abstracts: EPD: Hydrometallurgy, Metal Recovery	General Abstracts: EPD: High Temperature Processing	Aluminum Reduction Technology: Modelling and Design I	Aluminum Reduction Technology: Modelling II and General		Electrode Technology Symposium (formerly Carbon): Rodding and Coke Inventory	Southern 1
Aluminum Reduction Technology: Environmental and Plant Improvements	Aluminum Reduction Technology: Operational and Technology Improvements	Aluminum Reduction Technology: Slotted Anodes - Joint Session with Electrode Technology Symposium (formerly Carbon)	Aluminum Reduction Technology: Cell Fundamentals, Phenomena and Alternatives	Aluminum Reduction Technology: Anode Effects and Process Control I	Aluminum Reduction Technology: Inert Anode Operation and Low Temperature Electrolyte	Aluminum Reduction Technology: Process Control II and Bath Chemistry	Southern 2
Electrode Technology Symposium (formerly Carbon): Cathode Part I: Cathode Wear and Construction	Electrode Technology Symposium (formerly Carbon): Anode Technology and Production		Electrode Technology Symposium (formerly Carbon): Properties of Inert Anode Materials	Electrode Technology Symposium (formerly Carbon): Anode Baking Furnace Technology	Electrode Technology Symposium (formerly Carbon): Cathode Part II: Preheating and Cell Start Up	Electrode Technology Symposium (formerly Carbon): Cathode Part III: Titanium Diboride	Southern 3
Magnesium Technology 2007: Magnesium Globalization	Magnesium Technology 2007: Wrought Alloys and Forming Processes I: Deformation	Magnesium Technology 2007: Wrought Alloys and Forming Processes II: Rolling and Forming	Magnesium Technology 2007: Wrought Alloys and Forming Processes III: Extrusions	Magnesium Technology 2007: Alloy Development I	Magnesium Technology 2007: Alloy Development II	Magnesium Technology 2007: Corrosion and Coatings	Southern 4
	Magnesium Technology 2007: Automotive Applications and USAMP Programs	Magnesium Technology 2007: Casting and Solidification I	Magnesium Technology 2007: Casting and Solidification II	Magnesium Technology 2007: Primary Production, Recycling and Environmental/ Welding	Magnesium Technology 2007: Thermal Dynamics and Fundamental Research	Magnesium Technology 2007: Microstructure and Properties	Southern 5

2007 Nanomaterials: Fabrication, Properties and Applications: Session I.....	Oceanic 3	Mon AM	16
2007 Nanomaterials: Fabrication, Properties and Applications: Session II.....	Oceanic 3	Mon PM	63
2007 Nanomaterials: Fabrication, Properties and Applications: Session III	Oceanic 3	Tue AM.....	117
2007 Nanomaterials: Fabrication, Properties and Applications: Session IV	Oceanic 3	Tue PM	164
2007 Nanomaterials: Fabrication, Properties and Applications: Session V.....	Oceanic 3	Wed AM	223
2007 Nanomaterials: Fabrication, Properties and Applications: Session VI.....	Oceanic 3	Wed PM.....	274
8th Global Innovations Symposium: Metal Powders for Energy Production and Storage Applications: Session I in Conjunction with Materials for Clean Power Systems II - Hydrogen Storage	Oceanic 6	Wed AM	224
8th Global Innovations Symposium: Metal Powders for Energy Production and Storage Applications: Session II.....	Oceanic 6	Wed PM.....	276
8th Global Innovations Symposium: Trends in Materials and Manufacturing Technologies for Energy Production: Plenary	Australia 3	Mon PM	64
8th Global Innovations Symposium: Trends in Materials and Manufacturing Technologies for Energy Production: Session I.....	Australia 3	Tue PM	166
Advanced Metallic Composites and Alloys for High Performance Applications: Advanced Metallics.....	Europe 10	Mon AM	17
Advanced Metallic Composites and Alloys for High Performance Applications: Al Alloys and Composites.....	Europe 10	Tue PM	167
Advanced Metallic Composites and Alloys for High Performance Applications: Fe and Ni Alloys and Composites.....	Europe 10	Mon PM	65
Advanced Metallic Composites and Alloys for High Performance Applications: Metallic Composites	Europe 10	Wed PM.....	277
Advanced Metallic Composites and Alloys for High Performance Applications: Refractory Alloys and Composites.....	Europe 10	Tue AM.....	118
Advanced Metallic Composites and Alloys for High Performance Applications: Ti Alloys and Composites.....	Europe 10	Wed AM	225
Advances in Computational Materials Science and Engineering Methods: Dedicated Computational Methods.....	Europe 7	Thu AM.....	327
Advances in Computational Materials Science and Engineering Methods: Finite Element Method I	Europe 7	Wed AM	227
Advances in Computational Materials Science and Engineering Methods: Finite Element Method II.....	Europe 7	Wed PM.....	278
Advances in Computational Materials Science and Engineering Methods: Methods at the Atom Scale I	Europe 7	Mon AM	18
Advances in Computational Materials Science and Engineering Methods: Methods at the Atom Scale II.....	Europe 7	Mon PM	67
Advances in Computational Materials Science and Engineering Methods: Phase Field Methods I.....	Europe 7	Tue AM.....	119
Advances in Computational Materials Science and Engineering Methods: Phase Field Methods II.....	Europe 7	Tue PM	168
Advances in Microstructure-Based Modeling and Characterization of Deformation Microstructures: Characterization of Deformed Structures I.....	Europe 1	Mon AM	19
Advances in Microstructure-Based Modeling and Characterization of Deformation Microstructures: Characterization of Deformed Structures II.....	Europe 1	Tue AM.....	120
Advances in Microstructure-Based Modeling and Characterization of Deformation Microstructures: Characterization of Deformed Structures III	Europe 1	Wed PM.....	279
Advances in Microstructure-Based Modeling and Characterization of Deformation Microstructures: Modeling of Deformed Structures I.....	Europe 1	Mon PM	68
Advances in Microstructure-Based Modeling and Characterization of Deformation Microstructures: Modeling of Deformed Structures II.....	Europe 1	Tue PM	169
Advances in Microstructure-Based Modeling and Characterization of Deformation Microstructures: Modeling of Deformed Structures III	Europe 1	Wed AM	228
Alumina and Bauxite: Alumina Refinery Design and Development	Northern E4.....	Tue PM	171
Alumina and Bauxite: Alumina Refinery Safety and Integrity	Northern E4.....	Tue AM.....	122
Alumina and Bauxite: Bauxite, Digestion, Red Mud, Byproducts.....	Northern E4.....	Wed AM	229
Alumina and Bauxite: Role of Surface Chemistry in Enhancing Refinery Performance	Northern E4.....	Wed PM.....	280
Aluminum Alloys for Transportation, Packaging, Aerospace and Other Applications: Alloy Characterization	Northern A4	Wed PM.....	282
Aluminum Alloys for Transportation, Packaging, Aerospace and Other Applications: Alloy Development	Northern A4	Tue PM	172



Aluminum Alloys for Transportation, Packaging, Aerospace and Other Applications: Alloy Processing	Northern A4	Wed AM	230
Aluminum Alloys for Transportation, Packaging, Aerospace and Other Applications: Alloys Mechanical Behavior	Northern A4	Thu AM.....	327
Aluminum Alloys for Transportation, Packaging, Aerospace and Other Applications: Aluminum Applications	Northern A4	Mon PM	69
Aluminum Alloys for Transportation, Packaging, Aerospace and Other Applications: Aluminum Products	Northern A4	Tue AM	122
Aluminum Reduction Technology: Anode Effects and Process Control I.....	Southern 2.....	Wed AM	231
Aluminum Reduction Technology: Cell Fundamentals, Phenomena and Alternatives	Southern 2.....	Tue PM	173
Aluminum Reduction Technology: Environmental and Plant Improvements	Southern 2.....	Mon AM.....	21
Aluminum Reduction Technology: Inert Anode Operation and Low Temperature Electrolyte	Southern 2.....	Wed PM.....	283
Aluminum Reduction Technology: Modelling and Design I.....	Southern 1.....	Tue PM	174
Aluminum Reduction Technology: Modelling II and General	Southern 1.....	Wed AM	232
Aluminum Reduction Technology: Operational and Technology Improvements	Southern 2.....	Mon PM	70
Aluminum Reduction Technology: Process Control II and Bath Chemistry.....	Southern 2.....	Thu AM.....	329
Aluminum Reduction Technology: Slotted Anodes - Joint Session with Electrode Technology	Southern 2.....	Tue AM	123
Biological Materials Science: Bioinspired Materials	Europe 4	Mon AM.....	22
Biological Materials Science: Biological Materials I.....	Europe 4	Tue AM.....	124
Biological Materials Science: Biological Materials II.....	Europe 4	Thu AM.....	330
Biological Materials Science: Biological Materials/Bio-Medical	Europe 4	Tue PM	175
Biological Materials Science: Functional Biomaterials and Devices	Europe 4	Wed PM.....	284
Biological Materials Science: Implant Biomaterials	Europe 4	Wed AM	233
Biological Materials Science: Mechanical Behavior of Biomaterials	Europe 4	Mon PM	71
Biological Materials Science: Poster Session	Europe 4	Tue PM	176
Bulk Metallic Glasses IV: Alloy Development and Glass-Forming Ability	Asia 1	Tue AM	126
Bulk Metallic Glasses IV: Glass Science and Technology	Asia 1	Mon AM.....	23
Bulk Metallic Glasses IV: Mechanical Properties I.....	Asia 1	Mon PM	73
Bulk Metallic Glasses IV: Mechanical Properties II.....	Asia 1	Tue PM	177
Bulk Metallic Glasses IV: Mechanical Properties III	Asia 1	Wed PM.....	286
Bulk Metallic Glasses IV: Processing and Mechanical Properties IV	Asia 1	Thu AM.....	331
Bulk Metallic Glasses IV: Supercooled Liquids and Crystallization.....	Asia 1	Wed AM	235
Cast Shop Technology: Cast House Operations and Melting	Northern E1.....	Mon PM	74
Cast Shop Technology: Cast Shop Safety.....	Northern E1.....	Thu AM.....	333
Cast Shop Technology: Casting	Northern E1.....	Wed AM	237
Cast Shop Technology: Metal Treatment.....	Northern E1.....	Tue AM	127
Cast Shop Technology: Quality Measurements and Grain Refining	Northern E1.....	Tue PM	179
Cast Shop Technology: Solidification and Microstructure	Northern E1.....	Wed PM.....	288
Characterization of Minerals, Metals, and Materials: Characterization of Mechanical and Physical Properties of Materials I.....	Oceanic 8	Tue AM	128
Characterization of Minerals, Metals, and Materials: Characterization of Mechanical and Physical Properties of Materials II	Oceanic 8	Tue PM	179
Characterization of Minerals, Metals, and Materials: Characterization of Processing and Properties of Materials	Oceanic 8	Wed AM	238
Characterization of Minerals, Metals, and Materials: Characterization of Processing of Materials I.....	Oceanic 8	Wed PM.....	289
Characterization of Minerals, Metals, and Materials: Characterization of Processing of Materials II	Oceanic 8	Thu AM.....	334
Characterization of Minerals, Metals, and Materials: Characterization of Structure across Length Scales I.....	Oceanic 8	Mon AM.....	25
Characterization of Minerals, Metals, and Materials: Characterization of Structure across Length Scales II	Oceanic 8	Mon PM	75

Computational Thermodynamics and Phase Transformations: First Principles and Atomistic Calculations of Phase and Alloy Thermodynamics I	Europe 11	Mon AM	26
Computational Thermodynamics and Phase Transformations: First Principles and Atomistic Calculations of Phase and Alloy Thermodynamics II.....	Europe 11	Mon PM	77
Computational Thermodynamics and Phase Transformations: Microstructure Properties and Evolution I....	Europe 11	Tue AM.....	130
Computational Thermodynamics and Phase Transformations: Microstructure Properties and Evolution II ...	Europe 11	Tue PM	181
Computational Thermodynamics and Phase Transformations: Modeling of Phase Transformations I.....	Europe 11	Wed AM	239
Computational Thermodynamics and Phase Transformations: Modeling of Phase Transformations II	Europe 11	Thu AM.....	335
Computational Thermodynamics and Phase Transformations: Nanomaterials and Confined Systems I	Europe 11	Wed PM.....	291
Computational Thermodynamics and Phase Transformations: Nanomaterials and Confined Systems II.....	Europe 10	Thu AM.....	337
Degradation of Light Weight Alloys: Session I	Northern A3	Wed AM	240
Degradation of Light Weight Alloys: Session II.....	Northern A3	Wed PM.....	292
Diffusion in Advanced Materials and Processing: Atomistic and Multiscale Simulations.....	Europe 2	Mon AM	28
Diffusion in Advanced Materials and Processing: Energy Technology.....	Europe 2	Tue AM.....	131
Diffusion in Advanced Materials and Processing: Interfaces, Surfaces and Nanostructures	Europe 2	Mon PM	78
Diffusion in Advanced Materials and Processing: Intermetallics and Glasses	Europe 2	Wed PM.....	293
Diffusion in Advanced Materials and Processing: Materials Processing	Europe 2	Tue PM	182
Diffusion in Advanced Materials and Processing: Phenomenology and Experiments.....	Europe 2	Wed AM	241
Dynamic Behavior of Materials: Deformation I.....	Europe 3	Mon AM	29
Dynamic Behavior of Materials: Deformation II.....	Europe 3	Mon PM	79
Dynamic Behavior of Materials: Deformation III	Europe 3	Tue AM.....	132
Dynamic Behavior of Materials: Deformation IV	Europe 3	Tue PM	183
Dynamic Behavior of Materials: Fracture	Europe 3	Thu AM.....	338
Dynamic Behavior of Materials: Mechanical Properties I	Europe 3	Wed AM	243
Dynamic Behavior of Materials: Mechanical Properties II	Europe 3	Wed PM.....	294
Electrode Technology Symposium (formerly Carbon Technology): Anode Baking Furnace Technology	Southern 3	Wed AM	244
Electrode Technology Symposium (formerly Carbon Technology): Anode Technology and Production.....	Southern 3	Mon PM	81
Electrode Technology Symposium (formerly Carbon Technology): Cathode Part I: Cathode Wear and Construction	Southern 3	Mon AM	30
Electrode Technology Symposium (formerly Carbon Technology): Cathode Part II: Preheating and Cell Start Up.....	Southern 3	Wed PM.....	296
Electrode Technology Symposium (formerly Carbon Technology): Cathode Part III: Titanium Diboride.....	Southern 3	Thu AM.....	340
Electrode Technology Symposium (formerly Carbon Technology): Properties of Inert Anode Materials	Southern 3	Tue PM	185
Electrode Technology Symposium (formerly Carbon Technology): Rodding and Coke Inventory.....	Southern 1	Thu AM.....	341
Electrode Technology Symposium (formerly Carbon Technology): Slotted Anodes - Joint Session with Aluminum Reduction Technology	Southern 2	Tue AM.....	123
Electronic, Magnetic and Photonic Materials Division Symposium: Advanced Metallizations and Interconnect Technologies, in Honor of Prof. K. N. Tu's 70th Birthday: Advanced Metallizations and Interconnect Technology I.....	Pacific Hall B	Wed AM	246
Electronic, Magnetic and Photonic Materials Division Symposium: Advanced Metallizations and Interconnect Technologies, in Honor of Prof. K. N. Tu's 70th Birthday: Advanced Metallizations and Interconnect Technology II	Pacific Hall B	Wed PM.....	296
Friction Stir Welding and Processing IV: Session I.....	Northern E3.....	Mon PM	82
Friction Stir Welding and Processing IV: Session II.....	Northern E3.....	Tue AM.....	134
Friction Stir Welding and Processing IV: Session III	Northern E3.....	Tue PM	186
Friction Stir Welding and Processing IV: Session IV	Northern E3.....	Wed AM	247
Friction Stir Welding and Processing IV: Session V.....	Northern E3.....	Wed PM.....	297
Friction Stir Welding and Processing IV: Session VI	Northern E3.....	Thu AM.....	341
Frontiers in Solidification Science: Atomic Scale	Northern A3	Mon PM	83



Frontiers in Solidification Science: Microstructures I	Northern A3	Tue AM	135
Frontiers in Solidification Science: Microstructures II.....	Northern A3	Tue PM	188
Frontiers in Solidification Science: Nucleation and Crystal Structure	Northern A3	Mon AM.....	31
Frontiers in Solidification Science: Poster Session.....	Northern A3	Mon PM	84
Fundamentals of Shape Memory and Related Transitions: Atomistic and Microstructural Mechanisms	Europe 6	Tue PM	189
Fundamentals of Shape Memory and Related Transitions: Electronic Structure and Phonons.....	Europe 6	Tue AM	136
Fundamentals of Shape Memory and Related Transitions: Mechanical Behavior.....	Europe 6	Wed AM	248
Fundamentals of Shape Memory and Related Transitions: Multiscale Modeling and Applications.....	Europe 6	Wed PM.....	299
General Abstracts: Electronic, Magnetic, and Photonic Materials Division: GaN and Interconnects	Oceanic 7	Mon AM.....	32
General Abstracts: Electronic, Magnetic, and Photonic Materials Division: Magnetic and Ferroelectric Materials	Oceanic 7	Thu AM.....	343
General Abstracts: Electronic, Magnetic, and Photonic Materials Division: ZnO Thin Films and Liquid Crystals.....	Oceanic 4	Thu AM.....	344
General Abstracts: Extraction and Processing: High Temperature Processing.....	Southern 1	Tue AM	137
General Abstracts: Extraction and Processing: Hydrometallurgy, Metal Recovery	Southern 1	Mon PM	87
General Abstracts: Extraction and Processing: Hydrometallurgy, Wastewater Treatment	Northern E1.....	Mon AM.....	34
General Abstracts: Extraction and Processing: Pyrometallurgy, Base Metals.....	Northern E3.....	Mon AM.....	35
General Abstracts: Light Metals Division: Session I.....	Pacific Hall B	Mon AM.....	36
General Abstracts: Light Metals Division: Session II.....	Pacific Hall B	Mon PM	88
General Abstracts: Materials Processing and Manufacturing Division: Forming of Materials and Processes	Northern A4	Mon AM.....	37
General Abstracts: Materials Processing and Manufacturing Division: In Situ Synthesis and Rapid Prototyping	Northern A2	Wed AM	249
General Abstracts: Materials Processing and Manufacturing Division: Modeling and Simulation of Materials and Processes.....	Northern A2	Wed PM.....	300
General Abstracts: Materials Processing and Manufacturing Division: Processing and Microstructural Development	Northern A2	Thu AM.....	345
General Abstracts: Materials Processing and Manufacturing Division: Structure/Processing/Properties Relationships.....	Northern A1	Thu AM.....	346
General Abstracts: Structural Materials Division: Advances in Steel I.....	Europe 5	Tue AM.....	138
General Abstracts: Structural Materials Division: Advances in Steel II.....	Europe 5	Tue PM	190
General Abstracts: Structural Materials Division: Microstructure and Properties of Materials	Europe 5	Wed AM	250
General Abstracts: Structural Materials Division: Nickel Alloys and High Temperature Materials I.....	Europe 5	Wed PM.....	301
General Abstracts: Structural Materials Division: Processing and Properties of Light Metals.....	Europe 6	Thu AM.....	348
General Poster Session.....	N. H. Foyer.....	Mon PM-Wed PM.....	359
Hume-Rothery Symposium: Scattering Studies and the Fundamental Properties of Materials: Session I	Oceanic 7	Mon PM	89
Hume-Rothery Symposium: Scattering Studies and the Fundamental Properties of Materials: Session II	Oceanic 7	Tue AM.....	139
Hume-Rothery Symposium: Scattering Studies and the Fundamental Properties of Materials: Session III....	Oceanic 7	Tue PM	191
Hume-Rothery Symposium: Scattering Studies and the Fundamental Properties of Materials: Session IV....	Oceanic 7	Wed AM	252
Hume-Rothery Symposium: Scattering Studies and the Fundamental Properties of Materials: Session V....	Oceanic 7	Wed PM.....	303
Innovations in Electrometallurgy: Session I	Oceanic 5	Wed PM.....	303
Innovations in Electrometallurgy: Session II.....	Oceanic 5	Thu AM.....	349
Innovations in Measurement Science to Assess the Performance of New Materials in the Real-World: Advanced Measurement Techniques	Australia 3	Wed PM.....	304
Innovations in Measurement Science to Assess the Performance of New Materials in the Real-World: Characterization of Advanced Materials.....	Australia 3	Wed AM	253
Innovations in Measurement Science to Assess the Performance of New Materials in the Real-World: Fundamental Measurement Methods.....	Australia 3	Mon AM.....	38
Innovations in Measurement Science to Assess the Performance of New Materials in the Real-World: High Strain Rate Deformation	Australia 3	Tue AM	140

Innovations in Titanium Technology Symposium: Advances in Alloy Development	Asia 3	Wed AM	254
Innovations in Titanium Technology Symposium: Advances in Materials Processing	Asia 3	Tue PM	192
Innovations in Titanium Technology Symposium: Low Cost Materials and Processing	Asia 3	Mon AM	39
Innovations in Titanium Technology Symposium: Microstructure and Properties I	Asia 3	Wed PM	305
Innovations in Titanium Technology Symposium: Microstructure and Properties II	Asia 3	Thu AM	349
Innovations in Titanium Technology Symposium: Novel Materials and Processes I	Asia 3	Mon PM	90
Innovations in Titanium Technology Symposium: Novel Materials and Processes II	Asia 3	Tue AM	141
Integrated Computational Materials Engineering: Lessons from Many Fields: ICME in Materials Science	Oceanic 4	Wed AM	255
Integrated Computational Materials Engineering: Lessons from Many Fields: ICME in Other Fields	Oceanic 4	Wed PM	307
Intellectual Property in Materials Science: Patents, Tech Transfer and Licensing: Commercialization ...	America's Seminar	Tue PM	193
Intellectual Property in Materials Science: Patents, Tech Transfer and Licensing: Patents	America's Seminar	Tue AM	142
Internet and Other Electronic Resources for Materials Education: Session I	Oceanic 2	Mon AM	40
Magnesium Technology 2007: Alloy Development I	Southern 4	Wed AM	257
Magnesium Technology 2007: Alloy Development II	Southern 4	Wed PM	307
Magnesium Technology 2007: Automotive Applications and USAMP Programs	Southern 5	Mon PM	91
Magnesium Technology 2007: Casting and Solidification I	Southern 5	Tue AM	143
Magnesium Technology 2007: Casting and Solidification II	Southern 5	Tue PM	194
Magnesium Technology 2007: Corrosion and Coatings	Southern 4	Thu AM	350
Magnesium Technology 2007: Magnesium Globalization	Southern 4-5	Mon AM	40
Magnesium Technology 2007: Microstructure and Properties	Southern 5	Thu AM	352
Magnesium Technology 2007: Primary Production, Recycling and Environmental/Welding	Southern 5	Wed AM	258
Magnesium Technology 2007: Thermodynamics and Fundamental Research	Southern 5	Wed PM	309
Magnesium Technology 2007: Wrought Alloys and Forming Processes I: Deformation	Southern 4	Mon PM	92
Magnesium Technology 2007: Wrought Alloys and Forming Processes II: Rolling and Forming	Southern 4	Tue AM	144
Magnesium Technology 2007: Wrought Alloys and Forming Processes III: Extrusions	Southern 4	Tue PM	195
Materials in Clean Power Systems II: Fuel Cells, Solar, and Hydrogen-Based Technologies: Hydrogen Storage Materials in Conjunction with the 8th Global Innovations Symposium: Metal Powders for Energy Production and Storage Applications	Oceanic 6	Tue PM	197
Materials in Clean Power Systems II: Fuel Cells, Solar, and Hydrogen-Based Technologies: Materials for Clean Coal Power Generation and Gas Separation	Asia 2	Wed PM	310
Materials in Clean Power Systems II: Fuel Cells, Solar, and Hydrogen-Based Technologies: Materials for Solar Cells and Photovoltaic Systems	Asia 2	Thu AM	353
Materials in Clean Power Systems II: Fuel Cells, Solar, and Hydrogen-Based Technologies: Materials Oxidation/Corrosion and Protection	Asia 2	Wed AM	259
Materials in Clean Power Systems II: Fuel Cells, Solar, and Hydrogen-Based Technologies: PEMFCs	Asia 2	Mon PM	93
Materials in Clean Power Systems II: Fuel Cells, Solar, and Hydrogen-Based Technologies: Plenary Session	Asia 2	Mon AM	41
Materials in Clean Power Systems II: Fuel Cells, Solar, and Hydrogen-Based Technologies: SOFCs I	Asia 2	Tue AM	145
Materials in Clean Power Systems II: Fuel Cells, Solar, and Hydrogen-Based Technologies: SOFCs II	Asia 2	Tue PM	198
Materials Issues for Advanced Nuclear Systems: Energy Generation and Waste Issues	Europe 5	Mon AM	42
Materials Issues for Advanced Nuclear Systems: Material Characterization Issues	Europe 5	Mon PM	94
Materials Processing and Manufacturing Division Symposium: Mechanics and Materials Modeling and Materials Design Methodologies, in the Honor of Dr. Craig Hartley's 40 years of Contributions to the Field of Mechanics and Materials Science: Homogenization/Constitutive Behavior I	Northern A1	Mon PM	96
Materials Processing and Manufacturing Division Symposium: Mechanics and Materials Modeling and Materials Design Methodologies, in the Honor of Dr. Craig Hartley's 40 Years of Contributions to the Field of Mechanics and Materials Science: Homogenization/Constitutive Behavior II	Northern A1	Tue AM	146
Materials Processing and Manufacturing Division Symposium: Mechanics and Materials Modeling and Materials Design Methodologies, in the Honor of Dr. Craig Hartley's 40 Years of Contributions to the Field of Mechanics and Materials Science: Materials Design	Northern A1	Tue PM	199

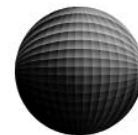


Materials Processing and Manufacturing Division Symposium: Mechanics and Materials Modeling and Materials Design Methodologies, in the Honor of Dr. Craig Hartley's 40 Years of Contributions to the Field of Mechanics and Materials Science: Microstructure Analysis and Representation I.....	Northern A1	Mon AM	44
Materials Processing and Manufacturing Division Symposium: Mechanics and Materials Modeling and Materials Design Methodologies, in the Honor of Dr. Craig Hartley's 40 Years of Contributions to the Field of Mechanics and Materials Science: Microstructure Analysis and Representation II	Northern A1	Wed PM	312
Materials Processing and Manufacturing Division Symposium: Mechanics and Materials Modeling and Materials Design Methodologies, in the Honor of Dr. Craig Hartley's 40 Years of Contributions to the Field of Mechanics and Materials Science: Nanostructure, Defects and Properties	Northern A1	Wed AM	260
Materials Processing Fundamentals: Powders, Composites, Coatings and Measurements.....	Northern A2	Tue PM	200
Materials Processing Fundamentals: Process Modeling.....	Northern A2	Mon PM	97
Materials Processing Fundamentals: Smelting and Refining.....	Northern A2	Tue AM	148
Materials Processing Fundamentals: Solidification and Deformation Processing	Northern A2	Mon AM	45
Materials Processing under the Influence of External Fields: Session I.....	America's Seminar	Mon AM	46
Materials Processing under the Influence of External Fields: Session II.....	America's Seminar	Mon PM	98
Materials Processing under the Influence of External Fields: Session III	America's Seminar	Wed AM	261
Materials Processing under the Influence of External Fields: Session IV	America's Seminar	Wed PM	313
Materials Processing under the Influence of External Fields: Session V	America's Seminar	Thu AM	354
Metrologies for Advanced Materials and Devices: Characterization, Measurement and Testing Science: Metrology for Micro and Nano Structures	Oceanic 6	Tue AM	149
Microstructural Processes in Irradiated Materials: Defect Clusters and Fundamental Radiation Effects	Europe 8	Thu AM	355
Microstructural Processes in Irradiated Materials: Dislocation - Obstacle Interactions and Radiation Induced Segregation.....	Europe 8	Mon AM	48
Microstructural Processes in Irradiated Materials: He Effects, Deformation and Fracture.....	Europe 8	Wed PM	314
Microstructural Processes in Irradiated Materials: Irradiation Effects in Ceramics	Europe 8	Mon PM	100
Microstructural Processes in Irradiated Materials: Modeling.....	Europe 8	Tue PM	201
Microstructural Processes in Irradiated Materials: Modeling, Microstructure and Embrittlement in Fe-Cr Alloys.....	Europe 8	Tue AM	150
Microstructural Processes in Irradiated Materials: Poster Session I.....	Europe 8	Tue PM	202
Microstructural Processes in Irradiated Materials: Poster Session II	Europe 8	Wed PM	316
Microstructural Processes in Irradiated Materials: Reactor Pressure Vessel Steels.....	Europe 8	Wed AM	263
National Academies ICME Study Community Town Hall Meeting.....	Oceanic 4	Wed PM	307
National Science Foundation Workshop: CyberInfrastructure to CyberDiscovery for Materials Science.....	Oceanic 4	Wed AM	256
Outreach Programs in Materials Science and Engineering: Outreach Programs at Universities	Pacific Hall A	Mon AM	49
Outreach Programs in Materials Science and Engineering: Outreach Programs in Industry and Government Laboratories.....	Pacific Hall A	Mon PM	101
Pb-Free Electronic Solders: Alloy Design, Characterization and Service Reliability: Electromigration and Void Formation.....	Oceanic 1	Tue AM	151
Pb-Free Electronic Solders: Alloy Design, Characterization and Service Reliability: Interfacial Effects	Oceanic 1	Mon AM	50
Pb-Free Electronic Solders: Alloy Design, Characterization and Service Reliability: Mechanical Characterization	Oceanic 1	Wed PM	317
Pb-Free Electronic Solders: Alloy Design, Characterization and Service Reliability: Microstructure and Characterization	Oceanic 1	Mon PM	102
Pb-Free Electronic Solders: Alloy Design, Characterization and Service Reliability: Processing and Reliability Issues.....	Oceanic 1	Wed AM	264
Pb-Free Electronic Solders: Alloy Design, Characterization and Service Reliability: Whisker Growth, Design, and Modeling.....	Oceanic 1	Tue PM	204
Phase Stability, Phase Transformations, and Reactive Phase Formation in Electronic Materials VI: Session I.....	Oceanic 2	Mon PM	104
Phase Stability, Phase Transformations, and Reactive Phase Formation in Electronic Materials VI: Session II.....	Oceanic 2	Tue AM	153

Phase Stability, Phase Transformations, and Reactive Phase Formation in Electronic Materials VI: Session III	Oceanic 2	Tue PM	205
Phase Stability, Phase Transformations, and Reactive Phase Formation in Electronic Materials VI: Session IV	Oceanic 2	Wed AM	265
Phase Stability, Phase Transformations, and Reactive Phase Formation in Electronic Materials VI: Session V.....	Oceanic 2	Wed PM.....	318
Plasticity from the Atomic Scale to Constitutive Laws: Atomistic Simulations of Dynamic Processes and Nano-Scale Plasticity	Europe 9	Tue AM.....	154
Plasticity from the Atomic Scale to Constitutive Laws: Dislocation Core Structure and Solute-Dislocation Interactions.....	Europe 9	Mon AM	51
Plasticity from the Atomic Scale to Constitutive Laws: Dislocation Ensembles	Europe 9	Tue PM	206
Plasticity from the Atomic Scale to Constitutive Laws: Dislocation Solute, Precipitate and Grain Boundary Interactions.....	Europe 9	Mon PM	105
Plasticity from the Atomic Scale to Constitutive Laws: Meso-Scale Plasticity	Europe 9	Wed AM	266
Plasticity from the Atomic Scale to Constitutive Laws: Rate Limiting Behavior and Informed Constitutive Laws	Europe 9	Wed PM.....	320
Properties and Performance of High Temperature Alloys and Coatings: Coatings and Oxidation I.....	Asia 4	Tue PM	208
Properties and Performance of High Temperature Alloys and Coatings: Coatings and Oxidation II	Asia 4	Wed AM	268
Properties and Performance of High Temperature Alloys and Coatings: Intermetallics and Multidiscipline.....	Asia 4	Wed PM.....	321
Properties and Performance of High Temperature Alloys and Coatings: Polycrystalline Alloys.....	Asia 4	Mon PM	106
Properties and Performance of High Temperature Alloys and Coatings: Single Crystal Alloys I.....	Asia 4	Mon AM	52
Properties and Performance of High Temperature Alloys and Coatings: Single Crystal Alloys II and Oxidation.....	Asia 4	Tue AM.....	155
Recent Developments in Semiconductor, Electro Optic and Radio Frequency Materials: Progress in Semiconductor Optoelectronics and Beyond.....	Oceanic 6	Mon PM	108
Recent Developments in Semiconductor, Electro Optic and Radio Frequency Materials: Recent Advances in Semiconductor Technologies	Oceanic 6	Mon AM	54
Recycling and Waste Processing: Aluminum	Australia 2.....	Wed AM	269
Recycling and Waste Processing: Automotive Recycling, Global Challenges and Opportunities.....	Australia 2.....	Tue AM.....	157
Recycling and Waste Processing: Batteries and Co/Ni.....	Australia 2.....	Mon PM	110
Recycling and Waste Processing: Materials Recovery from Wastes	Australia 2.....	Mon AM	55
Recycling and Waste Processing: Other Nonferrous	Australia 2.....	Wed PM.....	323
Recycling and Waste Processing: Precious Metals Recovery.....	Australia 2.....	Tue PM	209
Refractory Metals 2007: Oxidation and Thin Films	Europe 6	Mon PM	110
Refractory Metals 2007: Processing and Mechanical Deformation	Europe 6	Mon AM	57
Shape Casting: The 2nd International Symposium: Applications/Novel Processes.....	Northern E2.....	Wed PM.....	324
Shape Casting: The 2nd International Symposium: Liquid Metal/Solidification	Northern E2.....	Mon PM	111
Shape Casting: The 2nd International Symposium: Modeling	Northern E2.....	Wed AM	270
Shape Casting: The 2nd International Symposium: Process Design/Analysis.....	Northern E2.....	Tue AM.....	158
Shape Casting: The 2nd International Symposium: Structure/Property	Northern E2.....	Tue PM	210
Structural Materials Division Symposium: Mechanical Behavior of Nanostructured Materials, in Honor of Carl Koch: Fatigue, and Strengthening Mechanisms at Small Length Scale.....	Asia 5	Mon AM	58
Structural Materials Division Symposium: Mechanical Behavior of Nanostructured Materials, in Honor of Carl Koch: Microstructure and Mechanical Properties of Nanostructured Materials.....	Asia 5	Thu AM.....	357
Structural Materials Division Symposium: Mechanical Behavior of Nanostructured Materials, in Honor of Carl Koch: Plasticity and Deformation Mechanisms at Small Length Scale I	Asia 5	Tue AM.....	159
Structural Materials Division Symposium: Mechanical Behavior of Nanostructured Materials, in Honor of Carl Koch: Plasticity and Deformation Mechanisms at Small Length Scale II	Asia 5	Wed AM	271
Structural Materials Division Symposium: Mechanical Behavior of Nanostructured Materials, in Honor of Carl Koch: Plasticity and Deformation Mechanisms at Small Length Scale III.....	Asia 5	Wed PM.....	325
Structural Materials Division Symposium: Mechanical Behavior of Nanostructured Materials, in Honor of Carl Koch: Poster Session: Mechanical Properties of Nanostructured Materials	Asia 5	Tue PM	213



Structural Materials Division Symposium: Mechanical Behavior of Nanostructured Materials, in Honor of Carl Koch: Processing and Characterization of Materials Subjected to Severe Plastic Deformation	Asia 5	Mon PM	112
Structural Materials Division Symposium: Mechanical Behavior of Nanostructured Materials, in Honor of Carl Koch: Stability, Strain and Stress	Asia 5	Tue PM	211
The Material Recycling Industry: Global Challenges and Opportunities: Plenary Session	Southern 1	Mon AM	59
Towards Functional Nanomaterials: Synthesis, Characterization, and Applications: Directed Nano Fabrication	Oceanic 5	Mon AM	60
Towards Functional Nanomaterials: Synthesis, Characterization, and Applications: Nano Magnetism, Ferroelectric, Mechanics, and Other Properties	Oceanic 5	Mon PM	114
Towards Functional Nanomaterials: Synthesis, Characterization, and Applications: Nanoscale Superstructures, Metallic Nanoparticles and Plasmon	Oceanic 5	Tue AM	161
Towards Functional Nanomaterials: Synthesis, Characterization, and Applications: Nanowires and Nanotubes	Oceanic 5	Tue PM	220
Towards Functional Nanomaterials: Synthesis, Characterization, and Applications: Quantum Dots	Oceanic 5	Wed AM	273
Wide Band-Gap Semiconductor Nanostructures: Session I	Oceanic 4	Mon AM	62
Wide Band-Gap Semiconductor Nanostructures: Session II	Oceanic 4	Mon PM	115
Wide Band-Gap Semiconductor Nanostructures: Session III	Oceanic 4	Tue AM	162
Wide Band-Gap Semiconductor Nanostructures: Session IV	Oceanic 4	Tue PM	221



2007 Nanomaterials: Fabrication, Properties and Applications: Session III

Sponsored by: The Minerals, Metals and Materials Society, TMS Electronic, Magnetic, and Photonic Materials Division, TMS: Nanomaterials Committee
Program Organizers: Wobong Choi, Florida International University; Ashutosh Tiwari, University of Utah; Seung Kang, Qualcomm Inc.

Tuesday AM Room: Oceanic 3
 February 27, 2007 Location: Dolphin Hotel

Session Chairs: Seung Kang, Qualcomm Inc.; Young Hee Lee, Sungkyunkwan University

9:00 AM Keynote

Geometry-Controlled Carbon Nanotubes and Related Structures: *Sungho Jin*¹; ¹University of California at San Diego

For successful engineering applications of carbon nanotubes and related nanostructures, an ability to control their basic configurations is essential. In this talk, various processing techniques for controlling the nanotube geometry and microstructures such as the diameter, length, alignment, spacing, periodicity, 90° or zig-zag bending, single- or multi-branching, opening, cutting, shortening, and bonding will be discussed. Additional geometry modifications such as the removal of catalyst metal particles from aligned multiwall nanotubes for purification and uncontaminated electrochemical reactions, tip opening and filling of nanotubes for nanocomposite formation, and coating of nanotubes with high-density Pt catalyst nanoparticles will also be discussed. The implications of such geometry controls for physical, electronic, chemical, mechanical, and bio-related properties will be discussed in relation to potential technical applications such as field emission devices, sensors, nanosprings, nanosolenoids, AFM probes, fuel cell electrodes, electronic circuit nano interconnections, and nanocomposites.

9:40 AM Invited

Carbon Nanotube Field Emission X-Ray Technology for Biomedical Imaging and Homeland Security Applications: *Otto Zhou*¹; ¹University of North Carolina Chapel Hill

X-ray radiation is widely used for applications ranging from non-destructive testing, diagnostic medical imaging to security screening. The conventional x-ray source, based on the original design of Roentgen and Coolidge, has several intrinsic limitations due to the use of thermionic electron source. Recently we developed a field emission x-ray technology using carbon nanotube (CNT) emitters as the “cold” electron source. The device can generate temporally modulated x-ray radiation with a flux that is comparable to today’s commercial thermionic x-ray sources. We have also developed a multi-pixel x-ray source and demonstrated the feasibility of multiplexing radiography which has the potential to significantly increase the speed for tomographic imaging. The performance of the CNT field emission x-ray source will be presented. The applications of this new field emission x-ray technology have been demonstrated in devices including micro-CT scanner for in vivo small animal imaging. The results will be discussed.

10:05 AM

Carbon Nanotube Emission Enhancement by Microchannel Plate and Field Emission of Tungsten Oxide Multistage Field Emitters: *Raghunandan Seelaboyina*¹; Jun Huang¹; Wobong Choi¹; ¹Florida International University

In this work we report on, amplification technique for high current emission from thin multiwall carbon nanotubes and emission properties of tungsten oxide multistage field emitters. The nanotubes were synthesized by thermal chemical vapor deposition which demonstrated excellent field emission properties with a turn-on field ~1 V/μm and field enhancement factor ~9300. Emission was stable under DC bias with 2% average fluctuation. Total emission current was enhanced by 7.5 times when an electron multiplier microchannel plate was inserted between anode and cathode. Multistage field emitters consisted of tungsten oxide nanowires grown by thermal chemical vapor deposition on electrochemically sharpened tungsten tip. Field emission measurements of the emitters showed a low threshold field ~0.95 V/μm, high emission current 170 μA and a large field enhancement factor ~19800. High emission current of few

μA was also observed in relatively poor vacuum ~3x10⁻³ Torr, and emission properties were recoverable at 1x10⁻⁶ Torr.

10:20 AM

Health Hazards of Manufactured, Natural Environmental, and Other Anthropogenic Atmospheric Nanoparticulate Materials: Past, Present, and Future: *Lawrence Murr*¹; ¹University of Texas at El Paso

Beginning with chrysotile asbestos, the most versatile, multifunctional nanomaterial of all time (with more than 4000 commercial applications over more than 2000 years) and described by Pliny the Elder circa 70 AD as “the disease of slaves” in describing the plight of slave workers in asbestos mines, the plethora of health hazards for nanomaterials, particularly nanoparticulate materials, will be reviewed. In addition to asbestos manufacturing and commercialization, the hazards of asbestos as a geological contaminant and its connection to stomach cancers resulting from poor washing of talc from rice will be discussed. Other natural mineral dusts will be discussed as health hazards, including house dust. The potential for respiratory hazards as well as ingestion and dermal responses for a wide range of nanoparticulate materials in the environment will be examined based on current in-vitro and in-vivo studies, and future trends and precautions discussed in that context.

10:35 AM Break

10:50 AM Invited

Carbon Nanotube Cathodes for Microscopy and High Frequency Applications: *Ken Teo*¹; Mark Mann¹; William Milne¹; Eric Minoux²; Ludovic Hudanski²; Pierre Legagneux²; Oliver Groening³; Franck Peauger⁴; Dominique Dieumegard⁴; ¹University of Cambridge; ²Thales Research and Technology; ³EMPA; ⁴Thales Electron Devices

Plasma enhanced chemical vapour deposition can be used to grow carbon nanotubes with defined alignment, position, diameter, length and shape. This method is used to fabricate individual nanotubes at the end of tungsten needles as point electron sources, and arrays of nanotubes on flat surfaces as large area cathodes. The carbon nanotube point electron source is evaluated in terms of stability, noise, energy spread, emission pattern and brightness, and compared against state-of-the-art electron sources today. The performance of arrays of nanotubes is evaluated and the maximum current (or current density) reached for an array depends on the uniformity of the nanotubes and the current carrying capability of each nanotube. Our results show that peak current densities of 1-5A/cm² in dc or 1-12A/cm² at radio frequency (GHz). Direct modulation at 1.5GHz (Class D) and 32GHz (Class A) of the carbon nanotube cathodes was achieved.

11:15 AM

Decoration of Functionalized Single-Walled Carbon Nanotubes with Metal: *Qiang Zeng*¹; Enrique Barrera¹; ¹Rice University

This study is considered as a method for producing high conducting reinforcements for composite materials by using Single-walled Carbon Nanotubes (SWNTs). In this research, Homogenous dispersion and dense nuclear sites have been found to be necessary condition to form uniform coating on SWNTs. Several surface modification has been applied to achieve considerable improvement in the dispersion of purified single-walled carbon nanotubes. The results show that nickel could be successfully plated onto the activated surfaces of SWNTs through electroless plating. It was observed that high surface coverage of Pd-Sn catalytic nuclei is needed to form high quality coatings. The samples were characterized by using scanning electron microscopy (SEM), transmission electron microscopy (TEM), Raman spectroscopy, X-ray Photoelectron Spectroscopy (XPS) and energy-dispersive X-ray spectroscopy (EDX). It has been demonstrated that the surface modification is another way to control the coating quality. The metal-coated SWNTs are ideal for subsequent processing including composite consolidation or mixing.

11:30 AM

Spinning of Polymer Nano-Composite: Mostafa El-Ashry¹; Kareem Gouda¹; ¹British University in Egypt

Polymer nano-composites are attractive in many engineering and medical applications because of their distinctive mechanical, chemical, and electrical properties typically evident in nanomaterials. We propose a nano-composite fabrication method that can produce continuous polymer fibers that incorporate single wall carbon nanotube (SWCNT) and/or Multi-wall

carbon nanotube (MWCNT). This technique can spin nano-composites from precursor rheologies that would be considered "unspinnable" by any other current method. As such, this technique may allow the fabrication of novel composite structures, assist in the fabrication of nano-composite from new materials, and allow the use of novel chemical routes in nano-composites fabrication.

11:45 AM

Synthesis and Characterization of Ce-Doped YAG by Citrate-Nitrate Gel Combustion Process: *Xianzhong Guo*¹; *Xiaomei Guo*¹; *Kewen Li*¹; *Shanshan Liang*²; ¹Boston Applied Technologies, Inc.; ²Stony Brook University

Cerium doped yttrium aluminum garnet (YAG:Ce) powders were synthesized through a citrate-nitrate gel combustion process. The influence of heat-treatment and Ce content on the phase formation and photoluminescent properties of YAG:Ce was investigated by thermal analysis (DTA/TGA), powder X-ray diffraction (XRD), and luminescent measurement. The pure garnet phase was obtained directly from amorphous YAG:Ce precursors. The heat-treatment condition will affect the peak position and intensity of the emission of YAG:Ce phosphors. The peak position will shift towards red region, as increasing the Ce content in YAG, until cerium ions are saturated in the garnet structure.

Advanced Metallic Composites and Alloys for High Performance Applications: Refractory Alloys and Composites

Sponsored by: The Minerals, Metals and Materials Society, ASM International, TMS Structural Materials Division, ASM Materials Science Critical Technology Sector, TMS/ASM: Composite Materials Committee, TMS/ASM: Mechanical Behavior of Materials Committee

Program Organizers: Awadh Pandey, Pratt and Whitney Rocketdyne; Kevin Kendig, Air Force Research Laboratory; John Lewandowski, Case Western Reserve University

Tuesday AM Room: Europe 10
February 27, 2007 Location: Dolphin Hotel

Session Chair: John Lewandowski, Case Western Reserve University

9:00 AM Invited

Ductility and Impact Resistance of P/M Molybdenum-Rhenium Alloys: *Jochaim Schneibel*¹; *Gerhard Leichtfried*²; *Martin Heilmaier*³; ¹Oak Ridge National Laboratory; ²Plansee SE; ³Otto-von-Guericke University Magdeburg

Mo-Re alloys containing between 5 and 47.5 wt% Re were fabricated from Mo and Mo-Re powders by sintering and hot radial forging. Up to a concentration of 41 wt% Re, the Charpy ductile-to-brittle transition temperature decreased monotonically with increasing rhenium concentration. Between 10 and 41 wt% rhenium, the room temperature tensile ductility of recrystallized Mo-Re remained nearly constant with values on the order of 35 to 45%. This result differs from the low ductility values observed previously by Lundberg (1997) for compositions on either side of Mo-13 wt% Re. Possible reasons for this discrepancy will be discussed. JHS acknowledges support for this work by the Division of Materials Sciences and Engineering, U.S. Department of Energy, under contract DE-AC05-00OR22725 with Oak Ridge National Laboratory managed by UT-Battelle.

9:20 AM

A Nitride-Based Reaction for the Formation of a Three-Phase Mo-Si-B Alloy: *Joe Cochran*¹; *Michael Middlemas*¹; ¹Georgia Institute of Technology

Mo-Si-B intermetallic alloys have the potential of possessing both the oxidation resistance and mechanical properties required for the next generation of jet turbine engine blades. In a novel approach, three-phase alloys of α -Mo, A15 (Mo₃Si) and T2 (Mo₃SiB₂) have been produced through the reaction of molybdenum, Si₃N₄ and BN powders. Reaction of the starting materials was shown to occur between 1200°C and 1400°C. Densities at 95% of theoretical were achieved by sintering to 1600°C. This powder metallurgy approach yields a fine dispersion of intermetallics in a molybdenum matrix with grain sizes on the order of 1-4 μ m, which is not achieved through melt processing

routes. Electron back-scatter diffraction imaging was used to investigate the dispersion of the two different intermetallic phases within the molybdenum matrix. The reaction kinetics between molybdenum and the nitrides were determined using thermo-gravimetric analysis.

9:40 AM

Nano-Grained WC-Co Composite Powders by the Chemical Vapor Synthesis: *Taegong Ryu*¹; *Manoleta Mena*¹; *Hong Yong Sohn*¹; *Gilsoo Han*¹; *Zhigang Fang*¹; ¹University of Utah

A chemical vapor synthesis (CVS) process that has previously been used for preparing the aluminides of titanium and nickel, and other metallic and intermetallic powders has been applied to the preparation of WC-Co nanocomposite powder. The reduction and carburization of the vaporized chlorides by methane-hydrogen mixtures produced nanosized WC and Co composite powder, which sometimes contained W₂C, W and/or the η (Co₃W₃C) phase. The produced powders were treated in hydrogen to fully carburize the W₂C and W as well as remove excess carbon. The products were characterized using XRD, carbon analyzer, and TEM. The observed uniformity of mixing of the composite powder is important to ensure high quality of the bulk cemented tungsten carbide product after consolidation. The effects of temperature, reactant concentration, CH₄ to WCl₆ ratio, CH₄ to H₂ ratio, residence time, CoCl₂ and CO₂ contents, and the secondary treatment on the powder composition and particle size were determined.

10:00 AM

An Investigation on Oxidation Behavior and Microstructure of Plasma Sprayed W/Cu Composite: *Suk-Bong Kang*¹; *Hyun-Ki Kang*²; *Kwangjun Euh*¹; ¹Korea Institute of Machinery and Materials; ²Almati Company, Ltd.

Tungsten/copper composites have been used for heat dissipation materials in microelectronic device, heavy electric contacts, and warhead materials in military field. They have usually been made by the infiltration of a desired tungsten shape (skeleton) with liquid copper to achieve full densification. However, it needs several subsequent processing steps which require lots of energy and high cost. Compared to the infiltration, the plasma spraying process that directly sprays powders onto substrates has a considerable potential to be very profitable for the formation of thin or thick layers in some industrial applications. The purposes of this research are to decrease the porosity, to explore the oxidation between the surface and inner layer of composite which impairs the thermal conductivity in the heat sink materials, and to control the chemical composition uniformly in the plasma sprayed composites.

10:20 AM Break

10:40 AM

Research on Fabrication and Technique of New Carbon - Copper Composite Slider: *Lian Wei Yang*¹; *Jinhui Li*¹; *Guang Yao*²; ¹Tsinghua University; ²Northeastern University

Slider is quite important collecting electricity material of electric locomotive. Based on applied status and existed problem of current electric locomotive pantograph sliders, a new pantograph slider material was designed to meet the need of electric locomotive development, and different technique were compared to show their influence to the performance of slider. The results showed that performance of the new slider made by hot pressure technique was better. Not only was its resistance very low, but also its performance of friction, abrasion and impact toughness etc. was greatly improved compared to Germanic immersed metal slider with reduced friction coefficient 25 %, increased impact toughness 2.7 times and improved conductance 67 times; Its conductance improved 46.4 times; increased impact toughness 2.2 times compared to MC slider made in Japan.

11:00 AM

Mechanical Testing of the Molybdenum Solid-Solution Matrix in MoSiB Alloys: *Chris Rockett*¹; *Michael Middlemas*¹; *Joe Cochran*¹; ¹Georgia Institute of Technology

MoSiB alloys show promise as the next-generation turbine blade material due to their high-temperature strength and oxidation resistance afforded by a protective borosilicate surface layer. Powder processing and reactive synthesis of these alloys has proven to be a viable method and offers several advantages over conventional melt processing routes. To achieve both high-temperature oxidation resistance and satisfactory room-temperature mechanical strength, the microstructure must have well-dispersed intermetallics in a continuous



matrix of molybdenum solid-solution (Mo_{ss}). However, bend testing of pure Mo and Mo_{ss} samples has shown that, while the powder processing route can produce ductile Mo metal, the hardening effect of Si and B in solid-solution renders the matrix brittle. Testing at elevated temperatures (200°C) was performed in order to determine the ductile-to-brittle transition temperature of the metal as an indication of ductility. Methods of ductilizing the Mo_{ss} matrix such as annealing and alloying additions have been investigated.

11:20 AM

High Temperature Strength of Mo-Re-X Ternary Alloys: *Joachim Schneibel*¹; E. Felderman²; ¹Oak Ridge National Laboratory; ²Arnold Engineering Development Center

Additions of Re to Mo improve the room-temperature ductility, but do not significantly increase the strength at elevated temperatures (e.g., 1700 K). In this work, the influence of ternary alloying elements such as Zr, Al, Ti, Nb, Ta, Cr, Hf, and Si on the high temperature compression strength of Mo-Re-X alloys was evaluated. Hafnium was found to be a particularly effective – 2 at% Hf approximately doubled the 1700 K yield strength of Mo-41 wt% Re. Also, Hf additions up to 2 at% reduced the tensile stress at which room temperature twinning occurred. The room temperature ductility of specimens prepared from cast and annealed Mo-Re and Mo-Re-Hf was only a few percent, but higher ductility values are expected with improved material and specimen preparation.

11:40 AM

Improved Mechanical Properties of Ultrafine Grained Nb-1%Zr via Equal Channel Angular Extrusion (ECAE): *Guney Yapici*¹; Ibrahim Karaman¹; Hans Maier²; ¹Texas A&M University; ²University of Paderborn

Nb-1%Zr is widely used in a number of applications ranging from biomedical industry to space nuclear reactor concepts. Their relatively high operating temperature capability, chemical and biocompatibility and stability in nuclear environments make them attractive candidates over other alloy systems. In general, these applications require high strength and desired elastic modulus combined with enhanced ductility that Nb-1%Zr lacks in wrought condition. This talk will summarize our recent work on the ECAE of Nb-1%Zr for achieving target mechanical properties by engineering microstructure and crystallographic texture. Nb-1%Zr was processed up to 16 passes at room temperature without any shear localization. Post-processing of extruded billets with conventional forming techniques assisted by low temperature annealing treatments led to the formation of microstructures yielding both high tensile strengths and uniform strains (over 900 MPa and 20% ductility). Low cycle fatigue experiments showed stable response with improved cyclic stress range and number of cycles to failure.

12:00 PM

Phosphide Precipitates in Copper-Based Alloys: *Joon Hwan Choi*¹; ¹Korea Institute of Machinery and Materials

Several types of copper-based alloys having phosphorus with one or more transition metals such as manganese, nickel and iron were designed to have high strength with good electrical conductivity. A study on aging characteristics of the Cu-TM-P (TM= Mn,Ni,Fe) alloys showed that the molar ratios between the total amount of the transition metals and phosphorus to obtain an optimum combination of mechanical and electrical properties were close to 2:1. TEM analysis revealed precipitate phases formed during aging had M_2P (M = Mn and/or Ni and/or Fe) formulation and their crystallographic structures depended on the type of the elements. TEM analysis also showed there existed orientation relationships between the precipitates and copper matrix in non-recrystallized regions of the alloys.

12:20 PM

Comparison and Characterization of Copper-Graphite Composites Made with Cu-Coated and Uncoated Graphite Powders: *Liu Wei*¹; Yao Guangchun¹; Liu Yihan¹; ¹Northeastern University

Copper-graphite composites of graphite contents of 5, 10, 15, and 20 wt% made by powder metallurgy route using either Cu-coated graphite powders or mixture of copper and graphite powders. The Cu-coating process of graphite powders was carried out using electroless coating technique. Physical and mechanical properties, electrical conductivity, energy to fracture and wear behaviour, have been measured. It was found that composites made by Cu-coated and uncoated graphite have lower rates and friction coefficients than

those made from pure copper, and made by Cu-coated graphite have better mechanical properties than uncoated graphite. The technological conditions were also studied to determine the optimum conditions.

Advances in Computational Materials Science and Engineering Methods: Phase Field Methods I

Sponsored by: The Minerals, Metals and Materials Society, TMS Structural Materials Division, TMS: Biomaterials Committee, TMS/ASM: Computational Materials Science & Engineering

Program Organizers: Koen Janssens, Paul Scherrer Institute; Veena Tikare, Sandia National Laboratories; Richard LeSar, Iowa State University

Tuesday AM
February 27, 2007

Room: Europe 7
Location: Dolphin Hotel

Session Chair: Richard LeSar, Iowa State University

9:00 AM Introductory Comments

9:05 AM Invited

Phase-Field Modeling of Solid State Phase Transformations and Microstructure Evolution: *Long Qing Chen*¹; ¹Pennsylvania State University

Many of the technologically important materials are designed by controlling their phase transformations and/or microstructure evolution. Examples include the improvement of mechanical properties through solid state precipitation reactions in alloys such as Ni-based superalloys and the useful dielectric properties and electro-mechanical coupling effects by manipulating the phase transitions in ferroelectric crystals. This presentation will briefly review the applications of phase-field method to solid state phase transformations and microstructure evolution. A number of recent advances will be highlighted, including nucleation in the presence of long-range elastic interactions, ferroic transitions and domain structures thin film and bulk crystals, and multiscale modeling of alloy microstructure evolution in complex alloys.

9:40 AM Question and Answer Period

9:45 AM

A Comparative Study of Numerical Methods and Computational Tools for Phase Field Equations of Solidification: *Zhiheng Huang*¹; Paul Conway¹; ¹Loughborough University

A Partial Differential Equation (PDE) or coupled PDEs need to be solved in phase field microstructural modelling. Finite difference discretization in space is commonly used to solve such equations numerically. Spectral methods can also solve PDEs to a high accuracy on a simple domain. However, those two methods should be treated with care when the domain of interest is irregular. In such cases, finite volume method or finite element method is a natural alternative. A numerical algorithm implemented in a basic computer language such as C normally runs fastest. However, some high level computing environments or software packages provide the advantages of easy implementation and flexibilities in visualization. This paper provides a comparative study of using different numerical methods and computational tools to solve coupled phase field equations of solidification. The methodologies presented in this paper can be equally applied to other PDEs in phase field modelling.

10:10 AM Question and Answer Period

10:15 AM

A Level Set Simulation of Dendritic Solidification of Multi-Component Alloys: *Nicholas Zabaravski*¹; Lijian Tan¹; ¹Cornell University

A level set method combining features of front tracking methods and fixed domain methods is presented to model microstructure evolution in the solidification of multi-component alloys. Phase boundaries are tracked by solving the multi-phase level set equations. Diffused interfaces are constructed from these tracked phase boundaries using the level set functions. Based on the assumed diffused interfaces, volume-averaging techniques are applied for energy, species and momentum transport. Microstructure evolution in multi-component alloy systems is predicted using realistic material parameters. Techniques including fast marching, narrow band computing and adaptive

meshing are utilized to speed up computations. Several numerical examples are considered to validate the method and examine its potential for three-dimensional solidification modeling of practical alloy systems.

10:40 AM Question and Answer Period

10:45 AM Break

11:15 AM

Phase Field Modeling of Strained Heteroepitaxial Multilayer Thin Film Evolution: *Ramanarayan Hariharaputran*¹; Vivek Shenoy¹; ¹Brown University

Nanopatterns formed during multilayer growth by Asaro Tiller Grinfeld instability of strained/spacer layers or alternately strained layers are of current interest for their unique optical and electronic properties. Earlier theoretical studies were restricted to linear stability analysis to identify a phase stability diagram as a function of kinetic parameters with only surface diffusivity and simplified elastic state of the multilayer. Here, we present a new phase field model to simulate the non-linear evolution of strained multilayer growth. We observe three growth regimes namely, layered superlattice growth of alternate phases, aligned correlated islands and lateral composition modulation of the two phases which agree with experimental observations. We characterize our results in terms of kinetic parameters namely, deposition flux, surface and bulk diffusivities and material parameters like misfit strain and surface energies of the individual layers.

11:40 AM Question and Answer Period

11:45 AM

Multiscale Phase Field Modeling of Phase Transformations in Solids: *Valery Levitas*¹; Dong-Wook Lee¹; Dean Preston²; ¹Texas Tech University; ²Los Alamos National Laboratory

The following basic problems of modeling of martensitic phase transformations based on the Ginzburg-Landau approach are discussed: 1. New thermodynamic potentials for stress-induced martensitic phase transformations, both for small and large strains. 2. Analytical solutions for one-dimensional spatial variation of the order parameter: various types of static microstructures, their stability and physical interpretation. 3. Phase transformations in nanosize sample: surface effect, new microstructures, new functionally graded nanophases, barrierless surface-induced nucleation. 4. Finite element modeling martensite nucleation at dislocations and microstructure formation. Alternative phase field modeling approach is developed for the scale from 100nm and without upper limit. Martensitic microstructure evolution in a single and polycrystalline sample under uniaxial loading is found using finite elements method.

12:10 PM Question and Answer Period

12:15 PM

Computing Property Variability of Polycrystals Induced by Grain Size and Orientation Uncertainties: *Nicholas Zabaras*¹; *Sethuraman Sankaran*¹; ¹Cornell University

Multiscale computational methods bridging models at micro scale with macro properties is a problem of practical significance since many macroscopic properties depend strongly on geometrical variability of the micro-constituents. Probability distribution functions (PDFs) providing a complete characterization of microstructural variability in polycrystalline materials using limited information is difficult to obtain since this inverse problem is highly ill-posed. We use the maximum entropy principle to compute a PDF of microstructures based on given information about a microstructural system. Microstructural features are incorporated into the maximum entropy framework by obtaining data either from experiments or simulations. Grain size features are here extracted from a set of representative microstructures using phase-field simulations. Microstructures are sampled from the computed PDF using concepts from computational geometry and voronoi-cell tessellations. These microstructures are then interrogated using homogenization techniques to evaluate the variability of non-linear macro properties.

12:40 PM Question and Answer Period

Advances in Microstructure-Based Modeling and Characterization of Deformation Microstructures: Characterization of Deformed Structures II

Sponsored by: The Minerals, Metals and Materials Society, ASM-MSCTS: Texture and Anisotropy Committee, ASM-MSCTS: Texture and Anisotropy Committee

Program Organizers: Reza Shahbazian Yassar, Center for Advanced Vehicular Systems; Sean Agnew, University of Virginia; Jiantao Liu, Alcoa Technical Center

Tuesday AM Room: Europe 1
February 27, 2007 Location: Dolphin Hotel

Session Chairs: Reza Shahbazian Yassar, Center for Advanced Vehicular Systems; Matthew Miller, Cornell University

9:00 AM

Influence of the Interactions between Dislocation Mechanisms on Internal Strain Generation in HCP Zircaloy-2: *Feng Xu*¹; Mark Daymond¹; Rick Holt¹; ¹Queen's University

Zircaloy2 is an hcp alloy, used in nuclear industries for core components, e.g. pressure tubes in heavy water reactors and fuel cladding in heavy and light water reactors. Intergranular strains in Zircaloy2 can greatly affect mechanical performance. It is thus important to know how the material responds on macro- and microscopic scales to different external loadings, and what deformation mechanisms lead to the observed responses. We have used neutron diffraction to determine the lattice strain development/texture changes when the material was subjected to either compression or tension, in three directions relative to a parent texture, and elasto-plastic self-consistent models to interpret the data. Model parameters describing the deformation were obtained through simultaneous fitting of all experimental flow curves and internal strain data. Assessment of the data set demonstrated the importance of incorporating hardening effects arising due to interaction between different dislocation mechanisms. Substantial tensile twinning was inferred from intensity changes.

9:25 AM Invited

Measuring the Mechanical Response of Polycrystalline Alloys at the Crystal Level: *Matthew Miller*¹; ¹Cornell University

While multiscale models are being employed more regularly, truly multiscale validation experiments are much less common. Using new in-situ mechanical loading / diffraction techniques and technologies, it is now possible to measure lattice strains and quantify stress on the crystal level in-situ using synchrotron x-ray diffraction. This talk describes an experimental system and approach developed at Cornell and employed at the Cornell High Energy Synchrotron Source (CHESS) and the Advance Photon Source (APS). This system was designed to load polycrystalline samples while conducting x-ray diffraction experiments. A 0.5mm x 0.5mm beam of 50-100 keV synchrotron x-rays is used to interrogate an aggregate of grains. While loaded, the sample stage is rotated and strain pole figures are constructed. Lattice strain distributions functions (LSDFs) and crystal stresses are then derived. In this manner, the three-dimensional response of the crystals can be ascertained. This talk describes recent work on two phase titanium alloys.

9:50 AM

Application of the Artificial Intelligence Techniques in Modeling the Microstructure-Property Relationships of Materials: *Osama AbuOmar*¹; Reza Shahbazian Yassar²; Eric Hansen³; Kyla Stoltzing⁴; ¹Computer Science Department; ²Center for Advanced Vehicular Systems; ³Mississippi State University; ⁴Mechanical Engineering Department

The quantitative analysis of physically measured microstructural parameters plays an important role in establishing the microstructure-property relationship of materials. In the present research, various machine learning algorithms were used to establish the correlation between dislocation substructures and the materials' flow stress. Using Nye's dislocation density tensor, the densities of geometrically necessary dislocations were calculated and an algorithm was developed to extract the thickness of the dislocation (substructures) boundaries and the mean free path of the subcells. In the next



step the measured dislocation parameters were correlated with the materials flow stress using the artificial intelligence techniques.

10:10 AM

Characterization of Deformed Polycrystalline Cubic Alloys Using 2-Point Spatial Correlations: Christopher Hovaneč¹; Dejan Stojaković¹; Surya Kalidindi¹; Roger Doherty¹; ¹Drexel University

The vast majority of characterization methods rely solely on distribution functions which do not provide adequate information regarding the morphological features of the microstructure that are needed in establishing rigorous microstructure-property-processing linkages. It will be shown in this study that a richer description of the microstructure in polycrystalline metals can be attained by documenting the two-point correlation functions from Orientation Imaging Microscopy (OIM) scans obtained on a set of oblique sections made in the sample. This technique provides a rigorous three-dimensional statistical description of the first-order topological features in the microstructure. The relative advantages and disadvantages of this methodology will be discussed.

10:30 AM

A Novel Approach to the Rapid Population of Databases for Modeling of Microstructural Evolution and Mechanical Properties: Benjamin Peterson¹; Erin Barry¹; Santhosh Koduri¹; Peter Collins¹; Gopal Viswanathan¹; Vladimir Levit¹; Hamish Fraser¹; ¹Ohio State University

The microstructural evolution and mechanical properties of Timetal 550 (Ti-4Al-4Mo-1Zr-1Sn, wt%) has been investigated as a function of thermal history. The heat-treatment schedules have been varied in a controlled fashion using two different types of thermal-mechanical simulators, namely a Gleeble thermo-mechanical simulator and an Instron Electrothermo-mechanical tester (ETMT), each of which resistively heats the sample. The microstructures of samples heat-treated using these two techniques have been quantified using rigorous stereological procedures. These data have been used to populate databases relating thermal history, microstructure, and properties. These databases have been used to develop Bayesian Neural Network models, and these will be demonstrated. Finally, it will be shown that these models may be used to perform virtual experiments that yield information concerning the mechanisms of microstructural evolution.

10:50 AM Break

11:05 AM Invited

Grain Orientation, Deformation Microstructure and Flow Stress: Niels Hansen¹; X. Huang¹; G. Winther¹; ¹Risø National Laboratory

Dislocation structures in deformed metals have been analyzed quantitatively by transmission electron microscopy, high-resolution electron microscopy and Kikuchi line analysis. A general pattern for the microstructural evolution with increasing strain has been established and structural parameters have been defined and quantified. It has been found that two dislocation patterns co-exist in all grains, however, with very different characteristics dependent on grain orientation. This correlation with the grain orientation has been applied in modelling of the tensile flow stress and the flow stress anisotropy of FCC polycrystals. In conclusion some future research areas are briefly outlined.

11:30 AM

Rolling History Microstructural Analyses of Texture Gradients for 6022 Aluminum Sheet: Christina Burton¹; Mark Horstemeyer¹; Paul Wang¹; Reza Shabbazian Yassar¹; ¹Mississippi State University

This presentation covers the microstructural analyses of texture gradients of rolled 6022 aluminum sheet at various stages of the manufacturing process. The characterization of the history effects will provide a database for multiscale advanced material modeling. The rolling steps comprise reductions of a 6-inch billet to a 3-inch billet to a 1/8-inch sheet, an annealing process of the 1/8-inch sheet, and finally a reduction to the 1/32-inch finish gauge sheet. The texture gradients studied are taken from the center of the rolled thickness to the rolling surface of a hot rolled 6-inch billet and a hot rolled 3-inch billet. Characteristics of grain boundaries and texture gradients are measured by scanning electron microscope (SEM) analyses using a high resolution electron back scatter detector (EBSD) for the various stages of material.

11:50 AM

The ODF of the Recrystallization Texture and the 40<111> Transformed Rolling Texture of Al-Mn-Mg Alloy: Jiantao Liu¹; Joseph Fridy¹; Robert Dick¹; Thomas Rouns¹; Edward Llewellyn¹; ¹Alcoa Technical Center

It has been observed that either the Cube orientation {001}<100> or the P orientation {011}<566> could be the major recrystallization texture of the Al-Mn-Mg alloy sheet after cold rolling followed by annealing, depending on whether the intermediate heat-treatment (IHT) was imposed on the as received hot rolled sheet or not. In both cases, the orientation distribution function (ODF) of the deformation texture was transformed by 40<111> rotations. The transformed ODF was then compared to the ODF of recrystallization texture. In this way, the 40<111> orientation relationship between deformation texture and recrystallization texture was studied. Based on the 40<111> orientation relationship, the formation of the P orientation {011}<566> was discussed.

12:10 PM

Three Dimensional EBSD Characterizations of Deformed Materials: Matthew Nowell¹; Stuart Wright¹; ¹EDAX-TSL

Automated Electron backscatter diffraction (EBSD) or Orientation Imaging Microscopy (OIM) has been used by many researchers to characterize the spatial variance of orientation in deformed microstructures. The local variations in orientation provide an indication of residual plastic strain in the material. To date, the majority of studies correlating local orientation variations with strain have been performed on two dimensional planar sections and assumptions made on the character of strain based on local variations in orientation in the plane without any knowledge of the variations in the third dimension. Recent OIM scan performed on serial sections of deformed materials show that it is difficult to accurately infer the three-dimensional variation in local orientation and can, thus, lead to misleading assumptions on the spatial distribution of residual strain in deformed polycrystals. This study outlines the methodology behind the three dimensional characterization of material microstructures by OIM and shows results on deformed materials.

12:30 PM

Investigation of Plasticity in Nanoscale Metallic Multilayers by In-Situ Synchrotron Diffraction: Cahit Aydiner¹; Yun-Che Wang¹; Don Brown¹; Amit Misra¹; Jon Almer²; ¹Los Alamos National Laboratory; ²Argonne National Laboratory

Cu-Nb multilayer films have been studied for the first time by in-situ synchrotron X-ray diffraction (SXR) to investigate nanometer scale plasticity. Previous studies on this material system have shown that, as the layer thickness is reduced to tens of nanometers, glide of single dislocations substitute the dislocation pile-up at the interfaces, signifying a fundamental change in plasticity mechanism. To further our understanding of these mechanisms, elastic strain tensors were obtained in each phase during tensile tests with in-situ SXR. Samples of layer thicknesses of 5, 20, and 100 nanometers have been used to span the length scales of interest. The experimental data is interpreted by both an adaptation of elasto-plastic self-consistent model and polycrystalline finite element computations. In addition, strain rate dependence (in the quasi-static to 0.01 1/s range) of these mechanisms will be reported, which could now be investigated with SXR owing to a next generation fast area detector.

12:50 PM

Grain Refinement and Hardness Increase of Copper Subjected to High Pressure Torsion: Youshi Hong¹; Fengshou Shangguan¹; Ziling Xie¹; ¹Institute of Mechanics, Chinese Academy of Sciences

High Pressure Torsion (HPT) is a typical severe plastic deformation method to produce ultra-fine grains of metallic materials. An investigation was performed in this paper on copper specimens subjected to HPT treatment. An HPT apparatus was designed and made to install in a materials testing system. The pressure on specimen was 2GPa and the torque was applied by different revolutions from a quarter to 10. After the HPT treatment, grain size was measured by the technique of electron back scattered diffraction equipped with a scanning electron microscope. The result showed the grain size in the specimens with 8 and 10 revolutions was 270nm compared with the original value of 27.8 microns, i.e. it refined by two orders of magnitude. The micro-hardness testing on the specimen showed the hardness increased from 0.5GPa to 1.6GPa after HPT treatment. A model was proposed to describe the evolution relationship between grain refinement and shear strain.

Alumina and Bauxite: Alumina Refinery Safety and Integrity

Sponsored by: The Minerals, Metals and Materials Society, TMS Light Metals Division, TMS: Aluminum Committee
Program Organizers: Peter McIntosh, Hatch Associates; Jean Doucet, Alcan Inc; Morten Sorlie, Elkem Aluminium ANS

Tuesday AM Room: Northern E4
February 27, 2007 Location: Dolphin Hotel

Session Chair: Peter McIntosh, Hatch Associates

9:00 AM Welcome to 2007 Alumina and Bauxite Sessions

9:10 AM Session Introduction

9:15 AM Keynote

Leadership and Managing for Plant Safety and Integrity: *Joe Lombard*¹;

¹Managing Director Light Metals, Hatch Associates

Abstract not available.

9:45 AM

Inspection Techniques for Digestion Pressure Relief System: *William Harrington*¹; Garry Harrell¹; Bill Cohea¹; ¹Gramercy Alumina, LLC

Gramercy Alumina's refinery operates with a single high pressure Digestion unit. Pressure vessels contained therein are equipped with conventional pressure relief devices that discharge into dedicated branch and large diameter header piping systems. Activation of a slurry service relief valve has the potential of depositing process scale within the discharge piping network thereby reducing available cross-sectional area and diminishing capability to adequately relieve a high pressure event. Isolating piping to assess whether system integrity had been compromised following several years of operational service would require a total plant shutdown. In lieu of suspending operations, the plant developed and successfully implemented a program which facilitated inspection of the relief system's piping and headers while still in service. The established protocol relies heavily on techniques involving radiography, thermography, and gauging. This paper will present details and findings associated with the plant's on-line inspection of its Digestion unit pressure relief system.

10:10 AM

Thermography as a Predicting Method in Diagnosis of Scaling in Secondary Tanks and Vacuum Lines: *Ricardo Galarraga*¹; Royman Cañas¹; Jorge Minguett¹; ¹CVG Bauxilum

The possibility to predict incidents in main equipment should be fundamental in each organization. Some critical equipment represents a huge opportunity for testing with advanced technologies capable to foretell the behavior and warn about possible failures. In this paper the Thermography is used in Secondary Tanks and Vacuum Lines in order to detect the scale formation that hinders the normal flow of Hydrate slurry. The method described in this paper is a decision support tool, in order to avoid the abrupt loss of Tanks and interruption of operations during long periods. This way it has been possible to detect the obstruction of the equipment and to recover them without disrupting the Plant operation and reducing the operation costs. By early detecting procedures and adequate action plans, the incipient scaling are tackled and the loss of discharge of Tanks and the hydraulic loss associated to Vacuum systems has been completely controlled.

10:35 AM

Pressure Equipment Management: Management of Alumina Refinery Integrity and Operations Safety: *Peter Bletchly*¹; ¹Queensland Alumina Limited

Pressure equipment constitutes a significant investment in capital and a major proportion of potential high risk plant in many operations and this is particularly so in an alumina refinery. In many jurisdictions pressure equipment is also subject to statutory regulation that imposes obligations on owners of the equipment with respect to workplace safety. Most modern technical standards and industry codes of practice employ a risk based approach to support better decision making with respect to pressure equipment. For a management

system to be effective it must demonstrate that risk is being managed within acceptable levels. Pressure equipment is operated and maintained by diverse groups within most organizations and central to ensuring statutory compliance and management of risk are well documented and robust management systems that are clearly understood by all concerned. The management system must comprise elements for all stages of pressure equipment from design through fabrication, operation to disposal at end of life and include a strategy to manage non-conforming equipment. Queensland Alumina Limited has developed such a management methodology and successfully implemented its use across the operation. This methodology is included in the Plant quality system and is regularly audited by the third party quality auditor and the Statutory Authority. The methodology contains all the fundamental processes for managing pressure equipment in accordance with best practice codes, interfaces with legislation, previous operating experience and the Company's safety and environmental systems, yet still allows effective use of the equipment to underpin the Company's production goals.

11:00 AM Break

11:15 AM

The Role of Independent Audits in the Management of Aluminium Related Businesses: *Anthony Kjar*¹; ¹Gibson Crest Pty Ltd

Independent audits can be a valuable tool in challenging existing practice and achieving positive change. The author had led a wide range of audits on compliance with standards, assessing whether systems are capable of achieving desired outcomes and in value adding technical and commercial reviews. The focus of audits within a management framework is outlined and lessons learnt are discussed.

11:40 AM Keynote

Experiences from Other Chemical Process Industries for Safety and Integrity of High Pressure Refineries: An Address and Presentation from the Centre for Chemical Process Safety: *Speaker TBA*

Abstract not available.

12:10 PM Panel Discussion

12:55 PM Closing Comments

Aluminum Alloys for Transportation, Packaging, Aerospace and Other Applications: Aluminum Products

Sponsored by: The Minerals, Metals and Materials Society, TMS Light Metals Division, TMS: Aluminum Committee
Program Organizer: Subodh Das, University of Kentucky

Tuesday AM Room: Northern A4
February 27, 2007 Location: Dolphin Hotel

Session Chairs: Subodh Das, University of Kentucky; Zhong Li, Aleris International Inc

9:00 AM

Improvement of Quality of Trimmed Surface of Aluminum Panels: *Sergey Golovashchenko*¹; ¹Ford Motor Company

Trimming requires accurate alignment of the die shearing edges, typically 5-10% of the blank thickness. This clearance may be significantly larger due to insufficient stiffness of tooling and wear of the shearing edges. Increasing the clearance above the recommended value often leads to generation of burrs on the trimmed surface. These burrs may create difficulties for flanging and hemming operations. In addition, pieces of metal called slivers are generated during trimming process. Those pieces can be imprinted into the surface of stamped panels, which may require metal finish of every stamped exterior panel. Also, imperfections of the trimmed surface may reduce formability of the blanks significantly below Forming Limit Diagram. A modified trimming process significantly reducing the described imperfections will be discussed. Conventional and modified process will be compared for various clearances and trimming angles. Aluminum alloy 6111-T4, often used for exterior automotive panels, was used in this experimental study.



9:25 AM

Failure Analysis of Some Aluminium Alloys Used to Produce Aluminium Containers Especially Three Compartment and Airline Trays: Nick Singleton¹; Ebriham Alaradi¹; Mohamed Essa¹; ¹GARMCO

Aluminium is a widely used metal in various branches of industry like packing, construction, aerospace, etc. In this work, cracks during the forming of some semi-rigid foil food containers, especially the three compartment and airline casserole trays are investigated in aluminium alloys from the 3XXX and 8XXX series with different iron contents. It has been found that higher iron content up to 1.6% shows significant improvement in yield strength and improved formability (even if the die geometry is poor). This paper will focus on the influence of the iron, its strengthening effect on formability to prevent cracking during the pan forming process.

9:50 AM

Aluminum Products for Bridges and Bridge Decks: Subodh Das¹; J. Gilbert Kaufman¹; ¹Secat Inc

Aluminum alloys have been utilized for more than 70 years for bridges and bridge decks; some have been in service for more than 50 years. However, aluminum bridge systems have not been more widely used because decisions on bridge structures are invariably based upon first cost, which is higher for aluminum than for concrete or steel, not on life-cycle cost. Life cycle costs are significantly lower for aluminum bridges and bridge decks, primarily because lower cost is required for their maintenance, as compared with the very high cost of repainting or repaving steel and concrete bridges. In this paper, the history of use of aluminum for bridges and bridge decks will be reviewed, and their advantages leading to lower life-cycle costs detailed. Opportunities to quickly and efficiently renovate thousands of bridges across the United States with replacement aluminum decks will be itemized.

10:15 AM

Fatigue Crack Growth Behaviour of Aluminium Alloy 2219 Welded Plates: Ram Prasad¹; Ganji Narayana²; K. Sreekumar²; ¹Indian Institute of Technology Bombay; ²Indian Space Research Organization

The crack growth behaviour in high strength aluminium alloys have been a subject of research for the damage tolerant design requirements in aerospace structures. In this paper fatigue crack growth rate (FCGR) response of 2219 alloy in parent metal and weld zone has been investigated and correlated with fractographic features. At lower (up to 9 MPa \sqrt{m}) stress intensity factor range (ΔK), the weld zone exhibits more resistance to crack growth compared to parent metal. In the intermediate ΔK levels (10 to 13 MPa \sqrt{m}), the differences in the FCGRs in parent metal and weld zone was found to be negligible. Contrary to this at higher ΔK levels (> 13 MPa \sqrt{m}) the parent metal exhibited lower FCGRs than that of weld zone. The effect of crack closure loads on the FCGRs, the transition in the fracture surface morphology of parent and weld zone as a function of FCGR and ΔK are explained.

10:40 AM Break

10:50 AM

Study on Evolution Behaviors of Bubble in Aluminum Melt: Hongjie Luo¹; Guangchun Yao¹; ¹Northeastern University

The nucleating method of bubble in aluminum melt was studied in this paper. The driving force of bubble growth and its evolution behavior were also analyzed. The results show that the bubble formation in aluminum melt belongs to heterogeneity nucleation and the existence of solid particles provides necessary condition. The bubble growth achieves in the stage of constant temperature foaming mostly. The driving force of bubble growth comes from releasing hydrogen of TiH₂. Two periods can be divided in the stage of bubble growth. The major growth manner of bubbles is expansion in prior period and merging in final period. Bigger diameter bubbles grow up prior to smaller ones. The paper is about materials of aluminum foam.

11:15 AM

Study on Increasing Viscosity for Producing Foam Aluminum: Li Wei¹; ¹Department of Materials Science and Engineering, Shenyang Ligong University

Some of the factors which affect the foaming in a foamed aluminum casting process and microstructural evolution of metal foams have been investigated by applying the powder compact process in many literatures. But few studies on the effect of viscosity of the molten and on the mechanisms stabilizing the

pore formation have been undertaken. In this paper, foamed aluminum was preparation by powder metallurgy, the viscosity of the liquid metal was adjusted by Ca-addition into the metal, resulting in improvement of stabilization of bubble and uniformity of pore microstructure. The stabilizing mechanisms of the pore formation have been investigated, and the effect of Ca addition on porosity and pore microstructure is studied. Moreover, it has been proved that the effect of viscosity on the stabilizing of the molten is more important than oxide layer by means of dynamic observation on foaming course.

11:40 AM

Sound Absorption Property of Closed-Cell Aluminum Foam: Haijun Yu¹; Guangchun Yao¹; ¹Northeastern University

Closed-cell aluminum foams of different porosities and different thicknesses were prepared in this test; the sound absorption property was tested by utilizing standing waves tube, the sound absorption mechanism of which was studied, and the effect of porosity and thickness on its sound absorption property was also researched. It is found that the sound absorption property of Al-6Si closed-cell aluminum foam mainly depends on the Helmholtz resonator, the microphone and cracks of material. The porosity and thickness affect markedly on the sound absorption property of Al-6Si closed-cell aluminum foam: the sound absorption coefficient increases along with increasing porosity; increase of thickness can enhance the sound absorption coefficient at low frequency but reduce it at high frequency, but the contribution is not obvious for the whole sound absorption property, only appears the migratory phenomena of maximal sound absorption coefficient towards low frequency.

Aluminum Reduction Technology: Slotted Anodes - Joint Session with Electrode Technology

Sponsored by: The Minerals, Metals and Materials Society, TMS Light Metals Division, TMS: Aluminum Committee

Program Organizers: Geoffrey Bearne, Rio Tinto Aluminium Ltd; Stephen Lindsay, Alcoa Inc; Morten Sorlie, Elkem Aluminium ANS

Tuesday AM

Room: Southern 2

February 27, 2007

Location: Dolphin Hotel

Session Chair: Stephen Lindsay, Alcoa Inc

9:00 AM

Production and Performance of Slotted Anodes: Markus Meier¹; Raymond Perruchoud¹; Werner Fischer¹; ¹Research and Development Carbon Ltd

Historically, aluminium producers have been using slotted anodes for smelter technologies that require large size anodes. The slots helped to reduce the thermal stresses in the anodes and thus reduce the risk of cracking and to enable the gas bubbles to better escape from the anode bottom surface, which improves the pot stability and reduces the cell voltage drop. Today, slotted anodes are widely common also in smelters that use midsize anodes, mainly to take advantage of the lower instability level of the pots. To take maximum advantage of slotted anodes, numerous aspects need to be considered during anode manufacturing and usage. This paper describes the impact of slotted anodes on anode quality and performance in the pots both for an unadapted as well as an optimized anode production. With this background, the key anode requirements for optimum production figures of the entire smelter are outlined.

9:25 AM

Slot Cutting in Anodes: Jean-Jacques Grunspan¹; ¹Brochot SA

BROCHOT, a well known French-based company, has designed, manufactured and installed a new item in its line of equipment for anode handling systems in aluminium smelters. This is part of the continuous research and development to improve its equipment and customer service. The new item is a machine for cutting slots in the under-side of anodes for the electrolysis of aluminium. Electrolysis of aluminium releases gases at the anode which form a film on the surface and partially insulate it from the bath, thus reducing the efficiency of aluminium production. While the gas generated on the vertical faces of the anode escapes quite easily, that formed on the underside tends to remain longer, unless measures are taken to evacuate it. There is, therefore,

a strong trend in the aluminium industry towards making slots along the underside of the anodes so as facilitate this evacuation. Slots also provides an opportunity to control, to some degree, the direction and velocity of electrolyte that is driven by the bubble flow. This control can be enhanced by inclining the top of the slots.

9:50 AM

Modeling the Bubble Driven Flow in the Electrolyte as a Tool for Slotted Anode Design Improvement: *Dagoberto Severo*¹; *Vanderlei Gusberti*¹; *Elton Pinto*¹; *Ronaldo Moura*²; ¹PCE Ltd; ²ALBRAS Alumínio Brasileiro SA

Slotted anodes have been used in recent years by aluminum smelters in order to reduce gas bubble resistance at the anode/electrolyte interface. Bubbles are responsible also for part of the cell electric noise. The main objective of this study is to present a CFD model of the bubble driven flow in the electrolyte. The model is detailed enough to differentiate the effects of different anode and slot geometries. We consider the multiphase flow as a continuous liquid/dispersed gas pair, turbulent and steady state. A comparison with experimental measurements found in the literature is made. The model is applied to study options for the slotted anodes at ALBRAS. The simulations were done using the commercial code ANSYS CFX 10.0.

10:15 AM

The Effect of Implementing Slotted Anodes on Some Operational Parameters of a Pb-Line: *Ketil Rye*¹; *Ellen Myrvold*¹; *Ingar Solberg*¹; ¹Elkem Aluminum

"Slotted anodes" were implemented in February 2005 in one of the two potrooms of Line 2 in the Elkem Aluminium Mosjøen smelter. Forming slots in the anodes gives a better drainage of the process gas, which normally form large flat bubbles covering a significant part of the working anode area. Since gas is electrically insulating the net effect of the reduced gas coverage is a reduced lower electrical resistance over the ACD. However, the implementation of slotted anodes may also have some secondary effects outside the obvious effect on ACD and inter-polar resistance. This paper presents the observed effects on a range of operational parameters from a slotted anode implementation in a large group of pots. In summary, slotted anodes gave operational problems and increased anode cost. The use of slotted anodes was discontinued after 4 months.

10:40 AM Break**10:50 AM**

Development and Deployment of Slotted Anode Technology at Alcoa: *Xiangwen Wang*¹; *Gary Tarcy*¹; *Steve Whelan*¹; *Silvio Porto*¹; *Christopher Ritter*¹; *Bob Ouellet*¹; *Graham Homley*¹; *Andrew Morphet*¹; *Gilles Proulx*¹; *Stephen Lindsay*¹; ¹Alcoa Inc

Alcoa started slotted anode development and plant trials in 1998. Nearly all Alcoa prebake smelters are now running with slotted anodes. Implementation of slotted anodes has required little or no capital investment and has generally achieved improvements in current efficiency, power efficiency and pot stability. The success was not completely incident free and it became clear that the slotted anodes changed the behavior of many factors in the pot. There have also been issues involving anode quality. This paper provides a brief view of slotted anode development and deployment on different cell technologies at Alcoa. The chronological development is described along with comparative performance. Some of the negative aspects of slotted anodes in different technologies are also presented.

11:15 AM

The Impact of Slots on Reduction Cell Individual Anode Current Variation: *Geoffrey Bearne*¹; *Derek Gadd*¹; *Simon Lix*²; ¹Comalco Ltd; ²New Zealand Aluminium Smelter Ltd

Slotted anodes feature in many aluminium reduction line operations. It is generally accepted that slots in the bottom surface of anodes reduce gas coverage and hence bubble layer resistance. This provides an opportunity to lower cell resistance, and hence power input, while maintaining the anode-cathode distance. However, measuring the benefits of slotted anodes is difficult. One positive indication is a reduction in high frequency noise (the variation of around 1Hz) in measurements of individual anode currents. In this work, anode currents were measured at high frequency for four different prebake cell technologies (five anode sizes). The signals were compared, and used as input to a resistance model, to quantify the impact of slots. A technique

was developed to estimate the average gas coverage for slotted and unslotted anodes. It was found that longitudinal slots, in particular, result in a significant reduction in gas coverage and hence bubble resistance.

11:40 AM Panel Discussion

Senior representatives from the major aluminium companies will be invited to share their experiences with the production and use of slotted anodes in their plants, followed by an open discussion forum.

Biological Materials Science: Biological Materials I

Sponsored by: The Minerals, Metals and Materials Society, TMS Structural Materials Division, TMS/ASM: Mechanical Behavior of Materials Committee
Program Organizers: *Andrea Hodge*, Lawrence Livermore National Laboratory; *Chwee Lim*, National University of Singapore; *Eduard Artz*, University of Stuttgart; *Masaaki Sato*, Tohoku University; *Marc Meyers*, University of California, San Diego

Tuesday AM Room: Europe 4
February 27, 2007 Location: Dolphin Hotel

Session Chairs: *C.T. Lim*, National University of Singapore; *Kazuo Tanishita*, Keio University

9:00 AM

Effects of the Reinforcement Morphology on the Fatigue Properties of Hydroxyapatite Reinforced Polymers: *Robert Kane*¹; *Gabriel Converse*¹; *Ryan Roeder*¹; ¹University of Notre Dame

A variety of hydroxyapatite (HA) reinforced polymer biocomposites have been investigated for use as potential synthetic bone substitutes. While most studies have utilized a conventional equiaxed HA powder, HA whisker reinforcement was shown to result in improved tensile properties, and more closely mimicked the anisotropic material properties of bone tissue. The objective of this study was to investigate the fatigue properties of HA whisker versus powder reinforced polymers. High density polyethylene (HDPE) was reinforced with 20 and 40 vol % HA whiskers or powder using novel powder mixing and compression molding methods that resulted in uniform dispersion and whisker alignment. Specimens were tested in four-point bending fatigue under approximated physiological conditions. The use of HA whiskers improved the fatigue life by a factor of 4-5 compared to HA powder at both reinforcement levels. Therefore, HA whisker reinforced polymer composites may be useful as load-bearing synthetic bone substitutes.

9:20 AM

Design and Fabrication of 3-D Porous Bioactive Bone-Grafts via Fused Deposition Modeling Using Nanocrystalline Hydroxyapatite: *Monica Hopkins*¹; *Samar Kalita*¹; ¹University of Central Florida

Nanocrystalline calcium phosphates are materials of choice in bone engineering. In this research, we developed porous bioactive scaffolds with three-dimensional interconnectivity using nanocrystalline hydroxyapatite (HAp), doped with vital trace elements present in bone mineral. HAp nano-powder was synthesized using a low temperature water-based sol-gel technique. Dried white gel obtained was crushed into fine powder, doped with vital elements, and then calcined at 250-550°C. Phase evolution was studied using XRD technique. TEM observation confirmed particle size of 5-10 nm in the powder. 3-D porous scaffolds were fabricated through the indirect fused deposition modeling. In this process, porous polymeric molds with negative geometry of the desired structure were fabricated first. The molds were then infiltrated with doped nano-HAp slurry, dried and, sintered at 1300°C for 3 h. The resultant porous scaffolds were characterized for physical and mechanical properties using XRD, microscopy, immersion technique and compression testing. *In vitro* bioactivity was also assessed.



9:40 AM

Post-Selection Genetic Engineering of Inorganic-Binding Peptides for Practical Materials Applications: *Candan Tamerler*¹; Mustafa Gungormus²; Hanson Fong²; Deniz Sahin¹; Emre Oren²; Sibel Cetinel¹; Nevin Gul Karaguler¹; Mehmet Sarikaya²; ¹Istanbul Technical University; ²University of Washington

We are developing hybrid functional materials, composed of proteins and practical inorganics, by adapting genetic engineering and molecular biology protocols to materials science. The major components in these molecular biomimetic systems are peptides that are originally selected by combinatorial biology. Based on the homology of the strongly binding, experimentally selected peptides, we first create a bioinformatics-based scoring matrix. The inorganic functionality, that appears after the original selection constituting the first evolutionary cycle, can be improved by designing new sequences using the scoring matrix in silico, or by introducing mutations or bringing cycles of generations similar to natural evolution. We will explain various ways of tailoring peptide functionality using genetic engineering tools and present examples for practical applications, including nanobiosynthesis of inorganics, e.g., hydroxyapatite, towards tissue regeneration); directed immobilization of quantum dots and nanoinorganic particles for photonics, and enzyme immobilization. Supported by NSF-MRSEC and DURINT-ARO programs and TR-SPO.

10:00 AM

Physical, Mechanical and In-Vitro Characterization of Bioglass®-Hydroxy Apatite Bioceramics: *Hande Demirkiran*¹; Alonso Fuentes¹; Kytai Nguyen¹; Pranesh Aswath¹; ¹University of Texas at Arlington

Bioceramics with hydroxyapatite (HA) and Bioglass® (BG) were synthesized. Microhardness, compression and 4 point bend properties measured. New phases were characterized using X-ray diffraction. In vitro studies of the bioceramics were performed using two approaches: soaking the porous composites in simulated body fluid for 3 months, and cell culture studies for bone marrow stromal cell response. Differentiation of bone marrow stromal cells into osteoblasts was determined by alkaline phosphatase activity. After 4 days of culture, alkaline phosphatase activity was significantly greater for all of the cells cultured on the composites than on the controls. After 7 days, groups with Bioglass® content of 1%-10% had increased cell growth, with the 5% Bioglass® showing the greatest cell proliferation. In addition after 7 days of seeding, the enzyme activity of seeded cells had significantly increased for the composites containing 5%-25% Bioglass®, with 25% Bioglass® having the greatest amount of activity.

10:20 AM

Hydrothermal Healing Effect and the Reinforced Intermediate Layers on Improving the Bonding Strength of Plasma-Sprayed Hydroxyapatite Coatings: *Chung-Wei Yang*¹; Truan-Sheng Lui¹; ¹National Cheng Kung University

The effect of post-heat treatments and introducing intermediate bond coats on the characteristics of plasma-sprayed HA coatings (HACs) was investigated. The experimental results show that not only post-heat treatments but ZrO₂ bond coat can improve the bonding strength of HACs. The crystallinity and phase purity of HACs can be effectively increased with a low-temperature hydrothermal treatment. Furthermore, the crystallized HA is found to diminish the spraying defects of hydrothermal coating layers, and the 150°C hydrothermally-treated HACs show the highest strength because of its defect-healing effect. The Weibull distribution function provides a statistical method for determining the failure modes and reliability of the HACs. The strengthening HACs are generally reliable materials with a wear-out failure model. From the fractographic observation, the fracture surface of heat-treated HACs is different from the HA/bond coat layers. Hydrothermal HACs remain in tack on the substrate, and it represents a better reliability for further applications.

10:40 AM Break

10:50 AM Invited

Characterization of Structure-Property Relationships in Human Bone: *Robert Ritchie*¹; Joel Ager²; Guive Balooch²; ¹University of California; ²Lawrence Berkeley National Laboratory

We examine the micro-/nano-structural changes in the hierarchical structure

of bone accompanying the processes of aging, disease and clinical treatment, including steroid treatments, using multiscale experimental methods. We relate these structural changes to the toughness/fatigue properties of bone to obtain a quantitative and ultimately predictive picture of how bone resists fracture. To explain the deterioration in toughness induced by such biological factors, we evaluate the fracture properties at multiple length-scales, specifically at molecular/nano dimensions using vibrational spectroscopies and small angle x-ray scattering, at the microscale using electron microscopy, AFM/nanoindentation, and hard/soft x-ray tomography, and at the macroscale using R-curve and fatigue measurements. Specifically, we describe how clinical treatments with steroid hormones can lead to localized changes in the bone nanostructure (by forming regions of reduced mineralization), which prematurely “age” the bone and reduce its fracture resistance, whereas concurrent treatments with an amino-bisphosphonate can offset this degradation in structure and properties.

11:20 AM Invited

Bionic Design of Tube Formation in the Integrated Cellular Structure: *Kazuo Tanishita*¹; ¹Keio University

The vessel network formation is essentially required to achieve the function of reconstructed 3D cellular structure. Here we focused on the procedure of the tube formation of blood vessels and bile canaliculi in vitro and demonstrated the possibility of reconstructed liver tissue. Bile canaliculi (BC) are tubular structures that form the most proximal channels of the biliary tree and carry bile secreted by hepatocytes. BC are constructed by apical membranes of adjacent hepatocytes with the diameter of 1 μm. Small hepatocytes (SHs), which are known to be hepatic progenitor cells, are isolated from adult rat livers. With time in culture, many colonies of SHs develop into anastomosing networks, which may be BC. Furthermore we found out the shear stress stimulus promotes the micro-vessel formation and can be employed to form the capillary network in the reconstructed tissue.

11:50 AM

Delamination Behavior of Human Stratum Corneum: *Reinhold Dauskardt*¹; Kemal Levi¹; Kenneth Wu¹; Joy Baxter²; Helen Meldrum²; Manoj Misra²; Eugene Pashkovski²; ¹Stanford University; ²Unilever

The outermost layer of skin or stratum corneum (SC) has important mechanical function. Progressive delamination or desquamation of the SC is critical and has implications for skin adhering technologies. SC is subjected to damaging chemical exposure such as surfactants (e.g. soaps) that influence SC structure and mechanical behavior. Mechanics-based techniques are used to study the effect of surfactant treatments on delamination behavior of human SC. Cohesion energy is discussed as a function of temperature, hydration, chemical treatment and tissue depth. Time dependent delamination was used to understand kinetic mechanisms associated with corneocyte separation and related relaxation processes. The role of corneodesmosome density at cell boundaries was also explored following treatment with an exogenous enzyme with and without a protease inhibitor. Cohesion energy was observed to decrease after treatment with a recombinant chymotryptic enzyme (rSCCE). TEM of enzyme treated SC demonstrated a strong link between the cohesion energy and corneodesmosome density.

12:10 PM

Shape Memory Alloy Scaffolds for Bone Tissue Engineering: *Yuncang Li*¹; Jianyu Xiong¹; Peter Hodgson¹; Cui'e Wen¹; ¹Deakin University

Titanium alloy scaffolds for bone tissue engineering are receiving increasing attention because their porous structure and mechanical properties can be adjusted to match those of bone. In particular, there is an enormous potential to increase the life of such implant material if the porous structure can be imparted with shape memory properties. In the present study, TiNi scaffolds with a porous structure and high porosities up to 75% were fabricated by powder metallurgy. The porous structure was characterized by scanning electron microscope. The mechanical properties, the shape memory and superelastic effects were investigated by differential scanning calorimetry, nanoindentation and compressive tests. Results indicate that the porous TiNi scaffolds display an open-cell porous structure which provides new bone tissue ingrowth ability. The mechanical properties of the TiNi scaffolds can be tailored to match those of natural bone. Furthermore, the TiNi scaffolds show good shape memory and superelastic effects.

Bulk Metallic Glasses IV: Alloy Development and Glass-Forming Ability

Sponsored by: The Minerals, Metals and Materials Society, TMS Structural Materials Division, TMS/ASM: Mechanical Behavior of Materials Committee
Program Organizers: Peter Liaw, Univ of Tennessee; Raymond Buchanan, University of Tennessee; Wenhui Jiang, University of Tennessee; Guojiang Fan, University of Tennessee; Hahn Choo, University of Tennessee; Yanfei Gao, University of Tennessee

Tuesday AM Room: Asia 1
 February 27, 2007 Location: Dolphin Hotel

Session Chairs: Takeshi Egami, University of Tennessee; G. J. Fan, University of Tennessee

9:00 AM Keynote

Frustrating Business of Glass Formation: *Takeshi Egami*¹; ¹University of Tennessee

It is often believed that the f.c.c. and h.c.p. structures always represent the most ideal way to pack atoms. While this is true for hard spheres, it is hardly true for metals; many metals crystallize into the b.c.c. structure. The key is the atomic elasticity of metallic systems. As a result while the packing fraction of the dense-random-packed structure of hard spheres is only about 63%, that of soft spheres can be close to 74%, the packing density of the f.c.c. That is why when metal melts the volume changes only a few % or less. In this talk I show that the glass formation is a consequence of frustrated crystallization, and the atomic softness is crucial in accommodating frustration in the glassy structure. This recognition should help in finding the alloy system that forms stable metallic glasses, and facilitate understanding of the glass transition, atomic transport and mechanical deformation.

9:30 AM Invited

New Ternary Ni-Nb-Zr Bulk Metallic Glasses: Zhengwang Zhu¹; Haifeng Zhang¹; Wensheng Sun¹; *Zhuangqi Hu*¹; ¹Institute of Metal Research, CAS

A new ternary Ni-based bulk metallic glass (BMG) system, Ni-Nb-Zr, was developed. There exists a wide BMG forming region, in at%, 60<Ni<64, 28<Nb<38 and 0<Zr<9 with as-cast rods of at least 2mm diameter by using copper mould injection casting method. The maximum diameter of as-cast glassy rods reaches 3mm for all studied ternary Ni-based alloys. These BMG alloys exhibit high thermal stability and excellent mechanical properties. They possess high glass transition temperature, 900~880K, and high on-set crystallization temperature, 932~915K, which decrease with Zr content. They also show high hardness, typically HV~850, and high compressive fracture strength, 3~3.2GPa, along with some compressive plastic deformation of about 2%.

9:50 AM Invited

Glass Formation in Ternary and Quaternary Fe and Al Based Alloy Systems: *Yi Li*¹; ¹National University of Singapore

Bulk metallic glasses have been found mostly in multi-component systems, commonly more than three constituent elements. In addition, the glass forming ability (GFA) has a strong dependency on composition. Because of these, studying ternary and quaternary systems becomes crucial in finding large sized glasses as they offer the real starting point in the search. Fe and Al based alloys are most interesting as they are the two most common engineering alloys. Here we will show our latest results on the finding of bigger sized glassy samples in these ternary and quaternary systems. The importance of studying these base systems and the true elemental effect on glass forming ability will also be discussed.

10:10 AM Invited

Microstructural Characterization of Zr Bulk Metallic Glasses with a Pulsed Laser Local Electrode Atom Probe: *Michael Miller*¹; ¹Oak Ridge National Laboratory

Amorphous and devitrified zirconium-based bulk metallic glasses have been difficult to characterize with voltage-pulsed atom probes because of the brittle nature and poor electrical conductivity of these alloys. Recently, pulsed lasers have been reintroduced as an alternative method to field evaporation ions from

atom probe specimens. In addition to expanding the classes of materials that may be analyzed, laser pulsing also improves the mass resolving power under appropriate operating conditions. New atom probes have been developed that couple laser pulsing with significantly larger field of view single atom detectors. With these new systems, datasets that contain almost a quarter of a billion atoms have been collected from zirconium-based bulk metallic glasses. Focused ion beam based specimen preparation techniques have also been developed to fabricate atom probe specimens from a wide range of material forms including thin ribbons and gas atomized powders.

10:30 AM

Atomic Scale Characterization of Amorphous and Nanocrystalline Bulk Metallic Glasses: *Ananth Puthucode*¹; Hansoo Kim¹; Michael Kaufman¹; Rajarshi Banerjee¹; ¹University of North Texas

Bulk metallic glasses continue to receive considerable attention because of their relatively unique physical and mechanical properties and their potentially unique applications. Unfortunately, there remains considerable controversy concerning the role of phase separation and nanocrystallization on the strength and ductility of these materials. In this study, a range of different amorphous and nanocrystalline BMGs are being examined using both analytical high-resolution transmission electron microscopy and 3-D atom probe tomography. The specific issue being addressed is the competing influence of phase separation and nanocrystallization on the mechanical properties in these complex alloys. The direct comparison of the structural (TEM) and tomographic (3DAP) data should lead us to a clearer picture of the relationship between these microscopic features and the mechanical properties of this emerging materials class. *TEM and LEAP analyses performed using the analytical facilities in the Center for Advanced Research and Technology at the University of North Texas.*

10:45 AM

Atomistic Simulations and Structural Characterization of Binary Cu-Zr Glasses: *Ashwini Bharathula*¹; Katherine Flores¹; Wolfgang Windl¹; ¹Ohio State University

Recent theoretical and experimental models have shown that amorphous metal alloys have a preferred short-range order, typically found to be icosahedral or icosahedral-like, which may help to explain the formation of glassy alloys. In the present study, binary Cu-Zr amorphous alloys of known glass forming ability were modeled via molecular dynamics simulations at different quench rates. The resulting nearest-neighbor distributions and short-range ordering were analyzed using the Honeycutt-Anderson method. Additionally, variations in the free-volume distribution in these simulated alloys were monitored as the structures were quenched to room temperature at different cooling rates. These results are compared with the experimental open-volume distribution obtained for Zr-based bulk metallic glasses via positron annihilation spectroscopy.

11:00 AM Invited

A Model for the Nanoscale Structure in Partially Crystallized Bulk Metallic Glasses: Ling Yang¹; *Xun-li Wang*²; Alexandru Stoica²; ¹University of Cincinnati; ²Oak Ridge National Laboratory

Small angle X-ray scattering (SAXS) has been applied to study the devitrification of bulk metallic glasses. Three alloys with the composition of Zr_{52.5}Cu_{17.9}Ni_{14.6}Al₁₀Ti₅, Zr₅₀Cu₄₀Al₁₀ and Mg₆₅Cu₂₅Tb₁₀ were investigated. Although details differ, the SAXS patterns of all three samples show a characteristic interference peak. Assuming a log-normal particle size distribution, a core-shell model has been applied to fit the SAXS patterns successfully. The results show that Zr_{52.5}Cu_{17.9}Ni_{14.6}Al₁₀Ti₅, an excellent glass former, has the smallest average particles size with the finest particle size distribution. The same model can also describe small angle neutron scattering data reported by others, demonstrating the universality of the model. This research was supported by Division of Materials Sciences and Engineering, Office of Basic Energy Sciences, U.S. Department of Energy under Contract DE-AC05-00OR22725 with UT-Battelle, LLC.

11:20 AM Invited

Locating the Best Bulk Metallic Glass Former in Quaternary Alloy Systems Using a "3D-Pinpoint" Approach: *Jian Xu*¹; ¹Institute of Metal Research, Chinese Academy of Sciences

In recent years, alloy compositions with strong glass-forming ability have been developed in a number of systems, where centimeter-scale bulk metallic



glasses (BMGs) can be made. However, the search for large-size BMGs has been suffering from the lack of an established practical method to navigate in multi-component composition space. Recently, we developed a new method to track down the best BMG former in a composition tetrahedron (in a pseudo-ternary or quaternary system). We have made use of our 3D protocol to systematically assess the effects of the element substitution via the shapes of the contours of the BMG-forming zones in the composition tetrahedron. This effort allows us to discover new BMGs with large critical size (D_c) in quaternary systems, such as $Mg_{54}Cu_{28}Ag_7Y_{11}$ ($D_c=16mm$), $Mg_{57}Cu_{31}Y_{6.6}Nd_{5.4}$ ($D_c=14mm$), $Mg_{59.5}Cu_{22.86}Ag_{6.64}Gd_{11}$ ($D_c=27mm$), $Cu_{44.25}Ag_{14.75}Zr_{36}Ti_5$ ($D_c=10mm$), $Cu_{49.5}Ni_{5.5}Ti_{32}Zr_{13}$ ($D_c=6mm$), $Ni_{56}Co_3Nb_{36}Sn_5$ ($D_c=3mm$) and $Ti_{44.5}Zr_{7.8}Cu_{38}Ni_{10}$ ($D_c=3mm$). These findings are important in order to bring exotic laboratory wonders to marketplace.

11:40 AM

Glass Formation Mechanism of Minor Yttrium Addition in CuZr Alloys: *Yong Zhang*¹; ¹University of Science and Technology, Beijing

The paper studies the minor yttrium additional effect on the glass forming ability in a model alloy of (Cu0.48Zr0.48Al0.04)100-xYx by using a perturbation method. It is feasible to introduce the atomic level strain energy as a diminishment of the driven force for the crystal nucleation from the largely undercooled liquid. The atomic level strain energy is closely related to the atomic packing efficiency of the precipitated crystals. The prediction correlates well with the experimental results that less yttrium addition is needed to suppress the precipitation of crystal phase with higher atomic packing efficiency.

11:55 AM

Binary Eutectic Clusters and Glass Formation in Ideal Glass-Forming Liquids: *Z. P. Lu*¹; *C. T. Liu*²; *D. Ma*¹; *X.-L. Wang*¹; ¹Oak Ridge National Laboratory; ²University of Tennessee

A physical concept of binary eutectic clusters in "ideal" glass-forming liquids is proposed based on the characteristics of most well-known bulk metallic glasses (BMGs). Our approach also includes the treatment of binary eutectic clusters as basic units, which leads to the development of a simple but reliable method for designing BMGs more efficiently and effectively in these unique glass-forming liquids. As an example, bulk glass formers with superior glass-forming ability in the Zr-Ni-Cu-Al, Zr-Ir-Cu-Al and Zr-Fe-Cu-Al systems were identified with the use of the strategy. Furthermore, the basic concept of binary clusters was directly confirmed in the representative Zr-based amorphous alloys using high-energy x-ray and time-of-flight neutron diffraction techniques.

12:10 PM

Fabrication of Fe-Based Bulk Metallic Glass Components Using Laser Additive Manufacturing: *Shawn Kelly*¹; ¹Applied Research Laboratory, Pennsylvania State University

One of the current limitations in producing bulk metallic glass components of sufficient scale for structural application is the low critical casting thickness available with current amorphous alloy systems. Currently, iron-based glass forming alloys can be cast into fully amorphous ingots approximately 12mm in diameter. With laser additive manufacturing, material and heat are added incrementally, theoretically leading to the fabrication of much larger amorphous structures than currently achievable with casting alone. The paper will focus on thermal modeling and experimental processing of laser deposited Fe-based bulk amorphous metallic components.

12:25 PM

Predicting the Role of Diffusion in the Composition-Dependence of Crystal Nucleation in Glass Forming Systems: *Feng Jiang*¹; *James Morris*²; *Peter Liaw*¹; *Hahn Choo*¹; ¹University of Tennessee; ²Ceramics Division, Department of Metal, Oak Ridge National Laboratory

Bulk metallic glasses (BMGs) have received increased attention in recent years. The first and most important thing for BMG research is choosing the alloy composition. While compositions near the eutectic point to prepare BMGs are typically good, optimal alloys are often off-eutectic. Predicting the optimal composition from phase diagram is a current challenge. Here, we present a simple model that uses thermodynamic information for alloys to allow us to exam the role of alloy composition and diffusion rates on critical nuclei energetics and maximum undercoolings in strongly segregating eutectic

systems. We examine two separate limits. The first one is the "slow diffusion" limit, where the formation of the crystal phase is fast compared with the rate that chemical equilibrium is reached. The second one is the "fast diffusion" limit, where local equilibrium may be achieved rapidly compared to nucleation times. Under these different assumptions, we predict optimal compositions for glass formation.

12:40 PM

Critical Heat Flux and Instant Critical Cooling Rate of Bulk Metallic Glass Vit1 under Uni-Directional Heat Conduction Conditions: *Yuelu Li*¹; *Sumanth Shankar*¹; ¹Light Metal Castings Research Centre, McMaster University

Vit1 (Zr41.2Ti13.8Cu12.5Ni10Be22.5) is commercially one of the more significant of bulk metallic glasses (BMGs) and has found a variety of commercial applications because of its extraordinary glass forming ability. However, most of the critical cooling rates of BMGs reported in literature only reflect an average value for a bulk sample with little or no control over the heat flow direction. Further, past researches do not explicitly quantify the critical relationships among heat flux, cooling rate and thickness of amorphous layer. In this paper, results of experiments carried out to evaluate these relationships in a controlled uni-directional solidification set up will be presented. The effect of various heat transfer conditions upon the thickness of the amorphous layer was quantified. The critical heat flux and critical instant cooling rate as a function of solidification time was experimentally evaluated. Microstructure characterization and X-ray diffraction were used to evaluate the amorphous and crystalline layers.

Cast Shop Technology: Metal Treatment

Sponsored by: The Minerals, Metals and Materials Society, TMS Light Metals Division, TMS: Aluminum Committee

Program Organizers: David DeYoung, Alcoa Inc; Rene Kieft, Corus Group; Morten Sorlie, Elkem Aluminium ANS

Tuesday AM
February 27, 2007

Room: Northern E1
Location: Dolphin Hotel

Session Chairs: Pierre Le Brun, Alcan CRV; Bjørn Rasch, Hydro Aluminium R&D Sunndalsøra

9:00 AM Introductory Comments

9:05 AM

In-Line Salt Fluxing Process: A Final Solution to Chlorine Gas Utilization in Cast Houses: *Sebastien Leboeuf*¹; *Claude Dupuis*¹; *Bruno Maltais*²; *Marc-André Thibault*²; ¹Alcan Inc.; ²STAS

Over the past decades, the aluminium industry has been very active in developing and implementing metal treatment technologies such as TAC and RFI to reduce negative environmental, health and safety (EHS) impacts. However, most casthouses are still relying on the utilization of chlorine gas for in-line metal treatment. This requires maintaining an active chlorine network at considerable costs and EHS considerations. A new technology developed at Alcan Arvida Research and Development Centre (ARDC) in collaboration with Société des Technologies de l'Aluminium du Saguenay (STAS) has proven successful to achieve a complete elimination of chlorine and meet with the ultimate Alcan chlorine-free casthouse objective. This paper reviews the challenges to substitute chlorine gas utilization while achieving equivalent or better metal treatment performances. The in-line salt fluxing process is presented in term of equipment and process requirements. Preliminary metallurgical performances (hydrogen, alkali, inclusion removal) from pilot scale and industrial conditions are presented.

9:25 AM

The Almex HF Series Degassing and Metal Purification Systems: A Novel Approach to Vessel Design: *Shaun Hamer*¹; *Ravi Tilak*¹; ¹Almex USA Inc.

The requirement from batch type billet casthouses for a low cost, flexible and user friendly degassing unit has prompted the development of the Almex HF Series of degassing unit systems. Frequent alloy changes and minimal set-up times have forced the billet manufacturers to demand a system which will

keep pace with the production cycles. The HF Series of degassing units were developed to meet this demand and have been designed from the floor up to provide the optimum combination of performance and operating simplicity. These criteria demanded a fresh review of molten aluminum vessel design and have prompted a unique and revolutionary approach to vessel construction. This paper describes the characteristics and demands placed on the design of these systems and the engineering, materials and construction solutions implemented to meet these requirements.

9:45 AM

Porous Plug Technology for Degassing in Aluminum Foundry Ladles:

*Klaus Gamweger*¹; Reinhard Schwaiger²; ¹RHI AG; ²RHI

The treatment of molten metals with purging gases is a well established practice in non-ferrous metallurgy. In the aluminum industry, inert or reaction gases are blown into the melt using porous plugs at multiple steps in the process, including in melting and holding furnaces, and more recently in ladles. To enable effective degassing in foundry ladles a complete package was developed that includes porous plugs, refractory expertise, gas supply technology and gas control equipment. This paper shows the technological and economical advantages of the system compared to standard rotary lances. The benefits in degassing level, gas consumption, service life, maintenance and potential time savings are discussed.

10:05 AM

Kinetic Study of the Magnesium Removal from Molten Aluminum Using Ar-SF₆-O₂ Gaseous Mixtures:

*Alfredo Valdes*¹; ¹CINVESTAV

In this paper it is shown that pneumatically injected gaseous mixtures containing SF₆(g) are useful to oxidize the magnesium dissolved in molten aluminum alloys. Although the oxidation of magnesium with SF₆(g) is thermodynamically favorable, the addition of O₂(g) causes that ΔG is additionally reduced by -249.16 KJ/mol Mg. After chemical analysis of the final contents of magnesium in the treated alloys, the identification of compounds in the slag by x-ray diffraction, and chemical analysis of gaseous emissions produced, a scheme of reaction is proposed considering no emission of volatile fluorides or sulfides. Kinetic equations describing the magnesium removal rate are presented, taking into account that kinetics of the process is controlled by chemical reaction.

10:25 AM Break

10:45 AM

Simulation of Aluminium Filtration Including Lubrication Effect in Three Dimensional Foam Microstructures:

*Hervé Duval*¹; Carlos Rivière²; Emilie Lae²; Pierre Le Brun²; Jean-Bernard Guillot¹; ¹Ecole Centrale Paris; ²ALCAN

Numerical simulations of aluminium filtration through ceramic foam filters have been performed using a 3D lattice Boltzmann model of depth filtration. This model describes aluminium flow and inclusions transport and capture in a representative elementary volume of the filter. The lubrication effect arising when an inclusion approaches a solid surface is taken into account. In a first step, the model has been validated on experimental results provided by laboratory trials run on a filtration pilot and on industrial data from the literature. In a second step, a sensitivity study has been set up, in which the influence of the gravitational and interception numbers on the filtration coefficient has been investigated. Furthermore, the effects of the lubrication and of the roughness of the solid surfaces have been examined. Finally, scaling laws of the filtration coefficient have been derived and compared to theoretical results from the literature.

11:05 AM

PDBF: Proven Filtration for High-End Applications:

*Ghislain Le Roy*¹; ¹Novelis PAE

Novelis PAE offers on the market a filtering technology perfected over 20 years of development and sales called PDBF. Recent evolution covered the following areas: 1/optimising the filter bed stacking and operation to achieve the highest possible efficiency for in-line treatment 2/increasing the control of temperature thanks to a double heating system 3/widening the size range towards higher flow rates, up to 100 t/hour. Industrial results will be presented, together with typical operating costs.

11:25 AM

Removal of Intermetallic Particles for the Purification of Aluminium Alloys:

*Pierre Le Brun*¹; Christoph Kräutlein²; Georg Rombach³; Patrick Pouly⁴; Paul De Vries⁵; Jan Luyten⁶; ¹Alcan CRV; ²Institute of Makers of Explosives; ³Hydro Aluminium; ⁴Novelis; ⁵Corus Research and Development; ⁶VITO

The purification of molten aluminium has been studied in the framework of a collaborative program on recycling. In particular, the removal of elements like Fe, Mn and Si was targeted. One approach is to capture the element to remove in an intermetallic particle, which has subsequently to be removed. This paper reports on the removal of a large amount of deliberately created intermetallic particles (also called primary particles) from a molten aluminium bath. Several techniques have been considered in the work, including filtration, centrifugation, gravity separation, flotation. The applicability of these techniques is discussed, based on the experimental work that has been carried out. The model system used for the work reported is Al-Fe-Mn. This work has been funded within the Growth program of the European commission under the grant number GIRD-CT-2002-00728.

11:45 AM

Designing of Launder System during Aluminum Casting through CFD Simulation:

*Lifeng Zhang*¹; ¹Norwegian University of Science and Technology

Advanced computational fluid dynamics (CFD) models of turbulent fluid flow of liquid metals are applied to design the launder system during aluminum casting. In addition to the steady flow pattern, the computational models are developed to predict the transport and removal of inclusion particles and heat transfer. The models are three-dimensional and use the Eulerian-Lagrangian method for multiphase flow, the k- ϵ model for turbulence, species diffusion equation for alloy mixing, and the random walk method for particle transport. The effect of launder depth, shape, arrangement of inlet and outlet, and steel flow rate on residence time, mixing, inclusion removal and heat transfer are investigated. The designing of metallurgical vessels using CFD simulation is trying to get better metal quality and save energy.

Characterization of Minerals, Metals, and Materials: Characterization of Mechanical and Physical Properties of Materials I

Sponsored by: The Minerals, Metals and Materials Society, TMS Extraction and Processing Division, TMS: Materials Characterization Committee
Program Organizers: Arun Gokhale, Georgia Institute of Technology; Jian Li, Natural Resources Canada; Toru Okabe, University of Tokyo

Tuesday AM

Room: Oceanic 8

February 27, 2007

Location: Dolphin Hotel

Session Chairs: Peter Liaw, University of Tennessee; Oleg Senkov, UES Inc

9:00 AM Invited

The Interpretation of Tension Behavior in Ceramic Matrix Composites:

*Jeongguk Kim*¹; Peter Liaw²; ¹Korea Railroad Research Institute; ²University of Tennessee

The tensile fracture behavior of Nicalon fiber reinforced calcium aluminosilicate (CAS) glass-ceramic matrix composites (Nicalon/CAS) with two different types of samples; cross-ply and unidirectional specimens, were characterized using several analysis techniques. A nondestructive evaluation (NDE) technique, infrared (IR) thermography, was employed during tensile testing, and an IR camera was used for in-situ monitoring of progressive damages of composite samples in terms of the temperature evolution. The commercial finite element method (FEM) software was used for the simulation of tensile behavior of Nicalon/CAS composites. Microstructural characterization using scanning electron microscopy (SEM) was performed to investigate fracture mechanisms of the composites. In this investigation, several engineering analysis techniques were used to facilitate a better understanding of fracture mechanisms of Nicalon/CAS composites during tensile testing.



9:30 AM

Grain Boundary Engineering (GBE) of Shot-Peened Type 304 Stainless Steel: *Osama Alyoufi*¹; Dirk Engelberg²; T. Marrow²; ¹Kuwait University; ²University of Manchester

Grain boundary engineering of austenitic stainless steels through plastic strain and thermal annealing can be used to improve resistance to intergranular stress corrosion cracking. The effect of thermal annealing on shot peened Type 304 stainless steel has been examined using electron backscatter diffraction (EBSD) and X-ray diffraction (XRD). The objective was to evaluate the potential for surface property control by grain boundary engineering. The determination of near-surface plastic strain levels by EBSD and XRD are compared. The near-surface microstructures obtained by annealing were compared with microstructures obtained by bulk processing, and their corrosion and stress corrosion resistance were evaluated.

9:50 AM

On the Measurement of Yield Strength by Spherical Indentation: *Erik Herbert*¹; Warren Oliver¹; George Pharr²; ¹MTS Nano Instruments; ²University of Tennessee, Oak Ridge National Laboratory

Over the past 10 years, a number of investigators have proposed methods to measure the yield strength of metals using instrumented indentation experiments performed with a sphere. The objective of this work is to contribute to the experimental verification of four contemporary models by testing their ability to accurately determine the yield strength of the aluminum alloy 6061-T6 using a 385 nm radius sphere. The procedures proposed by Ma et al., and Cao and Lu were inconsistent with the experimental observations and could not be implemented. Yu and Blanchard's model overestimated the yield strength by approximately 55%. Field and Swain's procedure overestimated the tensile flow curve by roughly 40% which precluded obtaining a meaningful estimate of the yield strength. Among the most likely explanations for these surprisingly poor results are the effects of roughness and contaminants on the surface and an indentation size effect.

10:10 AM

Characterization of AlN Whiskers: *Pablo Caceres-Valencia*¹; ¹University of Puerto Rico-Mayaguez

Aluminum nitride whiskers have been synthesized using a modified vapor-liquid-solid (VLS) mechanism. The whiskers were synthesized with the aid of a catalyst, but a catalyst droplet was not found at the tip of the growing whiskers. It was speculated that the catalyst seeds were located at the base of the whisker rather than at its tip. Electron microscopy analysis indicated the two modes of growth mechanisms, namely the planar described by the <0-112>(-1101) growth planes and directions and the serrated described by the <0-111> fiber axis with a serrated morphology exposing the (0002) and (01-12) planes. Extensive twinning was detected during growth by SEM.

10:30 AM

Laser Shock Peening(LSP) of IN718 Superalloy: *Amrinder Singh Gill*¹; Vijay Vasudevan¹; S. Mannava¹; ¹University of Cincinnati

LSP is a surface engineering process that generates deep compressive residual stresses and microstructural changes, thereby improving fatigue strength, service lifetimes and crack propagation resistance of critical metal parts like aircraft engine fan and compressor blades. This study aims to develop an understanding of effects of LSP parameters on residual stress distributions and microstructural changes in an important aero-engine alloy, IN718. Coupons of alloy with and without a sacrificial/ablative layer were LSP-treated using GENIV system at GE Infrastructure Aviation. Depth-resolved characterization of macro residual strains and stresses and degree of cold work was achieved using high-energy synchrotron x-ray diffraction. Near-surface and through-the-depth changes in strain, texture and microstructure were studied using EBSD/OIM and by TEM of thin foils fabricated from specific locations using focused ion beam method. Local property changes were examined using microhardness and nanoindentation measurements. Results show relationship between LSP processing parameters, microstructure, residual stress distributions and hardness.

10:50 AM Break

11:10 AM

Wear Resistance of Modified Epoxy Composites Reinforced with Diamond Crystals: *Sergio Monteiro*¹; Gustavo Menezes¹; Ruben Jesus Rodriguez²; Felipe Lopes¹; Ana Lucia Skury¹; Guerold Bobrovnichii¹; ¹State University of the Northern Rio de Janeiro

Epoxy matrix composites containing dispersed particles of diamond crystals are being investigated as low cost tools for polishing decorative stones, such as marble and granite. Modifications in the epoxy structure by changing the stoichiometric hardener/resin percentage, phr, and the presence of diamond particles rendered the composite with the necessary mechanical strength for polishing operations. As important as the strength is the abrasive behavior. Therefore, the objective of this work was to investigate the wear resistance of modified epoxy composites reinforced with different amounts, up to 30 wt.%, of diamond particles. The results obtained showed a significant increase in wear resistance with the amount of incorporated diamond. Moreover, it was also found that an optimal condition occurred in association with phr above the stoichiometric ratio.

11:30 AM

Influence of the Micromorphology of Natural Fibers on the Reinforcement of Polymeric Composites: *Sergio Monteiro*¹; João José Rangel¹; ¹State University of the Northern Rio de Janeiro; ²Candido Mendes University

Fibers for composite reinforcement are usually simulated as a smooth and homogeneous cylinder with matrix interfacial bonding. This simulation applies reasonably well to synthetic fibers such as glass, carbon and aramid, in which the smoothness and homogeneity are processing requirements. By contrast, natural fibers with lignocellulosic composition like sisal, jute, hemp and many others display a more complex geometry, which can only be realized by means of a micromorphological characterization. In the present work, the influence of micromorphological features of natural fibers, associated with details superimposed to the basic cylindrical shape, was evaluated for the reinforcement effect on polymeric composites. Jute, sisal, ramie, curaua and coir lignocellulosic fibers were analyzed by SEM/EDS to characterize the role played by their surface features on the interfacial strength. The results have shown significant differences between synthetic and natural fibers due to micromorphological aspects.

11:50 AM

Fracture Behavior of Curaua Fiber Reinforced Polyester Composites: *Sergio Monteiro*¹; Ailton Ferreira¹; Regina Coeli Aquino²; Felipe Lopes¹; Jose Roberto d'Almeida³; ¹State University of the Northern Rio de Janeiro; ²Federal Center for Technological Education; ³Catholic University of Rio de Janeiro

Polymeric matrix composites reinforced with curaua continuous and aligned fibers have shown promising properties in comparison with other natural lignocellulosic fibers composites. Originally from the Amazon region, the fibers obtained from the leaves of the curaua plant (*Ananas Erectifolius*) are longer, thinner and stronger than most natural fibers. Actually, it has a great potential to be used as reinforcement of engineering composites. The objective of the present work was to investigate the fracture characteristics of polyester composites reinforced with up to 30 wt.% of continuous curaua fibers. The fracture surface of fiber aligned press molded rectangular specimens, ruptured in three-points bend tests, were analyzed by SEM. The results showed that the rupture strength is associated with a complex mechanism of individual interaction of the filaments, that composes each fiber, with the polymeric matrix. This interaction leads to an efficient load transfer during crack propagation.

12:10 PM

Study on the Tensile Properties of Copper Coated Carbon Fibers: *Zhuokun Cao*¹; Guangchun Yao¹; Yihan Liu¹; ¹Northeastern University of China

Copper coating whose thickness varies from 0.25µm to 1.6µm was obtained by electroless plating or electroplating methods, and the tensile properties of single-filament specimens were determined. The tensile test results indicate that stress-strain curves of these coated fibers turned out to be similar to the uncoated ones, but rupture elongation of the fibers would increase with the existence of copper coating. SEM observation on the fracture surface of specimens after tensile tests revealed that the coating formed in a electroless solution exhibit no plastic deformation contrast to obvious plastic deforming behavior of the copper layer obtain using electroplating method. Therefore, it

can be concluded that plasticity of the coated layer is not the major influencing factor for the increase of fracture elongation of the fibers. Further analysis revealed the fact that the improvement of tensile properties results from the reduction of the fibers' sensitivity on surface blemishes.

Computational Thermodynamics and Phase Transformations: Microstructure Properties and Evolution I

Sponsored by: The Minerals, Metals and Materials Society, ASM International, TMS Electronic, Magnetic, and Photonic Materials Division, TMS Materials Processing and Manufacturing Division, ASM Materials Science Critical Technology Sector, TMS: Chemistry and Physics of Materials Committee, TMS/ASM: Computational Materials Science and Engineering Committee

Program Organizers: Corbett Battaile, Sandia National Laboratories; James Morris, Oak Ridge National Laboratory

Tuesday AM Room: Europe 11
February 27, 2007 Location: Dolphin Hotel

Session Chair: Anthony Rollett, Carnegie Mellon University

9:00 AM Invited

Mesoscale Grain Boundary Properties from Molecular Dynamics Simulations: *Stephen Foiles*¹; ¹Sandia National Laboratories

Atomic-scale calculations have been used for many years to study the structure and energetics of grain boundaries at zero temperature. Recently, new techniques have been developed to examine mesoscale properties of boundaries at finite temperature such as the boundary free energy, stiffness and mobility. In particular, fluctuation methods have been employed to examine boundary stiffness and mobility and synthetic driving forces have been developed to examine boundary mobility. These approaches will be overviewed and new insights into boundary properties from these methods will be discussed. Sandia is a multiprogram laboratory operated by Sandia Corporation, a Lockheed Martin Company, for the United States Department of Energy's National Nuclear Security Administration under Contract DE-AC04-94AL85000.

9:30 AM

Statistical Characterization of Atomistic Motion during Grain Boundary Migration: *Hao Zhang*¹; David Srolovitz²; ¹Princeton University

The atomistic migration mechanism for a series of Sigma5 tilt grain boundary in nickel has been studied using molecular dynamics simulation. Three statistical measures were used to characterize the atomic motion: the non-Gaussian parameter, the mean first-passage time, and the van Hove correlation function. Three different types of displacements are classified. One of these is a string-like cooperative motion of atoms, predominately along the tilt axis. Statistical analysis shows that this cooperative motion occurs on a very short time scale and is intrinsic to the boundary rather than directly related to migration. The hopping of individual atoms across the boundary is shown to control the overall rate of grain boundary migration. Further simulations for general grain boundaries confirm that these two basic types of atom displacements that occur during migration are preserved on going from a highly symmetric, high angle boundary to general boundaries.

9:50 AM Invited

Characterization of Complex Microstructures for Computer Simulation: *Hamish Fraser*¹; Brian Welk¹; Santosh Koduri¹; Robert Williams¹; Peter Collins¹; Gopal Viswanathan¹; Vladimir Levit¹; ¹Ohio State University

Microstructural characterization has often been effected by recording a "typical" image from a two-dimensional section, which usually was the most "attractive" image, and qualitative descriptions of microstructural features would be reported. With the significant advances in computer simulation of microstructural evolution and microstructure/property interrelationships that have taken place in the recent past, it is now essential that accurate physical descriptions of microstructural features, including both average values as well as variations and their distributions, and mechanistic information regarding evolution be developed and employed. This paper describes research aimed

at providing accurate characterization of complex microstructures in a form suitable for use by computational models. Direct three-dimensional methods of characterization will be compared with results from rigorous stereological procedures. Methods for determining and representing the spatial variations in sizes of microstructural features will be outlined. Finally, the ongoing research into ways of describing microstructure in a digital form will be discussed.

10:20 AM Invited

A Framework for Automated 3D Microstructural Analysis and Representation: *Michael Groeber*¹; Michael Uchic²; Dennis Dimiduk²; Yash Bhandari¹; Somnath Ghosh¹; ¹Ohio State University; ²Air Force Research Laboratory, Materials and Manufacturing Directorate

Recently, significant advances in serial-sectioning have provided quantitative data describing the structure and crystallography of microstructures in 3D. The analysis and representation of this information can provide modeling efforts with a highly-refined and unbiased characterization of microstructure. The grain structure could be characterized and then translated directly into a 3D volume mesh for Finite Element Analysis. However, this approach requires a multitude of data sets to appropriately sample the heterogeneity observed in typical microstructures. One way to circumvent this issue is to develop computation tools that create synthetic microstructures that are statistically-equivalent. This study will discuss the development of programs that take a series of EBSD maps from a serial-sectioning experiment, and output a robust statistical analysis in 3D, as well as generate a host of synthetic structures. Importantly, the objective of this study is to provide a framework towards complete microstructure representation consistent with experimental data.

10:50 AM Invited

Measuring Facet Planes in Coarse Martensite in Low Carbon Steels by Combining 3D Reconstruction with EBSD: *George Spanos*¹; *David Rowenhorst*¹; R. Masamora¹; ¹Multi-Functional Materials Branch, Code 6355, Naval Research Laboratory

Coarse autotempered martensite forms in some low carbon steels (e.g., HSLA-100) and forms in-situ, at moderate to rapid cooling rates during both simulated and normal weld processing, and results in enhanced mechanical properties. This talk will present new techniques being employed at the Naval Research Laboratory to combine multiple serial sections and crystallographic observations taken from Electron Backscattered Diffraction (EBSD) maps, and then quantitatively reconstruct this microconstituent in 3D. These results include determining the crystallographic direction of interface normals in these crystals, particularly highlighting various 3D facets, as well as the principle growth direction.

11:10 AM Break

11:30 AM Invited

Three-Dimensional Simulation of Coarsening in Liquid Phase Sintering: *Sukbin Lee*¹; *Anthony Rollett*¹; Jeff Rickman²; ¹Carnegie Mellon University; ²Lehigh University

A three-dimensional, Potts model of liquid phase sintering in a system with full solid wetting is introduced to investigate the coarsening kinetics and microstructures associated with this process. Kinetic Monte Carlo simulation is used to probe coarsening dynamics and to obtain the properties of solid particles, including the volume of critical nuclei and the distribution of particle size as a function of time. It is found that the average particle volume increases linearly with time and that the particle size distributions are consistent with those obtained experimentally, as in the W-Ni-Fe and Sn-Pb systems. In obtaining these results careful consideration is given to the role of the initial microstructure in the subsequent evolution of the system.

12:00 PM

Modeling Abnormal Grain Growth in Nanocrystalline Nickel: *Elizabeth Holm*¹; David Follstaedt¹; Mark Miodownik²; ¹Sandia National Laboratories; ²King's College London

Nanocrystalline metals evince desirable mechanical properties, including high strength and hardness. However, they typically undergo abnormal grain growth at or near room temperature, and the resulting microstructural changes can alter properties. In pulse laser deposited nickel nanocrystalline films, abnormal grain growth is observed to increase with temperature, film thickness, electron beam exposure, and surface relief features. The basic mechanism or mechanisms of abnormal growth have not been identified in these materials.



We apply highly realistic, microstructural-scale computer simulations to examine several proposed abnormal growth mechanisms, including intrinsic boundary mobility variations, grain size gradients through the film thickness, surface energy effects, and geometry. We find one requirement for abnormal growth is the persistence of high mobility boundaries due to crystallographic, spatial, or thermal considerations. Alternately, the availability of low energy surfaces can also induce abnormal growth. These simulations provide new insight into abnormal grain growth in nanocrystalline metals.

12:20 PM

Thermodynamic Viewpoints on Nanograin Growth Kinetics: Xiaoyan Song¹; Lingmei Li¹; Juxing Zhang¹; Fu Guo¹; ¹Beijing University of Technology

The correlation of thermodynamics and grain growth kinetics of nanocrystalline metals was investigated both theoretically and experimentally. A model was developed to describe the thermodynamic properties of nano-grain boundaries, which could give reliable predictions in the destabilization characteristics of nano-grain structures and the slowing-down grain growth kinetics at a constant temperature. Both the temperature-varying and the isothermal nano-grain growth behaviors in the pure nanocrystalline Co were studied to verify the thermodynamic predictions. The experimental results that discontinuous nano-grain growth takes place at a certain temperature and grain growth rate decreases monotonically with time, confirm amply our thermodynamics-based description of the nano-grain growth characteristics. Therefore, we propose a thermodynamic point of view on the deviation of grain growth kinetics in nanocrystalline metals from those of polycrystalline materials.

12:40 PM

Heterogeneous Dislocation Distributions and Recrystallization Kinetics: A Phase-Field Study: Subbalakshmi Sreekala¹; Mikko Haataja¹; ¹Princeton University

During recrystallization, dislocation-free grains grow and invade areas with high dislocation density. In this work, we apply the phase-field method to model the isothermal recrystallization process as a phase transformation driven by the stored elastic energy. Dislocations are represented in two spatial dimensions in terms of a continuous Burger's vector field, and their contribution to the elastic energy density is explicitly incorporated. A key feature of our approach is that the driving force for grain growth becomes non-local in space due to the presence of long-ranged dislocation strain fields. We employ the model to examine the influence of various dislocation distributions (random, cellular and power-law correlated) on the growth of a recrystallized grain. Our results show that grain growth is typically highly anisotropic and irregular, in agreement with recent experiments. We also discuss how to extend this method to three spatial dimensions by invoking the full dislocation density tensor.

Diffusion in Advanced Materials and Processing: Energy Technology

Sponsored by: The Minerals, Metals and Materials Society, TMS Structural Materials Division, ASM Materials Science Critical Technology Sector, TMS: Alloy Phases Committee, TMS: High Temperature Alloys Committee, ASM-MSCTS: Atomic Transport Committee, TMS/ASM: Nuclear Materials Committee, TMS: Solidification Committee

Program Organizers: Yong-Ho Sohn, University of Central Florida; Carelyn Campbell, National Institute of Standards and Technology; Daniel Lewis, Rensselaer Polytechnic Institute; Afina Lupulescu, Union College

Tuesday AM
February 27, 2007

Room: Europe 2
Location: Dolphin Hotel

Session Chairs: Dennis Keiser, Idaho National Laboratory; Kyoko Kawagishi, NIMS - Japan

9:00 AM Invited

Substitutional and Interstitial Diffusion in α_2 -Ti₃Al(O): Evan Copland¹; David Young²; Brian Gleeson³; ¹NASA; ²University of New South Wales; ³Iowa State University

The reaction between Al₂O₃ and α_2 -Ti₃Al was studied with a series of Al₂O₃/ α_2 -Ti₃Al multiphase diffusion couples annealed at 900, 1000 and 1100°C. The

diffusion-paths were found to strongly depend on α_2 -Ti₃Al(O) composition. For alloys with low oxygen concentrations the reaction involved the reduction of Al₂O₃, the formation of a γ -TiAl reaction-layer and diffusion of Al and O into the α_2 -Ti₃Al substrate. Measured concentration profiles across the interaction-zone showed "up-hill" diffusion of O in α_2 -Ti₃Al(O) indicating a significant thermodynamic interaction between O and Al, Ti or both. Diffusion coefficients for the interstitial O in α_2 -Ti₃Al(O) were determined independently from the interdiffusion of Ti and Al on the substitutional lattice. Diffusion coefficients are reported for α_2 -Ti₃Al(O) as well as γ -TiAl. Interpretation of the results were aided with the subsequent measurement of the activities of Al, Ti and O in α_2 -Ti₃Al(O) by Knudsen effusion-cell mass spectrometry.

9:30 AM

Interdiffusion in Ni-Cr-X and Fe-Ni-Cr-X (X = Al, Si, Ge or Pd) Alloys at 700° and 900°C: Narayana Garimella¹; Michael Brady²; Yong-Ho Sohn¹; ¹University of Central Florida; ²Oak Ridge National Laboratory

Effects of alloying additions on the interdiffusion behavior of ternary Ni-Cr-X and quaternary Fe-Ni-Cr-X (X = Al, Si, Ge or Pd) alloys (fcc γ -phase) are investigated using solid-to-solid diffusion couples. Ni-Cr-X and Fe-Ni-Cr-X alloys with compositions of Ni-22at.%Cr, Ni-21at.%Cr-6.2at.%Al, Ni-22at.%Cr-4.0at.%Si, Ni-22at.%Cr-1.6at.%Ge, Ni-22at.%Cr-1.6at.%Pd, Fe-24.1at.%Ni, Fe-24.0at.%Ni-21.4at.%Cr, Fe-23at.%Ni-21at.%Cr-6at.%Al, Fe-23.2at.%Ni-21at.%Cr-3.9at.%Si, Fe-23.8at.%Ni-21.3at.%Cr-1.7at.%Ge, Fe-20at.%Ni-22at.%Cr-1.6at.%Pd were made using arc-melt and chill-cast. Solid-to-solid diffusion couples are assembled in Invar jig, encapsulated in Ar after hydrogen flushes, and annealed at 700°C and 900°C for 168 and 720 hours, respectively. Experimental concentration profiles are determined from polished cross-sections by using electron probe microanalysis with pure standards. Interdiffusion fluxes of individual components are determined directly from the experimental concentration profiles, and are integrated for the determination of average ternary and quaternary interdiffusion coefficients. Effects of alloying additions on the diffusional interaction in Ni-Cr-X and Fe-Ni-Cr-X alloys are examined with respect to the formation and growth kinetics of protective Chromia scale.

9:50 AM Invited

EQ Coating in Advanced TBC System for Ni-Base Superalloys: Kyoko Kawagishi¹; Akihiro Sato¹; Jistine Ang²; Kazuhide Matsumoto¹; Hiroshi Harada¹; ¹National Institute for Materials Science; ²University of British Columbia

In thermal barrier coating (TBC) systems for the Ni-base superalloy turbine blades of advanced gas-turbine engines, the interdiffusion between a conventional metallic bond coat and the substrate promotes the formation of secondary reaction zone (SRZ). It leads to the degradation of the mechanical properties of the blades. In this study, a new bond coat system, "EQ coating" is proposed. A stable phase such as γ' which is in equilibrium with the substrate is used as coating in order to minimize the diffusion between the coating and the substrate. Cyclic oxidation examinations of γ/γ' tie-line alloys clarified that 100% γ' alloy shows best oxidation resistance and indicated the possibility as the bond coat. SRZ and interdiffusion zone were not observed at the interface after the diffusion at 1100°C for 300h. Thus, it has been confirmed that the interdiffusion of alloying elements were suppressed by using our new bond coat system.

10:20 AM

Diffusion Characteristics at the 17-4 PH Steel-Nickel Interface: Arijit Laik¹; Prakash Gawde¹; Karanam Bhanumurthy¹; Gajanan Kale¹; ¹Bhabha Atomic Research Centre

Seal disc consisting of precipitation hardened 17-4 PH steel with Ni coating is an important component in advanced nuclear reactors. 17-4 PH steel and nickel specimens were diffusion bonded at 800°C and subsequently annealed in the temperature range 900 – 1100°C for different durations. The diffusion coefficients of the major elements Fe, Ni, Cr and Cu were evaluated using the Dayananda method for multi-component system. The interdiffusion coefficients for each of these elements were also evaluated using Boltzmann-Matano method assuming that the inter-element interaction is non-existent. The average effective interdiffusion coefficients varied between 2 to 117 X 10⁻¹⁶ m²/s. The temperature dependence of the diffusion coefficients for each element was determined assuming Arrhenius type of variation and the activation energies for diffusion of each element at various compositions were evaluated. Their range between 219 to 297 kJ/mol.

10:40 AM Break

11:00 AM Invited

Interdiffusion Behavior in Annealed RERTR Nuclear Fuel Plates: *Dennis Keiser*¹; ¹Idaho National Laboratory

Different fabrication techniques are being evaluated for producing advanced research reactor fuels. These include HIPing, friction stir welding, and transient liquid phase bonding. These techniques can be employed to bond together U-bearing alloys and Al alloys, thereby forming optimal diffusion couples. This talk will describe the multicomponent, multiphase diffusion that occurs when bonded samples are heat-treated at relatively high temperatures. The relative diffusion behavior for systems comprised of U, Mo, Si, and Al will be discussed, along with the types of phases that develop. The potential impact of this behavior on fuel performance in a reactor will be addressed.

11:30 AM

Assessment of Ternary Multicomponent Diffusion in Alloy 22 (Ni-Cr-Mo): *Alonso Jaques*¹; *Jeffrey LaCombe*¹; ¹University of Nevada, Reno

Diffusivity [D], and square-root diffusivity [r] matrices for the ternary Ni-Cr-Mo alloy in the approximate single-phase compositional range of Hastelloy C-22 (Alloy 22), surrounding, Ni-63 wt.%, Cr-22.3 wt.%, and Mo-14.7 wt.%. These data will contribute to our understanding of the long-term phase stability of Alloy 22, and its potential use as a corrosion barrier in nuclear waste packages. Experimental diffusion couple data were obtained at selected temperatures from a series of diffusion couples, and evaluated using the constant-diffusivity approach. Our approach treats the process as an optimization problem that simultaneously considers concentration profile data from numerous diffusion couples surrounding a single end-point composition. We make use of the mathematical characteristics of the analytical solution to this problem, reducing the number of parameters to be fitted. The parameter fitting is accomplished using a combination of heuristic and deterministic methods. Discussion of the sources of uncertainty in the diffusivity values is included.

11:50 AM Invited

Alloying Effect on Interdiffusion Layer Growth in U-Mo/Al Dispersion Nuclear Fuel: *Yeon Soo Kim*¹; *Gerard Hofman*¹; *Ho Jin Ryu*¹; ¹Argonne National Laboratory

U-Mo/Al fuel is being developed for research and test nuclear reactors. The main issue is the formation of interaction layers and pore formation at the interface between fuel and Al due to interdiffusion between U, Mo and Al. As a remedy, we proposed alloying of Si in matrix Al and Zr in U-Mo fuel. High temperature (~550°C) out-of-pile tests showed auspicious results. The anticipated results of in-reactor tests at low temperatures (~150°C) are now available. We observed that addition of Si up to 5 wt% in Al prevented pore formation completely while pure Al showed massive pore formation. In this paper, we will present the irradiation test results and corresponding analyses. We will also include a model to explain the Si effect.

12:20 PM

Interdiffusion Behavior in U-7wt.%Mo and U-10wt.%Mo Alloys in Contact with Al: *Emmanuel Perez*¹; *Nathan Hotaling*¹; *Yong-Ho Sohn*¹; *Dennis Keiser*²; ¹University of Central Florida; ²Idaho National Laboratory

U-Mo dispersion fuels in Al-base alloys are being developed that fulfill the requirements to use low enriched uranium in research reactors. In this study, interdiffusion behavior of U-Mo-Al system was examined with solid-to-solid diffusion couples of U-7wt.%Mo vs. Al and U-10wt.%Mo vs. Al. These couples were assembled in Invar steel jig, encapsulated in Ar after several hydrogen flushes, and annealed at 400, 500 and 600°C in a three-zone tube furnace for 24, 48 and 96 hours. Microstructural development of Al-rich intermetallic phases were examined by using scanning electron microscopy and experimental concentration profiles were determined from polished cross-section of these couples by using electron probe microanalysis with pure standards. Interdiffusion fluxes of individual components were determined directly from the experimental concentration profiles, and are integrated for the determination of integrated and average interdiffusion coefficients. Results are examined in the light of the formation and growth of potentially deleterious intermetallics.

Dynamic Behavior of Materials: Deformation III

Sponsored by: The Minerals, Metals and Materials Society, TMS Structural Materials Division, TMS/ASM: Mechanical Behavior of Materials Committee

Program Organizers: Marc Meyers, University of California; Ellen Cerreta, Los Alamos National Laboratory; George Gray, Los Alamos National Laboratory; Naresh Thadhani, Georgia Institute of Technology; Kenneth Vecchio, University of California

Tuesday AM Room: Europe 3
February 27, 2007 Location: Dolphin Hotel

Session Chairs: James Asay, Sandia National Laboratories; Lawrence Murr, University of Texas

9:00 AM Invited

Thermoplastic Deformation Localization in Impulse Loaded Metals: *Dennis Grady*¹; ¹Applied Research Associates

In the explosive-driven deformation of metal components, stability of the governing plastic constitutive behavior is crucial to uniform deformation of the material. When instability in the governing relations occurs, deformation localization can follow. In dynamic thermoplasticity adiabatic trapping of dissipated heat and concomitant thermal softening governs the localization process. This study extends previous work on high-rate thermoplastic shear localization. The rates and extent of temperature rise, and shear stress reduction in the localization process are pursued through plastic wave analysis. Solutions are used to calculate characteristic adiabatic shear-band thicknesses, spacings and localization times. Dimensional analysis is pursued where dimensionless ratios of the governing metal properties are formulated and related to the propensity of selected metals to undergo adiabatic shear localization. An extensive set of metals data is used to benchmark the analytic study. Predictions are compared with recent investigations of adiabatic shear localization in 304 stainless steel.

9:30 AM Invited

Shear Localization: A Historical Overview: *Stephen Walley*¹; ¹Cavendish Laboratory

The shear localization to be considered in this paper is not the slip that is seen in deformed crystals. Rather it is the phenomenon often given the name 'shear banding'. These often follow trajectories independent of the underlying microstructure. A summary of the necessary condition for shear localization was given by Zener & Hollomon in 1944. Their statement has never been bettered, but it may be generalized to structures as well as materials. There are many reasons for deformation-softening but they can be summed up as 'damage'. At a sufficiently high rate the heat diffusion length becomes comparable to the specimen size leading to thermal softening. Hence the term adiabatic shear banding (ASB). Such deformation localizes into a narrow zone of intense shear and the surrounding material hardly deforms at all. Heat and inertia are coupled in this problem and hence ASBs are a mixed material/geometry phenomenon.

10:00 AM Invited

Atomistic Calculations of Shock Induced Phase Transformations and Spall: *Michael Baskes*¹; *S. G. Srinivasan*¹; *Greg Wagner*²; ¹Los Alamos National Laboratory; ²Sandia National Laboratories

Shock waves in materials produce a number of interesting phenomena including phase transformations and spall. This presentation will discuss calculations of these phenomena at the atomic level using an embedded atom method potential. Using a flyer-plate geometry, many molecular dynamics calculations at different sample sizes, orientations, grain structure, and initial velocity were performed. The following observations about shock induced phase transformations may be made: (1) the fcc crystal transforms to a bcc-like crystal structure just behind the shock wave; (2) after a period of time, the bcc structure transforms to a layered hcp/fcc material; and (3) when the reflected shock wave traverses this material, the system mostly transforms back to fcc. Spall then occurs in this almost pristine material by void nucleation and growth at a grain boundary facet. The spall strength is found to be a strong function of the large strain rates in these computer experiments.



10:30 AM Break

10:45 AM Invited

Shear Banding in Bulk Metallic Glasses: *Lan-Hong Dai*¹; Long-Fei Liu¹; Yi-Long Bai¹; ¹State Key Laboratory of Nonlinear Mechanics, Institute of Mechanics, Chinese Academy of Sciences

Understanding shear banding behavior of bulk metallic glasses has been the subject of both theoretical and experimental investigations for number of years. However, the precise physical nature of the formation mechanism of shear bands still remains unclear. In this study, a systematic experimental and analytical study on shear banding in bulk metallic glasses was presented. Both quasi-static and dynamic forced-shear tests on Zr-based bulk metallic glass were carried out. The experimental results have demonstrated that strain rate has a significant effect on the formation of shear bands. Further shear instability analysis shows that the initiation of shear bands in bulk metallic glasses is totally controlled by the free volume softening at the quasi-static loadings, whereas for the dynamic loadings case, both the free volume softening and the adiabatic heating softening exert an influence.

11:15 AM

Dynamically Driven Phase Transformations in Composite Materials: *JeeYeon Plohr*¹; Brad Clements¹; Frank Addessio¹; ¹Los Alamos National Laboratory

A model developed for heterogeneous materials undergoing dynamically driven phase transitions in its constituents has been extended to allow for complex material micro-structure and evolution of damage. In this work, damage is described by interfacial debonding and micro-crack growth. We have applied the analysis to silicon carbide-titanium (SiC-Ti) unidirectional metal matrix composites. In these composites, Ti can undergo a low pressure and temperature solid-solid phase transition. We have carried out simulations to study the complex interplay between loading rates, micro-structure, damage, and the thermo-mechanical response of the system as it undergoes a solid-solid phase transitions.

11:30 AM

High-Strain Rate Compression Testing of Ice: Mostafa Shazly¹; *Vikas Prakash*¹; Bradley Lerch²; ¹Case Western Reserve University; ²NASA-Glenn Research Center

A modified SHPB was employed to study effect of strain rate on dynamic material response of ice. Disk shaped ice specimens were either provided by Dartmouth College, NH, and/or grown at CWRU. The SHPB was adapted to perform elevated strain rate tests in the strain rate range of 60 to 1400/s at test temperatures of -10 °C and -30 °C. Experimental results showed that the strength of ice increases with increasing strain rates. There is a slight influence of ice microstructure on its strength, but it is much less than the influence under quasi-static loading conditions. It is also observed that the end constraint and frictional effects do not influence the compression tests like they do at lower strain rates, and therefore the diameter/length ratio of the samples is not as critical. The strength of ice at high strain rates was found to increase with decreasing test temperatures.

11:45 AM

Constitutive Modeling and Validation for Pre-Strained Materials: *Shuh-Rong Chen*¹; George Gray¹; Paul Maudlin¹; Carl Cady¹; ¹Los Alamos National Laboratory

Materials used in defense applications usually are subjected to initial shock straining as a direct result of detonation of high explosives. The plastic deformation induced by shock under high pressure at high strain rate altered the state of material and in general introduced excessive defects (dislocation, twinning). The stress/strain responses characterized from and the constitutive relations derived for the material in un-deformed/annealed condition are no longer valid to accurately represent the current state of the shocked material. We investigated the pre-straining effects on mechanical properties of several materials (copper, stainless and 1018 steels, tantalum, uranium and its alloy) via flyer impact test, high-explosive driven impact test, and medium-rate rolling process. We will present a methodology to include shock effect in a constitutive model. Examples using tensile tests to study localization of pre-strained materials and validation of the constitutive model in finite-element-method simulation will be given.

12:00 PM

Comparison of Quasi-Static and Dynamic Fracture of Nitinol: *Fengchun Jiang*¹; Kenneth Vecchio¹; Raghavendra Adharapurapu¹; Justin Cheney¹; ¹University of California, San Diego

Apart from the wide use in the medical field as a functional material, Nitinol shape memory alloy (SMA) and its composites have a potential application in aerospace, electrical and mechanical engineering as structural material. The present study focuses on the fracture behaviors (fracture toughness and fracture mechanism) of NiTi SMA under impact loading conditions. To this end, a pre-cracked four-point bend specimen was employed to perform fracture test using a modified Hopkinson pressure bar loaded fracture test. The dynamic fracture initiation toughness was measured using this technique at loading rate of $\sim 10^6$ MPa/m/s. The comparison between quasi-static and dynamic fracture toughness tests revealed that the dynamic fracture toughness of NiTi is higher than that in quasi-static loadings. The micro-mechanisms of fracture under each loading condition were studied, and the results indicate the fracture mechanisms are different in quasi-static and dynamic loading conditions, but in a contrary manner than normally observed.

12:15 PM

Scaling Relationships and Dynamic Failure: *Mukul Kumar*¹; James Stöcken¹; Roger Minich¹; ¹Lawrence Livermore National Laboratory

Scaling relationships are experimentally observed between dynamic strength and void nucleation and growth rates for various microstructures in high purity copper. These are derived from analyzing velocity-time histories associated with 1-D gas gun experiments. While there has been a significant amount of discussion related to the pull-back on release and how it is related to the nucleation and early stages of spall failure, little or no attention has focused on the rebound in velocity after the first spall pull-back. A sharp contrast is observed in the rebound signal in the velocity-time trace from single crystals and polycrystalline samples suggestive of differences in void growth and energy release mechanisms between the microstructures. The magnitude and other characteristics of this pull-back will be discussed in the context of the driving pressure and an apparent rate dependence of the void growth process.

12:30 PM

The Influence of Stored Work on Shear Deformation in 1018 Steel: *Lisa Dougherty*¹; Ellen Cerreta¹; George Gray III¹; Carl Trujillo¹; Erik Pfeifl¹; ¹Los Alamos National Laboratory

As-received and pre-shocked 1018 steel was subjected to forced shear experiments under various conditions to determine the influence of stored work, temperature, and strain rate on shear deformation behavior, namely the development of shear localization and shear bands. The starting microstructures of the as-received material, examined in tension and compression through a range of strain rates and temperatures, and pre-shocked material, shock loaded at pressures just below (12 GPa) and just above (14 GPa) the epsilon-phase transition, were studied using scanning and transmission electron microscopy, and orientation imaging microscopy. Extensive twinning was observed in the 12 GPa shocked steel, whereas dense dislocation walls predominated in the 14 GPa shocked steel. Tests were performed to correlate these microstructural changes with mechanical behavior in compression and in shear. One consequence of this difference in microstructures is increased strain hardening with pressure.

12:45 PM

Microstructural Evolution during Deformation of a 10Ni-0.1C Steel: *Ping Wang*¹; K. Kumar¹; ¹Brown University

Microstructural evolution during deformation of a Fe-10 Ni-0.1C-Cr,Mo,V steel was examined. In the as-received condition, the steel has a lath martensite microstructure, and during quasi-static deformation, shear appears to be accommodated by lath rotation and lath thinning. During dynamic deformation, shear localization occurs and manifests by an optically visible shear band. Initially, the original microstructure is discernible within the band. With progression in severity of localization, there is evidence for a central region within the shear band composed of ~ 200 nm size equiaxed grains constituting austenite, with a low dislocation content, and heavily twinned ferrite. In the extreme situation, a crack "chases" the shear band, and examination of the resulting fracture surfaces provides evidence for the presence of a thin liquid film layer. Together, these observations provide a microstructural footprint for deformation progresses evolution shear localization, and a sense for the accompanying thermal profile within the shear band.

Friction Stir Welding and Processing IV: Session II

Sponsored by: The Minerals, Metals and Materials Society, TMS Materials Processing and Manufacturing Division, TMS: Shaping and Forming Committee

Program Organizers: Rajiv Mishra, University of Missouri; Murray Mahoney, Rockwell Scientific Company; Thomas Lienert, Los Alamos National Laboratory; Kumar Jata, US Air Force

Tuesday AM Room: Northern E3
February 27, 2007 Location: Dolphin Hotel

Session Chair: William Arbegast, South Dakota School of Mines and Technology

9:00 AM Invited

Analysis of Self-Reacting Friction Stir Welds in a 2024-T351 Alloy: Tomasz Neumann¹; Rudolf Zettler¹; Pedro Vilaça²; Jorge dos Santos¹; Luisa Quintino²; ¹GKSS Forschungszentrum; ²Technical University Lisbon

In this study the GKSS force controlled self-reacting unit has been employed to produce welds in a 4mm thick 2024 T351 aluminium alloy plates. Three pins geometries were investigated for their suitability in joining the workpieces. Processing temperatures were measured in both sides of the welded joint at a depth of 1mm from the top and bottom surfaces of the workpieces. Microhardness testing indicate that considerable thermal softening occurs in each side of the workpieces. A comparison of welding forces, welding temperatures and microhardness measurements performed in the same alloy for similar FSW parameters, produced using standard FSW technique indicates that the self-reacting welds have higher processing temperatures with slightly lower welding forces for both the weld travel and transverse to the weld travel direction. Temperature development in self-reacting FSW has been analysed using the "iStir" code.

9:20 AM

Mechanisms of Metal Flow Related Defect Formation in Friction Stir Welds: William Arbegast¹; Casey Allen¹; ¹South Dakota School of Mines and Technology

Friction Stir Welding has been described as a "controlled path extrusion" process with joint properties and quality governed by thermo-mechanical treatments and metal flow path formation. Five distinct metal flow paths have been identified within the FSW nugget (DXZ and TMZ), each with distinct processing temperatures and strain rates. These paths are independent of material type with similar metal flow seen in aluminum, titanium, nickel, and ferrous alloys. Experimental evidence for the existence of these paths and their effect on volumetric and geometric defect formation is described and related to processing parameters, pin tool designs, and metal flow path convergence.

9:35 AM

Development of a Torque-Based Weld Power Model for Friction Stir Welding: Jefferson Pew¹; Tracy Nelson²; Carl Sorensen²; ¹Exxon Mobile; ²Brigham Young University

The basis for modeling welding heat input is fairly well understood for most arc welding processes. To date, there is no definitive relationship to quantify the heat input for FSW. An important step in establishing a heat input model is exploring effects that process parameters have on power input. This study details the relationship between process parameters and torque for three different aluminum alloys: 7075, 5083 and 2024. A quantitative power input model is then created from the torque input. In addition, this study outlines and validates the use of variable spindle speed tests for determining torque over a broad range of parameters. Trends in the heat input model are determined from the power input model. These trends are verified by measurements of the weld heat affected zones. The methods described in this study can easily be used to develop torque models for different alloys and materials.

9:50 AM

Eulerian Simulation of Friction Stir Welding in 7075 Aluminum: L. Fournert¹; S. Guerdoux¹; Michael Miles²; T. Nelson²; ¹Ecole des Mines de Paris (CEMEF); ²Brigham Young University

This work is focused on the numerical simulation of the different stages

that are generally encountered in Friction Stir Welding (FSW): plunging of the pin into the plate, heating of the plate by the rotating tool, and welding by translation of the tool. The FORGE3® finite element was used to carry out fully coupled thermo-mechanical calculations, both in the plate and in the FSW tool. The model is based on a velocity/pressure formulation and uses tetrahedral elements and an Arbitrary Lagrangian Eulerian (ALE) formulation. The original mesh velocity computation, combined with automatic adaptive remeshing and a remap of the primary variables, leads to an accurate computation of the entire steady and non-steady FSW process. For validation purposes, experimental results and numerical simulations are compared for welding of AA 7075 under different process conditions.

10:05 AM

Transport Phenomena in Friction Stir Welding: Lyne St-Georges¹; Véronique Dassylva-Raymond²; László Kiss²; Alexandre Perron²; ¹REMAC Industrial Innovators; ²Université du Québec a Chicoutimi

The friction stir welding is a solid-state process where intense plastic deformations and temperature fluctuations are produced by a rotating tool. In this process, the plastic deformations and the temperature field have a significant impact on the microstructural modifications observed in the welded zone and consequently, on the final mechanical properties of the welded joint. To understand the effect of the tool rotation on the temperature and the velocity field, a three dimensional thermo fluid model has been developed and is presented for AA 6061-T6. The global shape of the velocity field is found to be similar to a Rankine combined vortex. The contribution of this nearly perfect potential vortex to the flow vorticity is negligible; the vorticity basically results from the translational movement of the tool. For the particles located near the weld axis, trajectories with complete revolutions around the tool and with only deviations around the tool are observed. For this latter case, the particles go from one side of the weld, pass around the tool and pursue their trajectory on the other side of the weld axis. Finally, the effect of the rotation of the tool on the temperature field is found to be significant on the temperature history of the welded joint. The tool rotation has a predominant effect when the rotational speed is relatively high compared to the traverse speed.

10:20 AM

Phase Space Analysis of Friction Stir Weld Quality: Enkhsaikhan Boldsaikhan¹; Antonette Logar¹; Edward Corwin¹; William Arbegast¹; ¹South Dakota School of Mines and Technology

The plot of a selected weld output versus its derivative defines a trajectory for a dynamical system that is related to weld quality. The ideal trajectory for the dynamical system is defined by the spindle frequency and is characterized by repeated orbits in an elliptical shape. The number of points in each orbit is also defined by the spindle frequency, and each orbit can be examined to determine the stability of the system during a weld. Multiple techniques, including calculation of the Lyapunov exponent for the dynamical system and statistical analysis of successive orbits, demonstrate the effectiveness of phase space analysis for determining weld quality. Examination of the phase space diagrams of welds without metallurgical defects show a tendency to convergence to the ideal trajectory and produce negative Lyapunov exponents as the system evolves. Welds containing defects produced non-stationary orbits and positive Lyapunov exponents, indicating divergence from the ideal orbit.

10:35 AM Break**10:50 AM**

In-Situ Neutron Diffraction Measurement of Temperature and Stress Fields in Friction Stir Processing of an Al Alloy: Zhili Feng¹; W. Woo²; X. L. Wang¹; D. W. Brown³; B. Clausen³; K. An¹; C. Hubbard¹; H. Choo²; S. A. David¹; ¹Oak Ridge National Laboratory; ²University of Tennessee; ³Los Alamos National Laboratory

We present the experimental approach and results of direct, experimental measurement of the temperature and thermal stress inside the stir zone during friction-stir processing of 6061-T6 aluminum plate using in-situ, time-resolved neutron diffraction measurements. A specially de-signed portable friction stir processing system was designed and built for this test. Measurements were made at different locations along the centerline of the processed region to reconstruct evolution of the temperature and stress as function of time as the material exits from the stir region. The design and implementation of the neutron measurement approach will be discussed. Decomposition of the



thermal and elastic strains from the lattice spacing changes measured using the neutron diffraction, for the first time, revealed the transient temperature and stress state under the tool shoulder during the FSP.

11:05 AM

Specific Energy and Temperature Mechanistic Models for Friction Stir Processing of Al - F357: P. Kalya¹; K. Krishnamurthy¹; Rajiv Mishra¹; John Baumann²; ¹University of Missouri; ²Boeing Company

Experimental analysis for microstructural modification of Al-F357 cast sheets in terms of process force and moment was carried out. Force and moment data were collected along with the surface temperature using an infrared camera. Least square model has been developed to represent the specific power (power per unit length of the weld) using the experimental results of measured torque. Tools with various shoulder surface area and various pin volumes were used in this study. Numerical analysis was carried out to determine the evolution of the surface temperature determine peak temperature. An empirical relationship has been developed between the modeled power and peak temperature. This work was performed under the NSF-IUCRC for Friction Stir Processing and the additional support of NSF, GM Pacific Northwest National Laboratory and Friction Stir Link for the UMR site is acknowledged.

11:20 AM

A Numerical Study of the Plunge Stage in Friction Stir Welding Using ABAQUS: Saptarshi Mandal¹; Justin Rice¹; Gene Hou¹; Abdelmageed Elmoustafa¹; ¹Old Dominion University

Although, there are several finite element (FEA) based models developed for friction stir welding (FSW), most of these models primarily concentrate on the phase of the weld where the tool is moving forward, eliminating the plunge stage. A better understanding of the plunge phase is extremely important with the growing role of friction stir spot welding and also for understanding tool wear in case of FSW of harder materials. This research develops a three dimensional FEA based model of the plunge stage using the commercial code ABAQUS to study the thermomechanical processes involved during the plunge. The strain rate and temperature dependent Johnson-Cook material law is used as the constitutive law. The heat source incorporated in the model involves friction between the material, the probe and the shoulder and also heat generated due to plastic deformation. A good correlation was found between the results obtained from ABAQUS and experimental data.

11:35 AM

Real-Time Classification of Friction Stir Weld Quality: Enkhsaikhan Boldsaikhan¹; Edward Corwin¹; Antonette Logar¹; William Arbegast¹; ¹South Dakota School of Mines and Technology

An essential step in the control of the friction stir welding process is real-time identification of weld quality and ability to detect developing changes in quality throughout the duration of a weld. A linear time sliding-window discrete Fourier transform was developed to generate feature vectors from machine outputs. Resulting vectors, which represent binned values from the DFT power spectrum, are presented to a previously trained neural network for classification and weld quality is recomputed approximately every 0.25 inches. The strength of the network response is used to signal shifts in weld quality. Although the weld could not be tested at the computation interval, evaluation of selected sections and of other non-destructive quality measurements derived from the system dynamics indicate that continuously-valued networks outputs are strongly correlated to changing weld quality. The real-time classification process correctly identified novel samples as good, bad, or transitioning from one type of weld to another.

11:50 AM

Minimizing Lack of Consolidation Defects in Friction Stir Welds: Srikrishna Chimbli¹; Dana Medlin¹; William Arbegast¹; ¹South Dakota School of Mines

Minimizing lack of consolidation defects in friction stir welds is important to develop maximum material properties within the weld, as well as maintaining consistent material properties along the length of a continuous weld. Process parameters such as travel speed, forge force, rotational speed, heel plunge depth, and tilt angle are important to control the thermal energy in the weld zone and minimize weld zone defects. In this evaluation, several weld process parameters were varied on butt welded 0.25 and 0.125 inch thick 7075 T7351 aluminum alloy and the resulting weld zone defects were

destructively characterized by traditional metallographic techniques. It was found that welds developed with higher heat indexes had fewer and smaller lack of consolidation defects. The most important variable to minimize lack of consolidation defects in this particular investigation was the forge force. The information learned from this evaluation will be used for future non-destructive evaluations.

Frontiers in Solidification Science: Microstructures I

Sponsored by: The Minerals, Metals and Materials Society, TMS Electronic, Magnetic, and Photonic Materials Division, TMS Materials Processing and Manufacturing Division, TMS: Chemistry and Physics of Materials Committee, TMS: Solidification Committee

Program Organizers: Jeffrey Hoyt, Sandia National Laboratories; Mathis Plapp, Ecole Polytechnique; Gabriel Faivre, CNRS; Shan Liu, Iowa State University

Tuesday AM Room: Northern A3
February 27, 2007 Location: Dolphin Hotel

Session Chair: To Be Announced

9:00 AM Invited

Coupled Growth in Polymer Systems: Rohit Trivedi¹; Jing Teng¹; ¹Iowa State University

Coupled growth is very commonly observed in many systems during solidification and solid-solid-transformations. The most widely used model is based on the considerations of volume diffusion in the parent phase and the interfacial energy. The effects of other physical processes, such as interface kinetics, interface diffusion and interface strain energy are often dominant in some systems. These different effects will be examined briefly with an emphasis on the experimental studies in polymer systems in which interface kinetics play a dominant role. Experimental studies on interface kinetic laws will first be presented which show that the kinetics are governed by the nucleation process, and they consume a majority of the available driving force for transformation. The scaling law between the spacing and velocity is found to be different from those in metallic systems, and a model will be presented to analyze the results.

9:30 AM Invited

Real-Time Observation of the Dynamics of Lamellar and Rod-Like Eutectic Microstructures: Silvere Akamatsu¹; Sabine Bottin-Rousseau²; Mikael Perrut²; Gabriel Faivre¹; ¹CNRS; ²University Paris VI

We present an experimental study of lamellar and rod-like eutectic microstructures in directional solidification of model, nonfaceted transparent alloys in thick samples. The solidification front is imaged in real time in an oblique view from the exterior (through the liquid and a container glass wall) with a long-distance microscope. I will present recent observations of the spatio-temporal dynamics of large, nearly periodic (isotropic) eutectic patterns beyond the onset of secondary instabilities as a function of the wavelength (lamella or rod spacing, relative to the minimum-undercooling spacing). The stability of steady, symmetric lamellar patterns is limited by a zig-zag instability (upper limit) and an Eckhaus instability (lower limit). In rod-like patterns, we observe a hexagonal packing with numerous, long-lived topological defects, depending on the history of the experiment. Our observations compare well with numerical results (M. Plapp and coworkers, Ecole Polytechnique, France).

10:00 AM Invited

Evolution of Eutectic Patterns during Coupled Growth of Al and Al₂Cu in Ternary Al-Cu-Ag Alloys: Ulrike Hecht¹; Victor Witusiewicz²; Anne Drevermann¹; Stephan Rex¹; ¹ACCESS Materials and Processes

Coupled, regular eutectic growth of Al and Al₂Cu from ternary Al-Cu-Ag liquid alloys has been investigated by unidirectional solidification of polycrystalline, bulk samples. In the selected ternary alloys the eutectic reaction is univariant, which implies constitutional supercooling that drives the morphological transition from planar to cellular eutectic patterns at the solid/liquid interface. Several key factors with influence on the morphological transition and the cellular growth patterns will be presented as follows: Based on thermodynamic data of the ternary system Al-Cu-Ag, the constitutional

supercooling criterium is analysed in comparison to the results of solidification experiments. The main focus is laid on EBSD-mappings that allowed analyzing the orientation relationships (OR) between the phases of the eutectic in different grains. The selected OR imprint upon the characteristics of both, lamellar domains and cellular patterns. The role of fault lines during destabilization of the solid/liquid interface will be discussed.

10:30 AM Break

10:50 AM Invited

Rapid Dendrite Growth in Undercooled Melts: Experiments and Modeling: *Dieter Herlach*¹; ¹German Aerospace Center

Containerless processing by electromagnetic levitation is applied to undercool bulk samples of metals and alloys essentially below their melting temperatures. Various techniques are utilized to measure the dendrite velocity as a function of undercooling. The experimental results are analysed within current theories of dendrite growth. In such a way non-equilibrium phenomena during rapid solidification of undercooled melts are investigated. Experimental results and their analysis within dendrite growth models are presented for the solidification of segregation-free microstructures, disordered superlattice structures of intermetallics and non-faceted microstructures of semiconductors.

11:20 AM Invited

Computational Studies of the Interaction of Solidification Fronts with Embedded Particles: *H. Udaykumar*¹; Justin Garvin¹; Yi Yang¹; ¹University of Iowa

The interaction between an advancing solidification front and a micron-size particle is an inherently multiscale heat and mass transport problem. Transport at the micro-scale couples with intermolecular interactions and lubrication forces in a thin layer of melt between the particle and the front to determine the overall dynamics of the interaction. A multiscale model is developed to simulate front-particle interactions for stable planar solidification fronts. The solution to the lubrication equations in the melt layer is coupled to the solution of the Navier-Stokes equations for the overall particle-front system. Techniques are developed for coupling the dynamics at the two disparate scales at a common "matching region". The interaction of unstable dendritic structures in pure materials and alloys with embedded ceramic particles is also studied using numerical computations.

11:50 AM

Crystal Anisotropy and Growth Directions of Cells and Dendrites in Directional Solidification: *Alain Pocheau*¹; Marc Georgelin¹; Julien Deschamps¹; ¹Institut de Recherche sur les Phénomènes Hors Equilibre

We consider the growth direction of cells and dendrites in directional solidification of a dilute alloy. It is known to vary with the pulling velocity from the direction of the thermal gradient to that of a principal crystalline axis, with important implications regarding the interface morphology and the structure of the resulting solid. We experimentally determine it in a succinonitrile alloy in the whole available range of variables made by the pulling velocity, the dendrite spacing, the thermal gradient and the mis-orientation angle between the thermal gradient and a relevant principal crystalline axis. Data reveal a non-linear collapse on a definite master curve which synthesizes the orientational response of cells and dendrites to growth conditions in the whole experimental range. The physical origin of the non-linearity of the collapse is pointed out and the nature of the master curve is clarified. Implications for solidification in heterogeneous environments are drawn.

12:10 PM

Damage Formation during the Deformation of a Solidifying Al-Mg Alloy: *Andre Phillion*¹; Peter Lee²; Steven Cockcroft¹; ¹University of British Columbia; ²Imperial College

When load is applied during solidification damage is accumulated in the form of voids. The evolution of this internal damage was measured via x-ray microtomography on interrupted semi-solid tensile test specimens. The 3D reconstructed images at each strain level were analysed to determine the location, size, morphology, and orientation of the damage. Child volumes representative of the typical microstructures were extracted and meshed for subsequent 3D finite element analysis. Using the 3D microstructural quantification and models, the key mechanisms influencing the nucleation and growth of damage in semi-solid aluminum alloys was studied.

Fundamentals of Shape Memory and Related Transitions: Electronic Structure and Phonons

Sponsored by: The Minerals, Metals and Materials Society, TMS Structural Materials Division, TMS: Chemistry and Physics of Materials Committee
Program Organizers: Michael Manley, University of California; James Morris, Oak Ridge National Laboratory

Tuesday AM Room: Europe 6
February 27, 2007 Location: Dolphin Hotel

Session Chair: Dallas Trinkle, University of Illinois

9:00 AM Introductory Comments

9:10 AM Plenary

Electron-Phonon Coupling in Shape Memory Alloys: *Stephen Shapiro*¹; ¹Brookhaven National Laboratory

All shape memory alloys undergo martensitic transformations that are strongly dependent upon the composition. A key question is, what is the driving force of the transformation? Inelastic neutron scattering studies of the phonon dispersion in a number of shape memory alloys (Ni-Ti, Ni-Al, Au-Cd, Ti-Pd, and Ni₂MnGa) have revealed anomalous phonon behavior that is a precursor to either the martensitic transition or the pre-martensitic phase. These observations, coupled with first principles calculations of the electronic structure and the electron-phonon coupling, show that the electron-phonon interaction drives the transformation. Fermi surface nesting is important and a recent study in Ni₂MnGa shows the presence of phasons, which are fluctuations of the phase of the charge density wave predicted by the calculations.

9:50 AM Invited

Electronic Structure and Anomalous Vibrational Effects in Heusler Compounds from First-Principles: *Alexey Zayak*¹; ¹University of Texas, Austin

First-principles calculations are used in order to investigate ferromagnetic Heusler alloys. Phonon dispersions of several systems are analyzed in order to discuss relations between characteristic features in their electron and phonon spectra. The phonon dispersions of the unstable compounds show that the optical Raman modes disperse at anomalously low frequencies, indicating a stronger polarizability of these systems. This unusual behavior reveals covalent interactions, acting as additional bonding features uncongenial to the cubic symmetry of the Heusler structure. This dominant effect originates from tiny features in the electronic DOS which are sensitive to the valence-electron-to-atom ratio and the external magnetic field. The overall picture reminds us some previous works where phonon renormalization in metals was attributed to the electron-phonon coupling and configurational frustration of the charge. This has a potential to unify separated pieces of our knowledge about Heuslers and get a better microscopic theory of the shape memory effect.

10:20 AM Invited

Electronic Instabilities in Shape-Memory Alloys: *Jason Lashley*¹; Peter Riseborough²; J. Smith¹; Cy Opeil³; Trevor Finlayson⁴; ¹Los Alamos National Laboratory; ²Temple University; ³Boston College; ⁴Monash University

Using a variety of experimental techniques that probe the thermodynamics and the electronic structure, we demonstrate that the martensitic transition is driven by instabilities in the conduction-electron gas. We investigate three nonmagnetic shape-memory alloys (InTi 24 at.% Ti, AuZn, and UNb 8 wt.% Nb) and one magnetic shape-memory alloy (Ni₂MnGa). In the nonmagnetic alloys the martensitic transition (MT) is significantly altered by the application of a magnetic field. Quantum oscillations in the speed of the longitudinal sound waves propagating in the [110] direction indicated a strong acoustic de Haas-van Alphen type effect. These results can be understood on the basis of successive Landau tubes sweeping through the Fermi surface modulate the screened pair potential and modulate the observed phonon frequencies. In the technologically important magnetic shape-memory alloy Ni₂MnGa, a pseudogap opens at the premartensitic transition temperature in photoemission spectra 0.3 eV below the Fermi energy at the premartensitic transition temperature.



10:50 AM Break

11:10 AM Invited

Boson Peak in Cu-Based Shape Memory Alloys: *Antoni Planes*¹; Lluís Manosa¹; Ricardo Romero²; Marcelo Stipcich²; Jason Lashley³; ¹Department ECM, Universitat de Barcelona; ²IFIMAT, Universidad de Centro de la Provincia de Buenos Aires; ³Los Alamos National Laboratory

A boson peak refers to an excess of low-energy modes in the vibrational spectrum of a given material with respect to the Debye prediction. It is revealed by thermodynamic quantities such as the heat capacity which shows a hump in the C/T^3 vs. T representation. This behaviour is typically observed in amorphous solids or glasses where resonant low-energy excitations originate from disorder. In the present paper we will present low-temperature heat capacity measurements that confirm the existence of a boson peak in Cu-based shape-memory alloys. We will also show that this behavior is associated with low-lying TA_2 -[110] phonon modes which provide these systems with an excess of vibrational entropy responsible for the stability of the bcc-based parent phase at high temperatures. This scenario is confirmed by experimental estimations of this excess of entropy. Results will be discussed within the framework of a model for the vibrational spectrum of these systems.

11:40 AM Invited

Phonon Mechanisms and Long-Range Elasticity in Shape Memory Alloys: *Avadh Saxena*¹; ¹Los Alamos National Laboratory

We have studied the crystallography and thermodynamics of shape memory alloys in which the structural phase transition is driven by either strain (e.g. in FePd) or shuffle modes (e.g. in AuZn). We identify both the transformation mechanisms and the relevant order parameters and study the free energy in order to explore the microstructure as well as the stress-strain constitutive response. Special emphasis is placed on the long-range elastic interaction arising from the elastic compatibility constraints and the softening of relevant phonons modes and elastic constants. Collaborators: T. Lookman, R. Ahluwalia, J.C. Lashley

12:10 PM

Temperature and Compositional Effects on the Phonons of Ni_{0.5}Ti_{0.5}-xFe_x (x = 0, 0.03): *Michael Manley*¹; Mark Asta¹; Dan Thoma²; James Smith²; Robert Hackenberg²; W. Hulst²; ¹University of California; ²Los Alamos National Laboratory

The beta-phase of NiTi has been shown to exhibit two types of phonon instabilities; a classical anharmonic phonon instability leading to the shape memory transition, and an electron-phonon driven soft mode that forms the intermediate R-phase. Both of these contribute to the thermodynamic stability of NiTi's solid state phases but each should be affected differently by temperature and composition. With an aim towards quantifying these contributions we performed a series of measurements of the phonon density of states (DOS) of Ni_{0.5}Ti_{0.5}-xFe_x (x = 0, 0.03) at temperature from 300 K to 575 K using inelastic neutron scattering. Furthermore, we compared the measurements with phonon DOS calculated using the first-principles approach of ab-initio molecular dynamics. These calculations involve molecular-dynamics simulations based on interatomic forces derived from density-functional theory, and are used to examine the origins of the composition and temperature dependencies of the phonon DOS measured experimentally.

General Abstracts: Extraction and Processing: High Temperature Processing

Sponsored by: The Minerals, Metals and Materials Society, TMS Extraction and Processing Division, TMS: Aqueous Processing Committee, TMS: Materials Characterization Committee, TMS: Pyrometallurgy Committee
Program Organizers: Boyd Davis, Kingston Process Metallurgy Inc; Michael Free, University of Utah

Tuesday AM
February 27, 2007

Room: Southern 1
Location: Dolphin Hotel

Session Chair: Boyd Davis, Kingston Process Metallurgy Inc

9:00 AM

Heavy Metals Behavior of Municipal Solid Waste Incineration Bottom Ash with Magnetic Separation: *Gi-Chun Han*¹; Nam-Il Um¹; Kwang-Suk You¹; Hee-Chan Cho²; Ji-Whan Ahn¹; ¹Korea Institute of Geoscience and Mineral Resources; ²Seoul National University

Although municipal solid waste incineration bottom ash has high potential for recycling as road material, leaching of heavy metals prevents its recycling. In general, some treatments such as screening, weathering, physical separation are used before bottom ash is recycled as road materials. Especially, magnetic separation is one of basic and important pretreatments. It can recover ferrous material and the material can be used without any treatments. And it can reduce problems to be expansive in recycling of bottom ash as a road material. This study focused on separation effect for heavy metals by magnetic separation. As the results, we found that Ni, Cr can be separated with ferrous material by magnetic separation and Cu, Pb can not be nearly affected.

9:25 AM

Emission Yields on Pyrolysis Followed by Combustion of Polyethylene in Steady Flow: *Cecilia Goncalves*¹; *Jorge Tenorio*¹; *Yiannis Leventidis*²; ¹University of Sao Paulo; ²Northeastern University

Certain high-volume waste plastics, such as polyethylene (PE), can be converted into a gaseous mixture of hydrocarbons upon pyrolysis under appropriate conditions, which can then be used as a fuel. This gaseous fuel can then be homogeneously mixed with air and can subsequently be burnt in a furnace under appropriate low-emission conditions. To investigate methods for minimizing such emissions, tests were carried out using a two-stage electrically-heated, drop-tube furnace, simulating pyrolysis followed by combustion under several temperatures of combustion (pyrolysis was kept at 1000°C) and injection rates of polymers. Light hydrocarbons were detected at the end of the pyrolyzer and oxidizer furnaces. CO₂, CO and O₂ were detected at the end of the oxidizer furnace. Light hydrocarbons were analyzed on gas chromatography and fixed gases on on-line analyzers.

9:50 AM

Utilization of Waste Glass in Alumina-Glass Composite: *Jiann-Yang Hwang*¹; Xiaodi Huang¹; Adele Garkida¹; Shangzhao Shi¹; Bowen Li¹; ¹Michigan Technological University

Scrap automobile GL20 tempered glass was crushed and sieved to various size fractions. A series of cold isostatic pressing trials were run in order to determine the relative compactibility of the powdered glass at various particle sizes. The -325 mesh was found most suitable for producing the composite material. Composites of alumina and glass powders were prepared at various proportions. These composites were then compacted by uniaxial pressing and cold isostatic pressing. Best results were achieved by cold isostatic pressing. The compacted powders were sintered at a temperature range of 650°C to 725°C. It was found that 695°C was the optimum sintering temperature. Composite glass parts produced with 10-20% v/o alumina were found to be sintered close to full density. Using an analysis of variance technique there was a statistically significant increase in hardness due the addition of alumina reinforcement.

10:15 AM Break

10:35 AM

New Testing Chamber at Messer Austria to Develop Burners for Ferrous, Nonferrous and Glass Production: *Michael Potesser*¹; Burkhardt Holleis²; Davor Spoljarić³; Helmut Antrekowitsch¹; Axel Scherello⁴; ¹University of Leoben; ²Messer Austria GmbH.; ³ELME Messer Gaas; ⁴Gaswärme-Institut e.V.

During the past, burners were eclipsed of metallurgical furnace optimizations. Since the energy cost is increasing and the environmental protection is going harder the burners are in the focus of several investigations and optimizations. One possible way is the combustion by oxygen. By using oxygen, the flame temperature increases and therefore fuel accordingly money (oxygen price included) could be saved by having a low amount of harmful substances like NO_x in the off gas. This paper describes a new burner chamber for the development of burners, which combust natural gas by oxygen or air by normal or diluted combustion hence low pollutants in the off gas (NO_x). The effectiveness of the burner characterized by off gas analyses, a simulation of the burner and in the new burner development chamber of Messer Austria GmbH. as well as future trends in the burner technologies were shown.

11:00 AM

Sulfurization of Rare-Earth Containing UO₂ Solid Solution by CS₂: *Nobuaki Sato*¹; Genki Shinohara¹; Akira Kirishima¹; Osamu Tochiyama¹; Soichi Sato²; ¹Tohoku University; ²Tokai Reprocessing Center, Japan Atomic Energy Agency

For the recovery of uranium from spent nuclear fuel by sulfide reprocessing process, decladding by voloxidation and separation of rare-earth elements by sulfurization were applied to the UO₂ spent fuel. During the voloxidation procedure, it was found that UO₂ was oxidized to U₃O₈ and some of the fission products, such as rare-earth elements formed solid solution with UO₂ at 1000°C. Then the sulfurization of the solid solution phase was examined at temperatures lower than 500°C, and found that U₃O₈ was reduced to form UO₂. However, the rare-earth containing UO₂ solid solution phase transferred to two phases, 1)UO₂ phase without rare-earth elements and UOS phase with rare-earths at 450°C. The conditions for selective sulfurization were also discussed.

11:25 AM

Solidification of Fluoride Solution in Aluminum Electrolyte Bath: Bowen Li¹; Xiaodi Huang¹; *Jiann-Yang Hwang*¹; ¹Michigan Technological University

The solidification of condensed CaF₂-AlF₃-NaF mixture in aluminum electrolyte bath was investigated by XRD and SEM. The condensed fluoride mixture crystallized quickly and formed layered structure with enormous intercrystalline pores after solidification. The main minerals in the solid are chiolite and cryolite. But they have different distribution along the cross section of the bath. The metallic distribution in the solid phases is also explored.

General Abstracts: Structural Materials Division: Advances in Steel I

Sponsored by: The Minerals, Metals and Materials Society, TMS Structural Materials Division, TMS: Advanced Characterization, Testing, and Simulation Committee, TMS: Alloy Phases Committee, TMS: Biomaterials Committee, TMS: Chemistry and Physics of Materials Committee, TMS/ASM: Composite Materials Committee, TMS/ASM: Corrosion and Environmental Effects Committee, TMS: High Temperature Alloys Committee, TMS/ASM: Mechanical Behavior of Materials Committee, TMS/ASM: Nuclear Materials Committee, TMS: Product Metallurgy and Applications Committee, TMS: Refractory Metals Committee, TMS: Superconducting and Magnetic Materials Committee, TMS: Titanium Committee
Program Organizers: Rollie Dutton, US Air Force; Ellen Cerreta, Los Alamos National Laboratory

Tuesday AM Room: Europe 5
February 27, 2007 Location: Dolphin Hotel

Session Chairs: Lisa Dougherty, Los Alamos National Laboratory; Veronica Livescu, Los Alamos National Laboratory

9:00 AM Introductory Comments

9:10 AM

Dilatometric Analysis of Phase Transformation during Heat Treatment of TRIP-Aided Cold Rolled Steels: *Dong-Woo Suh*¹; Chang-Seok Oh¹; Seong-Jun Park¹; Sung-Joon Kim¹; ¹Korea Institute of Machinery and Materials

TRIP-aided steels are subjected to two-stage heat treatment including the intercritical annealing and the isothermal treatment for bainite transformation. Since the microstructural evolution is greatly affected by the transformation kinetics during the heat treatment, quantitative understanding of transformation behavior is critical for microstructural control. Dilatometric analysis is one of the methods to investigate the transformation behaviors. Recently, the present authors suggested a dilatometric analysis model which considered the effect of non-isotopic volume change originating from the transformation-mismatch plasticity. It was successfully applied to the microstructural evolution during austenite decomposition. In this work, we expand the analysis model to investigate the transformation behaviors of TRIP-aided steels during the heat treatment. The transformation behaviors of the conventional CMnSi and the low Si CMnSiAl TRIP-aided steels are examined with the proposed model. The phase fractions evaluated by the dilatometric analysis show an agreement with those obtained by the metallographic and XRD analysis.

9:30 AM

Influence of Rolling Process in Secondary Hardening Co-Ni Steels: *Cho Ki Sub*¹; Kim Jeong Hoon¹; Sim Ho Seop¹; Lee Kon Bae¹; Yang Heong Ryeal²; Kwon Hoon¹; ¹Kookmin University; ²Inchun City College

Effects of rolling process on microstructure and mechanical properties were investigated in ultrahigh strength (9-13)Co-(8-11)Ni secondary hardening steels containing Mo and Cr. Heavy rolling in the unrecrystallized austenite region, direct quenching, and aging were mainly performed. In addition, the rolling in recrystallized and partially recrystallized regions and the re-austenitizing were conducted for comparison. The severe deformation in the unrecrystallized region resulted in both refinement of martensitic structure and increase in dislocation density. The former can contribute to enhancement in strength and toughness whereas strain hardening due to the latter can degrade the toughness. In as-quenched and aged conditions, both factors were considered in terms of toughness to strength balance. Of course, alloying additions primarily controlled mechanical properties in as-quenched and aged conditions.

9:50 AM

Multicomponent High-Strength Low-Carbon Ferritic Steel with Nanosize Precipitates: *Prakash Kollit*¹; Semyon Vaynman¹; Dieter Isheim¹; Morris Fine¹; David Seidman¹; ¹Northwestern University

The relationship between mechanical properties and microstructure are studied as a function of composition and aging time in precipitation hardened, multicomponent, high-strength low-carbon (HSLC) ferritic steels. Depending on the composition and thermal treatment, the steels can achieve yield strengths as high as 1192 MPa (173 ksi) and good Charpy V-notch impact toughness values at cryogenic temperatures. An essential microstructural strengthening component of the HSLC steels, are nanoscale Cu-Ni-Al-Mn precipitates, which are characterized at peak strength and hardness conditions employing local-electrode atom-probe (LEAP) tomography. The number density of precipitates is greater than 10²⁴ nm⁻³ and the volume equivalent radius is approximately 1 nm.

10:10 AM

Nitrogen Diffusion Hardening of Austenitic Stainless Steels: *Ozgur Celik*¹; Huseyin Cimenoglu¹; Eyup Sabri Kayali¹; ¹Istanbul Technical University

The application of austenitic stainless steel as an orthopedic implant material not only requires high corrosion resistance but also excellent wear behaviour within a corrosive environment such as body fluids to obtain biocompatibility and acceptability. The aim of this study was to harden the surfaces of AISI 304L, 316L, 316Ti austenitic stainless steels without forming an external chromium nitride layer. Nitriding was carried out in a fluidized bed type furnace in ammonia/nitrogen gas mixtures. Characterization of nitrated surfaces was made by hardness measurements, XRD and GDOS analysis, corrosion, wear and corrosion-wear tests. The presence of nitrogen modifies the corrosion behaviour in acid media and the stainless character is maintained. Finally it is concluded that formation of nitrogen supersaturated austenite (S-phase) at the outer surfaces of austenitic stainless steels yielded a significant improvement in both wear and corrosion-wear resistance besides hardness.



10:30 AM Break

10:50 AM

Reverse Austenite Transformation of Ultrafine Grained Ferrite-Pearlite Low Carbon Steel Fabricated by Equal Channel Angular Pressing: *Kyung-Tae Park*¹; Young Il Son²; Dong Shin³; Chong Lee⁴; Young Kook Lee⁵; ¹Hanbat National University; ²Agency for Defense Development; ³Hanyang University; ⁴Pohang University of Science and Technology; ⁵Yonsei University

Reverse austenite transformation characteristics of a low carbon steel consisting of ultrafine grained ferrite and severely deformed pearlite by equal channel angular pressing (ECAP) were investigated by using a dilatometry and compared to those of the steel having coarse grained ferrite and undeformed pearlite. Coarse grained steel exhibited two serial transformation stages, i.e. pearlite → austenite followed by ferrite → austenite. Contrarily, ultrafine grained steel transformed with three serial stages, i.e. carbon supersaturated ferrite → austenite, not-fully-dissolved pearlite → austenite, and ferrite → austenite. The differences of reverse austenite transformation characteristics between the two steels are discussed in association with mechanical carbon dissolution from pearlitic cementite during ECAP.

11:10 AM

Brittle Crack Susceptibility of Low Temperature Separator Vessel Material: *Ahmad Nawaz*¹; ¹Ghulam Ishaq Khan Institute

Low temperature separator vessel made from HSLA steel grade A516-70, is used in gas sector following the JT valve or the turbo-expander. Being at very low temperature (-7°F to -13 °F), it is susceptible to brittle fracture due to ductile to brittle transition. The influence of temperature on the failure behavior of this material has been studied. Moreover, since the low temperature separator is manufactured from welded sheets, therefore, affect of temperature on the failure behavior on the post weld heat treated (PWHT) sample have also been carried out. In particular, SEM examination revealed the type of fracture that occurred in the parent metal as well as PWHT sample. A significant increase in the impact toughness of the PWHT samples as compared to the parent metal was observed which was explained by optical micrographs as well as SEM examination.

11:30 AM

Temporal Evolution of the Nanostructure and Compositional Profiles in Multicomponent High-Strength Low-Carbon Steel: *Prakash Kollit*¹; David Seidman¹; ¹Northwestern University

The growth and coarsening kinetics of Cu-Ni-Al-Mn precipitates in precipitation hardened, multicomponent, high-strength low-carbon (HSLC) ferritic steel is characterized employing local-electrode atom-probe (LEAP) tomography. The mean radius $\langle R \rangle$, number density NV , supersaturation of the solute elements, volume fraction, compositional profiles, and solute partitioning are studied as a function of aging time. The precipitates in the underaged condition are found to be Cu-rich with significant quantities of Fe, Ni, Al, Mn, and Si. The precipitates evolve with time into almost elemental Cu precipitate cores with Ni-Al-Mn spheroidal shells in the overaged condition at 1024-hours. Iron and Si concentrations are found to decrease with aging time in the precipitate. Furthermore the observed experimental results for the exponents of the temporal power laws for radius and number density are found to deviate from the model values predicted by Lifshitz-Slyzov-Wagner (LSW) theory extended to multicomponent alloys (Umanstev and Olson).

Hume-Rothery Symposium: Scattering Studies and the Fundamental Properties of Materials: Session II

Sponsored by: The Minerals, Metals and Materials Society, TMS Electronic, Magnetic, and Photonic Materials Division, TMS: Alloy Phases Committee
Program Organizers: Patrice Turchi, Lawrence Livermore National Laboratory; Wolfgang Donner, University of Houston; J. Robertson, Oak Ridge National Laboratory

Tuesday AM Room: Oceanic 7
February 27, 2007 Location: Dolphin Hotel

Session Chairs: J. Robertson, Oak Ridge National Laboratory; Simon Billinge, Michigan State University

9:00 AM Invited

The Nanostructure Problem, and Some First Steps to Solve It: *Simon Billinge*¹; ¹Michigan State University

A diverse array of complex materials are driving the nanotechnology and molecular biology revolutions. To understand and design these materials, it is essential to perform high precision structural characterization at the nanoscale. Often, even sub-Angstrom changes in inter-atomic bond lengths have profound consequences for the chemistry and functionality of these structure-sensitive materials. Crystallographic methods are the gold standard for atomic structure determination, however a broad and growing class of materials do not yield to a crystallographic analysis. The scattering is diffuse and Bragg-peaks become broad and overlapped. This is “the nanostructure problem” which currently has no robust solution. I will discuss alternative, more broadly applicable, methods which are emerging for these problems. The complete solution will likely lie in a synthesis of different scattering, imaging and spectroscopic approaches bound up in a coherent computational framework.

9:30 AM Invited

The Investigation of the Structure and Optical Properties of Single Wall Boron Nitride Nanotubes: *Annick Loiseau*¹; ¹Office National d'Etudes et Recherches Aéropatiales - Centre National de la Recherche Scientifique

BN nanotubes are, as their carbon analogs, made of an hexagonal sheet wrapped into a cylinder, where boron and nitrogen atoms alternate at the vertices of the hexagonal network. Due to this chemical order, BN nanotubes display drastically different electronic properties since they are semiconducting with a large gap (~ 6 eV) and are therefore very promising for optoelectronic applications. ONERA has developed in 2001 the first synthesis route to BN single-wall nanotubes, making possible the study of their properties.¹ This lecture will review how different modes of transmission electron microscopy can be used in a combined way for determining their atomic structure, their composition, studying their formation mechanism and finally investigating the optical response of individual nanotubes and approaching their optical gap.²
¹R. Lee et al, Phys. Rev. B Rapid Comm 64, 121405-1 (2001); ²R. Arenal et al, Phys. Rev. Lett. 95 (2005) 127601.

10:00 AM Invited

The Tale of Inhomogeneous Nanodomains in Yttrium Barium Copper Oxide Superconductors: *Zahirul Islam*¹; ¹Argonne National Laboratory

As a copper-oxide based Mott insulator is doped, the long-range antiferromagnetism is destroyed, and superconductivity emerges above a certain doping level. Numerous experiments, however, indicate that these cuprates are inhomogeneous even in their superconducting state. In the case of YBa₂Cu₃O_{6+x} (YBCO), charge carriers are doped via oxygen stoichiometry variations. Systematic x-ray diffuse scattering experiments on YBCO revealed the presence of inhomogeneous short-range ordered modulations characterized by a wavevector of the form $\mathbf{q}=(q_x, 0, 0)$. These modulations correspond to correlated atomic displacements of Ba, Cu, and O atoms, respectively, due to oxygen-vacancy ordered “nanodomains”. These superstructures (“ORTHO” phases) form well above room temperature. Furthermore, “bowtie”-shape Huang diffuse scattering indicate characteristic strain at all compositions regardless of the average structure creating an intrinsically inhomogeneous lattice throughout the phase diagram. (APS is supported by DOE, Office of BES, Contract No. W-31-109-ENG-38.)

10:30 AM Break

10:50 AM Invited

X-Ray Scattering Study of Self-Organized InAs/GaSb Nanowire Arrays: *Jianhua Li*¹; Donna Stokes¹; Kevin Bassler¹; Simon Moss¹; ¹University of Houston

Recent experiments have demonstrated that although the lattice mismatch between InAs and GaSb is fairly small (~0.62%), well-ordered "InAs" nanowire arrays can be self-organized during the growth of InAs/GaSb superlattices which may be beneficial for device enhancement. To understand how to exploit this novel phenomenon, a detailed x-ray study of strain and composition of MBE grown InAs/GaSb superlattices on both GaSb and InAs (001) substrates was performed. Quantitatively the misfit strain, which is directly associated to composition mixing, inside the superlattice layer and at the interfaces has been determined. Our results suggest that the strain configuration of the superlattice layers and the interfaces, including their magnitude and sign, is a crucial factor governing the morphology of the system. We believe that with careful interface engineering the growth of self-assembled nanowire arrays in semiconductor heterostructures with a small lattice mismatch may be achieved for the optimization and/or development of new devices.

11:20 AM Invited

Computer Simulations of the Strained Growth of Nanostructured III-V Semiconductor Multilayers: *Kevin Bassler*¹; ¹University of Houston

Novel computational methods that have been developed for simulating the growth of almost lattice matched semiconductor multilayers will be described. Those methods have been used to study the self-organized formation of arrays of nanowires in both AlAs/InAs and InAs/GaSb superlattices due to strain induced lateral composition modulation. With these methods, not only can we find the unstable growth modes predicted by perturbation theory, but we can determine the final morphological structure of the multilayer. The methods also allow analysis of the effects of varying growth parameters, including the surface temperature of the growing multilayer. Results of our simulations will be compared to those of experimental x-ray diffraction studies of the same materials.

Innovations in Measurement Science to Assess the Performance of New Materials in the Real-World: High Strain Rate Deformation

Sponsored by: The Minerals, Metals and Materials Society, TMS Materials Processing and Manufacturing Division, TMS: Shaping and Forming Committee

Program Organizers: Mark Stoudt, National Institute of Standards and Technology; Lyle Levine, National Institute of Standards and Technology; Tusit Weerasooriya, Army Research Laboratory

Tuesday AM Room: Australia 3
February 27, 2007 Location: Dolphin Hotel

Session Chairs: K. Ramesh, Johns Hopkins University; Lyle Levine, National Institute of Standards and Technology

9:00 AM Invited

Materials Performance in the World Trade Center Disaster: *Frank Gayle*¹; Stephen Banovic¹; William Luecke¹; Tim Foecke¹; Chris McCowan¹; Tom Siewert¹; Dave McColskey¹; Richard Fields¹; ¹National Institute of Standards and Technology

At the request of the U.S. Congress, the National Institute of Standards and Technology conducted a major investigation of the World Trade Center disaster. The investigation addressed many aspects of the catastrophe, from occupant egress to factors affecting how long the Twin Towers stood after being hit by the airplanes, with the goal of gaining valuable information for structural design and code changes for the future. A key part of the investigation was the metallurgical analysis of structural steel from the Twin Towers. The analysis included characterization of mechanical properties, failure modes, and temperature excursions seen by the steel. This talk on the metallurgical investigation will describe the structure of the towers, recovered steel, and special issues faced in the analysis of the steel. In addition, major results and conclusions of the NIST Investigation will be presented.

9:30 AM Invited

Uncertainty Quantification of Material Properties of Two Types of Steels at Elevated Temperatures for Stochastic Modeling of Structures on Fire: *Jeffrey Fong*¹; James Filliben¹; Richard Fields¹; ¹National Institute of Standards and Technology

Using a least-square algorithm and a logistic function to fit five sets of open literature data, we construct a number of functions with uncertainty bounds for the material properties of two types of steel used in the World Trade Center, namely, Steel Type 1, a proprietary high-strength steel made in Japan, and Steel Type 2, a U.S.-made low-carbon steel named ASTM A36. By introducing a temperature distribution profile for a hypothetical fire environment similar to the published profile of the 1972 Hudson Terminal experiment with a 6 psf normal office fuel load, we obtain distribution functions for the variability of ultimate tensile strength and yield strength of Steel Type 1, and Young's modulus and yield strength of Steel Type 2. The relevance of the quantification of the uncertainty of material property data at elevated temperatures to the mathematical modeling of the performance of a structure on fire is discussed.

10:00 AM Invited

Developments in Crack-Arrest Toughness Measurement of Ferritic Steels: Richard Link¹; James Joyce¹; *Charles Roe*²; ¹United States Naval Academy; ²Naval Surface Warfare Center Carderock Division

Through-wall cracking is one definition of reactor vessel failure held by the US Nuclear Regulatory Commission. The ability to predict crack arrest as a determination of failure is therefore important and requires the measurement of crack-arrest toughness (CAT) for future reactor pressure vessel (RPV) steels. The US Navy has a similar need for CAT measurement to evaluate the application of steels with improved weldability. A previous ORNL-NIST collaborative effort made use of large specimens and plane strain finite element analysis to indirectly measure CAT of an RPV steel in the upper-transition regime with much success, but at a high expense. This effort takes advantage of our current understanding of constraint on initiation toughness, the weakest-link statistical description of ductile-to-brittle transition, and modern computational power to economize the specimen size and test costs. The results demonstrate an ability to measure CAT of steels with very low transition temperatures and surveillance-sized specimens.

10:30 AM

Measurement of Initiation Fracture Toughness as a Function of Loading Rate in Brittle Materials: *Tusit Weerasooriya*¹; Paul Moy¹; Wayne Chen²; ¹Army Research Laboratory; ²Purdue University

The fracture toughness of SiC and PMMA are studied at different loading rates. Rates of loading include quasi-static rates and high rates. Geometry of the test specimen for all the tests was designed following the ASTM Standard C 1421-01b, the standardized procedure to determine the fracture toughness of advanced ceramics. For experiments at lower rates, loading was applied using an Instron test machine conforming to the ASTM Standard. Experiments at high loading rates were conducted using a new experimental technique based on the split Hopkinson pressure bar. Using this technique, dynamic fracture toughness of brittle SiC and PMMA were obtained under valid conditions at high loading rates. In this presentation, the effect of loading rate on the fracture toughness of SiC and PMMA are discussed.

10:55 AM Break

11:05 AM Invited

Techniques for the Measurement of the High-Strain-Rate Deformations of Materials: *K. Ramesh*¹; ¹Johns Hopkins University

The primary issues that arise in very high strain rate testing are stress equilibration, inertial effects, wave dispersion, friction, and controllability of deformations. Here we address these issues during the development of a controlled technique for the measurement of material properties in a strain rate range that has been difficult to reach, 104 to 105 s⁻¹. A miniaturized Kolsky bar system that includes the input bar is developed, together with the use of the Laser Occlusive Radius Detector to obtain local measurements of specimen strain during the very high rate deformations. It is demonstrated that this miniaturized Kolsky bar system can be used to provide fully validated results. The technique is applied to the characterization of 6061-T651 aluminum, and the results are compared with the results obtained using a conventional Kolsky bar and high-strain-rate pressure-shear plate impact.



11:35 AM Invited

Dynamic Characterization of Shape-Memory Alloys: *Weinong Chen*¹; Bo Song¹; ¹Purdue University

Pulse-shaping techniques are developed for both the loading and unloading paths of a split Hopkinson pressure bar experiment to obtain valid dynamic stress-strain loops for engineering materials. Front and rear pulse-shapers, in association with a momentum trap, are used to precisely control the profiles of the loading and unloading portions of the incident pulse. The modifications ensure that the specimen deforms at the same constant strain rate under dynamic stress equilibrium during both loading and unloading stages of an experiment so that dynamic stress-strain loops can be accurately determined. The modified momentum trap prevents repeated loading on a specimen without affecting the amplitude of the desired loading pulse and without damaging the bar at high stress levels. Using the new technique, the temperature dependence of the dynamic compressive stress-strain behavior of a NiTi shape memory alloy has been determined at a high strain rate over a range of environmental temperatures.

12:05 PM Invited

Mechanical Testing at High Loading and Heating Rates Using an Electrically Pulse-Heated Kolsky Bar Technique: *Steven Mates*¹; ¹National Institute of Standards and Technology

A novel Kolsky Bar facility has been created at NIST to perform compression tests on metals at high strain rates and high heating rates to probe their non-equilibrium mechanical behavior. These data are needed for modeling the dynamic conditions that exist during high speed machining, in which heat generated by plastic work at the tool/chip interface diffuses ahead of the deformation zone, resulting in very large local heating rates ahead of the deformation zone. The Kolsky Bar facility uses direct electrical pulse heating of the sample to achieve heating rates of up to 6000 K/s with temperature control to within a few Kelvin. Details of the measurement technique are discussed, as are sample data obtained to date.

12:35 PM

Compensation of Inertial Effects Associated with Quartz Force Transducer Embedded Split Hopkinson Bar: *Daniel Casem*¹; Tusit Weerasooriya¹; Paul Moy¹; ¹US Army Research Laboratory

An aluminum split-Hopkinson bar is instrumented with quartz transducers and used to test low impedance soft material properties at high rates. Two transducers are used, one at the interface between the specimen and the input bar and the other at the interface between the specimen and the output bar. It is shown that the measured signal associated with the quartz transducer in the input bar contains a component due to the inertial effects of the gage and the loading platen. Three methods to actively compensate for this by are proposed: by differentiation of the strain gage measured interface velocity, by measurement of the strain gradient within the bar, and by adding a compensation crystal to the gage to remove the inertial component from the output. Ability to mitigate the inertial effects by these methods is presented.

Innovations in Titanium Technology Symposium: Novel Materials and Processes II

Sponsored by: The Minerals, Metals and Materials Society, TMS Structural Materials Division, TMS: Titanium Committee

Program Organizers: Mehmet Gungor, Concurrent Technologies Corporation; M. Ashraf Imam, Naval Research Laboratory; F. H. (Sam) Froes, University of Idaho

Tuesday AM

Room: Asia 3

February 27, 2007

Location: Dolphin Hotel

Session Chairs: Patrick Martin, Air Force Research Laboratory/MLLMD; Stephen Fox, TIMET

9:00 AM Invited

Processing Routes to Produce Titanium from TiO₂: *James Withers*¹; John Laughlin¹; Raouf Loutfy¹; ¹MER Corporation

The only commercial process to produce titanium metal is the metallothermic reduction of TiCl₄ by sodium (Hunter) and magnesium (Kroll). If titanium

could be produced from the ore/TiO₂ a saving for producing TiCl₄ and its special storage and handling would at least be achieved as well as the electrolytic requirement of producing the Na or Mg reductant. An approach is to carbothermally reduce TiO₂ to a lower oxide which provides several possible routes for a second electrolytic reduction step to produce titanium metal. Several potential electrolytic reduction routes for producing titanium from a carbothermic produced suboxide will be discussed with experimental results provided for each process route.

9:30 AM

The Production of Titanium from a Composite Anode: *James Withers*¹; John Laughlin¹; Raouf Loutfy¹; ¹MER Corporation

The DARPA Initiative in Titanium focused the enabling need for low cost primary titanium which resulted in several DARPA sponsored programs for investigation to produce low cost primary titanium. The composite anode process was one that received DARPA sponsorship. During Phase I, it was demonstrated titanium could be produced in a two-step process. TiO₂ was carbothermally reduced to TiO which was combined in an anode with carbon. The composite anode of TiO-C was electrolyzed in a fused salt to produce titanium particulate at the cathode and CO at the anode. The titanium was separated from the salt by vacuum evaporation and while hot, pressed into billets. The billets were secondarily processing by RMI and the titanium characterized. Processing will be discussed and the properties of titanium presented. This composite anode process is now in Phase II which is scaling-up to 500 lbs/day production of titanium.

9:50 AM

Net Shape Powder Metallurgy Processing Using ITP Titanium Powder: *Curt Lavender*¹; Yuri Hovanski¹; K. S. Weil¹; L. C. Jacobsen²; ¹Battelle Memorial Institute - Pacific Northwest National Laboratory; ²International Titanium Powder

Historically, titanium powder metallurgy has been limited by the cost and quality of available powders. Recent development activities by International Titanium Powder (ITP) have produce powders that have sufficient quality at costs projected to be less than \$5/lb. The purpose of this study was to evaluate ITP powder for use on direct press-and-sinter components. This presentation will cover several aspects of press and sinter powder metallurgy processing including milling for desired apparent and tapped densities, the effect of pressing pressure on green density and sintering response and powder and die lubrication. Mechanical properties data will be presented from MPIF tensile bars using a series of pressing pressures and sintering conditions. Lubrication effectiveness was evaluated by visual inspection and dimensional control statistics from gears made using a high-rate high-volume production die.

10:10 AM

Microwave Melting of Armstrong Process Titanium: *William Walden*¹; ¹Technikon, LLC

Microwave melting of titanium has the potential to redefine the applications of titanium castings, use less energy than any current melting technology used in production today, and improve the quality of the castings by providing a cleaner melt. The potential has been demonstrated for this technology, however, there are critical issues that need to be addressed prior to transition to pilot scale phase. In addition, this new melting technology using microwaves can be leveraged to allow direct melting of titanium powder, eliminating the usual multiple melt processes required for conventional vacuum melting furnaces. The author is working closely with International Titanium Powder (ITP) to expand the sets of technology necessary to bring inexpensive titanium cast products made with all domestically produced Armstrong titanium powder.

10:30 AM Break

10:45 AM Invited

A Novel Recycling Process of Titanium Metal Scraps by Using Chloride Wastes: *Haiyan Zheng*¹; Toru Okabe¹; ¹University of Tokyo

A novel process of recycling titanium metal scraps by utilizing the chloride wastes (e.g., FeCl₃ and AlCl₃) that are obtained as by-products of the Kroll process or any other chlorination processes was investigated in this study. This is important from the viewpoint of the increase in titanium metal scraps and chloride wastes in the future. Thermodynamic analyses and some primary experiments have been carried out in the previous researches. Based on the previous study, the experiments involved reacting titanium granules

and turnings with iron chloride (FeCl₂) in an evacuated sealed quartz tube under a reduced argon atmosphere over a temperature range of 900-1300 K. The analytical results of the obtained samples determined by ICP-AES, the potentiometric titration method, and XRD analyses indicate that the obtained titanium chloride can be easily separated from iron and other chlorides and then recovered.

11:10 AM

Effect of Al₂O₃ Addition on the Electro-Winning of Ti in DC-ESR Operation: *Masahiro Kawakami*¹; *Toshihide Takenaka*¹; *Takahiro Kawabata*¹; *Akihiro Matsuyama*¹; ¹Toyohashi University of Technology

The Electro-Slag Re-melting (ESR) unit has been operated in DC mode, where a graphite rod was used as anode and a steel plate was used as cathode. The slag was composed of the CaF₂-CaO-Al₂O₃ system. The TiO₂ powder was mixed with the slag. The slag composition was widely changed. The supplied current was 800 to 1 200 A. In the case where the slag composition was 20%CaO-30% Al₂O₃-CaF₂ and the current was 1 000 A, for example, the agglomerated electro-deposit was obtained. The amount was 68 g and the cathodic current efficiency was c.a. 40 %. The deposit contained c.a. 23% Al. Thus, the Ti-Al alloy was obtained by the present method. The effect of experimental conditions on the current efficiency was examined widely. The reaction kinetics was also discussed.

11:30 AM

A Fundamental Investigation on Recovery of Titanium-bearing Blast Furnace Slag: *Dong Haigang*¹; *Jiang Tao*¹; *Guo Yufeng*¹; *Li Guanghui*¹; ¹Central South University

There are lots of blast furnace slag including 22%~25% TiO₂ in China. Nowadays, there are no effective methods to recover this slag. To resolve the problem of effective utilization of Ti-bearing blast furnace slag, in this paper, based on full foundation of physical and chemical characteristics Ti-bearing blast furnace slag, Ti-bearing water quenching slag were systematically investigated by H₂SO₄ leaching. It was shown that the leaching rate of TiO₂ was 72.26% under the conditions of H₂SO₄ concentration 50%, reaction temperature 100°, reaction time 1h, L:S=10:1, raw material granularity -0.5mm and stirring speed 400r/min. The leaching mechanism was investigated from thermodynamic analysis, crystal shape and micrographic structure. The slag was activated by water quenching and formed lots of non-crystal substances which have good reaction activation helped to TiO₂ of leaching.

Intellectual Property in Materials Science: Patents, Tech Transfer and Licensing: Patents

Sponsored by: The Minerals, Metals and Materials Society, TMS Materials Processing and Manufacturing Division

Program Organizer: Steven Marsh, Dorsey & Whitney LLP

Tuesday AM Room: America's Seminar
February 27, 2007 Location: Dolphin Hotel

Session Chairs: Steven Marsh, Dorsey & Whitney LLP; Iver Anderson, Ames Laboratory and Iowa State University

9:00 AM Invited

Obtaining Patents and Using Them to Protect, Expand and Generate Funds for Your Business: *Gary Abelev*¹; ¹Dorsey and Whitney LLP

Patents grant a right to exclude others from practicing a patented invention for a limited time (approximately 20 years) in exchange for full public disclosure of the invention. Recognizing patentable innovations and obtaining patents can be beneficial to a business or research center in a variety of ways. A brief overview of the patent application process is presented. Approaches to using patents to protect technology and research efforts, as well as to generate revenue or settle disputes via licensing is also discussed.

9:30 AM Invited

Claim Strategies: Patenting Alloys and Other Material Compositions: *Steven Marsh*¹; ¹Dorsey and Whitney LLP

Patent claims define the precise scope of an invention that is afforded protection by a patent. Claim language and form can be critical when licensing

a patented invention or asserting infringement of a patent. A brief overview of claim structure is presented, including the benefits of filing both independent and dependent claims. Further details are provided relating to drafting and interpretation of claims that include ranges of certain elements, such as compositional ranges in materials. Advantages of including structural features as well as compositional language in patent claims for novel materials are also presented.

10:00 AM Invited

A View of the Nanotech Patent Landscape: *John Miller*¹; ¹Arrowhead Research Corporation

Abstract not available.

10:30 AM Break**10:45 AM Invited**

An Analysis of the Value of Patents during the Invention-Innovation Life Cycle: *Jainagesh Sekhar*¹; ¹University of Cincinnati

The talk examines the issue of when patents offer maximum value. The relationships between invention, innovation, productivity and activity are explored within the framework of this question. A case study of a radically innovating entrepreneurial company utilizing patents is examined. The effect of having patented technology on pricing issues are discussed.

11:15 AM Invited

University Spin-Off Companies: The Need for Rational Matches of the Inside and Outside Environments: *Rand German*¹; ¹Center for Advanced Vehicular Systems, Mississippi State University

Being a participant in the formation of ten companies, and now director of a program with focus on regional job creation has led to a clear understanding of the match between the two key environments that determines success in these ventures. With university intellectual property there can be a mismatch in knowledge and poor appreciation for the difficulties in commercialization. One of the failings comes from improper rationalization of the infrastructure, expectations, and resources. This mismatch occurs in technical knowledge, marketing, and underestimated commercialization barriers. Often the university provides no bridging support and simply expects cash flow from the patents. On the other hand, when the inventor leaves the university, it becomes easy to circumvent the patents. A partnership where both sides of the transaction understand the barriers is difficult to create, yet has proven most successful. This typically requires an equity position by the university.

11:45 AM Invited

Converting Science to Practice: Personal Experiences with Patent Licensing: *Iver Anderson*¹; ¹Iowa State University

One of the most satisfying aspects of research and discovery may lie beyond the boundaries of the clean laboratory environment: on the busy streets of the business world. In the work statement of a research project, the objective often will refer to the eventual application of the technology that your project will attempt to develop. If patentable intellectual property is the outcome of your research project, the patent process must proceed through the stage of licensing to allow access to the commercial arena. The licensing portal is a test of the utility of an invention and involves issues that are beyond the experience and control of a researcher. Skilled contracting and licensing specialists can establish these effective business relationships that implement laboratory discoveries. Some case histories will illustrate the licensing and tech transfer process. Support from Iowa State University Research Foundation and USDOE-BES, EERE, and FE (Ames Lab contract W-7405-Eng-82).



Magnesium Technology 2007: Casting and Solidification I

Sponsored by: The Minerals, Metals and Materials Society, TMS Light Metals Division, TMS: Magnesium Committee

Program Organizers: Randy Beals, DaimlerChrysler; Neale Neelameggham, US Magnesium LLC; Mihriban Pekguleryuz, McGill University; Alan Luo, General Motors Corporation

Tuesday AM
February 27, 2007

Room: Southern 5
Location: Dolphin Hotel

Session Chairs: Gerald Cole, LightWeightStrategies LLC; En-Hou Han, Chinese Academy of Sciences

9:00 AM

Mathematical Modeling and Experimental Investigation of Shrinkage Porosity in Squeeze Casting of Magnesium Alloy AM50A: *Fang Yu*¹; Shuping Wang¹; Naiyi Li²; Henry Hu¹; ¹University of Windsor; ²Ford Motor Company

A mathematical model has been developed to predict shrinkage porosity during squeeze casting of magnesium alloy. By employing a newly proposed criterion based on "burst-feeding" theory, this advanced model is able to predict the occurrence and forming location of shrinkage porosity under certain circumstances, i.e., a specified applied pressure and holding time. To verify the computational results, experiments have been carried out. In comparison of the prediction with the experimental results, a reasonable agreement was obtained. The shrinkage porosity prediction enables to optimize squeeze casting process parameters, such as applied pressure and holding time.

9:20 AM

Effect of Pressure Levels on Tensile Properties of Squeeze Cast Magnesium Alloy MG-AL-CA: *Henry Hu*¹; Masoumi Hohen¹; Naiyi Li¹; ¹University of Windsor

The focus of this study is on development of alternative manufacturing processes for potential high temperature magnesium-aluminium-calcium alloys. The effect of applied pressures on tensile properties of squeeze casting magnesium alloy Mg-5wt.%Al-1wt.%Ca has been investigated with applied pressure levels varying from 3 to 90 MPa. The experimental observation indicates that the applied pressure of squeeze casting not only reduces the porosity level of Mg-Al-Ca squeeze castings, but also eliminates their surface cracks. The results of tensile testing show that an increase in applied pressures enhances the tensile properties of the alloy. The microstructural analysis and density measurements imply that the material densification should be responsible for the reduction in porosity, the improvement in the tensile properties plus the elimination of surface cracking.

9:40 AM

Effects of Processing Variables on Flow Behavior of Semi-Solid Magnesium Alloys: *Hwa Chul Jung*¹; Kwang Seon Shin¹; ¹Seoul National University

The semi-solid casting process is an emerging process that is superior to conventional casting processes in the quality of products it produces. It makes casting products with high integrity and less porosity. Subsequent heat treatments can enhance the mechanical properties. In this study, the effects of various processing parameters on the flow behavior of semi-solid magnesium alloys were investigated and analyzed. A number of variables affect the flow and solidification behavior of semi-solid slurries such as solid volume fraction, geometry of the die, gate velocity and mold temperature. In order to produce semi-solid processed specimens, a horizontal universal testing machine was modified to a system similar to a die casting machine. In this system, as the semi-solid magnesium slurry was injected from sleeve into mold, the load was measured as a function of time and displacement. The load vs. time or displacement curves were analyzed at various processing parameters.

10:00 AM

Effect of Solid Fraction on Microstructure and Fluidity of AZ91D in New Type Semi-Solid Injection Process: *Kenji Miwa*¹; Rudi Rachmat¹; Takuya Tamura¹; Naoki Omura¹; ¹National Institute of Advanced Industrial Science and Technology (AIST)

We have developed new type semi-solid injection process, that is, runner-

less injection process which can increase the level of material yield. In order to investigate the effects of solid fraction, thickness of die cavity and injection speed on the microstructure and the fluidity of AZ91D alloy slurry in this process, semi-solid forming testing machine which has the same system as a runner-less injection machine has been made on an experimental basis. The temperature controlling system of this machine has been established to obtain the homogeneous solid-liquid coexisted state inside injection cylinder. AZ91D billets are injected into a permanent mold by this machine in the semi-solid state. High injection speed brings good fluidity and homogeneous microstructure due to the thixotropic effect based on high rate shearing in the part of nozzle and also inside the die cavity.

10:20 AM

Lost Foam Casting of Magnesium AM60B Alloy: *Qingyou Han*¹; Ralph Dinwiddie¹; Philip Sklad¹; Kenneth Currie²; Fred Vondra²; Mohamed Abdelrahman²; Graham Walford³; Dennis Nolan⁴; ¹Oak Ridge National Laboratory; ²Tennessee Technological University; ³Walford Technologies; ⁴Foseco-Morval

The lost foam casting process has been successfully used for making aluminum and cast iron thin walled castings of complex geometries. Little work has been carried out on cast magnesium alloys using the lost foam process. The article describes the research activities at Oak Ridge National Laboratory and Tennessee Technological University on lost foam casting of magnesium alloys. The work was focused on castings of simple geometries such as plate castings and window castings. The plate castings were designed to investigate the mold filling characteristics of magnesium and aluminum alloys using an infrared camera. The plate castings were then characterized for porosity distribution. The window castings were made to test the castability of the alloys under lost foam conditions. Significant differences between lost foam aluminum casting and lost foam magnesium casting have been observed.

10:40 AM Break

11:00 AM

The Role of Carbon for Grain Refinement in Mg-Al Based Alloys: *Young Min Kim*¹; Chang Dong Yim¹; Young Han Kim¹; Bong Sun You¹; ¹Korea Institute of Machinery and Materials

While there are many grain-refining methods including Zr addition, superheating, carbon inoculation and direct addition of nucleant particles, the addition of carbon-containing agents has been known as the most effective way for grain refinement in Mg-Al based alloys. Although several hypotheses for the mechanism of grain refinement by carbon addition have been proposed, no decisive evidence was reported yet. In this study, therefore, the mechanism of grain refinement in Mg-Al based alloys by various carbon inoculation methods was investigated. Grain size was measured by using color etchant and polarized light in optical microscope. EPMA and TEM analysis were carried out to elucidate the grain refinement mechanism of Mg-Al based alloys. No evidence for carbon segregation was found, but Al-Mn or Al-Fe compounds within Mg grains were observed from EPMA analysis. These compounds were formed in the melt before the formation of primary Mg, resulting in grain refinement by heterogeneous nucleation.

11:20 AM

Grain Refinement of Magnesium Alloys by Ultrasonic Vibration: *Anthony Ramirez*¹; Ma Qian¹; ¹Brunel University

Cavitation by ultrasonic vibration has been shown to be able to alter the solidification process of a wide range of materials. The influence of ultrasonic vibration on the grain refinement of different magnesium materials has been studied using an ultrasonic system with a frequency of 20 kHz. Ingot samples of pure magnesium, AZ31 (Mg-3%Al-1%Zn), and AZ91 (Mg-9%Al-1%Zn) with a diameter of 70 mm were produced with and without ultrasonic treatment. The melt temperature used was 730°C and the sonicating time was 180 seconds. Substantial grain refinement was observed in all ingot samples cooled in a hot claygraphite crucible under ultrasonic vibration. The average grain size of the 70 mm diameter ingot samples of AZ31 was found to decrease from about 2 mm to 150 μm or finer. Similar observations were made for AZ91. For pure magnesium, columnar grains (average length: 30 mm) were changed to nearly equiaxed grains (average grain size: 310 μm). The grain refinement mechanisms by ultrasonic vibration are discussed on the basis of the cavitation study established on water because of the similar densities and viscosities of water and molten magnesium.

11:40 AM

Hot Cracking of Mg-Al-Ca Alloy Castings: *Guoping Cao*¹; *Sindo Kou*¹; ¹University of Wisconsin

Ternary Mg-Al-Ca alloys are the base of a few new creep-resistant, light-weight Mg alloys for automobiles. Hot tearing in Mg-Al-Ca alloys was studied, including Mg-4Al-0.5Ca, Mg-4Al-1.5Ca, Mg-4Al-2.5Ca, Mg-4Al-3.5Ca, Mg-5Al-2.5Ca and Mg-6Al-2.5Ca, by constrained rod casting (CRC) in a steel mold. The hot tearing susceptibility decreased significantly with increasing Ca content but did not change much with the Al content. The temperature at which cracking occurred was determined by using instrumented CRC. It was higher in alloys more susceptible to hot tearing.

12:00 PM

Real-Time Monitoring of Hot Tearing of AZ91E Casting: *Guoping Cao*¹; *Sindo Kou*¹; ¹University of Wisconsin

Hot tearing in AZ91E, a widely used casting Mg alloy, was studied by using instrumented constrained rod casting (CRC) in a steel mold – with a load cell and thermocouple to monitor in real time the temperature at which hot tearing occurred. In order to understand the effects of casting parameters on hot tearing of AZ91E, different mold preheating and rod diameters were used. It was found that hot tearing occurred at about 500°C. When the preheating temperature was increased from 335°C to 385°C, the hot tearing severity decreased. The temperature versus fraction solid curve during casting was calculated based on the Scheil model, and it was found that hot tearing occurred at a fraction solid as low as 0.77.

12:20 PM

Magnesium Foam Produced by Foaming in Melt: *Haibin Ji*¹; *Guangchun Yao*¹; *Hongbin Li*¹; ¹Northeastern University

Metal foam possesses many advantages. The main methods of producing metal foam are: casting, powder metallurgical method, metalizing, sintering process, foaming in melt, eutectic directional solidification. The foaming in melt process is a better method that vesicant is directly added into the molten metal. Vesicant will separate out gas which can make the molten metal inflate. After cooled, metal foam is produced. In this experiment, Magnesium foam was produced by foaming in melt. After pure magnesium melted in cast iron crucible, Ca and Al were added to protect the melt from burning. The vesicant TiH₂ was added at 670°C, and the molten metal was whipped for 2 minutes. At the same time, argon gas was passed over. At last the molten metal foamed at 650°C for 3 minutes.

Magnesium Technology 2007: Wrought Alloys and Forming Processes II: Rolling and Forming

Sponsored by: The Minerals, Metals and Materials Society, TMS Light Metals Division, TMS: Magnesium Committee

Program Organizers: Randy Beals, DaimlerChrysler; Neale Neelameggham, US Magnesium LLC; Mihriban Pektuguleryuz, McGill University; Alan Luo, General Motors Corporation

Tuesday AM Room: Southern 4
February 27, 2007 Location: Dolphin Hotel

Session Chairs: Jennifer Jackman, Natural Resources Canada; Sean Agnew, University of Virginia

9:00 AM

Simulation of Hot Rolling of Magnesium Strip by Using Finite Element Technique: *Elhachmi Essadiqi*¹; *Guowu Shen*¹; *Claude Galvani*¹; *Kevin Spencer*¹; *Abdelbaset Elwazri*²; *Steve Yue*²; *Ravi Verma*³; ¹CANMET Materials Technology Laboratory; ²McGill University; ³General Motors Research and Development, Materials and Processes Laboratory

Finite element thermal and mechanical models were developed to simulate the thermal and mechanical behaviour of magnesium strip during hot rolling. The results of preliminary rolling trials were used to determine the required physical constants in the finite element simulation. Frictional and heat transfer processes during hot rolling were included in the simulation. Comparisons of predicted and experimental exit temperatures have been conducted for the magnesium alloy AZ31, for different combinations of rolling temperatures,

reduction rates and rolling speeds. There is good agreement between the predictions and the experimental results. In addition, the model was used to study some important issues in the hot rolling process, such as contribution of plastic work to temperature change, the effect of reduction rate on the heat transfer coefficient between the strip and roll, and the generation of internal stresses inside the magnesium strip.

9:20 AM

Effect of Hot Rolling Parameters on the Hot Tensile Behavior of AZ31 Magnesium Sheet: *Geremi Vespa*¹; *Ravi Verma*²; *Jon Carter*²; *Steve Yue*¹; ¹McGill University; ²General Motors Research and Development Center

In this work, the behavior under hot tensile deformation of magnesium AZ31 sheet rolled under a range of processing conditions was investigated. Specifically, as-cast material was held for 1 or 10 hours at 350, 400 and 450°C, rolled at those temperatures using roll speeds of 20 and 50 rpm and thickness reductions of 15 and 30% per pass. Hot tensile experiments on the rolled sheets were performed at 400 and 450°C at strain rates of 0.1, 0.01 and 0.001s⁻¹. Using the obtained flow curves and microstructures, the hot-tensile behavior was related to the processing conditions employed. It was found that rolling at 350°C with 30% reduction per pass yielded the finest microstructure and subsequently, the best hot deformation characteristics. These observations will be discussed in this article.

9:40 AM

Microstructure Evolution during Rolling of AZ31 Magnesium Alloy under Decreasing Temperature: *Faramarz Zareandi*¹; *Ravi Verma*²; *Stephen Yue*¹; *Elhachmi Essadiqi*³; ¹McGill University; ²General Motors Research and Development Center; ³CANMET Materials Technology Laboratory

Strength and ductility are desired characteristics in sheet materials for applications in the automobile industry. Such characteristics are developed during hot rolling of the as cast material to obtain sheet. Therefore, it is important to understand the evolution of microstructure when an as cast thick plate is rolled to a thin sheet. In this work, an as cast AZ31 magnesium alloy was rolled through six passes to reduce the thickness from 5 to 1 mm. The rolling was performed successively at quasi-isothermal temperatures of 450, 400, 350, 300, 250, and 200°C. Such a rolling process is associated with different deformation mechanisms as the temperature changes and, therefore, the evolution process of microstructure is affected. Recrystallization through necklacing is thought to be the principal mechanism of evolution at high temperatures whereas twins are more effective at low temperatures. Such evolution in terms of microstructure and texture is discussed in this paper.

10:00 AM

Effect of Grain Size on Elevated Temperature Deformation Behavior of AZ31 Magnesium Alloy: *Emilie Hsu*¹; *Ravi Verma*²; ¹McGill University; ²General Motors Research and Development Center

Deformation behavior of an AZ31 alloy sheet with grain sizes 8, 20 and 50 μm, generated by different cold rolling reductions followed by annealing, was investigated by tensile experiments at 350 - 450°C with strain rates 1x10⁻³ - 1x10⁻¹ s⁻¹. At 450°C and 1x10⁻³ s⁻¹, the alloy exhibited highest elongation of 265% for the specimen with 8 μm grain size and 152% for specimen with 50 μm grain size. The benefit of high elongation with small grains was eliminated at the fastest strain rate. Specimen with 8 μm grain size exhibited steady flow-stress behavior at high temperatures and slow strain rates, while at low temperatures with high strain rates, strain hardening followed by strain softening occurred in all specimens. The specimens with initial grain size of 50 μm exhibited significant grain refinement with increasing strain, suggesting potential for enhancement of ductility through in-situ grain refinement during deformation.

10:20 AM

Development of Magnesium Sheetmetal Forming Parts for Electronic Appliances: Case Studies: *Wonkyu Bang*¹; *Hwan Jin Sung*¹; *In Joon Kim*¹; *Dongkyun Choo*¹; *Woo Jin Park*¹; *In Ho Jung*¹; *Sangho Ahn*¹; ¹RIST

While magnesium alloys have long been drawing strong interest as the lightest structural materials available, their application has been limited mostly to die cast parts. A continuous multi-pass warm rolling process of strip cast AZ31B coils has recently been developed by RIST/POSCO in order to correspond the growing need for thinner gauged parts forming with enhanced productivity. In this study, comparative measurement and optimization of the



deep drawability has been conducted using AZ31B sheets of several different thermomechanical histories. Several sheetmetal parts for electronic appliances have been formed by using a servo press equipped with warm toolsets. Application of protective surface treatments has also been evaluated.

10:40 AM Break

11:00 AM

Mg Coil Production via Strip Casting and Coil Rolling Technologies: In Ho Jung¹; Wonkyu Bang¹; In Joon Kim¹; Hwan Jin Sung¹; Woo Jin Park¹; Dongkyun Choo¹; *Sangho Ahn¹*; ¹RIST

The request for low cost Mg sheet materials has been drastically increased for the applications to automotive and electronic industries. In order to satisfy this demand, POSCO and RIST launched the research program for the production of Mg sheet materials using the strip casting and coil rolling technologies. As results of the program, AZ31 Mg alloy strips of 600 mm width and 3.0 to 7.0 mm thickness have already been produced continuously to several Mg coils of up to 1220 mm diameter. Incorporating optimized preheating and reheating methods, a continuous multi-pass rolling process of strip cast AZ31 coils with the maximum width of 600 mm has been developed successfully. The final microstructure and mechanical properties of as-cast and as-rolled AZ31 sheet show that the new integrated process can produce highly qualified and cost-competitive Mg alloy sheets.

11:20 AM

Superplastic Behavior of Twin-Roll Strip Cast Mg Alloys: *Geun Tae Bae¹*; Sung Soo Park¹; Dae Hoon Kang¹; Nack Kim¹; ¹Pohang University of Science and Technology

Mg alloys have the great potential for application in transportation systems mainly due to their low density and high specific strength. It has been recently shown that twin-roll strip casting can efficiently produce the low cost, high performance wrought Mg alloy sheets having equivalent or better mechanical properties compared to conventional ingot cast Mg alloys. For the successful application of twin-roll strip cast Mg alloys, however, extensive research on superplastic forming of Mg alloys at elevated temperature is needed since the formability of Mg alloys is poor at room temperature. The present research is aimed at investigating the mechanical behavior of the twin-roll strip cast alloy sheets at high temperatures. It shows that twin-roll strip cast alloys have excellent superplasticity, more than 700% elongation at 330°C. Mechanisms of high temperature deformation will be discussed based on the results of load relaxation test and tensile test at high temperatures.

11:40 AM

Influence of Process Parameters on the Mechanical Properties of Rolled Magnesium ZM21-Sheets: *Kerstin Nestler¹*; Jan Bohlen¹; Dietmar Letzig¹; Karl Ulrich Kainer¹; ¹GKSS-Research Centre Geesthacht

The rolling process for sheet production is one of the required processes to promote the potential of magnesium alloys as semi-finished products. There exist a variety of process parameters which have a strong influence on the mechanical properties of the rolled sheets. Hence, it is of fundamental interest to understand the effects of the process parameters such as rolling temperature and the degree of deformation per pass on the deformation behaviour. Rolling trials were conducted using the magnesium alloy ZM21 in cast condition at different rolling temperatures. Furthermore, the degree of deformation per pass was modified and also the initial sample geometry was varied in order to change the number of rolling steps. Mechanical tests and metallographic characterisations were used to describe the influences of the process parameters on the mechanical properties depending on the orientation concerning the rolling direction of the ZM 21 sheets.

12:00 PM

Effect of Rolling Parameters on the Microstructure and Mechanical Properties of Mg-Zn-Y Alloys: *Ju Youn Lee¹*; Hyun Kyu Lim¹; Do Hyung Kim¹; Won Tae Kim²; Do Hyang Kim¹; ¹Yonsei University; ²Department of Applied Physics, Chongju University

Effect of rolling parameters such as rolling speed and reduction ratio on the microstructure and mechanical properties of Mg-Zn-Y alloys have been investigated in the present study. Depending on the rolling parameters, various types of microstructure, i.e. fine dynamic recrystallized grain structure or heavily twinned microstructure, can be obtained. In present research, as-rolled Mg-Zn-Y alloys have been fabricated by hot rolling with various

rolling speeds (32-64mm/s) and reduction ratio (10-30%). The resulting microstructure exhibited fine grain structure or twinned structure depending on the rolling parameters. For example, with increasing reduction ratio at low roll speed of 32mm/s, the grain size in as-rolled microstructure decreased from 6.6µm to 4.7µm. In the case of high rolling speed such as 64mm/s, a large amount of twinned structure still remained. Uniaxial tensile test at room temperature reveals that the mechanical property is strongly dependent on the rolling conditions.

12:20 PM

Workability of Cold-Rolling and Heat Treatment Characteristics of Mg-Li-Al Alloy: *Hong Bin Li¹*; Guangchun Yao¹; Zhiqiang Guo¹; Zhengang Liu¹; ¹Northeastern University

Microstructure, Cold-rolling workability, heat treatment characteristics and mechanical properties of Mg-xLi-1Al alloys were studied. Density of the studied alloys is in the range of between 1.19 g/cm³ and 1.62g/cm³. The alloys have excellent cold-formability and the reduction limit for cold-rolling of the β phase alloys with 16wt% and 22wt%Li can exceed 90% at room temperature. The properties and microstructures of Mg-9Li-1Al alloy were mainly studied. To get the alloy sheets as thin as possible they need annealing at different temperatures for 1h. Recrystallization behaviors of the alloys were investigated through microstructures observing and hardness measuring. The results show that the casting billets are suitable for continuous rolling after annealing at 573K for 1h, because the cold-rolling sheets are completely recrystallized at this time. The results of tensile tests show that the alloys have good strength and excellent elongation.

Materials in Clean Power Systems II: Fuel Cells, Solar, and Hydrogen-Based Technologies: SOFCs I

Sponsored by: The Minerals, Metals and Materials Society, ASM International, TMS Structural Materials Division, TMS/ASM: Corrosion and Environmental Effects Committee

Program Organizers: Zhengu "Gary" Yang, Pacific Northwest National Laboratory; Michael Brady, Oak Ridge National Laboratory; K. Scott Weil, Pacific Northwest National Laboratory; Yong-Ho Sohn, University of Central Florida

Tuesday AM
February 27, 2007

Room: Asia 2
Location: Dolphin Hotel

Session Chairs: Jiahong Zhu, Tennessee Technological University; Paul Jablonski, US Department of Energy

9:00 AM Invited

Glass-Ceramic Sealants for the Assembling of Solid Oxide Fuel Cell Stacks: *Sonja-Michaela Gross¹*; Thomas Koppitz¹; Uwe Reisinger¹; Eric Wanko¹; Josef Rimmel¹; ¹Research Centre Juelich

SOFCs are highly efficient energy conversion devices, producing electricity by electrochemical reaction of fuel gases with air. Besides, SOFCs have the advantage of low air pollutant emissions. Research Centre Juelich focus its research on planar anode supported SOFCs, having the prospect of high power density at low-cost production. Metallic components of stacks need to be joined by gas-tight and electrically insulating sealants. Glass-ceramics have shown to be an appropriate material for the sealing of stacks. When developing glass sealants, matching the CTEs of the joining partners is a predominant target to avoid stresses in the joint and attain thermal cycling ability. Another requirement is chemical inertness to the other stack materials. An overview on the sealing technology of Research Centre Jülich will be given. Beside of introducing the state-of-the-art design of SOFC stacks and sealants, methods and development strategies for new sealants will be picked out as a central theme.

9:35 AM Invited

SOFC Seal Development at Pacific Northwest National Laboratory: *Yeong-Shyung Chou¹*; Jeffrey Stevenson¹; Prabhakar Singh¹; ¹Pacific Northwest National Laboratory

Sealing for planar SOFCs is an extremely challenging task to advance the fuel cell technology. The seal has to satisfy many stringent requirements

not only for long-term operation, but also for repeated thermal cycling. In this presentation, we'll give a comprehensive study of two approaches: hybrid mica-based compressive seals and "refractory" sealing glasses. In the compressive mica seal approach, the origin of the primary leak path was examined. The effect of compressive stress and mica thickness were studied. Leak rates during long-term thermal cycling and long-term isothermal aging were evaluated. Materials degradation will be discussed. The refractory glass seal approach also be explained. Glass Compositions will be discussed in terms of thermal properties. Results for sealed coupons will be reported. Thermodynamic calculations of interfacial reactions will be compared with experimental results. Finally, leak test results for large samples will be reported to provide a more complete assessment of the seal.

10:10 AM

Effects of Atmospheres on Bonding Characteristics between Silver and Alumina: *Jin Yong Kim*¹; Jung Choi¹; John Hardy¹; K. Weil¹; ¹Pacific Northwest National Laboratory

Recently, silver-based reactive air brazing (RAB) has been developed as an effective alternative sealing technique for high temperature electrochemical devices such as solid oxide fuel cells. It was reported that bend strength of brazed joints significantly decreases after thermal aging in hydrogen at high temperature, while the air-treated samples exhibit no degradation in comparison with the as-brazed joints. In this study, the effects of atmospheres on the microstructure, mechanical properties, and bonding characteristics between silver and alumina have been investigated. The detailed results to date will be discussed.

10:35 AM Break**10:50 AM**

Stress Induced Disruption of SOFC Interfaces: *Yves Idzerda*¹; Alex Lussier¹; Joe Dvorak¹; Shane Stadler²; Johnathon Holroyd¹; Marco Liberati¹; Elke Arenholz³; Satish Ogale⁴; T. Wu⁴; T. Venkatesan⁴; ¹Montana State University; ²Southern Illinois University; ³The Advanced Light Source; ⁴University of Maryland

Interfacial stress is thought to have significant effects on electrical and oxygen transport properties of thin films of importance in solid oxygen fuel cell applications. In this work we investigate by X-ray absorption spectroscopy (XAS) and X-ray resonant scattering (XRS) how in-plane biaxial stress modifies the electronic and chemical structure of LaCaMnO (LCM), LaSrMnO (LSM), LaSrCoO (LSC), and LaSrFeO (LSF) thin films. The in-plane interfacial stress was controlled by deposition of these films on different lattice mismatched substrates or deposition of an overlayer material. The transition metal L-edge XAS and XRS data show that the strain response is to modify the interfacial composition of the SOFC film to achieve a better lattice match to the overlayer material, creating an interfacial region that is a severe barrier to oxygen and electron transport. This interface modification due to interfacial stress appears ubiquitous in multi-element systems that also exhibit multi-valency.

11:15 AM

Parametric Investigation of a New Planar Solid Oxide Fuel Cell Sealing Approach Using Finite Element Analysis: *K. Scott Weil*¹; Brian Koepfel¹; ¹Pacific Northwest National Laboratory

One of the critical issues in designing and fabricating a high performance planar solid oxide fuel cell (pSOFC) stack is the development of the appropriate materials and techniques for hermetically sealing the metal and ceramic components. We are currently developing a foil-based approach that appears to offer good hermeticity and mechanical integrity, while minimizing the generation of interfacial stresses in either of the joint substrate materials, particularly the ceramic cell. Prior experimental work conducted on small-scale samples demonstrated the viability of the concept. Here we present recent results from computational analyses undertaken to investigate potential issues associated with scaling up the seal to full-scale pSOFC stack dimensions/geometry.

11:40 AM

Shape Memory Alloy/Glass Composite Gas Seal for Solid Oxide Fuel Cells: *Christopher Story*¹; W. Reynolds¹; Kathy Lu¹; ¹Virginia Polytechnic Institute and State University

Widespread use of solid oxide fuel cells is hindered by a lack of long-term durability of seals between metallic and ceramic components. A large

mismatch between the thermal expansion coefficients of these components cause the seal between them to crack during thermal cycling. A novel gas seal is being developed which integrates 3D-printed TiNiHf shape memory alloy wires into a SrO-La2O3-Al2O3-B2O3-SiO2 glass matrix. The shape memory alloy wires create a thermal expansion gradient in the composite seal, and are also expected to heal cracks in the glass and provide transformation toughening. The seal production method and seal testing will be discussed in this presentation. The TiNiHf alloy has been produced by arc-melting and homogenization, followed by milling to a fine powder and 3D printing. The glass, after homogenization, has been sintered around the TiNiHf wire structure. The behavior of the composite seal during thermal cycling tests will be presented.

12:05 PM

Microstructure and Mechanical Properties of Ceramic Joints Brazed with Copper-Doped Ag-Al Based Braze Fillers: *Jin Yong Kim*¹; Jung Choi¹; John Hardy¹; K. Weil¹; ¹Pacific Northwest National Laboratory

Silver-aluminum based air braze has been investigated as an alternative braze sealing for high temperature devices. Addition of aluminum was designed to improve the dual atmosphere tolerance of silver based air braze. In the silver based braze filler, it has been reported that addition of copper (oxide) improves the wettability of molten silver on both ceramics and metals, resulting in improved bend strength of their joints. In this study, we attempted to add copper into various compositions of silver-aluminum based braze fillers. We will discuss the effects of copper addition on the microstructure and mechanical strength of brazed ceramic joints.

Materials Processing and Manufacturing Division Symposium: Mechanics and Materials Modeling and Materials Design Methodologies, in the Honor of Dr. Craig Hartley's 40 Years of Contributions to the Field of Mechanics and Materials Science: Homogenization/Constitutive Behavior II

Sponsored by: The Minerals, Metals and Materials Society, TMS Materials Processing and Manufacturing Division, TMS: Shaping and Forming Committee, TMS/ASM: Mechanical Behavior of Materials Committee
Program Organizers: Brent Adams, Brigham Young University; Hamid Garmestani, Georgia Institute of Technology

Tuesday AM Room: Northern A1
February 27, 2007 Location: Dolphin Hotel

Session Chairs: Robert Wagoner, Ohio State University; Charles Neu, Forensic Sciences Inc

9:00 AM

Control of Properties in Deformation Processes Using Multi-Scale Sensitivity Analysis: *Nicholas Zabarav*¹; Veera Sundararaghavan¹; ¹Cornell University

Material property evolution during processing is governed by the evolution of underlying microstructural features. We discuss an efficient multi-scale FEM analysis for tailoring properties in forming processes involving polycrystalline materials through control of texture evolution. The multi-length scale deformation process simulator allows for crystal elasto-viscoplasticity and simulation of texturing using continuum representations of the orientation distribution function. Sensitivity of microstructure field variables such as slip resistances and texture due to perturbations in forming parameters such as forging rates, die and preform shapes are exactly defined using multi-scale sensitivity analysis. An averaging principle is developed to compute sensitivity of stress and various material properties at the macroscopic level from microstructural sensitivity fields. These sensitivities are used within a gradient-based optimization framework for computational design of metal forming processes. Examples that illustrate efficiency of this approach in controlling yield strength distribution in the final product during complex 3D deformation processes are shown.



9:25 AM

Influence of Crystallographic Orientation in Fretting and Sliding

Contacts: *Richard New*¹; ¹Georgia Institute of Technology

Mechanical models of fretting and sliding contacts developed at the macroscopic scale are typically based on homogeneous, continuum assumptions, using simple plasticity laws, if plasticity is considered at all. More recently, sliding at the nanoscopic scale has been modeled using molecular dynamics simulations. Even with these recent advances, the bridge between the nanoscopic and macroscopic scale in these contact problems is immense and is a challenge for the materials design of surface layers, often critical for performance of engineering systems. This paper focuses on experimental results that are not well modeled at either of these extreme scales. The results are most likely described by intermediate scale models. Recent work using crystal plasticity constitutive models for modeling fretting and sliding contacts is highlighted as a possible methodology to describe the friction behavior of heterogeneous materials in which the microstructure and the scale of the deformation field due to friction are comparable.

9:50 AM

Meso-Scale Simulation of Dislocation - Grain Boundary Interactions:

*Myoung Gyu Lee*¹; Robert H. Wagoner¹; Brent L. Adams²; ¹Ohio State University; ²Brigham Young University

A novel meso-scale model has been formulated to predict quantitatively the strengthening introduced by polycrystallinity. Dislocation densities on each slip system are represented by superdislocations at the centers of finite elements which are used in a two-step numerical procedure. The first of these makes use of single-crystal constitutive response to enforce continuum equilibrium and compatibility. The second equilibrates the dislocation density distribution among the finite elements within a grain. The two steps proceed sequentially, and predict of dislocation distributions, inhomogeneous hardening, elastic and plastic incompatibility effects and grain-size strengthening. The predicted lattice curvature derived from dislocation distributions for small columnar assemblies of BCC crystals has been compared with that of corresponding measurements by OIM. Predicted and measured lattice curvatures peak near some grain boundaries and triple junctions, and the magnitudes agree reasonably well.

10:15 AM

On Modeling Texture Evolution and Yielding Asymmetry of Hexagonal Closed-Packed Metals:

*Oana Cazacu*¹; Brian Plunkett¹; Ricardo Lebensohn²; ¹University of Florida/REEF; ²Los Alamos National Laboratories

A model for describing the influence of evolving texture on the response of pre-textured metals for both quasi-static and dynamic loading conditions is proposed. Initial yielding is described using a recently developed yield criterion capable of simultaneously describing slip, twinning, and anisotropy. The anisotropy coefficients and the size of the elastic domain are functions of the accumulated plastic strain. The specific expressions for the evolution laws are determined using a multi-scale methodology i.e. experimental measurements of the crystallographic texture, polycrystalline calculations, and macroscopic scale interpolation techniques. Application of the model to the simulation of the three-dimensional deformation of a pure zirconium beam subjected to four-point bend tests along different directions is presented. Comparison between predicted and measured macroscopic strain fields and beam sections shows that the proposed model describes very well the difference in response between the tensile and compressive fibers and the shift of the neutral axis.

10:40 AM

The Effect of Plastic Anisotropy and Material-Hardening on the Springback: An Experimental and Numerical Study:

*Hesam Golmakani*¹; ¹Ferdoowsi University

One of the important parameters in material properties is the anisotropy of sheet metals which are created in the rolling process. In this study, the U-draw bending process for three different Aluminum and Steel alloys with 0, 45 and 90 cut-out orientations due to their rolling directions are investigated experimentally and numerically to investigate the effect of anisotropy on the springback and side wall curl. In order to perform draw-bending experiments, a special die is designed and employed. In addition, the material's hardening model shows the basic properties of the material during plastic deformation. Therefore three hardening models (isotropic, linear and nonlinear kinematics) are used to study the effect of the hardening assumptions on the simulation

results. The 3D simulation of springback is modeled by using the finite element code, Ansys. The accuracy of the simulation is verified by a comparison between the numerical and experimental results.

11:05 AM

The Properties and Performance of Enamel in the Prevention of Corrosion in Ferrous Materials:

*Richard Kwayisi*¹; ¹University of Science and Technology

This abstract is about the use of ceramic formulations from local sources, enamel, in the prevention of corrosion. This is to overcome the inability of ferrous materials to resist or withstand corrosion. Enameling is a heat treatment process that is applied to objects in a furnace. Enamel is defined as a vitreous, glass-like coating fused on to a metallic base. It is also defined as an inorganic finish fused to metal at temperatures sufficiently elevated to liquefy the coating and create a permanent bond with the substrate. Essentially, enamel is an alkali alumina-borosilicate (glass) to which other inorganic substances may be added to provide desirable physical properties such as resistance to acid and alkaline solutions, heat, corrosion and abrasion. The process of applying porcelain enamel to a fabricated steel product or component has an important relationship to the design of the piece. Thus it is important for designers and manufacturing engineers to understand the procedure even though the enameling process itself is a highly specialized method. Enamels are relatively inert to corrosive environments because they often contain oxides, sulphides and other components that occur in nature. Thus there is little driving force to make these materials corrode. Many of the corrosion that occurs in metals are electrochemical in nature; they require the flow of electrons. Enamels being poor in conductors are not susceptible to electrochemical corrosion as metal hence they serve as excellent anticorrosive coats. The basic ingredient in enamel finish called frit, is enameling glass. Enamel frits contain larger amount of B₂O₃, TiO₂, and ZrO₂ than glasses. The oxides Na₂O, MgO, CaO, etc and the other materials use in enamels have the properties to make the products high resistance to corrosion, aesthetic appearance, reduce friction and wear, provide high thermal stability and makes surfaces chemically inert.

11:30 AM

Towards Incorporating the Kinematic and Kinetic Effects of Net Burger's Vector in Crystal Plasticity:

*Jobie Gerken*¹; Paul Dawson²; ¹Los Alamos National Laboratory; ²Cornell University

Following a suggestion in the work of Craig S. Hartley, we have incorporated, in addition to the classical elastic and plastic deformation, a long range deformation term in the multiplicative decomposition of the deformation gradient that is due to a bilinear distribution of a net Burger's vector in a region about a material point. Using the Volterra edge dislocation solution, this long range deformation is shown to be a function of gradient of the net Burger's vector. Relating the net Burger's vector to slip gradients, the long range deformation is a function of second order gradients of slip and therefore relates the kinetics of the plastic and long range deformations. It's shown, through simulation of a plate with varying boundary conditions, that long range effects significantly affect the resulting patterns of plastic deformation. The results show regions of slip localization that isolate regions of nearly constant long range deformation.

TUESDAY AM

Materials Processing Fundamentals: Smelting and Refining

Sponsored by: The Minerals, Metals and Materials Society, TMS Extraction and Processing Division, TMS: Process Technology and Modeling Committee, EMPMD Council, TMS: EPD Council
Program Organizer: Princewill Anyalebechi, Grand Valley State University

Tuesday AM Room: Northern A2
 February 27, 2007 Location: Dolphin Hotel

Session Chair: To Be Announced

9:00 AM

In-Situ Analysis of the Direct Reduction Process of Wustite by Solid-State Carbon in TEM: *Ishikawa Nobuhiro*¹; *Aoyagi Takeshi*¹; *Furuya Kazuo*¹; *Kimura Takashi*¹; *Mitsuoka Nayuta*²; *Inami Takashi*²; ¹National Institute for Materials Science; ²Ibaraki University

The method of in-situ analysis of the direct reduction of iron oxides by solid state carbon in a transmission electron microscope (TEM) was invented. This method was performed using wustite as an iron-oxide and carbon-deposition as a solid state carbon. The fracture surface was utilized to get the clean surface of wustite. The carbon was deposited on the fracture surface of wustite to contact with wustite. The preparations of the specimen was done with the size of thin foil of TEM sample. In-situ observation was performed at elevated temperature. The Fe precipitation at the boundary of wustite and carbon. The growth of Fe-precipitates into the carbon layer was also observed.

9:15 AM

Kinetics of the Pressure Leaching of Sulfidized Chalcopyrite in H₂SO₄-O₂ Media: *Rafael Padilla*¹; *Paola Pavez*¹; *Maria Ruiz*¹; ¹University of Concepcion

An environmentally friendly route to copper extraction from chalcopyrite by a combination of pyrometallurgy and hydrometallurgy is the sulfidation process which consists of roasting chalcopyrite with sulfur at 350 – 400°C and subsequent leaching of the sulfidized material to dissolve the copper. In the framework of this alternative, the leaching kinetics of the sulfidized chalcopyrite concentrate in autoclave was studied. The pressure leaching was carried out with H₂SO₄-O₂ solutions in the temperature range 100 - 150°C, and partial pressures of oxygen from 101 to 1216 kPa. The results indicated that the copper dissolution rate increases with increasing temperature and partial pressure of oxygen from 506 to 1216 kPa. The leaching kinetics was analyzed by using a modified shrinking core model $1-(1-0.45X)^{1/3} = kt$, which represented well the experimental data. The determined activation energy was 65 kJ/mol and the rate dependency on the partial pressure of oxygen was of first order.

9:30 AM

Experimental Study of CO₂ Sequestration by Steelmaking Slag: *Henry Rawlins*¹; *Kent Peaslee*¹; *Von Richards*¹; *Simon Lekakh*¹; ¹University of Missouri-Rolla

Steelmaking processes intensively use carbon-containing materials and generate a significant amount of carbon dioxide emissions. The U.S. steel industry produces ~1.75 tons CO₂ for every ton of steel shipped. At the same time, steelmaking processes use calcium and magnesium oxide containing minerals for slag formation, which are excellent CO₂ capture agents. The goal of this investigation was to experimentally study carbon dioxide sequestration by steelmaking slag with simultaneous acceleration of the slag stabilization processes in preparation for re-use as a construction material. Thermogravimetric methods and a slurry reactor were used to study reaction kinetics. The degree of slag carbonization was evaluated for industrial and synthetic slags in wet and dry processes.

9:45 AM

Effect of Na₄O₇P₂ on Cu Powder Preparation from Copper Oxide Slurries: *Hun Chung*¹; *Jong Ahn*¹; *Tri Hoang*²; *Dong Kim*¹; *Jae Lee*¹; *Jong Kim*²; ¹Korea Institute of Geoscience and Mineral Resources; ²Chungnam National University

In order to generate monodisperse particle system, two requirements are

considered; firstly, a complete separation of nucleation and growth steps for the formation of particles; secondly, an avoidance of their aggregation during the nucleation and growth. The former would be fulfilled if a short burst nucleation is rapidly induced while the latter has been often achieved by either adding suitable protective organic agents or controlling the zeta potential of particles. Sodium diphosphate as a surfactant was used in producing well dispersed 100 to 200 nm copper powders from copper oxide slurries with an addition of hydrazine as a reduction agent. In the wet chemical process, it was found that the synthesized metallic copper particles contain a thin oxidized surface layer, and sodium phosphate significantly affects the zeta potential of the Cu surfaces. The high dispersity of the produced powders was obtained with the use of appropriate sodium phosphate additions.

10:00 AM

Study on Hydrogen-Enriching Gas Reforming in Smelting Reduction Iron-Making Process: *Nan Wang*¹; ¹Northeastern University

For the two-step smelting reduction iron-making process, the advantages of hydrogen-enriching gas reforming are not only to lower the export gas temperature from final reduction vessel to satisfy the requirement of pre-reduction operation, but also to improve the kinetic conditions of pre-reduction and increase reduction efficiency. In order to attain better match between pre-reduction and final reduction operation in the two-step smelting reduction process, a static model of hydrogen-enriching gas reforming has been developed in this work. The interrelation of inlet and outlet composition and temperature of reforming gas, materials consumption under different reforming conditions are analyzed by using this model. The calculation results show that the hydrogen-enriching gas reforming can realize an effectively utilization of surplus physical heat energy of gas mixture and decrease of system energy consumption. Furthermore, reduction potential of reducing gas mixture and hydrogen ratio are also increased through hydrogen-enriching gas reforming.

10:15 AM

The Role of Iron in the Pressure Leaching of White Metal: *Maria Ruiz*¹; *Eduardo Gallardo*¹; *Rafael Padilla*¹; ¹University of Concepcion

During the treatment of white metal by pressure leaching with sulfuric acid and oxygen, the presence of iron in the leaching solution has a significant effect in the leaching rate. In this study, experiments were carried out in a titanium auto clave to clarify the role of iron in the leaching of white metal produced in a Teniente Converter reactor. The effect of iron (FeSO₄) additions to the leaching solution was studied in the range 100 to 150°C, using an oxygen partial pressure of 1013 kPa and 3 gpl of white metal. The results indicated that below the melting point of elemental sulfur (about 119°C) the addition of even 1 gpl of iron produced a large increase in the leaching rate (at 110°C the copper dissolution after 90 min increased from 49 to 73%). However, at higher temperatures the presence of iron is detrimental to the leaching rate.

10:30 AM Break

10:45 AM

Passivation Behaviour of Copper Anodes with Various Chemical Composition: *Zaki Mubarak*¹; *Helmut Antrekowitsch*¹; *Gregor Mori*¹; ¹University of Leoben, Austria

Anode passivation is one of the existing problems faced by copper refineries with the increase of current density and impurities content of the anodes. In the present work, passivation behaviours of copper anodes with distinctive chemical compositions were studied in simulated industrial electrolytes with potentiodynamic, galvanostatic polarisations and microscopic analysis. The contents of oxygen, lead, silver, nickel and antimony were found to have major influence on the anode passivation. High-oxygen anode exhibited a lower passivation resistance indicated by the lower peak and minimum current densities and time to passivation. Moreover, the increase of lead, silver, nickel and antimony contents generally enhanced the vulnerability of the anodes to passivation. Scanning electron microscopy (SEM), energy-dispersive X-ray (EDX) and X-ray diffraction (XRD) analyses detected the presence of copper sulphate, copper oxide, lead sulphate, silver powder, nickel oxide, nickel sulphate, antimony oxide and nickel-antimony bearing complex oxide on the passive anode surface after polarisation.



11:00 AM

Preliminary Investigation into the Effect of Green Compact Microstructural Design on the Density of Combustion Synthesized Aluminide Composites: Na Wang¹; *Khaled Morsi*¹; ¹San Diego State University

The combustion synthesis of aluminide intermetallics and their composites has been investigated for some time. The addition of ceramic reinforcements to the powder compact has been previously known to have a detrimental effect on the density of the final composite product after combustion synthesis. This paper discusses new strategies for elemental powder design that can result in improved densities of combustion synthesized nickel aluminide-titanium carbide composites without the application of external pressures. The paper discusses powder processing and the effect of elemental powder/green compact microstructural design on the microstructure of the combustion synthesized product.

Metrologies for Advanced Materials and Devices: Characterization, Measurement and Testing Science: Metrology for Micro and Nano Structures

Sponsored by: The Minerals, Metals and Materials Society, TMS Electronic, Magnetic, and Photonic Materials Division, TMS: Thin Films and Interfaces Committee

Program Organizers: Choong-Un Kim, University of Texas at Arlington; Nugehalli Ravindra, New Jersey Institute of Technology; Bhushan Sopori, National Renewable Energy Laboratory; Dia-Eddin Arafah, University of Jordan; David Field, Washington State Univ

Tuesday AM Room: Oceanic 6
February 27, 2007 Location: Dolphin Hotel

Session Chairs: David Field, Washington State University; Choong-un Kim, University of Texas

9:00 AM Introductory Comments

9:10 AM Invited

Atomic Force Microscopy Nanometrology and In-Situ Mechanical Testing - Challenges and Opportunities: *Xiaodong Li*¹; ¹University of South Carolina

Atomic Force Microscopy (AFM) has been widely used to measure the nanometer-scale topography of surfaces. The AFM technique offers digital data storage, ability to post-process data to obtain a range of spatial resolutions, and use of incoherent illumination sources, providing a base for integration with the currently available digital image correlation (DIC) operation platforms to map the local deformation variation at very small scales. We have developed a nano/micro mechanical tester that can be integrated into the commercial AFM to carry out small scale mechanical tests inside the AFM and simultaneously image the deformed/fracture sample in-situ. The DIC technique has been used to process the AFM images and quantitatively measure local, nanoscale deformation. The AFM scanner drifts, non-linearity, the relative movements between the scanner and the sample, the environment change, and the viscoelastic behavior of the test materials, may contribute to the AFM image quality and impose great challenges.

9:40 AM Invited

Metrology for Interconnect Reliability in Microelectronic Devices: *Nancy Michael*¹; Dongmei Meng¹; Woong Ho Bang¹; Liangshan Chen¹; Choong-un Kim¹; Y.-J. Park²; Laura Matz²; ¹University of Texas; ²Texas Instruments, Inc

Several technological challenges have emerged and pose significant threats to the desired progress of nanoscale microelectronics technology nodes. An important but often ignored challenge is metrology: the extreme scale of components makes characterization difficult and time-consuming. Interconnect reliability characterization is one of these challenging areas. Nanoscale node interconnects are integrated with porous dielectric and minimal barrier thickness, and thus, are prone to failures such as compromised barrier and dielectric cracking. It is critical to detect the potential for such failure during manufacturing, yet currently practiced metrologies have limited capability. In this paper, we describe a method to detect the defects which can lead to interconnect failures. Specifically, this method can detect the presence

of defects in the barrier and also can trace changes in the pore structure of low-k dielectric materials. The working principle of this method, based on electrochemical principles, and related evidence will be presented.

10:10 AM

Tunable Refractive Index Anti-Reflection Nano Silica Coatings via Sol-Gel Acid and Base Catalyzed Chemistry: *Abhilash Vincent*¹; Erik Brinley¹; Ajay Karakoti¹; Sudipta Seal¹; ¹University of Central Florida

Due to their tunable refractive index properties, porous silica (SiO₂) is considered to be one of the best anti-reflective optical coatings for laser mirrors. In this work we present a systematic and cost effective approach to fabricate anti-reflection SiO₂ coatings with a transmission of 99% on boron silicate glass at ambient atmospheric conditions through acid and base catalyzed sol-gel chemistry. The effect of porosity and the micro-structure evolution on the optical transmittance is studied in depth. The particle growth of silica nano particle under different pH conditions of solution precursor is investigated using tapping mode Atomic Force Microscopy (TMAFM) and is correlated with their optical properties. The mechanical strength and Young's Modules of these coating are analyzed through AFM scratch resistance and AFM nanoindentation techniques and are investigated as a function of various synthesis parameters.

10:35 AM Break

10:45 AM Invited

Recent Advances in Radiation Pyrometry: Nugehalli Ravindra¹; *Anthony Fiory*¹; ¹New Jersey Institute of Technology

Radiation pyrometry continues to be the standard technique for non-contact, real-time measurement of temperature in materials processing. An overview of the various approaches to measurement of temperature using such non-contact methods is presented here. Various industry approaches including the multi-wavelength imaging pyrometry and ripple pyrometry are discussed. Examples of emissivity models and their correlation to radiation pyrometry are presented. A summary of the various radiation pyrometers, their applicable range of temperatures and process applications is presented.

11:10 AM Invited

Relationship of Intrinsic Luminescence to Recombination Lifetime in Silicon Wafers: *Richard Ahrenkiel*¹; ¹University of Denver

In recent years, the intrinsic luminescence of silicon has been used as a method to characterize the recombination lifetime of crystalline silicon. The assumption is made that the steady state photoluminescence (PL) at 1.15 eV (1.07 μm) is proportional to the recombination lifetime. In this work, we measured the PL intensity at 1.1 eV of a number of single crystal wafers with resistivities in the 1 to 100 ohm-cm range under constant excitation intensity. We then measured the recombination lifetime of the same wafer set by both microwave reflection and resonant coupled photoconductive decay (RCPCD) in both air ambient and in a iodine/methanol. Plots of the measured lifetime versus the PL intensity showed no correlation between the two quantities. In fact, there is an anti-correlation in that the shortest lifetime had the most intense PL signals and vice versa. Some fundamental physical reasons can be explain an anti-correlation relationship.

11:40 AM Invited

Diagnostics and Process Monitoring Techniques for Solar Cell Production: *Bhushan Sopori*¹; ¹National Renewable Energy Laboratory

During last several years, photovoltaic (PV) energy production and consumption have grown at a very rapid rate of about 40% per year, reaching one gigawatt per year. This has spurred an urgent need for process monitoring in the commercial production of solar cells to help improve yield and reduce the cost of PV energy. In the past, the PV industry has typically used minimal process monitoring, employing techniques that were developed for the microelectronics industry. However, there is a need for developing new diagnostic techniques specifically for PV production - techniques capable of high throughput, applicable to wafers with rough or textured surfaces, and with low operating cost. This paper will review various diagnostic techniques currently used in the PV industry for process control, followed by new methods that are being developed, to be deployed in the PV industry in the near future. These techniques may be categorized into three groups: (i) measurement of physical parameters of wafers and cells, such as sawing quality, texture etching, diffusion for junction formation, antireflection coating, and metallization;

TUESDAY AM

(ii) measurement of electronic properties such as minority-carrier lifetime, process and material nonuniformities, and cell parameters; and (iii) other control parameters such as propensity for breakage of wafers and aesthetic appearance of cells and modules. *This work has been authored by employees of the Midwest Research Institute under Contract No. DE-AC36-99GO10337 with the U.S. Department of Energy. The United States Government retains and the publisher, by accepting the article for publication, acknowledges that the United States Government retains a non-exclusive, paid-up, irrevocable, worldwide license to publish or reproduce the published form of this work, or allow others to do so, for United States Government purposes.

12:10 PM**Characterization of Solar Cell Substrates Using Diode Array Technique:**

*Jesse Appel*¹; *Bhushan Sopori*²; *Przemyslaw Rupnowski*²; *Anna Duda*²; *Lorenzo Roybal*²; *Vishal Mehta*¹; *N. M. Ravindra*³; ¹National Renewable Energy Laboratory and New Jersey Institute of Technology; ²National Renewable Energy Laboratory; ³New Jersey Institute of Technology

In current manufacturing regimes, silicon solar cells are made from low-cost silicon wafers, which are produced in one of three ways: low-grade, Czochralski-type single-crystal wafers; multicrystalline silicon wafers grown by casting; or shaped ribbons produced by directional solidification. These materials contain high concentrations of impurities and defects, which lead to spatial variations in the material properties. A detailed characterization of the substrates is needed to understand the nature of defects and impurities and their influence on solar cell performance. Although many techniques can be applied to map material properties, the influence of the various materials on cell performance is difficult to determine. We have developed a technique to fabricate arrays of edge-passivated diodes (small-area solar cells), which can be probed using an automatic prober to generate dark and illuminated I-V characteristics of each device. These devices can be readily used for other measurements, such as measurement of minority-carrier diffusion length, light or electron beam induced current, C-V analyses, and DLTS. The data from diode arrays are used to study influence of defects and impurities on cell performance and to predict the highest large-area cell performance. *This work has been authored by employees of the Midwest Research Institute under Contract No. DE-AC36-99GO10337 with the U.S. Department of Energy. The United States Government retains and the publisher, by accepting the article for publication, acknowledges that the United States Government retains a non-exclusive, paid-up, irrevocable, worldwide license to publish or reproduce the published form of this work, or allow others to do so, for United States Government purposes.

12:35 PM Invited

The Analysis on a Solder-Ball Shear Test: *Woong Ho Bang*¹; *Choon-Sik Kang*²; *Kyu Hwan Oh*²; *Choong-Un Kim*¹; ¹University of Texas at Arlington; ²Seoul National University

The solder ball shear test is a destructive testing method in which a solder bump is shear-fractured in a direction parallel to bump/metallization interface. It measures the shear-fracture strength of a solder bump that estimates the mechanical reliability of solder joints in electronic packages. Through experiments, finite elements method and fracture mechanics approaches, we have analyzed the ball shear test of which result can be affected by several factors: the effect of a solder ball size on the testing result has been particularly focused on. The analyzed results and discussion will be presented in present talk.

Microstructural Processes in Irradiated Materials: Modeling, Microstructure and Embrittlement in Fe-Cr Alloys

Sponsored by: The Minerals, Metals and Materials Society, TMS Structural Materials Division, TMS/ASM: Nuclear Materials Committee
Program Organizers: Charlotte Becquart, University of Lille; Gary Was, University of Michigan; Brian Wirth, University of California

Tuesday AM Room: Europe 8
February 27, 2007 Location: Dolphin Hotel

Session Chairs: Roger Smith, Loughborough University; Gary Was, University of Michigan

9:00 AM Invited

Multiscale Modelling of Radiation Damage and Phase Transformation: The Challenge of FeCr Alloys: *Lorenzo Malerba*¹; *Alfredo Caro*²; *Janne Wallenius*³; ¹Belgian Nuclear Research Center; ²Lawrence Livermore National Laboratory; ³KTH

FeCr alloys are model materials to investigate mechanisms of microstructure evolution under irradiation of high-Cr ferritic/martensitic steels for nuclear applications. The endeavour of modelling their atomic-level behaviour under irradiation faces serious difficulties. Fe is ferromagnetic and Cr is antiferromagnetic, challenging the applicability of DFT. In FeCr the short-range order parameter changes sign from negative to positive at a critical concentration and a large miscibility gap between two coherent phases exists. The interplay between these thermodynamic features and point-defects determines the system microstructural evolution under irradiation. Modelling this requires new formalisms and tools to account for point-defects and thermodynamics in concentrated alloys. Here we review recent efforts made in this direction producing advanced interatomic potentials for FeCr and discuss still open issues on FeCr modelling. Some significant results obtained studying radiation damage in FeCr alloys are presented and discussed according to their capability of providing keys for experiment interpretation.

9:35 AM

Simulation of Radiation Damage in FeCr: *Carolina Björkas*¹; *Niklas Juslin*¹; *Kai Nordlund*¹; ¹Accelerator Laboratory, University of Helsinki

Steel in fusion reactors will suffer radiation damage. In order to develop steels better suited for reactor walls, it is vital to understand and control the defects formed by energy transfer from particles from the plasma. We use molecular dynamics simulations to study iron-chromium, comparing different potentials. We present threshold energies, the lowest energies required to form defects, and compare differences in interstitial production between pure iron and iron-chromium. This is also an important test for new potentials. The effect of chromium quantity on the cascade damage and defect types have been studied for 0.5 - 50 keV cascades on up to 1.5 million atoms. We find that all potentials predict practically the same total Frenkel pair production, but show pronounced differences in the chromium content in interstitials. We will also compare simulated and experimental ion beam mixing coefficients, and discuss whether this can be used to validate interatomic potentials.

9:55 AM

Point Defects and Precipitation in Fe-Cr Alloys: *Magdalena Caro*¹; *Harun Dogo*²; *Ryan Till*³; *Alfredo Caro*¹; ¹Lawrence Livermore National Laboratory; ²Naval Postgraduate School; ³Arizona State University

The behavior of Fe-Cr alloys under irradiation is in part controlled by the characteristics of point defects generated by high energy collision. Radiation enhanced diffusion and radiation induced precipitation are among the mechanisms that lead to changes in the microstructure under irradiation, and thus controlling effects such as swelling and a' precipitation. Point defects in Fe-Cr alloys are diverse in nature due to their interaction with a variety of local solute configurations. Ab initio results indicate that the magnetic structure of the alloy is critical in determining this energetics. The ability to model these properties with classic potentials is still to be proven. In this work we perform a detailed comparison between ab initio and classic values of a variety of point



defects configurations, testing in this way the extent to which classic potentials can be reliable used for radiation damage studies.

10:15 AM

Atomistic Simulations of Radiation-Induced Defect Processes and Segregation in Fe-Cr Systems: *Srinivasan Srivilliputhur*¹; Carolyn Tomchik²; Alfredo Caro³; M. Baskes¹; M. Caro³; S. Maloy¹; J. Stubbins²; ¹Los Alamos National Laboratory; ²University of Illinois; ³Lawrence Livermore National Laboratory

Atomistic simulations of alloys using empirical models often incorrectly model basic thermodynamic properties. Recently, Caro et al.¹ proposed a general approach to develop many-body classical potentials that incorporate complex formation energy curves in alloys. This enabled them to correctly predict the order versus segregation tendency in the Fe-Cr system. We use this new model to study 25 keV displacement cascades in Fe-Cr systems using molecular dynamics at room temperature. Compositions of interest lie between 8 and 20 atomic-% chromium. This range was chosen because both the atomistic model and experiments show precipitation of the alpha-prime phase at ~12 atomic-% Cr. We examine the effect of Cr concentration on the defect evolution, segregation behavior, and second phase precipitation in the early stages of damage. The irradiated Fe-Cr systems are compared with pure iron. ¹A. Caro, D.A. Crowson, and M. Caro, Phys. Rev. Lett. 95, 075702 (2005).

10:35 AM Break

10:55 AM Invited

Microstructural Response of a 9 Cr Oxide Dispersion Strengthened Steel to Heavy Ion Irradiation: *Todd Allen*¹; Jian Gan²; Jeremy Busby³; Michael Miller³; Shigeharu Ukai⁴; S. Thevuthasan⁵; S. Shutthanandan⁵; ¹University of Wisconsin; ²Idaho National Laboratory; ³Oak Ridge National Laboratory; ⁴Hokkaido University; ⁵Pacific Northwest National Laboratory

Ferritic-martensitic (FM) alloys are expected to play an important role as cladding or structural components in Generation IV systems. Oxide dispersion strengthened ferritic-martensitic steels have been developed to operate at higher temperatures than traditional FM steels, with nanometer scale oxide particle providing the high temperature strength. The stability of these oxides under irradiation is important. Heavy-ion irradiation has been used to determine the oxide stability over a temperature range of 500-700°C to doses of 150 dpa. Microstructures are analyzed with transmission electron microscopy and atom probe tomography. Grain boundary composition changes were measured by FEG-STEM. At all temperatures, the average oxide size decreases but the oxide density increases. Research at the Oak Ridge National Laboratory SHaRE User Facility was sponsored by the Office of Basic Energy Sciences, U.S. Department of Energy, under contract DE-AC05-00OR22725 with UT-Battelle, LLC.

11:30 AM

The Mechanism of Irradiation Hardening Accompanied by No-Loss-of-Elongation in ODS Steels: *Akihiko Kimura*¹; ¹Kyoto University

Generally, irradiation induces hardening accompanied by loss of elongation, which is explained in terms of acceleration of plastic localization. However, recent irradiation studies clearly showed that the hardening was not accompanied by loss of elongation in oxide dispersion strengthening (ODS) steels. In this paper, experimental evidences of the no-loss-of-elongation are shown for high Cr-ODS steels irradiated in JMTR, JOYO and HFIR, and the mechanism of the hardening with no-loss-of-elongation is proposed based on the deformation behavior of the steels, such as anisotropy in elongation, deformation bands characteristics, homogeneous/inhomogeneous deformation, moving dislocation morphology, structure of nano-particles and so on. High performance of the ODS steels under irradiation can be correlated with the dispersion of nano-sized oxide particles in high density.

11:50 AM

Irradiation Embrittlement in the Absence of Irradiation Hardening: *R. Klueh*¹; M. Sokolov¹; ¹Oak Ridge National Laboratory

Ferritic/martensitic steels are candidate materials for future fusion reactor first wall and blanket structures. A major problem is the hardening that occurs when the steels are irradiated by neutrons below 425-450°C. This hardening is observed as an increase in yield stress that results in embrittlement observed as an increase in ductile-brittle transition temperature

in a Charpy impact test. Based on observations that showed little change in strength at irradiation temperatures above 425-450°C, the general conclusion has been that no embrittlement occurs above these temperatures. In a recent irradiation study of a reduced-activation steel, embrittlement was observed after irradiation at 500°C. Earlier studies on a conventional steel also showed effects above the irradiation-hardening temperature. Indications are these "embrittlement effects" are caused by precipitation that is accelerated by irradiation. Experimental observations have been analyzed with computational thermodynamics calculations to illuminate the problem and determine how best to ameliorate the effects.

12:10 PM

Heavy-Ion Irradiation Damage in FeCr Alloys: *Michael Jenkins*¹; Zhongwen Yao¹; Zhongwen Yao¹; Sen Xu¹; Marquis Kirk²; ¹University of Oxford; ²Argonne National Laboratory

Fe-Cr model alloys with 0-18%Cr have been irradiated *in-situ* with 100 keV Fe⁺ and Xe⁺ ions at 20°C and 300°C in the IVEM-Tandem Facility at Argonne National Laboratory. So far only room-temperature Fe⁺ experiments on polycrystals have been analysed in detail. In all materials the threshold dose for visible damage was about two orders of magnitude higher than in fcc metals such as copper and so well into the cascade overlap region, although the threshold dose for visible damage in Fe-Cr alloys was considerably lower than in pure Fe. Loops with Burgers vectors of type $a/2\langle 111 \rangle$ and $1/2\langle 111 \rangle$ were both present. There is some evidence that their nature is vacancy. This paper will discuss some interesting dynamical observations, and the results of a further series of *in-situ* experiments just completed. We shall also describe results from bulk irradiations of the same materials irradiated with 2MeV Fe⁺ ions at 300°C.

Pb-Free Electronic Solders: Alloy Design, Characterization and Service Reliability: Electromigration and Void Formation

Sponsored by: The Minerals, Metals and Materials Society, TMS Electronic, Magnetic, and Photonic Materials Division, TMS: Electronic Packaging and Interconnection Materials Committee

Program Organizers: Fu Guo, Beijing University of Technology; K. Subramanian, Michigan State University; Sung Kang, IBM Corporation; Srinivas Chada, Medtronic; Laura Turbini, University of Toronto; Jin Yu, Korea Advanced Institute of Science and Technology

Tuesday AM Room: Oceanic 1
February 27, 2007 Location: Dolphin Hotel

Session Chairs: Chih Chen, National Chiao Tung University; Darrel Frear, Freescale Semiconductor

9:00 AM

Effect of Electromigration on the Mechanical Characteristics of Ultra-Thin Solder Joints: *C. E. Ho*¹; Deep Choudhuri¹; Adam Southworth¹; Andre Lee¹; K. Subramanian¹; ¹Michigan State University

Electromigration (EM) has become a serious reliability concern in solder joints experiencing current densities over 10e+3 Amp/cm². Specifically, an extreme thin/thick divergence in the Cu circuit/solder bump configuration can induce "current crowding", which will vary the current density within the solder by orders of magnitude, aggravating the influence of EM substantially. In order to minimize such a risk, modification to joint geometry, such as thicker UBM or Cu pillars with an ultra-thin solder coating (~20 μm), are being explored to re-adjust the current path to be straight and uniform before it enters the solder. This study is aimed at gaining a better understanding of (1) chemical reaction with consumable solder, and (2) mechanical characterization with and without the EM in such joint configurations to address reliability issues that arise from such modifications.

9:20 AM

Kinetic Study of Grain Rotation Induced by Electrical Current in Pure Tin: *Albert T. Wu¹; Ming-Hsun Chen¹; Wen-Lin Shih¹; C. Robert Kao²;*
¹National Taipei University of Technology; ²National Taiwan University

Tin is the dominant element in lead-free solder. Electromigration causes evolution of microstructure has been studied by synchrotron white beam x-ray diffraction and a model was established. In our study, the morphology of white tin (β -Sn) stripe was observed to change gradually after current stressing at elevated temperature with increasing time. The phenomenon may be contributed from the anisotropic property of β -Sn. The angle of grain rotation was measured to analyze the torque generated by the vacancy concentration along grain boundaries due to the difference of resistance of tin along a- and c-axis. We propose a kinetic study to implement the model and provide a more comprehensive understanding of the behavior of Sn-based lead free solder under electromigration.

9:40 AM

Effect of Thickness of Cu under-Bump-Metallization on the Electromigration Lifetime of Flip-Chip Solder Joints: *Shih-Wei Liang¹;*
Yuan-Wei Chang¹; Chih Chen¹; ¹National Chiao Tung University

The thick electroplated Cu up to 80 μ m has been adopted for the under bump metallization (UBM) of Pb-free solders due to metallurgical reliability concerns and its high electrical conductivity. However, the current-density and temperature distribution in the flip-chip solder joints with thick Cu UBMs during electromigration is not clear. Three-dimensional thermo-electrical analysis was employed to simulate the current-density and temperature distributions for the eutectic SnPb solder bumps with 0.5- μ m, 5- μ m, 25- μ m, 50- μ m, and 100- μ m Cu UBM. It was found that hot spots in solder and current crowding effect were almost eliminated when the Cu thickness was over 50 microns. Simulated at stressing current of 0.6 A under 70 $^{\circ}$, the estimated mean-time-to-failure of the joints with a 50- μ m-thick Cu column was 6.7 times longer than that of joints with a 0.5- μ m thick Cu column.

10:00 AM

Additive Effect on the Kirkendall Void Formation in Eutectic SnAg Solder Joint on Common Substrates: *Feng Gao¹;* Tadashi Takemoto¹;
¹Osaka University

The Sn-3.5Ag eutectic solder doped with 0.2Co-0.1Ni additives was soldered on the common substrates, namely, OSP and NiAu surface finishes. The evolution of the microstructure at the interfacial region during isothermal solid aging was explored. In particular, the Kirkendall voids were emphasized due to its critical effect on the solder joint reliability. For OSP surface finish, the remarkably depressed Cu₃Sn phase was observed for the Sn-3.5Ag-0.2Co-0.1Ni/OSP solder joint, while the Kirkendall voids were still present after isothermal solid aging at higher temperature. While for NiAu surface finishes, it seemed no severe effect of additives on the interfacial microstructure, as well as the subsequent Kirkendall voids. The additives (Co, Ni) were all detected in the intermetallic for OSP while rarely probed for NiAu surface finish. This might impact the intermetallic phase stabilization and the relevant interdiffusion behavior, and thereby influence the formation of Kirkendall voids at the interface.

10:20 AM

Effect of Electromigration on UBM Consumption in Lead Free Solder Joints Tested at Room Temperature: *Yen-Liang Lin¹;* C. Robert Kao²;
Yi-Shao Lai³; ¹National Central University; ²National Taiwan University;
³Advanced Semiconductor Engineering, Inc.

The UBM consumption in lead free solder joints accelerated by electromigration was investigated. The solder used was Sn₃Ag_{1.5}Cu and the joints had a nominal diameter of 125 micron. The UBM on the chip had a Cu/Ni(V)/Al metallization, and the surface finish on the substrate side was Au/Ni. Our studies showed that when the test vehicle stressed with a constant 2.08 A current at room temperature, producing a nominal current density of 45000 A/cm² (basing on the opening area of the contact window), the die temperature will jump to 120 $^{\circ}$ C due to Joule heating. Under current stressing, a rapid consumption of Ni UBM occurred only after 40 hours and the joints failed due to the formation of poor conductive layer after UBM exhaustion. However, Ni UBM adhered well after 100 hours at 120 $^{\circ}$ C when no electric current was applied. In other words, electric current play an important role on UBM consumption.

10:40 AM Break

10:50 AM

Electromigration in SnCu Solder Stripes: *Chien-An Chen¹;* C. C. Wei¹; Chih Chen¹;
¹National Chiao Tung University

To measure the critical length of electro-migration in SnCu solder stripes, we used focus ion beam (FIB) to cut the stripes into several segments of different lengths, from 5 μ m to 200 μ m. The stripes underwent a heat treatment of aging at 150 $^{\circ}$ for 5 hr, and then was applied a desired current at 100 $^{\circ}$, to achieve a current density of 2×10^4 A/cm². After current stressing, voids form on the cathode end and hillocks form on the anode end. Atomic force microscope was employed to measure the depletion volume, which enables us to calculate electromigration rate. In this study, we used the Blech structure to measure the electromigration rate and critical length of the SnCu solder stripes. The results will be presented in the conference.

11:10 AM

EM (Electromigration) Effect on the Interfacial Reaction of EL-Ni (Electroless Ni)/Au UBM and Sn1.8Cu Solder: *Yao-Chun Chuang¹;* Cheng-Yi Liu¹;
¹National Central University

EM effect at the interface between Sn(Cu) solders/Ni(P) were studied. During this talk, two main parts will be present: (1) EM effect on interfacial reaction between Ni(P) bond pad and Sn(Cu) solders. We found that the self-formed Cu-Sn compound layer on the Ni(P) bond pad was damaged by the current stressing, which can not prevent the EM-induced dissolution on Ni(P) bond pad. Also, the Ni₃P layer formation was found to be enhanced by EM. The detail EM effect on the interfacial reaction between Ni(P) bond pad and Sn(Cu) solders will be discussed. (2) Enhancement of current crowding due to the asymmetrical structure of bond pads of flip-chip solder joints. The current distribution simulation shows the asymmetrical structure of bond pads of flip-chip solder joints will cause serious current crowding at the corner of solder bump. The current simulation results agree with our experimental results very well.

11:30 AM

Electromigration Study of Flip-Chip Solder Joints Using Kelvin Bump Structure: *Yuan-Wei Chang¹;* Chih Chen¹;
¹National Chiao Tung University

Electromigration in solder joints has been studied extensively in recent years. Kelvin structure has been used for years to monitor the variation of Al and Cu interconnects, but there are few studies on observing the variation of bump resistance with Kelvin structure during electromigration. Instead of Daisy-chain structure which has been used to study solder joint for long time, Kelvin structure can detect the slight change of resistance in specific circuit. During electromigration, the variation in solder joint, such as void formation and thickness change of IMC can cause the change in bump resistance. We fabricated Kelvin bump probes and used it to measure the change of bump resistance during electromigration. 3D finite element modeling was also performed to simulate the bump resistance increase which was due to the variation in single solder joint. This approach facilitates the systemic study of failure mechanism in flip-chip solder joints due to electromigration.

11:50 AM

Electromigration Study of SnAgCu Using Solder Stripe: *Yung-Ching Hsu¹;*
¹National Chiao Tung University

SnAgCu has become the most promising Pb-free candidate to replace Pb-containing solders. However, one of the fundamental electromigration parameters, critical length, has not been measure because it is very difficult to prepare short solder stripe. In this letter, solder stripes of various lengths, including 5,10,15,20,30,100 and 200 μ m can be fabricated by employing focus ion beam. Length dependent electromigration behavior was observed, which implies that there may be back stress under stressing. The stripes were stressed at $2-4 \times 10^4$ A/cm² at 100-150. The critical length can be obtained.

12:10 PM

Investigation of Void Nucleation and Propagation during Electromigration in Flip-Chip Solder Joints: *Sheng-Hsiang Chiu¹;* Chih Chen¹;
¹National Chiao Tung University

Void nucleation and propagation in the solder joint during electromigration was investigated in this study. SnPb solder joints with 5- μ m Cu/3- μ m Ni under-bump-metallization (UBM) were adopted. As the stressing time increased, the voids formed in the current crowding region and they propagated toward the rest of the UBM opening. Furthermore, cross-sectional SEM images of the



solder bump indicated that voids were observed in the solder near the entrance point of the Al trace, and it propagated as the stressing time increased. The velocity void propagation was measured, and it is found that the velocity was low in the initial stage. Then it increased afterwards and it decreased in the middle stages. The details will be presented during the conference.

Phase Stability, Phase Transformations, and Reactive Phase Formation in Electronic Materials VI: Session II

Sponsored by: The Minerals, Metals and Materials Society, TMS Electronic, Magnetic, and Photonic Materials Division, TMS: Alloy Phases Committee
Program Organizers: Sinn-Wen Chen, National Tsing Hua University; Srinivas Chada, Medtronic; Chih-ming Chen, National Chung Hsing University; Young-Chang Joo, Seoul National University; A. Lindsay Greer, University of Cambridge; Hyuck Lee, Korea Advanced Institute of Science and Technology; Daniel Lewis, Rensselaer Polytechnic Institute; Katsuaki Sugauma, Osaka University

Tuesday AM Room: Oceanic 2
 February 27, 2007 Location: Dolphin Hotel

Session Chairs: Hyuck Lee, Korea Advanced Institute of Science and Technology; Katsuaki Sugauma, Osaka University

9:00 AM Invited

Prevention of Sn Whisker Formation by Surface Treatment of Sn Plating: *Katsuaki Sugauma*¹; Keun-Soo Kim²; Yuuhi Yorikado¹; Masanobu Tsujimoto²; Isamu Yanada²; ¹Osaka University; ²C. Uyemura and Company, Ltd.

Establishment of lead-free plating technology and whisker countermeasures is one of the critical problems remaining to be solved for lead-free electronics packaging. Recent researches have revealed the mechanisms of Sn whisker formation and growth. However, more researches are required to find acceptable methods to prevent Sn whisker formation. In this study, a new approach to prevent the Sn whisker, by surface treatment on Sn plating, was proposed. Two Ni layers of different thickness were plated on the surface of the Sn plating. These samples and pure Sn plating samples were stored in room ambient environment for 300 days. Sn whiskers were observed on pure Sn plating samples after 7 days, however, no Sn whisker was observed on Ni/Sn plating samples after 300 days. Comparing with pure Sn plating, Ni/Sn plating is much stable against Sn whisker formation.

9:25 AM Invited

Detachment of Interfacial Intermetallic Compound Layer in Solder Joints: *Kejun Zeng*¹; ¹Texas Instruments

Formation of an interfacial layer of IMC after soldering process is essential for solder joint reliability. The IMC layer should remain at the interface in the subsequent packaging processes. Detaching of IMC crystals from interface may degrade the joint reliability. Many papers have been published on the phenomenon of IMC detachment in solder joints. It may be due to complete consumption of the soldering metal and dewetting of the metal beneath, or the stress buildup in the IMC layer after extended reflow. Another case of IMC detachment in solder joints is presented in the present paper. After an industrial reflow process, in addition to the interfacial Cu₆Sn₅ layer on the Ni/Au plated Cu pad, another Cu₆Sn₅ layer formed in the bulk solder near pad. Influences of the Ni thickness and reflow process on the IMC detachment have been investigated. Its formation mechanism and effect on joint reliability will be discussed.

9:50 AM

Investigation of Dissolution Behavior and Kinetics of Metallic Substrates and Intermetallic Compounds in Molten Lead-Free Solders: *Yee-Wen Yen*¹; Yu Tseng²; Chiapng Lee²; Chien-Chung Jao²; Wei-Kai Liou¹; Chung-Yu Lee¹; Chun-Lei Hsu¹; ¹National Taiwan University of Science and Technology, Graduate Institute of Materials Science and Technology; ²National Taiwan University of Science and Technology, Department of Chemical Engineering

Dissolution Behavior and kinetic of metallic substrates-Cu, Ag and the intermetallic compound (IMC)-Ag₃Sn in molten Sn, Sn-3.0Ag-0.5Cu, Sn-58Bi and Sn-9Zn at 300, 270 and 240°C were investigated in this study.

Dissolution rate of both Cu and Ag in molten solder is Sn>Sn-3.0Ag-0.5Cu>Sn-58Bi>Sn-9Zn. Plane Cu₃Sn and scalloped Cu₆Sn₅ phases in Cu/solders and the scalloped Ag₃Sn phase in Ag/Solders can be observed at metallic substrate/solder interfaces and the dissolution mechanism is controlled by the grain boundary diffusion. For Sn-9Zn/Cu systems, the plane Cu₅Zn₈ layer formed at the interface. AgZn₃, Ag₅Zn₈ and AgZn phases were found at the Sn-9Zn/Ag system and the dissolution mechanism is controlled by the lattice diffusion. Massive Ag₃Sn phases dissolved into solders and formed during solidification processes in Ag₃Sn/Sn or Sn-3.0Ag-0.5Cu systems. AgZn₃ and Ag₅Zn₈ phases formed at the Sn-9Zn/Ag₃Sn interface. More Zn atoms diffuse through Ag-Zn IMCs and make (Ag,Zn)Sn₄ and Sn-rich region form between Ag₅Zn₈ and Ag₃Sn.

10:10 AM

Interfacial Reactions between the Molten Sn-Zn and Sn-Cu Solders and the Fe Substrate: *Yu-Chih Huang*¹; Sinn-wen Chen¹; ¹National Tsing Hua University

Wave soldering is a predominant joining technology for electronic products. Due to their higher melting temperatures, the processing temperatures with Pb-free solders are higher than those with Sn-Pb solders. Higher processing temperatures result in intensive dissolution and interaction between solders and the solder pot materials which are usually different kinds of steels. Interfacial reactions in the Sn-Cu/Fe and Sn-Zn/Fe couples are investigated in this study. FeSn₂ phase is formed in the Sn-Cu/Fe couples reacted at 250°C. There is no significant growth of the reaction layer with longer reaction time, and FeSn₂ phase pellets are observed in the solder matrix. δ phase and ζ phase are formed in the Sn-Zn/Fe couples reacted at 220°C. Iron has the higher dissolution rate with molten Sn-Zn solder; however, the dissolution rates of iron in molten solders are still relatively low compared with those of commonly used substrates, such as Cu and Ni.

10:30 AM Break

10:50 AM

Sn-Cu Intermetallic Layer Thickness Measurement Using Electrochemical Method: *Ker-Chang Hsieh*¹; Min-Hsien Lu¹; ¹National Sun Yat Sen University

The tin has been widely used as coating materials for copper metal finishing in electronic industries. X-ray and electrochemical methods are used to estimate the thickness of tin layer. It is also important to characterize the growth rate of Cu₃Sn and Cu₆Sn₅ intermetallic that related with the whisker growth and joint reliability. In this study, we apply the sequential electrochemical reduction analysis (SERA) technique to determine the individual thickness of pure tin layer, Cu₆Sn₅ and Cu₃Sn. Further, the depletion rate of tin layer at high temperature aging and the growth situation of intermetallic compounds will be discussed.

11:10 AM

Effect of Strain and Thermomechanical Fatigue on Allotropic Transformation in Sn and Sn-Based Alloys: *Deep Choudhuri*¹; C. E. Ho¹; Adam Southworth¹; Andre Lee¹; K. Subramanian¹; ¹Michigan State University

Body-Centered Tetragonal (β) to Diamond Cubic (α) phase transformation occurs in Sn at temperatures below 13.2°C. Pb-free solder alloys used in electronic interconnects have β-Sn as the major constituent. Transformation from ductile β-Sn to brittle α-Sn will adversely affect solder joint reliability under low temperature service conditions. This study investigated the effect of imposed strains and Thermomechanical Fatigue (TMF) on β-Sn to α-Sn allotropic transformation. Bulk specimens of Sn and Sn-based alloys were strained to different extents, and maintained at low temperatures for long time durations. Furthermore, solder joints containing Sn-based solder and bulk specimens of the same alloys were subjected to TMF with different dwell times at low temperature extreme. The evolution of microstructure present in bulk and joint configurations, characteristic X-ray intensity and residual strength measurements were carried out to facilitate the analysis.

11:30 AM

Lattice Parameter Changes and Phase Reactions for AuIn₂: A. Noori¹; A. Pangan¹; *Mark Goorsky*¹; Rajinder Sandhu; P. Chang-Chien²; M. Yajima²; X. Zeng²; R. Tsai²; ¹University of California; ²Northrup Grumman Space Technology

The gold – indium phase diagram has been studied for important eutectic reactions involving the formation of AuIn₂ compounds for materials integration applications. In this work, we investigated the lower temperature reactions (annealing temperature < 200°C.) of gold – indium multilayer structures deposited on semiconductor substrates. Previous studies focused on temperature above 200°C. X-ray diffraction shows that the as-deposited structures possess the thermodynamically stable AuIn₂ peaks as well as Au and In. Further annealing at 140 - 200°C leads to slight increases in the amount of AuIn₂ formed, but more importantly, to a shift in the AuIn₂ peaks to smaller lattice parameter with increased annealing time or temperature. This decrease corresponds to a strain on the order of 10-2 after annealing for 20 minutes at 180°C and the change in lattice parameter is a kinetically limited process with an activation energy of approximately 0.9 eV.

11:50 AM

Enhanced Wettability of Oxidized Copper with Lead-Free Solder by Ar-H2 Plasmas for Flip Chip Bumping: *Yung-Sen Lin*¹; Chun-Hao Chang¹; Wei-Jih Lin¹; ¹Feng Chia University

Enhanced wettability of oxidized copper (Cu) with lead-free solder 96.5Sn-3Ag-0.5Cu by Ar-H2 plasmas was investigated. The solderability test demonstrates that the wettability of oxidized Cu with lead-free solder 96.5Sn-3Ag-0.5Cu was significantly improved from no wetting of copper for oxidized at 260°C/1 hr to 100% wetting of Cu treated by Ar-H2 plasmas at certain plasma settings. The wettability of Cu with lead-free solder 96.5Sn-3Ag-0.5Cu was found to be highly dependent on the surface characteristics of Cu. The enhanced wettability of Cu with lead-free solder 96.5Sn-3Ag-0.5Cu by Ar-H2 plasmas is due mainly to the decreased surface energies of Cu. Auger Electron Spectroscopy (AES) shows the atomic composition of oxygen on Cu can be decreased from 20% for the oxidized Cu to 0% at the depth 18 nm from the top surface of the Cu modified by Ar-H2 plasmas.

12:10 PM

Crystalline Analyses of the Stress-Induced Void during Self-Annealing in Cu Interconnects: *Heung Nam Han*¹; Hyo-Jong Lee¹; Jae Hun Kim¹; Kyu Hwan Oh¹; Sun-Jung Lee²; ¹Seoul National University; ²Samsung Electronics Company

For highly integrated semiconductor, the transition from aluminum to copper interconnects requires more strict estimation for the interconnect reliability. In particular, the void generation in wide pattern is one of recent issues in the copper interconnect. In this study, a crystallographic measurement was performed on the stress-induced void. The planar EBSD analysis showed that the void was initiated at the triple junction of the grain boundaries, regardless of the contact position by via pattern. The void grew along a grain boundary, and the voided region was confirmed to be one or two of the grains joining at the triple junction, which had the relatively high equi-biaxial elastic modulus for its plane normal direction. It was found that the void rarely occurred at {100} plane normal grains. In order to confirm the crystalline orientation of the void, a stepwise cross-sectional crystalline analysis was carried out by using FIB technique.

Plasticity from the Atomic Scale to Constitutive Laws: Atomistic Simulations of Dynamic Processes and Nano-Scale Plasticity

Sponsored by: The Minerals, Metals and Materials Society, TMS Structural Materials Division, TMS/ASM: Computational Materials Science and Engineering Committee

Program Organizers: Christopher Woodward, US Air Force; Michael Mills, Ohio State University; Diana Farkas, Virginia Tech

Tuesday AM Room: Europe 9
February 27, 2007 Location: Dolphin Hotel

Session Chairs: Diana Farkas, Virginia Tech; William Gerberich, University of Minnesota

9:00 AM Invited

Moving Dislocations in Disordered Alloys: *Alfredo Caro*¹; Jaime Marian¹; ¹Lawrence Livermore National Laboratory

Using atomistic simulations of dislocation motion in Ni and Ni-Au alloys we report a detailed study of the mobility function as stress, temperature and composition vary. We analyze the results in terms of analytic models of phonon radiation and their selection rules for phonon excitation. We find a remarkable agreement between the location of the cusps in the stress - velocity relation and the velocity of waves propagating in the direction of dislocation motion with polarization along the Burger's vector. Temperature dependence follows the phonon damping models. Alloying hardening effects appear in the static Peierls stress as well as in the dynamics. Work performed under the auspices of the U.S. Department of Energy by the University of California Lawrence Livermore National Laboratory under contract No. W-7405-ENG-48.

9:30 AM

Dynamic Emission of Dislocations Loops in Fcc Crystals: *Dan Mordehai*¹; Guy Makov²; Itzhak Kelson³; ¹Commissariat à l'Énergie Atomique; ²Nuclear Research Center Negev; ³Tel Aviv University

The mechanisms that control the plastic deformation at high strain rates remain unknown due to the difficulty of performing experimental metallurgical observations during the deformation. One of the key questions is, what is the generation mechanism of shock-induced dislocations using molecular dynamics simulations we have studied screw dislocations in Cu (fcc) single crystal. We have observed that under a shear stress of about 1.5GPa the cores of the partial dislocations are no longer planar on the slip plane, but spread on to the cross-slip plane. If the stress is increased further the dislocation emits dynamically faulted loops on to the cross-slip plane. This emission process results in stacking faults along the secondary plane, which we believe provides a new insight of how shocked metals plastically deform. These two phenomena, the non-planar core and the dynamic emission of dislocations, are discussed in the framework of the anisotropic elasticity theory.

9:50 AM

From Micro to Macro Plasticity: Stefan Brandstetter¹; Steven Van Petegem¹; *Helena Van Swygenhoven*¹; ¹Paul Scherrer Institute, Switzerland

The macroscopic yield stress is defined as the stress for which the strain deviates 0.2% away from linear elasticity. Materials usually exhibit plastic deformation at stresses well below the yield stress, the so-called microplastic regime. In polycrystalline metals it is taken for granted that the majority of grains are plastically deforming at the macroscopic yield, however there is no easy method to verify this assumption. Using in-situ XRD spectra measured during in deformation of nanocrystalline and ultra-fine grained Ni, it is shown that the amount of strain assigned to microplasticity can significantly exceed the usual 0.2% definition of the macroscopic yield stress, when grain sizes reach the nanometre range. In other words, for electrodeposited nanocrystalline Ni, the usual 0.2% definition does not correspond with the onset of macroscopic plasticity. The deformation mechanisms at atomic scale responsible for such behaviour are discussed in terms of suggestions from molecular dynamics simulations.



10:10 AM

Contact-Induced Shear Localization in Nanocrystalline Al by Atomistic Simulation: *Virginie Dupont*¹; Frederic Sansoz¹; ¹University of Vermont

Plastic flow serration has been observed in the indentation response of nanocrystalline metal films. This behavior usually corresponds to a shear localization process via the propagation of shear bands. The relationship between contact response and shear banding mechanism, however, has not been fully addressed in nanocrystalline metals. The goal of this investigation is to study the atomic mechanisms leading to shear localization during indentation of nanograined Al. Molecular statics and dynamics simulations are used to model the 2D indentation of Al columnar thin films with a rigid cylindrical indenter. Different grain sizes (5 – 10 nm) and Embedded Atom Method potentials for Al are studied. Our results show that shear banding arises from both grain boundary sliding and intragranular slip. At large depths of indentation, we show that shear banding can lead to grain growth by coupled motion of grain boundaries.

10:30 AM

Atomistic Simulations of Nanoporosity in <100> and <110> Tilt Grain Boundaries in Cu and Al: *Garritt Tucker*¹; Mark Tschopp¹; David McDowell¹; ¹Georgia Institute of Technology

The objective of this work is to investigate the correlation between nanoporosity and grain boundary structure as well as the role of nanoporosity in dislocation emission at grain boundaries. We present a stereologically-based methodology for calculating the grain boundary nanoporosity that also allows for the calculation of spatial statistics within the boundary plane. We use molecular statics with embedded atom method potentials for Cu and Al to generate various <100> and <110> symmetric tilt grain boundaries. Additionally, certain grain boundaries possess a higher degree of nanoporosity connectivity and the use of two-point correlation functions, lineal path functions, and visualization techniques are implemented to quantify the structure. The implications of the connectivity of nanoporosity on the emission of dislocations from grain boundary regions are also explored.

10:50 AM Break

11:10 AM Invited

A Quasicontinuum Study of Scale Effects in Uniaxially Compressed Au Nanopillars: *Jaime Marian*¹; Jaroslaw Knap¹; Michael Ortiz²; ¹Lawrence Livermore National Laboratory; ²California Institute of Technology

Recent measurements of plastic yielding in micro-sized single crystals reveal a dramatic size effect for a wide range of materials. It is known that when the sample size approaches the scale over which dislocation cell structures form, the flow behavior of fcc metals can be significantly altered. This carries important implications when studying plastic processes in the presence of strong strain gradients, such as those encountered during nanoindentation, testing of nanowires, etc. The recent development of new nanoscale fabrication, testing and characterization technologies has enabled researchers to study the mechanical properties of engineering materials a few microns in size. These studies emphasize the need to consider both the sample geometry as well as the internal structure to determine the strength of a micro-sized material. In spite of this, the atomic-sized plastic defects generated during these tests have not yet properly characterized and much work remains to be done in order to improve our understanding of the microplasticity at this level. In this sense, the Quasicontinuum (QC) method suggests itself as an ideal tool to access all lengthscales involved in problem and provide direct comparison with experiments. A study of size effects in Au nanopillars under uniaxial compression is presented, where the intricacies of dislocation nucleation and propagation, resulting in slip steps are detailed. Appropriate constitutive responses are given and the variation of the yield stress with diameter size is rationalized in terms of geometric features of the pillars, rather than the intrinsic microstructure.

11:40 AM

Effects of Twin Boundaries on the Slip Activity of Nanosized FCC Metallic Pillars: Konstantin Afanasyev¹; Frederic Sansoz¹; ¹University of Vermont

Significant size effects have been observed in the plastic deformation of nanosized metallic wires and pillars. Fabricated FCC metal nanowires are usually made of a large number of twin interfaces. It is now known that size directly influences crystal slip activity in metallic nanopillars; however, the

role of twin interfaces on this process is still unclear. This paper presents several atomistic simulations aiming at a fundamental understanding of the plasticity mechanisms at play during compression and pure bending of twin-dominated metal nanopillars. We perform classical molecular dynamics simulations on 12 nm-diameter cylindrical pillars with EAM potentials for Au and Ni. Particularly, we investigate the effects of twin density on the atomic mechanisms of dislocation slip and overall constitutive behavior. We find that the nanopillar plasticity can be significantly changed and new deformation mechanisms, such as interface migration, observed in the presence of twin interfaces.

12:00 PM

Tension Compression Asymmetry and Size Effects in Nanocrystalline Ni Nanowires: *Joshua Monk*¹; Diana Farkas¹; ¹Virginia Tech

We investigate size-effects in polycrystalline nickel nanowires using molecular dynamics and an EAM potential. Both compressive and tensile deformation tests were performed for nanowires with radii ranging from 8 nm to 18 nm and a grain size of 10 nm. The wires contained up to five million atoms and were tested using a strain rate of 3.33×10^8 s⁻¹. The results are compared with similar tests for a periodic system, which models a macroscopic sample size of the same nanocrystalline material. The results indicate that the wires present significantly lower flow stresses than the macroscopic counterparts. Significant tension compression asymmetry was also observed, which is strongly dependent on the wire size. The results are discussed in terms of the various plasticity mechanisms operating in nanocrystalline metals.

12:20 PM

Dislocations and Their Interactions in Nanocrystalline Grains: *Evan Ma*¹; X. L. Wu²; ¹Johns Hopkins University; ²Institute of Mechanics

Dislocations and mechanical twins, the main carriers of plastic deformation, are well characterized for conventional single-crystal or polycrystalline metals. In the other extreme when the metals turn amorphous, there are no well-defined dislocations. Then what happens for nanocrystalline metals, with crystallites but tiny grain sizes on the order of 10 nanometers? We have carried out extensive TEM examinations to study the characters, configurations, interactions and storage, and formation mechanisms of dislocations [APL 88 (2006) 231911] and deformation twins [APL 88 (2006) 061905 and Script Mat. 54 (2006) 1685] in nanocrystalline Ni with an average grain size of 20 nm. The preferential deformation in the vicinity of grain boundaries and twin boundaries, for dislocation storage and accommodation of large plastic strains that decompose nanograins [unpublished], will also be discussed.

Properties and Performance of High Temperature Alloys and Coatings: Single Crystal Alloys II and Oxidation

Sponsored by: The Minerals, Metals and Materials Society, TMS Structural Materials Division, TMS: High Temperature Alloys Committee, TMS/ASM: Corrosion and Environmental Effects Committee, TMS/ASM: Mechanical Behavior of Materials Committee

Program Organizers: Qiang Feng, Beijing University of Science and Technology; Timothy Gabb, NASA Glenn Research Center; Doug Konitzer, General Electric Aviation; Roger Reed, Imperial College London; Bruce Pint, Oak Ridge National Laboratory; Sammy Tin, Illinois Institute of Technology; Shiela Woodard, Pratt and Whitney

Tuesday AM Room: Asia 4
February 27, 2007 Location: Dolphin Hotel

Session Chairs: Pierre Caron, ONERA; Roger Reed, Imperial College

9:00 AM Invited

Linking the Processing, Properties and Chemistry of Advanced Single Crystal Ni-Base Superalloys: *Sammy Tin*¹; ¹Illinois Institute of Technology

Remarkable improvements in performance and efficiency of advanced turbine engines can be attributed to technological developments pertaining to the turbine blades located in the high pressure or "hot stage" of the engine. Additional improvements in thermal efficiency of advanced turbine engines are possible if the temperature capability of these complex multi-component

TUESDAY AM

Ni-base alloys can be significantly extended. A new class of single crystal Ni-base superalloys containing high concentrations of refractory elements and platinum-group metal additions has recently been developed for use in ultra-high temperature applications. Developing an improved fundamental understanding of the solidification characteristics and deformation mechanisms is a major challenge. An overview of recent investigations aimed at linking the processing, properties and chemistry of novel Ni-base superalloys will be presented and discussed.

9:25 AM

Effect of HIPping on the Deformation Anisotropy and Fracture of Single Crystal Ni-Base Superalloys: *Fereshteh Ebrahimi*¹; Eboni Westbrooke¹; Micheal Kessler¹; ¹University of Florida

In this study the effects of loading orientation and hot isostatic pressing (HIPping) on the deformation and fracture of a Ni-base superalloy single crystal were evaluated at room temperature. The results indicate that HIPping significantly affects the critical resolved shear stress (CRSS) anisotropy, slip band evolution and the fracture behavior of this material. The CRSS values measured in samples loaded along the $\langle 111 \rangle$ and $\langle 123 \rangle$ orientations were increased, however HIPping did not influence the CRSS for samples loaded along the $\langle 100 \rangle$ orientations. This phenomenon is attributed to the dependency of shear localization between the pores and/or eutectic pools on their relative orientation to the loading axis. It was also found that the yield strength measured parallel to the primary dendrites was higher than the strength evaluated perpendicular to them. In this presentation, these results are discussed in the light of microstructural, compositional and fractographical analyses using electron microscopy techniques.

9:45 AM

Modelling the High Temperature Creep Behaviour of the Single Crystal Nickel-Based Superalloy CMSX4 <001>: Hector Basoalto¹; Bernd Vermeulen¹; Jeffery Brooks¹; Gina Coventry²; *Steve Williams*³; Julian Mason-Flucke²; Stephen Bagnall²; ¹QinetiQ Ltd.; ²Rolls-Royce plc.

Over the past decade, Rolls-Royce plc has been increasingly using the single crystal nickel-based superalloy CMSX4 in turbine components such that it is in widespread use in service today. The prediction of service life of these parts is highly dependent on having good material behaviour models. The paper describes the development of a uniaxial creep model for the single crystal superalloy CMSX4 along the $\langle 001 \rangle$ orientation. The advanced model presented here is based on the current Rolls-Royce hyperbolic tangent creep equations. The model is able to capture the tertiary dominated creep behaviour above 850°C, as well as, the low temperature creep behaviour of CMSX4, where incubation periods of several hundred hours and primary strain in excess of 5% are observed. This allows the use of the creep model over the entire stress/temperature range of interest for prediction of creep behaviour in turbine vanes, turbine blades and turbine segments.

10:05 AM

On the Creep and Phase Stability of Advanced Ru-Bearing Ni-Base Single Crystal Superalloys: *An-Chou Yeh*¹; Akihiro Sato²; Atsushi Sato¹; Hiroshi Harada¹; ¹National Institute for Materials Science; ²Ishikawajima-Harima Heavy Industries

Ruthenium additions have lead to the development of new Ni-base single crystal superalloys with high refractory content and enhanced phase stability at elevated temperatures. This new trend of alloy development increases negative γ/γ' lattice misfit, which can promote formations of γ' raft and fine interfacial dislocation network for effective strengthening against creep at temperatures above 1000°C. Recent studies have shown Ru-bearing superalloys achieving significant advantage of creep resistance over current commercial alloys. However, questions are remained for alloy designers as to the optimal amount of Ru content and the magnitude of lattice misfit for future alloy developments. The present article attempts to address these issues by examining creep and phase stability of several Ru-bearing alloys. In conclusions, the indirect strengthening effects due to Ru, i.e. lattice misfit, needs to be balanced with the rafting tendency and TCP phase formations to achieve good creep performances across a wide temperature range.

10:25 AM

Detection of Fatigue Damage Accumulation in a Single Crystal Nickel-Base Superalloy: *Jianzhang Yi*¹; Christopher Torbet¹; Tresa Pollock¹; J. Jones¹; Divine Kumah¹; Naji Hussein¹; Roy Clark¹; ¹University of Michigan

Nickel-base superalloys are utilized for the most critical components in aircraft engines. Reliability of these components could be improved with the development of fast diagnostic tools and reliable life prediction methodologies. In the present study, we report the applicability of a portable ultrasonic testing system combined with x-ray imaging to quantify the damage evolution in single crystal Ni-base superalloy. The capability has been demonstrated of image fatigue cracks originating in coatings details of microstructural features in 200 μ m thick foils of single crystal superalloy using a synchrotron x-ray source. Further investigation is underway to explore the possibility of detecting fatigue crack initiation and propagation in the alloy using a femtosecond laser induced x-ray source.

10:45 AM

Characterization of LCF Damage in Ni-Based Superalloys for Airfoil Applications: *Clarissa Yablinsky*¹; Katharine Flores¹; Michael Mills¹; James Williams¹; ¹Ohio State University

Ni-based superalloys are used for turbine airfoil applications due to their excellent high temperature properties. Alloy design has historically focused on creep resistance as the critical design parameter. Recently, the focus has shifted to fatigue resistance, resulting in the need to better understand the effects of alloy design on fatigue crack initiation and propagation. In this study, coated and uncoated single crystal Rene N5 specimens were cycled in strain control in the temperature range of 1800-2000°F. Changes in the size and distribution of γ' precipitates were characterized using high resolution scanning electron microscopy (SEM). Fracture surfaces were also characterized via SEM. Bulk and local deformation mechanisms were examined using transmission electron microscopy (TEM) and specimens selectively prepared using a focused ion beam (FIB). These fatigue deformation mechanisms will be compared with those operating during creep at similar temperatures.

11:00 AM Break

11:15 AM Invited

Compositional Effects on the Cyclic Oxidation Resistance of Superalloys: *James Smialek*¹; Timothy Gabb¹; Charles Barrett¹; ¹NASA

Cyclic oxidation is an important aspect of superalloy performance, and composition provides the most direct control. Conventional superalloys are generally composed of base elements [Ni-Co-Cr-Al], refractory elements [Nb-Mo-Ta-W-Re], oxygen-active elements [Ti-Zr-Hf-Y-La], light elements [B,C], and occasionally [V-Mn-Ru-Si], with P and S trace impurities. 1100°C oxidation was assessed by scale growth and spallation, combined as an attack parameter, K_s , and used to rank 30+ commercial alloys. Less than 4 mg/cm² weight loss occurred for high 5-6% Al and 3-9% Ta, and low Ti <1% (wt.%). Conversely, alloys exhibiting weight loss of 200-300 mg/cm² contain low <3.5% Al, no Ta, and high >3% Ti. The Cr effect can be somewhat masked because of its inverse correlation with Al. Multiple linear regression to a polynomial fit helped quantify complex oxidation effects within a ten element compositional space. Accordingly, single crystal alloys do exhibit excellent behavior as predicted, especially with low-sulfur, Y-Hf-doped modifications.

11:40 AM

Cyclic Oxidation of Ru-Containing Single Crystal Superalloys at 900°C: *Qiang Feng*¹; Brian Tryon²; Tapash Nandy²; Tresa Pollock²; ¹University of Science and Technology Beijing; University of Michigan; ²University of Michigan

Ru-containing single crystal superalloys have recently been developed for potential applications of blade alloys in aircraft engines. Cyclic oxidation experiments were conducted at 900° on a series of Ru-containing single crystal superalloys with different levels of Ru (3.5-9 at.%) and Cr (0-8 at.%). The oxides and morphology of oxidized surfaces were characterized. High levels of Cr additions (8 at.%) significantly improved oxidation resistance, equivalent to the second generation single crystal alloys, while increased levels of Ru adversely affected the oxidation performance. A multi-layered scale formed on the alloy surface, and it generally consisted of an external layer of NiO, an intermediate layer of spinel and an alumina inner layer. High levels of Cr additions promoted the formation of a continuous and protective



alumina layer adjacent to the superalloy. These experimental results are compared with those of the same alloys at 1100°. The oxidation mechanisms will be also discussed.

12:00 PM

The Effect of Co and Refractory Element (Re+W) Contents on Cyclic Oxidation of Ru-Containing Single Crystal Superalloys at 1100°C: *Shuwei Ma¹; Dipak Das¹; Tresa Pollock¹; ¹University of Michigan*

Cyclic oxidation behavior of Ru-containing single crystal superalloys with two levels of Co and refractory elements (Re+W) has been investigated at 1100°C in air. The phase constitution and the evolution of the oxide layers have been studied by using XRD and EPMA. The outer portion of the oxide scale consists of either spinel (NiAl₂O₄) or a mixture of NiO and spinel depending on the alloy composition. Ta₂O₅ particles were found to coexist in the spinel layer in case of alloys with higher levels of Co. While the effect of Re+W is not very apparent, a lower Co content is found to promote the formation of a continuous Al₂O₃ inner layer which results in an increase in the oxidation resistance of the superalloy. Among the alloys examined in the present study, the best oxidation resistance is provided by the one which has a combination of low Co (2.5at.%) and high Re+W (4at.%).

12:20 PM

Microstructure and Oxidation Behavior of Aluminide Coated Ru-Containing Superalloys: *Dipak Das¹; Kenneth Murphy²; Tresa Pollock¹; ¹University of Michigan; ²Howmet Research Center*

Ruthenium-bearing Ni-based single crystal superalloys are currently being developed for their use as gas turbine engine parts at high temperatures. In the present investigation, microstructural aspects and oxidation behaviour of several aluminide coated Ru-containing Ni-based single crystal alloys have been studied. Alloys have been selected based on their contents of Ru, Cr and the refractory elements (W+Re). The coating was applied by using a high temperature low activity aluminizing method. The coated alloys were cyclically oxidized at 1100°C in air. In as-coated condition, the coating in all the cases was found to have the typical two-layer structure. In addition, a secondary reaction zone (SRZ) was also observed below the coating in case of all the alloys. The degradation of coating microstructure and changes in SRZ during oxidation have been studied.

12:40 PM

The Effects of Silicon on the Oxidation Resistance of Ni-Base Superalloys: *Atsushi Sato¹; Hiroshi Harada²; Tadaharu Yokokawa²; Kyoko Kawagishi²; Hachiro Imai¹; ¹Shibaura Institute of Technology; ²National Institute for Materials Science*

A recently developed nickel-base single crystal superalloy possesses unrivalled high temperature creep properties due to its high Re and Ru content. On the other hand, the addition of such elements considerably degrades the superalloy's oxidation resistance; thus, effective measures to prevent this degradation are required. Adding yttrium to the superalloy at ppm levels showed substantial improvements; however, it is extremely difficult to reproduce consistent yttrium levels during casting. Hence, we tried to find a more reliable method to improve superalloy oxidation resistance. We have previously established that an addition of 1.0-1.9 wt.% silicon dramatically improves the oxidation resistance of 5th generation superalloys, as this promotes the formation of alumina and completely suppresses the formation of nickel oxide and spinels. In this study, the effects of silicon, aluminium and chromium on a nickel-base superalloy's oxidation resistance are quantitatively evaluated.

Recycling and Waste Processing: Automotive Recycling, Global Challenges and Opportunities

Sponsored by: The Minerals, Metals and Materials Society, TMS Extraction and Processing Division, TMS Light Metals Division, TMS: Recycling and Environmental Technologies Committee

Program Organizers: Mark Schlesinger, University of Missouri; Robert Stephens, Teckcominco, Inc.; Donald Stewart, Alcoa Technology; Ray Peterson, Aleris International; Jan van Linden, Recycling Technology Services, Inc.; Subodh Das, SECAT; Abdel Serna-Vasquez, Aleris International; Cynthia Belt, Aleris International Inc; John Pickens, Alumitech/Aleris International; John Hryn, Praxair; Richard Kunter, Richard S. Kunter and Associates; Andreas Siegmund, Quemetco Metals Inc.; Masao Suzuki, AI Tech Associates

Tuesday AM
February 27, 2007

Room: Australia 2
Location: Dolphin Hotel

Session Chairs: Jan Van Linden, Recycling Technology Svc Inc; Cynthia Belt, Aleris International Inc

9:00 AM Invited

Effect of Global Trade on Recycling and Recycling Technology: *Wijnand Dalmijn¹; ¹Dalmijn*

In the last decade the volume of recycled materials in the world has increased significantly. This increase was caused by a combination of legislation, technology and economy. An example of the influence on recycling of the legislation is in Europe where product responsibility and recycling percentages of products are specified and the landfilling cost is increased in order to promote the long term goal of zero landfilling. An example of this policy is in Germany where zero landfilling is being implemented. With increasing recycling volumes the technology of wet and dry bulk sorting had to be optimized and new separation equipment designed such as eddy current separators. Tom meet the specifications of the customers, quality control systems were designed and implemented for example in the aluminum industry as well as the glass recycling industry. Separators based on sensor technology like color cameras and metal detectors.

9:25 AM Invited

Future Developments in Car Recycling in the Netherlands: *David Bebelaar¹; Mark van Veldhuizen¹; ¹Automotive Recycling Nederland*

Auto Recycling Nederland (ARN) was established in 1993 by the automobile and automobile related branch organizations in the Netherlands in anticipation of the producers' responsibility stipulated in de European ELV directive. Ever since, ARN is the officially recognized authority for the recycling of cars in the Netherlands. Under the direction of ARN the requirements to realize an 85% recycling rate were met years before the implementation date of the directive. This was achieved predominantly by dismantling and recycling a list of hazardous and other materials on top of the metal content of cars. ARN is now facing the next challenge of the directive to meet a 95% recycling target which in the Netherlands will be due in 2007. This cannot be achieved by simple continuation of the strategy of 'pre shredder' dismantling of materials. The strategy is therefore adjusted and the efforts will be concentrated on the treatment of shredder waste to meet the additional recycling quota. Studies of different post shredder separation processes and tests run by ARN show that higher than 85% results are achievable with technology presently existing. How much higher is depending however not only upon technology but primarily on the marketability of the output fractions. Whether it is feasible to implement such technology in the Netherlands will depend on the economic parameters. Increasing the landfill cost will have a positive efforts but can also have a negative influence on the economy of the car cycle. But above all market forces like the seemingly endless demand for secondary materials in China dictates what the nearby future will look like.

9:55 AM Invited

A Mechanical Separation Process to Recover Metals and Polymers from Shredder Residue: *Joseph Pomykala Jr.¹; Bassam Jody¹; Edward Daniels¹; Jianhong Yang¹; Jeffrey Spangenberg¹; ¹Argonne National Laboratory*

Shredder residue is a byproduct from the recovering of metals from end of life vehicles, home appliances and other metal containing materials. The five million tons of shredder residue produced annually in the United States is presently land filled. Shredder residue contains about 5-10% by weight metal pieces that are larger than 9 mm in size. It also contains about 5-10% by weight metal and metal oxide fines smaller than 9mm. To meet the challenges of automotive materials recycling, the U.S. Department of Energy is supporting research at Argonne in cooperation with the Vehicle Recycling Partnership of USCAR and the American Plastics Council. Argonne National Laboratory has developed a mechanical separation process for separating and recovering the metals as well as other materials such as polymers from the shredder residue. Argonne also tested a process to produce reduced iron from the fines. This paper describes the Argonne processes.

10:25 AM Break

10:35 AM Invited

Elemental Analysis and Chemical Composition Based Material Separation: *Adam Gesing¹; ¹Gesing Consultants Inc*

The need for elemental analysis and chemical-composition-based material separation will be demonstrated for scrap metal alloys including aluminum alloys. Sorting of a few known alloys in the manufacturing scrap stream will be compared to the batching of a secondary alloy from an unknown mixture of post-consumer scrap. The capabilities of LIBS, XRF and PGAA (neutron activation) for quantitative elemental analysis will be compared. The analytical capability requirements of process control and high-speed sorting will be contrasted. Examples of successful sorting applications utilizing each of the three technologies will be discussed.

11:05 AM Invited

DE-XRT Imaging for Automatic Particle Sorting: *Tako de Jong¹; ¹Delft University of Technology*

The concept of imaging based on dual-energy X-ray transmission (DE-XRT) for automatic particle sorting was developed by Delft University of Technology. This technique can be applied for the concentration of certain types of polymers as well as for the removal of halogen and heavy-metal containing components from organic mixtures prior to thermal treatment. Examples are the removal and concentration of PVC and flame retardant resins from plastic mixtures and the removal of critical contaminants from solid recovered fuel (SRF). Today state-of-the-art automatic X-Ray sorters are equipped with DE-XRT technology and are capable of processing large volumes of material. These features make X-ray sorting an economically attractive option for waste processing. Experimental data on separation efficiencies will be presented and some examples of industrial applications will be discussed.

11:35 AM Invited

The Success of Vehicle Recycling in North America: *Richard Paul¹; ¹Lear Automotive EEDS Spain S.L.*

This presentation will discuss the results of evaluating the North American automotive recycling infrastructure and calculating vehicles processed, materials recycled, parts reused, and shredder residue landfilled. Data and other available information regarding these procedures and material volumes will be used for a report on the success of vehicle recycling. Vehicle recycling, component reuse and metal recovery is important to governments, vehicle manufacturers, suppliers, material recyclers, dismantlers, and shredders. The highly efficient car recycling infrastructure serves to divert materials from landfill and recycle metals from high volume consumer product and serves as an alternative source of low cost components for repair of vehicles that might otherwise be taken out of service. Although North America has no single comprehensive, automotive specific law similar to Europe or Japan, they are myriad federal, state and local regulations which require vehicle pretreatment, fluid collection, separation of selected materials of concern and landfill restrictions. The analysis will provide insights on current levels of performance at North American automotive recycling centers, vehicle recyclability, component reuse, material recycling, vehicle pretreatment and handling of hazardous materials.

12:00 PM Panel Discussion

Shape Casting: The 2nd International Symposium: Process Design/Analysis

Sponsored by: The Minerals, Metals and Materials Society, TMS Light Metals Division, TMS: Aluminum Committee, TMS: Solidification Committee

Program Organizers: Paul Crepeau, General Motors Corporation; Murat Tiryakioglu, Robert Morris Univ; John Campbell, University of Birmingham

Tuesday AM Room: Northern E2
February 27, 2007 Location: Dolphin Hotel

Session Chair: Makhlof Makhlof, Worcester Polytechnic Institute

9:00 AM Introductory Comments

9:10 AM

Advanced Intermetallic Materials and Processes: Overview of the IMPRESS Integrated Project: *David Jarvis¹; Daniela Voss¹; Nicholas Lavery¹; ¹European Space Agency*

IMPRESS is part of the European Commission's 6th Framework Programme and stands for Intermetallic Materials Processing in Relation to Earth and Space Solidification. The main scientific objective of the project is to gain a better understanding of the complex links between materials processing, material structure and resultant properties of intermetallic compounds. In order to achieve this objective, the IMPRESS project combines a wide range of activities including improved casting technology, fundamental studies of solidification both terrestrially and in space, the creation of reliable thermodynamic and kinetic databases, thermophysical property measurements, multiscale computer modelling, structure characterisation, mechanical property testing and industrial product development. With the knowledge generated, the project aims to develop and test 40cm investment-cast TiAl turbine blades for aero-engines and stationary gas turbines. For blade manufacturing the principal melt processes under study are tilt casting, counter-gravity casting and centrifugal casting.

10:00 AM

Quantitative XCT Evaluation of Porosity in an Aluminum Casting: *Joseph Wells¹; ¹JMW Associates*

Traditional destructive sectioning and NDE techniques including radiography and ultrasound provide insufficient 3D qualitative and quantitative porosity diagnostics, characterization, and visualization capabilities. Improved methods are required for efficiently assessing the detailed nature, extent and distribution of porosity in research, product development, prototyping and first-items manufactured inspection stages of engineering materials and structures. One quite powerful and recent NDE modality which has been demonstrated to be most advantageous in the 3D diagnostics of volumetric porosity is industrial x-ray computed tomography, XCT. With this non-invasive approach, very large numbers of irregular shaped pores can be individually characterized according to spatial coordinates, surface area, volume, aspect ratio, and size distributions. In addition, virtual transparency image processing techniques permit the 3D visualization of all pores insitu within the object casting. Examples of such porosity characterization and the cognitive visualization of same using the XCT modality in a representative aluminum casting are presented and discussed.

10:25 AM

Naturally Pressurised Filling System Design: *John Campbell¹; ¹University of Birmingham*

The conventional unpressurised and pressurised filling system designs employed to fill moulds under gravity perform poorly, creating generous quantities of entrainment defects (bubbles, bifilms and sand inclusions), and so efficiently degrading castings and their properties. The new concept of the naturally pressurised system is described, and its successes and limitations are examined. It seems that there is no good solution at the present time to the gravity pouring of steel castings using a bottom-teemed ladle, explaining the widely experienced upgrading costs suffered by heavy steel foundries. It is



clear that ultimately, foundries should be designed to avoid the pouring of melts at any point during the melting or casting process. Thus new melt handling technology is required for the designs of foundries, and only counter-gravity filling of moulds is seen to be capable of routinely producing substantially defect-free castings.

10:50 AM Break

11:10 AM

Improved Soundness and Mechanical Properties Obtained by Solidification under Pressure in A206: *Pavan Chintalapati*¹; John Griffin¹; ¹University of Alabama at Birmingham

The goal of this study is to achieve forging properties with the benefits of cast structural components. The effect of applying 10 atmospheres of pressure during solidification on the soundness and mechanical properties on A206 aluminum was studied. Experimental wedge shaped castings were solidified in no-bake molds at 1 and 10 atmospheres pressures. A wedge shaped casting provided a range of porosity and controlled solidification front. Radiography verified that pressure increased soundness by an order of magnitude. Tensile coupons were removed from selected cooling rates. Elongation improved by ~50 to 550% and tensile strength increased ~11 to 60% when pressurized during solidification. Similar improvements in cast properties of other alloys are possible under the correct metallurgical conditions. This paper discusses how to achieve these metallurgical conditions for complex three-dimensional production castings.

11:35 AM

The Design of L-Shaped Runners for Aluminium Gravity Casting: *Fu-Yuan Hsu*¹; Mark Jolly²; John Campbell²; ¹Auspicious Company Ltd; ²University of Birmingham

The purpose of this research is the development of guiding principles and rules for the design of running systems for aluminium gravity castings, employing both the “virtual” experiment, a computational modelling package, and the “physical” experiment, the real-time X-ray radiography study. Guidelines for the designing of L shaped junctions are developed. Five geometries of L-junctions have been studied for the design of runners and multiple-gate systems. Progressive filling along the L shaped geometry has been achieved by reducing the area of the “dead zone”. Higher flow rate and less turbulent filling of the mould cavity can be achieved by the new L shaped junction design. In a multiple-gate system uniform distribution of flow rate through each gate into the mould cavity has been accomplished. Quantification of a running system is explored by the estimation of the coefficient of discharge Cd and the loss coefficient K for individual components.

12:00 PM

Analysis of a Confluence Weld Defect in an Aluminum Casting Alloy: *Oscar García-García*¹; Miguel Sanchez-Araiza²; Manuel Castro-Román¹; José Escobedo B¹; ¹CINVESTAV; ²Castech S.A. de C.V.

A leakage problem in an aluminum cast cylinder head was studied. Metallographic characterization showed the presence of a confluence weld defect caused by the meeting of two different metal streams not able to join together. Process key variables such as pouring temperature, mould temperature, etc., were analyzed to determine their influence on the occurrence of the problem. Computer simulation of the filling process suggested that air entrapment could be related to the origin of the defect. Additionally, core outgassing was found to be an important factor increasing the local pressure at the area of interest. Optimization of process key variables contributed significantly to reduce the scrap rate. However, the complete elimination of the defect required a major change in casting design, which was made by considering both; the formation mechanism of the confluence weld defect and the increase of local pressure due to core outgassing during the filling operation.

12:25 PM

Study of Mould Temperature Effect on the Incidence of Porosity in a Cast Cylinder Head: *Jacobo Vargas Orihuela*¹; Manuel Castro-Roman¹; Martin Herrera-Trejo¹; Miguel Sanchez-Araiza²; ¹CINVESTAV; ²Castech S.A. de C.V.

Software simulation allows detecting casting zones with susceptibility to foundry defects. Some defects are only detected when casting is manufactured at high production rates. The changes needed to eliminate the problem imply

economic lost and time waste. The present work analyzed the possibility of detecting low incidence defects zones by simulation. Simulation was calibrated with experimental data obtained from cooling curves, measured during the filling and solidification process, at the zones where potential defects appeared. The effect of changes on the mold temperature was considered. Variations of mold temperature were made by delaying the time between castings. Cooling of the mold, before pouring a subsequent casting, was allowed both with and without the first casting inside of the mold. The information obtained from simulations was compared with experimental results. It was found that after delaying the molding process, the number and extension of zones with porosity defects were increased.

Structural Materials Division Symposium: Mechanical Behavior of Nanostructured Materials, in Honor of Carl Koch: Plasticity and Deformation Mechanisms at Small Length Scale I

Sponsored by: The Minerals, Metals and Materials Society, TMS Electronic, Magnetic, and Photonic Materials Division, TMS Materials Processing and Manufacturing Division, TMS Structural Materials Division, TMS: Chemistry and Physics of Materials Committee, TMS/ASM: Mechanical Behavior of Materials Committee, TMS: Nanomechanical Materials Behavior Committee

Program Organizers: Xinghang Zhang, Texas A&M University; Yuntian Zhu, Los Alamos National Laboratory; Michael Rigsbee, North Carolina State University; C. Suryanarayana, University of Central Florida; Haiyan Wang, Texas A&M University; C. T. Liu, Oak Ridge National Laboratory

Tuesday AM
February 27, 2007
Room: Asia 5
Location: Dolphin Hotel

Session Chairs: Xinghang Zhang, Texas A&M University; K. Jimmy Hsia, National Science Foundation

9:00 AM Invited

Plastic Deformation at the Micron Scale: Strain Gradients and Dislocation Source-Controlled Plasticity: *William Nix*¹; ¹Stanford University

Crystals are almost always stronger when plastic deformation is confined to small volumes. One manifestation of this is found in the indentation size effect (ISE), which can be understood in terms of the gradients of strain that accompany deformation in small indentations. Here we review strain gradient hardening and the role of geometrically necessary dislocations (GNDs) in that hardening process. We also describe recent measurements of the GNDs in small indentations with microbeam x-ray diffraction. Recent experiments have shown that gold single crystal pillars in the micrometer size range show significant size effects, with smaller being stronger, when the pillars are tested in uniaxial compression, without significant strain gradients. These size effects suggest that plasticity is dislocation source-controlled, wherein smaller volumes are stronger because fewer sources of dislocations are available. The evidence for source-controlled plasticity is reviewed and recent attempts to describe the corresponding size effects on strength are described.

9:20 AM

A Simple Analysis of Partial Dislocations: *K. Jimmy Hsia*¹; Huajian Gao²; ¹National Science Foundation; ²Brown University

Peierls-Nabarro model for full dislocations resolves the controversy of singular dislocation field near the core of dislocation. It also gives an estimate of the dislocation core dimension. More importantly, it gives an estimate of the resistance stress to dislocation motion in an otherwise elastic material. Taking this approach to studying the partial dislocations, one can anticipate results that may shed light to the magnitude of the resistance stress to the motion of partial dislocations. In this paper, we develop a model to study the spreading of partial dislocations. Perturbation solutions of the governing equation are obtained. The result is consistent with the Peierls solution for a full dislocation. In particular, partial dislocations undergo constriction when they encounter barriers as in the case of cross-slip or their interactions with twin or grain boundaries. The increase of the resistance to partial dislocation motion is of tremendous importance.

9:35 AM Invited**A Remarkable Microstructure in Phase-Transformed Ta Thin Films:** *Shefford Baker*¹; Robert Knepper¹; Ray Fertig¹; ¹Cornell University

Thin Ta films were deposited on oxidized Si substrates in an ultra high vacuum environment by magnetron sputtering. These films were thermally cycled in-situ and their stress-temperature behaviors were recorded using a substrate curvature method. The microstructures of the films were studied using x-ray diffraction, electron backscattered diffraction (EBSD), and transmission electron microscopy (TEM). As-deposited films were in the metastable tetragonal beta phase, but transformed to the stable alpha phase at high temperatures. Phase transformed films were found to have microstructures characterized by continuous orientation gradients and discontinuous grain boundaries. A rotation pole figure (RPF) method was developed to analyze the EBSD data. A model for the generation of the microstructure is presented and the roles of oxygen content and film stress on the phase transformation and on the final microstructures are discussed. New possibilities for device fabrication using Ta films are described.

9:55 AM**Strength Limits and Deformation of Ultrathin Copper and Silver Films:** Wen Chung Li¹; *T. John Balk*¹; ¹University of Kentucky

Although it is well known that deformation behavior of metal thin films differs strongly from that of bulk metals, knowledge of fundamental mechanisms is not complete, especially for nanoscale thin films. Copper and silver films, 25 nm to 1 μm in thickness, were deposited onto silicon wafers and thermally cycled to sub-ambient temperatures to systematically assess the strength limits of nanoscale thin films and the persistence of the strength plateau at low temperature. Thermomechanical behavior of thin films will be correlated with dislocation motion and interaction with grain boundaries, as observed by in situ and post mortem transmission electron microscopy. Comparison of thermomechanical data with a model proposed by Nix suggests that orthogonal dislocation obstacles play a larger role than parallel obstacles, especially for thicker films and lower plastic strains. These interrelated findings will be discussed in the context of a microstructure-based understanding of thin film stress evolution.

10:10 AM**Etch-Induced Nanoscale Flaws Influence the Strength of Several Silicon Microfabrication Technologies:** *Brad Boyce*¹; David Miller¹; Kenneth Gall²; Conrad Stoldt³; ¹Sandia National Laboratories; ²Georgia Institute of Technology; ³University of Colorado, Boulder

Several commercially-available processes for silicon microelectromechanical systems may have similar underpinning failure origins. In Sandia's SUMMiT V process, each of the five layers has a different strength, with the topmost layer being more than twice as strong as the first deposition layer. While several possible explanations have been considered, the most plausible explanation is the layer-dependent surface topography, controlled by the etch condition. Atomic force microscopy has revealed 90 nm deep "curtaining" crevices on the sidewalls, consistent with critical flaw predictions; and the layer-dependent strength scales inversely with surface roughness. As an extension, a study of etching processes applied to MUMPs polysilicon has shown that often-used gold overlayers induce galvanic corrosion of silicon, producing a porous surface morphology. Due to this etch-induced degradation, fracture strength decreases drastically with etch immersion time. Finally, in bulk-micromachined single crystal silicon-on-insulator, strength is also shown to correlate with die-to-die variability in BOSCH etch-induced topography.

10:25 AM**Orientation Effects on Properties of Wear Tested Single Crystal Nickel:** *Neville Moody*¹; Megan Cordill²; Somuri Prasad¹; William Gerberich²; ¹Sandia National Laboratories; ²University of Minnesota

Strength, friction, and wear control the performance and reliability of nickel based microdevices under sliding contacts. However, the effects of frictional contacts and wear are undefined. To address these effects, we have begun a program using nanoscratch and nanoindentation to study wear on <001> and <111> oriented single crystal nickel. Nanoscratch techniques were used to generate wear patterns as a function of load and cycles. Nanoindentation was used to measure properties in each wear pattern. The results for <001> single crystal nickel showed there was a strong increase in hardness with increasing applied wear load that was accompanied by a change in surface deformation.

The <111> single crystal nickel exhibited similar behavior, but at a higher work hardening rate. In this presentation, we will show how crystal orientation affects deformation processes and properties under sliding contacts. This work was supported by Sandia National Laboratories under USDOE contract DE-AC04-94AL85000.

10:40 AM Break**10:50 AM Invited****Life of a Dislocation in a Nanocrystalline FCC Metal: Experiments and Simulations:** *Helena Van Swygenhoven*¹; ¹Paul Scherrer Institute, Switzerland

Molecular dynamics simulations of nc-Al will be presented suggesting that grain boundary dislocation sources can not be represented by Frank-Read sources. Simulations also suggest that nucleation and propagation are separated processes where propagation is hindered by a pinning-depinning, a thermally activated mechanism and not purely mechanically driven as suggested in some mesoscopic models (Acta Mat 54(2006)1975). The computational part of the talk is followed by an overview of experiments (Mat.Today 9(2006)) designed to validate simulation results such as in-situ X-ray diffraction profile analysis, a technique allowing to capture footprints of dislocations at low temperature (APL 87(2005)) and the recent questioning of the validity of the 0.2% yield stress as the onset of macroscopic plasticity (Adv. Mat. 18(2006)). Furthermore stress relaxation measurements and dip-test measurements (APL, 2006 in-press) allowing to separate internal and effective stresses and to evidence negative creep will be discussed in terms of suggestions of molecular dynamics.

11:10 AM**Shear Plasticity Model for Nanocrystals:** Anna Kolesnikova¹; Ilya Ovid'ko¹; *Alexey Romanov*²; ¹Institute of Problems of Mechanical Engineering; ²Ioffe Physico-Technical Institute

Plastic deformation of nanocrystalline materials demonstrates some specific features including instability of dislocations in nanograins, shear along grain boundaries, unique work-hardening behavior, etc. In this work we consider a macroshear of nanocrystalline material as interplay between localized shear and misorientation band development. On the mesoscopic scale we investigate the dislocation-disclination configurations formed at nanograin boundaries and junctions under the action of the external stresses. It is demonstrated that there exists an energy release in the process of defect structure transformations at nanograin boundaries. These defect structure transformations proceed via one-axis disclination dipole nucleation at the grain versus so-called U-configuration, which is built by a disclination quadrupole and a dislocation dipole. The one-axis disclination dipole nucleation is assisted diffusion accommodation process along the grain boundaries. One-axis disclination configurations contribute to nanograin rotations. The dependence of the external stress at which the moving dislocation crosses the nanograin on grain size is demonstrated.

11:25 AM Invited**Mechanical Property Evaluation at the Micro-Scale Using FIB Fabrication Methods:** *Michael Uchic*¹; Dennis Dimiduk¹; Robert Wheeler²; Paul Shade³; Hamish Fraser³; ¹Air Force Research Laboratory; ²UES, Inc.; ³Ohio State University

Focused Ion Beam microscopes have been an indispensable tool in the development of new mechanical testing methods that operate at the micro- and nano-meter length scales. Over the past five years, some of the authors have developed and refined a micro-compression test methodology that has been used to characterize the mechanical properties of metallic materials. This talk will present selected applications of this methodology to various materials systems, including ultra-fine-grained Ni. Lastly, we will show recent efforts to implement a prototype mechanical test system for performing micro-compression experiments inside a SEM.

11:45 AM Invited**Length Scale Effects in the Deformation of Metals:** *Cynthia Volkert*¹; Nicolas Cordero¹; Erica Lilleodden¹; Alex Donohue²; Frans Spaepen²; ¹Forschungszentrum Karlsruhe; ²Harvard University

Recent developments in micro-mechanical testing methods involving the use of focused ion beam machining and nanoindentation offer unique opportunities to systematically study deformation of small samples. We have performed compression tests on micron and sub-micron columns made by ion



beam machining from a variety of materials, including single crystalline Cu, amorphous PdSi, and multilayer films made of a-PdSi and Cu. The results illustrate a number of different length scale effects including increases in strength due to sample size (single crystal Cu) and grain size (Cu in multilayer samples), and changes in deformation mechanism (amorphous PdSi). A brief discussion of possible causes of the size effects in the amorphous and crystalline metals and their implications for composite design will be presented.

12:05 PM

Statistical Nature of Surface Dislocation Nucleation: Ting Zhu¹; Ju Li²; Amit Samanta²; Austin Leach¹; Ken Gall¹; ¹Georgia Institute of Technology; ²Ohio State University

Recent compression experiments on single-crystal pillars with diameters ~ 300 nm have revealed strength approaching the ideal surface strength [Acta Mater. 53, 1215] of materials. This raises a fundamental question on the role of free-surface dislocation nucleation, competing against more traditional dislocation sources like the Frank-Read source. Dislocation nucleation is a rate process where thermal fluctuations are pitted against a nucleation energy barrier, whose magnitude is controlled by the local stress. Atomistic reaction pathway calculations (free-end nudged elastic band and dimer methods) are performed to identify the saddle-point states of surface nucleation. We show the activation volume of nucleation is characteristically on the order of $10b^3$, where b is the Burgers vector, under common laboratory experiment conditions of activation energy ~ 0.7eV. Using the atomistic results as input, we relate the nucleation stress probabilistically to temperature, applied strain rate and pillar size.

12:20 PM

Experiments and Dislocation Dynamics Simulations of Plasticity in BCC Metal Micro-Pillars: Julia Greer¹; Christopher Weinberger²; Wei Cai²; ¹Palo Alto Research Center (PARC); ²Stanford University

While size effects in sub-micron crystal plasticity can be explained by the presence of strain gradients, recent uniaxial micro-compression experiments of FCC metals (e.g. gold) suggest that size effect exists even in their absence. To investigate the effects of crystal structures on this type of size effect, we perform similar micro-compression experiments on BCC metals and compare the results with Dislocation Dynamics (DD) simulations. Freestanding molybdenum micro-pillars are created by focused ion beam (FIB) machining and are subsequently compressed using Nanoindenter with a diamond flat punch. The image stresses from the free surface in DD simulations are computed efficiently by a new algorithm that takes advantage of Fast Fourier Transform and a set of analytic solutions. The anisotropy of (edge and screw) dislocation mobility in BCC metals lead to interesting effects on microstructure and flow stress.

Towards Functional Nanomaterials: Synthesis, Characterization, and Applications: Nanoscale Superstructures, Metallic Nanoparticles and Plasmon

Sponsored by: The Minerals, Metals and Materials Society, TMS Electronic, Magnetic, and Photonic Materials Division, TMS: Nanomaterials Committee
Program Organizers: Zhiming Wang, University of Arkansas; Alexander Govorov, Ohio University; Andrey Rogach, Ludwig-Maximilians-Universität München

Tuesday AM
February 27, 2007

Room: Oceanic 5
Location: Dolphin Hotel

Session Chairs: Alexander Govorov, Ohio University; Hugh Richardson, Ohio University

9:00 AM Invited

Nanoscale Superstructures from Nanowires and Nanoparticles: Nicholas Kotov¹; Jaebeom Lee¹; Alexander Govorov²; ¹University of Michigan; ²Ohio University

Many biomedical fields that require evaluation of local concentrations and other parameters for intricate geometries. This is difficult to accomplish

using traditional sensor deployment schemes, which often require substrate and wires. In this presentation, we address these problems by designing a nanoscale sensing device from different types of nanoparticles and nanowires connected by molecular springs made from flexible PEG oligomers. The polymeric linkers afford continuous and dynamic change of conformations in such structures leading to the variations of the distance between the nanoscale colloids reversibly changes depending on conditions or analyte concentration and can be evaluated by fluorescence measurements. Plasmon-exciton interactions result in tremendous enhancement of luminescence and for some systems in characteristic wavelength shift depending on the analyte concentration. Understanding plasmon-exciton interactions creates a knowledge base for other technologies such as lasing in nanomaterials, energy conversion, and nanoscale electronics.

9:30 AM Invited

Thermo-Optical Properties of Nanoparticles Embedded in Ice: Characterization of Heat Generation and Melting: Hugh Richardson¹; Alexander Govorov¹; Zachary Hickman¹; Alyssa Thomas¹; Martin Kordesch¹; ¹Ohio University

We investigate the system of optically-excited gold nanoparticles (NPs) in an ice matrix aiming to understand heat generation and melting processes at the nanoscale level. NPs of various sizes are studied with Raman and photoluminescence spectroscopy. Along with the traditional spectroscopic methods, we introduce thermo-optical spectroscopy based upon the phase transformation of ice. With this, we can measure, not only the optical response of the NPs, but also thermal response. The heat generation is dependent upon the mesoscopic character of different clusters of NPs. The gold NPs are immobilized on a glass substrate and single particle spectroscopy is used to determine the location, number and geometry of different sized gold NP clusters. The thermal properties of the optically-excited gold clusters are established by combining theoretical calculations with experimental results. Our approach yields a quantitative measure of the amount of heat generated for single and small clusters of optically-excited gold NPs.

10:00 AM Invited

Thermodynamically Driven Controlled Self-Assembly of Fluorescent Semiconductor Nanocrystals within Polycrystalline Superstructures with Desired Optical Properties: Alyona Sukhanova¹; Alexander Baranov¹; Vladimir Oleinikov²; Mikhail Artemyev¹; Dmitry Klinov²; Igor Nabiev¹; ¹Université de Reims Champagne-Ardenne; ²Shemyakin-Ovchinnikov Institute of Bioorganic Chemistry, Russian Academy of Sciences

Self-assembly of colloidal nanocrystals (NCs) make it possible to obtain structures with high level of ordering and permit construction of patterns to be used in optoelectronics, photonics and biosensing. Thermodynamically driven self-organization allow large-scale production of nanowires and ordered 2D or 3D NC superlattices with little infrastructural investment. Among the nanosized building blocks, fluorescent NCs quantum dots (QDs) and rods (QRs) are especially appealing, because their photoluminescence quantum yield approximate 70% and their photostability and absorption determine brightness much higher than that of organic fluorophores, offering the quantum structures with advanced optical properties. We describe an operation and analyze the mechanism of "lab-in-drop", droplets of the aqueous solutions of QDs and QRs, in which a variety of superstructures with desired structural and optical properties may be produced. We will further demonstrate that organic dyes may be thermodynamically pre-crystallized and their NCs form the superstructures similar to those described for QDs.

10:30 AM

Wavelength Tuning of Surface Plasmon Resonance by Annealing Silver-Copper Nanoparticles: Makoto Hirai¹; Ashok Kumar¹; ¹University of South Florida

Silver-copper (Ag-Cu) nanoparticles have been synthesized by irradiating laser light on Ag and Cu plates. The peak absorption attributed to surface plasmon resonance (SPR) of the Ag-Cu nanoparticles appeared at 763 nm, which was approximately 200 nm higher wavelength than that of Ag nanoparticles. With increase in the annealing temperature from 300 to 548 K, the peak absorption attributed to SPR of the Ag-Cu nanoparticles shifted continuously from 763 to 437 nm. This fact proved that the peak absorption attributed to SPR can be tuned in the whole visible region by changing the annealing temperature only. Moreover, from the results of atomic force

microscopy and grazing angle x-ray diffraction, the SPR wavelength tuning is conjectured due to not the change in the surface morphology of the Ag-Cu nanoparticles but the increase in the electric conductivity of the nanoparticles induced by the precipitation of Cu atoms.

10:45 AM Break

10:55 AM Invited

Nanometals for Molecular Beacons and Optical Molecular Rulers:

*Geoffrey Strouse*¹; ¹Florida State University

Nucleic acids (RNA, DNA, etc) can change conformation to initiate disease states. Whether in Tuberculosis, Diphtheria, or simply the self-catalytic process in hammerhead RNA; such structural changes form the basis of molecular beacons for disease state detection. While optical techniques such as Forster Resonance Energy Transfer (FRET) are viable probes of conformation change, the interactions are limited to encounters typically < 10 nm. Nano-surface energy transfer (NSET) between a donor dye and the surface of a metal below 2 nm allows distances on the order of 21 nm to be sampled and more importantly utilized for kinetic analysis of a biomechanical event. A major advantage of NSET is the ability to observe simultaneous quenching events from several appended dyes, which in essence allows one to triangulate structure. We will explore the application and theoretical basis of NSET.

11:25 AM Invited

The Nanooptics of Metallic Nanoparticles: *Garnett Bryant*¹; ¹National Institute of Standards and Technology

Understanding the nanooptics of metallic nanoparticles is critical for applications in nanometrology, nanosensors, near-field imaging, nanoantennas, nanooptical communication, and metamaterials where large optical response by nanoscale structures is needed. This response is provided by surface plasmons that are excited in these confined structures. I discuss the plasmonic excitations of single and coupled metallic nanoparticles based on fully retarded calculations of their electromagnetic response. Results compared with experiment show that classical theory provides an excellent model. Similar resonances in isolated and coupled nanoparticles mask important differences in their response. For isolated particles, the response is dipole-like charge oscillation. In coupled systems, the interparticle gaps break the intraparticle symmetry, distort intraparticle dipolar response, and localize charge at the gaps. Interaction across gaps significantly redshifts the response and dramatically increases near fields. These effects become singular in the limit of nearly touching nanoparticles. Examples are discussed to illustrate these effects.

11:55 AM Invited

Peptide Coated Nanoparticles for Catalysis and Sensing Applications:

*Joseph Slocik*¹; Jeffrey Zabinski, Jr.¹; David Phillips¹; Rajesh Naik¹; Alexander Govorov²; ¹Air Force Research Laboratory; ²Ohio University

Nature exemplifies a great deal of control in the synthesis and assembly of inorganic materials. As a result, numerous synthetic approaches which mimic their biological counterpart have been inspired. In particular, peptides represent an encouraging approach given the vast matrix of biological templates and exquisite features of peptides. These features include programmable sequences, hydrophilic domains, variable isoelectric points, metal binding groups, and molecular recognition sites. For example, CoPt, Au, and Pt nanoparticles have been synthesized with sequences derived for these materials. With this toolbox of unlimited sequences, we have designed multi-functional peptides for the synthesis of gold particles, bimetallic catalysts, and nanoparticle sensors. Peptide coated gold nanoparticles are attractive for catalysis and sensing due to the peptide surface which can be used as additional templates or sensing elements. In the latter, these responded to a variety of targets both colorimetrically and conductively. Targets included metal ions, vapors, and chemical species.

12:25 PM

Microscopic Models of Hybrid Nanocrystals: Exciton-Plasmon Interactions and Photonic Properties: *Alexander Govorov*¹; Wei Zhang¹; Garnett Bryant²; ¹Ohio University; ²National Institute of Standards and Technology

We investigate the optical properties of hybrid superstructures composed of metal and semiconductor nanoparticles (NPs), and bio-linkers/polymers. Different architectures for a hybrid nano-complex result in qualitatively

different optical response. In many studies, metal NPs quench semiconductor NP photoluminescence (PL). However, a plasmon enhancement can be achieved by organizing many Au NPs into a spherical or cylindrical shell around a CdTe NP.^{1,2} We compute electromagnetic fields induced inside a NP superstructure using a multipole expansion approach to describe the optical response of these hybrid complexes. Plasmon enhancement of emission appears due to the increased photon-absorption probability (Ag structures) or from the stimulated emission processes (Au structures). ¹J. Lee, A. O. Govorov, J. Dulka, and N. A. Kotov, *Nano Lett.* 4, 2323 (2004). ²A. O. Govorov, G. W. Bryant, W. Zhang, T. Skeini, J. Lee, N. A. Kotov, J. M. Slocik, and R. R. Naik, *Nano Lett.* 6, 984 (2006).

12:40 PM

Self-Organized Periodic Array of Single Crystal Oxide Nano Islands:

*Michael Rauscher*¹; L. Zimmerman¹; S. Dregia¹; J. Lee¹; S. Akbar¹; ¹Ohio State University

We have deposited a gadolinium doped ceria thin film on an yttria-stabilized zirconia substrate using RF magnetron sputtering. Subsequent spalling of the thin film and a high temperature anneal combine to create a periodic array of single crystal islands with regular size, shape, and distance from their nearest neighbors. The features can be used as a template to transfer the pattern to other materials of interest, with the high strength of the material allowing for superior durability and fidelity of pattern transfer. In its current form, the nanostructure may find use in manipulation of single proteins and single molecules of DNA, as well as in nanoscale analytics. We predict the ability to establish long-range periodicity in the alignment of the islands creating a regular 2D network of nanochannels. These structures represent a tunable, self-assembling, low-cost, non-cleanroom means of producing nanoscale features suitable for nanofluidic channel fabrication and numerous other applications. In this work, we discuss the conditions necessary to create the novel nanostructure, and highlight the influence of annealing on the structure features. We have performed preliminary characterization of the system to determine its intrinsic usefulness for a range of optical, electronic, magnetic, and biological nanofluidic applications. We also discuss early efforts to create nanofluidic devices based on the pattern.

Wide Band-Gap Semiconductor Nanostructures: Session III

Sponsored by: The Minerals, Metals and Materials Society, TMS Electronic, Magnetic, and Photonic Materials Division, TMS: Electronic Materials Committee, TMS: Nanomaterials Committee, TMS: Thin Films and Interfaces Committee, TMS: Young Leaders Committee

Program Organizers: Ashutosh Tiwari, University of Utah; Haiyan Wang, Texas A&M; Minseo Park, Auburn University

Tuesday AM

February 27, 2007

Room: Oceanic 4

Location: Dolphin Hotel

Session Chairs: Florian Solzbacher, University of Utah; Nori Sudhakar, North Carolina State University

9:00 AM Invited

Toward the Achievement of Tailor-Made Solid-State Lighting with a Phosphor-Less Technology Based on InGaN/GaN Quantum Wells:

*Mitsuru Funato*¹; M. Ueda¹; K. Nishizuka¹; Y. Kawakami¹; Y. Narukawa²; T. Mukai²; ¹Kyoto University; ²Nichia Corporation

Semiconductor emitters inherently provide nearly monochromatic output light, and consequently present white light emitting diodes (LEDs) consist of an InGaN/GaN blue LED pumping a yellow phosphor. On the other hand, our approach is to use InGaN/GaN multi-facet structures to produce highly efficient multi-color emissions. When the {11-22} planes together with the conventional (0001) planes naturally appear as microfacets through the regrowth process on patterned (0001) GaN templates, InGaN/GaN quantum wells (QWs) grown on the {11-22} microfacets showed a higher emission efficiency [APL85, p.3122 (2004)] and rainbow color mixture [APL87, #231901 (2005)]. Furthermore, the synthesis of the emission spectrum from each microfacet QW, which differs from each other, enabled to produce



a desired output color including white [APL88, #261920 (2006)]. These observations lead us to believe that our proposed structure is promising for solid-state lighting that requires tailored color of emission.

9:35 AM Invited

MgZnO Nanoalloys: Optical, and Phonon Properties at Ambient and Extreme Conditions: Leah Bergman¹; Matt McCluskey²; Tsvetanka Zheleva³;

¹University of Idaho; ²Washington State University; ³Army Research Laboratory

The MgZnO alloy system may provide a new UV optically tunable family of wide bandgap materials. ZnO has the hexagonal wurtzite structure of bandgap ~ 3.3 eV while MgO has the NaCl cubic structure of bandgap ~ 7.5 eV; alloying above the solubility limit was recently realized. We present studies on the photoluminescence and Raman properties of MgZnO nanocrystallites, for Mg composition up to 25%, and of size ~30 nm. The photoluminescence was found to exhibit a 0.30 eV blueshift for our composition range, and the PL emission was analyzed in accordance to an excitonic-type recombination. Additionally, the LO Raman mode was found to exhibit a blueshift of ~ 33 wavenumbers as is expected for an alloy system. Temperature and pressure response of the nanoalloys will be discussed as well.

10:10 AM Invited

Advanced Carbon Materials for Vacuum Microelectronics and Thermionic Energy Converter Applications: Sanju Gupta¹; ¹Missouri State University

Carbon, the sixth most abundant element in the universe, has its appeal due to its versatile nature of chemical bonding resulting in diverse forms where diamond (tetragonal) and graphite (trigonal) are well-known allotropes. Unprecedented worldwide activity in nanostructured carbons is initiated by the discovery of C60 molecule and development of arc-discharge technique producing nanotubes followed by nanocrystalline diamond synthesized by varying traditional gas phase chemistry for poly-diamond. I will present recent activities related to chemical vapor deposited nanodiamond and nanotubes. Room temperature electron emitting materials (cold cathodes) are of vital importance enabling a variety of applications: flat panel displays, RF amplifiers, radar, electric propulsion for microsattelites, and portable X-ray sources for medical and security diagnostics. Traditional field emission (I-V) properties and temperature dependent field emission microscopy (T-FEEM) enabling real-time imaging of electron emission from nanotubes and nanodiamond will be presented. T-FEEM findings will be related to vacuum thermionic energy converters.

10:35 AM Invited

Nanoscale Magnetic Properties of Self-Assembled Magnetic Particles in Single and Multilayered Structures: Dhananjay Kumar¹; Alok Gupta¹;

¹North Carolina A&T State University

We have developed a smart thin film processing method based upon pulsed laser deposition to fabricate nanocrystalline magnetic materials with accurate size and interface control and improved magnetic properties. Using this method, single and multilayered samples having Fe and Ni particles in 5-60 nm size range have been produced by embedding these nanoparticles in thin films matrices of nonmagnetic layers such as wide band-gap Al₂O₃. By controlling the size distribution in confined layers, it was possible to tune the magnetic properties from superparamagnetic to ferromagnetic in a controlled way. The measurement of coercivity as a function of particle size indicates that the transition from single- to multi-domain region occurs at a lower particle size in later than in former which is thought to be due to stronger magnetic interaction among particle in multilayer structures. This work has been carried out under NSF-NIRT grant (DMR-0403480) at NCAT State University.

11:00 AM Break

11:20 AM

Effect of Al Doping on the Properties of Zn(Cu)O Based Diluted Magnetic Semiconductors: Deepayan Chakraborti¹; John Prater²; Jagdish Narayan¹;

¹North Carolina State University; ²Army Research Office

We report systematic studies on epitaxial growth and effect of Al doping on properties of Zn(Cu)O based dilute magnetic semiconducting thin films deposited onto sapphire c-plane single crystals. Epitaxial thin films were grown using pulsed laser deposition technique and x-ray diffraction and high resolution transmission electron microscopy were employed to study characteristics of thin film epitaxy, defects and interface with the sapphire substrate. Magnetic

measurements including magnetization as a function of applied magnetic field and temperature have been performed in a superconducting quantum interference device (SQUID) magnetometer and resistivity measurements have been conducted using four point probe resistivity measurement system. Room temperature ferromagnetism was observed in Zn(Cu)O thin films and doping with Al (n type) shows a decrease in both resistivity and saturation magnetic moment. This study provides us with new insight into analyzing the magnetic properties of these materials considering carrier induced and F-center mediated exchange mechanisms.

11:45 AM

Process Control and Gas Phase Dynamics during Laser Synthesis of ZnO Nanocrystals: Masashi Matsumura¹; Mevlut Bulut¹; Renato Camata¹;

¹University of Alabama, Birmingham

Zinc oxide (ZnO) nanocrystals are finding applications in numerous UV materials, nanodevices, and sensors. Here we combine laser ablation and aerosol processing to improve control over the synthesis of ZnO nanocrystals. Using differential mobility analysis we study the gas-phase dynamics of nanoparticles formed during KrF pulsed laser ablation of ZnO targets in inert atmospheres. Background pressures in the 70-760 Torr range and laser fluences of 1-5 J/cm² were used. Ablation at low laser fluences (<2 J/cm²) yields gas-suspended nanoparticle populations exhibiting bimodal size distributions with first peak at 5-15 nm and second at 35-50 nm. A bimodal model consisting of a set of population balance equations was developed to explain this observation. The model accounts for events inside the laser plume, where both nucleation and coagulation occur, and subsequent events outside the plume, where nucleation ceases. Model predictions are in good agreement with size distributions measured by differential mobility analysis.

12:10 PM

Optical and Electrical Properties of Ga-Doped Mg_{0.15}Zn_{0.85}O Thin Films: Wei Wei¹; Chunming Jin¹; Vikram Bhosle¹; Andy Doraiswamy²; Roger Narayan²; Jagdish Narayan¹;

¹North Carolina State University; ²University of North Carolina at Chapel Hill

Transparent oxide semiconductors are important materials for the electrical, optical and opto-electrical applications, such as conductive contacts, solar cells, laser diodes, ultraviolet lasers and thin-film transistors. Gallium- and aluminum- doped zinc oxide (ZnO) thin films have generated an immense interest as a new transparent oxide semiconductor material. In this report, we present our studies on as-deposited and annealed Ga-doped magnesium zinc oxide (MgZnO) thin films on amorphous fused silica substrates deposited by pulsed laser deposition. The samples were annealed in both vacuum and O₂ ambient. The structures of as-deposited and annealed films were characterized by X-ray diffraction (XRD) and transmission electron microscopy (TEM). The annealing effects on the optical properties of the films were studied by transmission, absorption, and photo-luminescence measurements. The annealing effects on electrical properties were also studied by Hall effect measurements and resistivity measurements.

12:35 PM

Silicon Carbide White Light Emitting Diodes: Sachin Ber¹; Nathaniel Quick²; Aravinda Kar¹; ¹University of Central Florida; ²Applicote Associates, LLC

White light emitting diodes (LEDs) have been successfully fabricated for the first time in silicon carbide substrates (4H:SiC and 6H:SiC) using a novel laser doping technique. Chromium (Cr), aluminum (Al) and nitrogen (N) were used as dopants. Cr and Al act as acceptors while N as a donor. Donor acceptor pair recombination between Al and N emits blue light output, while Cr and N recombination yields violet and green to red broadband output. The electroluminescent spectrum of the entire structure in a 4H:SiC substrate shows a white light broad spectrum extending from 400 nm up to 800 nm covering the entire visible light spectrum typical of white light. These LEDs were further analyzed by current-voltage and capacitance-voltage characteristics, Hall effect measurement, deep level transient spectroscopy and secondary ion mass spectroscopy for their electrical, optical and material properties.

1:00 PM

Pulsed Laser Deposition of Chromium-Doped Zinc Selenide Thin Films and Nanostructures for Mid-Infrared Laser Applications: Jonathan Williams¹; Renato Camata¹; ¹University of Alabama at Birmingham

Intra-shell transitions in divalent metal ions such as Cr²⁺, Fe²⁺, and Ni²⁺ (transition metals) incorporated in the lattice of wide band-gap II-VI semiconductors offer excellent prospects for affordable laser sources in the 3-5 μ m spectral range, a wavelength regime in high demand for numerous applications. In this study we have targeted the creation of Cr-doped ZnSe thin films and nanodots by pulsed laser deposition (PLD). Films and nanodots with nominal Cr concentration in the 10¹⁹-10²⁰/cm³ were deposited at various temperatures on GaAs (450-550 $^{\circ}$) and sapphire (600-700 $^{\circ}$) substrates through KrF excimer ablation of hot-pressed targets containing appropriate stoichiometric mixtures of Zn, Se, and Cr species in a helium background environment (10-4 Torr). Deposited films and dots were analyzed using X-ray diffraction to determine quality of crystalline structure and energy dispersive X-rays to assess the actual Cr concentration incorporated into the films. Photoluminescence measurements were carried out to evaluate emission in mid-infrared.

2007 Nanomaterials: Fabrication, Properties and Applications: Session IV

Sponsored by: The Minerals, Metals and Materials Society, TMS Electronic, Magnetic, and Photonic Materials Division, TMS: Nanomaterials Committee
Program Organizers: Wonbong Choi, Florida International University; Ashutosh Tiwari, University of Utah; Seung Kang, Qualcomm Inc.

Tuesday PM Room: Oceanic 3
February 27, 2007 Location: Dolphin Hotel

Session Chairs: Stephen Pearton, University of Florida; Seung Kang, Qualcomm Inc.

2:00 PM **Invited****Magnetism and Transport in Epitaxially Grown Fractals and Nanodots of Transition Metal Alloys and Compounds:** R. Budhani¹; ¹Condensed Matter – Low Dimensional Systems Laboratory, Indian Institute of Technology Kanpur

Magnetic materials in zero, one and two dimensional geometries such as clusters consisting of a few thousand atoms, wires with nanometer scale diameter and ultra thin films respectively, have been at the centre stage of condensed matter/materials physics, and are the basis of a myriad of technologies. The fundamental interest in low dimensional magnetic materials emanates from the fact that a macroscopic property such as magnetization, which is a consequence of the cooperative response of millions of spins, can be altered in a non-trivial manner if a large fraction of these spins are made to reside on the surfaces or interfaces of a magnetic entity. The dynamics of electron spin in low dimensional systems gives rise of a variety fascinating effects which can be the basis for a large number of technologies. One of the promising ways to synthesize low dimensional structures such as self-organized nanodots and self-similar fractals is through stress engineered epitaxial growth. We have successfully used pulsed laser ablation technique to grow low dimensional structures of high coercivity alloys such as CoPt and oxides of the La_{1-x}Sr_xMnO₃ family on single crystal substrates which provide either tensile or compressive strain. A suitable choice of growth temperature, vapor flux and lattice mismatch optimizes the balance of the surface, interface and elastic energies of the growing film and leads to the formation of self-organized and self-similar structures. This talk will focus on the dynamics of magnetic relaxation and spin-dependent electron transport in such structures.

2:25 PM **Invited****Functional Magnetic Nanostructures:** Srikanth Hariharan¹; ¹University of South Florida

Magnetic nanostructures are considered as basic building blocks in spin-electronic devices and high-density data storage. In practical applications, functional nanostructures generally consist of particle aggregates that are assembled or embedded in non-magnetic media. Precise mapping of

fundamental parameters like the magnetic anisotropy and switching fields over a wide range in temperature and magnetic fields, is essential to understand the influence of relaxation, interactions, surface structure and other phenomena that govern the dynamic magnetic properties in these systems. RF transverse susceptibility experiments, developed by us, provide a very sensitive and unique way to probe these features. This talk will feature our studies of the spin dynamics in functional magnetic nanostructures ranging from ordered arrays, polymer nanocomposites to ferrofluids. The potential broader applications of magnetic nanoparticles in RF devices, magnetic refrigeration and novel energy conversion will be discussed. Research supported by grants from NSF and DARPA/ARO.

2:50 PM

Domain Structures and Induced Magnetic Properties of Isolated and Interacting Iron (Fe) Ellipsoids inside Carbon Nanotubes: Prabeer Barpanda¹; ¹Rutgers University

Carbon nanotubes have attracted significant attention owing to its unique combination of mechanical strength and tunable electronic properties. Often, the single wall nanotubes (SWNT) are produced by catalysis taking iron as a precursor. This process results in introduction of residual iron nanoparticles inside the grown SWNT. The existence of these ferromagnetic iron nanoparticles can be used to introduce magnetic properties to SWNT, which can be used in various applications. In the current study, the domain structure of 20-200 nm long ellipsoidal iron nanoparticles has been investigated as a function of its size, ellipticity and aspect ratio, using a 3-D FFT modeling technique. The small size and high shape anisotropy forces a single domain structure. The coercivity of iron ellipsoids upon application of external magnetic field has been correlated to the possible interaction with covering nanotubes. Eventually, the magnetic interaction of two closely spaced ellipsoids inside SWNT has been scrutinized.

3:05 PM

Synthesis, L₁₀ Ordering, and Magnetic Properties of Fe₅₀Pt₃₅Rh₁₅ Nanoparticles: Mohammad Shamsuzzoha¹; Zhiyong Jia¹; David E. Nikles¹; J. W. Harrell¹; ¹University of Alabama

Fe₅₀Pt₃₅Rh₁₅ nanoparticles in the size range of 2 to 3.5 nm with the disordered fcc (A1) structure were prepared by the simultaneous reduction of platinum acetylacetonate, iron acetylacetonate and rhodium acetylacetonate. Upon annealing, the nanoparticles transformed to the fct (L₁₀) phase at temperatures that are lower than those observed in pure FePt nanoparticles. Maximum ordering was achieved at a temperature of about 500 $^{\circ}$ C. As prepared nanoparticles were superparamagnetic, but progressively became ferromagnetic with heating by partially transforming into the high-anisotropy L₁₀ structure. The coercivity reached a maximum of around 6000 Oe at an annealing temperature of about 500 $^{\circ}$ C.

3:20 PM

High-Temperature Magnetic Material: Nanostructured ϵ -Phase Fecon: Raghmani Ningthoujam¹; Nameo Gajbhiye²; Nori Sudhakar³; A. K. Nigam⁴; ¹Chemistry Division, Bhabha Atomic Research Centre, Mumbai; ²Chemistry Department, Indian Institute of Technology; ³Physics Department, Indian Institute of Technology; ⁴Tata Institute of Fundamental Research Centre

The Fe-Co-N alloy in hexagonal close packing structure (ϵ -phase) is a potential candidate for high-temperature magnetic materials applications such as inductive heads by virtue of their high saturation magnetization, high Curie-temperature and low coercivity. Here, the interesting structural and magnetic properties of the nanostructured ϵ -Fe_{3-x}CoxN (x = 0.4) system are presented. The magnetic phase is further probed by Mössbauer study which shows a mixture of sextet and doublet patterns for Co-doped ϵ -Fe₃N. The sextet pattern originates from the α -Fe particle coming out of nitride matrix and a hyperfine field of 40 Tesla is observed. The doublet is a characteristic of the superparamagnetic nature of Co-doped ϵ -Fe₃N system. ZFC and FC magnetizations show a blocking temperature of 74 K for Co-doped ϵ -Fe₃N. The magnetization and T_c increase with Co-doping.

3:35 PM **Break**



3:40 PM Invited

GaN_xZnO and InN Nanowires for Gas Sensing Systems: *Stephen Pearton*¹;

¹University of Florida

A variety of wide bandgap semiconductor nanowires have been examined for gas sensing applications. The transport properties of single nanowires shows them to be n-type in all cases. The most sensitive system for hydrogen detection is ZnO. A comparison of the sensitivities for detecting hydrogen with Pt-coated single ZnO nanorods and thin films of various thicknesses (20-350 nm) will be discussed. The Pt-coated single nanorods show a current response approximately a factor of three larger at room temperature upon exposure to 500ppm H₂ in N₂ than the thin films of ZnO. The power consumption with both types of sensors can be very small (in the nW range) when using discontinuous coatings of Pt. Once the Pt coating becomes continuous, the current required to operate the sensors increases to the μW range. The sensors can be integrated into a self-contained wireless hydrogen sensor system powered using ambient vibrations and light.

4:05 PM Invited

Incorporating Nanotechnology Innovations into Daily Life: *Reyad Sawaf*¹; ¹QuarTek Corporation

Nanotechnology innovations are being introduced in many technologies to provide better performance in many sectors. New generations of plastic like materials that are biodegradable are being introduced into consumer products that are more environmentally friendly. Nanoditives added to polymers to create consumer and environmental friendly polymers that can be incorporated in packaging, housing, medical devices, and many more applications. Which nanomaterials offer the best antimicrobial properties for certain applications? How can we create an antimicrobial environment in the home, the hospital, and on the job through nanotechnology? These applications and many more will be discussed.

4:30 PM

Functionalized Nanoelectrode Array on Microtip for Enzyme-Free Detection of Specific Analytes: *Somenath Roy*¹; *Aparna Datta Roy*¹; *Harindra Vedala*¹; *Wonbong Choi*¹; ¹Florida International University

The present study focuses on the fabrication of ultra sensitive nanoelectrode arrays on a tungsten microtip probe for fast and efficient detection of specific analytes in biological samples. Uniquely designed for in-vivo and in-vitro applications, this sensor assembly offers the dual advantages including the invasive attribute of a microtip as well as the ultra high detection capability associated with the array of carbon nanotubes or oxide nanowires grown on the microtip. In addition, the enzyme-free approach precludes the possibility of biofouling and protein denaturation related instability, which are characteristics to majority of the enzymatic sensors. Multi-walled carbon nanotubes (MWNs), or tungsten-oxide nanowire arrays are grown on the tungsten microtip by thermal CVD process. Surface functionalization of the nanoelectrode array is achieved through deposition of metal (Ru, Pt and Au) nanoparticles by electrochemical technique. Amperometric techniques are employed for quantitative detection of cholesterol and uric acid in human plasma.

4:45 PM

Precision Nanofabrication of Protein Nanostructures for Applications in Tissue Engineering and Drug Delivery: *Jiayu Liang*¹; *Shelley Dougherty*¹;

¹Worcester Polytechnic Institute

Based upon the need for more thorough nanoscale research we are developing simple, inexpensive, and scalable nanofabrication methods which accommodate different types of materials through the use of porous anodized aluminum oxide (AAO). Using optimized manufacturing conditions we have fabricated AAO with uniform, highly ordered arrays of 20 nm and 50 nm diameter pores. These AAO membranes have been coated with thin layers of gold via e-beam evaporation and used to produce protein nanotubes. Briefly, the inner walls of the AAO pores are treated with a binding agent that immobilizes proteins and allows the protein to form a tube structure within the pores. The protein coating remains within the pores to form a composite nanomaterial, or is liberated to yield free standing protein nanotubes with different nanostructures. Potential applications of those protein nanostructures include applications in tissue engineering and drug delivery will be briefly discussed.

5:00 PM

Critical Factors in the Microfluidic Production of Semiconductor Nanocrystals: *Fiona Doyle*¹; *Jeffrey Winterton*¹; ¹University of California

One of the most serious barriers to the widespread application of semiconductor nanocrystals is the current inability to manufacture them in realistic quantities. Nearly all advanced applications using these materials will require significant quantities of readily available high quality nanocrystals with tightly controlled properties, but current production techniques are limited to laboratory settings, restricted to milliliter volumes, and generally require post production processing to achieve the necessary size distributions. Microfluidic production techniques present an attractive alternative to conventional methods because they afford substantial improvements in the control over local reaction environments and could dramatically increase production rates by parallelization. However, microfluidic methods also present a unique set of challenges that must be fully understood for these methods to be implemented effectively. We are investigating the relationships between microreactor configurations and nanocrystal growth kinetics to identify factors critical to increasing production of high quality materials in order to meet demand.

5:15 PM

A General Route to Porous Nanostructured Oxides: *Qing Yang*¹; ¹University of Science and Technology of China

Porous nanostructured materials have attracted much attention because of their potential for advanced applications in catalysis, separation technologies, electronic engineering, and manufacturing of optical devices. The chemical synthesis of inorganic materials with porous structures has been especially motivated by the requirements to reveal their structure- and morphology-dependent properties and to achieve their specific applications. Up to now, the porous nanomaterials such as silica, alumina, silicate/aluminosilicate, oxides, and carbon etc have been obtained through various strategies including hydrothermal, sol-gel, template-assisted ones. In the present work, a simple process of precursor calcinations was employed for the fabrication of several porous nanostructured oxides such as MgO, Fe₂O₃, CeO₂, Y₂O₃, CuO, LaMnO₃ etc. Experiments demonstrated that the conditions of reaction temperature, use of capping materials, concentration of reactants played important role in the growth of the final products. Meanwhile, the growth mechanism and possible chemical properties of the oxides were tentatively investigated.

5:30 PM

Core-Shell AgCo Cluster Assembled Materials: *Marc Hou*¹; *Evgueny Zhurkin*²; *Thibaut Van Hoof*¹; ¹Université Libre de Bruxelles; ²St Petersburg Technical University

Small AgCo clusters are modelled by Metropolis Monte Carlo. They are formed by a Co core surrounded by a non-crystalline Ag shell. Their assembling by deposition with 0.1, 0.25 and 0.5 eV per atom kinetic energy is modelled by Molecular Dynamics. The nanostructure morphology strongly depends on the deposition energy. The films formed by deposition at 0.25 and 0.5 eV/at. are stable once detached from their substrate and they are used to model bulk cluster assembled systems. Slow isothermal mechanical deformation is modelled realistically and we find that a uni-axial tensile stress generates no cracks and improves elastic properties. Pores resulting from the deposition shrink but the structural features of the Co and the Ag systems are not altered by the deformation. As a consequence, superplasticity is found, whereby the Ag system takes over most of the deformation.

5:45 PM

Synthesis of Nanosized Tungsten and Tungsten Carbide Powder: *Guo Zhimeng*¹; *Luo Ji*¹; *Hao Lu*¹; *Lin Tao*¹; *Lu Guangfeng*¹; ¹School of Materials Science and Engineering, University of Science and Technology Beijing

Nanosized tungsten powder was synthesized by means of different methods and conditions with nanosized WO₃ powder; the powder and the intermediate products were characterized by using XRD, EM, TEM, B.E.T and SAXS (X-ray diffractometer/Kratky small angle scattering goniometer). It has been shown that nanosized WO₃ can be completely reduced to WO₂ at 600° after 40min, and WO₂ can be reduced to W at 700° after 90min, moreover, W particle's mean size is less than 40nm. Furthermore, the process of WO₃>WO₂>W excelled the process of WO₃>W which can stably get nanosized tungsten powder with less grain size. As nano-tungsten powder and ethanol as carburizer, nano-WC powder is synthesized by gas

phase carbonization at low temperature. It is studied the mechanism of nano-tungsten powder's carbonization by nano-carbon black, acetylene, carbinol and ethanol, and the carbonization craft is determined. When the temperature is below 1050°, nano-tungsten powder cannot be carbonized completely to get nano-WC powder by nano-carbon black in the hydrogen atmosphere. At the temperature below 950°, nano-WC powder can not be produced by the carburization agent of carbinol. Nano-tungsten powders can be carbonized by ethanol to get nano-WC particle at the temperature over 900° and by controlling the flow rate of ethanol, carbon build-up at high temperature can be avoided. Finally using tungsten powders of 30nm, ethanol gas flow rate of 100ml/min and hydrogen flow rate of 1L/min and holding at temperature of 900° for 90 minutes, nanoWC powder is produced whose area of specific surface is 12.483m²/g, mean size is 74.9nm by SAXS, total carbon content is 6.18% and the particles are approximately spherical.

8th Global Innovations Symposium: Trends in Materials and Manufacturing Technologies for Energy Production: Session I

Sponsored by: The Minerals, Metals and Materials Society, TMS Materials Processing and Manufacturing Division, TMS: Global Innovations Committee

Program Organizers: Joy Hines, Ford Motor Company; David Bahr, Washington State University; John Smugeresky, Sandia National Laboratories

Tuesday PM Room: Australia 3
February 27, 2007 Location: Dolphin Hotel

Session Chair: David Bahr, Washington State University

2:00 PM

The Distribution of Oxygen in mc-Silicon Ingots for Solar Cell Applications: *Marisa Di Sabatino*¹; Eivind Ovrelid²; Espen Olsen²; ¹Norwegian University of Science and Technology; ²SINTEF

Multi crystalline silicon is one of the most used materials for solar cell application. The quality and efficiency of solar cells depend, among other factors, on impurity content in general and oxygen content in particular. This work aim to study the distribution of oxygen along different ingots produced in laboratory. The ingots were mc-silicon doped with boron (p-type) and phosphorous (n-type). Oxygen content was measured by an FT-IR equipment on selected samples for each ingot. A recently developed mathematical model based on the Scheil equation was used for evaluating the distribution of oxygen and the values were compared with the experimental results. The mathematical model shows deviation from the experimental results which lead to conclude that, in order to predict the distribution of oxygen, the evaporation of SiO has to be taken into account.

2:25 PM

In Situ Passivation during High Pressure Gas Atomization of Improved MRE₂Fe₁₄B for High Performance Permanent Magnet Applications: *Peter Sokolowski*¹; Iver Anderson²; Wei Tang²; Yaqiao Wu²; Kevin Dennis²; Matthew Kramer¹; R. McCallum¹; ¹Iowa State University; ²Ames Laboratory

A modified gas atomization chamber allows for a novel approach to in situ passivation of solidified particle surfaces through injection of a reactive gas, nitrogen trifluoride (NF₃). The ability to control surface chemistry during processing of fine RE-Fe-B powders leads to advantages over current processing methodologies. In particular, the capability to coat particles while "in flight" may eliminate the need for post atomization treatment, otherwise a necessary step for oxidation and corrosion resistance. Formation of rare earth (RE) type fluorides on the surface was evidenced through electron spectroscopy (XPS) and auger analysis. Gas fusion analysis on coated powders (dia. <45µm) indicated a reduced oxygen concentration of 580ppm. Thermogravimetric analysis (TGA) revealed a decreased rate of oxidation at elevated temperatures up to 300°C. Passivation of RE-containing powder would be required for large-scale manufacturing of bonded magnets for use in high performance applications. Support from DOE-EERE-FCVT through Ames Lab contract W-7405-ENG-82.

2:50 PM

Magnetostriction Studies in Single Crystals of Iron-Gallium Alloys: *Tanjore Jayaraman*¹; Nakorn Srisukhumbowornchai²; Swieng Thuanboon¹; Sivaraman Guruswamy¹; ¹University of Utah; ²King Mongkut's University of Technology Thonburi

Gallium addition to iron results in a dramatic increase in the magnetostriction of Fe. Fe-Ga alloys are of immense current interest for use in sensor and actuator applications due to their attractive combinations of large low-field magnetostriction, high mechanical strength, ductility, toughness, and low associated cost. In our earlier work using polycrystalline and textured Fe-Ga alloys, it was shown that magnetostriction of Fe is dramatically increased by addition of non-magnetic Ga. Here a detailed study on single crystals of Fe-Ga alloys with compositions between Fe-15 at.% Ga and Fe-27.5 at.% Ga is reported. Single crystals of were grown using Bridgman single crystal growth technique. Rocking curves in conjunction with detector and phi scans were used for orientation determination. Single crystals were oriented within 0.25 degrees off the desired orientation. Measurements of magnetic properties and magnetostriction coefficients 3/2(π100) and 3/2(π111) are reported.

3:15 PM

Studies of Magnesium Oxide-Coated Lithium Cobalt Oxide Materials: *Jinlin Lu*¹; Xiuqing Zhai²; Yan Fu²; ¹Shenyang Institute of Chemical Technology; ²Northeastern University

Lithium cobalt oxide (LiCoO₂) powders, utilized as cathode materials in lithium-ion secondary batteries, have been synthesized through the high temperature heating process. However, the discharge capacity decreases quickly, especially after circulating many circles. In order to improve the long cycle capability of LiCoO₂, excess magnesium oxide-coated LiCoO₂ materials were synthesized by homogeneous precipitation. The testing result shows that the long cycle property of LiCoO₂ coated by magnesium oxide is better than that of the pure LiCoO₂.

3:40 PM Break

3:55 PM

Corrosion Behavior of Iron-Gallium Alloys in Aqueous Environments: *Tanjore Jayaraman*¹; Nakorn Srisukhumbowornchai²; Michael Free¹; Sivaraman Guruswamy¹; ¹University of Utah; ²King Mongkut's University of Technology Thonburi

Iron-gallium alloys have attracted lots of attention for use in sensor and actuator applications due to an excellent combination of large low-field magnetostriction, high mechanical strength, good ductility and low cost. In our earlier studies on magnetostriction of polycrystalline, textured and single crystals of Fe-Ga alloys we have shown that Fe-Ga alloys are excellent alternative to existing rare earth based giant magnetostrictive materials for use in a wide range of sensors and actuator applications. This paper reports the very first measurements of the corrosion behavior of Fe-Ga and Fe-Ga-Al alloys in a wide range of corrosive environments from strongly acidic to basic environments that include seawater, and various concentrations of HNO₃, H₂SO₄, NaOH and HCl. In general, the corrosion behaviors of these alloys were found to be excellent.

4:20 PM

Investigation of Steel-Compound-Parts Manufactured by Indirect Impact Extrusion: Bernd-Arno Behrens¹; Friedrich-Wilhelm Bach²; Kai Moehwald²; Armin Kueper¹; ¹Institute of Metal Forming and Metal Forming Machine Tools (IFUM), University of Hanover; ²Institute of Materials Science (IW), University of Hanover

Due to the high output of production lines and the superior metal properties of steel, many automotive components are forged. Because of the high dynamic and tribological loads of gears a hard surface layer of the teeth is needed to increase wear resistance. Simultaneously the bulk material needs to stay ductile to prevent fracture of the teeth. To adjust the material properties of forged gears in this way the so-called Compound-Forging was invented. For this process slugs made from non-tempering steels, like case-hardening steels, are forged together with tube-sections made from tempering steels. During the forming process both materials are forge-welded together. In this paper a die-concept for the investigation of the applicability of Compound-Forging to indirect impact extrusion is presented. The aim of this process is to transfer the technology to not only forge gear wheels but also forge shaft-like parts with hard surfaces and ductile bulk material.



4:45 PM

Development of Advanced Thermal Barrier Coatings for Mo-Si-B

Materials: Joshua Jackson¹; David Olson¹; Brajendra Mishra¹; Angelique Lasseigne¹; ¹Colorado School of Mines

The development of an advanced thermal barrier coating for Mo-Si-B turbine materials will be discussed. The controlling kinetics are characterized to enable deposition of a controlled-thickness thermal barrier coating with a functionally graded architecture. Deposition of aluminum, including silicon, silica, and mullite particulate, is made possible at low temperatures, to prevent excessive diffusion reactions, by use of organic electrolysis. The reaction kinetics of diffusion and subsequent oxidation to form mullite-based thermal barrier coatings are explored.

5:10 PM

Processing Gas Turbine Components with High Pressure Water Jet:

William Thompson¹; ¹Springfield Manufacturing LLC

High pressure, multi axis water jet processes are being applied to a wide range of gas turbine hot gas path components. Removal of the environmental coatings applied by thermal spray processes can be removed without generating toxic waste. Water jet machining removes all impurities from the substrate resulting in a surface prepared for subsequent metallurgical operations. Cooling schemes can be generated via water jet after parts have been coated, rather than employing a variety of maskants to prevent intrusion of coatings in cooling passages. No metallurgical damage such as recast layer, intergranular attack, or pitting occurs in water jet applications. This presentation illustrates how high pressure water jet has evolved to become the choice of environmentally sensitive turbine manufacturers.

5:35 PM

Hydrogen Effects on Laser Engineered Net Shape (LENS) Repaired

Weldments: Paul Korinko¹; Thad Adams¹; ¹Savannah River National Laboratory

Laser Engineered Net Shape (LENS[®]) processing is a unique process that uses powder metals that are fused into a net shaped product in-situ using a laser beam. LENS[®] can be used to build new parts or as a repair process and is being considered as an innovative repair method to improve process efficiencies and to reduce manufacturing times. For this project, LENS[®] was used as a repair technique for mismachined components. Stainless steel pressure vessel components were prepared with oversized bores and intentionally introduced linear gouges. The damaged areas were repaired with LENS materials, machined to the required diameter, resistance forge welded, exposed to hydrogen and burst tested. The LENS[®] process as it pertains to repairing stainless steel components, the hydrogen charging, the proof testing, and post test metallurgical evaluation will be discussed. This work was conducted for the Department of Energy under contract DE-AC09-96SR18500.

Advanced Metallic Composites and Alloys for High Performance Applications: Al Alloys and Composites

Sponsored by: The Minerals, Metals and Materials Society, ASM International, TMS Structural Materials Division, ASM Materials Science Critical Technology Sector, TMS/ASM: Composite Materials Committee, TMS/ASM: Mechanical Behavior of Materials Committee

Program Organizers: Awadh Pandey, Pratt and Whitney Rocketdyne; Kevin Kendig, Air Force Research Laboratory; John Lewandowski, Case Western Reserve University

Tuesday PM

Room: Europe 10

February 27, 2007

Location: Dolphin Hotel

Session Chair: Kevin Kendig, US Air Force

2:00 PM

Precipitation of Al₃(Sc,Zr) Particles in an Al-Zn-Mg-Cu-Sc-Zr Alloy during Heat Treatment:

Marat Shaghiev¹; Svetlana Senkova¹; Oleg Senkov¹; ¹UES, Inc.

It has been recently shown that small additions of Sc and Zr to 7000 series aluminum alloys may considerably improve both strength and ductility, which

is associated with precipitation of fine coherent Al₃(Sc,Zr) particles. These particles also increase resistance to recrystallization and promote formation of a stable refined microstructure. The Al₃(Sc,Zr) particles precipitate from a supersaturated solid solution during first heat treatment and cannot be dissolved after that, while the strengthening effect depends on their size and number density. Therefore, it is necessary to optimize precipitation of the Al₃(Sc,Zr) particles, in order to achieve superior balance of mechanical properties. In the present work, the effect of heat treatment conditions on microstructure and tensile properties of a developmental 7000 series aluminum alloy SSA018 modified with Sc and Zr was studied, with special emphasis on the analysis of size and number density of the Al₃(Sc,Zr) particles, and the strengthening mechanisms were discussed.

2:20 PM

Aluminum - Intermetallic Particulate Composites:

G.S. Murty¹; Brian Gordon¹; ¹Touchstone Research Laboratory

Aluminum (Al) matrix composites are attractive for various structural applications due to their excellent specific properties. The work being presented involved developing a new type of Al matrix composite with intermetallic particulate reinforcement produced by standard rapid solidification and powder metallurgy processing. The uniqueness of this type of composite lies in the compatibility between the metal matrix and the intermetallic phase. As a result, the mechanical properties are superior to other composites with ceramic particulates. The objectives of this work were to process the composites and explore their mechanical properties in order to identify the composite and process parameters that give the best combination of properties. The results to date demonstrate that this material has a higher specific strength than 7075-T73 at temperatures greater than 200F, and a specific strength similar to Ti-6Al-4V at 500F.

2:40 PM

Carbon Fiber with Ni-Coated Reinforced Aluminum Matrix Composites:

Han Bianhua¹; Tianjiao Luo¹; Chunlin Liang¹; Guangchun Yao¹; Yihan Liu¹; ¹Northeastern University

The aluminum matrix composites reinforced by carbon fiber have attractive properties. But manufacture of aluminum matrix composites reinforced by carbon fiber have been limited by low wettability and interfacial reaction between carbon fiber and molten aluminum. The nickel coated carbon fibers can improve the wettability between carbon fibers and aluminum, and can inhibit the harmful interfacial reaction for its stable coating structure, so nickel plating is a simple and easy method to improve the surface behaviour of carbon fiber. This paper introduces the process of electroplating with nickel on carbon fiber. Microscopic structure of nickel coating and the effect of nickel plating rate and coating structure with the solution composition, current density and electroplating time have been studied. The principle of nickel plating is also researched. The aluminum matrix composites is reinforced by carbon fiber with nickel coating, and the composite effect between aluminum and carbon fiber is observed.

3:00 PM

Fabrication of Carbon Nanotube Reinforced Aluminum Alloy Matrix

Composite: Chitoshi Masuda¹; Yu-Usuke Nishimiya¹; ¹Waseda University

Maluti-walled carbon nanotube reinforced Al-12wt%Si eutectic aluminum alloy matrix composite was fabricated by powder metallurgy and consolidated by SPS method and the microstructures were examined. The amounts of carbon nanotubes in powder milled by ball milling analyzed by chemical analysis were nearly equal to those added. The Knoop hardness of the powders milled and the composites increased with increasing the amount of carbon nanotubes up to about 5wt%. The density of composites measured by Archimedes method was more than 95% up to the amount of carbon nanotubes of 5wt%. The Young's modulus of the composites evaluated by a ratio of longitudinal ultrasonic wave velocity to transverse one also increased up to about 100MPa for the carbon nanotubes of 5wt%, while for over the carbon nanotubes the Young's moduli was tended to be saturated with increasing the amount of carbon nanotubes up to about 10wt%. The elastic moduli of composites estimated using the rule of mixture were nearly equal to the experimental values. The strengths of the composite containing the amount of carbon nanotubes of 2 and 5wt% evaluated on the basis of the linear relationship between hardness and tensile strength were about 470-534 MPa and 690 MPa, respectively, while for the unreinforced materials was about 200 MPa. The estimated strength drastically

increased due to the content of carbon nanotubes. The observation of TEM revealed that the carbon nanotubes were dispersed in the matrix.

3:20 PM Break

3:40 PM

Filament Winding of Metal Matrix Composites: *Brian Gordon*¹; ¹Touchstone Research Laboratory

Metal matrix composites (MMCs) are important for applications requiring better specific properties and a higher temperature capability than what can be achieved with conventional monolithic metals and organic composites. A method for producing MMC components using a low-cost filament winding process and test results to date are presented. Hydrostatic burst testing has been conducted on 4-inch diameter cylinders produced with both hoop and helical plies under conditions that produce either a uniaxial or biaxial stress state in the cylinder wall. In addition, axial tension and torsional testing have been completed on cylinder specimens. This testing will lead to the development and refinement of predictive models that can be used for designing pressure vessels for various defense and commercial applications. The MMC filament winding process is in the process of being scaled up for producing larger specimens for continued testing and characterization.

4:00 PM

Reinforcement Homogeneity and the Fracture of Discontinuously Reinforced Aluminum: *Garth Wilks*¹; *J. E. Spowart*¹; ¹Wright Patterson Air Force Base

Deformation processing (extrusion) is used to homogenize reinforcement distribution in a discontinuously reinforced aluminum matrix composite (DRA 6092/SiC/25p). Reinforcement distribution is quantified using the homogenous length scale technique. Toughness from several orientations of three different extrusions is measured via chevron notch short rods in peak aged material. It is shown that extrusion has a positive influence on reinforcement homogeneity and toughness in each orientation. Generally, a strong positive relationship between fracture toughness and fracture surface roughness is also observed. A fractal analysis technique is developed and used on fracture surface profilometry data to quantify crack path deflection. This crack path deflection is explained by microstructural observations, and used to incorporate the influence of reinforcement distribution into the Majumdar & Pandey model for fracture in DRA.

4:20 PM

In Situ Fiber Strength Distribution in Nextel-Reinforced Aluminum Matrix Composites: *Joseph Butler*¹; *Jeffrey Schultz*¹; *Stephen Kampe*¹; ¹Virginia Tech

The fracture surfaces of individually-tested alumina Nextel™ continuous composite fibers were examined and a measurement of critical flaw size was attempted. From this information, an empirical relationship between flaw size and fracture strength was developed. A comparison to similar data obtained from identical fibers but embedded within the matrix of a MetPreg™ continuous fiber aluminum matrix MMC enables the assessment of the influence of processing on the resulting fiber strength distribution in the MMC. The results indicate that the average in-situ strength of the fibers is increased when incorporated within the metal matrix composite.

4:40 PM

Thermal Management of Cast Carbon Fiber-Al Composites: *Pradeep Rohatgi*¹; *Vindhya Tiwari*¹; *Nikhil Gupta*²; ¹University of Wisconsin; ²Polytechnic University

A modified squeeze cast process is used to synthesize the carbon fiber-Al 2014 alloy composites. Carbon fibers are extended out of the mold and cooled to increase the rate of heat extraction from the solidifying melt. Such an arrangement minimizes the effect of difference in the thermal expansion coefficients of carbon fibers and the matrix alloy. The resulting composites are remelted and solidified. The effect of heat extraction on solidified layer on the fiber surface is analyzed theoretically and experimentally. The analysis is conducted at various melt temperatures to observe the effect of temperature on the thickness of the solidified layer with respect to the cooling rate. The resulting composites are found to have better quality than that obtained from the traditional squeeze cast process.

Advances in Computational Materials Science and Engineering Methods: Phase Field Methods II

Sponsored by: The Minerals, Metals and Materials Society, TMS Structural Materials Division, TMS: Biomaterials Committee, TMS/ASM: Computational Materials Science & Engineering

Program Organizers: Koen Janssens, Paul Scherrer Institute; Veena Tikare, Sandia National Laboratories; Richard LeSar, Iowa State University

Tuesday PM Room: Europe 7
February 27, 2007 Location: Dolphin Hotel

Session Chair: Koen Janssens, Paul Scherrer Institute

2:00 PM Introductory Comments

2:05 PM Invited

A 3D Cellular Automaton Dislocation Model for FCC Crystals and Its Role in Multiscale Materials Modeling: *Qizhen Li*¹; *Peter Anderson*²; ¹University of Nevada, Reno; ²Ohio State University

Dislocation motion plays a big role in mechanical properties of crystalline materials and dislocation dynamic modeling helps us understand the various behaviors of dislocations. We introduce a three-dimensional cellular automaton (CA) model here to study the evolution of dislocation configurations in FCC single crystals. Three examples are employed to illustrate the features of our model. The three examples are Frank-Read source operation in an infinite, isotropic, elastic material with isotropic and also anisotropic line energy, and dislocation cross slip in the vicinity of a fixed dislocation that is parallel to and repels the initial dislocation line. A comparison is made between our CA dislocation model and other dislocation dynamics models. We also explain the relation among atomistic modeling, dislocation dynamics modeling and continuum modeling, and indicate the position of our model in multiscale materials modeling.

2:40 PM Question and Answer Period

2:45 PM

Phase Field Modeling of Microstructural Evolution in Titanium Alloys: *Ning Ma*¹; *Yunzhi Wang*¹; ¹Ohio State University

In this presentation we review our recent efforts in developing the phase field modeling techniques into designer tools for microstructural engineering in Titanium alloys such as Ti-64 and Ti-6242 during thermal processing. In particular, a mobility database for these alloys has been developed. Effect of anisotropy in interfacial energy and mobility on the formation of sideplate colony and basketweave structures are examined in three-dimensions. The models developed are integrated with Pandat thermodynamics database through a flexible data passing scheme. The work is supported by AFRL under Metals Affordability Initiative (MAI) project.

3:10 PM Question and Answer Period

3:15 PM

Coupled Composition-Deformation Phase-Field Method for Biological Membranes: *Chloe Funkhouser*¹; *Francisco Solis*²; *Katsuyo Thornton*¹; ¹University of Michigan; ²Arizona State University

We present a method for modeling phase transition and corresponding morphological evolution of binary lipid membranes with planar and spherical background geometries. The composition field is coupled to the deformations of the background geometry by the introduction of composition-dependent spontaneous (preferred) curvatures and bending stiffness in the Helfrich Hamiltonian. The evolution of the composition field is described by a Cahn-Hilliard-type equation, while the deformation field is described by a damped relaxation. Our method explicitly treats the full nonlinear form of the local geometric invariants of the surface: the local metric, mean curvature, Gaussian curvature, and the differential operators associated with them. The model is applied to examine morphological evolution and stability of lipid membranes.



3:40 PM Question and Answer Period

3:45 PM Break

4:15 PM

Microscopic Phase-Field Simulation of Morphological Evolution in $Ni_{75}Al_xV_{25-x}$ Alloy: Yongsheng Li¹; Zheng Chen¹; Yanli Lu¹; Yongxin Wang¹; ¹Northwestern Polytechnical University

The Ni_3X style precipitates play an important role in enhancing the mechanical properties of alloy. The morphology evolution and coarsening dynamics of gamma prime and theta in $Ni_{75}Al_xV_{25-x}$ alloys are studied by using the microscopic phase-field model based on the Onsager-type dynamic equation. Due to the anisotropy elastic interactions between the precipitates, the particles align along the dominant directions at spatial. The variations of average diameters of gamma prime and theta indicates that the growth and coarsening are dominant at the early and late-stage respectively. The well-known LSW law (Lifshitz-Slyozov-Wagner) is not obtained in the elastic interaction systems. In addition, the dynamic scaling regimes of late-stage coarsening are attained, which demonstrates that the scaling behavior of structure function is also applicable for the elastic interaction systems. The simulated results are very similar to the experimental observations.

4:40 PM Question and Answer Period

4:45 PM

Phase Field Study for Self-Assemble of the Second Phase Particles in Coherent Phase Transition: Pil-Ryung Cha¹; Jin-You Kim²; ¹Kookmin University; ²Seoul National University

Phase field model has attracted many scientists due to its ability in describing the complex pattern formations occurring in Nano- and Meso-scales. In this presentation, we are going to introduce the phase field model and to review our recent development and application of phase field model for self-assembled second phase particles in coherent phase transition. We describe the phase field study for the effect of the misfit strain on the growth shape and alignment of the coherent precipitates in Ni-base superalloy system. We observe that coherent misfit strain and anisotropy of elastic constants induce the interface instability that brings about the particle splitting and the self-assembled alignment of particles. Finally we discuss about the mechanisms of the particle splitting and alignment.

5:10 PM Question and Answer Period

5:15 PM

Phase Field Based Microstructural Evolution Modeling of Binary and Ternary Nb-Si Alloys: Sujoy Kar¹; Sundar Amancherla¹; Bernard Bewlay²; Ying Yang³; Austin Chang³; ¹GE India Technology Center Pvt Ltd; ²GE Global Research; ³University of Wisconsin

Nb-Si based alloys have been studied extensively over the last decade and are regarded as the next generation alloys for high-temperature structural applications due to their low density and better properties. Microstructures of these alloys can be complex and vary significantly with the addition of elements such as Ti and Hf. Hence an improved understanding of the phase stability and the microstructural evolution of these alloys is essential for optimization of these alloys for high-temperature applications. In the present paper we describe the binary and ternary microstructural evolution modeling results on the dendritic, eutectic and peritectic solidification of the Nb-Si based alloys, obtained using phase-field simulations. The effect of parameters viz. heat extraction rate, the ratio of the diffusivity of the solute in liquid to solid, the interfacial energy of liquid and solid interface on the microstructural evolution during solidification is discussed in detail.

5:40 PM Question and Answer Period

Advances in Microstructure-Based Modeling and Characterization of Deformation Microstructures: Modeling of Deformed Structures II

Sponsored by: The Minerals, Metals and Materials Society, ASM-MSCTS; Texture and Anisotropy Committee, ASM-MSCTS; Texture and Anisotropy Committee

Program Organizers: Reza Shahbazian Yassar, Center for Advanced Vehicular Systems; Sean Agnew, University of Virginia; Jiantao Liu, Alcoa Technical Center

Tuesday PM Room: Europe 1
February 27, 2007 Location: Dolphin Hotel

Session Chairs: Mark Horstemeyer, Mississippi State University; Stuart Wright, EDAX-TSL

2:00 PM

Microstructural Modeling of Grain Subdivision and Large Strain Failure Modes in F.C.C. Crystalline Materials: Omid Rezvanian¹; Mohammed Zikry¹; A.M. Rajendran¹; ¹North Carolina State University

The major objective of this research is to develop a unified physically-based representation of microstructures in f.c.c. materials to investigate finite inelastic failure modes and scenarios at different physical scales that occur due to a myriad of factors, such as texture, grain size and shape, grain subdivision, heterogeneous microstructures, and grain boundary misorientations and distributions. The microstructurally-based formulation is based on coupling a multiple-slip crystal plasticity formulation to three distinct dislocation densities, which pertain to statistically stored dislocations (SSDs), geometrically necessary dislocations (GNDs), and grain boundary dislocations (GBDs). This dislocation density based multiple-slip crystal plasticity formulation is then coupled to specialized finite-element methods to predict the scale-dependent microstructural behavior, and the localized phenomena that may contribute to failure initiation for large inelastic strains. The evolution of these dislocation-densities is used to predict how crystallographic and noncrystallographic microstructures relate to intragranular and intergranular failure at different scales.

2:20 PM Invited

Atomistic Processes of Phase Transformation and Dynamic Recrystallization in Intermetallic Titanium Aluminide Alloys: Fritz Appel¹; ¹GKSS Research Centre Geesthach

Intermetallic titanium aluminide alloys are multiphase assemblies with complex microstructure and constitution, involving gamma-TiAl, alpha-2, beta, B2 and orthorhombic phases. The earlier stages of phase transformation and dynamic recrystallization occurring upon hot-working were investigated at the atomic scale by high-resolution electron microscopy. Accordingly, the conversion of the microstructure is triggered by a particular deformation state and non-equilibrium phase composition. The beta/B2 is apparently unstable under tetragonal distortion, which gives rise to the formation the B19 phase via distinct shuffle displacements. These processes lead to a modulated microstructure, which is comprised of several stable and metastable phases. The phase transformations are accomplished by the propagation of ledges and the formation of twin structures. Large ledges can apparently easily be rearranged into intermediate metastable structures, which serve as precursor for the nucleation of new grains.

2:45 PM Invited

Elastic-Plastic Self-Consistent Model Including Grain Reorientation Due to Twinning: Bjorn Clausen¹; Carlos Tome¹; Donald Brown¹; Sean Agnew²; ¹Los Alamos National Laboratory; ²University of Virginia

Over the last decades self-consistent polycrystal deformation models have successfully been used to investigate deformation behavior of metals. The elastic-plastic self-consistent model (EPSC) is traditionally used at low degrees of deformation, less than 10% strain, as it does not take into account the lattice rotations due to slip or twinning. In the present work, the EPSC model has been extended to include the grain reorientation due to twinning, enabling the application of the model to cases where twinning is the predominant deformation mechanism in the early stages of plasticity. One

such case is compressive loading of extruded magnesium; due to the texture formation during extrusion, most grains are favorably oriented for twinning when compressed along the extrusion axis. Neutron diffraction measurements of internal strains in extruded magnesium during compressive loading have been used in combination with the model predictions to investigate the initial stress state in the twins.

3:10 PM

Forming Limit Diagram Prediction for Non-Cubic Metals: Application to Magnesium Alloys: *C. John Neil*¹; Sean Agnew¹; ¹University of Virginia

The poor formability of non-cubic metals, such as magnesium alloys, is often attributed to their strong single crystal plastic anisotropy and frequently strong crystallographic texture. The Marciniak-Kuczinski (M-K) approach to forming limit diagram (FLD) prediction, based upon plastic instability within a pre-existing flaw has been widely applied to examine the effect of basic materials constitutive parameters on formability. In particular, the role of crystallographic texture has been successfully incorporated utilizing polycrystal plasticity (Taylor-type) models for cubic metals. In this study, the M-K approach has been applied to the case of hexagonal close packed magnesium alloys using a viscoplastic self-consistent (VPSC) polycrystal simulation tool. The effect of texture on the formability of magnesium alloys is explored and optimal textures for specific forming operations are presented. Further attention is given to the effects of forming temperature and strain rate, and constitutive parameters, such as rate sensitivity and slip system activity.

3:30 PM Invited

Internal State Variable Modeling of Structure-Property Relationships in Deformed Microstructures: *Mark Horstemeyer*¹; Kiran Solanki¹; ¹Mississippi State University, Center for Advanced Vehicular Systems

Proper identification of microstructure-property constitutive relationships and their associated uncertainties is a crucial step in developing physics based modeling, and performing numerical simulation of deformation and failure in materials. An effective method to capture the microstructure-property relationship is by use of internal state variable evolution equations, where a multiscale hierarchy of numerical simulations coupled with experiments presented in ascending spatial size scale can be used to determine the functional forms of the macroscale plasticity and damage progression in ductile metals. A methodology is presented in which a cascade of different spatial size scale finite element analyses coupled with experiments at each scale is performed to determine final failure of a structural component. A discussion of different length scales will be presented related to rate and temperature dependent plasticity and damage evolution in ductile metals. This modeling concept will be shown to address a broad range of engineering problems.

3:55 PM Break

4:10 PM

Microstructure Modeling for the Superalloy Ingot Breakdown Process: *Alexander Bandar*¹; Ravi Shankar¹; Li Cai¹; Wei-Tsu Wu¹; Donald Weaver²; ¹Scientific Forming Technologies Corporation; ²Air Force Research Laboratory, Metals Processing Section (AFRL/MLLP)

A microstructure evolution model is presented, integrated into the Finite Element Modeling (FEM) software package DEFORMTM. Recrystallization, precipitation, phase transformation, and grain growth, during and after thermomechanical deformation, are predicted via a phenomenologically-informed Cellular Automata (CA) algorithm. Strain, strain rate, and temperature are computed via FEM and provided as inputs to the model. Inverse Analysis (IA), used to determine unknown materials constants via iterative backwards-calculation from known experimental results, is demonstrated as an effective technique to determine constants for work hardening and recovery, and for critical dislocation densities necessary to nucleate recrystallization. Results of a CA technique to predict microstructure evolution during cogging of nickel-base superalloy U-720 are presented; however, the model is designed to accommodate a range of alloys, thermomechanical processes, and other microstructure evolution algorithms such as Monte Carlo (MC) or Phase Field (PF) methods as well. Limitations of the model and future work are also discussed.

4:30 PM

Modeling the Mechanical Behavior of Hexagonal Materials: Application to Zirconium: *Gwenaelle Proust*¹; Irene Beyerlein¹; George Kaschner¹; Carlos Tome¹; ¹Los Alamos National Laboratory

Hexagonal materials deform plastically by a variety of slip and twinning modes. The relative contribution of these mechanisms depends strongly on texture, temperature and strain rate. In this work, we propose to further elucidate the complicated competition and interactions between twinning and slip deformation modes as a function of temperature for high purity zirconium. We present here a constitutive model which focuses on the microstructural effects of twinning on hardening, and accounts for the temperature dependence of the slip and twin mechanisms. We implement this hardening model in our visco-plastic self consistent (VPSC) polycrystal model to simulate the response of Zr when the temperature or the strain path are changed. We use tensile and compressive experimental data realized along different loading directions at temperature regimes varying between 76K and 450K to adjust the constitutive parameters of the constitutive model.

4:50 PM Invited

Observation and Modeling of Dislocation Structure Evolution During Deformation of Aluminum: *David Field*¹; Ioannis Mastorakos¹; Colin Merriman¹; ¹Washington State University

As deformation proceeds in commercial purity Aluminum a rich dislocation structure develops. This structure can be observed by TEM or EBSD methods, among others. This work extends the crystal plasticity formulation of Arsenlis, et al (cf. JMPS 52 (2004), 1213) to three dimensions and compares the results with experimental observations of structure evolution by EBSD. The excess dislocation density is readily determined using EBSD techniques and this measure is directly correlated with that predicted by the model. Discussion of extending the model to include strengthening particles is included.

5:15 PM

Multiscale Characterization and Modeling of Ductile Fracture in Cast Aluminum Alloys: *Somnath Ghosh*¹; Valiveti Dakshinamurthy¹; Hu Chao¹; Jie Bai¹; ¹Ohio State University

This paper will present a multiple scale materials characterization with multiple-scale modeling for ductile fracture of cast aluminum alloys. Image reconstruction technique is introduced to obtain high resolution microstructures from low resolution SEM/optical microstructure images. Multiscale characterization tools are proposed with novel characterization parameters, specifically aimed at micromechanical modeling. Using domain refinement functions of microstructural characteristics, successive domain partitioning is performed. Subsequently a multi-level computational model is developed for multi-scale analysis of ductile fracture. The method combines macroscopic coupled plastic-damage modeling with displacement based FEM with a microstructurally explicit modeling of ductile fracture by the Voronoi cell FEM. Three computational levels of hierarchy with different resolutions are introduced to reduce modeling and discretization errors. Numerical examples are solved to demonstrate the effectiveness of the model in predicting ductile failure.

5:35 PM

The Effect of Colony Orientation on Deformation Behavior and Slip Transmission during Hot Working of Ti-6Al-4V Single-Colony Samples: *Ayman Salem*¹; S. Semiati¹; ¹US Air Force Research Laboratory

The deformation behavior of individual alpha/beta colonies of Ti-6Al-4V has been established under hot working conditions. Constant strain-rate uniaxial compression tests were conducted on samples cut from single-colony crystals that were grown using a float zone technique. Each sample was oriented for slip along a different prismatic slip system in the alpha-phase. The mechanical behavior exhibited a strong dependence on colony orientation. The apparent anisotropy in the critical resolved shear stress was explained based on the burgers orientation relationship between the alpha (hcp) and beta (bcc) phases of the colonies and hence the orientations of alpha slip directions relative to those in the beta phase.



Alumina and Bauxite: Alumina Refinery Design and Development

Sponsored by: The Minerals, Metals and Materials Society, TMS Light Metals Division, TMS: Aluminum Committee

Program Organizers: Peter McIntosh, Hatch Associates; Jean Doucet, Alcan Inc; Morten Sorlie, Elkem Aluminium ANS

Tuesday PM Room: Northern E4
February 27, 2007 Location: Dolphin Hotel

Session Chair: Milind Chaubal, Sherwin Alumina Company

2:00 PM Session Introduction

2:05 PM

Alumina Yield in the Bayer Process-Past, Present and Prospects: *Roelof Den Hond*¹; Iwan Hiralal²; Ab Rijkeboer³; ¹Alcor Technology; ²Hiracon Consultancy; ³Rinalco Consultancy

During the past decades a large number of alumina plants were successful in economically increasing the productivity of the Bayer liquor loop. Over a period of 25 years the benchmark precipitation yield has increased from 70 g/l to 90+ g/l, whilst producing sandy alumina. However with the theoretical maximum precipitation yield at 160 g/l there is still a wide gap to be closed. This paper provides an overview of past developments, the present status and the prospects, resulting from increased process knowledge and emerging technologies. It is envisaged that benchmark precipitation yield will soon cross the 100 g/l level.

2:30 PM

Capital Cost: To Be or Not to Be: *Peter-Hans Ter Weer*¹; Anthony (Tony) McCabe²; ¹TWS Services and Advise BV; ²Global Alumina

The capital cost of a bauxite and alumina project is a key parameter in meeting corporate threshold economic criteria and in many cases may "make or break" a project. Although capital costs of projects tend to be quoted and compared, a consistent basis is often lacking and "apples" are compared with "pears". This paper addresses elements of capital cost estimates of bauxite and alumina projects and their effect on project economics.

2:55 PM

Chemical Reaction Engineering in the Bayer Process: *Daniel Thomas*¹; ¹WorleyParsons

Chemical reaction engineering provides an important link between chemistry (kinetics, thermodynamics) and economics (capital cost, productivity, efficiency). The key elements are interpretation of (batch) laboratory data, application of the resultant models to continuous operations, and industrial equipment selection (and costing). When successfully combined, these tools allow optimisation of the business case for both new refinery designs and brownfield upgrades. As both computational tools and fundamental chemical understanding improve, there is opportunity for improved application of chemical reaction engineering to the Bayer process. This paper presents some case studies and examples of potential applications.

3:20 PM

Energy Consumption in Bayer Process: *Songqing Gu*¹; Lijuan Qi¹; ¹Zhengzhou Research Institute of Chalco

The energy consumption in Bayer process is studied in this paper. It is found by thermodynamic analysis of Bayer process that the theoretical energy consumption for diasporic bauxite is only a little higher than that for gibbsitic bauxite. Calcination, evaporation and digestion can be identified as the highly energy consuming processes in alumina production. The energy consumption differences in various refineries using Bayer process are brought about by the following factors: (1) Systematic energy consumption depending on the concentration system and temperature system in whole Bayer cycle; (2) Heat recovery efficiency and heat loss impacted by the heat utilization during calcinations, evaporations and temperature changes of bauxite slurry or liquor, the heat transfer efficiency in preheaters and the heat insulation of high temperature vessels and pipes as well; (3) Energy efficiency of equipment

including the specific energy consumption and electrical efficiency of such equipment as stirs, pumps and fans etc.

3:45 PM Break

4:00 PM

Outlooks for the Future in Bauxite Processing: *Vadim Lipin*¹; *Vladimir Kazakov*²; ¹Saint Petersburg State Polytechnical University; ²St. Petersburg State Technologic University of Vegetable Polymers

Problem of energy consumption decrease and improvement of quality of resulting products is the central at upgrading of Bayer process. The overcoming of these problems basically is reached on technological units of autoclave digestion of bauxite and decomposition of aluminate liquor. A role of other units (milling of bauxite, thickening and washing of red mud, evaporation of spent liquor, etc.) have the followed importance. Besides modern approaches to new product reception from bauxites and to the decision of solid wastes problem are shown.

4:25 PM

Pressure Decantation at Gramercy Alumina: *Patricia Landry*¹; Hugh Edwards¹; ¹Gramercy Alumina

Gramercy Alumina restarted in July 2001, using a Double Digestion of Jamaican bauxite, employing Alcan pressure decantation technology. Low temperature digestion slurry is decanted in pressure vessels using synthetic flocculant to separate a clarified overflow and a consolidated mud underflow. The overflow reports to the digestion flash train. The underflow is pumped to the high temperature desilicator/digesters. Demand for throughputs and supersaturation levels above original design has challenged operation and process personnel since start-up. Physical changes to the decanter's piping and controls have improved underflow pumping capabilities to accommodate the above-design throughputs and significant bauxite quality changes. Optimizing flocculant injection placement and dosage level has reduced consumption to half the start-up levels. Despite advances that enabled above original design production levels, relatively short decanter operating cycles and high scaling rates still pose significant operating and maintenance limitations. These improvements and the ongoing challenges are the subject of this presentation.

4:50 PM

New Super Mills for Bauxite Grinding at the Gove Alumina Refinery: *Colin Thorpe*¹; ¹Alcan Bauxite and Aluminum Technology, Alcan Engineering

This paper is to talk about the selection of large rod mills to minimise the number of mills with overall power reductions. The Alcan Gove refinery installs three new rod mills, two mills online with an additional mill on standby to meet 3.8 mtpa Al. In the Definitive Feasibility Study, Alcan Engineering had analysed the existing 2 compartment rod/ball mills operating at the Gove site. Survey results from these mills had been used as the basis for predicting the capacity of these existing mills and the capacity of a number of alternative circuits to meet Alcan Gove expansion from 2.0 mtpa to 3.8 mtpa Al. The design capacity of each mill is 650 wet metric tonnes per hour (WMTPH) at specified grinding performance. Each mill has a 2000 kW drive making these mills the largest rod mills. The new rod mills commissioned in 2005 exceeded the design requirements of the Alcan Gove expansion whilst achieving the desired grinding performance.

5:15 PM

Design Developments for Fast Ramp-Up and Easy Operation of New Large Calciners: *Michael Missalla*¹; *Roger Bligh*¹; *Michael Stroeder*¹; *Cornelis Klett*¹; ¹Outokumpu Technology Ltd

Four new generation Outokumpu calciners with capacities up to 3300 t/d alumina have been commissioned and ramped up quickly from first hydrate "feed-on" to full capacity The shortest taking just 3 days. The calciners, some the largest yet built by Outokumpu, have been found to be significantly easier to operate than older designs while also providing improved performance. The paper discusses the design developments leading to this easier operation and improved performance – specifically, the flowsheet development, design of the fluid bed cooler, use of windboxes and automation. The contributions from installation and pre-commissioning procedures, and importantly from the customer's team are also discussed. The status of the two new 3500 t/d calciners at Alcan Gove will also be described.

5:40 PM Closing Comments

Aluminum Alloys for Transportation, Packaging, Aerospace and Other Applications: Alloy Development

Sponsored by: The Minerals, Metals and Materials Society, TMS Light Metals Division, TMS: Aluminum Committee

Program Organizer: Subodh Das, University of Kentucky

Tuesday PM Room: Northern A4
February 27, 2007 Location: Dolphin Hotel

Session Chairs: Subodh Das, University of Kentucky; Shridas Ningileri, Secat Inc

2:00 PM

New Aluminum Alloy for the Next Generation Aircraft: *Julian Gheorghie¹*; ¹Universal Alloy Corporation

This paper will present some of the challenges that the new aluminum alloys are facing, many of these challenges being caused by a very tough carbon-fiber composite competition. Both systems have unique features not exhibited by the competitor system. Due to the very different nature of the two systems is many times difficult to make a head-to-head comparison. When making such assessment mechanical and corrosion properties, specific weight, acquisition and maintenance cost have to be taken in consideration. Aluminum alloy systems have the advantage of being a well established technology, therefore the integration of any new alloy system into a new aircraft design is considerable less expensive when compared to the composite alternative. The mechanical and corrosion properties of a newly developed alloy as well as some of its current applications will be presented. The aging behavior as it relates to the mechanical and corrosion properties will also be presented.

2:25 PM

Towards Microstructurally Based Models for Sheet Formability and Fracture of Al Alloys: *David Wilkinson¹*; Mukesh Jain¹; Jidong Kang¹; Haixiao Hu¹; ¹McMaster University

The formability of Al alloy sheet can be influenced by numerous metallurgical parameters including alloy composition, grain size and shape, texture and intermetallic particles. We have attempted to address these parameters in a systematic way that will lead to the development of models for formability and fracture which are based on material microstructure. To date we have focused on the role of constituent particles that are prevalent in both 5xxx and 6xxx alloys and which are known to reduce tensile ductility. In this presentation we will update this work and present preliminary data aimed at including texture as an additional parameter.

2:50 PM

A Kind of New Aluminum Alloy Research: *Hua Shen¹*; Zhi Guo Dong¹; Weidong Yang¹; Guangchun Yao¹; ¹School of Materials and Metallurgy

Aluminum is noticed because it is of low density, high stress, easy machining and rich resource and so on. But it is of poor corrosion-resisting, hardness and mechanical strength, thus its application is limited. Al-Mg-Mn-RE complex alloy was studied by someone. In this work, a new element of Cr was added to aluminum base alloy, then it was compared with aluminum and Al-Mg-Mn-RE alloy in corrosion-resisting, hardness and mechanical strength, finally the better property was found. This was because Cr was of particular character in aluminum base alloy by observing the microstructures of alloys. Corrosion-resisting, hardness and mechanical tests were carried out at room temperature. The results showed that corrosion-resisting, hardness and mechanical strength all rose while the elongation worsened.

3:15 PM

Development of Superplasticity in an Al-Mg-Sc Alloy: *Jaya Prasad¹*; *Subramshu Bhattacharya²*; ¹IIT Madras

Superplasticity is the ability of polycrystalline materials to exhibit, in a relatively isotropic manner, large elongations prior to failure, under appropriate conditions of temperature and strain rate. This behaviour can be utilised in the shaping and forming of components, parts and structures that cannot be easily or economically produced from materials of normally limited ductility. Recent interest in replacing steel with aluminium in auto-body sheet-metal parts has

led to Al-Mg based non-heat treatable alloys becoming potential candidates for automotive applications. In this work an Al-4wt.%Mg-0.25wt.%Sc alloy capable of exhibiting superplastic behaviour was developed. Using an appropriate casting schedule and a suitable thermomechanical processing route, fine-grained sheets of the alloy were produced. Tensile tests were carried out to characterize the high temperature deformation behaviour. It was demonstrated that the present alloy exhibits reasonably large elongations with a high sensitivity of the stress to the strain rate, typical of superplastic materials.

3:40 PM Break

3:50 PM

Production of AA6061 Billets for Thixoforming: *Yücel Birol¹*; ¹Marmara Research Center

Thixoforming offers the possibility of forming complex aluminum parts with an exceptional quality and a reduction of processing steps. The production of a fine, equiaxed, globular microstructure is a must for the success of thixoforming. Thermomechanical processing produces such a microstructure through recrystallization of heavily deformed billets and a subsequent heat treatment in the mushy zone. In the Cooling Slope (CS) casting route, on the other hand, molten metal with a suitable superheat is cast over a water-cooled, inclined metal plate into a permanent mould to produce the thixotropic material. Both thermomechanical processing and the CS casting routes were employed to produce AA6061 thixotropic feedstock which were then formed in the semi solid state. The effect on the final microstructures of cold work in the thermomechanical processing route and the effect of CS length, casting temperature in the CS casting route were investigated.

4:15 PM

Application of a New Constitutive Model for the FE Simulation of Local Hot Forming of Age Hardening Aluminium Alloys: *Asbjørn Mo¹*; *Sylvain Gouttebroze¹*; *Øystein Grong²*; *Ketil Pedersen¹*; *Hallvard Fjær³*; ¹SINTEF; ²Norwegian University for Science and Technology; ³Institute for Energy Technology

In local hot forming processes, the material is subjected to local heating while being simultaneously deformed. The softening behaviour that age hardening alloys exhibit at elevated temperatures can then be exploited in order to effectively carry out certain critical forming operations. A new constitutive model is presented that relates the flow stress to the strain rate, temperature, and microstructure in age hardening aluminium alloys. The model accounts for the accumulation and annihilation of dislocations, as well as for the changes in the volume fraction and size distribution of the hardening precipitates. The model is applied in case studies to which histories of strain rates and temperatures typical for local hot forming are input. The calculated flow stress history is compared to similar histories obtained by a simpler, and in FE codes more commonly used, material behaviour modelling. Consequences of not accounting directly for the mentioned microstructural aspects are discussed.

4:40 PM

The Influence of Particle Size to the Preparation of Foam Aluminum by Powder Metallurgy Method: *Zhiqiang Guo¹*; *Guangchun Yao¹*; *Yihan Liu¹*; ¹School of Materials and Metallurgy, Northeastern University

There are many factors influence the preparation of foam aluminum. In this paper influences of particle sizes to powder metallurgy method were studied. Three different sizes of powders were applied: $d < 0.074\text{mm}$; $0.074\text{mm} < d < 0.147\text{mm}$; $0.147\text{mm} < d < 0.295\text{mm}$. Mix powders with foaming agent (TiH₂) respectively, press them into precursors. And then do foaming experiments. It can be concluded with the increasing of powder diameter, reunion phenomena of TiH₂ became serious. TiH₂ particles reunited together. In foaming process, some places that TiH₂ reunited expanded violently. A portion of pore walls became thinner fleetly because of the shortage of resilience, pore walls began to rupture, collapse occurred. The results showed that high porosity and stability foam aluminum materials can be obtained by using particles with small diameter ($d < 0.074\text{mm}$).



5:05 PM

Friction Stir Welding of Aluminum Alloys 6061-T6 and 6101-T6: *Carter Hamilton*¹; Stanislaw Dymek²; ¹Miami University; ²Akademia Górniczo - Hutnicza University of Science and Technology

Tin plated 6061-T6 and 6101-T6 aluminum extrusions were friction stir welded in a corner configuration. A banded microstructure of interleaved layers of particle-rich and particle-poor material comprised the weld nugget. Transmission electron microscopy revealed the strong presence of tin within the particle-rich bands, but TEM foils taken from the TMAZ, HAZ and base material showed no indication of Sn-containing phases. Since tin is limited to the surface of the pre-weld extrusions, surface material flowed into the nugget region, forming the particle-rich bands. Similarly, the particle-poor bands with no tin originated from within the thickness of the extrusions. Mechanical testing of specimens excised from the as-welded panels resulted in consistent failure on the retreating side of the weld, approximately 10 mm from the weld nugget. SEM analysis of the fracture surfaces revealed typical ductile rupture; however, when the excised specimens were solution heat treated and aged, the specimens consistently failed within the weld nugget and revealed two distinct modes of fracture consistent with the particle-rich and particle-poor layers of the nugget. This investigation correlates the mechanical performance of friction stir welded 6061-T6 and 6101-T6 panels with the fracture behavior and the microstructural characteristics of the weld nugget. Factors leading to the development of the banded microstructure are identified.

Aluminum Reduction Technology: Cell Fundamentals, Phenomena and Alternatives

Sponsored by: The Minerals, Metals and Materials Society, TMS Light Metals Division, TMS: Aluminum Committee

Program Organizers: Geoffrey Bearne, Rio Tinto Aluminium Ltd; Stephen Lindsay, Alcoa Inc; Morten Sorlie, Elkem Aluminium ANS

Tuesday PM

Room: Southern 2

February 27, 2007

Location: Dolphin Hotel

Session Chair: Gary Tarcy, Alcoa Inc

2:00 PM

Bubble Noise from Søderberg Pots: *Marianne Jensen*¹; Tor Pedersen¹; Kjell Kalgraf¹; ¹Elkem Aluminium ANS

High frequency measurements of voltage were introduced at Elkem Aluminium Lista in order to find the effect of noise from the release of gas bubbles from the anode – bubble noise. On a Søderberg pot the bubble noise represents a fairly large portion of the total pot noise. Hence it is important to understand what impacts the bubble noise in order to understand and control the Søderberg pot in a better way. The bubble noise varies quite a lot over time and between pots. The variations are related to different process conditions. Looking at number of anode problems and carbon dust generation there is a correlation between the bubble noise and the quality of the Søderberg anode. The metal quality is also strongly impacted by a change in the bubble noise. Several process conditions have been investigated, presented and discussed in the paper.

2:25 PM

Theory of Bubble Noise, Bath Height, and Anode Quality: *Kjell Kalgraf*¹; ¹Elkem Aluminium Research

Many papers have studied the effect of bubble noise upon flow, current efficiency, alumina distribution, bath velocity distribution, overvoltages, frequencies generated, etc. Few papers have dealt with bubble noise, anode quality, and bath height. Some of the relationships turn out to be counterintuitive. We present a theory relating bubble noise to anode quality and bath height, showing that bubble noise goes down when bath height increase and when gas leaks through the anode increase. Gas leaks through the anode are related to bath height and to the number of cracks in the anode, i.e. anode quality. The dependence of bubble noise on gas leaks is less for a prebake pot than for a Søderberg pot. Bubble noise is an indicator of anode quality. The rate of decline with bath height is 2.8-3.8 mV/cm of bath in Søderberg pots and 0.5-1 mV/cm in prebake pots in agreement with measurements.

2:50 PM

Electrode Processes of Sulphur Species in Molten Salts: *Pavel Fellner*¹; Marta Ambrová¹; Jomar Thonstad²; Jana Jurisová¹; ¹Slovak University of Technology; ²NTNU

The effect on the cathode and anode reactions when adding sodium sulphate to molten chlorides and fluorides was investigated by chronopotentiometry and cyclic voltammetry in the temperature range 820°C–1000°C. The cathode process was explained under the assumption that Na₂SO₄ thermally dissociates into Na₂O and SO₃, which is the electroactive species. The formation of sulphide was observed. The influence of sulphide on aluminium electrolysis will be discussed. The anode reaction of sulphate depends on the electrode material. On gold electrodes, no electrochemical activity of sulphate was observed. However, when a platinum anode was used, sulphate was oxidized to oxygen and SO₃ that decomposed thermally. When a normal carbon anode was used, the presence of COS and SO₂ in the anode gas leaving the laboratory aluminium cell was observed.

3:15 PM

Interaction of Heat Resistance Concrete with Low Melting Electrolyte KF-AIF₃(CR=1,3): *Yurii Zaikov*¹; Alexander Chuikin¹; Alexander Redkin¹; Andrei Khramov¹; Nikolai Shurov¹; Vasilii Kryukovskii²; ¹Institute of High Temperature Electrochemistry; ²Russian Aluminum Company Rusal

The kinetics of heat resistance concrete interaction with low melting electrolyte KF-AIF₃ (CR=1,3) was investigated at 700 and 750°C. The experiments were carried out by continuous weighting method. The interaction of concrete with melt components was found. The kinetics of this interaction depends on alumina contents in a melt, temperature and the way of concrete preparation. The corrosion rate was found to be 12±3 cm/year. This value was obtained by calculation based on 7 hours experiments. The electrolysis of aluminum from low melting electrolyte in heat resistance concrete container have been carried out during 60 hours.

3:40 PM Break

3:55 PM

Effect of Ca in Characterization of Bath Electrolyte by the X-Ray Methods: *Frank Feret*¹; ¹Alcan Inc

Determination of total Ca (as CaF₂) in bath electrolyte by XRF is discussed and so is the effect of Ca on measured XRD intensities. The XRD effect was calculated for two bath specimens of different composition and can be presented in the numerical form: $C_j = K_{11}i_j (1 + 0.024 \text{ CaF}_2)$. The impact of Ca on formation of calcium cryolite is explained and formulae for calculating excess AIF₃ (ExAIF₃) in these compounds are given. The traditional equation used for controlling bath chemistry $\% \text{ExAIF}_3 = 0.2424 \text{ \%Chiolite} + K (\% \text{CaF}_2 - \% \text{Fluorite})$ was critically examined and is considered no longer valid. Occurrence of two diverse Ca-cryolite (NaCa_{1.5}AIF₇ and NaCaAIF₆) phases in bath electrolyte samples was identified as the reason for experimental K constant being different from theoretical $K = 0.717$. Effect of spectral interference of the 2.955 Å line of NaCa_{1.5}AIF₇ on chiolite's 2.909 Å peak is also discussed.

4:20 PM

Aluminium Production Process Options with a Focus on the Application of Hydrogen Diffusion Anodes: *Sankar Namboothiri*¹; Mark Taylor¹; John Chen¹; Margaret Hyland¹; Mark Cooksey²; ¹Light Metals Research Centre; ²CSIRO Light Metals Flagship

One of the disadvantages of the Hall-Héroult process that uses pre-bake technology for producing aluminium is the need for periodic carbon anode replacement. This results in voltage instability, varying cell geometry, and variations in the rate of electrolysis. Furthermore, greenhouse gases are formed as a by-product. Due to these shortcomings, alternative technologies such as inert anodes have been investigated and tested, but with little success to date. The use of hydrogen as the anode in aluminium electrowinning has merit, as aluminium can be produced at a reversible potential similar to that with a carbon anode, while also overcoming the disadvantages as outlined above. This paper reviews the various process options for aluminium electrowinning, with the focus on the use of hydrogen at the anode. A thermodynamic analysis, considering various gas-electrode-electrolyte system options, was performed to identify a system with the optimum operating parameters for hydrogen anodes in aluminium production.

4:45 PM

Ionic Liquid Electrowinning of Aluminum -Modeling of Batch Reactor:Mingming Zhang¹; Ramana Reddy¹; ¹University of Alabama

A mathematical modeling was developed for the batch reactor of aluminum electrowinning in ionic liquid electrolyte. This model describes the deposition process by incorporating the mass transport of participating ionic species, homogeneous chemical reactions within the diffusion layer, and the associated electrochemical kinetics. A number of process parameters adversely affecting the current distribution were evaluated for optimal reactor performance, including current and potential distributions, ohmic loss, concentration profiles, fluid flow distribution, and electrode configurations. The optimized parameters were then used in designing the electrochemical reactor. The batch reactor system, which incorporates also non-linear electrode kinetics and fluid-flow due to forced convection, was modeled numerically via finite volume method. A comprehensive fluid dynamic software ("Fluent") integrated with electrochemical module has been used to simulate the reactor. Effects due to different reactor configurations, different electrolyte properties, and various flow conditions and current densities are presented and critically discussed.

5:10 PM

Refining Aluminum Process in Ionic Liquids: Huimin Lu¹; Yongheng Wang¹; ¹Beijing University of Aeronautics and Astronautics

In this paper, the authors studied the refining aluminum process in the ionic liquids, which were prepared by 1-methyl-3-butyl imidazolium chloride (BMIC) and anhydrous aluminum chloride (AlCl₃), with copper cathode and aluminum alloy anode. In the experiments, the cell voltage range was from 1.1V to 1.7V, the concentration ratio range of AlCl₃ to BMIC from 1.3 to 1.9 and the electrolysis temperature at 105±2°. After analyzing the deposits by SEM and XRD, the optimum parameters of the electrolyte concentration ratio and the cell voltage were found out. The current densities increased with the increase of the cell voltage and the concentration ratio. However, the best cathode morphology was obtained at 1.3V~1.5V with the concentration ratio 1.6, the current efficiency (CE) reached 89.5% and specific energy consumption was 4.66kWh/kg Al when the cell voltage was 1.4V.

Aluminum Reduction Technology: Modelling and Design I

Sponsored by: The Minerals, Metals and Materials Society, TMS Light Metals Division, TMS: Aluminum Committee

Program Organizers: Geoffrey Bearne, Rio Tinto Aluminium Ltd; Stephen Lindsay, Alcoa Inc; Morten Sorlie, Elkem Aluminium ANS

Tuesday PM

Room: Southern 1

February 27, 2007

Location: Dolphin Hotel

Session Chair: Martin Segatz, Hydro Aluminium GmbH

2:00 PM

CFD Modelling of Electrolyte Flow in Aluminium Reduction Cells: Yuqing Feng¹; Mark Cooksey¹; M. Schwarz¹; ¹Commonwealth Scientific and Industrial Research Organisation

A CFD model has been developed to study the effect of design parameters (e.g. inter-anode gap, the presence of slot) on bath flow of an aluminium reduction cell, where a full scale air-water model of part of a cell has been used as a test bed. Two inter-anode gaps (20 mm, 40 mm) in combination with two anode configurations (no slot and a 15 mm wide longitudinal slot) have been considered. Further to the model validation using PIV measurement taken under similar conditions, the effect of inter-anode gap and the presence of a slot on bath flow have been investigated quantitatively in terms of the amount of gas in the anode-cathode distance (ACD) under the anode, and net flow in the ACD and in the inter-anode gaps and slot.

2:25 PM

Modeling the Effect of the Anode Changing Sequence with a Non-Linear Shallow Water Stability Model: Vanderlei Gusberti¹; Dagoberto Severo²; Schneider Andre²; Elton Pinto²; Antonio Vilela¹; ¹LASID - PPGEM - Programa de Pos Graduação em Engenharia Metalúrgica, Minas e Materiais; ²PCE Ltd

Numerical simulation of the magnetohydrodynamic (MHD) stability of the aluminum electrolysis cell has become an important tool for improving its design and operation efficiency. This paper presents a non-linear transient shallow water stability model and its application to the study of the stability of an existent cell. In the model, current density in the liquid metal pad, magnetic field generated by the currents inside the cell and subsequently, metal-bath interface wave shape are calculated at each time step. Anode changing greatly disturbs cell stability. During the anode changing sequence, large current density disturbances occur, which produce a different MHD stability pattern after each anode change. We use the model to investigate the effect of different anode changing patterns on MHD stability of the metal-bath interface. With the predictions of the model, it was possible to develop a new anode change sequence that improves cell stability.

2:50 PM

Analysis of the Formation of Magnetic Forces in the Metal Pad: Marcus Gustafsson¹; Dariusz Kacprzak¹; Mark Taylor¹; ¹University of Auckland

The electrical currents in an aluminium reduction cell (external busbars as well as internal currents) produce strong magnetic fields. The interaction of these magnetic fields with the current distribution in the cell give rise to Lorentz forces in the molten metal and the electrolyte. These forces create steady-state fluid flows, deform the metal pad surface and introduce transient phenomena like interfacial waves. These are called magnetohydrodynamic (MHD) effects. Finite Element Methods allow for the calculation of Lorentz Force Densities that show the MHD effects. These plots are useful to show the results of the calculations, but do not help to identify where they originate from. This presentation will show how to use a simple method to determine which parts of a reduction cell contribute most significantly to the resulting Lorentz Forces, which is of importance when creating or modifying a design of a reduction cell.

3:15 PM

Simulation of Cell Thermoelectric Field with Consideration of Electrochemical Reactions: Gennady Arkhipov¹; Vitali Pingin¹; Yaroslav Tretyakov¹; ¹Energy Technology Centre, Russia

Mathematical modeling of thermoelectric field is an important task of development and improvement of aluminium cells. A aluminium cell is a complicated thermodynamic system characterized with numerous electrochemical, physical and other processes. Estimation unit of electrochemical reactions in melt was developed to take into account electrochemical reactions in cell thermoelectric estimations and energy balance. The estimation unit was included in the AN-SYS program. The paper compares thermoelectrical fields calculated with and without account of electrochemical reactions in the melt.

3:40 PM Break

3:55 PM

Numerical Simulation of Electrical Joints in the By-Pass System of 230 kA Cells at CVG VENALUM: Ulises Ortega¹; Juan Salazar²; Juan Gonzalez²; ¹National Polytechnic University UNEXPO; ²CVG VENALUM

Modeling and simulation were performed on an electrical joint, part of the by-pass system of 230 kA cells at CVG VENALUM. The aim of the study was to obtain the contact pressure in the joint for different amperage values, taking into account thermal expansion and the influence of parameters as surface roughness and hardness. For this purpose, a FEM code was used including interface contact elements for the thermo electrical and thermo mechanical non-linear analyses. As part of this study both electrical and thermal contact resistance values were found using experimentally developed correlations. Both resistances are functions of contact pressure, which depends on the joint's temperature. A preliminary model was developed to determine contact resistances at a constant pressure value. A thermo electrical model was then run and used as input a thermo mechanical run, to determine contact pressure variations with temperature, allowing for the contact resistances to be readjusted.



4:20 PM

Development and Progress of 300 kA Aluminum Reduction Cells in Yichuan Aluminum Smelter Plant: *Ren Bijun*¹; Zhuxian Qiu²; Songling Dai¹; ¹Yichuan Electric-Power and Aluminium Group; ²Northeastern University

The state-of-the-art of Chinese aluminum electrolysis industry is reviewed for the past 25 years. The properties of the 300kA large scale aluminum reduction cells in Yichuan aluminum smelter plant were introduced in detail. At the present paper, some problems of Chinese aluminum electrolysis were analyzed. By using some novel technologies and materials to build the cell, lower cathode voltage drops and the good side-ledge are formed to prolong the cell lift time. By some improving techniques of alumina concentration control, superheat temperature control and computer specialist diagnosis, the alumina concentration in the melt of 1.5-2.5wt%, superheat temperature of 6-10°C could be realized indeed. As a result, the aim of 94% CE, 13000kWh/t-Al DC consumption and over 2000 days cell lift-time have been achieved in this large scale cell in this plant.

4:45 PM

A New Model for MHD Instabilities in Aluminum Reduction Cells: *Mehdi Kadkhodabeigi*¹; Yadollah Saboohi¹; ¹Sharif University of Technology

A new model for investigating the interfacial MHD instabilities in aluminium reduction cells based on Shallow Water approximation and linear stability analysis is proposed and the effect of different parameters of the cell on its instability phenomenon is considered. This work has two features that are: (a) the terms of linear friction have been considered in molten layers so that we can see the stabilizing effects of these. (b) we have considered the effect of lateral boundaries on the stability of cell. Based on this model a very important dimensionless parameter is found. This parameter is the most important factor in the field of instability of cell. By use of mathematical programming the best geometry for designing new cells and retrofitting the existing cells, respect to minimization of MHD instabilities and electrical energy consumption is obtained.

Biological Materials Science: Biological Materials/ Bio-Medical

Sponsored by: The Minerals, Metals and Materials Society, TMS Structural Materials Division, TMS/ASM: Mechanical Behavior of Materials Committee

Program Organizers: Andrea Hodge, Lawrence Livermore National Laboratory; Chwee Lim, National University of Singapore; Eduard Artz, University of Stuttgart; Masaaki Sato, Tohoku University; Marc Meyers, University of California, San Diego

Tuesday PM
February 27, 2007

Room: Europe 4
Location: Dolphin Hotel

Session Chairs: Peter Fratzl, Max Planck Institute of Colloids and Interfaces; Sungho Jin, University of California, San Diego

2:00 PM Introductory Comments

2:05 PM Invited

Nanobiomechanical Approaches to Studying Cancer: *C.T. Lim*¹; ¹National University of Singapore

Cancer is a leading cause of death in many countries including the US and this number is anticipated to rise even higher with time. At the cell level, cancer can be characterised by the uncontrolled cell growth and proliferation in the human body. The invasions of surrounding tissues by the process of metastasis also greatly magnify the extent of the damage which ultimately spreads to the rest of the body. Here, we use nanobiomechanical approaches to study breast cancer with the aim of better understanding the pathophysiology of this disease from a biomechanics perspective. With the aid of emerging biophysical techniques, we aim to study the change in the biomechanical properties of cancer cells in terms of their stiffness, cell-cell adhesion as well as biorheological properties. It is hoped that through this, we can provide useful information for the further study on the detection, diagnosis and treatment of cancer.

2:35 PM Keynote

Advanced Biomaterials for Regenerative Medicine: *Samuel Stupp*¹; ¹Northwestern University

Advances in regenerative medicine throughout this century will have great impact on human longevity, quality of life, and the economy. The targets may include, brain repair, heart regeneration, insulin-producing tissue to cure diabetes, the possibility to offer humans new cartilage, bone, and teeth in adulthood, among others. One of the scientific challenges in regeneration is the supramolecular crafting of a three-dimensional artificial matrix to actively control cell function. Ideal biomaterials for the extracellular space need to orchestrate information flow to receptors in highly dynamic fashion. This opportunity in materials innovation will be an exciting one as interactions among signaling pathways are unraveled. The signaling targets could include those linked to cell survival, stem cell differentiation, proliferation, specific cell recruitment, or those involved in the growth of blood vessels on demand to feed cells. This lecture will describe supramolecular biomaterials using a diverse set of molecules that self-assemble into one-dimensional nanostructures.

3:15 PM Invited

Significantly Accelerated Osteoblast Cell Growth on Aligned TiO₂ Nanotubes: *Sungho Jin*¹; Brian Oh¹; ¹University California at San Diego

Proper control of nanostructures can produce a very large surface area and topographical features on biomaterials suitable for cell adhesion and growth. Vertically aligned yet laterally spaced TiO₂ nanotubes have been utilized to grow MC3T3-E1 osteoblast cells. The adhesion/propagation of the cell is substantially enhanced by the topography of the TiO₂ nanotubes with the filopodia of growing cells going into the nanotube pores, producing a locked-in cell structure.¹ The presence of the nanotube structure induced a significant acceleration in the growth rate of osteoblast cells by as much as ~300-400%, as evidenced by SEM-based cell counts, and cell viability assays such as Trypan Blue Exclusion, MTT, and Alkaline Phosphatase (ALP) activity test. The effect of various biological and materials parameters for optimal cell viability will be discussed. ¹S. Oh, C. Daraio, L. H. Chen, T. R. Pisanic and S. Jin, *J. of Biomed. Mater. Res.* 78A, 97 (2006).

3:45 PM Break

4:05 PM Invited

Integration of "Bio" in the Materials Science and Engineering Program at Georgia Tech: *Naresh Thadhani*¹; Robert Snyder¹; ¹Georgia Institute of Technology

The inherent interdisciplinary nature of materials science and engineering has been responsible for the survival and revival of many previous Metallurgical and Ceramic Engineering academic programs. Incorporation of "Bio" in materials science and engineering programs needs to occur through the same interdisciplinary notion, while maintaining the core structure-property-performance paradigm. The School of Materials Science and Engineering (MSE) at Georgia Tech has integrated "bio" into the academic program by recruiting core MSE faculty and leveraging the strengths of core "bio" faculty from various units at Georgia Tech and Emory University, through joint appointments. In this presentation, we will describe how this integration is providing multidisciplinary research opportunities for students in areas such as tissue engineering, genetic patterning, bio-manufacturing, bio-implants, medical devices, and disease detection, diagnosis, and treatment. Educational programs focusing on bio-materials and bio-properties at the graduate and undergraduate levels will also be discussed, in addition to our future direction.

4:35 PM

Materials Science and Engineering Using Genetically Engineered Proteins and Peptides: *Candan Tamerler*¹; *Mehmet Sarikaya*¹; ¹University of Washington

Polypeptides are materials makers in biology as transporters, nucleation/growth modifiers, scaffolds, and agents for communication among cells and biomacromolecules (lipids, DNA, polysaccharides, and proteins). Biological materials include soft tissues as functional units (enzymes and motor proteins) and systems (muscles, skin, and neurons) In hard bone and dental tissues proteins constitute scaffolds and control inorganic material formation and structuring (morphogenesis, crystallography, and hierarchy). Just like in biology, materials for practical applications could be made using genetically

engineered polypeptides with specific binding to desired inorganic materials that control synthesis, fabrication, and function. Using combinatorial mutagenesis, we select polypeptides that bind to metals and ceramics and use them as molecular erectors. Here we will demonstrate biocombinatorial selection of inorganic binding peptides, their genetic tailoring for specific function, and utilization as molecular MSE tools for bionanofabrication, functional immobilization on patterned substrates, and molecular probing towards technology and medicine.

4:55 PM

Direct Contact Cytotoxicity Assays for Filter-Collected, Carbonaceous Nanoparticulate Material and Observations of Lung Cell Response: *Karla Soto*¹; K. Garza¹; Y. Shi¹; L. Murr¹; ¹University of Texas, El Paso

Standard cytotoxicity assays for nanoparticulate material involve suspension of dilution sequences which are often difficult to achieve with many soots and some carbon nanotube aggregates, all of which are variously represented in indoor and outdoor environments. We have developed a methodology for exposing cell cultures to filter collections directly. Preliminary results for carbonaceous nanoparticulate materials collected on glass filters (with 1-3 μm diameter fibers) from a natural gas burner (laboratory) enclosure have exhibited significant cytotoxic responses for human epithelial (lung) cell (A549) viability for high-flow, blue-flame (HFBBF), low-flow, blue-flame (LFBBF), and incomplete high-flow, yellow-flame (HFYF) combustion nanoparticles consisting of aggregated, branched, primary spherules (30 to 35 nm diameter) composed of intercalated fragments of grapheme and polycyclic aromatic hydrocarbons (PAH); with a pyrene/fluoranthene ratio of ~ 6.3 and total PAH content of 18, 101, 142 ppm for LFBBF, HFBBF, and HFYF, respectively.

5:15 PM

Structure and Mechanical Properties of Crab Exoskeletons: *Po-Yu Chen*¹; Albert Lin¹; Marc Meyers¹; ¹University of California, San Diego

The structure and mechanical properties of the exoskeletons of Sheep crab (*Loxorhynchus grandis*) and Dungeness crab (*Cancer magister*) are discussed. The exoskeleton of crabs is a complex composite consisting of highly mineralized chitin-protein fibers arranged in a twisted plywood/Bouligand pattern. There is a high density of ductile tubules in the vertical direction that stitch the structure together, allowing self-healing. Tensile tests in longitudinal, transverse, and vertical directions were applied to determine the mechanical properties of crab exoskeletons. Specimens were tested under hydrated and dehydrated conditions. Chemical treatments were used to remove proteins and minerals respectively to evaluate how the constituents affect the overall properties. Micro- and nano-indentation as well as three-point-bend tests were performed to measure the hardness and fracture toughness. Fracture surfaces after tests were examined using scanning electron microscopy. The fracture mechanism is discussed and modeled. Research Support: NSF DMR 0510138.

5:35 PM

The Electronic Properties of Metal-Labeled DNA: *Chenzhong Li*¹; ¹Florida International University

DNA is close to an ideal nano wire because of its narrow diameter, flexibility, and electronic properties. In addition, the self-assembly properties of DNA have been exploited to generate 2D and 3D structures on surfaces and in solution. In order to improve the conductivity of DNA meanwhile to maintain their molecular recognition properties, a novel metal DNA complex has been developed. The electron transfers properties of immobilized DNA monolayer and the DNA-metal hybrids on the electrode surface were investigated by electrochemical and AC impedance techniques. We found electron transfer via the metal DNA film is faster than that of the native DNA film and the metal ions can modulate the electrochemical properties of DNA monolayers. The results are consistent with an ion-assisted long-range polaron hopping mechanism for electron transfer. Attempts have also been made to develop a biosensing system for DNA mismatch detection.

Biological Materials Science: Poster Session

Sponsored by: The Minerals, Metals and Materials Society, TMS Structural Materials Division, TMS/ASM: Mechanical Behavior of Materials Committee
Program Organizers: Andrea Hodge, Lawrence Livermore National Laboratory; Chwee Lim, National University of Singapore; Eduard Artz, University of Stuttgart; Masaaki Sato, Tohoku University; Marc Meyers, University of California, San Diego

Tuesday, 5:55 PM Room: Europe 4
February 27, 2007 Location: Dolphin Hotel

Application of Magnesium Alloys as Implant Material: *Ozgur Duygulu*¹; Ali Arslan Kaya¹; R. Alper Kaya²; Gizem Oktay¹; Frank Witte³; ¹TUBITAK Marmara Research Centre, Materials Institute; ²Sisli Etfal State Hospital, Clinic of Neurosurgery; ³Department of Orthopaedic Surgery, Hannover Medical School

Magnesium alloys are a new candidate to be used as degradable implants. These alloys are biocompatible with low toxicity, dimensionally comparable to the cortical bone substance and fast corroding making them potentially a good choice as an implant material. Thus, the idea of having a hybrid implant material composed of titanium with magnesium outer layer to utilize the most advantageous properties of both materials also seems attractive. However, Ti and Mg do not have solubility in each other nor do they form an intermetallic compound, leaving limited solutions for joining. In one attempt titanium was coated with magnesium via arc PVD. Diffusion bonding technique was also used while employing reactive interlayers of other elements to help create bonding between Mg and Ti. It may be suggested that using magnesium alloys as bone implant and in novel hybrid implant materials composed of magnesium and titanium alloys may emerge in the future.

The Effect of Crystallographic Texture on Cell-Attachment Behavior and Mechanical Properties of Hydroxyapatite Coatings: *Hyunbin Kim*¹; Renato Camata¹; Sukbin Lee²; Gregory Rohrer²; Anthony Rollett²; Kristin Hennessy¹; Susan Bellis¹; Yogesh Vohra¹; ¹University of Alabama at Birmingham; ²Carnegie Mellon University

Naturally occurring apatite in human hard tissues often exhibits preferred crystallographic orientations. These textures are believed to influence the biological and biomechanical properties of hard tissues. Serendipitous occurrences of texturing have also been observed in synthetic hydroxyapatite (HA) coatings for implants. In this study, we present evidence that c-axis-textured HA coatings exhibit improved bioactivity and mechanical properties. We developed a method that enables the deposition of highly textured HA by controlling the laser fluence and plume direction of incidence in pulsed laser deposition. X-ray pole figures revealed formation of HA grains with the c-axis preferentially aligned perpendicularly to the substrate in coatings deposited with high laser fluence and normal incidence of plume. Human mesenchymal stem cells attached in greater numbers to the HA coatings with c-axis texture, as compared with randomly-oriented coatings. Nanoindentation results showed enhancement of hardness and Young's modulus in c-axis-textured HA coatings, compared to randomly-oriented coatings.

3-D Porous Resorbable Tricalcium Phosphate Mandible Bone-Graft via Fused Deposition Modeling (FDM): *Joseph Cardello*¹; Monica Hopkins²; Samar Kalita²; ¹Timber Creek High School; ²University of Central Florida

In this research, a porous resorbable mandible bone-graft was fabricated. Initially, tricalcium phosphate (TCP) bioceramic powder was synthesized using a simple precipitation process. Amorphous powder was doped with magnesium ions, an essential element of the bone mineral, to enhance its properties and stabilize the b-phase at elevated sintering temperatures. The powder was then calcined, and the resulting powder was uniaxially compressed, sintered, then measured for density and tested for hardness and biaxial strength. Next, a negative mold of a section of the human mandible was made in an FDM machine using a 3-D STL image constructed from CT scan data by Mimics software. The mandible mold was then infiltrated with slurry of the Mg-doped b-TCP powder. The infiltrated green mold was dried, and then sintered to obtain the bioceramic mandible graft. The graft was later characterized for physical and mechanical properties and compared with that of a real mandible.



Matrix Metalloproteinase Influence on Titanium Implant Osseointegration:

Lindsey VanSchoiack¹; Julie Janes²; Veronica Shubayev³; James Earthman¹;
¹University of California Irvine; ²San Diego VA Healthcenter; ³University of California San Diego

Biomaterial and biological material interactions are controlled by biocompatibility, material property differences, and chemical interactions. These factors are intrinsic to the materials being integrated; suture and skin, implant and bone, polymer and organ. Regulating cellular and molecular processes in the integrating tissues may improve the interaction and stability of the complex formed by the biomaterial and the body. Matrix Metalloproteinases (MMPs) are a family of extracellular proteases known to control bone resorption. We studied the effects of a synthetic MMP inhibitor therapy on the healing and osseointegration of titanium implants in the femurs of rats over several time points and observed significant differences in osseointegration levels between groups. As anticipated, compared to the natural time course of implant osseointegration the experimental group exhibited greatly accelerated stability and integration. This study suggests that MMP inhibition may facilitate osseointegration and that controlling extracellular matrix remodeling may improve material integration with living tissues.

Simulation of the Stress State in the Forceps in Aspekt Improve Its Ergonomics:

Szota Michal¹; Jassinski Józef¹; Lacki Piotr¹; Jeziorski Leopold¹;

¹Czestochowa Technical University

In order to design forceps properly it is necessary to optimise many parameters and consider the functions, which forceps should fulfil. Of course, some simplifications are necessary respecting calculation methodology. In the paper solution procedure of such a problem has been presented. The presented solution allows for precise determination of the geometrical dimensions according to the functional requirements that forceps should fulfil. The presented numerical analysis describes small range of the forceps application but the used algorithm can be applied in any other type of forceps. The carried out calculations allow for determination of the geometrical parameters with reference to the expected spring rate. The charts elaborated on the basis of the calculations are very useful during a design process. The numerical calculations show an essential problem, namely change in contact surface as a function of load. The observed phenomenon can affect the forceps functioning badly.

Bulk Metallic Glasses IV: Mechanical Properties II

Sponsored by: The Minerals, Metals and Materials Society, TMS Structural Materials Division, TMS/ASM: Mechanical Behavior of Materials Committee

Program Organizers: Peter Liaw, Univ of Tennessee; Raymond Buchanan, University of Tennessee; Wenhui Jiang, University of Tennessee; Guojiang Fan, University of Tennessee; Hahn Choo, University of Tennessee; Yanfei Gao, University of Tennessee

Tuesday PM Room: Asia 1
 February 27, 2007 Location: Dolphin Hotel

Session Chairs: A. L. Greer, University of Cambridge; J. Eckert, Technische Universität Darmstadt

2:00 PM Keynote

Shear Bands in Metallic Glasses: A. L. Greer¹; ¹University of Cambridge

As is well known, plastic deformation of metallic glasses at ambient temperature is inhomogeneous, shear being concentrated into bands approximately 10 nm thick. This presentation will review recent work on the mechanism of operation of shear bands, important for optimizing the plasticity of the glasses. Measurements of the temperature rise at shear bands suggest values for the stress acting during shear. The diffusion of heat from a band gives a heat-affected zone much wider than the band thickness. It is then of interest to analyze the origin of the thickness, which cannot be controlled thermally. Finally it will be shown that heavy surface deformation can induce intense shear banding with beneficial effects including a compressive residual stress in surface layers, and promotion of more uniform plasticity from pre-nucleated shear bands.

2:30 PM Invited

Investigations of Plastic Deformation Processes in a Bulk Metallic Glass: Katharine Flores¹; Ashwini Bharathula¹; Michael Uchic²; ¹Ohio State University; ²US Air Force Research Laboratory

Improving the structural reliability of bulk metallic glass components requires a detailed understanding of the relationship between plastic flow behavior and glass structure. In the present work, we examine the structural changes associated with homogeneous and inhomogeneous flow in a Zr-based bulk metallic glass using a variety of experimental techniques, including positron annihilation spectroscopy. Previous PAS results indicate that the open volume in this glass falls into three distinct categories: densely packed interstitial-like holes, loosely packed flow defects, and vacancy-like voids. The evolution of these open volume regions with deformation will be discussed. Additionally, the elastic and plastic behavior of the glass has been characterized at the microscale. Pillars with micron-scale diameters were micromachined using a Focused Ion Beam (FIB) milling technique. Their mechanical behavior was studied in compression and the deformation characterized by SEM. These results will be discussed in light of the observations regarding open volume distribution.

2:50 PM Invited

Ductile Foreign-Particle-Reinforced Bulk Metallic Glasses and the Tailoring of Their Properties: Jörg Löffler¹; ¹Swiss Federal Institute of Technology-Zurich

We present a new class of foreign-particle-reinforced bulk metallic glasses (BMGs) in which a fully amorphous Vit 105 (Zr_{52.5}Cu_{17.9}Al₁₀Ni_{14.6}Ti₅) matrix has been reinforced with 25-44 μm graphite particles of 3-20 vol.%. The samples were produced via a multi-step melt processing route, and good particle distribution was achieved via a levitation mixing procedure. By adjusting the processing parameters part of the graphite was transformed into ZrC, which allows a systematic change in mechanical properties. We found that graphite generates a decrease in hardness, whereas carbide formation leads to an increase compared to the monolithic matrix material. The best mechanical properties were observed at low volume fractions of graphite, where high plastic deformation of up to 18.5% was achieved without sacrificing the high yield strength (1.85 GPa) of the BMG. To our knowledge, this composite displays the highest combination of yield strength and ductility so far reported for foreign-particle-reinforced BMGs.

3:10 PM Invited

Microscopic Deformation Mechanisms in Metallic Glasses: Mo Li¹; ¹Georgia Institute of Technology

Despite extensive studies made in the past, the deformation mechanisms in amorphous metals have not been clearly understood. What are the underlying "defects" that promote the plastic deformation? What is the role of the adiabatic heating? Under what conditions should the nano voids form? Must the shear banding occur? Those questions, along with many others related applications, have been at the very center of active researches in the past fifteen years. In this talk, we try to answer some of those questions from extensive atomistic modeling and theoretical analysis. We show that volumetric change indeed accompanies the deformation and is an integral part of the plastic deformation in metallic glasses. We also show the conditions and thermodynamics of the void formation. We show the atomic scale characterizations of shear bands and its formation mechanisms. The localized deformation in metallic glasses is a unique consequence of the non-crystalline materials.

3:30 PM

Nanometer Scale in Homogeneity and Enhancement of Plasticity in Bulk Metallic Glasses: Do-hyang Kim¹; H. Chang¹; E. Park¹; Won Tae Kim²; ¹Center for Noncrystalline Materials, Yonsei University; ²Cheongju University

Addition of alloying element having positive enthalpy of mixing with constituent elements can induce the two-glass phase separation in glass forming alloys. Phase separation into two amorphous phases can result in various types of microstructures ranging from droplet-type to interconnected-type structures. Moreover, it has been shown that addition of small amount of element having positive enthalpy of mixing with the constituent elements can induce nm scale inhomogeneity, leading to the enhancement of plasticity. In the present study, it will be shown that ternary alloy systems such as Ni-Nb-Zr, Cu-Zr-Be exhibit enhanced plasticity in the limited composition range, indicating that nm scale inhomogeneity in the amorphous phase can play a

role in modifying the deformation behavior of the amorphous phase. Detailed structural study, for example, by EXAFS, shows that addition of alloying element having positive enthalpy of mixing with some of the constituent element leads to the structural change, exhibiting enhancement of plasticity.

3:45 PM

Spall Strength of a Zirconium-Based Bulk Metallic Glass: *Fuping Yuan*¹; Vikas Prakash¹; John Lewandowski¹; ¹Case Western Reserve University

In the present study, a series of plate impact experiments were utilized to obtain the spall strength of a zirconium-based bulk metallic glass (BMG), Zr_{41.25}Ti_{13.75}Ni₁₀Cu_{12.5}Be_{22.5}, both under compression and pressure-shear shock wave conditions. The bulk metallic glass samples were shock loaded by utilizing Ti-6Al-4V flyer plates to around 7 GPa. Normal plate impact, and combined pressure and shear experiments with skew angles ranging from 12 to 20 degrees, were conducted to study the effects of normal shock compression and combined compression and shear on the BMG's spall strength. The results indicate that the spall strength of the BMG decreases with increasing compressive stress and shear stress. Scanning electron microscopy of spall surface was used to understand the modes of spall failure following normal shock compression and combined compression and shear loading on the BMG.

4:00 PM Invited

Design of Ductile Bulk Metallic Glasses and Composites: *Jurgen Eckert*¹; ¹Darmstadt University of Technology

Improving the ductility and toughness of bulk metallic glasses (BMGs) is one of the main goals necessary to be achieved for further promoting the use of these materials for engineering applications. This can be rationalized by creating heterogeneous materials with different type and length-scale of heterogeneities. As examples, recent results obtained for Cu- and Ti-base BMGs and composites will be given. Some guiding principles for the design of such alloys will be presented and the resulting phases and microstructures will be described. Moreover, the impact of a heterogeneous microstructure for affecting the deformation mechanisms will be discussed and related to the intrinsic properties of the respective phases and the global mechanical response of the material.

4:20 PM Invited

Plastic Deformation Behavior of Bulk Metallic Glass Composites Containing Spherical bcc Phase Precipitates: G. Sun¹; G. Chen¹; G. Chen²; ¹Nanjing University of Science and Technology; ²Joint Laboratory of Nanostructured Materials and Technology, Nanjing University of Science and Technology, State Key Laboratory for Advanced Metals and Materials, University of Science and Technology Beijing

Zr-based BMG composites with spherical β -crystalline particles showing significantly improved ductility at room temperature were prepared through an self-developed method. The plastic deformation behavior of Zr-based spherical β phase/BMG composites is discussed by observing detailed shear-band structures formed in the specimen surfaces, which were subjected to different plastic strain. The mechanism of plasticity improvement of the BMG composites which contain spherical β phase was revealed by comparison of the surface appearance of the deformed compression specimens between the Zr-based dendritic and spherical β phase/BMG composites.

4:40 PM

Yield Point of Metallic Glass: *Ju Li*¹; Futoshi Shimizu¹; Shigenobu Ogata²; ¹Ohio State University; ²Osaka University

Shear bands form in most bulk metallic glasses (BMGs) within a narrow range of uniaxial strain $\sim 2\%$. We propose this critical condition corresponds to embryonic shear band (ESB) propagation, not its nucleation. To propagate an embryonic shear band, the far-field shear stress must exceed the quasi steady-state glue traction of shear-alienated glass until the glass-transition temperature is approached internally due to frictional heating, at which point ESB matures as a runaway shear crack. The incubation lengthscale necessary for this maturation is estimated to be $\sim 10^2$ nm for Zr-based BMGs, below which sample size-scale shear localization does not happen. We model 4 metallic glasses: a binary Lennard-Jones system, two binary embedded-atom (EAM) potential systems, and a quaternary EAM system. Despite vast differences in the structure and interatomic interactions, the four MD calculations give yield strain predictions of 2.4%, 2.1%, 2.6% and 2.9%, respectively.

4:55 PM

The Influence of Pd on Fatigue Behavior of Zr-Based Bulk-Metallic Glasses: *Gongyao Wang*¹; P. Liaw¹; Y. Yokoyama²; M. Freels¹; A. Inoue²; R. Buchanan¹; C. Brooks¹; ¹University of Tennessee; ²Tohoku University

Zr-based bulk-metallic glasses (BMGs) exhibit good glass-forming abilities and excellent properties. Although Zr₅₀Cu₄₀Al₁₀ shows good mechanical behavior, the fatigue behavior is poor. In order to improve the fatigue behavior of Zr₅₀Cu₄₀Al₁₀ BMGs, some small additive elements like Ni, Pd were add into alloys. In our lab, fatigue behaviors were studied on Zr₅₀Cu_{40-x}Al₁₀Pd_x [X: 0–7 atomic percent (at%)] BMGs. The uniaxial tension-tension fatigue experiments were performed on the button-head notched or tapered fatigue specimens. The relationship between the fatigue behavior and Pd content was developed. The fatigue-endurance limit of Zr₅₀Cu₃₇Al₁₀Pd₃ was found to be the highest with a value of 983 MPa among the BMGs studied. A mechanistic understanding of the fatigue behavior of these Zr-based BMGs is suggested. A possible relationship between the ratio of the fatigue-endurance limit to the tensile strength and the ratio of the shear modulus to the bulk modulus will be attempted.

5:10 PM

A Correlation between Atomic Packing Density and Plastic Deformation of Cu-Zr Amorphous Alloys: An Atomistic Simulation Study: *Young-Min Kim*¹; Byeong-Joo Lee¹; ¹Pohang University of Science and Technology

Currently, the plasticity and its origin is one of the major concerns in developing ductile amorphous alloys. Even with a great deal of research effort, the mechanism of plastic deformation in amorphous alloys is not clearly known yet and no common agreement has been made. As an effort to confirm the validity of the free-volume theory on the plasticity of amorphous alloys, in the present study, we investigated the correlation between atomic packing density and plasticity of amorphous alloys using molecular dynamics simulations based on MEAM potentials. An atomistic scheme to evaluate the plasticity of amorphous alloys was developed and applied to various Cu-Zr alloys. A lowest plastic deformation was obtained in an alloy with a highest atomic packing density, and based on this, the atomic packing density which can be easily computed by an atomistic approach could be proposed as a means to predict plastic deformability of amorphous alloys.

5:25 PM

In-Situ Neutron Scattering Measurement of Stress-Strain Behavior of a Bulk Metallic Glass: *Timothy Wilson*¹; Bjorn Clausen²; Jennifer Elle³; Thomas Proffen²; Don Brown²; ¹University of Tennessee; ²Los Alamos National Laboratory; ³University of Idaho

Traditional diffraction stress analysis is difficult to apply to BMG components because they lack the long-range order necessary to produce sharp diffraction patterns, and thus, the internal strains for BMG have not been examined until recently. In this work, in-situ neutron scattering was used to measure the local elastic internal strain distribution in a Zr₅₇Nb₅Cu_{15.4}Ni_{12.6}Al₁₀ BMG as a function of a known applied stress. Various techniques were used to evaluate the internal strain. The strain was determined in both reciprocal space, by examining changes in the 1st broad diffraction peak, and in real space, by measuring changes in the atomic pair distribution function (PDF). The resulting "lattice" strain response is in good agreement with macroscopic elastic modulus and Poisson's ratio. These results can be used to help understand the elastic deformation of BMGs as well be used to help evaluate current models of BMG deformation.

5:40 PM

Mechanical Properties of Al Based Amorphous Alloys with Nano-Dispersion Synthesized by Mechanical Alloying and Consolidated by Equal Channel Angular Pressing: D. Roy¹; S. Bera¹; Z. Zúberová²; R. Hellmig²; *Yuri Estrin*²; I. Manna¹; ¹Indian Institute of Technology; ²Clausthal University of Technology

Mechanical alloying is a flexible processing route to producing equilibrium and metastable engineering alloys, including nanocrystalline and amorphous materials, in bulk quantity. While several amorphous and bulk amorphous alloys have been synthesized by mechanical alloying, a successful strategy to consolidate these novel alloys into bulk/solid components is still awaited. In this work, we synthesized Al based ternary amorphous alloy composites with either in-situ nano-intermetallic precipitates or ex-situ nano-ceramic dispersion by mechanical alloying. The milled powder was then consolidated by equal channel angular pressing (ECAP). The microstructure and the



physical/mechanical properties of both the milled product and compacted samples were characterized at appropriate stages. The characterization routine included microstructural studies by SEM and TEM, compositional micro-analysis by EDS, phase evolution/identification by XRD, and mechanical property studies. The results show that combination of mechanical alloying and ECAP could be a suitable approach to developing Al based amorphous alloy components with nanometric dispersion.

Cast Shop Technology: Quality Measurements and Grain Refining

Sponsored by: The Minerals, Metals and Materials Society, TMS Light Metals Division, TMS: Aluminum Committee

Program Organizers: David DeYoung, Alcoa Inc; Rene Kieft, Corus Group; Morten Sorlie, Elkem Aluminium ANS

Tuesday PM
February 27, 2007

Room: Northern E1
Location: Dolphin Hotel

Session Chairs: Rein Vainik, Opticast Aluminium AB; Jeffrey Wiesner, Alcoa Inc

2:00 PM Introductory Comments

2:05 PM

A Novel, Inexpensive and Rugged Probe for Measuring Gas Bubbles in Liquid Metals: Piero Marcolongo¹; James Evans¹; Dana Walker²; D. Corleen Chesonis²; ¹University of California; ²Alcoa

Gas bubbles play roles in many liquid metal processing operations e.g. in the gas fluxing of aluminum to remove impurities. An understanding of the behavior of such units depends on knowing how the bubbles are dispersed in the metal. Various bubble probes have been used in the past but all seem prone to problems. This paper describes a probe consisting of a narrow ceramic tube inserted into the metal and connected to an inert gas supply. Small bubbles are created at the immersed end of the tube; their formation is heard by a microphone in the gas supply line. These bubbles, henceforth "probe bubbles", are not the bubbles to be measured. The latter are much larger and, as they pass up over the immersed end of the probe, these large bubbles change the sound of the probe bubble. The phenomena involved have been examined in water and aluminum.

2:25 PM

Method Developed for Quantitative Assessment of Inclusions in Aluminium Billets: Majed Jaradeh¹; Torbjorn Carlberg¹; ¹Mid Sweden University

A technique, based on sodium hydroxide hot macro etching, has been developed to deep etch non-metallic inclusions in a way that makes them visible on a macro scale. The distribution of inclusions in transverse sections along DC-cast Aluminium billets could thus be studied. The technique has obvious advantages over other common analysis methods in giving a macroscopic spatial distribution of inclusions in a relatively simple way. The paper describes the development of the new technique and some applications. An analysis was made of how different inclusions behave during prolonged strong etching. Light optical microscopy, TEM and SEM/EDX have been used to identify specific inclusions.

2:45 PM

Improvement in Hydrogen Measurement Technique for Molten Aluminum: Todd Gansemer¹; Brian Reynolds¹; Jim Hart²; D. Corleen Chesonis²; ¹Alcoa Davenport Works; ²Alcoa Technical Center

The hydrogen content of molten aluminum can be assessed through in-line measurements using equipment such as Alscan, Telegas, or Notorp and through laboratory methods such as Leco Nitrogen Carrier Fusion or Hot Vacuum Subfusion Extraction (HVE). It is generally recognized that differing hydrogen results can be obtained by different methods. The Alscan method has been observed to have a bias relative to other methods that produces higher hydrogen measurements. The extent of this bias appears to depend on ambient humidity and temperature. An explanation for the bias has been discovered and an equipment modification to eliminate it has been developed and extensively tested through comparisons with Notorp and Leco.

3:05 PM Break

3:25 PM

Grain Refinement of Al-Si Casting Alloys: Geoffrey Sigworth¹; Catherine Smith²; Mark Easton³; Joseph Barresi⁴; Tim Kuhn¹; ¹Alcoa Inc; ²Comalco Research and Technical Support; ³Monash University; ⁴Comalco Aluminium Ltd

When the technical information on the grain refining of aluminum-silicon casting alloys is reviewed, it becomes evident that today's practices are employed primarily for historical reasons. In particular, the high Ti levels (c. 0.1%) in A356 and A357 alloys date from the years when the modern Al-Ti-B grain refiners did not exist. This paper reviews the history of grain refining in Al-Si alloys and an improved practice is outlined. It is important to understand that titanium can be present in two forms. One dissolves in aluminum; the other is nearly insoluble. With today's powerful Al-Ti-B refiners, there is no reason for large additions of soluble titanium. Experimental data is presented for A356 alloy. Lowering the dissolved Ti levels has no deleterious effect, and offers the potential of a significant cost saving.

3:45 PM

Refinement of Al-Si Eutectic Grains: A Novel Method to Produce High Integrity Al-Si Castings: Liming Lu¹; Kazuhiro Nogita²; Stuart McDonald³; Arne Dahle⁴; ¹CSIRO Minerals; ²Australian Research Council Centre of Excellence for Design in Light Metals, University of Queensland; ³Cooperative Research Centre for Cast Metals Manufacturing; ⁴University of Queensland

Eutectic modification with Sr, Na or Sb yields a refined fibrous silicon morphology which can improve the tensile ductility of cast Al-Si alloys. However, many companies choose not to use modifiers due to increased scrap rates and negligible beneficial effects on the mechanical properties because of alterations in the porosity characteristics of the castings. Here we report a novel method to modify Al-Si alloys which reduces the porosity of the castings while maintaining the well-modified silicon structure, thus producing consistent high performance Al-Si castings. This new invention is based on the grain refinement of the Al-Si eutectic grains, or cells.

4:05 PM

Impact of Grain Refining on SemiSolid Metal Processing: Shahrooz Nafisi¹; ¹Facility for Electron Microscopy Research

Desired microstructure for semi solid metal (SSM) processing contains primary particles free of dendrites and almost in the globular form with minimum entrapped eutectic. The crucial matter is the form and size of primary particles and more spherical and lesser size give better flowability during component shaping process with the added additional benefit of superior mechanical properties. In this study, with simultaneous conventional and SSM processing of aluminum alloys, most important and critical parameters for refiner employment will be explained.

Characterization of Minerals, Metals, and Materials: Characterization of Mechanical and Physical Properties of Materials II

Sponsored by: The Minerals, Metals and Materials Society, TMS Extraction and Processing Division, TMS: Materials Characterization Committee

Program Organizers: Arun Gokhale, Georgia Institute of Technology; Jian Li, Natural Resources Canada; Toru Okabe, University of Tokyo

Tuesday PM
February 27, 2007

Room: Oceanic 8
Location: Dolphin Hotel

Session Chairs: Sergio Monteiro, UENF; Toru Okabe, University of Tokyo

2:30 PM

Characterization of Surface-Treated and Cold Worked Nickel-Base Superalloys: Hyojin Song¹; Peter Nagy²; Vijay Vasudevan¹; ¹Department of Chemical and Materials Engineering, University of Cincinnati; ²Department of Aerospace Engineering and Engineering Mechanics, University of Cincinnati

The intentional introduction of near-surface compressive residual stresses, using methods like shot peening, laser shock peening, is well known for enhancing the resistance to fatigue crack nucleation and growth of turbine

engine parts. Recently, nondestructive quantitative eddy current conductivity measurements have been successfully utilized to measure the state and degree of residual stress in shot-peened and cold worked nickel-base superalloys. However, the difficulty in separating the macro residual stress (elastic) and cold work (plastic) contributions to the conductivity has militated against the achievement of a complete analysis of the measured frequency-dependent apparent eddy current conductivity (AECC) results, and, furthermore, there is a lack of basic understanding of how intrinsic and extrinsic factors like microstructural changes brought about by surface and/or cold-work treatments affect the conductivity. The present study combines measurements of electrical resistivity/conductivity with detailed characterization of microstructure, residual stress distributions and quantitative analysis of surface-treated and cold worked Ni-base superalloys.

2:50 PM

Microstructural Characterization of Nitride Coatings: Julien Nazon¹; Valérie Flaud¹; Joël Sarradin¹; Jean-Claude Tedenac¹; Nicole Fréty¹; ¹Université Montpellier II - CNRS - UMR 5617 - LPMC

Microstructural characterization of tantalum and chromium nitride coatings was investigated. Nitride coatings were deposited onto steel substrates using the reactive sputtering process route. Material microstructure was characterized using different techniques, i.e. X-Ray Diffraction (XRD), Scanning Electron and Atomic Force Microscopies (SEM, AFM), Secondary Ion Mass Spectrometry (SIMS) and Rutherford Backscattered Spectrometry (RBS). Particular attention was paid to the study of coating growth mechanisms determined from AFM investigations, as well as to the study of coating residual stresses calculated from XRD experiments.

3:10 PM

Comparison of the Influence of Hydrogen on the Mechanical Behavior of API X52, X65 and X70 Steels: Miguel Barron¹; Victor Cortes¹; Julio Juarez²; Guillermina Gonzalez²; ¹Universidad Autonoma Metropolitana Azcapotzalco; ²Universidad Nacional Autonoma de Mexico

It was studied the influence of hydrogen on the mechanical behavior of API X52, X65 and X70 steels by means of tensile testing. Cylindrical specimens were machined from tubes currently employed in the Mexican oil industry, and heat treated for stress relief and homogenization during one hour at 650°C. Hydrogen was introduced in some specimens by cathodic charge in an electrochemical cell using a 0.5M H₂SO₄ aqueous solution and 50 mA m⁻² of current density during 24 hours. Besides, CS₂ was employed in order to prevent the formation of molecular gaseous hydrogen. Afterwards, specimens with and without hydrogen were subjected to tensile tests in an Instron machine using a strain rate of 1x10⁻⁴ s⁻¹. From the experimental results the corresponding strain hardening index was determined for each of the aforementioned steels, and it was observed that the X70 steel is more sensitive to hydrogen embrittlement.

3:30 PM

Comparison between Traditional and Innovative Steels for Large Plastic Moulds: Donato Firrao¹; Maurizio Chiarbonello¹; Paolo Matteis¹; Giovanni Mortarino¹; Pasquale Russo Spena¹; Giorgio Scavino¹; Graziano Ubertalli¹; Maria Ienco²; Gabriella Pellati²; Maria Pinasco²; Enrica Stagno²; Riccardo Gerosa³; Barbara Rivolta³; Agostino Silvestri³; Giuseppe Silva³; Adriano Tavasci³; Elisa Tata⁴; Severino Missori⁴; Roberto Montanari⁴; Andrea Ghidini⁵; ¹Politecnico Di Torino; ²Università di Genova; ³Politecnico di Milano; ⁴Università di Roma Tor Vergata; ⁵Lucchini Sidermeccanica S.p.A.

Moulds for plastic automotive components such as bumpers and dashboards are usually machined from large pre-hardened steel blooms. Due to the blooms size, the heat treatment of the standard 1.2738 steel produces mixed microstructures (continuously varying from surface to core) and a very low fracture toughness, that makes this steel sensible to the defects that may occur in the moulds. In the present work, two alternative steels are investigated: a quenched and tempered microalloyed steel, and a precipitation hardenable steel. Whereas the former can be subjected to the same mould production cycle currently employed for the 1.2738 steel, the latter should be hardened by a subcritical treatment after machining. The microstructures and the ensuing mechanical behavior of steels samples, representative of different positions inside large bloom, or of different heat treatment conditions, have been examined by metallographic techniques, by fracture toughness and tensile tests, and by ensuing fractographic examinations.

3:50 PM

A Thermal Characterization of Composites Behaviors on HASTELLOY® C-22HSTM Alloy: E-Wen Huang¹; Fengxiao Liu¹; Michael Benson¹; Peter Liaw¹; Hahn Choo¹; Lee Pike²; Dwaine Klarstrom²; ¹University of Tennessee; ²Haynes International, Inc.

Corrosion-resistant nickel-based alloys are widely used in engineering applications because of their excellent resistance to a wide variety of corrosive environments. The HASTELLOY® C-22HSTM alloy is an aged-hardened, nickel-based, corrosion-resistant superalloy that is strengthened by Ni₂(Cr,Mo) long-range ordered precipitates in a face-centered cubic matrix. In the present study, the tensile behavior of C-22HS alloy was examined by a real-time IR-Camera, as a thermal monitor, at room temperature. The surface thermal evolution was determined as a function of applied strain. This thermal evolution demonstrates that the C-22HS alloy behaves as a composite. The diffraction study of C-22HS alloy also supports this real-time thermal study. Acknowledgements: The National Science Foundation, International Materials Institutes (IMI) Program (DMR-0231320), with Dr. Carmen Huber as the program director, supports this work.

4:10 PM

Evaluation of Structural Strength in Carbody of Freight Car: Jeongguk Kim¹; Jung-Won Seo¹; Sung-Tae Kwon¹; Sung-Cheol Yoon¹; Young Joon Kim¹; ¹Korea Railroad Research Institute

In order to verify the structural strength of newly manufactured carbody of a freight car in railway application, the structural strength assessment of a carbody was performed using engineering analysis techniques. The freight car was designed with A570 steel for the transportation of cold-rolled coils in steel making company. Prior to the evaluation of structural strength, commercial finite element method (FEM) software was used for the stress and structural analyses on stress distribution in a carbody of freight car. The strain gages were attached on the carbody based on the FEM results. The actual vertical loading test and horizontal compression loading test were conducted, and the results were compared with the previous FEM results. In this investigation, the evaluation method for the structural strength in a structural component has been introduced using several engineering techniques, and experimental and theoretical results were compared.

4:30 PM Break

4:50 PM

A Comparison Between Mechanical Testing for Clayey Ceramic Strength Characterization: Carlos Mauricio Vieira¹; Eduardo de Carvalho¹; Sergio Monteiro¹; ¹State University of the Northern Fluminense

The mechanical strength is an important property for technological characterization of materials and a fundamental requirement for clayey ceramics such as those used for building construction. Owing to the inherent nature of the porous conventional red ceramics, the norms specify compression tests in cylindrical specimens for the mechanical characterization of clayey ceramics. Another simple test performed on cylindrical specimens that has been suggested as a better alternative to evaluate the mechanical properties, applies a diametrical compression in which tensile stresses played a major role. In the present work, a comparison between these two mechanical testing was carried out to characterize the strength and other related properties in a common clayey ceramic used for red brick fabrication. The results displayed the advantages and also exposed the limitations of both tests as a standard specification for red ceramic products.

5:10 PM

Characterization of Clayey Ceramic Incorporated with Eucalyptus Firewood Ash: Carlos Mauricio Vieira¹; Mônica Borlini¹; Sergio Monteiro¹; ¹State University of the Northern Fluminense

This work has for its objective to evaluate the effect of incorporation of eucalyptus firewood ash on the physical and mechanical properties of a clayey ceramic. Mixtures of kaolinitic clay from the municipal area of Campos of Goytacazes, State of Rio de Janeiro, Brazil, were prepared with additions of 0, 5 and 10% in weight of ashes from firewood. Ashes with particle sizes lower than 149 mm (100 mesh) and 75 mm (200 mesh), were used in each incorporated composition. Specimens were 20 MPa uniaxially press-molded and fired at 900°C. The firing properties evaluated were diametrical shrinkage, water absorption and mechanical strength by diametrical compression. The



results showed that the ash incorporation caused significant changes in the physical and mechanical properties of the clayey ceramic, which do not impair its use as bricks.

5:30 PM

Fabric Rupture Mechanism of Jute Sackcloth Used as Reinforcement in Polyethylene Composites: *Sergio Monteiro*¹; Amanda Lima¹; Luis Augusto Terrones¹; José Roberto d'Almeida²; ¹State University of the Northern Rio de Janeiro; ²Catholic University of Rio de Janeiro

Used jute sackcloth is being investigated as a possible reinforcement of recycled polyethylene matrix composites. This would allow the reutilization of two types of waste materials commonly discarded in many countries. Owing to previous employment of the jute sackcloth, the fabric has flaws that interfere with the mechanical behavior of the composite. In this work, a fracture mechanics approach to fabrics behavior under load has been used to interpret the possible rupture mechanism in jute sackcloth composites. Composites made of new and used sackcloth were bent tested and the results showed differences that could be explained by fracture mechanics.

5:50 PM

Characterization of the Rupture Mechanisms of Coir Fibers in Polyester Composites: *Sergio Monteiro*¹; Luis Augusto Terrones¹; Felipe Lopes¹; Jose Roberto d'Almeida²; ¹State University of the Northern Rio de Janeiro; ²Catholic University of Rio de Janeiro

The fibers obtained from the shell of the coconut fruit, known as coir fibers, are regarded as a residual by-product and, traditionally discarded into the environment. Nowadays, however, coir fibers have been considered as reinforcement phase in polymeric composites for applications that do not demand structural resistance. In the present work, an investigation has been conducted on the possibility of using coir fiber reinforced polyester matrix composites as load carrying elements. This investigation was concentrated on the characterization of the fibers' rupture mechanisms when embedded in the polyester matrix. The results have shown that the surface morphological aspects of the coir fibers play an important role on its ability to transfer the load imposed onto the matrix.

6:10 PM

Microstructures and Mechanical Properties of Sn-3.0Ag-0.5Cu-xNi Solders: *Fei-Yi Hung*¹; Truan-Sheng Lui¹; Li-Hui Chen¹; Cheng-Wei Chan¹; ¹National Cheng Kung University

The effect of Ni content on the microstructure and the tensile deformation mechanisms of a potential lead-free solder, Sn-3.0Ag-0.5Cu-xNi ($x=0, 0.1, 0.2, 0.3$ wt.%), are examined in this study. The results show that both Sn-Cu-Ni and Sn-Cu-Ni-Ag intermetallic compounds increased with increasing the Ni content. The IMCs existed mostly formed in the proeutectic Sn-rich phases. Notably, the Cu content of the bar-like Sn-Cu-Ni phase was lower than that of the particle-like Sn-Cu-Ni-Ag phases. In addition, the tensile deformed resistance of Sn-3.0Ag-0.5Cu-xNi solders decreased as increasing the Ni content. Adding Ni obtained the finer structures, however the hard massive Sn-Cu-Ni deteriorated the tensile deformed resistance.

Computational Thermodynamics and Phase Transformations: Microstructure Properties and Evolution II

Sponsored by: The Minerals, Metals and Materials Society, ASM International, TMS Electronic, Magnetic, and Photonic Materials Division, TMS Materials Processing and Manufacturing Division, ASM Materials Science Critical Technology Sector, TMS: Chemistry and Physics of Materials Committee, TMS/ASM: Computational Materials Science and Engineering Committee

Program Organizers: Corbett Battaile, Sandia National Laboratories; James Morris, Oak Ridge National Laboratory

Tuesday PM Room: Europe 11
February 27, 2007 Location: Dolphin Hotel

Session Chair: Dane Morgan, University of Wisconsin

2:00 PM Invited

Density Functional Approach for Modeling Elasto-Plastic Effects in Solidification: *Nikolas Provatas*¹; Peter Stefanovic¹; Ken Elder²; ¹McMaster University; ²Oakland University

We review the so-called "phase field crystal" methodology as an alternative to traditional phase field modeling for systems where elasto-plastic and diffusive processes are important. We begin with a new modified phase field crystal model (MPFC) [P. Stefanovic, M. Haataja and N. Provatas, Phys. Rev. Lett. 96, 225504 (2006)] recently developed to couple rapid elastic relaxation effects to diffusion-limited phase transformation kinetics in pure materials. The MPFC model is used to demonstrate the role of externally imposed strains on grain growth and texture development during solidification of nano-crystalline solids. We then present a new extension of the phase field crystal methodology to binary alloys, demonstrating the application of this methodology to the study solidification and solid-state transformations in alloy systems.

2:30 PM Invited

Grain Boundary Segregation and Prewetting Studied by Phase-Field and Atomistic Methods: W. J. Boettinger¹; *Y. Mishin*²; J. A. Warren¹; P. L. Williams²; ¹National Institute of Standards and Technology; ²George Mason University

Grain boundaries (GBs) in metallic alloys are often enriched in a solute. As the bulk composition approaches the solidus line, the segregated GB layer becomes increasingly disordered and may turn into a thin liquid layer. This eliminates resistance to GB sliding with a profound impact on mechanical properties. A similar problem arises during alloy crystallization when impinging grains either form a GB or remain separated by a thin liquid layer. This so-called prewetting transition was studied by the phase-field method, mostly in pure metals, but was never addressed by combining atomistic and phase-field approaches. We apply two different phase-field models to examine transitions between GB segregation and GB prewetting in Cu-Ag alloys. The same transitions have been studied and observed by grand-canonical Monte Carlo simulations using an embedded-atom Cu-Ag potential. Comparison of the continuum and atomistic results reveals generic features of GB prewetting and demonstrates advantages of the combined approach.

3:00 PM

Phase-Field Modeling of Microstructural Evolution during Solidification in Al-Sc Alloys: *you-hai wen*¹; Sarath Menon¹; Chris Woodward²; ¹UES, Inc.; ²Air Force Research Laboratory/MLLM

The addition of small quantities of Sc to Al alloys is known to dramatically reduce grain size in Al castings. Two possible mechanisms for this grain size refinement have been proposed: the heterogeneous nucleation of the fcc-Al solid solution phase on Al₃Sc particles that form first during solidification or a strong chemically-dependent anisotropy of solid-liquid interfacial energy on the nucleation and growth of the fcc phase. Here the relative roles of heterogeneous nucleation and anisotropic interfacial energy on dendritic growth are studied using a phase-field model. The role of crystallographic orientation of the nucleating phase is incorporated and preliminary results on the solidification behavior of a binary Al-0.375at%Sc alloy are discussed. Simulations show that the nature of distribution of the Al₃Sc particles has a

very strong effect on the evolving microstructure while significant variation in anisotropic interfacial energy does not appear to have any noticeable effect on the solidification microstructure.

Diffusion in Advanced Materials and Processing: Materials Processing

Sponsored by: The Minerals, Metals and Materials Society, TMS Structural Materials Division, ASM Materials Science Critical Technology Sector, TMS: Alloy Phases Committee, TMS: High Temperature Alloys Committee, ASM-MSCTS: Atomic Transport Committee, TMS/ASM: Nuclear Materials Committee, TMS: Solidification Committee

Program Organizers: Yong-Ho Sohn, University of Central Florida; Carelyn Campbell, National Institute of Standards and Technology; Daniel Lewis, Rensselaer Polytechnic Institute; Afina Lupulescu, Union College

Tuesday PM Room: Europe 2
February 27, 2007 Location: Dolphin Hotel

Session Chairs: Daniel Lewis, Rensselaer Polytechnic Institute; Richard Sisson, Worcester Polytechnic Institute

2:00 PM Invited

Unusual Mechanochemical Mechanisms, Thermodynamics and Kinetics of Some Phase Transformations and Chemical Reactions in Solids: *Valery Levitas*¹; ¹Texas Tech University

Three unusual cases of diffusive phase transformations and chemical reactions in solids are considered that are related to new mechanochemical mechanisms: 1. The beta-delta transformations in energetic crystal HMX via the virtual melting that occurs 120K below the melting temperature (Levitas, Smilowitz, Henson and Asay, PRL and APL, 2005; JCP and JPCB, 2006). 2. Pressure-induced crystal-crystal phase transformation and amorphization in some materials (including quartz, coesite, and jadeite, germanium and silicon, as well as BN and graphite) via the virtual melting that may occur 1000K below the melting temperature (Levitas, PRL, 2005). 3. The fast oxidation of aluminum nanoparticles covered by an initial oxide shell (Levitas, Asay, Son and Pantoya, APL, 2006). In this case, traditional diffusive mechanism is substituted with a complex mechanochemical process resulted in dispersion of atomic scale liquid aluminum clusters, oxidation of which is not limited by diffusion. The above mechanisms explain numerous unusual experimental phenomena.

2:30 PM Invited

The Influence of Solid State Diffusion on Microstructural Development During Solidification: *John DuPont*¹; ¹Lehigh University

The extent of solid state diffusion that occurs during solidification has a significant effect on the development of the final microstructure. In fact, many solute redistribution models are developed based on the extent of diffusion expected in the solid state during solidification. The lever law and Scheil equation provide simple models for calculating solute redistribution and microstructural development at the extreme cases for binary systems. Other models are available in which intermediate behavior is expected, and a new model has recently been developed for calculations in ternary systems. This paper will review the influence of solid state diffusion on the development of microstructure during solidification. Important examples on microstructure and properties will be given, along with a review of solute redistribution models available for estimating the final microstructure under a range of solidification conditions. Useful approaches for selecting the model most suitable for a given application will also be presented.

3:00 PM

Reactivity of the Ag-28Cu Braze Alloy with Titanium: *Myriam Sacerdote-Peronnet*¹; Jérôme Andrieux¹; Olivier Dezellus¹; Françoise Bosselet¹; Jean-Claude Viala¹; ¹University of Lyon

Joining titanium base alloys is an important issue to be addressed in the scope of producing low weight high strength components for use at medium temperature (600°C). With a melting point of 780°C, the eutectic alloy Ag-28Cu (28wt% Cu or 40at% Cu) has already shown good wetting and bonding characteristics with regard to conventional brazing of titanium base parts

at temperatures higher than 850°C. In the present contribution, attention is focussed on the reactivity of that eutectic alloy with titanium between 780 and 850°C. For semi-infinite diffusion couples, reaction layer sequences of various types were characterized between 780 and 850°C. Using the diffusion path concept, attempts were made to relate these sequences with the phase equilibria reported in the Ag-Cu-Ti ternary phase diagram, that we have recently assessed using Thermocalc and experimental literature data.

3:20 PM Invited

Diffusion in the Al₂O₃-TiO₂ System under Pulsed Current Applications: *Dat Quach*¹; *Vladimir Kodash*¹; *Joanna Groza*¹; ¹University of California

Isothermal diffusion couple experiments between bulk Al₂O₃ and TiO₂ polycrystals have been performed at 1436 and 1500°C with and without a pulsed current application. The current application increases the rate of diffusion and reaction to form an intermediate compound, Al₂TiO₅. The incubation time for compound formation is shortened and in the order of a few minutes. This enhancement is partially due to changes in the stoichiometry and defect structures of TiO₂ under a reducing atmosphere during the experiments. While these changes significantly boost the electrical conductivity of nonstoichiometric TiO₂, the pulsed current application may affect the coupled counterdiffusion of Al³⁺ and Ti⁴⁺ ions and enhance Ti⁴⁺ diffusion.

3:50 PM Break

4:00 PM

Thermal Stability of Tantalum Nitrides Diffusion Barriers: *Julien Nazon*¹; *Joël Sarradin*¹; *Jean-Claude Tedenac*¹; *Nicole Fréty*¹; ¹Université Montpellier II - CNRS - UMR 5617 - LPMC

Diffusion of copper through tantalum nitride has been studied. Tantalum nitride and copper thin layers were successively sputtered onto silicon substrates. Process parameters were chosen to get a layer thickness of 150 nm for tantalum nitride and 100 nm for copper. Microstructure of multilayers materials was characterized after vacuum annealing from 500 to 700°C using different techniques, i.e. X-Ray Diffraction (XRD), Scanning and Transmission Electron Microscopies (SEM, TEM), Secondary Ion Mass Spectrometry (SIMS) and Rutherford Backscattered Spectrometry (RBS). The diffusion mechanisms were determined from this experimental approach associated to a thermodynamical approach.

4:20 PM

Elemental Diffusion Behavior for the Sn-37Pb and Sn-3.0Ag-0.5Cu Joints with Cu and Ni Substrates during Aging: *Po-Jyun Huang*¹; *Kai-Jheng Wang*¹; *Jenq-Gong Duh*¹; *Mysore Dayananda*¹; ¹National Tsing Hua University

Sn-37Pb and Sn-3.0Ag-0.5Cu solder alloys are widely used in today's microelectronic packages. In this study, isothermal interdiffusion in Sn-37Pb and Sn-3.0Ag-0.5Cu solder joints with Cu and Ni substrates after aging at 150°C was investigated. Diffusion structures and concentration profiles were examined by Field-Emission Electron Probe Microanalyzer (FE-EPMA). For Cu substrate, Cu₆Sn₃ and Cu₃Sn IMCs formed in both Sn-37Pb and Sn-3.0Ag-0.5Cu joints. For Ni substrates, Ni₃Sn₄ IMC was revealed in the Sn-37Pb/Ni joints. In the Sn-3.0Ag-0.5Cu/Ni joints, both (Ni,Cu)₃Sn₄ and (Cu,Ni)₆Sn₃ IMCs formed at soldering interface. Concentration profiles for each constituent along a specific trace line in joints were evaluated by detailed quantitative analysis with FE-EPMA. The interdiffusion fluxes of each element in the joint were calculated from the concentration profile with the aid of MultiDiFlux program. Effects of solder alloys on the elemental diffusion behavior in the joint assembly were probed and discussed.

4:40 PM

Reaction Paths and Diffusion Paths in Fe/Al-Si Joints Obtained with Various Silicon Contents: *Myriam Sacerdote-Peronnet*¹; *Jean-Claude Viala*¹; ¹University of Lyon

The Al-Fe-Si phase diagram is a key system for the development of metallic components and various products such as aluminium alloy parts locally reinforced with iron base inserts, hot dip aluminized steel sheets or laser beam welded aluminium/steel structures. To obtain Fe/Al-Si bimetallic materials with optimized properties, it is necessary to acquire a thorough understanding of their interface chemistry. In this context, an experimental study has been undertaken by immersing ferrous substrates in aluminium-silicon liquids with various Si contents (from 4 to 25 wt% Si) at temperatures ranging from 600 to 800°C. Different types of reaction zones were characterized depending on the



temperature and the silicon content of the aluminium alloy. For each of them, we will relate the reaction layer sequences observed at the interfaces with the Al-Fe-Si phase diagram using the diffusion path concept.

5:00 PM

Calculation of Carburizing Kinetic Parameters from the Carbon Concentration Profiles Based on Direct Integration of the Flux: *Olga Karabelchtchikova*¹; Mohammed Maniruzzaman¹; Richard Sisson¹; ¹Worcester Polytechnic Institute

Understanding the effect of process parameters on the mass transfer coefficient and carbon diffusivity in austenite is very important for the gas carburizing process control and optimization. A method for direct flux integration has been proposed in this paper to calculate the kinetic parameters from the experimental concentration profiles. 8620 steel discs were gas carburized at different levels of the atmosphere carburizing potential and at different austenizing temperatures. Analyses of the carburized parts included weight gain, micro-hardness and carbon concentration profile. Time-dependent weight gain and surface carbon content measurements allowed calculation of the instantaneous mass transfer coefficient, while carbon profiles corresponding to different carburizing times were used to calculate the concentration dependent carbon diffusivity. The calculated mass transfer coefficient and carbon diffusivity values were compared to those reported in the literature and served as input to the carburizing model validating the predicted results by the experimental concentration profiles.

5:20 PM

Diffusion Models for Boronizing Processes: Wycliffe Graham¹; Roumiana Petrova¹; Henry White²; ¹New Jersey Institute of Technology; ²Stony Brook University

Boronizing is a technically important elevated temperature metallurgical phenomenological process which is employed to reduce coking and improve the wear resistance of materials. In this study, we present a singly infinite multicomponent/ multiphase diffusion model to describe our experimental system. We assume (1) local equilibrium between adjacent phases separated by an interface, (2) motion of the diffusion plane at a particular position is proportional to the square root of the annealing time, (3) time invariant terminal concentrations, (4) no volume change in mixing due to interdiffusion, (5) sequence of phases appearing during diffusion correspond to the phase equilibria for the system, and (6) the composition of the phases across a boundary correspond to the equilibrium values in the phase diagram. We will present both experimental and theoretical results from our studies of boronizing of steel and refractory materials.

Dynamic Behavior of Materials: Deformation IV

Sponsored by: The Minerals, Metals and Materials Society, TMS Structural Materials Division, TMS/ASM: Mechanical Behavior of Materials Committee

Program Organizers: Marc Meyers, University of California; Ellen Cerreta, Los Alamos National Laboratory; George Gray, Los Alamos National Laboratory; Naresh Thadhani, Georgia Institute of Technology; Kenneth Vecchio, University of California

Tuesday PM
February 27, 2007

Room: Europe 3
Location: Dolphin Hotel

Session Chairs: Stephen Walley, Cavendish Laboratory; K. Ramesh, Johns Hopkins University

2:00 PM Invited

DRX: The Dynamic Deformation Regime: *Lawrence Murr*¹; ¹University of Texas, El Paso

Severe plastic deformation, especially involving high-strain-rates ($>10^3$ s⁻¹) occurs by solid-state flow which is accommodated by dynamic recrystallization (DRX), either in a continuous or discontinuous mode. This flow can be localized in shear instability zones (or adiabatic shear bands) with dimensions smaller than 20 microns, or include large volumes with flow zone dimensions exceeding centimeters. This paper will illustrate these microstructural features using optical and electron metallography to examine a host of dynamic

deformation examples: high velocity and hypervelocity impact and crater formation, rod penetration into thick targets (which includes rod and target DRX flow and mixing), large projectile-induced target plug formation and failure, explosive welding, and friction welding and processing.

2:30 PM

Shock and Recovery of Polymers and Particulate Composites: *Eric Brown*¹; Philip Rae¹; George Gray¹; Carl Trujillo¹; ¹Los Alamos National Laboratory

Polymers are increasingly being utilized as monolithic materials and composite matrices for structural applications historically reserved for metals. High strain rate applications in aerospace, defense, and automotive industries have led to interest in the shock response and the ensuing changes in polymer structure due to shock prestraining in a range of polymers and particulate composites. We present an experimental methodology for soft-recovery shock-loading coupled with mechanical and chemical post-shock analysis of these materials. Gas launched plate impact experiments have been performed on pedigree PTFE 7C momentum trapped shock assemblies to probe the effect of shock induced crystalline phase transitions in polymers. The technique is extended to recovery of an inert mock material for PBX 9501. Despite a highly ductile matrix, this composite exhibits low strain to failure under mechanical loading. Preliminary results on additional fluoropolymers will also be presented.

2:45 PM

Dynamic Behavior of Ceramic Powders: *Tracy Vogler*¹; Daniel Sandoval¹; Thomas Buchheit¹; Moo Lee¹; John Borg²; Dennis Grady³; ¹Sandia National Laboratories; ²Marquette University; ³Applied Research Associates

The behavior of ceramic powders under dynamic loading is of interest for a variety of applications. Several ceramic powders have been studied using a variety of techniques including planar shock loading, static compression, and nanoindentation to measure fundamental physical behavior. In addition, powder-filled metal cylinders were tested in a cylindrically convergent configuration using explosives and in normal impact to test available constitutive models for the powders. Post-test examination of recovered powders is used to quantify the mechanisms of deformation and compaction. We will present some of the key results of this investigation and attempt to draw some general conclusions about the dynamic behavior of granular materials and the suitability of existing models for simulations of multiaxial loading of ceramic powders. Sandia is a multiprogram laboratory operated by Sandia Corporation, a Lockheed Martin Company for the United States Department of Energy's National Nuclear Security Administration under contract DE-AC04-94AL85000.

3:00 PM

Meso-Scale Hydrodynamic Calculations of Porous Granular Material: *John Borg*¹; Tracy Vogler²; ¹Marquette University; ²Sandia National Laboratories

Meso-scale hydrodynamic calculations have been conducted in order to gain further insight into the dynamic compaction characteristics of granular ceramics. From the calculations a numerically derived shock response (Hugoniot) has been obtained and compared to experimentally obtained Hugoniot in order to assess the viability of the computational method. A parametric study has been done in order to assess the sensitivity of computationally derived Hugoniot to micro material characteristics such as strength, volume fraction, and particle size distribution. A discussion as to the shortcomings in the meso-scaling modeling technique, as well as ways, future considerations are included.

3:15 PM

Shock Compression of Iron Nanoparticles: *Chengda Dai*¹; Daniel Eakins¹; Naresh Thadhani¹; ¹Georgia Institute of Technology

The shock compression of iron nanoparticles is investigated to explore its potential as a soft magnetic constituent exchange-coupled with a hard phase for fabrication of nanocomposite permanent magnets. Recovery and instrumented experiments were performed in this work on ferromagnetic nanoparticles (25 nm) of iron. Recovery experiments were performed using three-capsule plate-impact geometry with the powders quasi-statically pre-pressed at various initial densities. Maximum densification attained at impact velocity of 1120 m/s (5mm-SS304 flyer) was around 84% theoretical maximum density. The recovered compacts showed retention of nano-scale structure with some growth

of the nanoparticles. Shock Hugoniot measurements were performed using PVDF stress gauges sandwiching the powder samples of known thickness to determine the stress amplitude and shock wave velocity. The results illustrate that the full-compaction pressure of nano-Fe particles is much higher, relative to the micro-scale Fe particles reported in literature, even after accounting for strength differences.

3:30 PM Break

3:45 PM

Laser Compression: A New Frontier in Shock Research: *Marc Meyers*¹; B. Remington¹; D. Lassila¹; J. McNaney¹; E. Bringa¹; ¹University of California

Laser compression provides pressures ranging from a few to hundreds of GPa at pulse durations of the order of nanoseconds or fractions thereof. It can be applied in both shock and quasi-isentropic mode. The short duration ensures a rapid decay of the pulse and quenching of shocked sample in times that are orders of magnitude lower than in conventional explosively driven plate impact experiments. Systematic experiments carried out in specimens well suited for transmission electron microscopy characterization are revealing that laser compression, by virtue of a much more rapid cooling, enables the retention of a deformation structure closer to the one existing during shock. The smaller pulse length decreases the propensity for localization. The limitations of laser experiments are also discussed. Research Supported by LLNL.

4:00 PM

The Mechanical Response of Pure Iron at High Strain Rates under Dominant Shear Loading: *Daniel Rittel*¹; Guruswami Ravichandran²; ¹Technion; ²Caltech

The mechanical behavior and microstructure of pure iron subjected to dominant shear loading has been characterized over a wide range of strain-rates. Pure iron is highly strain-rate sensitive. It exhibits marked strain-softening that is unexpected for the annealed material, but is identical to that of iron preshocked at 40 GPa. The microstructure undergoes significant refinement with increasing strain-rate, from large initial grains (50micron), through dislocation cells and large twinning, and finally microtwins and dynamically recrystallized 200 nm grains at the higher strain-rates. In-situ temperature measurements indicate the release of an external heat source, other than the thermomechanical conversion of plastic work, which is identified as dynamic recrystallization. The present results suggest the operation of the alpha-epsilon phase transition that is known to occur during hydrostatic or shock loading at 13 GPa.

4:15 PM

Dynamic Response of Cellular Materials Characterized with High Speed Imaging: *Hideaki Kusano*¹; Toshihiko Mukai²; ¹Shimadzu Corporation; ²National Institute for Materials Science

Cellular materials have a potential for absorbing impact energy. To effectively absorb the impact energy, a material is required to exhibit an extended stress plateau. In this study, closed-cellular Al foams have been examined at high strain rates. The mechanical response was characterized by split Hopkinson pressure bar. Simultaneously, the deformation behavior of cellular Al alloy was also monitored by the ultra high speed video camera, Shimadzu HPV-1, with the sampling time of 1~4 micro seconds. The deformation behavior was co-related with the mechanical response. The localized deformation behavior could cause larger stress drop after yielding in compression. Secondly, the high speed imaging was also applied for the characterization of acrylic resin cube with or without perforations. The effect of existing perforations was co-related with the mechanical response of the polymer cube. As a result, the effect of geometrical imperfection on the dynamic response of cellular material will be addressed.

4:30 PM

Dynamic Response of a Multilayer Prismatic Cellular Metal to Underwater Blast: *Zhensong Wei*¹; Anthony Evans²; ¹University of California, Santa Barbara

The objective of the present article is to characterize the response to water blast of a low relative density, multilayered corrugated core by combining insights from experiments and 3D simulations. The cellular metals have been fabricated using corrugations with 00/90 lay-up orientation and bonded by means of a transient liquid phase bonding method. Characterization of the dynamic crushing of the cores has revealed that, at low rates, interlayer

interactions induce a buckling-dominated, soft response. This softness is eliminated at high rates because inertial stabilization transitions the response to yield-control. The experiments conducted using the Dynocrusher test facility impart a soft response, consistent with lower rate crushing mechanisms. The 3D simulations and the Dynocrusher measurements are in broad agreement. The predictions of crushing strain, pulse amplitude/duration and impulse delivery rate correspond closely with the measurements. The application of core homogenization schemes has also been investigated.

4:45 PM

Mechanical Property and Energy Absorption of Aluminium Foams under Dynamic and Quasi-Static Compression: *Yuncang Li*¹; Jianyu Xiong¹; Mark Forrest¹; Peter Hodgson¹; Cui'e Wen¹; ¹Deakin University

Aluminium foams possess a unique combination of physical, mechanical, thermal, electrical and acoustic properties. In particular, they are lightweight and show excellent energy absorption. This makes them attractive in applications where crashworthiness and weight are critical, e.g. automotive industry and lightweight armour protection. In the present study, aluminium foams with superior mechanical properties and good energy absorption capacity were prepared through both the reinforcement of the matrix material and the resin-impregnation of the aluminium foams. The deformation behaviours and the energy absorption under dynamic and quasi-static compression of the aluminium foams were investigated. Results indicate that the stress of the aluminium foams under dynamic loading increased noticeably with the increasing of the strain rate. Furthermore, the resin-impregnation of the aluminium foams is a promising technique to improve the mechanical properties and the energy absorption capacity.

5:00 PM

Research on Dynamic Compressive Property of Aluminum Foam with Different Matrix: *Haijun Yu*¹; Guangchun Yao¹; Yihan Liu¹; ¹Northeastern University

Closed-cell aluminum foam (CCAF) with Al matrix and Al-6Si matrix was prepared in this test; the microcosmic pattern and phase composition of matrix were studied, and the dynamic compressive property was researched. The results show that the microcosmic pattern of CCAF with Al matrix is simple, existing basically as small pieces (Al₂₀CaTi₂); whereas the microcosmic pattern of CCAF with Al-6Si matrix is complex, mainly existing as large pieces (Al₃.21Si_{0.47} or CaAl₂Si₃), long needles (Al₃Ti) and small white flakes (Al₂O₃). Dynamic compressive results show that the stress—strain curves of CCAF with Al matrix are smooth, zone of fractures having obvious trace of being torn; whereas the stress—strain curves of CCAF with Al-6Si matrix are not smooth, some curve fluctuating markedly, and zone of fracture indicates obvious fracture characteristics of brittle material. With the increase of relative density, the trend of yield strength and apparent Young's modulus also increase.

5:15 PM

Design Space Exploration for Dynamic Testing of Foams in Split Hopkinson Pressure Bar: Siladitya Pal¹; *Spandan Maiti*¹; Ghatu Subhash¹; ¹Michigan Technological University

Substantial research over the years has established that the major parameters influencing stress equilibrium in split Hopkinson pressure bar (SHPB) set-up are specimen length, incident bar-specimen and specimen-transmission bar impedance mismatch, pulse shape and its duration and loading rate. General guidelines have been documented for testing ductile materials and ceramics. But such guidelines for porous materials (e.g., foams) which can exhibit large deformation without failure to extreme brittleness, are still emerging. In this study, an explicit dynamic finite element framework has been developed to model wave propagation in a SHPB and evaluate the effects of foam geometry (cell size and distribution), specimen dimensions, material properties, loading duration, and bar materials on the stress equilibration process. This computational model can simulate various loading conditions and experimental set-up geometries for a range of foam material behavior, thus capable of providing necessary design parameters for conducting dynamic experiments.



5:30 PM

Dynamic Buckling in Shock Loaded Metallic Prismatic Cores and Their Imperfection Sensitivity: *Enrico Ferri*¹; Anthony Evans¹; ¹University of California-Santa Barbara

Dynamic compression of thin 304 SS plates is investigated in a sandwich structure configuration by suddenly imparting a constant velocity to the front face. Such structures, which would buckle elastically under quasi static compression, are stabilized by inertia under intense dynamic loading. This stabilization enables the plate to deform plastically, enhancing its energy-absorption. The plates were tested at velocities up to 160 m/s. The transmitted stresses were measured with a Hopkinson bar and the buckling was monitored with high speed camera. The bucklewave length was found to be inversely proportional to the imposed velocity. The transmitted stresses exhibited a plateau level corresponding to the material yield strength at the relevant strain-rate and are independent of the imposed velocity but scale with the core height. Thereafter the stress drops abruptly. The duration of the transmitted stress pulse has been related to the time taken for propagation of the bucklewaves.

5:45 PM

Explosive Shock-Wave Consolidation of Aluminum Powder/Carbon Nanotube Aggregate Mixtures: Optical and Electron Metallography: *Wayne Salas*¹; Noe Alba Baena¹; Lawrence Murr¹; ¹University of Texas at El Paso

The formation of conventional metal-matrix composites from carbon nanotubes has proven to be difficult because of their agglomeration and inability to disperse. We have explored the explosive consolidation of 150 µm aluminum powder/multiwalled carbon nanotube (MWCNT) aggregates (including multiconcentric fullerenes) at volume percentages of 2 and 5%. These consolidated mixtures formed 2-phase, monolithic systems with the MWCNT aggregate material spreading along the Al grains and forming carbon phases at the Al triple points. The Al powder particle (or grain) hardness increased from HRE 22 to HRE 40 for the consolidated Al while the 2-phase system hardness dropped from HRE 40 to HRE 39 and 33 respectively for 2% and 5% (volume) MWCNT aggregate additions. TEM and FESEM observations illustrate a peculiar, laminate-like structure of the consolidated MWCNT aggregate material which is easily delaminated causing intergranular (Al) failure. The Al grains exhibit a shock-induced dislocation substructure (0.5-3 µm) and recrystallized sub-grains.

6:00 PM

Characterization of Micro and Nano Second Phase/2-Phase Regimes Created by Explosive Shock-Wave Consolidation of Powder Mixtures: *Noe Alba Baena*¹; Wayne Salas¹; Lawrence Murr¹; ¹University of Texas at El Paso

Mechanically mixed and green compacted (80%) powders of Al (150 µm)/SiC or Al₂O₃ (30 µm and 30 nm) in volume fractions of 2, 4 and 21% were explosively consolidated in cylindrical fixtures utilizing ANFO to form stacks of 2-phase, cylindrical monoliths 50 mm x 32 mm (diameter); including pure Al powder reference monoliths. The Al reference monoliths had a Vickers hardness (HV) of 46 in contrast to the starting powder hardness of 25. Correspondingly the Rockwell hardness for 21% SiC and Al₂O₃ mixtures in Al increased by ~60%, from the Al reference (single-phase) monolith; while the elongation declined by ~60%. The prominent Al intergranular-like fracture within the 21% (volume) SiC or Al₂O₃ phase regime was observed by FESEM. At 21% (volume) SiC a distinct 2-phase Al/SiC regime was formed with fracture occurring prominently in the SiC consolidated phase. Microstructures for these systems were also observed by optical metallography and TEM.

Electrode Technology Symposium (formerly Carbon Technology): Properties of Inert Anode Materials

Sponsored by: The Minerals, Metals and Materials Society, TMS Light Metals Division, TMS: Aluminum Committee

Program Organizers: John Johnson, RUSAL Engineering and Technological Center LLC; Morten Sorlie, Elkem Aluminium ANS

Tuesday PM

Room: Southern 3

February 27, 2007

Location: Dolphin Hotel

Session Chair: Alexander Gusev, RUSAL

2:00 PM Introductory Comments

2:05 PM

Corrosion Behavior of Nickel Ferrite-Based Ceramics for Aluminium Electrolysis Cells: *Xiao Yan*¹; Mark Pownceby¹; Geoff Brooks²; ¹Commonwealth Scientific and Industrial Research Organisation; ²Swinburne University of Technology

NiFe₂O₄-based ceramic materials of different compositions were fabricated from NiO, Fe₂O₃, and nitrides using the solid state synthesis technique at elevated temperatures. The materials were tested in a stirred finger test apparatus at 980°C in synthetic cryolite-Al₂O₃ melts in the presence and absence of molten aluminium. The factors affecting corrosion rates of the materials were investigated experimentally under various conditions. These included composition and porosity of the materials, rotating speed of the samples, duration of testing, and Al₂O₃ content of the electrolyte melts. The materials and baths before and after testing were characterized using XRD, XRF, ICP, and EPMA techniques, respectively. The microstructure of the materials before and after testing was compared and very good characteristics were observed. The results indicated that the corrosion resistances of the NiFe₂O₄-based ceramics against the electrolyte melts used and molten aluminium are very high. The mechanism of corrosion of the materials is discussed.

2:30 PM

Effect of Cu Content on the Corrosion Behaviour of Cu/(10Ni-90NiFe₂O₄) Cermets in Aluminum Electrolysis: *Tian Zhongliang*¹; *Lai Yanqing*¹; Li Xinzheng¹; Li Jie¹; Liu Yexiang¹; ¹School of Metallurgical Science and Engineering

Cu/(10Ni-90NiFe₂O₄) cermet inert anodes with metal Cu content of 0, 5, 10, 15 and 20% were prepared and their corrosion behavior in Na₃AlF₆-Al₂O₃ melts was investigated in laboratory electrolysis tests. The results indicate that the content of metal Cu in anodes had little effects on the steady-state concentrations of Ni in electrolyte, the concentration of Fe decreases from 304ppm to 206ppm and that of Cu increases from 21ppm to 70ppm with the content of metal Cu increasing from 0 to 20%. Considering the corrosion resistance, among NiFe₂O₄ based cermet anodes with different content of metal Cu, 5Cu/(10Ni-90NiFe₂O₄) cermet behaves best and should be further studied. Post-examination shows that metal Cu at the anode surface is oxidized, which improve its corrosion resistance, and doesn't leach preferentially during electrolysis.

2:55 PM

Effect of Additive and Grain Composition and on Properties of Inert Anodes: *Jinhui Xi*¹; Yingjie Xie²; Guangchun Yao²; Yihan Liu²; ¹China University of Mining and Technology; ²Northeastern University

In order to improve the distributions of metal phase in cermet inert anodes and then increase the properties of inert anodes, in this study, additive and grains graduation were adopted. Firstly, additive V₂O₅ was added to Fe₂O₃ and NiO powder when prepare NiFe₂O₄. Then NiFe₂O₄ ceramic with V₂O₅ was crushed, and the different size of grains been blended together when prepare cermet inert anodes. It is found that the properties of the samples with grain graduation are better than that of samples without grain graduation. More importantly, when appropriate grain graduation according to certain-sized sample is used, metal Ag can form the network structure in the ceramic matrix. The optimized distribution of Ag can be beneficial to increasing the properties of samples. In addition, additive V₂O₅ can make the distribution of the metal phase more ideal.

TUESDAY
PM

3:20 PM

Al-Ti-O-X Cermet as Inert Anode for Aluminium Electrolysis: Xiaozhou Cao¹; Zhongning Shi¹; Hongmin Kan¹; Xianwei Hu¹; Zhaowen Wang¹; Zhuxian Qiu¹; ¹Northeastern University

A new Al-Ti-O-X cermet inert anode was investigated for aluminium electrolysis. The anode was fabricated by cold-press and sintered at 1600°C in Ar atmosphere with Al₂O₃, TiO₂ and metal as raw materials. The phase and microstructure of anode were analyzed by XRD and SEM. The results shows a new phase (Al₂TiO₅) created in the anode, metal phase dispersed in ceramic phase which can increase anode electric conductivity. Anode material was tested in electrolyte molten salt. Al-Ti-O-X cermet anode shows good anti-corrosion and stable cell voltage during the course of electrolysis test.

3:45 PM

Effect of Copper Content on Microstructure and Mechanical Properties of Cu/(10NiO-NiFe₂O₄) Cermets: Zhang Gang¹; Li Jie¹; Lai Qing¹; Zhang Yong¹; Tian Liang¹; Ye Long¹; Liu Xiang¹; ¹Central South University

Cu/ (10NiO-NiFe₂O₄) cermets were fabricated by using cold pressing sintering method. The phase composition and microstructure and effect of metallic content on the relative density and mechanical properties such as bending strength and fracture toughness were studied. The results showed that the cermets were consisted of Cu, NiO and NiFe₂O₄. Within the range of metallic content from 0 to 20wt. %, there was a durative increase for the fracture toughness and a break for the relative density and bending strength with the increase of metallic content. A maximal relative density with 95.85% and bending strength with 200.34MPa and fracture toughness with 3.55 MPa•m^{1/2} could be achieved at the metallic content of 5wt. %, 15wt. % and 20wt. %, respectively. The ratio of Fe/Ni is about 2.58~2.84 in NiFe₂O₄ and 0.24~0.29 in NiO. The metallic composition is consisted of Cu, Fe and O element.

4:10 PM Break

4:30 PM

Study on the Conductivity of Fe-Ni-Al₂O₃ Cermet Inert Anode: Xiaozhou Cao¹; Zhongning Shi¹; Xianwei Hu¹; Xiaodong Lu¹; Zhaowen Wang¹; Zhuxian Qiu¹; ¹Northeastern University

Al₂O₃ was used as ceramic matrix of inert anode in order to lighten the corrosion of anode and reduce the pollution of anode material to aluminium product, meanwhile adding Fe and Ni metals to improve the electrical conductivity of anode. Fe-Ni-Al₂O₃ cermet inert anode was prepared by powder metallurgy and electric conductivity was measured by four-electrode method. Study on the effect of metal content temperature and microstructure to electric conductivity of anode. The results show the anode has the property of high-temperature semiconductor and the conductivity of anode increases with the temperature rising. The mechanisms of conductivity were discussed according to the experiments.

4:55 PM

Analysis on Electrolysis Corrosion from the Electric Mechanism of Cermet Inert Anode Based on Nickel Ferrate: Tao Luo¹; Zhao-wen Wang²; ¹Sun-Stone Carbon Technology Center; ²School of Materials and Metallurgy, Northeastern University

Such inert anode comprises NiFe₂O₄, NiO and metallic Ni and Cu. Because the NiFe₂O₄ and NiO are semiconductors, the cermet anode also presents the speciality of semiconductor, and the electrical conductivity suddenly ascends at about 750°C. NiFe₂O₄ is a kind of N-type semiconductor, which electric mechanism is due to charging and discharging electron of Fe³⁺ ions to Ni²⁺ ions around them. So the Fe³⁺ ions own much more activity than others, which results in the un-proportional loss of Fe element compared with Ni element in the nickel ferrate spinel matrix during the electrolysis.

Friction Stir Welding and Processing IV: Session III

Sponsored by: The Minerals, Metals and Materials Society, TMS Materials Processing and Manufacturing Division, TMS: Shaping and Forming Committee

Program Organizers: Rajiv Mishra, University of Missouri; Murray Mahoney, Rockwell Scientific Company; Thomas Lienert, Los Alamos National Laboratory; Kumar Jata, US Air Force

Tuesday PM

Room: Northern E3

February 27, 2007

Location: Dolphin Hotel

Session Chair: Tracy Nelson, Brigham Young University

2:00 PM Invited

Microstructures and Mechanical Properties of Friction Stir Welded AA5182 and AA5754 Aluminum Tailor-Welded Blanks: Yen-Lung Chen¹; ¹General Motors

The microstructures and mechanical properties of friction-stir-welded AA5754-O and AA5182-O aluminum tailor welded blanks have been characterized. All samples failed in the base metal region except in those cases where there was a severe undercut at the weld toe. Microhardness measurements showed that there was a maximum hardness increase of 16-30% in the thermomechanically affected zone (TMAZ) over the base metal, mainly due to the work hardening effect of the friction stir welding process and the grain refining effect in the weld nugget. The weld nuggets consisted of small, equiaxed grains, about 8 μm in diameter. In this study the higher hardness of the friction-stir welds than the base metals should help prevent failure in the weld during forming of the tailor-welded blanks. Furthermore, the fine grains in the weld nugget should be beneficial to the ductility of the weld.

2:20 PM

Formability and Springback Evaluation of Friction Stir Welded Automotive Sheets: Wonoh Lee¹; Junehyung Kim¹; Daeyong Kim²; Chongmin Kim³; Sangjoon Park¹; Michael L. Wenner³; Kazutaka Okamoto⁴; R.H. Wagoner⁵; Kwansoo Chung¹; ¹Seoul National University; ²Hyundai-Kia Motors; ³General Motors; ⁴Hitachi America, Ltd.; ⁵Ohio State University

Formability and springback of automotive friction stir welded TWB (tailor welded blank) sheets were experimentally and numerically investigated for aluminum alloy 6111-T4, 5083-H18 and DP-steel sheet samples, which were friction-stir welded with the same and different thicknesses. To represent mechanical properties, anisotropic yield function Yld2004-18p and the combined isotropic-kinematic hardening law were utilized. In order to examine formability, deformation until failure in three applications including the simple tension test with various weld line directions, the hemisphere dome stretching test and the cylindrical cup drawing test were measured and simulated. For springback, two types of weld line combinations, longitudinal and transverse TWBs, were prepared for three springback tests, the unconstrained cylindrical bending, 2-D draw bending and OSU draw-bend tests. The numerical code performed reasonably well in analyzing all verification tests, while the magnitude of springback was largely dependent on the ratio of the yield strength with respect to Young's modulus and thickness.

2:35 PM

Formability Analysis of Locally Surface-Modified Al 5052 Sheets: Chang Lee¹; Suk Kang²; Heung Han²; Sung-Joon Kim¹; Kyu Oh²; ¹Korea Institute of Machinery and Materials; ²Seoul National University

Microstructural characteristics of Al 5052 sheets whose surface were locally modified by the concept of SFJ (Surface Friction Joining) were analyzed. Severe shear deformation and residual heat are two main variables for the microstructure change of the modified region, so that the mechanical property can also be changed. It is noteworthy that the formability of the surface-modified sheets is greatly improved compared with as-received sheets. The formability is improved as the tool diameter is increased, and these results are indicated by LDH (Limiting Dome Height) test. EBSD analysis was carried out to evaluate relationship between microstructural change and mechanical properties. PQ (pattern quality), which is one of the representative EBSD results, was introduced for the plastic deformation measurement. The average PQ gap during LDH test was measured for modified region and base material,



respectively. It is found that more plastic deformation is accommodated at modified region during LDH test.

2:50 PM

Numerical Simulation of the Static and Dynamic Response of Corrugated Sandwich Structures Made with Friction Stir Welding and Superplastic Forming: Karim Muci Kuchler¹; Sajith Kumar Annamaneni¹; Darrell Herling²; William Arbegast¹; ¹South Dakota School of Mines and Technology; ²Pacific Northwest National Laboratory

Sandwich structures have the potential to find applications in vehicles or vessels subjected to impulsive loadings. A key element of those structures is the geometry of the top and bottom surfaces and the geometry of the core. To justify the use of a sandwich structure instead of a monolithic plate, it is necessary to demonstrate that it will have a superior performance under the expected loading conditions while maintaining the same weight. It has been shown that through the combination of friction stir welding and superplastic forming, different types of corrugated sandwich structures can be obtained. In this paper, numerical simulations are used to perform an initial comparison of the static and the basic dynamic characteristics of two of those structures against a monolithic plate of the same material and weight. Based on the results of the simulations, conclusions are drawn regarding the possible applications of the corrugated sandwich structures.

3:05 PM

Mechanical Properties of Friction Stir Welded Metal Matrix Composites at Cryogenic Temperatures: Chris Vickery¹; Sara Hagie¹; Michael Langerman¹; William Arbegast¹; Casey Allen¹; ¹South Dakota School of Mines and Technology

Aluminum metal matrix composites (MMC's) are known to possess thermal conductivities that are dependent on the volumetric loading and type of the ceramic reinforcement. Exploiting this characteristic in designing thermally insulating metallic structures requires the ability to join these materials while maintaining the desirable properties across the joint at service temperatures. Friction stir welding has been demonstrated to successfully joint MMC's while maintaining uniform particle distributions and austensibly thermal properties that are consistent with the parent material. Friction stir welds in butt and lap joints in alumina reinforced aluminum MMC with 10 and 20 volume percent have been tested under cryogenic conditions to determine static tensile strength of the welded joint. For comparison, tensile properties of the parent materials at room temperature and cryogenic temperature, and of the welded joints at room temperature were also obtained.

3:20 PM

Effect of Processing Parameters on Microstructure of the FSW Nugget: Joseph Querin¹; Judy Schneider¹; ¹Mississippi State University

Friction stir welding is a thermo-mechanical process that utilizes a non-consumable rotating pin tool to stir the edges of a weld seam together. Within the recrystallized zone of the weld nugget, contrasting bands are commonly observed using optical microscopy. Although the mechanisms resulting in the formation of these contrasting bands are unclear, they may result from variations in the thermo-mechanical processing that the material experiences. Orientation image mapping (OIM) is used in this study to determine the size and crystallographic orientations of the refined grains associated with the banded regions. Corresponding variations in hardness are determined using nano-indentation measurements.

3:35 PM Break

3:50 PM

Friction Stir Lap Joining of Al 7075 with Sealant: Tim Li¹; George Ritter¹; Nick Kapustka¹; Richard Lederich²; ¹Edison Welding Institute; ²Boeing Company

The implementation of friction stir welding (FSW) as a rivet replacement technology has drawn a tremendous interest from the aerospace industry in recent years. The traditional riveting process is labor intensive and costly, and mechanical properties of FSW lap joints are superior to the riveted ones. However, the inherent issue of crevice corrosion in FSW lap joints must be resolved before FSW lap joining can be fully implemented on aircraft structures. A desirable approach to this problem is to apply sealant between two metal sheets prior to FSW. In this paper, FSW lap joining with a sealant was conducted on 0.080-in. (2 mm) thick Al7075-T7 sheet. No crevice corrosion

was observed at the faying surfaces of all FSW lap joints after exposure to salt fog spray for 500 hr. This feasibility study has shown promising results for resolving the inherent crevice corrosion issue for bringing FSW lap joints into production.

4:05 PM

Friction Stir Lap Welds of AA6111 Aluminum Alloy: Manasij Yadava¹; Rajiv Mishra¹; Y. Chen²; X. Gayden²; Glenn Grant³; ¹University of Missouri; ²General Motors; ³Pacific Northwest National Laboratory

A study of the hooking defects in friction stir welded lap joints of AA6111 aluminum alloy was conducted. In this study, 1.0 mm sheets of AA6111 aluminum alloy were welded in lap joint configuration by friction stir welding (FSW). Different tools and process parameters were used to study the effects of these variables on defect configuration, and therefore weld strength. Lap-shear tests were performed in the as-welded and heat treated conditions. Hooking defects on both the advancing and retreating side have been correlated with the FSW process variables. Heat treatment response of welds was observed to vary with process parameters. Process variables were optimized for maximum strength in the heat treated condition. This work was performed under the NSF-IUCRC for Friction Stir Processing and the support of NSF, Boeing, GM, Pacific Northwest National Laboratory and Friction Stir Link for the UMR site is acknowledged.

4:20 PM

Friction Stir Welding of an Aerospace Magnesium Alloy: Xinjin Cao¹; M. Jahazi¹; M. Guerin¹; ¹Institute for Aerospace Research

Hot rolled AZ31B-H24 sheets with a thickness of 4.95 mm were joined using an MTS ISTR friction stir welding machine. The cavity defects in the butt joints were studied and two mechanisms are observed. The pores are thought to be due to volume deficiency, and/or poor material flow and mixing. Excessive metal loss may cause subsurface pores which usually occur at the upper half of the welding nugget at the advancing side. Poor material flow and mixing may form internal pores which are usually elongated and curved, with the concave side in the welding direction. The grain size in the weld nugget was observed to be larger than that in the thermal-mechanically affected zone or heat-affected zone due to recrystallization, causing a drop in Vickers microindentation hardness.

4:35 PM

Friction Stir Joining of Thermoplastics: Saritha Mattapelli¹; William Arbegast¹; Robb Winter¹; ¹South Dakota School of Mines and Technology

Over the last several years we have investigated the joining of thermoplastic polypropylene using the Friction Stir Joining (FSJ) technique. Our work has focused on optimizing the FSJ process parameters, specifically material travel speed, material pre-heating temperature, material pre-heating time, pin tool rotation speed, and pin tool thread pitch. The FS joint was characterized using optical microscopy, scanning electron microscopy, and differential scanning calorimetry (DSC); and for tensile strength and percent elongation. As a result of this research a process map was developed which shows that higher quality joints are obtain at high pin tool rotation speeds and low material travel speed. It was observed that the tensile strength of the friction stirred joints was ~90% of the parent material. DSC shows that crystallinity appears to vary through the FS joint. Work is currently ongoing to spatially resolve crystalline density, flow patterns, and the temperature distribution through the FSJ part.

4:50 PM

Friction Stir Welding of Bulk Metallic Glasses – Vitreloy 106A: Rakesh Suravarapu¹; Katharine Flores²; William Arbegast¹; Stanley Howard¹; ¹South Dakota School of Mines and Technology; ²Ohio State University

The objective of this work was to determine if the metallic glass (BMG), Vitreloy 106A, could be friction stir processed and retain its amorphous nature in the welded region and, if so, to establish the processing window. Small (3x3 in.) room-temperature and preheated material was friction stir processed with selected processing parameters ranging from 300 to 800 RPM and travel speeds of 0.5 to 2 in. per minute using PCBN and W-Re pin tools. X-ray diffraction and differential scanning calorimeter methods were used to determine that the extent of devitrification decreased with increased average specific heat input, pseudo heat index I (RPM/IPM * Plunge) and pseudo heat index II (RPM/IPM * Forge). Friction stir plunges did not cause devitrification. Linear welds ranged from 38 to 79 % devitrified, with better plasticization for

preheated welds which were approximately 50% devitrified. Improved results are thought possible with larger samples.

Frontiers in Solidification Science: Microstructures II

Sponsored by: The Minerals, Metals and Materials Society, TMS Electronic, Magnetic, and Photonic Materials Division, TMS Materials Processing and Manufacturing Division, TMS: Chemistry and Physics of Materials Committee, TMS: Solidification Committee

Program Organizers: Jeffrey Hoyt, Sandia National Laboratories; Mathis Plapp, Ecole Polytechnique; Gabriel Faivre, CNRS; Shan Liu, Iowa State University

Tuesday PM Room: Northern A3
February 27, 2007 Location: Dolphin Hotel

Session Chair: To Be Announced

2:00 PM Invited

Faceted Twinned Bicrystalline Si Dendrites in Al-Si Alloys: *Ralph Napolitano*¹; Choonho Jung²; Emrah Simsek³; ¹Materials Science and Engineering, Iowa State University; Materials and Engineering Physics, Ames Laboratory; ²Iowa State University; ³Ames Laboratory

Mechanisms of selection controlling the morphology of faceted bicrystalline primary silicon "dendrites", grown directionally in Al-Si alloys, are investigated. In particular, we examine twin boundaries within the dendritic core, consider the detailed atomistic structure, and propose a twin-plane migration mechanism, where a complex configuration of high-mobility coherent twin boundaries provides the morphological responsiveness required for dendritic array development and optimization. We employ Bridgman-type growth experiments along with serial milling, electron microscopy, electron probe microanalysis, and backscattered electron diffraction to investigate the dendrite tip conditions, branching and splitting mechanisms, overall array adjustment, microsegregation patterns, orientation relationships, and the growth of the interdendritic fcc Al phase.

2:30 PM Invited

In Situ and Real Time Study of Directional Solidification by Synchrotron Imaging in Al-Based Alloys: *Henri Nguyen-Thi*¹; Guillaume Reinhart¹; Nathalie Manginck-Noël¹; Hyejin Jung¹; Bernard Billia¹; Adeline Buffet²; Thomas Schenk³; Jürgen Härtwig²; José Baruchel²; ¹L2MP-University Paul Cézanne; ²ESRF; ³LPM-Ecole des Mines de Nancy

The properties of Al-based alloys are largely controlled by the microstructure left during the growth process, with the accompanying solute segregation profile. Understanding the patterns that form during the growth process is not only of high technological interest but also scientifically important. In situ and real-time observation of the solid-liquid interface is crucial to deepen our understanding of dynamical phenomena that occur during the solidification process. To achieve this goal, directional solidification experiments in both Al-Ni₃5wt% and Al-Si₇0wt% alloys were carried out at the European Synchrotron Radiation Facility (ESRF) in Grenoble (France). By using the combination of synchrotron X-ray Radiography (SXR) and Synchrotron White-Beam X-Ray Topography (SWBXR), we are able to characterize both geometrical and crystallographic information for the same solidification microstructure. These techniques give critical information on dynamical phenomena and crystallographic properties of the solidifying microstructure during either columnar or equiaxed growths and the columnar-to-equiaxed transition (CET).

3:00 PM Invited

Fine Structures: Feedback Control of Unstable Binary Alloy Microstructures: *Wolfgang Losert*¹; Silvere Akamatsu¹; Herman Singer¹; Andrew Pomerance¹; Michael Newey¹; Antonio Pons²; Alain Karma²; ¹University of Maryland; ²Northeastern University

We present an experimental and simulation study of feedback control of unstable cellular patterns in directional solidification (DS) of a dilute binary alloy in a two-dimensional geometry. The control scheme consists of applying local, transient heating spots of constant power close to cell tips which

protrudes ahead of the average position. Phase field simulations show that such a control scheme can stabilize spacings an order of magnitude below the threshold of a period-doubling instability. In DS experiments, we use a transparent succinonitrile-coumarin 152 alloy in thin samples. With automatic, real-time tracking of cell tips, and by using moveable, micron sized laser spots for local heating, we obtain a long-lasting stabilization of uniform cellular arrays well into the unstable range with minimal heating, as predicted by numerical calculations.

3:30 PM Break

3:50 PM Invited

Morphological Similarity between Macro-Step Pattern in Sublimation and Interface Pattern in Solidification: Seong Gyoon Kim¹; Jin Yang²; *Won Tae Kim*³; ¹Kunsan National University; ²Sapphire Technology Company; ³Cheongju University

Diffusion induced instability of solid/liquid interface during solidification of metals or alloys is well established. Depending on the growth condition planar, cellular, cellular dendritic, and dendritic patterns can be formed. In this study we report another example of pattern evolution caused by the diffusion induced instability. During the sublimation of sapphire, various macro-step patterns were observed from smooth lines, faceted lines, cellular form, isolated dendrites and dendritic array. The evolution of the patterns was analyzed in terms of temperature dependences of evaporation rate and ad-atom diffusivity. The morphological transitions between the various macro-step patterns showed striking similarity to the transition of solid/liquid interface patterns observed in solidification of materials. The secondary arm spacing behind the leading tip was in agreement with the wave length determined by stability analysis of macro-step. Phase-field simulation of step flow with Burton-Cabrera-Frank (BCF) model reproduced all the features of dynamics of the observed pattern evolution.

4:20 PM Invited

Measurements of Experimentally Grown Three-Dimensional Xenon Multiplets and Comparative Phase Field Simulations: *Herman Singer*¹; Irina Singer¹; Joerg Bilgram¹; ¹Swiss Federal Institute of Technology ETH

We investigate in our in situ experiments 3D xenon crystals during free growth into pure supercooled melt. Changes of growth morphologies are induced by a perturbation of the thermal diffusion field in the surrounding melt of the crystal. Apart from the dendritic morphology, seaweed and doublon morphologies and for the first time transitions from dendritic to triplet structures (first predicted by [Abel et al., PRE 55, 7789 (1997)]) were observed experimentally. Quantitative measurements of the 3D reconstruction of dendrites and doublons will be given. For dendrites we find excellent agreement between the experimentally measured thickness of dendritic fins and analytical predictions of Brener and Temkin [PRL 71, 3653 (1993)]. With 3D phase field simulations it was possible to reproduce the experimental procedure and to verify that doublon and triplet structures can grow in a stable way even in the presence of anisotropic surface free energy as found for experimental substances.

4:50 PM

Growth of Equiaxed Dendritic Crystals Settling in an Undercooled Melt: *Arnoldo Badillo*¹; *Christoph Beckermann*¹; ¹University of Iowa

The growth of single equiaxed dendritic crystals settling in an undercooled melt is examined by performing experiments with transparent succinonitrile-acetone alloys. The crystals are dropped in a tall glass cylinder containing the undercooled melt. Using two traveling cameras, the crystal settling speed, dendrite arm orientations, and dendrite tip growth velocities are measured as a function of time. It is found that the dendrite tip growth velocity is a strong function of the orientation of the dendrite arm and the relative flow speed between the melt and the crystal. However, the average of the six primary dendrite arm growth velocities is nearly identical to that predicted by the standard diffusion theory. Furthermore, the variation of the internal solid fraction of the settling equiaxed crystals, calculated from the measured settling speeds, is well predicted using a model for convective heat and mass transfer from a volume-equivalent sphere.



5:10 PM

Quantifying Dendritic Coarsening in Three Dimensions: *Amber Genau*¹; Peter Voorhees¹; Dimitris Kammer¹; ¹Northwestern University

Although dendritic coarsening is extremely common and plays a major role in determining the mechanical properties of metallic alloys, it has not been extensively studied because of the difficulties measuring topologically complex structures. Using serial sectioning and three-dimensional reconstruction techniques, the evolution of isothermally coarsened solid-liquid mixtures in Pb-Sn alloys was analyzed in three dimensions. Both qualitative and quantitative analysis will be presented, including a new method for evaluating the spatial distribution of interfacial curvatures in systems with complex structures. The spatial distribution of curvature is vital to fully understanding the process of coarsening because diffusion dictates that the evolution of a structure is driven not only local curvature but also by the proximity of other curved interfaces. Probability density plots of the interfacial curvature distribution and of anisotropy as measured by the distribution of interface normals will also be presented for a range of volume fraction alloys.

Fundamentals of Shape Memory and Related Transitions: Atomistic and Microstructural Mechanisms

Sponsored by: The Minerals, Metals and Materials Society, TMS Structural Materials Division, TMS: Chemistry and Physics of Materials Committee
Program Organizers: Michael Manley, University of California; James Morris, Oak Ridge National Laboratory

Tuesday PM Room: Europe 6
February 27, 2007 Location: Dolphin Hotel

Session Chair: Avadh Saxena, Los Alamos National Laboratory

2:00 PM Introductory Comments

2:10 PM Invited

Structural Transformations and Gigantic Magnetostriction in Fe-Ga Alloys: *Armen Khachatryan*¹; Dwight Viehland²; ¹Rutgers University; ²Virginia Tech

The Fe-Ga BCC alloys with ~15-20 at % Ga have a giant magnetostriction that may exceed 20x that of α Fe. Application of the coherent thermodynamics to this system predicts the special type of decomposition between two solubility limits of the BCC phase described by the equilibrium phase diagram and the coherent phase diagram. This decomposition is controlled by excess vacancies playing the role of the third component. It involves the local Bain distortion and eventually produces a dispersion of nano-size magnetic tetragonal clusters of the FCT phase. The reorientation of these clusters under the applied magnetic field produces macroscopic strain interpreted as a giant extrinsic magnetostriction. The proposed theory predicts two concentration ranges where such a magnetostriction may occur (~10-20 at%Ga and 25-27 at%Ga) and the atomic structure of the clusters in both ranges. The estimates for the magnetostriction are in good agreement with the observations.

2:40 PM

Tracing Phase Transition and "Memory" in Ferromagnetic Shape-Memory Alloys under External Fields: *Yandong Wang*¹; Yang Ren²; E-Wen Huang¹; Gang Wang³; Zhihua Nie³; Hahn Choo¹; Peter Liaw¹; Liang Zuo³; ¹University of Tennessee; ²Argonne National Laboratory; ³Northeastern University

A magnetic-field control of the shape-memory effect has been demonstrated in the ferromagnetic Ni-Mn-Ga and Ni-Co-Mn-In alloys with the Heusler structure. Although considerable attention has been devoted to the processing of ferromagnetic materials for optimal performance properties, the underlying mechanism that controls the shape-memory effect remains unclear. In particular, the interactions between crystallographic textures and stresses and their influences on the functional performance in polycrystalline SMAs are less understood. Here we use the synchrotron-based high-energy X-ray diffraction to study the in-situ behavior of phase transition for revealing the underlying mechanisms of the role of various stresses and textures on 'memory' at the

scale of multi-scale microstructures. In particular, the mutual interactions of multiple external (temperature, stress, and magnetic) fields on the phase transformation characterizations will be studied in-situ for the first time in the state-of-the-art instrumentation established at the 11-ID-C beamline, APS. Some important findings will be reported.

3:05 PM

Magnetic Domain Walls and Anti-Phase Boundaries in Ni-Mn-Ga Ferromagnetic Shape Memory Alloys: *Sai Prasanth Venkateswaran*¹; Noel T. Nuffer¹; Marc DeGraef¹; ¹Carnegie Mellon University

The ferromagnetic shape memory alloy Ni₂MnGa has an ordered Heusler structure at room temperature. As in most materials with this structure type, rapidly cooled (quenched) samples have a large density of anti-phase boundaries (APBs), both on the Heusler and B2 sublattices. In this work, we set out (1) to show that APBs are present, and (2) to determine whether or not magnetic domain walls and APBs interact in this system. Although APBs are not visible with conventional dark field imaging methods, they do become visible in the Fresnel imaging mode; every APB is decorated by a magnetic domain wall. Through image simulations, we will show evidence for the presence of two types of magnetic image contrast: one associated with the APBs and the other with conventional 180 degree domain walls.

3:30 PM Break

3:50 PM Invited

Martensitic Alpha to Omega in Titanium: Atomic Pathway and Impurity Effects: *Dallas Trinkle*¹; Richard Hennig²; Srilliputhur Srinivasan³; Robert Albers³; John Wilkins⁴; ¹University of Illinois, Urbana-Champaign; ²Cornell University; ³Los Alamos National Laboratory; ⁴Ohio State University

Pure titanium transforms under pressure to the brittle omega phase, a transformation that must be suppressed for engineering applications. Impurities, such as 1% oxygen in commercial Ti alloys, greatly affect this transformation. The theoretical understanding of transformation suppression relies on: (1) finding the atomic pathway of the martensitic transformation in pure titanium and (2) using this pathway that traps the impurities to estimate their effect. A systematic approach generates all possible pathways; they are successively pruned by energy estimates using elastic theory, tight-binding and first-principles methods. This final method reduces seven possibilities to the lowest energy pathway. The speed of the diffusionless martensitic transformation traps dilute impurities, providing candidate pathways for alloyed materials. Ab initio refinements yield the change in both the relative stability of and the energy barrier between the phases due to impurities. The resulting microscopic picture explains the suppression of the transformation in commercial Ti alloys.

4:20 PM Invited

Reaction Coordinate Theory of Martensitic Transformation: Chen Shen¹; Ju Li¹; *Yunzhi Wang*¹; ¹Ohio State University

The behavior of shape memory alloys is controlled by the underlying mechanisms of martensitic transformations. In this presentation we formulate a reaction coordinate theory to study nucleation mechanisms during martensitic transformations, which can describe generally curved paths in both transformation strain space and real space. With the incorporation of phase field microelasticity theory and ab initio calculations of the optimal transformation path (in a multi-dimensional space of cell vectors and internal coordinates) of a representative cell that brings the parent phase into the product phase during a martensitic transformation, the activation energy and critical nucleus of martensite are computed using a modified nudged elastic band method. It is shown that the configuration of a martensite embryo could differ significantly from that of a fully grown martensitic plate of invariant plane habit. Examples of both homogeneous and heterogeneous nucleation will be discussed.

4:50 PM

Characterization of a New Phase in a Ti-30Ni-20Pt High Temperature Shape Memory Alloy Using DSC, TEM and 3-D Atom Probe Tomography: *Michael Kaufman*¹; Sarah McMurray²; David Diercks¹; Anita Garg³; Ronald Noebe³; ¹University of North Texas; ²Western Kentucky University; ³NASA Glenn Research Center

A new phase observed in a nominal Ti-30Ni-20Pt high temperature shape memory alloy (HTSMA) has been characterized using transmission electron

microscopy and 3-D atom probe tomography. This phase forms homogeneously in the B2-structured austenite phase by a nucleation and growth mechanism. At 500 °C the precipitate phase coarsens from ~30nm after 4h to ~250nm after 1000h and results in a concomitant increase in the martensitic transformation temperature of the base alloy. Although the structure of this phase typically contains a high density of faults making characterization difficult, it appears to be trigonal (-3m point group) with $a \sim 1.28$ nm and $c \sim 1.4$ nm. Its composition is slightly depleted in Pt relative to the matrix. The implications of this phase on the stability, transformation temperatures, and overall SMA properties will be highlighted accordingly. *Work performed using the analytical facilities in the Center for Advanced Research and Technology at the University of North Texas.*

5:15 PM

Alternate Transformation Pathways in NiTi: *James Morris*¹; Maja Krcmar²; Y. Y. Ye³; C. L. Fu¹; ¹Oak Ridge National Laboratory; ²Grand Valley State University; ³Ames Laboratory

Recent calculations suggest an orthorhombic structure for the ground state of NiTi, obtained from the B19 structure by tilting to approximately 107°. We show that this structure is the B33 structure, and that the phase transformation from the B19 phase can occur through an infinite number of pathways. Ab initio calculations suggest that any of these can occur through a homogeneous deformation that has no energy barrier at T=0 K. These pathways arrive from a geometric relationship between the parent and product phase, related to both possible dislocation dissociations in the parent phase, and low-energy stacking faults in the product phase. The possible transformation pathways suggest a specific role of dislocations and low-angle grain boundaries in the two-way shape memory effect. This research is sponsored by the Division of Materials Science and Engineering, Office of Basic Energy Sciences, US Department of Energy under Contract No. DE-AC05-00OR-22725 with UT-Battelle.

General Abstracts: Structural Materials Division: Advances in Steel II

Sponsored by: The Minerals, Metals and Materials Society, TMS Structural Materials Division, TMS: Advanced Characterization, Testing, and Simulation Committee, TMS: Alloy Phases Committee, TMS: Biomaterials Committee, TMS: Chemistry and Physics of Materials Committee, TMS/ASM: Composite Materials Committee, TMS/ASM: Corrosion and Environmental Effects Committee, TMS: High Temperature Alloys Committee, TMS/ASM: Mechanical Behavior of Materials Committee, TMS/ASM: Nuclear Materials Committee, TMS: Product Metallurgy and Applications Committee, TMS: Refractory Metals Committee, TMS: Superconducting and Magnetic Materials Committee, TMS: Titanium Committee

Program Organizers: Rollie Dutton, US Air Force; Ellen Cerreta, Los Alamos National Laboratory

Tuesday PM Room: Europe 5
February 27, 2007 Location: Dolphin Hotel

Session Chairs: Robert Field, Los Alamos National Laboratory; Amy Clarke, Los Alamos National Laboratory

2:00 PM Introductory Comments

2:10 PM

Investigation of Specific Compositional Elements as the Bases for the Specimen Bias in Fracture Toughness Reference Temperature for Reactor Pressure Vessel Steels: *Randy Nanstad*¹; John Merkle¹; ¹Oak Ridge National Laboratory

There is strong interest from the nuclear industry to use the precracked Charpy single-edge notched bend, SE(B), specimen (PCVN) to enable determination of the reference temperature, T_0 , with reactor pressure vessel surveillance specimens. Unfortunately, for many different ferritic steels, tests with the PCVN specimen (10x10x55 mm) have resulted in T_0 temperatures 10 to 25°C lower than T_0 values obtained using data from compact, C(T), specimens. Various micromechanics evaluations have been conducted to explain the observations, with crack tip constraint being the commonly identified factor.

Preliminary observations of this bias for a number of different reactor pressure vessel steels, both base metals and welds, have identified certain compositional differences that may contribute to such observations. The fracture toughness data are reviewed and the chemical compositional differences are compared with the results of analysis showing the dependencies of the biases.

2:30 PM

Mechanical Properties and Strain Hardening Behavior of Microstructures Produced by Quenching and Partitioning (Q&P) Processing: *Amy Clarke*¹; John Speer²; David Edmonds³; Kejian He³; Fernando Rizzo⁴; David Matlock²; ¹Los Alamos National Laboratory; ²Colorado School of Mines; ³University of Leeds; ⁴Pontifícia Universidade Católica-Rio de Janeiro

The quenching and partitioning (Q&P) process has been developed to employ carbon transport from martensite to austenite during a partitioning treatment after initial quenching between M_s and M_f . Quenching within this temperature range produces specific fractions of martensite, while the partitioning treatment promotes stabilization of remaining austenite through carbon enrichment. Carbon-enriched retained austenite is of current commercial interest, especially with respect to transformation-induced plasticity (TRIP) steels, since the transformation of austenite to martensite results in high work hardening rates and favorable strength/ductility combinations. Q&P processing is an alternative processing approach to conventional austempering for producing microstructures with retained austenite. Mechanical properties of austenite/martensite mixtures produced by Q&P processing of sub-sized tensile samples of a 0.19C-1.59Mn-1.63Si (wt. pct.) steel composition are presented, and are compared to other advanced high strength steel grades. Instantaneous strain-hardening curves are highlighted to examine the effect of martensite and retained austenite on strain-hardening during tensile deformation.

2:50 PM

Effect of Prior Microstructure and Heating Rate on Austenite Formation in Spheroidized 52100 Steel: *Kester Clarke*¹; Chester Van Tyne¹; E. Buddy Damm²; Martin Mataya³; David Matlock¹; ¹Colorado School of Mines; ²Timken Company; ³Los Alamos National Laboratory

The effect of the prior microstructure and heating rates (ranging from 100°C/s to 1000°C/s) on austenitization kinetics was studied using spheroidized AISI 52100 steel with two size distributions of spheroidized carbides. The initial microstructure was characterized using light optical microscopy, electron microscopy, and microprobe analysis. Dilatometry was used to determine the on-heating transformation kinetics, including the transformation start time, transformation completion time, complete carbide dissolution time, and time to homogenous austenite. Light optical and electron microscopy was used to evaluate the evolving austenite microstructure. Results indicate that the effect of prior microstructure is significant. In particular, the effect of the prior microstructure on the austenitization kinetics increases with heating rate. Solid solution alloying elements appear to play a key role in the austenitization kinetics.

3:10 PM

Effects of Ni Contents on Continuous Cooling Transformation Behavior and Mechanical Properties of Low Carbon HSLA Steels: *Juseok Kang*¹; Chang Woo Lee¹; Seong Soo Ahn¹; Chang Yong Yoo¹; Chang Gyung Park¹; ¹Pohang University of Science and Technology

Continuous cooling transformation behaviors and resulting mechanical properties were studied for low carbon HSLA steels containing three different level (1~3 wt. %) of Ni contents. Thermo-mechanical processing simulations with varying cooling rate from 0.3°C/s to 50°C/s were conducted by using Gleeble. Bainite-like microstructures of acicular ferrite and bainitic ferrite were easily developed with increasing Ni contents due to hardenability increasing effects of Ni. At the slowest cooling rate of 0.3°C/s, γ to α phase transformation was delayed with decreasing Ni contents due to occurrence of pearlite and quasi-polygonal ferrite phase transformation. When cooling rate was higher than 1°C/s, however, γ to α phase transformation was accelerated as Ni contents decreased. A nucleation from hardened residual austenite can be sluggish in high Ni containing steels. Bainitic ferrite based microstructure showed superior tensile strength around 1200Mpa. However, those steels revealed lower upper shelf energy due to its high dislocation density.



3:30 PM Break

3:50 PM

Effects of Specimen Thickness and Notch Shape on Drop Weight Tear Test and Charpy Impact Test Properties of API X70 and X80 Line-Pipe Steels: Sang Yong Shin¹; Byoungchul Hwang²; Sunghak Lee¹; Nack J. Kim¹; Ki Bong Kang³; ¹Pohang University of Science and Technology; ²Korea Institute of Machinery and Materials; ³POSCO

Effects of specimen thickness and notch shape on drop weight tear test (DWTT) and Charpy V-notch (CVN) impact test properties of API X70 and X80 line-pipe steels fabricated by varying hot-rolling conditions were investigated. The DWTT results indicated that the steels rolled in the single phase region had the higher upper shelf energy (USE) than the steel rolled in the two phase region because their microstructures consisted of acicular ferrite, which was similar to the CVN test results. The DWTT energy transition temperature (ETT) of the steel rolled in the two phase region was the lowest because it had finer effective grain size and lowest volume fraction of hard secondary phases. The ETT increased with increasing specimen thickness because of the increase in the constraint state, and the ETT of the chevron-notch DWTT was slightly higher than that of pressed-notch DWTT.

4:10 PM

Cementite Dissolution and Delamination of Hyper-eutectoid Pearlite Steel Filaments for Tire Cords: Yang Yo Sep¹; Park Seong Yong¹; Bae Jong Gu²; Park Chan Gyung¹; ¹POSTECH; ²Trefilarbed Korea

Effects of microstructural parameters on the delamination of steel filaments with various true strain and carbon content have been experimentally investigated. The filaments were fabricated by cold drawing process with the true strain range from 4.12 to 4.32 and the carbon contents of 0.82 and 1.02 wt.%. Torsional ductility of the filaments was measured by using torsion-torque tester. Microstructural parameters, such as lamellar spacing, the thickness and morphology of cementite, were identified by using both transmission electron microscopy (TEM) and voltage-pulsed atom probe tomography. Delamination phenomenon was observed in the filaments with 1.02 wt.% C regardless of true strain, while it was not observed in the filaments with 0.82 wt.% C. As the true strain and carbon content increased, the lamellar spacing ($\bar{\epsilon}P$) and cementite thickness (t_c) decreased. Spherical-shaped cementites and clusters of thicker cementite were also found in the filament with 1.02 wt.% C. In order to elucidate the occurrence of delamination, its microstructural dependence was discussed in terms of microstructural parameters mentioned above.

4:30 PM

Rail Base Corrosion Analysis as a Major Factor that Shortens the Service Life of Rail in North American Transit Systems: Francisco Robles-Hernandez¹; G. Plascencia²; Kevin Koch¹; D. Jaramillo²; ¹Transportation Technology Center Inc.; ²CIITEC-IPN

In the present paper the results of the rail base corrosion study conducted on several transit systems across North America are presented. This type of corrosion shortens rail life considerably and can result in catastrophic rail failure. Rail base corrosion is characteristic of tracks located in tunnels or undergrounds as a result of a combination of environmental factors such as severe humidity, dissolved salts from the underground, accumulation of salts at the tie plates and clips (base of the rail), the returned current, leaks or stray currents from the non-grounded rails, etc. In contrast, transit systems that have no humidity, but particularly open air tracks, present limited to non-rail base corrosion. One approach of the present study was the simulation of controlled laboratory conditions using a similar electrolytic environment as the created at the base of the rail in order to understand the mechanisms that accelerate rail base corrosion. The second approach is a numerical simulation of the states of stresses created at the corroded/eroded locations at the base of the rail. As a conclusion it can be said that both the environmental conditions (humidity and deposited salts) combined with electrical leaks at the tie plates and clips are the major reasons for the formation of an electrolytic or galvanic system that accelerates the corrosion considerably. This result in the formation of stress concentrators, that in many cases are hidden therefore difficult to detect and compromising the integrity of the track, thus safety.

Hume-Rothery Symposium: Scattering Studies and the Fundamental Properties of Materials: Session III

Sponsored by: The Minerals, Metals and Materials Society, TMS Electronic, Magnetic, and Photonic Materials Division, TMS: Alloy Phases Committee
Program Organizers: Patrice Turchi, Lawrence Livermore National Laboratory; Wolfgang Donner, University of Houston; J. Robertson, Oak Ridge National Laboratory

Tuesday PM Room: Oceanic 7
February 27, 2007 Location: Dolphin Hotel

Session Chairs: Alphonse Finel, ONERA; Rozaliya Barabash, Oak Ridge National Laboratory

2:00 PM Invited

Diffuse Scattering of Bulk Alloys and the Near-Surface Microstructure: Bernd Schönfeld¹; Gernot Kostorz¹; ¹ETH Zurich

Diffuse scattering using x-rays or neutrons offers quantitative access to short-range order parameters and the static atomic displacements. While the method has been successfully applied to studies of bulk alloys, grazing-incidence diffraction now gives access to the near-surface microstructure. A survey will be given on the microstructure of Pt-Rh alloys near the surface, in comparison with the local atomic arrangement in the bulk. Local order is found in all cases investigated till now, with differences in the location of the maxima of short-range order scattering between (110) and (111) surfaces; a tendency towards the bulk '40' microstructure is only seen for the (110) surface. Static atomic displacements are more difficult to be evaluated as the species dependence must be considered. The 3λ x-ray method allows the achievable precision to be assessed. These aspects will be illustrated for some selected systems where measurements at three wavelengths were performed on bulk samples.

2:30 PM Invited

Diffuse Scattering Studies of Local Atomic Environments in Alloys: J. Robertson¹; ¹Oak Ridge National Laboratory

The concepts of order and disorder are fundamental to understanding the many physical properties exhibited by various materials. These concepts are somewhat ambiguous but often provide needed insight into the relationship between how the atoms are arranged in a material and its bulk properties such as phase stability, electrical resistance and magnetism. In this talk I will be discuss local atomic arrangements in crystalline binary solid solutions and how information about the local order can be obtained from diffuse x-ray and neutron diffuse scattering measurements. The crystal lattices are assumed to be either simple face-centered cubic (fcc) with four atoms per unit cell or body-centered cubic (bcc) with two atoms per unit cell. However, the methods presented here can be generalized to include other lattice symmetries and be applied to extremely complex crystals where only a small subset of the atomic sites are chemically disordered.

3:00 PM Break

3:20 PM Invited

Quantitative Phase Field Modeling of Precipitation: Alphonse Finel¹; Yann Le Bouar²; Umut Salman¹; ¹Office National d'Etudes et de Recherches Aérospatiales; ²Centre National de la Recherche Scientifique

Phase Field modeling of microstructural evolution in alloys has already a long and successful history. One of the basic ingredients of the theory is the introduction of continuous fields that describe the local state of the alloy. These fields have a meaning only at a mesoscopic scale, because their definition requires some spatial averaging procedure. An important consequence of this point of view concerns the way we construct the Phase Field equations. We will show that a quantitative Phase Field modeling of the nucleation and growth mechanism requires a careful determination of the Phase Field ingredients (free energy functional, mobility coefficients, noise term). We will also discuss a Phase Field analysis of a displacive transformation, namely the proper martensitic transition, where inertial effects play in principle a crucial role.

3:50 PM Invited

Genesis of the Cluster Expansion Method: *Didier de Fontaine*¹; ¹University of California

William Hume-Rothery was one of the first to apply theoretical methods derived from quantum mechanics and classical thermodynamics to the elucidation and rationalization of alloy phase equilibria. At the time, could he have anticipated how the field would have evolved at the start of the new millennium? Probably not. He could hardly have foreseen the huge computational power unleashed on the solution of the Schrödinger equation in non-trivial situations, on the handling of reliable statistical thermodynamic algorithms and on computer simulation techniques. Such tools are now at our fingertips, literally, to the point that we can now anticipate the derivation of alloy phase diagrams from first principles, i.e. from the knowledge of atomic numbers of the constituents only, for example. In particular, one tool that was forged in recent times is that of the Cluster Expansion, whose genesis and applications I shall briefly describe.

4:20 PM Invited

Predicting Short-Range Order and Its Effects on Alloy Properties via Direct First-Principles Calculations: *Duane Johnson*¹; *D. Biava*¹; ¹University of Illinois

We use a new electronic-structure method to include directly the effects of short-range order (SRO) and detail its impact on alloy electronic and structural properties.^{1,2} We then show how to predict directly the SRO parameters at finite temperatures. Results are obtained via a KKR method using the dynamical cluster approximation DCA, a proper generalization of the coherent-potential approximations (CPA), implemented in 3D systems in our KKR-CPA code.¹ The method may be used to address size-effects in alloys, either by direct calculation or by linear-response theory, as done for SRO using the KKR-CPA. We exemplify some of the various calculations and effects in various alloy systems, such as Cu-Zn, Cu-Au, and Ni-Al. ¹D.A. Biava, et al., Phys. Rev. B 72, 113105 (2005); and references therein. ²Subhradip Ghosh, et al., Phys. Rev. B 73, 085106 (2006). ³M. Jarrell and H. Krishnamurthy, Phys. Rev. B 63, 125102 (2001).

4:50 PM Invited

The Role of Displacement Short Range Order in the Determination of Higher Order Correlation: *Yevgeniy Putzyrev*¹; *Donald Nicholson*¹; *G. Stocks*¹; *G. Ice*¹; ¹Oak Ridge National Laboratory

Scattering experiments are routinely used to measure pair correlation in solid solutions. Only in special cases can model structures that reproduce the pair correlation be used to determine higher order correlations. However, the requirement that measured displacement short range order also be reproduced by the model further constrains the possible higher order correlation. The determination of further restrictions on higher order correlation relies on the use of a model for atomic displacement in terms of local environment. We illustrate this procedure for a 1-d lattice-liquid using a simple displacement model and for NiFe using ab initio calculations to relate atomic displacements to local environment. 1) Frank H. Stillinger and Salvatore Torquato, J. Phys. Chem. B 108 19589 (2004). This work sponsored by DOE-OS through the Office of Basic Energy Sciences (BES) was performed at Oak Ridge National Laboratory which is managed by UT-Battelle, LLC under Contract No. De-AC05-00OR22725.

Innovations in Titanium Technology Symposium: Advances in Materials Processing

Sponsored by: The Minerals, Metals and Materials Society, TMS Structural Materials Division, TMS: Titanium Committee

Program Organizers: Mehmet Gungor, Concurrent Technologies Corporation; M. Ashraf Imam, Naval Research Laboratory; F. H. (Sam) Froes, University of Idaho

Tuesday PM Room: Asia 3
February 27, 2007 Location: Dolphin Hotel

Session Chairs: Taras Lyssenko, International Titanium Powder; Richard Dashwood, Imperial College London

2:00 PM Invited

Advances in Titanium Metal Injection Molding: *Francis Froes*¹; ¹University of Idaho

The approaches to production of titanium powder injection molded parts are reviewed. Historically, oxygen levels have been too high for structural use (particularly with the Ti-6Al-4V alloy). However, recent advances in starting powders, binders and sintering facilities now allow oxygen levels in the Ti-6Al-4V alloy to be controlled to about 0.2 wt % oxygen. This should result in significant expansion of the titanium PIM market place into aerospace, automobiles, surgical instruments, dentistry, communication devices (such as computers and cell phones), knives and guns.

2:30 PM

Titanium Powder Metallurgy Composite Materials for Armor and Structural Applications: *Volodymyr Duz*¹; *Vladimir Moxson*¹; *Jane Adams*²; *Walter Roy*²; *Stephen Luckowski*³; ¹ADMA Products Inc; ²US Army Research Laboratory; ³US Army ARDEC

This presentation covers the recent developments in blended elemental (BE) titanium Powder Metallurgy (P/M) to produce the low cost titanium components and composite Titanium alloys for armor and structural applications. Titanium alloys exhibit many attractive properties for defense applications, but their use is limited by high cost of titanium components produced by conventional metallurgical processes. A PM approach is viable route for cost effective fabrication of titanium alloys as well as low cost Metal matrix composites (MMCs), reinforced by ceramic particles. The results achieved in this study demonstrated that high density Titanium alloys can be manufactured by room temperature consolidation followed by vacuum sintering and the properties of the Titanium alloys are meeting the Military specifications. Increased modulus of elasticity by an innovative addition of the various reinforcing particulates and microstructure modifications by various post treatments will also be presented.

2:50 PM Invited

Sintering Behavior of Titanium Powders: *Stephen Gerdemann*¹; *David Alman*¹; ¹United States Department of Energy

Powder-metallurgy processes such as conventional press-and-sinter, powder forging, and powder-injection molding, offer the potential for manufacturing near-net-shape titanium parts without costly and difficult forming and machining operations. Understanding how powders behave during sintering is essential to achieving full density. An extensive series of dilatometry experiments was conducted to examine the sintering behavior of cold-pressed CP titanium and Ti 6-4 powders. Three different sizes of sponge fines (<150, <75, and <45 micron), two hydride-dehydride powders (<75 and <45 micron), gas-atomized Ti, and a powder from the new Armstrong process developed by International Titanium Powder (ITP) were pressed into cylinders and run in a dilatometer at different temperatures. The microstructures of the sintered Ti cylinders were examined. Differences between powders and between sintering behavior are discussed with the aim of identifying the conditions required to achieve maximum density via press-and-sinter processing.

3:15 PM Break



3:30 PM

Compaction of Titanium Powders: *Stephen Gerdemann*¹; David Alman¹;
¹United States Department of Energy

Understanding how powders behave during compaction is essential to achieving full density in powder metallurgy processing. Three sizes of CP titanium sponge fines (<150, <75, and <45 micron), two sizes of hydride-dehydride powders (<75 and 45 micron), one gas atomized CP Ti, powder from International Titanium (ITP), and one Ti 6-4 powder were cold-pressed in a single-action cylindrical die. By measuring the movement of the die plunger, the applied force, and the final density, it is possible to calculate the density at any given pressure, and from this, to generate a plot of green density obtained vs. pressure applied. The ITP powder had the lowest initial density, but pressed to a density similar to the other powders. The initial density of the Ti 6-4 powder was similar to that of the other powders, but its final pressed density was only 80%, compared to 90% for the other powders.

3:50 PM

The Adiabatic High Velocity Compaction of Titanium Powder: *Gordon Goranson*¹; ¹LMC Inc.

LMC's High Velocity Mechanical Press compacts titanium powders to net shape components with reduced sintering time and temperature, or no sintering. One Tool – One Impact – One Part. The patented impact unit achieves ram velocities up to 100 meters per second creating adiabatic phenomena in powder to dislocate molecules and rejoin them in a solid state. Material yield is maximized. Surface finish is determined by the tooling. High cycle rates are achieved. No lubricants. Part densities have been achieved to over 99%. The LMC process will produce (1) pellets that can be controlled for processing by smelters for extrusions, rolled or machined, (2) near net shape billets to be finished machined, and (3) net shape parts. Presses capable of components to 20 kilos. The process is fully commercialized for cutting, blanking, and forming. Environmentally friendly. No recyclables, minimum material waste and reduces energy consumption up to 90% compared to conventional presses.

4:10 PM

Microstructural Engineering of Pure Titanium for Improved Monotonic and Cyclic Response: *Guney Yapici*¹; Ibrahim Karaman¹; Hans Maier²; ¹Texas A&M University; ²University of Paderborn

Occasionally, pure titanium lacks the optimum mechanical properties for demanding engineering applications for industries ranging from biomedical to transportation. Here we present a remedy to this problem by using equal channel angular extrusion (ECAE) where bulk billets are extruded through two perpendicular channels of equal cross section achieving simple shear deformation. Grade-2 Ti was processed up to 12 ECAE passes at 300°C without shear localization in a quest for reaching strength levels comparable to that of Ti-6Al-4V with higher ductility levels. TEM analysis revealed microstructural evolution at the nano to micro regime. Post-processing mechanical response of the extruded samples is investigated to reveal the processing-microstructure-property relationships. Additional deformation of extruded billets with conventional forming techniques assisted by low temperature annealing treatments resulted in both high tensile strengths and uniform strains (900 MPa and 30% ductility). Low cycle fatigue experiments showed improved cyclic stress range and number of cycles to failure.

4:30 PM

Laser Processed Porous Ti for Biomedical Applications: Amit Bandyopadhyay¹; *Vamsi Balla*¹; Felix Espana¹; Susmita Bose¹; ¹Washington State University

The need for unique mechanical and functional properties for different metallic implant materials necessitates the use of novel design and manufacturing approaches. Particularly for load bearing hip or knee implants, high fatigue resistance and compressive strength is necessary, while a low modulus is important to reduce stress shielding. We have fabricated porous Ti samples in the porosity range from 25 to 70 vol% by controlling Laser Engineered Net Shaping (LENSTM) process parameters with three dimensionally interconnected pores in the size range of 60–700µm. The Young's modulus of laser processed porous Ti samples can be tailored in the range of 2 and 50 GPa by changing the LENSTM process parameters and porosity, which matches that of human cortical bone. The presence of finer and acicular α in the microstructure also resulted in high hardness (194±14 Hv).

Our talk will focus on process-structure-property correlation of these porous Ti samples for bone-implants.

Intellectual Property in Materials Science: Patents, Tech Transfer and Licensing: Commercialization

Sponsored by: The Minerals, Metals and Materials Society, TMS Materials Processing and Manufacturing Division

Program Organizer: Steven Marsh, Dorsey & Whitney LLP

Tuesday PM Room: America's Seminar
February 27, 2007 Location: Dolphin Hotel

Session Chair: Gary Abelev, Dorsey & Whitney LLP

2:00 PM Invited

Protection and Licensing of Biomaterials: Lessons Learned from Case Studies: *Frances Toneguzzo*¹; ¹Massachusetts General Hospital

Two case studies involving the licensing of biomaterials in the healthcare field will be presented. The first case study will be directed toward biomaterials for the orthopedic industry and will highlight issues of intellectual property, managing protection and licensing of improvements, co-exclusive licensing strategies and managing licensing relationships. The second case study will focus on biomaterials as drug delivery systems for women's health and address issues of emerging technologies and industries as well as general licensing and intellectual property matters.

2:30 PM Invited

Commercialization of Technologies from University Research: *Peter Pritchard*¹; ¹Center for Economic Growth

The role of university-generated intellectual property is evolving into a more serious endeavor, with increased investment by many universities to achieve commercialization of this IP. A few established research universities have been wildly successful in generating revenues through their licensing programs, while others who entered the licensing arena in the last decade are struggling to achieve modest revenues. The success of university tech transfer operations can depend on a few key factors: quality and nature of the research being conducted, amount of time the university has been engaged in licensing, and the strength of an individual researcher's relationships with industry. Several observations are provided on the relationships and skills necessary to successfully commercialize university-generated technology for the public benefit.

3:00 PM Invited

An Investor's View of Intellectual Property in Academic Start-Up Companies: *Amir Nashat*¹; ¹Polaris Venture Partners

Start-up ventures based on university technology contain two key components: the academic inventors of the technology and their university-owned intellectual property. A successful startup requires that all of the important components come together to form a durable partnership. This talk will give an overview on the relationships between the inventors, the university, the company and the investors. The session will discuss each of these aspects individually, as well as provide real-world examples based on Polaris Venture Partners' experience starting over 15 university-based companies over the past decade.

3:30 PM Break

3:45 PM

Roundtable Discussion of Patent, Licensing and Tech Transfer Issues

Magnesium Technology 2007: Casting and Solidification II

Sponsored by: The Minerals, Metals and Materials Society, TMS Light Metals Division, TMS: Magnesium Committee

Program Organizers: Randy Beals, DaimlerChrysler; Neale Neelameggham, US Magnesium LLC; Mihriban Pekguleryuz, McGill University; Alan Luo, General Motors Corporation

Tuesday PM Room: Southern 5
February 27, 2007 Location: Dolphin Hotel

Session Chairs: Helmut Kaufmann, Aluminium Ranshofen GmbH; Naiyi Li, Ford Motor Company

2:00 PM

Microstructure and Mechanical Properties of Magnesium Alloy AM60 and Its Cast Processing Conditions: *Hong Tae Kang*¹; Naiyi Li²; ¹University of Michigan-Dearborn; ²Ford Motor Company

Effects of casting technique on microstructure and mechanical properties of magnesium alloys AM60 were investigated. The magnesium alloys AM60 were produced by high-pressure die cast (HPDC) with two different casting processors. Each HPDC produced magnesium alloy AM60 with thickness of 2 mm. Tensile test results showed that the specimens from the processor A are stronger than those from the processor B. The fatigue tests were also conducted by load control according to ASTM E466 standard procedure with zero to max loading. After fatigue testing, the failed surfaces of the specimens were observed by SEM. The fatigue test results showed that specimens from the casting processor A are more consistent than those from processor B. From this study, it was clearly observed that the flow rate of the molten magnesium affects to the microstructure and mechanical properties of the magnesium alloys AM60.

2:20 PM

Shear Defects in High Pressure Die Castings: *Christopher Gourlay*¹; Arne Dahle¹; ¹CRC for Cast Metals Manufacturing

Magnesium alloy high pressure die castings (HPDC) commonly contain bands of positive macrosegregation, porosity and occasionally tears that follow the outer contour of the casting. These bands have been shown to influence properties of some products. It is therefore important to understand the origin of these defects to develop means of controlling their occurrence. Here we compare these HPDC defects with microstructures that form during rheometry experiments using AZ91 as an example alloy. The deformation mechanisms when partially solid alloys are sheared during vane rheometry are outlined and related to the formation of shear bands in HPDC.

2:40 PM

Influences of the Process Defect on the Material Properties of a Thin-Walled Cast Structure: *Saravanan Subramanian*¹; Ronald Cooper¹; Dan Houston¹; Patrick Blanchard¹; Nicholas Warrior²; ¹Ford Motor Company; ²University of Nottingham

High pressure magnesium die casting is widely reported as producing parts that exhibit large local variation in part properties. Defects introduced during filling and solidification are reported to be the cause of such property variation. In particular pore band defects, caused by micro shrinkage are of primary concern. The bands effectively create a laminate structure through the casting thickness. Mechanical properties and microstructure have been shown to vary within each layer. Therefore, to investigate this phenomenon further, die cast components were prepared and test samples were milled from different layers within the casting thickness. Bulk porosity measurements were recorded for each layer. Furthermore, the standard tensile sub size samples were prepared and tested under uni-axial tensile loading conditions. This paper presents the variations in mechanical properties through the thickness direction. An analytical model is also proposed to approximate the failure strain based on the pore band characteristics.

3:00 PM

Magnesium Metal Matrix Composites (Mg-MMC) Produced by Innovative Die Casting Process: *German Gertsberg*¹; Eli Aghion²; Amir Arnon²; Nir Moskovitch¹; ¹Magnesium Research Institute; ²Ben Gurion University

Magnesium Metal Matrix Composites (Mg-MMC) may offer improved properties for applications requiring increased tensile strength and wear resistance. The use of Mg-MMC as structural material can become quite attractive for commercial applications, especially if they are adequately produced by die casting process. The aim of the research was to develop an innovative die casting process technology for AZ91C and SiC particles. This was done by a systematic study which was able to define the optimal die casting process parameters, such as melt temperature, shot-sleeve filling ratio, die temperature, and lubrication schedule. In addition, a unique method for introducing SiC particles into the molten alloy was developed to insure homogenous dispersion of the particles. This method was based on a special bottom entry feeding device. The wear resistance in terms of weight loss was evaluated using a special "Block on Ring" experimental set-up that was specially designed for this assignment.

3:20 PM

Research on Preparation Process of Super Light Mg-9Li-1Zn Alloy/Al Cladding Plate: *Guoyin Zu*¹; Hongbin Li¹; Guangchun Yao¹; ¹School of Materials and Metallurgy

The corrosion resisting property of Mg-Li alloy is quite bad and the mechanical property is also bad, author prepared the Mg-9Li-1Zn/Al composite plate using cold-rolling. Author studied the technology of cold-rolling and the annealing system of Mg-9Li-1Zn/Al composite plate, and analyzed the recrystallization behaviour of Mg-9Li-1Zn sheet for different annealing system, and tested the mechanical properties. The results show that the critical reduction of Mg-9Li-1Zn/Al composite plate is about 50% , and the best reduction is about 60~65%. After annealing a phases can obviously spheroidize, and the complete recrystallization occurs after annealing at 300°C for 3h, and at the same time the microstructure and properties of the composite plate are the best. The density of Mg-9Li-1Zn/Al composite plate is 1.6~1.7g/cm³, it still has the character of lightness, at the same time the corrosion resisting property can rise largely.

3:40 PM

Effect of Mn Addition on Microstructure and Properties of As-Casting Mg-Li-Al Alloy: *Hong Bin Li*¹; Guangchun Yao¹; Haibin Ji¹; Zhiqiang Guo¹; Zhengang Liu¹; ¹Northeastern University

Mg-xLi-Al alloys with Mn addition from 0.2 to 1.5wt% were produced and studied in this paper. The density of the alloys is very low and between 1.21 g/cm³ and 1.64g/cm³. The microstructures of alloys change from single α , ($\alpha+\beta$), to single β phase with lithium content rising from 5 to 22wt%. The results of the tensile tests show that the strength decreases with lithium content rising, while the elongation increases sharply. LA92 alloy with Mn addition was mainly studied. It is known that adding Mn can form some new phases in alloy by microstructure observation, SEM with EDS and X-ray analysis. The results of tensile tests show that The UTS and YS can rise by 26.8% and 22.7%, respectively, when 0.5wt% Mn is added. It is clarified that too much Mn addition can result in forming too much new hard phases and worsening the tensile properties.

4:00 PM

Advances in Magnesium Injection Molding (Thixomolding®): M. Scharrer¹; A. Lohmueller¹; *Robert Singer*¹; ¹Neue Materialien Fürth GmbH

Magnesium Injection Molding (Thixomolding®) is a relatively new casting process that competes with high pressure die casting. Various advantages have been demonstrated in the past like reduced porosity, lower distortion and closer tolerances. The improvement is due to lower casting temperatures near the liquidus or in the semi-solid regime. The present paper will introduce two further advantages of the Thixomolding technology. Firstly, the closed system in combination with the intensive mixing in the barrel is beneficial for casting alloys containing elements that are known to be prone to oxidation, segregation or evaporation in conventional die casting. Data will be presented for AJ- and AS-type alloys which demonstrate an improvement in mechanical properties for thixomolded material. In addition the low temperature level can reduce die sticking and hot cracking and improve die life. In a second part of the paper another important advantage of Thixomolding will be demonstrated. As



the processing technology is similar to polymer injection molding, hot runner systems can be developed which gives Thixomolding another unique selling point. Scrap can be greatly reduced, heating energy and raw material is saved and flow length can be reduced dramatically. Results will be presented for a first hot runner system that has been installed on our 220 t – Thixomolding machine.

4:20 PM

Effect of Severe Plastic Deformation on Thixomolded AZ91D Mg Alloy: Xiang Li¹; Amit Ghosh¹; Ray Decker²; ¹University of Michigan; ²Thixomat, Inc.

Severe plastic deformation is imparted to thixomolded AZ91D alloy plate by two processes: (i) pure compression at 120 °C and (ii) Alternate Biaxial Reverse Corrugation (ABRC) at 300 °C followed by flattening at 280 °C. Basal slip and twinning dominate deformation process within primary solid fraction of the thixomolded material, but not in the fine grain eutectic structure. Twinning helps subdivision of grains but the angle between the twinning plane and compression axis increases with increasing strain, as more slip occurs to accommodate plastic flow. ABRC process produces ultra-fine grained AZ91D alloy with improved homogeneous grain structure and improves continuous distribution of α Mg with the β phase as strengthening second phase is generated and significantly improves the final mechanical properties. These structures provide higher strength and higher tensile elongation compared to as-thixomolded material, and exhibits very high hardness. (Work supported by National Science Foundation under DMR Award 0314218).

4:40 PM

Rheo-Diecasting (RDC) of Magnesium Alloys: Zhongyun Fan¹; Guojun Liu¹; Yun Wng¹; Souxun Ji¹; Amitabha Das¹; ¹Brunel University

A new semisolid metal processing technology, rheo-diecasting (RDC) has been developed for production of Mg-alloy components with high integrity. The RDC process innovatively combines the dispersive mixing power of a twin-screw mechanism for creation of high quality semisolid slurry and the high efficiency, low cost nature of the high pressure die casting (HPDC) process for component shaping. In this paper we present the RDC process and the resulting microstructure and mechanical properties of various Mg-alloys. Solidification behaviour of Mg-alloys in the RDC process and the co-relationships between microstructure and mechanical properties of RDC Mg-alloys are also discussed. It was found that the RDC process is capable of producing Mg-alloy samples with close-to-zero porosity and a fine, uniform microstructure throughout the entire sample irrespective of the section thickness. Compared with those obtained by other existing processing techniques, the RDC samples have substantially improved or equivalent mechanical properties, and are heat treatable.

5:00 PM

Rheoforming Technologies for Processing Wrought Magnesium Alloys: Zhongyun Fan¹; Shouxun Ji¹; Yun Wang¹; Shaoming Zhang¹; Amitabha Das¹; ¹Brunel University

The current applications of Mg in the automotive industry constitute almost 100% cast components without any significant contribution from wrought products. The main barriers to the penetration of wrought Mg alloys into motor vehicles are poor deformability, low productivity and high cost. To overcome such barriers, a group of new processing technologies, collectively named rheoforming, have recently been developed by BCAST at Brunel University, for production of high quality wrought Mg-alloy products in various forms. The rheoforming technologies include DC rheocasting (DCRC), twin roll rheocasting (TRRC), and rheoextrusion (RE). The primary aim of rheoforming technologies is to achieve a cast body with fine and uniform microstructure free from chemical segregation and cast defects. In this paper we present the rheoforming technologies and the experimental results on microstructure and mechanical properties of rheoformed wrought Mg-alloys.

5:20 PM

Study of Processing Map on Mg-3Al-1Zn Alloy Prepared by Low Frequency Electromagnetic Casting: Yingxin Wang¹; Xiaojin Zeng¹; Wenjiang Ding¹; Alan A. Luo²; Anil K. Sachdev²; ¹Shanghai Jiaotong University; ²General Motors Research and Development Center

Processing map of the AZ31 magnesium alloy prepared by low frequency electromagnetic casting has been constructed, which shows the peak power

dissipation efficiency of 34% corresponding to the optimized working conditions with a temperature of 773K and a strain rate of 0.001s⁻¹. The instability of AZ31 alloy is controlled by twinning, flow localization and cracking induced by DRX; the safety, controlled by DRX. The extrusion experiment validates the veracity of the processing map, which indicates the processing map can be used to predict the microstructural evolution of AZ31 alloy during deformation.

Magnesium Technology 2007: Wrought Alloys and Forming Processes III: Extrusions

Sponsored by: The Minerals, Metals and Materials Society, TMS Light Metals Division, TMS: Magnesium Committee

Program Organizers: Randy Beals, DaimlerChrysler; Neale Neelameggham, US Magnesium LLC; Mihriban Pekguleryuz, McGill University; Alan Luo, General Motors Corporation

Tuesday PM Room: Southern 4
February 27, 2007 Location: Dolphin Hotel

Session Chairs: Karl Kainer, GKSS Research Center; Ravi Verma, General Motors Corporation

2:00 PM

Extrudability of Magnesium Alloys: Dale Atwell¹; Matthew Barnett¹; ¹Cooperative Research Centre for Cast Metals Manufacturing (CAST)

Magnesium alloys are slow to extrude relative to aluminium alloys. However, few quantitative comparisons of the actual processing limits are available. Through generating extrusion limit diagrams, a series of commercial magnesium alloys (M1, ZM21, AZ31, AZ61 and ZK60) were compared with a common “fast extruding” aluminium alloy (AA6063). The maximum extrusion speed of the M1 alloy, whilst still avoiding cracking, is shown to be similar to AA6063. However, alloys ZK60 and AZ61 were only able to be extruded at a rate ~3 % of that of AA6063. Thus, with increasing alloying addition the relative extrudability severely declined. The variation in the extrusion parameters used also significantly influenced the mechanical properties of the extrudate.

2:20 PM

Quality-Affecting Parameters in the Direct Extrusion of Magnesium Alloys: Wim Sillekens¹; ¹TNO Science and Industry

While the interest in magnesium sections (profiles) is growing, the underlying extrusion technology is still in an early stage of development. More in particular, many of the processing aspects need still to be explored with the aim of bringing productivity as well as quality to a level competitive to aluminium to enable a more widespread use. Several avenues can be distinguished in addressing this issue, ranging from new alloys and feedstock preparation methods through alternative extrusion methods to tailored processing and tooling. With direct extrusion being the primary option for mainstream production, this paper deals with the main processing parameters that affect the quality of magnesium sections. Laboratory extrusion trials were conducted into the influence of process and material conditions on the extrudability of the alloys AZ31 and ZM21, specifically regarding surface quality. Except for variations in speed and temperature, these conditions do also include modifications in die geometry, atmosphere at the die exit and cleanliness of the container. Results show that parameters such as the geometry of the die bearing are of major concern, but also confirm that some basic measures of good housekeeping need to be maintained in order to get reproducible and reliable results.

2:40 PM

The Effect of Severe Plastic Deformation on the Mechanical and Corrosion Behavior of Mg Alloys: Dan Eliezer¹; Guy Ben-Hamu¹; Loter Wagner²; ¹Ben-Gurion University of the Negev; ²Technical University of Clausthal

The quest for ever higher performance in structural applications has resulted in the outgoing development of new or improved materials with novel crystallographic textures, microstructures, and compositions. Due the promise of excellent properties such as superplasticity, high strength, good ductility, enhanced high cycle fatigue life, and good corrosion resistance, interest has

TUESDAY PM

grown in nanostructure bulk materials. In recent years, bulk nanostructure materials processed by methods of severe plastic deformation (SPD) such as Equal Channel Angular Extrusion (ECAE) have attracted the growing interest of specialists in materials science. The main object of this research is to compare the mechanical properties and corrosion behavior of Magnesium alloys after ECAE process. Hardness, tensile, AC and DC polarization tests were carried out on the extruded rods, and the microstructure was examined using optical, electron microscopy and EDS. The relation between the microstructure, corrosion behavior and the mechanical properties will be discussed in details.

3:00 PM

The Effect of Texture on the Mechanical Properties of AZ31 Mg Alloy by Equal Channel Angular Extrusion: *Li Jin*¹; Dongliang Lin¹; Xiaoqin Zeng¹; Wenjiang Ding¹; ¹Shanghai Jiaotong University

The texture and mechanical properties of AZ31 Mg alloy processed by equal-channel angular extrusion (ECAE) were investigated. These alloys were subjected to one to eight passes, in which a single passage yielded an effective strain of ~1.15, at 498K. The microstructures of these alloys were examined by transmission electron microscopy (TEM), electron back-scattered diffraction (EBSD) and X-ray diffraction (XRD). The results show that the higher Schmid factors of dominant texture in the alloy on slip system, the higher elongation of AZ31 Mg alloy at room temperature. However, the strength of AZ31 Mg alloy can not only be decided by the texture evolution, and the grain boundary structure have important role on the increasing of yield stress and ultra tensile strength.

3:20 PM

Deformation Behavior of ECAPed AZ31 Mg Alloy at Low Homologous Temperature: *Hyunseok Lee*¹; Daewoo Kim¹; Wonkyu Bang²; Youngwon Chang¹; ¹Pohang University of Science and Technology; ²Research Institute of Industrial Science and Technology

Equal Channel Angular Pressing (ECAP) is one of very effective techniques that can produce relatively large bulk material with ultra-fine grained microstructure. In this study, the ECAP process was applied to an AZ31 magnesium cast alloy. After 4 ECAP passes at 523 K, a fine grained microstructure could be obtained. A series of tensile and load relaxation test were conducted with the ECAPed material at temperatures ranging from 523 K to 623 K. The alloy exhibited superplastic deformation behavior and a characteristic sigmoidal flow curve at each test temperature. The deformation mechanisms were investigated using both the mechanical test results and related microstructure observations within the framework of the internal variable theory, recently proposed by Chang et al.

3:40 PM Break

4:00 PM

Initial Ballistic Evaluation of the Magnesium Alloy AZ31B: *Tyrone Jones*¹; Matthew Burkins¹; William Gooch¹; Rick DeLorme²; ¹US Army Research Laboratory; ²Magnesium Elektron, North America

Wrought magnesium alloys, which maintain various niche market applications due to their unique properties, have been the subject of a heightened level of research and development for potential application in the automotive market. However, little data is available on their ballistic properties. In order to fill this gap, the US Army Research Laboratory (ARL) and Magnesium Elektron North America, Incorporated (MENA) conducted a cooperative effort to evaluate magnesium alloy AZ31B, which was commercially available in a wrought form. MENA produced the rolled product and conducted the mechanical testing, while ARL performed the ballistic testing. Some limited ballistic data is provided for this alloy in various tempers.

4:20 PM

The Influence of Grain Size on Yielding Asymmetry of Extruded AZ31 Magnesium Alloy: *Jingtao Wang*¹; De Liang Yin¹; ¹Nanjing University of Science and Technology

Yielding asymmetry between tension and compression is typical in many wrought magnesium alloys. To clarify the influence of grain size on yielding asymmetry, AZ31 magnesium alloy with different grain size were prepared through extrusion followed by annealing treatment. Uniaxial tension and compression tests were carried out at room temperature to evaluate the yielding asymmetry of this alloy. Optical microscopy and TEM were used to investigate the microstructure change just after yielding point. It is found that

yielding asymmetry decreases significantly with decreasing grain size. Optical microscopic observation shows that twinning area fraction decreases with decreasing grain size, suggesting tensile twinning, which has strong polarity to deformation direction, is not easy to occur at smaller grain size and thus the yielding asymmetry decreases accordingly with decreasing grain size. Further, quantitative analysis concerning grain size and yielding strength was made according to the results of mechanical property tests and TEM observations.

4:40 PM

The Role of Texture in Yielding Asymmetry of Extruded AZ31 Magnesium Alloy: De Liang Yin¹; *Jingtao Wang*¹; ¹Nanjing University of Science and Technology

Yielding asymmetry is a typical characteristic of wrought magnesium alloys with compression yield strength less than tensile yield strength along extruding direction. To reveal the role of texture in yielding asymmetry of wrought magnesium alloy, AZ31 magnesium alloy with various textures were prepared using different extrusion ratios. Uniaxial tension and compression tests were carried out to evaluate the yielding asymmetry of this alloy. Orientation distribution function was employed to determine the extrusion texture and optical microscopy was used to observe the deformed microstructure. It is shown that yielding asymmetry increases with strengthening basal fibrous texture which favors tensile twinning in compression and suppresses this twinning along extruding direction. Optical microscopic observation confirmed that twinning area fraction after tension was greater than that after compression just after yielding point, which confirms that the yielding asymmetry is ascribed to the polarity of tensile twinning at various basal fibrous textures.

5:00 PM

Anisotropic Properties of Thixoextruded AZ31 Mg Wrought Alloy: *Young-Ok Yoon*¹; Jin Kyu Lee¹; Hyung-Ho Jo¹; Shae K. Kim¹; ¹Korea Institute of Industrial Technology

Mg alloys are expected to increase in automotive application due to demands for vehicle mass reduction. At present, Mg alloys used in the automotive industry are predominantly in the form of die cast parts. However, Mg wrought alloys, particularly in the field of extrusion process, will be necessary to support the growing interest for lightweight automotive components. Especially, AZ31 Mg wrought alloy shows low extrusion speed and high extrusion pressure when extruded conventionally. The aim of this study is to characterize a thixoextruded AZ31 Mg wrought alloy bar in terms of its anisotropic behavior through the optical microscope, mechanical test and x-ray texture measurement. Especially, 4 point bending tests are carried out on a thixoextruded AZ31 Mg wrought alloy bar in order to investigate the anisotropic behavior of the mechanical properties.

5:20 PM

Control of Grain Size and Precipitate Shape on Fracture Toughness in Mg-Zn-Zr Alloy: *Hidetoshi Somekawa*¹; Alok Singh¹; Toshiji Mukai¹; ¹National Institute for Materials Science

For structural applications, it is important to examine the mechanical properties of magnesium alloys satisfy with both reliability and safety. One of the distinction methods is the investigation of fracture toughness. It has been reported that the fracture toughness in magnesium alloys are lower than that in commercial aluminum alloys. Therefore, the improvement method of fracture toughness needs to be development for the future applications. Recently, the grain refinement has been used to improve the mechanical properties in magnesium alloys, because of reduction in formation of deformation twins. In addition, it is well known that the existence of precipitates influences the mechanical properties of metallic materials. However, the synergistic effect on fracture toughness in magnesium alloys have not been investigated yet. In this study, the control of grain size and precipitate shape were achieved to enhancement for fracture toughness in commercial Mg-Zn-Zr alloy, ZK60, produced by direct extrusion process.



Materials in Clean Power Systems II: Fuel Cells, Solar, and Hydrogen-Based Technologies: Hydrogen Storage Materials in Conjunction with the 8th Global Innovations Symposium: Metal Powders for Energy Production and Storage Applications

Sponsored by: The Minerals, Metals and Materials Society, ASM International, TMS Structural Materials Division, TMS/ASM: Corrosion and Environmental Effects Committee

Program Organizers: Zhenguo "Gary" Yang, Pacific Northwest National Laboratory; Michael Brady, Oak Ridge National Laboratory; K. Scott Weil, Pacific Northwest National Laboratory; Yong-Ho Sohn, University of Central Florida

Tuesday PM Room: Oceanic 6
February 27, 2007 Location: Dolphin Hotel

Session Chairs: Zhigang Fang, University of Utah; Chun Lu, Pacific Northwest National Laboratory

2:00 PM Invited

Exploration of Magnesium Borohydride for On-Board Hydrogen Storage: Grigori Soloveichik¹; Matthew Andrus¹; Jun Cui¹; Yan Gao¹; John Lemmon¹; Thomas Raber¹; Job Rijssenbeek¹; Malgorzata Rubinsztajn¹; Suchismita Sanyal¹; *Ji-Cheng Zhao*¹; ¹GE Global Research

Mg borohydride is a promising material for on-board hydrogen storage. It contains 14.8 wt.% hydrogen and can desorb all of it at < 450°C. Mg borohydride decomposes in a two-step process: the 1st step forms MgH₂, boron and H₂, and the MgH₂ further decomposes in the second step to form Mg and H₂. The 2nd step is readily reversible. The viability of Mg borohydride as a hydrogen storage material depends on the reversibility of the 1st step: reaction of MgH₂, boron and H₂ to form the Mg borohydride. Work is underway to identify the crystal structure of Mg borohydride which is important for computational screening of dopants (elemental substitution for Mg) using density functional theory. Preliminary data show an orthorhombic crystal structure and detailed work is underway. We are using our robust combinatorial methodology to perform dopant and catalyst screening to try to make Mg borohydride fully reversible.

2:35 PM Invited

Effects of Mechanical Activation on Dehydrogenation of the Lithium Amide and Lithium Hydride System: Ruiming Ren¹; Tippawan Markmaitree²; William Osborn²; *Leon Shaw*²; Z. Gary Yang³; ¹University of Connecticut/Dalian Jiaotong University; ²University of Connecticut; ³Pacific Northwest National Laboratory

The dependence of the dehydrating reaction of the LiNH₂ and LiH mixture on the degree of mechanical activation was investigated. Different degrees of mechanical activation were obtained via different conditions of high-energy ball milling. The enhanced reaction kinetics was related to changes in the characteristics of the powder mixtures induced by high-energy ball milling. The more mechanical activation, the more reduction in the onset, peak, and completion temperatures for the dehydrating reaction. Mechanical activation could lead to a decrease in the activation energy of the dehydrating reaction. A 60% reduction in the activation energy was achieved by high-energy ball milling at room temperature for 24 hours. High-energy ball milling also effectively prevented escaping of NH₃ from the LiNH₂ and LiH system. A proposal on dual roles of LiH was put forward to explain the mechanism of the dehydrating reaction and all of the phenomena observed in this study.

3:10 PM

Modification of Light Metal Complex Hydrides for Improved Storage Properties: *Chun Lu*¹; Jinyong Kim¹; Zhenguo Yang¹; Leon Shaw²; ¹Pacific Northwest National Laboratory; ²University of Connecticut

Light metal complex hydrides with a promising storage capacity are considered as potential candidates for onboard hydrogen storage application. These storage materials however often demonstrate a slow hydrogen uptake and release kinetics that needs to be improved for practical use. To this end, effort has been carried out to modify the exemplary compound system of

lithium nitride hydride with additives. This paper will present the effects of the additives on hydrogen storage properties of the Li-N-H system and discuss the benefits of the additives for the storage application.

3:35 PM Break

3:50 PM Invited

High Capacity Mg-Based Hydrogen Storage Materials: *Peter Notten*¹; Peter Kalisvaart²; Paul Vermeulen²; ¹Philips Research and Eindhoven University; ²Eindhoven University

It has been identified that hydrogen storage is one of the key drivers, enabling the future hydrogen economy. High-capacity hydrogen storage materials will play a dominant role in future gas phase and electrochemically driven devices, such as Fuel Cells and NiMH batteries. Significantly higher gravimetric storage capacities are, however, required to accomplish the necessary breakthroughs. It has recently been shown that more than 6.5 wt.% of hydrogen can electrochemically be absorbed and desorbed at high rates at room temperature in fluorite-based Mg-compounds. It has been argued that, in contrast to the well-known rutile-structured Mg-alloys these MgX materials (X=Sc,Ti,V,Cr) have a much more open crystal structure facilitating fast hydrogen transport. In this presentation the electrochemically induced hydrogenation aspects of these new materials will be addressed.

4:25 PM

Hydrogen Absorption on Gamma Irradiated Powders: *Luis Muga*¹; Barbara Galuszka-Muga¹; ¹TOFTEC Inc.

This project proposes a different approach to enhance hydrogen absorption by modifying powdered carbon, boron nitride and other materials *via* gamma irradiation prior to and/or during exposure to pressurized hydrogen gas at ambient temperatures. The electronic environment at surface and interior sites is activated by penetrating radiation thus creating non-equilibrium conditions *via* Compton recoils. These effects imply bond disruption, free radical formation, and internal site activation, conditions conducive to enhanced hydrogen physisorption. A description of the experimental setup (gas handling manifold, pressurized sample cartridges, sample pretreatment, modification of irradiation facility and gas desorption protocol) is given. Calibration procedures are described and a measure of the attainable precision of absorbed gas recovery from gram amounts of irradiated material is presented.

4:50 PM

NMR Study of Mechanically Activated Li-N-H System: *Chun Lu*¹; Jianzhi Hu¹; Zhenguo Yang¹; Leon Shaw²; ¹Pacific Northwest National Laboratory; ²University of Connecticut

Mechanical activation via high energy ball milling has been often used for fabrication and synthesis of hydrogen storage materials. To gain insight into the effects of mechanical activation, Li-N-H system was taken as example and studied using the advanced NMR tool. Lithium hydride (LiH), amide (LiNH₂) and their mixture (2LiH+LiNH₂) were mechanically activated via attrition milling for different times. The mechanically activated samples, along with those without mechanical activation, were then investigated via in situ ¹H and ⁶Li NMR spectroscopy at elevated temperatures. This paper will report details of this work and discuss mechanistic understanding on the effects of mechanical activation of the materials and their storage properties.

Materials in Clean Power Systems II: Fuel Cells, Solar, and Hydrogen-Based Technologies: SOFCs II

Sponsored by: The Minerals, Metals and Materials Society, ASM International, TMS Structural Materials Division, TMS/ASM: Corrosion and Environmental Effects Committee

Program Organizers: Zhenguo "Gary" Yang, Pacific Northwest National Laboratory; Michael Brady, Oak Ridge National Laboratory; K. Scott Weil, Pacific Northwest National Laboratory; Yong-Ho Sohn, University of Central Florida

Tuesday PM Room: Asia 2
February 27, 2007 Location: Dolphin Hotel

Session Chairs: Yves Idzerda, Montana State University; Lichun Chen, Technical Materials Inc

2:00 PM Invited

Evaluation of a Surface Treatment on the Performance of Crofer 22 APU in a SOFC Button Cell: *David Alman*¹; Christopher Johnson¹; Paul Jablonski¹; ¹Department of Energy

Crofer 22 APU is a 22 weight percent Cr ferritic stainless steel developed at Forschungszentrum Jülich and manufactured by ThyssenKrupp for application as an interconnect in SOFC. We have developed a cerium oxide surface treatment which greatly enhances the oxidation resistance of this and many other alloys. Minimizing scale growth is helpful for improving the performance in interconnect application; however, the overall performance is dependant upon such things as scale thickness, scale resistivity, etc. We report on the in-cell performance of cerium treated and conventional Crofer 22 APU and discuss the results in terms of the microstructure and scales that form.

2:35 PM Invited

Advanced PVD Nanocomposite Protective Coatings for SOFC Metallic Interconnects: *Paul Gannon*¹; Max Deibert¹; Vladimir Gorokhovskiy²; Richard Smith¹; Zhenguo Yang³; Preston White¹; Edward Musz¹; Stephen Teintzel¹; ¹Montana State University; ²Arcomac Surface Engineering, LLC; ³Pacific Northwest National Laboratory

In an effort to enable inexpensive ferritic steels as interconnects (bi-polar plates) in planar solid oxide fuel cell (SOFC) stacks, advanced large area filtered arc physical vapor deposition (LAFAD) of MCrAlYO nanocomposite ceramic protective coatings is being investigated (M = Ti, Co, Mn and/or Ni). Coatings were applied to T430 steel specimens and subjected to various SOFC relevant exposures. The coatings' adhesion, microstructure, composition, area specific resistance and Cr volatility were evaluated as a function of exposure and compared with uncoated counterparts, using a variety of surface and cross section analysis techniques (SEM/EDS/EBSD; RBS; XRD). Significant improvement in simulated SOFC interconnect performance was observed with coated vs. uncoated specimens. Coating deposition processes, basic coating properties and SOFC interconnect protection mechanisms are discussed.

3:10 PM

Improvement of Oxidation Resistance of Ferritic Fe-Cr Alloy for SOFC Interconnects: *Akihiro Toji*¹; Toshihiro Uehara¹; ¹Hitachi Metals, Ltd.

A ferritic Fe-22Cr alloy with a small addition of La and Zr, ZMG232, which has good oxidation resistance and good electrical conductivity at 750-1000°C, was developed as a metallic interconnect material. Recently, further long-term stability of oxidation resistance of interconnect material has been required. So in order to improve the oxidation resistance, the effect of alloying elements on properties of ZMG232 was basically investigated. As a result, it was found that the oxidation resistance of ZMG232 at 750-1000°C in air was extremely improved by decreasing both of Si and Al contents. The developed alloy, ZMG232L, has about half of oxidation weight gain of ZMG232, and much thinner thickness of oxide layer than ZMG232.

3:35 PM

Evaluation of Model 6-22 Cr Ferritic and Austenitic Stainless Steel Alloys: *Paul Jablonski*¹; David Alman¹; ¹Department of Energy

Commercial stainless steels typically contain 0.5-1 weight percent silicon and lesser amounts of aluminum, generally as a carry over product from

the manufacturing processes. These reactive elements can form electrically resistive layers within the SOFC interconnect as an oxidation product. By starting with high purity materials and utilizing careful melt shop practices we were able to formulate a series of ferritic and austenitic stainless steel alloys containing between 6 and 22 Cr. We report on their performance in simulated SOFC environments and compare these results to commercial alloys with similar levels of Cr but containing Si and other "tramp" elements.

4:00 PM Break

4:15 PM

Issues Related to Scale Area Specific Resistance (ASR) Measurement of Interconnect Alloys: *Jiahong Zhu*¹; ¹Tennessee Technological University

With recent trend in reducing the solid oxide fuel cell (SOFC) operation temperature to the range of 600-800°C, metallic alloys (e.g. ferritic Fe-Cr alloys) have been promoted as SOFC interconnect materials. In addition to the consideration of coefficient of thermal expansion (CTE) and oxidation resistance, the oxide scale area specific resistance (ASR) is a major parameter for assessing the performance of the interconnect alloys. Unfortunately, the measurement of ASR has not been standardized and there are some disparities existing in the literature with regard to the methodology for scale ASR measurement. In this talk, several issues related to the ASR measurement are described and discussed, such as the selection of contact paste, dc vs. ac technique, and the contribution of contact resistance to the overall ASR. The measurement of scale ASR in the reducing (anode) atmosphere is also discussed.

4:40 PM

Electrical Contacts and Interfacial Resistance between Electrodes and Metallic Interconnects in SOFCs: *Guan-Guang Xia*¹; Zhimin Nie¹; Zhenguo "Gary" Yang¹; Jeff Stevenson¹; ¹Pacific Northwest National Laboratory

In SOFCs, electrical contact layers are often used between electrodes (anode or cathode) and interconnect in order to promote electrical contact and facilitate stack assembling. For a minimized power loss and satisfied performance, the contact layers have to be stable under SOFC operating conditions and chemically compatible with electrodes and interconnects that are often constructed from high temperature oxidation resistant alloys in planar SOFCs. In comparison, the electrical contacts at the cathode side appear to be more susceptible to degradation in stability and performance due to the oxidizing environment. In our work, a series of candidate contact layer materials were selected, and their electrical performance has been evaluated in air. Their stability in the cathode side environment and interactions with different cathode compositions and interconnect candidate alloys have also been studied. This paper will present details of this work.

5:05 PM

X-Ray Analysis of SOFC Degradation from Hydrogen Sulfide Exposure: *Alexandre Lussier*¹; Y. U. Idzerda¹; S. Sofie¹; ¹Montana State University

Experimental data shows that the deleterious effect of hydrogen sulfide exposure on solid oxide fuel cell performance is typically irreversible, yet the poisoning mechanism is still poorly understood. In the case of the traditional Ni/YSZ anode, post-mortem analysis of cells degraded by H₂S reveals no sulfur in the anode by conventional analysis techniques. We use X-ray Absorption Spectroscopy (XAS) to achieve improved sensitivity and detection of sulfur to elucidate the specific poisoning mechanism. Cell performance tests confirm the irreversible damage to traditional Ni/YSZ fuel cell anodes with less than 10 ppm H₂S, however, many Ni/CeO₂ fuel cell anodes suffered initial degradation in performance, but recovered in pure hydrogen. Furthermore, one Ni/CeO₂ cell showed complete tolerance to sulfur at greater than 300 ppm H₂S with no drop in performance for a duration of 100 hours. Post-mortem analysis revealed the development of cerium oxy-sulfide, however, the correlation between oxy-sulfide formation and resistance to cell degradation is not completely recognized. We will present our most recent results of XAS analysis and sulfur tolerance test performance on nickel based SOFC anodes.



Materials Processing and Manufacturing Division Symposium: Mechanics and Materials Modeling and Materials Design Methodologies, in the Honor of Dr. Craig Hartley's 40 Years of Contributions to the Field of Mechanics and Materials Science: Materials Design

Sponsored by: The Minerals, Metals and Materials Society, TMS Materials Processing and Manufacturing Division, TMS: Shaping and Forming Committee, TMS/ASM: Mechanical Behavior of Materials Committee
Program Organizers: Brent Adams, Brigham Young University; Hamid Garmestani, Georgia Institute of Technology

Tuesday PM Room: Northern A1
 February 27, 2007 Location: Dolphin Hotel

Session Chairs: David McDowell, Georgia Institute of Technology; Hamish Fraser, Ohio State University

2:00 PM

Challenges and Prospects for Materials Design: *David McDowell*¹; ¹Georgia Institute of Technology

Presently, a materials design revolution is underway in which classical materials selection is replaced by design of material microstructure to achieve certain performance requirements, subject to constraints on other properties. The materials design approach advocated here invokes the notion of robust design, i.e., insensitivity of the desired response to various sources of uncertainty. It utilizes decision theory and the notion of compromise decision support, leading to Pareto optimal solution sets. To this end we have developed notions of multilevel design and Type III robust design, addressing configuration of simulations/evaluations and uncertainty of models or database information. We close with an overview of Georgia Tech's AFOSR Multi-University Research Initiative (MURI) on Design of Multifunctional Energetic Structural Materials, a distributed collaborative materials design effort that employs modeling tools ranging from ab initio methods to molecular dynamics to mesoscopic and macroscopic continuum models.

2:25 PM

Digital Material Frameworks for Material Design and Property Prediction: *Matthew Miller*¹; Paul Dawson¹; ¹Cornell University

Dr. Hartley has been instrumental in emphasizing the need for accelerated material development formulations and for supporting the development of digital material representation frameworks. This talk summarizes our work conducted under Dr. Hartley's Materials Engineering for Affordable New Systems program, which we have continued to develop. Our "digital material" is centered on a relational database of material structure information in the form of distributions. There are tools for building (instantiating) and loading virtual samples drawn from the digital material, analogous to the processes used in a physical laboratory. Mechanical properties are derived from the predicted response; hence, designers are able to iterate on the material structure for optimal properties. New experimental techniques have enabled the measurement and storage of actual microstructures. A new material representation framework we are working on for titanium alloys that encompasses both the statistical structure of the digital material and measured microstructural volumes is also described.

2:50 PM

Invertible Microstructure-Property-Processing Linkages Using Spectral Methods: *Surya Kalidindi*¹; Hari Kishore Duvvuru¹; Marko Knezevic¹; Massimiliano Binci¹; ¹Drexel University

Effective properties of materials are derived from the details of the underlying microstructure spanning several hierarchical length scales. A complete description of the microstructure is experimentally impractical at the current time; it is also unwarranted in many engineering design applications. Instead, statistical descriptions of the microstructure are often employed in composite theories (or homogenization theories) to predict the effective overall properties of the material. Models also exist for accurate prediction of the evolution of these statistical descriptions of microstructure under certain prescribed

processing operations. This paper presents a new and highly efficient spectral framework, called Microstructure Sensitive Design, for building invertible microstructure-property-processing linkages.

3:15 PM

On The Design and Control of Properties in Polycrystalline Materials Using Process-Texture-Property Maps: Nicholas Zabaravski¹; *Veera Sundararaghavan*¹; ¹Cornell University

We put forth a methodology to generate graphical representations of texture-property relationships in polycrystalline materials during deformation processing. Graphical representations when combined with linear analysis techniques form a powerful method for property optimization. The orientation distribution function is represented using finite element interpolation techniques that allow matrix representation of the microstructure-property relationships using linear upper-bound relations. Computations of texture evolution based on model reduction are then used to derive texture-property-process maps for various deformation processes. Universe of textures realized from a deformation process is shown to be optimally visualized as simple polygons in the reduced texture space. Various optimization problems are solved in this representation using graphical cross-plots or linear programming. These include identification of textures with extremal properties and identification of processing paths for reaching a desired property. Statistical learning techniques that allow optimization of properties that depend on higher-order features of the microstructure are described.

3:40 PM

Progress in Materials Modeling and Some Future Needs: Hamish Fraser¹; Somnath Ghosh¹; Michael Mills¹; *James Williams*¹; ¹Ohio State University

At the end of the 20th century there was growing recognition of the need for high fidelity modeling tools to accelerate materials development. These tools could supplant multiple empirical iterations that were commonly used to develop new materials. In response to this need, there has been a renewed effort to develop a variety of material modeling tools that compliment newly available experimental capabilities. Included are phase field modeling methods for describing microstructure evolution, finite element and crystal plasticity models for analyzing mechanical behavior, improved thermodynamic computational methods for defining equilibrium and sophisticated statistical methods such as neural networks for dealing with complex alloys where first principle methods are not yet ready. This talk will review the progress made in materials modeling over the past ~5 years using examples. It will close with some suggestions regarding high impact materials modeling needs that will sustain progress in this vital area.

4:05 PM

Application of Microstructure Sensitive Design in Fuel Cell Electrodes: *Dongsheng Li*¹; Hamid Garmestani¹; ¹Georgia Institute of Technology

A statistical continuum mechanics formulation is presented by means of Green's function method to predict the electrical and mechanical properties of fuel cell electrodes. This model is applied within the framework of microstructure sensitive design (MSD) to guide the design of the microstructure in porous lanthanum strontium manganite (LSM) fuel cell electrode. To satisfy the property requirement and compatibility, porosity and its distribution can be adjusted under the guidance of MSD to achieve optimized microstructure. Processing parameters can be adjusted to tailor the microstructure to achieved desired properties.

4:30 PM

Design and Control of Microstructure in Controlled Drug Release Systems: *David Saylor*¹; Chang-Soo Kim¹; Dinesh Patwardhan¹; James Warren²; ¹U.S. Food and Drug Administration; ²National Institute of Standards and Technology

A popular method of controlling drug release is to incorporate the drug into a polymer matrix, which becomes a diffusion barrier, limiting the drug release rate. It has been demonstrated that the microstructure that evolves during manufacture significantly impacts the release kinetics. However, because the relationships between processing conditions, microstructure, and release kinetics are not well understood in these systems, the product development and approval processes are currently governed by limited, empirically derived correlations. We have, therefore, developed a phase-field theory for microstructure evolution in these systems. Calculations based on theory

TUESDAY PM

Microstructure Sensitive Design (MSD) is a novel mathematical framework that facilitates development of invertible linkages between statistical description of the material's microstructure and its effective properties. Property closures are an important outcome of the MSD methodology, and delineate the complete set of theoretically feasible effective (homogenized) anisotropic property combinations in a given material system. In this paper, these concepts are employed in the delineation of effective property closures involving yield strength, ultimate tensile strength, uniform ductility, energy dissipated before necking, and the Lankford parameter R for a range of cubic and hexagonal metals. These novel closures demonstrate clearly the versatility of the MSD framework.

4:55 PM

Property Closures for Uniform Ductility and Ultimate Tensile Strengths of Polycrystalline Cubic and Hexagonal Metals: *Marko Knezevic*¹; *Surya Kalidindi*¹; ¹Drexel University

Microstructure Sensitive Design (MSD) is a novel mathematical framework that facilitates development of invertible linkages between statistical description of the material's microstructure and its effective properties. Property closures are an important outcome of the MSD methodology, and delineate the complete set of theoretically feasible effective (homogenized) anisotropic property combinations in a given material system. In this paper, these concepts are employed in the delineation of effective property closures involving yield strength, ultimate tensile strength, uniform ductility, energy dissipated before necking, and the Lankford parameter R for a range of cubic and hexagonal metals. These novel closures demonstrate clearly the versatility of the MSD framework.

5:20 PM

Computational Systems Design of Hierarchically Structured Materials: *Gregory Olson*¹; ¹Northwestern University

Abstract: A systems approach integrates processing/structure/property/performance relations in the conceptual design of multilevel-structured materials. Using examples of high performance alloys, numerical implementation of materials science principles provides a hierarchy of computational models defining subsystem design parameters which are integrated via computational thermodynamics in the comprehensive design of materials as interactive systems. Recent initiatives integrate materials science with quantum physics and applied mechanics, and address the acceleration of the full materials design, development and qualification cycle. Under the AFOSR-MEANS program, efficient exploitation of predictive science has demonstrated a YAG-passivating Nb alloy with oxidation resistance at 1300°C. Principal barriers to the adoption of the new paradigm of science-based materials engineering are primarily cultural, and will require substantial reform of undergraduate materials education.

Materials Processing Fundamentals: Powders, Composites, Coatings and Measurements

Sponsored by: The Minerals, Metals and Materials Society, TMS Extraction and Processing Division, TMS: Process Technology and Modeling Committee, TMS: EMPMD Council, TMS: EPD Council
Program Organizer: Princewill Anyalebechi, Grand Valley State University

Tuesday PM

Room: Northern A2

February 27, 2007

Location: Dolphin Hotel

Session Chair: Prince Anyalebechi, Grand Valley State University

2:00 PM

Plasma Synthesis of Ultrafine Nd-Fe-B Magnetic Particles: *Edgar Vidal*¹; *Alejandro Gonzalez*²; *Judith Gomez*¹; *Patrick Taylor*¹; ¹Colorado School of Mines; ²Universidad Simon Bolivar

Ultrafine magnetic particles have been synthesized using oxides of neodymium, boron and iron as precursors. Methane was used as the reducing agent in the thermal plasma system in order to promote the formation of the magnetic particles. The effect of processing parameters on the chemical and morphological characteristics are presented.

2:15 PM

Synthesis of Biomimetic TiC Fibers Using Cotton as Bio-Templates: *Sutham Niyomwas*¹; ¹Prince of Songkla University

Biomimetic titanium carbide fibers with woodlike microstructure has been prepared by carbothermal reduction reaction of charcoal/silica composite

in argon atmosphere, which were fabricated by vacuum-assisted infiltrating titanium oxide sol into hollow fiber bio-template from natural fibers of cotton. The morphology of resulting TiC fiber, as well as conversion of wood fiber to ceramic fiber, has been investigated by SEM, XRD, TGA and DTA techniques. Experimental results show that the biomimetic fiber morphology of cotton fiber charcoal is remained in the TiC fibers.

2:30 PM

Properties of Magnesia-Calcium Zirconate Refractories Prepared by Nano-Technology: *Min Chen*¹; ¹Northeastern University

Magnesia-chromite brick has been widely used in cement rotary kilns and slag line of VOD furnace for its excellent properties of high refractoriness and slag resistance and thermal shock, but the environment problems caused by hexavalent chrome have resulted in several technological innovations to develop new type refractories for substitution of magnesia-chromite brick, and magnesia-calcium zirconate refractories is one of these substitutions. However, the application of magnesia-calcium zirconate refractories has been influenced by the high price with increasing the content of ZrO₂ in the refractories. In the present work, the effect of the addition of nano-size ZrO₂ powder on properties of MgO-CaO refractories was investigated. The results showed that homogeneous microstructure with fine calcium zirconate grains well dispersing was formed and the thermal shock resistance of the refractories could be appreciably improved with a less amount of ZrO₂ addition.

2:45 PM

Synthesis of Porous Composites by Self-Propagating High Temperature Synthesis of TiO₂-B₂O₃-Al System: *Sutham Niyomwas*¹; ¹Prince of Songkla University

The TiB₂-Al₂O₃ porous composites were obtained in situ by self-propagating high temperature synthesis (SHS) of TiB₂-B₂O₃-Al System. The reaction was carried out in a SHS reactor under static argon gas at the pressure of 0.5 MPa. The standard Gibbs energy minimization method was used to calculate the equilibrium composition of the reacting species. The effects of increasing aluminum mole ratio to the precursor mixture of TiO₂, B₂O₃ and Al were investigated. XRD and SEM analyses indicate complete reaction of precursors to yield TiB₂-Al₂O₃ as product composite.

3:00 PM

Residual Strains of Steel Tubular Specimens after Subject to Torsion and Tension Using Neutron Diffraction: *Xin Luo*¹; *D. Penumadu*¹; *Ke An*²; *Camden Hubbard*²; *F. Tang*²; *H. Choo*¹; *Peter Liaw*¹; ¹University of Tennessee; ²Oak Ridge National Laboratory

Studying on residual strain under 1-D loading, typically pure tension, by using diffraction-based methods has been well studied in the past. However, very little work has been done so far about the residual strain due to pure torsion or under 3-D loading conditions. Torsion provides unique opportunity to probe mechanical behaviors of materials under pure shear stress, and in combination with axial load, provides a mechanism to rotate principal stresses in a controlled fashion. Thus, complete three-dimensional mechanical behavior can be investigated by controlling the major principal stress rotation to characterize anisotropic materials. Steel tubular specimens were first subjected to either pure torsion or pure tension that corresponds to a target equivalent strain invariant. These specimens then were investigated using the neutron residual stress facility (NRSF2) at ORNL. Residual strain in terms of changes in the lattice spacing was measured in radial and circumferential direction with a gage volume of 1×2×1 mm³, and along axial direction with a gage volume of 2×1×2 mm³. Two monochromators of Si220 (2.67Å) and Si331AF (1.73Å) were used. Results are analyzed for the hkl reflections of 110 and 211, both of which are reported to be weakly affected by intergranular strain for tension stress path from prior literature. Results indicate considerable difference in the measured residual strain variation between the tubular specimens subjected to torsion versus tension. This study is first of its kind for evaluating residual strains in generalized loading conditions and also helped to demonstrate the need for having a multi-axial loading system (axial and torsional) for the anticipated residual stress testing facility for the Spallation Neutron Source users.



3:15 PM

Synthesis of Fibrous Nickel Cobaltite Spinel from Ammoniacal Complex Nickel-Cobalt Oxalate: *Jing Zhan*¹; Chuanfu Zhang¹; ¹Central South University

A nickel-cobalt oxalate complex precursor containing ammonium for the synthesis of fibrous nickel cobaltite was obtained by coordination coprecipitation technique. SEM, XRD pattern, thermal analysis and IR spectroscopy were used in the characterization and the evaluation of some aspects of the formation mechanism of fibrous morphology of the precursor. The effects of different Ni/Co ratios, decomposition temperature and decomposition time on the phase constitute of final product were addressed. The crystallinity, purity, and surface morphology of the as-prepared NiCo₂O₄ fibers were investigated by XRD, IR, SEM, respectively. Finally, Structure of nickel cobaltite spinel examined by X-ray absorption spectroscopy (XPS) indicates, as expected, that Ni occupies the octahedral sites of the spinel structure while Co occupies both tetrahedral and octahedral sites. The result of the surface examination by xps shows that the surface composition is different from nominal bulk composition.

3:30 PM Break

3:45 PM

Synthesis of Dense CaO Clinker from Lightweight CaCO₃ with Oxides Addition: *Nan Wang*¹; ¹Northeastern University

CaO clinker was sintered from lightweight CaCO₃ powder by adding fine MgO and ZrO₂ powders, respectively. The results showed that the CaO derived from lightweight CaCO₃ was highly sinterable and compact CaO clinker with relative density above 96% was obtained, but further increment of compactness was restrained due to the occurrence of abnormal CaO grain growth. The densification of clinker was promoted due to the behavior of oxides addition on restraining the grain growth of CaO, and the microstructure of CaO clinker underwent a restructuration process with the amount increasing of oxides addition. Homogeneous microstructure, with well growing MgO grains occupying most of the boundary triple points of CaO grain formed with addition of 20%MgO. Especially when 20%ZrO₂ was added, CaZrO₃ layer formed around CaO grains. The hydration resistance of the clinker was appreciably improved due to promotion of densification, formation of CaO solid solution and modification of microstructure.

4:00 PM

The Formation of β -PP Crystals in a Compatibilized Blend of Isotactic Polypropylene and Polyamide-6: *Ronghua Zhang*¹; ¹City University of Hong Kong

A blend (referred to as Blend-0.3) of β -nucleated isotactic polypropylene (PP) and polyamide-6 (PA6) compatibilized with maleated polypropylene (MA-g-PP) was prepared by twin-screw compounding and followed by injection moulding. The injection moulded sample was studied by differential scanning calorimetry (DSC) and wide angle x-ray diffraction (WAXD). It was observed that high β -PP content can develop in Blend-0.3 at low cooling rate. The β -crystallinity measured by DSC was in agreement with the WAXD results. From analyzing the crystallization kinetics, it was revealed that the rate of crystallization for the β -PP crystals in Blend-0.3 was very slow. This is the major reason for the observed difficulties in obtaining high β -PP content in Blend-0.3 at normal cooling rates. The higher crystallization temperature of β -PP than that for α -PP explains why the high β -PP content can develop in Blend-0.3 when it was cooled down at lower cooling rates.

Microstructural Processes in Irradiated Materials: Modeling

Sponsored by: The Minerals, Metals and Materials Society, TMS Structural Materials Division, TMS/ASM: Nuclear Materials Committee
Program Organizers: Charlotte Becquart, University of Lille; Gary Was, University of Michigan; Brian Wirth, University of California

Tuesday PM Room: Europe 8
February 27, 2007 Location: Dolphin Hotel

Session Chairs: Brian Wirth, University of California; Charlotte Becquart, University of Lille

2:00 PM Invited

A Comparison of Cluster Dynamics Modeling by Reaction Rate Theory and Kinetic Monte Carlo: *Roger Stoller*¹; Stanislav Golubov¹; Christophe Domain²; Charlotte Becquart³; ¹Oak Ridge National Laboratory; ²Electricite De France; ³University of Lille

The multiscale modeling scheme encompasses models from the atomistic to the continuum scale. Phenomena at the mesoscale are typically simulated using reaction rate theory (RT), Monte Carlo (MC), or phase field models. These mesoscale models are appropriate for application to problems that involve intermediate length scales, and timescales from diffusion to long-term microstructural evolution (~years). Recent advances in computational power have expanded the domain MC models. Although the RT and MC models can be used simulate the same phenomena, some of the details are handled quite differently in the two approaches. A direct comparison of the RT and MC descriptions has been made in the domain of point defect cluster dynamics modeling, such as is relevant to both the nucleation and evolution (growth) of radiation-induced defect structures. The relative merits of the two approaches will be discussed along with issues such as their computational efficiency.

2:35 PM

Microstructural Evolution of Binary Alloys under Irradiation: *Arnoldo Badillo*¹; Yang Liu¹; Pavel Krasnochtchekov¹; Robert Averback¹; Pascal Bellon¹; ¹University of Illinois at Urbana-Champaign

The evolution of a compositional microstructure of a concentrated binary alloy under irradiation is simulated using a continuum kinetic model, which considers a vacancy and interstitial transport mechanism for atomic diffusion. The model is based on the coarse graining of a simple atomistic model, where point defects, both isolated and clustered, are included. A phase field model is obtained by the linearization of the kinetic model, which allows for quantitative predictions of the evolution of the microstructure under irradiation. Atomistic Monte Carlo simulations are performed to test the results of the phase field model. The effect of irradiation-induced displacement cascades on the chemical composition, is modeled by the introduction at a controlled rate of spherical zones, from where only a fraction of the point defects created in the cascade events, are allowed to escape due to recombination and interaction with clusters inside the spherical zones.

2:55 PM

Computer Simulation of Cascade Damage in Pure Iron and Fe-C: Andrew Calder¹; *David Bacon*¹; Alexander Barashev¹; Yuri Osetsky²; ¹University of Liverpool; ²Oak Ridge National Laboratory

Three issues associated with cascade damage in iron are presented. First, cascades of PKA energy in the range 5-20keV have been simulated for temperature up to 600K using an interatomic potential (Ackland et al., J. Phys.: Condens. Matter 2004) for which the energy difference between the $\langle 110 \rangle$ dumbbell interstitial and the $\langle 111 \rangle$ crowdion is close to the value from ab initio calculation. We compare the damage with that obtained earlier with potentials for which the interstitial energy difference is small. Second, cascades in iron containing carbon interstitial solute have been simulated. Carbon is found to have no significant influence on defect numbers, but a high proportion of self-interstitials are associated with it. Finally, the effect on damage of PKAs of elements of high (Bi) and low (C) mass has been investigated. Mass, rather than interatomic potential, is revealed to be influential: fewer defects are created by PKAs of heavy atoms.

TUESDAY PM

3:15 PM

Defect Kinetics in Electron Irradiated Steels: A Multiscale Modeling: *Chu Chun Fu*¹; Laurent Joly¹; Jean-Louis Bocquet¹; Alain Barbu¹; Francois Willaime¹; ¹SRMP CEA

Microstructural evolution of nuclear materials are governed by the kinetics of defects produced by irradiation. The population of vacancies, self-interstitials, and their clusters can however be followed only indirectly, e.g. by macroscopic resistivity measurements. By combining ab initio and kinetic Monte Carlo methods, we simulated the abrupt resistivity changes — the recovery stages — observed upon annealing after electron irradiation in ultra pure and C-doped iron. We investigate the effects of carbon — one of the principal component in the steel — on the defect population evolution. In agreement with experimental evidences, C atoms are effective traps of isolated vacancies and a weaker attraction are found between C and self-interstitial atoms. Stages related to carbon migration and clustering with self-defects are identified and interpreted. We also show a significant change of resistivity when C atoms are isolated or clustered with vacancies which directly affects the appearance of the Stage III.

3:35 PM Break

3:55 PM Invited

Fitting Interatomic Potential Functions to Quantum Mechanical Calculations Using Neural Networks: *Roger Smith*¹; Ed Sanville¹; Steven Kenny¹; Ajeev Bholoa¹; ¹Loughborough University

A methodology is presented for developing empirical potential functions without postulating a functional form. Instead, a neural network is employed to learn the functional relationships of potential energy surfaces from the local geometric arrangement of atoms. This is illustrated by training on thousands of data points derived from tight-binding for different silicon systems including both small clusters and bulk structures. The model successfully fitted energy variations of the different test cases as a function of bond distances, bond angles, lattice constants and elastic properties for both equilibrium and non-equilibrium small cluster and bulk structures. This indicates a robust and consistent methodology for fitting empirical potentials which can be applied to a wide range of materials independent of the type of bonding or their crystal structure. The extension of the methodology to data obtained from density functional theory will also be described.

4:30 PM

Effect of Interatomic Potential on the Behavior of Dislocation-Defect Interaction Simulation in Irradiated Fe: *Seyed Masood Hafez Haghghat*¹; Jan Fikar¹; Robin Schäublin¹; ¹Centre de Recherches en Physique des Plasmas-Ecole Polytechnique Federale de Lausanne

Molecular dynamics simulation is one of the most useful methods to model defect generation and subsequent change in mechanical properties in material that will suffer irradiation in the future fusion reactors. This work is aimed at showing the influence of the empirical interatomic potential on the simulated shearing of α -Fe containing an edge dislocation and an irradiation-induced defect. The recent potentials derived by Ackland et al. (1997), Mendelev et al. (2003) and Dudarev-Derlet (2005) are used to identify critical parameters. The stress-strain responses of a sample containing one edge dislocation and a nanometric void are compared under imposed strain rate and temperatures from 10 to 700 K at constant volume. Potentials give different rates of decrease of obstacle strength with increasing temperature. Results are analyzed in terms of dislocation core structure, void surface structure and thermal expansion. Implications for the choice of the potential are given.

4:50 PM

Independence of the Long Term Point Defect Cluster Growth on Displacement Cascades Features: *Marc Hou*¹; Abdelkader Souidi²; Charlotte Becquart³; Christophe Domain⁴; Lorenzo Malerba⁵; ¹Université Libre de Bruxelles; ²Centre Universitaire Dr. Moulay Tahar de Saïda; ³Université de Lille 1; ⁴Electricité de France R&D; ⁵SCK.CEN

Displacement cascades in iron are generated by means of the MARLOWE Binary Collision Approximation with primary energies ranging from 5 to 100 KeV. They serve as input for modelling long term evolution by means of the LAKIMOCA Object Kinetic Monte Carlo. The number densities of vacancy and interstitial clusters formed on the long term are not significantly dependent on the primary knock on energy. We also show that they are insensitive to

subcascade formation, to cascade morphology and spatial extension as well as to the clustering of point defects induced by the displacement cascade generation. It is therefore suggested that the knowledge of a limited number of low energy displacement cascades is sufficient to predict the point defect cluster growth on the long term, using the dpa as a scaling factor. This work is a cooperative project carried out in the frame of the European integrated project PERFECT.

5:10 PM

Non-Linear Dynamics of Microstructure Evolution and Pattern Formation in Irradiated Crystals: *Woo Chung Ho*¹; ¹Hong Kong Polytechnic University

As irradiation proceeds, crystal defects accumulate and interact, and the microstructure evolves from that of a normal engineering material to that uniquely characteristic of a component after many years of exposure. Remarkable patterns with nano-scale structures often appear, with phase-transition characteristics. Microstructure evolution of metals during irradiation is discussed from the point of view of non-linear dynamics of a complex stochastic system of interacting crystal defects. We show that the kinetic equations representing the diffusion-controlled accumulation of crystalline defects and the resulting evolution of irradiated microstructures often shows complex behavior and symmetry-breaking occurs due to the instability of the spatially homogeneous solution. Pattern formation such as defect walls and void lattices occurs due to the non-linearity of the system in a way similar to phase transformations in thermodynamic systems evolving under the thermodynamic state function such as free energy.

Microstructural Processes in Irradiated Materials: Poster Session I

Sponsored by: The Minerals, Metals and Materials Society, TMS Structural Materials Division, TMS/ASM: Nuclear Materials Committee
Program Organizers: Charlotte Becquart, University of Lille; Gary Was, University of Michigan; Brian Wirth, University of California

Tuesday, 5:30 PM Room: Europe 8
February 27, 2007 Location: Dolphin Hotel

Atomistic-Scale Understanding of Hardening Mechanism in Fe-Cr Alloys: *Jae-Hyeok Shim*¹; Chan Sun Shin²; Whung Whoe Kim²; Brian Wirth³; ¹Korea Institute of Science and Technology; ²Korea Atomic Energy Research Institute; ³University of California, Berkeley

High Cr ferritic/martensitic steels are being considered as a structural material for future generation nuclear reactors due to their good mechanical properties at high temperatures and resistance to swelling. It is known that these steels suffer from irradiation hardening and embrittlement below about 673 K, even at moderate dose. In addition, neutron irradiation is known to promote the precipitation of Cr-rich bcc phases with nanometer size during thermal aging, when the Cr content in Fe is larger than about 7 wt %. Despite the importance of understanding hardening mechanism in Fe-Cr alloys, it is not well known how solute Cr atoms and Cr nano-precipitates in Fe induce hardening of these alloys. In this study, the effect of solute Cr atoms and Cr nano-precipitates on dislocation glide in Fe is investigated using molecular dynamics simulations. The results will elucidate how much Cr nano-precipitates formed during irradiation contribute to irradiation hardening.

Diffusion of Defects Stimulated by In-Situ High-Energy Electron Irradiation: Experiment and Theory: Zhongwen Yao¹; Marquis Kirk²; Chung Woo³; Sergei Dudarev⁴; Michael Jenkins¹; ¹University of Oxford; ²Argonne National Laboratory; ³Hong Kong Polytechnic University; ⁴EURATOM/UKAEA Fusion Association

In-situ heavy-ion irradiations of Fe and FeCr alloys has been carried out in the Argonne National Laboratory IVEM-Tandem Facility. Thin foils were irradiated with 100keV Fe⁺ or Xe⁺ ions at room-temperature or 300°C, and the development of radiation damage microstructures was monitored by electron microscopy. Dislocation loops were observed to form in all cases, although loops once formed also disappeared during the ion irradiation, sometimes abruptly and sometimes apparently more gradually. Subsequently



a difference was noted between regions which had been observed in the electron microscope during ion irradiation, and thus had been exposed to simultaneous sub-threshold (200kV) electron irradiation, and regions outside the area covered by the electron beam. In regions exposed to electrons the final density of dislocation loops was considerably lower. We shall show that these observations may be understood in terms of athermal diffusion of point-defect clusters, stimulated by the electron beam.

Dislocation Interactions with Helium Bubbles: Hyon-Jee Lee¹; Brian Wirth¹; Ian Robertson²; ¹University of California, Berkeley; ²University of Illinois, Urbana-Champaign

Molecular dynamics simulations of the interaction between gliding dislocations and helium bubbles are presented. An examination of various factors, including dislocation type (edge, screw and mixed), temperature, stacking fault energy, bubble size and helium pressure lead to the conclusion helium bubbles are strong obstacles to dislocation motion. Low pressure bubbles are sheared, and the interaction is controlled by departure side pinning. With increasing helium pressure, the bubbles become over-pressurized and the interaction and detachment mechanism is controlled by the interaction of the dislocation with the interfacial distortion, including prismatic loops, and Orowan type detachment can be observed. The molecular dynamics simulations are compared to in-situ TEM observations.

Microstructural Characterisation of Ion Irradiated Ultra-High Purity Iron by Experimental And Modeling Methods: Mercedes Hernández-Mayoral¹; María José Caturla²; ¹Centro de Investigaciones Energéticas, Medioambientales y Tecnológicas; ²Universidad de Alicante

Basic processes occurring in metals under irradiation are studied by experimental characterisation and computer simulations. Ion irradiation experiments performed under well known and controlled irradiation conditions on iron of different purities are presented. Evolution of damage with dose is studied from 0.05 to 1 dpa, at a fixed dose rate of 2×10^{-4} dpa/s, and 300°C. Experimental results obtained by Transmission Electron Microscopy show that defects are formed by irradiation at all the considered doses. At the higher doses these defects are identified as $a\langle 100 \rangle$ and $a/2\langle 111 \rangle$ dislocation loops. Density and size of defects increased up to 0.5 dpa, while at 1 dpa defect density decreases due to loop coarsening and dislocation network formation. These experiments are modeled using Kinetic Monte Carlo with input data from ab initio and molecular dynamics. Possible mechanisms for loop formation and growth during irradiation are discussed.

Modeling Point Defect Interactions in Fe-Cr Alloys: Brian Wirth¹; Hyon-Jee Lee¹; Jae-Hyeok Shim²; Kevin Wong¹; ¹University of California, Berkeley; ²Korea Institute of Science and Technology

Fe-Cr alloys are a leading candidate material for Generation IV and Fusion reactors. Complete understanding of their response to irradiation, including the radiation induced segregation of Cr, requires knowledge of point defect and point defect cluster interactions with Cr solute atoms and impurities. In this work, we present results from a hierarchical modeling approach of defect cluster behavior in Fe-Cr alloys. The modeling includes ab initio electronic structure calculations performed using the VASP code with projector-augmented electron wave functions using PBE pseudo-potentials and a collinear treatment of magnetic spins, molecular dynamics using semi-empirical Finnis-Sinclair type potentials, and kinetic Monte Carlo simulations of coupled defect and Cr transport responsible for microstructural evolution. The modeling results are compared to experimental observations in both binary Fe-Cr and more complex ferritic-martensitic alloys, and provide a basis for understanding the observations of Cr enrichment and depletion at grain boundaries in various irradiation experiments.

Molecular Dynamics Study of Interstitial C Atoms in BCC Iron: Migration and Interaction with Radiation-Produced Point Defects and Defect Clusters: Kanit Tapasa¹; Alexander Barashev¹; David Bacon¹; Yuri Osetsky¹; ¹University of Liverpool

Properties of interstitial C atoms and their interaction with irradiation-produced defects in bcc-iron obtained by MD simulations using empirical potentials are presented. Comparison is made with the published data from ab initio calculations and experiments on the recovery of electron-irradiated pure Fe and Fe-C alloys. The interpretation of the recovery stages is discussed. The effect of carbon atoms on the configuration, relative stability and migration

of $1/2\langle 111 \rangle$, $1/2\langle 110 \rangle$ and $\langle 100 \rangle$ interstitial clusters is presented. Carbon atoms are predicted to enhance the relative stability of $\langle 100 \rangle$ over $1/2\langle 111 \rangle$ clusters, but not sufficiently to explain their common occurrence in irradiated iron. The mobility of $1/2\langle 111 \rangle$ clusters is significantly reduced or prevented (for the period of simulation) by attraction to C atoms. Jumps of C atoms along the cluster periphery similar to those in the core of a straight edge dislocation are observed. The mechanism and parameters of this motion have been determined.

Mutual Interaction of Interstitial Loops in α -Fe and Fe-Cr Alloys: Dmitry Terentyev¹; Lorenzo Malerba¹; ¹SCK-CEN

Under irradiation, two types of dislocation loops are known to form in Fe and Fe-Cr alloys: $1/2\langle 111 \rangle$ and $\langle 100 \rangle$. The nucleation and growth of these loops defines the evolution of the microstructure in many respects. Thus, microstructure evolution models (rate theory or kinetic Monte Carlo) require information on reactions with other defects, which mobile loops can undergo. In this work a molecular dynamics study of SIA loops motion and mutual interactions in Fe and FeCr alloys is presented. The comparative calculations have been carried out using two recently proposed interatomic potentials for pure Fe and Fe-Cr potential based on the ab initio calculations of the mixing enthalpy. Highlighting the effect of 'magnetism' introduced in one of the applied potentials is one goal of the study. The other goal is to examine the influence of Cr atoms on the reactions that dislocation loops undergo.

Nanocrystalline Materials: Enhancing Radiation Tolerance: Tong Shen¹; Shi Feng¹; Ming Tang¹; James Valdez¹; Yong Wang¹; Kurt Sickafus¹; ¹Los Alamos National Laboratory

Radiation damage has been studied almost exclusively in single-crystalline and conventionally polycrystalline (PC) materials. In this presentation, we examine irradiation-induced microstructural changes in single-phase nanocrystalline (NC) $MgGa_2O_4$ compounds. We find that radiation tolerance in NC samples exhibit significant improvements when compared with their PC counterparts. The PC $MgGa_2O_4$ is amorphized at a dose of 12 dpa while the NC $MgGa_2O_4$ is not amorphized following a much higher dose of 96 dpa. We correlate the enhanced radiation tolerance to suppressed accumulation of point defects in NC grain interiors and analyze the thermodynamic and kinetic origins for the enhanced tolerance. We believe this structural approach to enhancing radiation tolerance – namely, creating a large volume fraction of grain boundaries which act as defects sinks – should be generally applicable to many other materials – metals, ceramics and semiconductors – and may lead to new materials developments in the nuclear community.

Optimization of DBTT of Eurofer ODS Steel by Controlled Heat Treatment: Zheng Lu¹; Roy Faulkner¹; ¹Loughborough University

Eurofer ODS steel is potential candidate for fusion reactor application due to its excellent swelling resistance and high temperature properties. One of the main issues is that high fluence neutron irradiation induces a significant increase of ductile-to-brittle transition temperature (DBTT) at temperatures below 400°C which restricts their application. The aim of this study is to lower the initial DBTT of Eurofer ODS steel by heat treatment optimization. Two heats of Eurofer ODS steels, FZK and Heat-HXX-1115, with different C contents were normalized at 980, 1040, 1100, 1150, 1300°C and tempered at 550, 650, 750, 850°C, respectively. The microstructure is characterized by optical microscopy, FEGTEM and OIM-EBSD techniques. The effect of normalizing and tempering temperature on grain size, precipitation, grain boundary chemistry, grain boundary orientation, hardness, and DBTT are investigated. Monte Carlo models of precipitation are used with thermodynamic software MTDATA to forecast the phase evolution kinetics in Eurofer ODS.

Pb-Free Electronic Solders: Alloy Design, Characterization and Service Reliability: Whisker Growth, Design, and Modeling

Sponsored by: The Minerals, Metals and Materials Society, TMS Electronic, Magnetic, and Photonic Materials Division, TMS: Electronic Packaging and Interconnection Materials Committee

Program Organizers: Fu Guo, Beijing University of Technology; K. Subramanian, Michigan State University; Sung Kang, IBM Corporation; Srinivas Chada, Medtronic; Laura Turbini, University of Toronto; Jin Yu, Korea Advanced Institute of Science and Technology

Tuesday PM Room: Oceanic 1
February 27, 2007 Location: Dolphin Hotel

Session Chairs: Nikhilesh Chawla, Arizona State University; Srinivas Chada, Medtronic

2:00 PM

Effect of Stress on Whisker Growth in Matte Sn: *Adam Southworth*¹; C. E. Ho¹; Deep Choudhuri¹; Andre Lee¹; K. Subramanian¹; ¹Michigan State University

A major reliability issue in the implementation of Pb-free electronics is growth of Sn whiskers. In the microelectronics industry, whisker growth is of concern when they reach a length of about 50 μm . Their growth is often attributed to compressive stresses that develop in the Sn layer. Such stresses develop over time, and their magnitude will be affected by variables such as the (i) thickness and quality of surface finish, (ii) environmental factors such as temperature and humidity, (iii) interfacial chemical reactions, and (iv) mechanically induced stresses. In the present investigation copper sheets coated with matte Sn were bent to various curvatures and incubated isothermally. Periodic evaluations with SEM were carried out to characterize the whisker growth. This study explores the effects of imposed mechanical stress and humidity on Sn whisker growth so as to gain a better understanding of their roles on whisker growth in Sn.

2:20 PM

Indentation Load Effects on Whisker Growth in Sn_{3.5}Ag Solders: *John Nychka*¹; Fuqian Yang¹; Rong Chen¹; Yan Li¹; ¹University of Kentucky

Metallic whiskers, which form under normal service conditions in lead-free solders, typically cause short circuit failures due to the growth of whiskers across electrical leads – failures that lead to unpredictability, unreliability, and economic losses. It is well known that applied compressive stresses result in whisker formation in solder alloys; this work focuses on determining the effects of local residual stresses on the formation and growth of whiskers in lead-free solder, specifically Sn_{3.5}Ag. Attempts to more accurately observe the formation and growth of whiskers under approximated service conditions are required to evaluate the effects of microstructure, and mechanical and electrical stresses. Toward this goal, localized residual stresses were induced by varying the indentation load. Indented specimens were then heat treated to grow whiskers. Whisker formation and growth were characterized by scanning electron microscopy to determine the areal whisker density as a function of the indentation load.

2:40 PM

Reliving Sn Whiskers Growth by Reflow: *Cheng-Chang Wei*¹; P. C. Liu¹; Cih Chen¹; Jeffrey Lee²; P. C. Chen³; ¹National Chiao Tung University; ²Integrated Service Technology; ³Advanced Semiconductor Engineering

Currently, in the electronic packaging industries, Pb-free solders are replacing eutectic tin-lead. Most of components suppliers are looking forward the pure tin plated or tin-alloys electroplating as an alternative for the tin-lead plating. However, the lead-frame could grow long tin whiskers, which cause serious reliability issue in microelectronics devices. In this study, we investigated the annealing and reflowing process, trying to mitigate the growth of whiskers by the temperature/humidity storage test components. The annealing and reflowing conditions test were 220° thermal treatment; 268° reflowing treatment. It is found that the intermetallic compound formation seems not the major reason to assist the whiskers formation. Instead, whiskers grew near the corrosion region. After the 220° thermal treatment, the growth

of whisker was relived slightly. We found the reflowing process could retard the whiskers growth effectively by forming an equi-axed grain structure and some of stress could be relived during tin re-crystallization process.

3:00 PM

Tin Whisker Growth Driven by Electric Current: *Yu-Wei Lin*¹; C. Robert Kao¹; Yi-Shao Lai²; ¹National Taiwan University; ²Advanced Semiconductor Engineering Group

The effect of electromigration on the tin whisker growth was studied. The substrate used in this experiment was a p-type silicon wafer. Sputtering was used to deposit a 1 micron copper film on the substrate. Then lithography process was applied to define the copper circuits. Afterward, immersion tin was used to exchange the copper for tin. The thickness of the final tin film was 1 micron. Three different widths of tin lines, 50 microns, 100 microns, and 200 microns, were designed on the sample, producing current density ratio of 4:2:1. It was found that both the current density and the temperature had strong effects on the number of tin whiskers. In addition, the current crowding effect will influence the behavior of whisker growth. The current density distribution was the key factor determining the regions where tin whiskers grew. The electromigration flux and the effective charge were calculated.

3:20 PM

Diffusion-Controlled Whisker Growth: *Fuqian Yang*¹; ¹University of Kentucky

Whisker growth plays an important role in determining the performance and lifetime of micro/nano electronic devices. It has been accepted that the whisker growth is a stress relaxation process in materials. Tu in 1994 proposed that the fracture of surface oxide led to the relief of localized stresses and estimated the growth rate of whiskers based on grain diffusion. In this work, we consider the contribution of lattice diffusion to the whisker growth. Assuming that the material is subjected to constant applied stress, we solve the lattice diffusion and obtain the growth rate of whiskers. In contrast to the whisker growth controlled by the grain boundary diffusion, the growth rate is inversely proportional to size of the whisker. The difference in the dependence of the growth rate on the size of the whisker provides us a technique to determine the mechanism controlling the growth of metallic whiskers and nanowires.

3:40 PM Break

3:50 PM

Origin of Surface Defects in Final Finishes of PCB by an Electroless Nickel Immersion Gold (ENIG) Process: *Bae-Kyun Kim*¹; Seong-Jae Lee¹; Jong-Yun Kim¹; Kum-Young Jee¹; Yeo-Joo Yun¹; Mi-Yang Kim¹; Song-Hae Park¹; Jong-Soo Yoo¹; ¹Samsung Electro-Mechanics

Surface defects in PCB can be defined as corroded holes of nickel plate layer, such as pinholes or circled dark area so-called black pad, after electroless nickel immersion gold (ENIG) process. Once corroded voids are created at the nickel/gold interfaces, the bonding strength of solder joints becomes weak. It results in failure of wire bondability or soldering solderability in PCB. Previous experimental data with process control factors, such as phosphorus content, pH and temperature in nickel bath, may help us to understand the mechanism of the defect generation. However, in spite of many characterizations about the defects, the overall mechanism and relationship between process control factors have not been properly understood. In this paper, key findings about the relationship between the electron drain sources in gold layers and the defect generation are demonstrated. Based on these results, more reasonable root causes for PCB joint failures are uniquely proposed.

4:10 PM

Experimental Investigation and Thermodynamic Calculation of the Phase Equilibria in the Sn-Bi-Ni Ternary System: *Yoshikazu Takaku*¹; Ikuo Ohnuma¹; Zhanmin Cao²; Yuji Miyabe³; Ryosuke Kainuma⁴; Kiyohito Ishida¹; ¹CREST-JST, Tohoku University; ²University of Science and Technology Beijing; ³Department of Materials Science, Tohoku University; ⁴CREST-JST, IMRAM, Tohoku University

Sn-58Bi alloy is practically utilized as a low-temperature solder which is often connected on a Ni layer on a Cu substrate. Therefore, phase diagrams of the Sn-Bi-Ni system are indispensable to investigate the interfacial reaction and soldering phenomena. However, very few studies on the phase equilibria in the ternary system have been carried out. In this study, the phase equilibria of Sn-Bi-Ni system, including three isothermal sections in the Sn-rich



portion as well as two vertical sections, were investigated by means of DSC and metallographic analysis. Experimental results exhibited the formation of a metastable NiSn phase at 673 K, which transforms into a stable Ni₃Sn₄ phase by further heat-treatment. Thermodynamic calculation was carried out by CALPHAD (calculation of phase diagrams) method. Thermodynamic parameters for describing the Gibbs energy of each phase were optimized, which results in good agreement between calculated equilibria and experimental data.

4:30 PM

Modeling of Materials Properties of Multi-Component Lead-Free Solder

Alloys: Nigel Saunders¹; Zhanli Guo¹; Peter Miodownik¹; Jean-Philippe Schille¹; ¹Sente Software Ltd.

The worldwide movement in the electronics industry to implement lead-free solders (LFS) has created a demand for fundamental property data that accurately describe the behaviour of these alloys and can be used to develop appropriate manufacturing and reliability models. To generate all the data required experimentally is costly and time-consuming, if always possible at all. Therefore, it is highly desirable to develop computer-based models that can calculate such properties as a function of alloy chemistry, temperature and other influential factors. In the present work models have been created such that a full set of physical and thermophysical properties can now be calculated, including coefficient of thermal expansion, densities, various moduli, thermal conductivity, liquid surface tension and wettability, all as a function of composition and temperature (extending into the liquid state) for solder alloys from the multi-component system Sn-Ag-Al-Au-Bi-Cu-In-Ni-Pb-Sb-Zn.

4:50 PM

Materials and Design Optimization of Integral Heat Spreaders and Solder Thermal Interface Materials in Advanced Intel CPU Packaging:

Thomas Fitzgerald¹; Carl Deppisch¹; Fay Hua¹; ¹Intel

This paper provides a historical overview of both the Integral Heat Spreaders (IHS) and Solder Thermal Interface Materials (STIM) used by Intel. The first IHS used on a CPU package at Intel was certified 1999. This paper briefly explains how the Intel IHS design for solder TIM packaging has evolved and has been optimized to (1) improve package performance, (2) solve reliability issues and (3) reduce part cost. This paper also provides an historical overview of the materials selection process, and explains why Indium was chosen as STIM material. This paper also outlines some of the current challenges for both IHSes and solder-TIM, and briefly discusses future IHS designs, including the potential of a solder-in-lid solution.

5:10 PM

The Effect of a Solder Bump Size on the Ball-Shear Test Results:

Woong Ho Bang¹; Choon-Sik Kang²; Kyu Hwan Oh²; Choong-Un Kim¹; ¹University of Texas at Arlington; ²Seoul National University

Solder-ball shear experiments for different bump sizes have been carried out. The results indicate shear force level that increases with a solder ball size but fracture mode that is more brittle at larger solder bumps. The FEM analysis incorporating the viscoplasticity of a solder bump proposes that, not only is the bump/metallization adhesion strength is the strength that determine the ball shearing force, but also the visco-plastic deformation of a solder bump affects the solder-ball shearing force: a larger ball experiences larger deformation amount during a ball shear test with the consequence of the increased shear force result. Through the fracture mechanics approaches, the more brittle fracture mode at larger solder bumps has been found to be due to an increased bump rotation moment that opens crack tip at a crack initiation site. The result and discussion will be discussed in detail at present talk.

Phase Stability, Phase Transformations, and Reactive Phase Formation in Electronic Materials VI: Session III

Sponsored by: The Minerals, Metals and Materials Society, TMS Electronic, Magnetic, and Photonic Materials Division, TMS: Alloy Phases Committee
Program Organizers: Sinn-Wen Chen, National Tsing Hua University; Srinivas Chada, Medtronic; Chih-ming Chen, National Chung Hsing University; Young-Chang Joo, Seoul National University; A. Lindsay Greer, University of Cambridge; Hyuck Lee, Korea Advanced Institute of Science and Technology; Daniel Lewis, Rensselaer Polytechnic Institute; Katsuaki Suganuma, Osaka University

Tuesday PM

Room: Oceanic 2

February 27, 2007

Location: Dolphin Hotel

Session Chairs: A. Greer, University of Cambridge; Chih Ming Chen, National Chung-Hsing University

2:00 PM Invited

Electromigration Effects on Intermetallic Compound Growth: *A. L. Greer¹; H. T. Orchard¹; ¹University of Cambridge*

It is now well known that an imposed electrical current normal to the interface between two metals can influence the growth of intermetallic compounds at the interface. Recent observations of compound formation at Au wire bonds onto Al-based metallization will be reported. These show that sensitive electrical measurements can be correlated with microstructural studies. An analysis of the kinetics of growth of a compound is based on electromigration effects on the interdiffusion within a compound itself. This provides a basis for understanding the asymmetric effects of direct currents of opposite polarity. Particular insights can be gained from studies in which the polarity is reversed. Effects on void development and on multiple intermetallic phases will also be considered.

2:25 PM Invited

Electromigration of Sn Based Alloy Solders: Incubation Time, Threshold Current Density and Driving Forces: *Young Chang Joo¹; ¹Seoul National University*

Electromigration of flip chip solder has become an important reliability threat for microelectronic devices. Because flip chip solders consists of two or three elements with more than one phases, their electromigration behavior may be complicated. We have analyzed the electromigration behavior of various Sn based solder materials, such as pure Sn, eutectic SnPb, Sn5.0Pb95 and pure Pb, using the edge drift structures. The change in composition during electromigration, existence of incubation time, and length dependence of threshold current density are investigated. An incubation stage for edge drift was observed in eutectic SnPb electromigration. However, no incubation time has been observed in single composition system. The threshold current densities of Pure Sn were inversely proportional to the line lengths. However, eutectic SnPb solder did not show the typical line length dependences. This suggests that there are more than one back-flux forces in multi-phase system. Possible driving forces during electromigration are discussed.

2:50 PM

Electromigration in CuSn Intermetallic Compound: *ChengFeng Chen¹; Chin Chen¹; ¹National Chiao Tung University, Department of Materials Science and Engineering*

Flip Chip Technology is one of the most important packaging methods for high current density IC device. While current density applied increased, solder joint has become a critical issue on device reliability. Furthermore, as the bump size continues to shrink, the effect of the intermetallic compound (IMC) on the electromigration becomes more pronounced. In this study, Blech structure of CuSn IMC with about 105 A/cm² at elevated temperature of 300° is investigated. Voids was found in the cathode end and hillocks was found in the anode end. We can measure the drift velocity of the IMC by measuring the depletion volume. The details will be presented in meeting.

3:10 PM

Enhanced Electromigration Effects in the Eutectic SnBi Solder by the Addition of 1 wt% Copper: *Chih Ming Chen*¹; *Chih-chieh Huang*¹; ¹National Chung-Hsing University

Fast and non-uniform grain coarsening in the eutectic SnBi solder is undesirable since such a violent microstructural change may affect the solder properties severely. By adding only 1 wt% copper, the rate of the grain coarsening is greatly suppressed. The suppression effect is due to the formation of many fine Cu-Sn particles that act as the obstructers against the grain growth. However, the copper addition results in an enhancement effect on the electromigration-induced Bi segregation at the anode side of the solder. Compared to the eutectic SnBi solder, the Bi segregation rate is faster in the Sn-57wt%Bi-1wt%Cu solder. The Bi segregation at the anode side may result in the strength reduction due to the brittleness of Bi and the more serious Joule heating due to the higher resistivity of Bi.

3:30 PM Break

3:50 PM

Thermomigration of Pb in Eutectic SnPb Flip Chip Solder Joints: *Fan-Yi Ou Yang*¹; *K. N. Tu*¹; ¹University of California, Los Angeles

Thermomigration is defined as mass flow driven by a temperature gradient. It is an irreversible process. A temperature difference of 1°C across a solder joint with 10 μm in height will produce a temperature gradient of 1000°C/cm, which cannot be ignored. When electromigration is combined with thermomigration in flip chip solder joints, fast failure due to large void formation at the cathode and the hot end occurs. Here, thermomigration in eutectic SnPb flip chip solder joints will be presented. Redistribution of Sn and Pb has been observed, with Pb being the dominant diffusing species and moving to the cold end. No linear concentration gradient in either Pb or Sn is observed, contrary to classical Soret effect. The lamellar structure becomes finer after thermomigration, indicating an increase in lamellar interfaces and in free energy. The molar heat of transport of Pb has been calculated to be 79 kJ/mole.

4:10 PM

Electromigration in Gold Bumps on Flexible Substrates under High Current and High-Electrical Field: *Chung Kuang Lin*¹; *S. W. Liang*¹; *Chih Chen*¹; ¹National Chiao Tung University

Au bumps has been the most important packaging technology for optoelectronic devices. The gold bumps exposes to high-electrical field under operation. In this study, the electromigration behavior was investigated under high bias voltage, which is 40V under 85% humidity at 85°. Because the spacing between the Au bumps has only 5-7μm, under the high electric field, Au may migrate on the surface of passivation. It is found that the gold bump may form lateral bulge under the bias of 40V. For the high current testing, we applied current of about dozens of mA on gold bumps. It is found that failure occurred at the Al leads on the ITO substrate under about 70mA testing conditions. The temperature increase due to Joule heating was measured by an infrared microscope, and it was found that serious Joule heating occurred in the Al leads due to poor heat dissipation of the ITO substrate.

4:30 PM

Electrical Resistivity and Interfacial Behavior of Bi-Ag/Cu High Temperature Solder Joints: *Jenn-Ming Song*¹; *Kar-Kit Lew*¹; *Hsin-Yi Chuang*¹; ¹National Dong Hwa University

Pb-3~5wt%Sn is now the conventional solder material for high temperature soldering applications. However, for the environmental concerns the development of Pb-free high temperature solders is urgent. Bi-Ag based solder is one of the proposed alloys to replace high Pb solders mainly due to their proper melting temperature. This present study investigated the interfacial reaction between Bi-11wt%Ag alloys and Cu substrate. The results demonstrate that grain boundary grooving and even penetration occurred at Bi-Ag/Cu interfaces. Cu-rich precipitates with a composition of Cu-40Bi-(3~6)Ag appeared within the joints. The dissolution of Cu substrate followed a linear relationship with the reaction time in the early stage and then the amount of dissolved Cu remained constant when the saturation of Cu was achieved. Another aim of this study was to evaluate the electrical performance of the Bi-Ag/Cu joints. For this purpose, the properties of Pb-5Sn/Cu joints were also examined for comparison.

4:50 PM

Effect of Soldering Reaction on the Electrical Properties of Bismuth Telluride/Cu Junctions: *Chien-Neng Liao*¹; *Wen-Jin Chen*¹; *Jing-Hua Li*¹; ¹National Tsing Hua University

To form thermoelectric refrigerators, thermoelectric elements, in general, are attached to Cu conductors by soldering technique. Contact resistance of thermoelectric heterojunctions is known to have strong impact on module performance, especially when the modules have short or thin-film type thermoelectric elements. In this study the effects of soldering reaction and subsequent thermal aging on electrical contact resistivity of bismuth telluride/Cu metallization are investigated. The preliminary results show that eutectic Pb-Sn solder joints appeared to have higher contact resistivity than Sn-Ag-Cu solder joints. The intermetallic compound (IMC) formed at the thermoelectric heterojunction during soldering reaction is identified to be SnTe compound with certain amount of Sb and Bi by electron probing analysis. The growth kinetics of the IMC during thermal aging will be investigated. The impact of Ni diffusion barrier in between thermoelectric elements and Cu metallization on the contact resistivity and the evolution of interfacial microstructure will also be explored.

5:10 PM

Thermomigration in Eutectic SnPb and SnAg Solder: *Hsiang-Yao Hsiao*¹; *Chih Chen*¹; ¹National Chiao Tung University

Due to serious joule heating in flip-chip solder joints during accelerated electromigration, the applied high current may cause a non-uniform temperature distribution in a flip chip solder joint, which may cause thermomigration in an electromigration experiment. Both SnPb and SnAg solder joints with 5-μm Cu UBM was adopted to study thermomigration. The thermomigration behavior in eutectic SnPb alloy was observed after stressed by 1.5 A at 70°C. We design the test structure of flip chip solder joints which will enable us to conduct thermomigration with and without electromigration. Furthermore, we used infrared microscope to measure the joule heating effect under the current stressing conditions. Thus, the thermal gradient and migration flux can be measured.

5:30 PM

Electrochemical Properties of the Sn-9Zn-1.5Ag-1Bi and Cu Substrate in 3.5wt % NaCl Solution: *Chih-Yao Liu*¹; *Moo-Chin Wang*²; *Min-Hsiung Hon*¹; ¹National Cheng Kung University; ²National Kaohsiung University of Applied Sciences

The electrochemical properties at interface between the Sn-9Zn-1.5Ag-1Bi on Cu substrate in 3.5wt % NaCl solution has been investigated. The Sn-9Zn-1.5Ag was also tested for comparison. The phase formation observed in two solders by an X-ray diffractometer (XRD), an scanning electron microscope (SEM), an energy dispersive spectrometer (EDS) and a transmission electron microscope (TEM). The corrosion products of SnCl₂, ZnCl₂, ZnO and SnO were observed in the Sn-9Zn-1.5Ag and Sn-9Zn-1.5Ag-1Bi solder alloy. The adhesion strength are decreased 7.84 ± 0.28 to 6.28 ± 0.21 MPa for Sn-9Zn-1.5Ag-1Bi after electrochemical test. The Sn-9Zn-1.5Ag-1Bi solder alloy were higher equilibrium potential and corrosion resistance than Sn-9Zn-1.5Ag solder alloy.

Plasticity from the Atomic Scale to Constitutive Laws: Dislocation Ensembles

Sponsored by: The Minerals, Metals and Materials Society, TMS Structural Materials Division, TMS/ASM: Computational Materials Science and Engineering Committee

Program Organizers: Christopher Woodward, US Air Force; Michael Mills, Ohio State University; Diana Farkas, Virginia Tech

Tuesday PM Room: Europe 9
February 27, 2007 Location: Dolphin Hotel

Session Chairs: Jeff Simmons, US Air Force; Vaclav Vitek, University of Pennsylvania

2:00 PM Invited

Dislocation Mean Free Paths Determined Using DD Simulations: *Benoit Devincere*¹; *Ladislav Kubin*¹; *Thierry Hoc*²; ¹CNRS; ²Ecole Centrale Paris

Within a multiscale materials modeling framework, effort has been devoted



to establishing a plasticity model that draws its physical bases at the scale of dislocation processes. The objective is to obtain ability to retrieve all the complexity of strain hardening fcc single crystals or polycrystals. The involved material parameters are statistical quantities that can be rigorously determined from a representative volume element deformed by DD simulations. Results are presented on the dislocation mean free paths (DMFP), which govern the evolution of dislocation densities in slip systems. It is shown that the DMFP depends on: the density of obstacles piercing slip planes, the probability for making a junction and the strength of interactions between slip systems. Values for the DMFP were determined for different tensile axis. The simulation results are discussed with respect to existing experimental data on single crystals and their implications for constitutive laws of plastic deformation is commented.

2:30 PM

Dynamical Scaling in a Simple 1-D Model of Dislocation Activity: Jack Deslippe¹; Raymond Tedstrom²; *Murray Daw*²; D. Chrzan¹; T. Neeraj³; M. Mills⁴; ¹University of California Berkeley; ²Clemson University; ³Exxon; ⁴Ohio State University

We examine a simple, 1-D model of dislocation activity, including a stress-activated source and mutually interacting dislocations. We demonstrate, through numerical and analytical steps, that the dislocations emitted from a 1-D stress-activated source evolve toward a distribution which is self-similar in time, and we derive the power-law forms and distribution function. We show that the asymptotic distribution is a step-function, and the dislocation front moves out linearly in time. The spacing between dislocations in the asymptotic distribution is uniform and increases logarithmically in time. The number of dislocations increases as $t/\ln(t)$, and the strain increases as $t^2/\ln(t)$.

2:50 PM Invited

Is It Worth Observing Dislocations in the Microscope?: *Patrick Veysiere*¹; ¹Centre National De La Research Science

This talk is comprised of three parts: (1) Some properties of dislocation contrast, useful for comparison with models and with simulation experiments, are restated. (2) Examples of TEM analyses of deformation microstructures are discussed in selected systems. The particular role played by dipolar configurations is emphasized. (3) Properties of dipoles are analyzed under isotropic and anisotropic elasticity in cubic systems. Several static properties are examined (e.g. the equilibrium angle and the dependence of this on dipole character and anisotropic elasticity). It is shown in addition that given a dipole height, the passing stress is a maximum in the screw orientation. Implications on dislocation interaction under constrained deformation conditions are examined.

3:20 PM

Scale-Dependent Chemical Mixing Forced by Plastic Deformation in Solids: *Pascal Bellon*¹; R. Averback¹; S. Odunuga¹; P. Krasnochtchekov¹; Jia Ye¹; ¹University of Illinois

We showed recently that the chemical mixing forced by sustained plastic deformation in solids cannot be described by a forced diffusion process at all length scales. In analogy with standard tools to study chemical mixing by convective and turbulent flows, we propose to analyze this forced mixing by studying the evolution of separation distances of pair of atoms, the so-called Richardson's pairs. Here, we derive and solve the evolution equation for a point source in a solid subjected to repeated shearing by dislocation glide. We demonstrate that the mixing is superdiffusive up to a cross-over length scale where it becomes diffusive. We validate these predictions by molecular dynamics and kinetic Monte Carlo simulations. We show that the cross-over from superdiffusive to diffusive mixing makes it possible to identify a characteristic length scale for the carriers of plastic deformation. We apply this technique to the determination of dislocation slip distances in nanomaterials and to the determination of shear transformation zones in amorphous alloys.

3:40 PM Break

4:00 PM Invited

Algorithmic Developments Enabling Strain Hardening Simulations in Dislocation Dynamics: *Tom Arsenlis*¹; ¹Lawrence Livermore National Laboratory

Dislocation dynamics simulations methods have the potential of directly connecting the physics of dislocations with evolution of strength and strain hardening in crystalline materials. The challenge in connecting the aggregate

behavior of dislocations to strain hardening with these simulations has been and remains one of computability. In this presentation, we focus on dislocation dynamics algorithm development in pursuit of extending the simulation technique to strains on the order of 10% in simulation volumes on the order of $10^3 \mu\text{m}^3$. Three computational strategies investigated to increase the computability of dislocation dynamics simulations: minimization of the computational expense of the simulation time step iteration, maximization of the simulation time step size, and improved strong scaling characteristics on parallel computing architectures. The discussion focuses on the algorithmic advances incorporated in the ParaDiS code project and strain hardening simulation results relevant for continuum crystal plasticity constitutive model development.

4:30 PM

In-Situ Neutron Diffraction Studies of Ductile Rare Earth B2 Intermetallics: *Scott Williams*¹; Don Brown²; Bjorn Clausen²; Alan Russell³; Karl Gschneidner³; ¹Iowa State University; ²Los Alamos National Laboratory; ³Ames Laboratory

The low room temperature ductility and fracture toughness of most intermetallic compounds severely limit their engineering use. Although special processing and testing methods can improve intermetallics' ductility, inherent ductility is the exception rather than the rule. Recent findings at Ames Laboratory suggest that a group of rare earth intermetallics of the B2 (CsCl-type) crystal structure possess significant ductility at and below room temperature. In this study, B2 rare earth intermetallics' plasticity was studied by in-situ neutron diffraction on SMARTS at LANSCE. Results showed no evidence of phase transformation or twinning. Unusual Bragg diffraction peak intensity changes during deformation suggest that mosaicity influences extinction, providing a novel method for evaluating deformation mechanisms. Intergranular strain behavior was compared with that of traditional BCC $\{110\}\langle 111 \rangle$ slip and with predictions from Elasto-Plastic Self Consistent (EPSC) modeling. The results indicate that deformation mechanisms other than $\{110\}\langle 111 \rangle$ slip account for the plastic behavior observed.

4:50 PM Invited

Deformation Mechanisms Based on Nanoscale Plastic Instabilities: *William Gerberich*¹; Megan Cordill¹; William Mook¹; ¹University of Minnesota

Insight into discretized dislocation behavior at the earliest stages of nanoindentation has led to a proposed approach for dealing with submicron plasticity mechanisms. With the reality of nanoindentation in situ in the transmission electron microscope and advanced atomic force microscopy, the rapid development of experimental data of immediate use to computational algorithms is at hand. Discretized "single dislocation" events in silicon and nickel single crystal volumes of less than 50 nm have now been detected. Additionally, multiple dislocation avalanches have been detected in nickel single crystals which lead to a thermally-activated mechanism approach not previously discussed. With regard to strain hardening, the impact of back stresses on activation energies and activation volumes at the 100 nm length scale and less are discussed.

5:20 PM

Dislocation Nucleation and Pileup from Surface Steps under Contact: *Yanfei Gao*¹; Honghui Yu²; ¹University of Tennessee; ²City College of New York

We present a micromechanical dislocation model of contact-induced deformation of a surface step or ledge. The Stroh formalism of anisotropic elasticity and conservation integrals are used to evaluate the driving force on the dislocation. The driving force together with a dislocation nucleation criterion is used to construct a contact-strength map of a surface step in terms of contact pressure, step height, surface adhesion and lattice resistance. Results show that dislocations in certain slip planes can be easily nucleated but will stay in equilibrium positions very close to the surface step, while dislocations in some other slip planes easily move away from the surface into the bulk. Different slip planes, if acting separately, give rise to different degrees of surface hardening. Amazingly, we find that the cooperation between different slip planes can make it order-of-magnitude easy to multiply and pileup dislocations, a phenomenon named latent softening.

Properties and Performance of High Temperature Alloys and Coatings: Coatings and Oxidation I

Sponsored by: The Minerals, Metals and Materials Society, TMS Structural Materials Division, TMS: High Temperature Alloys Committee, TMS/ASM: Corrosion and Environmental Effects Committee, TMS/ASM: Mechanical Behavior of Materials Committee

Program Organizers: Qiang Feng, Beijing University of Science and Technology; Timothy Gabb, NASA Glenn Research Center; Doug Konitzer, General Electric Aviation; Roger Reed, Imperial College London; Bruce Pint, Oak Ridge National Laboratory; Sammy Tin, Illinois Institute of Technology; Shiela Woodard, Pratt and Whitney

Tuesday PM Room: Asia 4
February 27, 2007 Location: Dolphin Hotel

Session Chairs: K. Jimmy Hsia, National Science Foundation; Doug Konitzer, GE Aviation

2:00 PM Invited

Advances in Turbine Coatings and Alloys - Turbine Design Benefits: *David Litton*¹; ¹Pratt and Whitney

Recent advances in coating and alloy materials and processing for turbine parts will be reviewed in the context of the advantages that they provide to turbine designers. The properties and interactions of thermal barrier coatings, bondcoats, and superalloys will be correlated to the life-limiting failure modes of turbine hardware in the various missions for which turbine engines are designed, and the environments in which they operate. The benefits to turbine hardware designs derived from advances in coatings processing technology will also be discussed. Benefits derived from advances in modeling will be reviewed briefly. Finally, trends in future turbine designs will be predicted with respect to the demands they will place on materials technology.

2:25 PM

Influence of Cobalt on the Interaction between a Fourth Generation Single Crystal Superalloy and Its Protective Coating: *Odile Lavigne*¹; *Pierre Caron*¹; *Catherine Ramusat*¹; ¹ONERA

In turbine blades with a thermal barrier coating, the interdiffusion zone between the single crystal (SC) nickel-base superalloy and its aluminide bond coat may include a secondary reaction zone (SRZ) extending over several hundred micrometers and reducing the effective load-bearing section. We have investigated the influence of a 10wt% cobalt addition in MC-NG fourth generation SC alloy, originally cobalt-free and likely to form SRZ, on both interdiffusion zone and bond coat microstructural evolutions. Cobalt addition reduces the SRZ amount in the as-coated material. Moreover, the growth rate of the SRZ during high temperature/long time exposures is significantly reduced. In the same time, the rate of transformation of the β -NiAl bond-coat into γ -Ni₃Al phase is decreased. Some hypotheses on the role of cobalt in the interdiffusion processes between the superalloy and the bond coat are suggested, based on local chemical analyses and microstructural observations.

2:45 PM

A Study of the Roles of Nickel and Aluminium in SRZ Formation: *Jestine Ang*¹; *Atsushi Sato*²; *Kyoko Kawagishi*³; *Toshiharu Kobayashi*³; *Hiroshi Harada*³; ¹University of British Columbia; ²Shibaura Institute of Technology; ³National Institute for Materials Science

We are developing overlay bond coats that do not induce secondary reaction zone (SRZ) formation in their underlying 5th generation nickel-base superalloy substrates, for application in hot section jet engine components. The main causes of SRZ formation are not clearly understood. Since nickel and aluminium form the basis of both nickel-base superalloys and overlay coatings, our first step is to investigate how the interdiffusion of nickel and aluminium at the bond coat/ substrate interface affects SRZ formation in multi-component systems. To accomplish this, alloys were cast with identical element activities as a representative 5th generation superalloy, with the exception of nickel and aluminium activities, which were suppressed and increased respectively, to different extents. An EQ coating was also cast to serve as a control specimen. The results from our diffusion couple and isothermal oxidation tests will be presented.

3:00 PM

Mechanical Properties of "EQ Coating" Coated Ni-Base Single Crystal Superalloys: *Akihiro Sato*¹; *Kyoko Kawagishi*²; *Yasuhiro Aoki*³; *Kazuhide Matsumoto*²; *Toshiharu Kobayashi*²; *Hiroshi Harada*²; *Mikiya Arai*³; ¹National Institute for Materials Science/Ishikawajima-Harima Heavy Industries Company, Ltd.; ²National Institute for Materials Science; ³Ishikawajima-Harima Heavy Industries Company, Ltd.

A new bond coat system, "EQ Coating", designed to be in thermodynamic equilibrium with the Ni-base superalloy substrate has been developed in National Institute for Materials Science, Japan. Previous studies indicated that minimal interdiffusion occurred between EQ coating based on γ/γ' tie-line composition and the substrate. EQ coating based on γ' composition showed promising oxidation resistance. In this study, EQ coating based on γ' composition was applied to a 4th generation superalloy, TMS-138 by spray process. Microstructure changes and mechanical properties at high temperatures were investigated. The results indicated that no Secondary Reaction Zone (SRZ) was observed beneath the coating after 300 hours at 1100°. The creep rupture life of 3mm width - 1mm thickness specimens at 1100°/137MPa condition was same as that of non-coated specimens; although the creep life of the conventional Pt-aluminide coated specimens was almost one-fifth of that of non-coated specimens.

3:20 PM Invited

Observations of the Microstructure and Mechanical Behavior of Two-Phase NiCoCrAlY Bond Coats: *Budhika Mendis*¹; *Chris Eberl*¹; *Kevin Hemker*¹; ¹Johns Hopkins University

Technological benefits of thermal barrier coatings (TBC) are derived from their ability to sustain high thermal gradients while maintaining structural integrity in extremely hostile environments. Final failure is generally associated with top coat spallation, but the overall performance of a TBC is closely related to the behavior of its bond coat. Here we address the microstructural stability and attendant mechanical properties of a commercial "two-phase" LPPS NiCoCrAlY bond coat. TEM micro-diffraction and energy-filtered imaging have uncovered the presence of very fine γ -Ni₃Al precipitates and the formation of additional phases with thermal cycling. Microsample tensile tests point to the existence of impressive room temperature strength and ductility and a significant loss of strength at elevated temperatures. Attempts to incorporate these observations into overall spallation models will be outlined. The support of The Air Force Office of Scientific Research under the MEANS-2 Program (Grant No. FA9550-05-1-0173) is gratefully acknowledged.

3:45 PM Invited

Microstructure and Property Analysis of Magnetron Sputter Deposited NiAlHf and NiAlPtHf Coatings for High Temperature Applications: *Patrick Coleman*¹; *Xiao Li*¹; *Bo Ning*¹; *Feng Huang*¹; *Mark Weaver*¹; ¹University of Alabama

In recent years, several Ni-Al-Hf and Ni-Al-Pt alloys have been promoted as promising bond coats in thermal barrier coatings systems. In this study, the microstructures and properties of Ni-Al-Hf and Ni-Al-Pt(Hf) coatings magnetron sputter deposited onto CMSX-4, aluminum oxide, and silicon substrates have been investigated in the as-deposited condition and following isothermal oxidation and annealing treatments at temperatures ranging from 1273 to 1423 K. The microstructural changes of the coatings after annealing and isothermal oxidation tests were examined by scanning electron microscopy (SEM), transmission electron microscopy (TEM), and X-ray diffraction (XRD) analysis. In both coating systems, post deposition annealing at 1273 K resulted in recrystallization, grain growth, and precipitation which altered their respective oxidation resistances. This talk will summarize our recent results on these two coating compositions.

4:10 PM Break

4:25 PM Invited

Surface Rumppling of Aluminide Coatings: Causes and Preventions: *Brian Gleason*¹; *Daniel Sordelet*²; ¹Iowa State University; ²Ames Laboratory

Nickel-rich β -NiAl and (Ni,Pt)Al coatings tend to progressively develop unwanted surface undulations ("rumppling") during repeated thermal cycling. Key factors affecting the occurrence and extent of β -coating rumppling are shown to be (i) thermal expansion mismatch between the coating and the underlying superalloy substrate and (ii) complete or partial transformation



of the β to martensite and/or γ' -Ni₃Al. In the case of $\beta \rightarrow \beta'$ martensite transformation, rumpling is found to be important only if the transformation temperature is sufficiently high to allow for deformation by creep. Factors affecting the transformation temperature will be assessed based on structural and physical property measurements, together with first-principles calculations. The prevention of rumpling is most directly assured by minimizing or even removing β as a coating constituent. Focusing on β removal, the merits and recent developments at ISU of Pt+Hf-modified $\gamma + \gamma'$ coatings are discussed.

4:50 PM

Synthesis and Oxidation Behavior of Platinum-Enriched $\gamma + \gamma'$ Bond Coatings on Ni-Based Superalloys: *Ying Zhang*¹; Justin Stacy¹; Lirong Liu¹; Bruce Pint²; Allen Haynes²; Ben Nagaraj²; Brian Hazel³; ¹Tennessee Technological University; ²Oak Ridge National Laboratory; ³General Electric Aircraft Engines

“Simple” Pt-enriched $\gamma + \gamma'$ coatings were synthesized on René 142 and single-crystal N5 Ni-based superalloys by electroplating a thin layer of Pt followed by a diffusion treatment in vacuum at 1150-1175°C. For the superalloys containing 13-14 at.% Al, the typical Al content in the “simple” $\gamma + \gamma'$ coating was in the range of 16-19 at.%. In general, the alumina scale adherence to these $\gamma + \gamma'$ coatings was not as uniform as to β -(Ni,Pt)Al coatings on the same superalloy substrate. Modified $\gamma + \gamma'$ coatings with ~22 at.% Al have been developed by introducing a secondary short-term aluminization step via pack cementation. The cyclic oxidation behavior of the modified $\gamma + \gamma'$ coatings is being investigated at 1100-1150°C to determine if a higher Al content will improve the oxidation behavior.

5:10 PM

Microstructural Changes of Bond-Coated Ni-Base Superalloys Caused by Coating Process and Subsequent Heat Cycles: *Hideyuki Murakami*¹; Akihiro Yamaguchi¹; Yingna Wu¹; Seiji Kuroda¹; ¹National Institute for Materials Science

Recent demand in increasing the efficiency of gas turbines has led the component materials, i.e. coated Ni-base superalloys, to be exposed at much higher operating temperatures. Therefore there is a great demand for improving the protective performance of bond coat materials. When performing bond-coating, however, some microstructural changes of coatings and substrates caused by the bond coating process and subsequent heat treatment can cause deterioration of thermomechanical properties of the coated materials. This study introduces some microstructural changes of substrates caused by LPPS and aluminizing procedures. The effect of heat treatment on microstructural changes of coatings and substrates are also discussed.

5:30 PM

The Effect of Hf Content on the Phase Content, Oxidation Behavior and Phase Transformation-Induced Deformation of Two Phase Ni-Al and Ni-Pt-Al Alloys: *Bruce Pint*¹; Scott Speakman¹; Ian Wright¹; Lirong Liu²; Ying Zhang²; ¹Oak Ridge National Laboratory; ²Tennessee Technological University

Increasing the Hf content in cast, two phase Ni-(30-35at.%)Al and Ni-Pt-Al alloys from 0.05at% to 0.4% was found to significantly effect the influence of thermal cycling on oxidation behavior at 1000-1200°C. Using in-situ high temperature x-ray diffraction, the Hf content affected the $\gamma + \beta \leftrightarrow \beta$ transformation observed near 1150°C. After oxidation, alloys with low Hf-content showed β phase depletion near the alloy surface while high Hf-content alloys showed primarily β phase near the surface along with Hf internal oxidation. High Hf content alloys also showed less macroscopic deformation after 1h cycles at 1100-1150°C.

5:50 PM

Prediction of Microstructure Evolution between Ir Coatings and Ni-Al Alloy Substrates Using a Phase-Field Model: *Machiko Ode*¹; Taichi Abe¹; Hideyuki Murakami¹; Hidehiro Onodera¹; ¹National Institute for Materials Science

Ir has some attractive characteristics for oxidation resistant coating materials. For instance, Ir has the highest melting temperature among PGMs, excellent chemical stability and low oxygen diffusivity. However, when the coated materials are exposed at elevated temperature, microstructural changes are inevitable due to the accelerated interdiffusion of alloying elements between the coatings and substrates. In the present study, microstructure

evolution is numerically predicted using a phase-field model. Ir/Al-Ni alloy systems are adopted as coating/substrate materials, respectively. The effects of temperature, diffusion coefficient and coating thickness on the growth rate of the secondary reaction layer and the precipitation site are studied. The growth rate increases proportional to the coating layer thickness and the position of the secondary reaction layer shifts depending on both diffusion coefficients and temperatures.

Recycling and Waste Processing: Precious Metals Recovery

Sponsored by: The Minerals, Metals and Materials Society, TMS Extraction and Processing Division, TMS Light Metals Division, TMS: Recycling and Environmental Technologies Committee

Program Organizers: Mark Schlesinger, University of Missouri; Robert Stephens, Teckcominco, Inc.; Donald Stewart, Alcoa Technology; Ray Peterson, Aleris International; Jan van Linden, Recycling Technology Services, Inc.; Subodh Das, SECAT; Abdel Serna-Vasquez, Aleris International; Cynthia Belt, Aleris International Inc; John Pickens, Alumitech/Aleris International; John Hryn, Praxair; Richard Kunter, Richard S. Kunter and Associates; Andreas Siegmund, Quemetco Metals Inc.; Masao Suzuki, AI Tech Associates

Tuesday PM Room: Australia 2
February 27, 2007 Location: Dolphin Hotel

Session Chairs: Richard Kunter, Richard S. Kunter and Associates; John Krstulich, CAMP

2:30 PM

Recovery of Precious Metals by Using Chemically Modified Waste Paper: *Katsutoshi Inoue*¹; *Hidetaka Kawakita*¹; ¹Saga University

New adsorption gels were prepared by chemically immobilizing functional groups of primary amine or ethylenediamine on crushed waste paper. Adsorption behaviors of these chemically modified waste paper gels were investigated for various metal ions from water at varying pH and from varying concentration of hydrochloric acid solution. Both gels exhibited very high selectivity to precious metals, gold, palladium and platinum, over base metals in the adsorption from hydrochloric acid solution; the selectivity was higher than commercially available anion exchange resins. The maximum adsorption capacities of these gels for palladium and platinum were found to be found greater than 1 mol/kg-dry gel.

3:00 PM

Kinetics and Mechanism of the Reaction between Pt(IV) Complex Ions and Sodium Tiosulfate in Aqueous Solution: *Krzysztof Paclawski*¹; *Krzysztof Fitzer*¹; ¹AGH University of Science and Technology

One of the way of separation of the noble metals, such as Au and Pt, existing in the aqueous solutions containing HCl in the form of different complexes, is the application of the selective reduction of the Pt(IV) complex ions in the presence of Au(III) complexes. The reductant which can work selectively in such a system can be sodium tiosulfate. In this work, the kinetic studies of the redox reaction between Pt(IV) chloride complexes and sodium tiosulfate were carried out. The influence of many different factors for the rate of reaction, e.g. pH, temperature, reductant itself, and Pt(IV) ions concentration, were tested. From the obtained experimental data, values of the rate constants, activation parameters (energy, enthalpy and entropy of activation) as well as the rate law of the reaction were determined. Also, the mechanism of this reaction was suggested.

3:30 PM

Recovery of Gold by Using Biomass Wastes Containing Polyphenol Compounds: *Katsutoshi Inoue*¹; *Hidetaka Kawakita*¹; ¹Saga University

New recovery method of gold from chloride media was developed by using adsorption gels prepared from biomass wastes containing polyphenol compounds: waste persimmon peel and lignophenol which is prepared from wood wastes by immobilizing phenol groups on wood lignin by a simple method. Gold can be recovered as elemental gold from hydrochloric acid over a wide concentration region while other precious metals such as platinum and

palladium as well as base metals are not practically adsorbed. The maximum adsorption capacities of gold on persimmon peel gel and lignophenol gel were as high as 4.5 and 1.9 mol/kg-dry gel, respectively.

4:00 PM Break

4:15 PM

Dissolution Rates of Pt-Zn Intermetallic Compounds in Acid: *Hideaki Sasaki*¹; Masao Miyake¹; Hisao Kimura¹; Masafumi Maeda¹; ¹University of Tokyo

The dissolution behaviors of Pt-Zn intermetallic compounds in acid were examined to develop an efficient process for recovery of Pt from scraps. Pure Pt sheets were reacted with Zn vapor in a sealed reactor with a temperature gradient, and Pt-Zn intermetallic compounds were synthesized. The anodic dissolution rate of the Pt-Zn compound in acid was measured by channel flow double electrode technique using the compound as a working electrode. This technique made it possible to measure the dissolution rate of Pt from the Pt-Zn compound separately from the total dissolution rate of the compound, and revealed that the apparent dissolution rate of Pt was about 100 times higher from the Pt-Zn compound than from pure Pt.

Shape Casting: The 2nd International Symposium: Structure/Property

Sponsored by: The Minerals, Metals and Materials Society, TMS Light Metals Division, TMS: Aluminum Committee, TMS: Solidification Committee

Program Organizers: Paul Crepeau, General Motors Corporation; Murat Tiryakioglu, Robert Morris Univ; John Campbell, University of Birmingham

Tuesday PM

Room: Northern E2

February 27, 2007

Location: Dolphin Hotel

Session Chair: Glenn Byczynski, Nemak Canadian Operations

2:00 PM Introductory Comments

2:10 PM

Stresses in the Eutectic Si Particles of Sr-Modified A356 Castings Loaded in Tension: *John Griffiths*¹; Edward Oliver²; Michael Fitzpatrick³; Trevor Finlayson⁴; David Viano¹; Qigui Wang⁵; ¹CSIRO; ²CCLRC Rutherford Appleton Laboratory; ³The Open University; ⁴Monash University; ⁵General Motors Powertrain Engineering

During tensile tests of A356 castings, the eutectic Si particles cleave, the number of broken particles increasing with strain until complete fracture of the alloy. Controversy exists about (a) how the particles fracture and (b) how they contribute to the yield stress and work-hardening rate. These controversies centre on the particle stresses. Surprisingly, there have only been two direct measurements of these stresses and both were limited to applied strains of ~1%. Discussion about how the particles affect the plastic flow and fracture properties is, therefore, speculative. We report the results of in situ neutron diffraction measurements of the strains in the Si particles during tension and compression testing. A range of dendrite arm spacings was tested to investigate the well-known effect of this variable on ductility and a range of heat-treatments was used to investigate effects of the strength of the Al dendrites.

2:35 PM

The Effect of Si Content on the Size and Morphology of Fe-Rich and Cu-Rich Intermetallics in Al-Si-Cu-Mg Alloys: *Carlos Caceres*¹; Birgir Johannesson²; John Taylor¹; Adrian Canales³; Marcos Cardoso³; Jose Talamantes³; ¹University of Queensland; ²Icelandic Technological Institute; ³Corporativo Nemak

Recent studies have shown that the β -Al₅FeSi and θ -Al₂Cu phase intermetallic particles are refined and dispersed in the presence of high silicon, hence improving the ductility of Al-Si-Cu-Mg alloys. In alloys with low Si content, the Fe- and Cu-rich particles form long and closely intertwined clusters which lead to low ductility. At high Si contents, the intermetallic phases appear more dispersed and the clusters of particles are small and isolated from

each other, hence the increased ductility. In this work experiments involving ternary Al-Si-0.8Fe alloys are presented, which suggest that Si alone is not responsible for the refining of the Fe-rich and Cu-rich intermetallics in the earlier alloy. This indicates that a synergistic interaction with other elements, possibly Sr and Mn, may be necessary for the refining of the intermetallics to occur. Possible alternative mechanisms are discussed.

3:00 PM

On the Use of General Extreme Value (GEV) Distribution in Fracture of Al-Si Alloys: *Murat Tiryakioglu*¹; ¹Robert Morris University

The use of the General Extreme Value distribution in the fracture of Al-Si alloys was demonstrated. Analysis of data from the literature showed that the size and aspect ratio of damaged Si particles in Al-Si alloys follow the Gumbel distribution. Thirteen of the fourteen datasets from the literature for size of defects on fracture surfaces of cast Al-Si alloys were also found to follow the Gumbel distribution. The use of the correct statistical distribution should improve the accuracy of fracture-mechanics based models to predict fatigue life of cast Al alloys.

3:25 PM

Effect of Processing on the Structure and Properties of Squeeze Cast Al-7Si-0.3Mg Alloy: *Kumar Sadayappan*¹; Fragner Werner²; ¹CANMET - Materials Technology Laboratory; ²ARC - LKR

Squeeze casting of Al-Si alloy was carried out using an UBE 350 HVSC machine. Effects of process variables such as melt modification, casting temperature and pressure on the mechanical properties were evaluated using a step plate casting. The operating temperatures of the melt and tools were found to have significant influence on properties of the casting than the squeeze pressure. The segregation of the eutectic liquid which can be effectively controlled by process temperatures is one of the reasons cited for the scatter in properties. The results from the investigation are presented and discussed.

3:50 PM Break

4:10 PM

Effect of Various HIP Conditions on Bilayers and Mechanical Properties in Aluminum Castings: *James Staley*¹; M. Tiryakioglu¹; John Campbell²; ¹Robert Morris University; ²University of Birmingham

Manufacturers of near net shape aluminum castings use hot isostatic pressing (HIP) to improve their castings' mechanical properties. HIP can close porosity and improve mechanical properties but typical HIP parameters for aluminum castings may not be able to heal bifilms. Bilayers are essentially pre-oxidised cracks in the casting, which lower and increase scatter of mechanical properties. Therefore, typically HIPed aluminum castings with bifilms are not as reliable as wrought parts partly due to HIP's inability so far to completely mitigate the effects of bifilms. This research investigates the effects of various HIP conditions on bilayers and mechanical properties of aluminum castings affected by bifilms. Castings were non-HIPed or HIPed at typical, solution heat treat or eutectic melting temperatures and tensile and fatigue tested. Weibull statistics are used to quantify the castings' reliability and microscopy and fractography are used to investigate healing of bifilms and to correlate microstructure to test results.

4:35 PM

The Influence of Oxide Inclusions on the Post-HIP Fatigue Properties of Two Al-Si-Mg Castings: *Stephen Mashl*¹; ¹Bodycote IMT Inc

Advances in hot isostatic pressing (HIP) process techniques and equipment have reduced processing costs, especially for aluminum castings. This decrease in cost has resulted in a broadening of the HIP market and, correspondingly, an increase the types and quality of castings which go through HIP. Trials evaluating the effect of HIP on separate groups of aluminum castings can produce mixed results. Improvement in post-HIP fatigue resistance can be large, small, or non-existent. Investigation revealed that non-metallic inclusions, particularly oxides, have a significant effect on the HIP response of an aluminum casting. This study reviews existing theory on the relative influence of porosity and inclusions on fatigue life and, using experimental data from a program aimed at integrating HIP and heat treat into a single process, shows how variations in oxide concentration can decrease or eliminate the improvement in fatigue life normally associated with hot isostatic pressing.



5:00 PM

Structure, Properties, Processing Relations in Cast, Solutionized, and Aged Al-Si-Cu-Mg Alloys: Yong Ma¹; Jian Fang¹; Harold Brody¹; ¹University of Connecticut

Parallel approaches are being followed to develop quantitative knowledge, criteria, and data for the interrelations among casting and heat treatment process parameters, microstructure, and tensile properties for multicomponent, multiphase aluminum alloys. In one measured tensile properties for alloys with a variety of cast microstructures and thermal treatments are fit to simple relations and a limited set of process and microstructure parameters to find a strong, statistically significant correlation. Then another set of castings with a similar processing conditions are made, the properties measured, and the validity of the empirical process design relation tested. The second approach is to use optical and electron microscopy and calorimetry to understand the influence of process parameters on microstructure and, in turn, on properties. Thermal and physical models of alloy behavior are tested against measured microstructures and properties, iteratively, to build the desired knowledge and data bases for phenomenologically-based process design modules.

5:25 PM

Development of Novel Al-Si-Mg Alloys with 8 to 17 wt% Si and 2 to 3.5 wt% Mg: Xiaochun Zeng¹; Sumanth Shankar¹; Makhlof Makhlof²; ¹Light Metal Castings Research Centre, McMaster University; ²Advanced Casting Research Center - Metal Processing Institute, Worcester Polytechnic Institute

Based on our recent understanding of the evolution of eutectic phases in Al-Si hypoeutectic alloys a new family of alloys are being developed to obtain superior properties of the cast component. The alloy will contain 8 wt% to 17 wt% Si coupled with 2 wt% to 3.5 wt% Mg. These alloys were developed based on our understanding of the effect of various iron containing phases on the nucleation of the eutectic phases in Al-Si hypoeutectic alloys. High levels of Mg was added for two reasons, firstly to prevent the formation of β (Al,Fe,Si) intermetallic phase and promote the formation of p (Al,Fe,Si,Mg) phase during solidification, and secondly to alter the rheological properties of the alloy leading to better fluidity and mould filling characteristics of these alloys. In this paper, the mechanical properties and casting behavior of few of the compositions in the above-mentioned compositional ranges will be presented.

Structural Materials Division Symposium: Mechanical Behavior of Nanostructured Materials, in Honor of Carl Koch: Stability, Strain and Stress

Sponsored by: The Minerals, Metals and Materials Society, TMS Electronic, Magnetic, and Photonic Materials Division, TMS Materials Processing and Manufacturing Division, TMS Structural Materials Division, TMS: Chemistry and Physics of Materials Committee, TMS/ASM: Mechanical Behavior of Materials Committee, TMS: Nanomechanical Materials Behavior Committee

Program Organizers: Xinghang Zhang, Texas A&M University; Yuntian Zhu, Los Alamos National Laboratory; Michael Rigsbee, North Carolina State University; C. Suryanarayana, University of Central Florida; Haiyan Wang, Texas A&M University; C. T. Liu, Oak Ridge National Laboratory

Tuesday PM Room: Asia 5
February 27, 2007 Location: Dolphin Hotel

Session Chairs: C. Liu, Oak Ridge National Laboratory; Kevin Hemker, Johns Hopkins University

2:00 PM Invited

On the Thermal Stability of Nanostructured Materials: Stabilizing Defects by Solute Segregation: Reiner Kirchheim¹; ¹Institut fuer Materialphysik

The interaction of solute atoms with defects like vacancies, dislocations and grain boundaries is treated in a generalized concept based on the work of W. Gibbs and C. Wagner related to surface adsorption. It can be shown that the formation energy of defects is reduced by solute segregation with a concomitant increase of defect density. The effect is the larger the larger

the chemical potential of the solute is. This could be especially the case in nanostructured alloys produced far away from equilibrium, i.e. by mechanical milling or various deposition techniques. The general concept is used to interpret a variety of experimental results.

2:20 PM

Effect of Annealing and Deformation on the Mechanical Behavior of Nanostructured Metals: Xiaoxu Huang¹; Naoya Kamikawa¹; Niels Hansen¹; ¹Riso National Laboratory

Nanostructured metals produced by plastic deformation to large strain are different from the conventional polycrystal by the presence of relatively high concentration of low angle dislocation boundaries and interior dislocations in the structure. Recovery annealing is therefore expected to modify the structure and the mechanical behavior. An unusual phenomenon, namely annealing induced increase in strength and decrease in ductility, has been observed in nanostructured metals. It has been proposed (e.g. X. Huang et al.312 (2006) 249) that slight deformation instead of annealing can be used to optimize the mechanical properties. In this paper, we present our recent investigations on the effect of annealing and deformation on the mechanical behavior of nanostructured metals, which prove our proposal and lead to a discussion on the strengthening mechanisms of nanostructured metals.

2:35 PM

Thermal Stability of Sputter-Deposited Cu Foils with Nanoscale Growth Twins: O. Anderoglu¹; A. Misra²; H. Wang¹; R. Hoagland²; Xinghang Zhang¹; ¹Texas A&M University; ²Los Alamos National Laboratory

Recently, we have reported on the synthesis of sputter-deposited bulk Cu foils with a high density of growth twins of around 5 nm spacing within the columnar grains of 40-80 nm in diameter.¹ These nanotwinned Cu foils exhibited high tensile strengths of around 1.2 GPa. Here we will report on the thermal stability of nanotwinned structures in Cu. Vacuum annealing at temperatures up to 600°C for one hour resulted in no significant change in the twin density, whereas the average columnar grain size increased to a few hundred nanometers. The coarsening of the nanotwinned versus high-angle grain boundary nanostructures will be discussed in terms of their respective boundary energies. The effect of annealing on the hardness and electrical resistivity of nanotwinned Cu foils will also be discussed. ¹Zhang, X; Wang, H; Chen, XH; Lu, L; Lu, K; Hoagland, RG; Misra, A; Appl. Phys. Lett., 88 (2006) 173116.

2:50 PM Invited

Observations of Room Temperature Stress-Assisted Grain Growth in Nanocrystalline Al Thin Films: Daniel Gianola¹; Kevin Hemker¹; ¹Johns Hopkins University

Recent studies have emphasized the importance of microstructural evolution during the deformation of fully dense nanocrystalline materials. In the current study, submicron free-standing aluminum thin films were fabricated using DC magnetron sputtering and surface and bulk micromachining techniques that alleviated the challenges usually associated with the mechanical testing of submicron free-standing thin films. Results obtained from these films demonstrate unique mechanical behavior, where discontinuous grain growth results in a fundamental change in the way in which the material deforms. In situ X-ray diffraction and post mortem transmission electron microscopy point to the importance of stress-assisted room temperature grain growth in transforming the underlying processes that govern the mechanical response of the films; nanoscale deformation mechanisms give way to microscale plasticity. The efficacy of impurity pinning of grain boundaries and the effect of applied strain rate on the kinetics of grain growth are also being investigated and will be discussed.

3:10 PM

Atomic Mechanism of Stress-Assisted Grain Coarsening during Indentation of a Nanostructured Metal: Frederic Sansoz¹; Virginie Dupont¹; ¹University of Vermont

Recent experimental studies have reported an abnormal grain coarsening phenomenon in nanocrystalline metals under high applied stress. More specifically, during micro-indentation, this coarsening effect was found to occur faster at cryogenic temperatures. The underlying mechanism governing this behavior remained an open question. We investigate the atomic mechanism at play during indentation-induced grain growth by molecular simulations.

The cylindrical indentation of nanocrystalline columnar Al films is modeled with different average grain sizes (5-10 nm). We show that stress-driven grain growth can be obtained in the athermal limit during nanocrystalline aluminum indentation. We find that the grain growth results from rotation of nanograins and propagation of shear bands. Together, these mechanisms are shown to lead to the unstable migration of the grain boundaries via process of coupled motion. The calculation of the atomic-level shear stress acting on the interfaces during the shear band propagation is also used to explain the coarsening behavior.

3:25 PM

Stress-Induced Grain Growth in a Bulk Nanocrystalline Ni-Fe Alloy: A High-Energy X-Ray Diffraction Study: *Guojiang Fan*¹; L. F. Fu²; Y. D. Wang³; G. Y. Wang¹; H. Choo⁴; P. K. Liaw¹; Y. Ren⁴; N. D. Browning⁵; ¹University of Tennessee; ²University of California; ³Northeastern University; ⁴Argonne National Laboratory; ⁵Lawrence Berkeley National Laboratory

A high-energy x-ray diffraction (HEXRD) technique has been employed to investigate plastic deformation of a bulk nanocrystalline (nc) Ni-Fe alloy under the uniaxial compression and tension, respectively. The evolution of the crystallite domain sizes, microstrains, and the texture components has been monitored quantitatively by using HEXRD. The results indicate that both uniaxial compression and tension lead to a grain growth in the bulk nc Ni-Fe alloy. During the compressive tests, the nc grains grow preferentially along a certain direction. During the tensile tests, grain growth was observed in the uniformly deforming region, and a substantial grain growth occurs in the area very close to the fracture surface. The stress-induced grain growth was accompanied by a texture development in the deformed specimen. The present study will show that HEXRD is a powerful tool to investigate the deformation mechanisms in bulk nc metals and alloys.

3:40 PM Break

3:50 PM Invited

Atomistically-Informed Mesoscale Simulation of Coupled Grain Growth and Grain-Boundary Diffusion Creep in Nanocrystalline Materials: *Dieter Wolf*¹; ¹Idaho National Laboratory

Molecular-dynamics simulations have been used to elucidate the intricate, highly non-linear coupling between grain-boundary diffusion creep and grain growth in nanocrystalline metals. We demonstrate how the materials-physics based insights into the underlying deformation and grain-growth mechanisms extracted from these simulations can be incorporated into a mesoscopic simulation model, thus overcoming the length and time-scale limitations inherent to the MD approach. The objects evolving in space and time in the mesoscale simulations are the discretized grain boundaries and grain junctions rather than the atoms themselves, involving characteristic length and time scales governed by grain-boundary processes and parameters rather than atom vibrations. This then enables analysis of the intricate interplay between grain growth and grain-boundary diffusion creep for a system containing a large number of grains with arbitrary sizes.

4:10 PM

The Use of X-Ray Diffraction to Determine Slip and Twinning Activity in Commercial-Purity (CP) Titanium: *Tamas Ungar*¹; Krisztián Nyilas¹; Michael Glavicic²; Levente Balogh¹; Ayman Salem²; S. Semiatin²; ¹Eotvos University; ²Air Force Research Laboratory

High resolution laboratory and special synchrotron X-ray diffraction techniques were used to characterize slip and twinning activity in extruded billets of commercial-purity (CP) titanium. The subgrain size was of the order of a few-hundred nanometers. The laboratory diffraction experiments evaluated the fractions of $\langle a \rangle$, $\langle c \rangle$, and $\langle c+a \rangle$ type dislocations, the average dislocation density (ρ), subgrain size, and the size distribution without twinning. X-ray line profile analysis was used to evaluate stacking faults and twinning assuming $\{10\bar{1}\}$, $\{11\bar{2}\}$, and $\{102\}$ habit planes. Novel synchrotron x-ray diffraction experiments (ESRF synchrotron in Grenoble, France) also enabled the characterization of deformation behavior in individual grains in the polycrystalline CP-Ti, and hence resulted in an accurate description of slip activity.

4:25 PM Invited

Tailoring and Patterning the Grain Size of Nanocrystalline Alloys: *Christopher Schuh*¹; Andrew Detor¹; Jason Trelewicz¹; ¹Massachusetts Institute of Technology

Nanocrystalline alloys that exhibit grain boundary segregation can access thermodynamically stable states with the average grain size dictated by the alloying addition. Here the Ni-W system is discussed, in which the W content controls grain size over a very broad range: ~2-140 nm. Based upon this observation, we introduce a new synthesis technique allowing for precise composition control during the electrodeposition of Ni-W alloys which, in turn, leads to precise control of nanocrystalline grain size. This technique offers new possibilities for understanding the structure-property relationships of nanocrystalline solids, such as the breakdown of Hall-Petch strength scaling, and also opens the door to a new class of customizable materials incorporating patterned nanostructures. Efforts in modeling nanostructure stabilization for weakly segregating systems are also discussed.

4:45 PM

Stored Energy and Recrystallization Temperature of High Purity Copper after Equal Channel Angular Pressing: *Jingtao Wang*¹; Yue Zhang¹; Chang Cheng¹; ¹Nanjing University of Science and Technology

Equal channel angular pressing (ECAP) at room temperature was conducted at room temperature to impose high strain into high purity copper. Differential Scanning Calorimetry (DSC) was used to estimate the stored energy from ECAP and recrystallization temperature. It was found that the stored energy increases upon ECAP processing until a peak is reached at 12 passes of ECAP, and a slight decrease in stored energy was observed at higher ECAP passes. The recrystallization temperature decreases upon the increase of the stored energy up to ~50 J/mol, and reaches a stable value of ~210°C. Partial annealing of an ECAP processed (8 passes) sample by heating to ~185°C at a heating rate of 20°C/min released the stored energy from ~55J/mol to ~18J/mol, without substantial change on the recrystallization temperature of the sample. Microstructure and Mechanical properties evolution of copper samples upon ECAP passes was also investigated.

5:00 PM

A Novel In-Situ Composite Structure in TiAl Alloys: *Fritz Appel*¹; Michael Oehring¹; Jonathan Paul¹; ¹GKSS Research Centre Geesthach

Phase decomposition and ordering reactions in beta/B2-phase containing TiAl alloys were utilized to establish a novel, previously unreported, type of in-situ composite. The characteristic constituents of this composite are laths with a modulated substructure that are comprised of several stable and metastable phases. The modulation occurs at the nanometer-scale and thus leads to a significant refinement of the material. Microstructural control can be achieved by conventional thermo-mechanical processing and results in a structurally and chemically very homogeneous material with excellent mechanical properties. The physical metallurgy of this novel type of alloy has been assessed by high resolution transmission electron microscopy and mechanical testing. Particular emphasis is paid on transformation induced toughening mechanisms that operate at low temperature and the structural stability of the composite under creep conditions.

5:15 PM

Characteristics of Nanostructured Ni3Al during Annealing: *Jiangwei Ren*¹; Aidang Shan¹; Junbao Zhang²; Junliang Liu²; Hongwei Song²; ¹School of Materials Science and Engineering, Shanghai Jiao Tong University; ²Baosteel Iron and Steel Company, Ltd.

Intermetallic compounds are very attractive to material researchers for their special dislocation structure. Nanostructure is unique in structural characteristics. Accordingly, it is interesting to explore the structural characteristics of nanostructured intermetallics. In this research, surface mechanical attrition treatment (SMAT) has been employed to produce nanostructured surface in intermetallic Ni₃Al. Through the severe plastic deformation, the grain of intermetallic was refined from several hundred micrometers to about ten nanometers. And the original ordered crystal structure changed to disorder. Annealing behavior of Ni₃Al nanocrystalline was studied. Annealing was performed at 300-700°C. The microstructure change and ordering behavior of nanostructure of Ni₃Al was examined by scanning electronic microscope (SEM), X-ray diffraction (XRD) and transmission electronic microscope (TEM). The results showed that nanostructured Ni₃Al undergoes disorder to



order transformation during annealing and the grain size keeps to be stable up to a certain temperature and grow quickly after that.

5:30 PM

Texture Evolution and Deformation Mechanisms in the Largely Deformed Bulk Nano-Metals: Yanling Yang¹; Yandong Wang¹; Hahn Choo²; Nan Jia¹; Yandong Liu²; Liang Zuo¹; Peter Liaw²; ¹Northeastern University; ²University of Tennessee

Evolution of crystallographic textures after deformation is closely related to the mechanisms of deformation in polycrystalline materials. Of those various mechanisms to control the plastic deformation in bulk nano-metals (BNMs), the diffusion-assisted grain boundary sliding and/or diffusion-assisted grain rotation are the common ones, instead of the dislocation-motion-mediated grain rotation in the coarse-grained materials. However, it is an open question whether the deformation mechanism will change during large plastic deformation (over 20% strain) in the BNMs. In this presentation, we will talk about the investigation on the evolution of texture in a largely-deformed nc Ni material fabricated by a pulsed-electrodeposition technique with initial grain size of around 20 nm. The homogeneous deformation was achieved by cross-rolling at room temperature. The comparisons among the texture evolution of the nc-grained samples and its coarse-grained counterparts, in combination of the dislocation-slipping-based plastic deformation simulations, give the quantitative mechanisms of deformation in the bulk materials.

5:45 PM

Interface Diffusion Phenomena in Advanced Nanostructured Materials: Yury Kolobov¹; Maxim Ivanov¹; Konstantin Ivanov¹; ¹Belgorod State University

The particular features of the effect of grain boundary sliding activation by directed diffusion fluxes of atoms along grain boundaries are discussed. The interaction and interference of diffusion processes - grain boundary sliding and migration - as the factors determining the development of plastic deformation at conditions considered are analyzed. It is shown that the unique properties of bulk nanostructured metals and alloys obtained by severe plastic deformation are the result of two factors: ultrafine size of the grains and nonequilibrium state of their boundaries. The determining role of diffusion-controlled processes on grain boundaries in grain boundary sliding development during creep and superplastic flow of nanostructured metals and alloys is proved. The regularities of low temperature or/and high-strain rate superplasticity manifestation in the materials indicated were investigated.

Structural Materials Division Symposium: Mechanical Behavior of Nanostructured Materials, in Honor of Carl Koch: Poster Session - Mechanical Properties of Nanostructured Materials

Sponsored by: The Minerals, Metals and Materials Society, TMS Electronic, Magnetic, and Photonic Materials Division, TMS Materials Processing and Manufacturing Division, TMS Structural Materials Division, TMS: Chemistry and Physics of Materials Committee, TMS/ASM: Mechanical Behavior of Materials Committee, TMS: Nanomechanical Materials Behavior Committee

Program Organizers: Xinghang Zhang, Texas A&M University; Yuntian Zhu, Los Alamos National Laboratory; Michael Rigsbee, North Carolina State University; C. Suryanarayana, University of Central Florida; Haiyan Wang, Texas A&M University; C. T. Liu, Oak Ridge National Laboratory

Tuesday, 6:05 PM Room: Asia 5
February 27, 2007 Location: Dolphin Hotel

Session Chairs: Yuntian Zhu, Los Alamos National Laboratory; Deliang Zhang, University of Waikato

Annealing Calorimetry as a Tool for Defect Analysis in Nanometals: Daria Setman¹; Elena Korznikova²; Erhard Schaffer¹; Michael Zehetbauer¹; ¹University of Vienna; ²Ufa State Aviation Technical University, and Institute of Metals Superplasticity Problems, Russian Academy of Sciences

Recently methods of annealing calorimetry have been successfully applied in determining the type and density of lattice defects in nanomaterials especially

those produced by Severe Plastic Deformation (SPD), and in measuring the temperature shifts of phase transitions which often occur in connection with nanocrystallisation and/or SPD. The identification of lattice defects requires to measure stored energies $E(\text{stor})$ being typically a factor 10 smaller than phase transition energies, at a resolution of the order $dE(\text{stor}) = 0.05 \text{ J/g}$, and a resolution in activation energy determination of smaller than $dQ = 0.1 \text{ eV}$. Both conditions are met by modern power compensating differential scanning calorimeters provided careful investigations of base lines are performed. The paper reports on density measurements of SPD induced monovacancies, vacancy agglomerates and dislocations in several nanometals and alloys with different lattice types, and on determinations of activation enthalpies which allow for conclusions on the migration mechanisms of these defects.

Asymmetric Cross Rolling: A Potential Severe Plastic Deformation of Processing Ultrafine-Grained Materials: Bin Chen¹; ¹SJTU

The shear strain and its directions were thought to play an important role in processing ultrafine grain size during severe plastic deformation (SPD). Asymmetric rolling, however, has a shear deformation zone in the middle section of deformation zone. Accordingly, asymmetric cross rolling, a new rolling method was developed by us. And its experiments have been conducted to investigate its effects on microstructure and mechanical properties of AZ31. The influencing factors such as velocity ratio of rolls, rolling route and rolling temperature were investigated. It was found that the shear strain of asymmetric cross rolling contributes to refinement of grain size. Samples rolled by asymmetric cross rolling have finer grain size than that rolled by common rolling.

Combination of ECAP and Aging Treatment to Strengthen AZ80 Magnesium Alloy: De Liang Yin¹; Jingtao Wang¹; Li Kui Weng¹; ¹Nanjing University of Science and Technology

Both ECAP and aging treatment have the potential to improve the mechanical properties of some magnesium alloys. In this work, the two methods were combined to strengthen this material. Experiment shows that ECAP of AZ80 can lead to grain refinement and significant improvement of strength and ductility of the material. Microstructure and mechanical properties of AZ80 magnesium alloy were further examined in combination conditions of ECAP and aging treatments. It is found that, ECAP for 8 passes at 360°C followed by aging treatment at 150°C is more effective in producing materials with good mechanical properties. TEM analysis reveals that large amount of discontinuous precipitates appear in some grain boundaries and then grow into the interior of these grains, which has special orientation to the matrix, suggesting that mechanical properties are closely related to the precipitation process.

Dynamic Equal-Channel Angular Pressing of Ti for Producing Ultrafine-Grained Structure: Evgeniy Shorokhov¹; Igor Zhgilev¹; Alexander Gurov¹; Dmitry Gunderov²; ¹Russian Federal Nuclear Center; ²Ufa State Aviation Technical University

A new method of severe plastic deformation of materials, dynamic equal-channel angular pressing (DECAP), is developed. Unlike the conventional ECAP, the energy of explosion products is used as a working substance instead of the press. During the experiments a sample of commercially pure Ti was accelerated using the gun up to the velocity of 300 m/s and then it was pressed in the matrix through the channels which were bent at an abrupt angle. The samples were loaded up to 4 times. After DECAP the strength of titanium is increased by approximately two times. Such strengthening of titanium is reached also during the static ECAP. After one cycle of DECAP the formation of very nonuniform microstructure is noted. The size of the structural elements refined to about one micron and smaller. After four cycles of DECAP ultrafine-grained structure is formed.

Dynamic Torsional Deformation of Ultra-Fine-Grained Dual Phase Steel Fabricated by Equal Channel Angular Pressing: Yang Gon Kim¹; Byoungchul Hwang²; Sunghak Lee¹; Dong Shin³; ¹Pohang University of Science and Technology; ²Eco-Materials Research Center, Korea Institute of Machinery and Materials; ³Hanyang University

Dynamic torsional deformation behavior of an ultra-fine-grained dual phase steel fabricated by equal channel angular pressing (ECAP) was compared with that of an ECAP'ed ultra-fine-grained low-carbon steel. The ECAP'ed low-carbon steel consisted of very fine, elongated ferrite-pearlite grains of

~0.5 μm in size, and the ECAP'ed dual phase steel consisted of very fine ferrite-martensite grains of ~1 μm in size. The dynamic torsional test results indicated that maximum shear stress of the dual phase steel was lower than that of the low-carbons steel, but that fracture shear strain was higher in the dual phase steel. Some adiabatic shear bands were observed at the gage center of the dynamically deformed torsional specimen of the low-carbon steel, although they were not found in the dual phase steel. These results suggested that the ECAP'ed ultra-fine-grained dual phase steel could be a good way to increase the fracture resistance under dynamic loading as the formation of adiabatic shear bands was reduced or prevented.

Effect of Grain Boundary Recovery on Tensile Properties of Nanostructured CP-Ti Produced by Compressive Deformation at LNT: Xiaojing Xu¹; ¹Jiangsu University

The effect of grain boundary recovery on tensile properties of nanostructured commercially pure titanium (Nanostructured CP-Ti) was investigated. The nanostructured CP-Ti was produced by multi-step compressive deformation at liquid nitrogen temperature (LNT). An annealing treatment, with the attempt that recovery occurred only at grain/twin boundaries, was conducted by heating the nanostructured CP-Ti very slowly (0.5 K/min) up to a low temperature of 573K. Tensile testing illustrates the annealing treatment decreased both strength and ductility. A calculation based on Taylor equation shows that the theoretical decrease of strength due to the annealing-resulted reduction of dislocation density is obviously lower than the actual decrease of strength. These above results suggest that the non-equilibrium grain/twin boundaries appeared to increase the strength and ductility, and the lattice dislocations trapped into grain boundaries that are associated with non-equilibrium state of grain/twin boundaries made a more effective strengthening than general lattice dislocations in present nanostructured CP-Ti.

Effect of Hot Isostatic Pressing on a Cryomilled Aluminum Alloy and Boron Carbide Nanocomposite: Rustin Vogt¹; Julie Schoenung¹; Piers Newberry¹; ¹University of California Davis

The addition of ceramic particulate reinforcement via cryomilling can result in Al alloys with extremely high strength. In the present study, boron carbide (B₄C) was cryomilled with Al 5083 to form a metal matrix composite powder with a nanocrystalline grain structure. This powder was blended with un-milled, gas-atomized Al 5083 powder to increase ductility, and then consolidated by hot isostatic pressing (HIPping), followed by extrusion. The change in the cryomilled microstructure and properties during consolidation is characterized and described. The HIP temperature was varied between 350 and 500° to investigate its effect on the microstructure and mechanical properties of the final material, as determined by optical and electron microscopy; hardness, tensile and compressive testing. An increase in the HIP temperature led to a decrease in strength and an increase in ductility, which is related to an increase in the average grain size.

Effect of Low Temperature Annealing Twins on Mechanical Properties of nc-Ni: Indranil Roy¹; Hsiao-Wei Yang¹; Linh Dinh¹; Farghalli Mohamed¹; ¹University of California, Irvine

Fully dense bulk nc-Ni specimens having an average grain size of 100 nm were subjected to isothermal annealing at 573 K for different holding times to induce varying volume fractions of annealing twins within the microstructure. For smaller holding times, transmission electron (TEM) micrographs indicate that, while there is limited grain growth, a larger volume fraction of annealing twins is induced. With increasing holding time, there is an increase in grain size and an annihilation of the annealing twins. Following annealing treatments, specimens with different volume fractions of twins were tested under uniaxial tension at 393 K with a strain rate of 10⁻³ s⁻¹. The mechanical data show that both the strength and ductility of nc-Ni decrease with a decrease in the annealing twin density.

Effect of SiC Film on Tensile Properties of Nanostructured CP-Ti Produced by Compressive Deformation at LNT: Xiaojing Xu¹; Honghong Shao¹; Jianchang Gao¹; ¹Jiangsu University

The effect of SiC film on tensile properties of nanostructured commercially pure titanium (Nanostructured CP-Ti) was investigated. The nanostructured CP-Ti was produced by multi-step compressive deformation at liquid nitrogen temperature (LNT). The SiC film was deposited on the nanostructured CP-Ti substrate using radio-frequency magnetron sputtering technique at room

temperature. The film presents an amorphous structure and its thickness is about 2 micron. The interface between the film and the nanostructured CP-Ti substrate presents a high bonding force of more than 21N. Tensile testing shows that the film improved the ductility considerably and simultaneously did not decrease the strength. SEM observation shows the interface kept bonding even at the fracture tip of tensile specimen. These above results illustrate that the ductility of nanostructured materials can be enhanced by an appropriate surface film technique if the film can help to resist the development of necking.

Effect of Strain Rate on the Tensile Behavior of Ultra-Fine Grained Pure Aluminum: Mingliang Wang¹; Aidang Shan¹; Jiangwei Ren¹; ¹Shanghai Jiao Tong University

Ultra-fine grained pure aluminum was produced through 4 times ECAP plus cold rolling under liquid nitrogen temperature. Tensile test was performed under a strain rate range of 10⁻⁶ to 10⁻¹/s with samples cut from rolled sheet. The response of tensile properties to strain rate was analyzed. It was found that the deformation induced instability is sensitive to the strain rate. The ductility decreases while the yield strength increases with increase of the strain rate. The observed phenomenon was explained based on the contribution from both inner grain dislocation activity and grain boundary sliding.

Effects of the Number of Equal-Channel Angular Pressing Passes on the Anisotropy of Ultra-Fine Titanium: Alexander Korshunov¹; Tamara Kravchenko¹; Lev Polyakov¹; Andrey Smolyakov¹; Irina Vedernikova¹; Alexander Morozov¹; ¹Russian Federal Nuclear Center- All-Russian Research Institute of Experimental Physics

Annealed commercially pure titanium was processed by four passes of equal-channel angular pressing (ECAP) at a temperature of 450°C using route BC. Pressed samples had a square section with a side length of 8 mm. Anisotropy was analyzed based on the conventional yield strength at compression in three mutually perpendicular directions. Compression tests were performed with static loading at room temperature and at 450°C. The tests were conducted with the as-received material, and after 1, 2, 3 and 4 passes. Anisotropy of the as-received condition holds out at further pressing and makes about 25 percent. Anisotropy after all the passes is similar both for room and elevated temperature. Anisotropy characteristics are observed to change during the third pass. The anomalous change in anisotropy during the third pass is also evidenced by the analysis of microhardness measurements in different section planes of the samples.

Fabrication and Tensile Properties of Ultrafine Grained Dual Phase Steels: Dong Shin¹; Duck Young Hwang¹; Kyung-Tae Park²; Young Gun Ko³; Chong Lee³; ¹Hanyang University; ²Hanbat National University; ³Pohang University of Science and Technology

Ultrafine grained (UFG) ferrite-martensite dual phase steels were fabricated by equal channel angular pressing and subsequent intercritical annealing treatment. Their room temperature tensile properties were examined and compared to those of coarse grained and UFG steels. The strength of UFG dual phase steels were much higher than that of coarse grained counterpart, but total elongation were not degraded. More importantly, the present UFG dual steels exhibited rapid strain hardening unlike most UFG materials. The addition of small amount of vanadium increased the strength and elongation of the present UFG dual phase steels, and it was found that the vanadium addition was beneficial to further improvement of their mechanical properties. An excellent combination of strength, elongation and strain hardening of the present UFG dual phase steels was explained in terms of their specific microstructural features.

Fabrication of WC-Co Cermets by Laser Engineered Net Shaping: Yuhong Xiong¹; John Smugeresky²; Leonardo Ajdelsztajn¹; Julie Schoenung¹; ¹University of California, Davis; ²Sandia National Laboratories

The Laser Engineered Net Shaping (LENS[®]) technology is an extension of rapid prototyping technologies into direct fabrication of engineering parts. Bulk tungsten carbide-cobalt (WC-12 wt.% Co) cermets were produced without any molds using the LENS[®] technology, starting from granules consisting of WC crystallites (with a grain size ranging from nanocrystalline to microcrystal) in a Co matrix. Microstructure and hardness property were investigated. Experimental results revealed that decomposition and decarburization of WC was limited during laser deposition. It was also found



that the process parameters, including laser power, traverse speed and working distance, have significant influence on the microstructure of cermets. Both uniform microstructure with small WC crystallites and microstructure with alternate layers (containing small and large WC crystallites) were observed when processing conditions differ. Thermal behavior of the LENS® process, shape change and coarsening of WC crystallites were investigated to study the mechanisms of microstructural evolution of the cermets.

Features of the Formation of the Microstructure of the V-4%Ti-4%Cr Alloy under Severe Plastic Deformations: *Ivan Ditenberg*¹; *Alexandr Tyumentsev*¹; *Yury Pinzhin*¹; ¹Institute of Strength Physics and Material Science SB RAS

Transmission electron microscopy was used to examine the microstructure formed under severe deformations in V-4Ti-4Cr alloys rolled at room temperature. Microband nanostructured states and high-energy defect substructures have been detected that feature a high curvature of the crystal lattice, a high density of partial disclinations at the microband boundaries, and local internal stresses reaching E/30 (E being Young's modulus). It has been shown that important features of the microband structure are the prevailing reorientation of the microbands around type <110> directions and the high density of large-angle boundaries. It has been supposed that these features result from the plastic deformation and reorientation of the crystal lattice through mechanisms of local martensitic type reversible transformations (direct plus reverse transformations accompanied by a change of the reverse transformation system) in fields of high local stresses.

Flexible Electronics: From Printed Nano-Silver Inks to Organic Thin Film Transistors (OTFTs) on Polymer Substrates: *Julia Greer*¹; *Ana Arias*¹; *William Wong*¹; *Michael Chabiny*¹; *Robert Street*¹; ¹Palo Alto Research Center (PARC)

Organic thin-film transistors (OTFTs) on flexible substrates can enable manufacturing of low-cost displays due to their flexibility and low-temperature processing. Inkjet-printed nano-particles, initially in dispersion of ~40 nm-sized silver clusters in solvent, sinter rapidly when cured at low homologous temperatures, due to high surface area/volume. Upon solvent evaporation, Ag particles come in contact and begin sintering, forming a continuous conductive percolation network. Unique low-temperature sintering characteristic of nano-features enables utilizing these inks as interconnects. Results of experiments investigating mechanical stress, microstructure, and resistivity of thin porous films produced from nano-particle inks are presented. Power law dependence of resistivity on strain and porosity was established as a function of time and temperature through competing sintering and grain growth/crystallization mechanism(s). Transfer characteristics and carrier mobilities of OTFTs on plastic substrates under mechanical bending are also discussed.

Highly Improved Ductility Achieved by Phase Transformation in Ultrafine-Grained Steel: *Sheng Cheng*¹; *Hahn Choo*¹; *Xun-li Wang*¹; *Peter Liaw*¹; ¹University of Tennessee

It has been recognized that the low ductility of nanostructured (NS) and ultrafine-grained (UFG) metals has originated from the poor strain hardening. However, by introducing the phase transformation into the NS and UFG metals, the strain hardening can be greatly improved, and, therefore, a combination of the excellent strength and ductility can be achieved. In our UFG steel, a tensile elongation of ~40% with a yield stress of ~1,000 MPa has been obtained. The strain-hardening behavior has been investigated as a function of the phase-volume fraction, dislocation structures, etc. A preferential phase transformation is found to be associated with the strain localization. The effect of the strain rate on the strain localization and preferential transformation is discussed. This work was supported by the National Science Foundation Major Research Instrumentation (MRI) Program (DMR-0421219) and International Materials Institutes (IMI) with Dr. C. Bouldin and Dr. C. Huber as the Program Directors, respectively.

Improvement of Room Temperature Superplasticity in Zn-22%Al Alloy: *Shao Hua Xia*¹; *Jia Wang*¹; *Jingtao Wang*¹; ¹Nanjing University of Science and Technology

Zn-22%Al alloy with sub-micrometer grain was obtained by three different processing of quenching + aging, quenching + ECAP 4 passes and 8 passes equal channel angular pressing (ECAP) at room temperature. The samples were tensiled in a broad strain rate range of 1×10⁻⁴ to 1s⁻¹ at room

temperature. The three kinds of alloy samples exhibit good superplasticity at room temperature. At strain rate of 4×10⁻³s⁻¹, the specimens after quenching + 4 passes and 8 passes of ECAP reach a high elongation of 360% and 325% respectively; while, at a high strain rate of 1×10⁻¹s⁻¹, the elongation of these two alloy samples is still higher than 150%. Besides high elongation, at strain rate of 4×10⁻²s⁻¹, a high value of strain rate sensitivity of 0.35~0.4 was observed in all these three kinds of alloys. A room temperature, grain growth during ECAP was also observed in the alloy.

In-Situ Observation of Tensile Deformation of Bimodal Al 5083: *Byungmin Ahn*¹; *Steven Nutt*¹; ¹University of Southern California

The tensile properties and deformation response of bimodal structured nanocrystalline Al 5083 alloy were investigated using a micro-straining unit. Atomized Al 5083 powder was ball-milled in liquid N₂ to obtain a nanocrystalline structure, and blended with 15% unmilled coarse-grained powder to achieve bimodal structure. The powder blend was hot vacuum degassed to remove residual contaminants, consolidated by either cold (CIP) or hot isostatic pressing (HIP), and then forged. The microstructure was observed in-situ using an optical microscope. The investigation of tensile and fracture of bimodal structure suggests unusual deformation mechanisms and interactions between ductile coarse-grain bands and nanocrystalline regions.

Mechanical Behavior of Bulk Ultrafine Grained Zr Processed by Severe Rolling: *Ling Jiang*¹; *Michael Kassner*¹; *Oscar Ruano*²; *Teresa Pérez-Prado*²; ¹USC; ²CENIM, CSIC

The aim of this work is to investigate the mechanical behavior of bulk ultrafine grained Zr processed by severe rolling. Mechanical properties such as strength, ductility, strain hardening and strain rate sensitivity have been evaluated at room temperature and compared with those of coarse grained Zr. The correlation between the microstructure and the mechanical behavior has been investigated. The predominant deformation mechanisms are discussed on the light of the these findings.

Mechanical Properties of Long-Length Nanostructured Metallic Rods Produced by Continuous ECAP: *Georgy Raab*¹; *Dmitry Gunderov*¹; *Yuntian Zhu*²; *Terry Lowe*²; *Ruslan Valiev*¹; ¹Ufa State Aviation Technical University; ²Los Alamos National Laboratory

We have recently established an ability to produce long rods of nanostructured metals via a hybrid severe plastic deformation technique that combines continuous equal-channel angular pressing based on the Conform® process (ECAP-C) with other metal forming methods. Using a new ECAP-C die-set with a capability of processing at temperatures in the range of 20-450°C and pressing velocity up to 60 mm/s we produced several rods of nanostructured copper and titanium with lengths up to 3 meters. In this work we report the mechanical properties of rods processed using various processing parameters and routes. Special attention is paid to homogeneity of mechanical properties (strength, ductility, fatigue) along the length of the rods. We find that ECAP-C results in a level of mechanical properties similar to or even higher than conventional ECAP.

Mechanical Properties of Nanostructured fcc/bcc Multilayer Films: *E. G. Fu*¹; *N. Li*¹; *A. Misra*²; *R. Hoagland*²; *Xinghang Zhang*¹; ¹Texas A&M University; ²Los Alamos National Laboratory

Nanoscale metallic multilayers exhibit maximum hardness at layer thickness of around 2 – 5 nm. Molecular dynamics simulations (Hoagland et al., Scripta Mat., 2004) have shown that the interface barrier stress to the transmission of individual glide dislocations may define the limiting strength of nanolayered materials. We have experimentally investigated the layer thickness dependence of the hardness of several fcc / bcc systems, such as Cu/V, Cu/Nb and Al/Nb with different interface properties. The multilayered films were synthesized via magnetron sputtering technique, with individual layer thickness varying from 1 to 200 nm. The as-deposited fcc/bcc multilayer films had Kurdjumov-Sachs orientation relationship: {111}fcc // {110}bcc; <110>fcc // <111>bcc. The maximum hardnesses obtained in each of the three systems are interpreted in terms of the differences in the respective moduli and the interface properties.

Mechanistic Explanation for Strain Softening Phenomenon Observed in Nanocrystalline or Ultrafine-Grained Metals: *Feng Tang*¹; *Julie Schoenung*¹; ¹University of California

Strain hardening, which is attributed to the enhancement of dislocation

interaction with increasing plastic deformation, is a common phenomenon observed in single crystal or polycrystalline metals. In contrast, strain softening has recently been observed in metals with grain sizes that range from tens to hundreds of nanometers. This new-found phenomenon is peculiar, and the understanding of its mechanism may provide new opportunities to improve the mechanical properties of nanocrystalline or ultrafine-grained metals. In the present study, a mechanism based on the formation of residual internal stresses caused by dislocation creation and absorption at grain boundaries is proposed to explain the strain softening phenomenon in nanocrystalline and ultrafine-grained metals. With these residual internal stresses, in order to create new dislocations at grain boundaries for further plastic deformation, lower external stress is required when compared with that without the residual internal stresses, which results in strain softening.

Molecular Dynamic Simulations of Plastic Deformation in Nanocrystalline Aluminum-Lead Alloy: *Seonhee Jang*¹; *Yojna Purohit*¹; *Douglas Irving*¹; *Clifford Padgett*¹; *Ronald Scattergood*¹; *Donald Brenner*¹; ¹North Carolina State University

The mechanical behavior of pure nanocrystalline metals has been studied extensively. However, nanocrystalline alloys have received little attention either experimentally or theoretically. To understand the mechanical properties in nanocrystalline metal and its alloy, we first developed pure Al and immiscible Al-Pb alloy models with columnar structure composed of hexagon-shaped grains and carried out the first principles calculation to fit the parameters for interatomic potentials into modified embedded atom method. We also carried out the Monte Carlo technique to observe how Pb atoms affect the mechanical behavior of Al nanostructure. Simulation results for pure Al and for dilute Al-Pb alloys will be presented. Results are discussed in terms of dislocation emission, stacking faults formation and grain boundary structures with different grain sizes and grain boundary segregation effects on the deformation mechanisms. Comparison will be made to recent experimental results on these alloys.

Nano- and Ultrafine-Structured Metastable Beta-Titanium Alloys Processed by Severe Plastic Deformation: *Wei Xu*¹; *Xiaolin Wu*¹; *Mariana Calin*²; *Kenong Xia*¹; *Jürgen Eckert*²; ¹University of Melbourne; ²Technische Universität Darmstadt

Severe plastic deformation in the form of equal channel angular pressing (ECAP) and cold rolling was employed to produce nano- and ultrafine-structured metastable beta-titanium alloys with different phase stability against beta to alpha^{*} martensitic transformation. After plastic deformation, the grains were easily refined to the nanoscale (50–100 nm) in alloys with low stacking fault energy in which martensitic transformation and mechanical twinning were favored. A single plastic deformation mechanism such as dislocation slip was unable to easily result in such a fine microstructure and thereby a hybrid mechanism consisting of at least two concurrent deformation modes was most likely operative. Since the instability of the bcc beta phase increases with decreasing stacking fault energy, it was believed that deformation-induced martensitic transformation and twinning played a crucial role. Complicated interactions between dislocation slip, martensitic transformation and twinning may have facilitated the refinement by dividing the original coarse grains into nanometre-sized blocks.

New Opinion on Microstructure and Hardening Mechanism of Ti-Si-N Nanocomposite Coatings: *Ming Kong*¹; *Geyang Li*¹; ¹Shanghai Jiao Tong University

Ti-Si-N nanocomposite coating is currently a hot topic in the field of superhard coatings. Earlier theoretical hardening mechanism with regard to this nanostructured material was the nc-TiN/a-Si₃N₄ mode: equiaxed crystalline TiN of several nanometers in diameter surrounded by less than 1-nanometer amorphous Si₃N₄ interfacial layers. The present study employing transmission electron microscope observed a TiN/Si₃N₄ nanocomposite coating with high hardness, and surprisingly found that rather than amorphous as was the common opinion, the several-monolayer-thick Si₃N₄ interfacial phase had crystalline structure and formed low-energy coherent interfaces with TiN nanocolumnar crystals. A parallel simulation utilizing two-dimensional nanostructured TiN/Si₃N₄ multilayered coatings also implied that at a thickness of less than 0.7 nm, sputter-deposited amorphous Si₃N₄ was forced to crystallize and formed coherent interfaces with TiN, accompanied by a remarkable enhancement in coatings' hardness. A possible strengthening

mechanism with regard to nanocomposites was proposed based on the current comprehension on the hardening of nanomultilayers.

Numerical Simulations and Comparison with Experiment of the ECAE Process Multi Pass: *Andrey Smolyakov*¹; *Alexander Korshunov*¹; *Vyacheslav Soloviev*¹; ¹Russian Federal Nuclear Center- All-Russian Research Institute of Experimental Physics

Numerical simulations of ECAE process carried using DRACON code (VNIIEF) based on variation-difference method of solving continuum mechanics equations have shown that satisfactory agreement between experimental and numerical data on deformed billet state can be achieved by using experimental data in the development of physical model.

OIM Study of Micro-Structure and Texture Heterogeneity during ECAP in Copper: *Alexander Zhilyaev*¹; *Srinivasan Swaminathan*²; *Georgy Raab*³; *Terry McNelley*²; ¹Centro Nacional de Investigaciones Metallúrgicas; ²Naval Postgraduate School; ³Ufa State Aviation Technical University

The heterogeneous deformation of annealed copper subjected to equal channel angular pressing (ECAP) was studied by Orientation Imaging Microscopy. Microstructure and microtexture of partially pressed Cu billet have been recorded and analyzed at inner and outer corners as well as in the middle of shear zone. Special case of distinctly inhomogeneous deformation of prior annealing twins by interpenetrating slip bands was observed, and some twin-matrix interfaces displayed stair-like offsets. The intense local deformation within the annealing twins exhibits characteristics of dislocation slip and not deformation twinning.

Post-ECAP Annealing of Al-Si Alloys: *Przemyslaw Szczygiel*¹; *Hans Roven*¹; *Oddvin Reiso*²; ¹Norwegian University of Science and Technology; ²Hydro Aluminium AS

Experiments were conducted to investigate the post-ECAP annealing response of three generic Al-Si alloys with varying silicon content. The alloys were deformed by ECAP up to 4 passes and microstructural changes during deformation and annealing were studied by microscopic techniques (OLM, SEM, TEM). Measured hardness evolution gave indication of changes in the mechanical behaviour due to recovery/recrystallization processes. Influence of ECAP strain, particle fraction and annealing temperature on microstructure and properties evolution of the current SPD materials and their thermal stability is discussed. The importance of particles on recrystallization of materials severely deformed by ECAP is considered by relating recrystallized microstructures to respective particle distributions.

Precipitate Shape and Coherency Loss Mechanisms in Au-Rh Alloys: *Peihua Jing*¹; *Hyon-Jee Lee*¹; *Jae-Hyeok Shim*²; *Brian Wirth*¹; *I. M. Robertson*³; ¹University of California, Berkeley; ²Korea Institute of Science and Technology; ³University of Illinois

In precipitate hardened materials, the strength and creep properties are controlled by dislocation interactions, which depend on the precipitate interfacial structure. We present the results of atomistic simulations specifically designed to investigate the precipitate shape, coherency loss and dislocation bypass mechanisms in a Au-Rh alloy with a large lattice misfit. Semi-empirical Sutton-Chen type interatomic potentials have been used for pure Au and Rh; Au-Rh cross potential has been derived to accurately describe the elastic properties of Au-Rh alloy, the Au-Rh mixing enthalpy and interfacial energy. The results provide insight into the precipitate coherency loss mechanisms and the effect of precipitate coherency on dislocation interaction and bypass.

Rate Dependent Behavior of Ultrafine Grained Magnesium Alloy: *Kyle Azevedo*¹; *Shailendra Joshi*¹; *K.T. Ramesh*¹; *Evan Ma*¹; ¹Johns Hopkins University

Nanostructured magnesium ZK60 alloys are promising candidates for lighter and stronger structures. In this work, we investigate the mechanical response of ultrafine-grained ZK60 alloy processed by ECAP (8 passes). The macroscopic response is observed over a wide range of strain rates from 10⁻³ s⁻¹ (servohydraulic) to 10⁴ s⁻¹ (Kolsky bar) under compression. Using a high-speed camera, the high rate deformation process is investigated. The deformed microstructures are correlated with the associated macroscopic responses. The results indicate rate dependent hardening comparable to some other hexagonally close-packed metals. Final failure occurs through shear irrespective of the strain rate.



Residual Stress Analysis for As-Deposited Soft High Moment Fe65Co35/Ru Laminated Thin Films: *Jinmei Dong*¹; Subhadra Gupta¹; ¹University of Alabama

A series of Fe65Co35/Ru laminated thin Films were sputtered on Si (100) wafers by DC magnetron sputtering in the optimized sputtering conditions. The structure and magnetic properties were characterized by XRD and VSM, almost all the laminated films exhibit well-defined uniaxial anisotropy and soft magnetic properties with saturation magnetization > 2T. The film residual stress was measured by Flexus Thin Film stress tester. ANOVA models were used to analyze the effect factors of residual stress: The stress of the films is homogeneous ($P > 0.05$); No significant differences of residual stress between different lamination orders ($P > 0.05$) for fixed individual materials thickness: However, there are significant differences of residual stress between different film thickness ($P < 0.05$). Based on the above analysis, a regression model was set up to trace the residual stress for different Fe65Co35/Ru laminated thin films.

Strain-Hardening Behavior of Ultrafine Grained Microalloyed Steels Produced by Severe Plastic Deformation: *Maurizio Vedani*²; Sergio Arnaboldi¹; Paola Bassani²; Ausonio Tuissi²; ¹Politecnico di Milano; ²Consiglio Nazionale delle Ricerche- Istituto per l'Energetica e le Interfasi

A study is presented on grain refinement by severe plastic deformation of three Nb-V microalloyed steels differing in their Nb content. Steel samples having a square section of 30x30 mm were cut from continuously cast billets and hot rolled in a temperature range 1000-850°C to reduce their section down to 12x12 mm. The obtained samples were then severely deformed by caliper rolling at 500°C, to obtain wires having a section of 1.9x1.9 mm and a grain size in the range 0.4-0.8 micrometers in the as rolled state. Annealing treatments at 600°C were then performed on the UFG steel samples for times varying from 5 minutes up to 2 hours. Investigations on thermal stability of the structure and on mechanical behaviour of the annealed steels was then carried out as a function of steel composition and annealing time.

Strain Hardening Behavior of an Ultra-Fine Grained Aluminum Alloy: *Troy Topping*¹; Andrew Newbery¹; Zhuhui Zhang¹; Enrique Lavernia¹; ¹University of California, Davis

Aluminum alloys with nanocrystalline and ultra-fine grain (UFG) size are of immense interest because of their high strength – typically more than 30% stronger than conventionally processed alloys. For this study, the microstructure and mechanical behavior of UFG Al 5083 plate, produced by the quasi-static forging and rolling of cryomilled powder, has been investigated and compared to course-grained Al 5083 - in particular, the ability to strengthen the UFG material further by strain hardening. Annealing treatments were varied to investigate the thermal stability of the UFG material and to obtain a dislocation-free condition without significant grain growth. Both the UFG and conventional material were then cold worked to increase their strength. It is found that the UFG structure decreases the range of strength that can be obtained from strain hardening. The microstructural evidence suggests this is due to limited dislocation accommodation in the small grains.

Strengthening Mechanisms of Bulk Nanostructured Ag Prepared by Powder Metallurgy and Subsequent Compressive Deformation at LNT: *Xiaojing Xu*¹; Jinqi Cao¹; ¹Jiangsu University

Bulk nanostructured Ag was produced by Powder Metallurgy and subsequent Multi-Step Compressive Deformation at liquid nitrogen temperature (LNT), and its strengthening mechanisms was investigated by estimating the contribution of different structure defects (lattice dislocation, grain boundaries) to strength. The dislocation strengthening contribution was calculated by using Taylor equation, where dislocation density was estimated in terms of the coherent diffraction domain size and the lattice microstrain that were obtained from XRD line breadth analysis. The grain boundary strengthening contribution was calculated by using Hall-Petch relationship. These theoretical results show that dislocation strengthening and grain boundary strengthening made a contribution of about ~ 40.0% and ~ 45.8%, respectively. Since the friction stress of lattice also made a contribution of ~ 7.8% to strength, it is extrapolated that other strengthening mechanisms, such as twin boundary and non-equilibrium boundaries, appeared to make a very low contribution to strength.

Stress Relaxation Mechanisms in Materials with NanoInclusions: Vladimir Chaldyshev¹; *Anna Kolesnikova*²; Alexey Romanov¹; ¹Ioffe Physico-Technical Institute; ²Institute of Problems of Mechanical Engineering

Plastic-elastic distortions in materials with nanoInclusions (or quantum dots) often are the cause of degradation of structural, optical and electronic properties of these materials. The major role in plastic-elastic state of such heterostructures plays the mechanical stress relaxation processes. In our report a relaxation of mechanical stresses in structures with nanoInclusions are investigated. The relaxation is connected with dislocation loops nucleation: single misfit dislocation loop, continuous distribution of these loops at the matrix/inclusion boundary caused to the change of inclusion self-deformation, and (or) dislocation loop-satellite formation in the vicinity of the inclusion. In the framework of considered relaxation mechanisms the critical sizes of inclusions in which the relaxation is energetically profitable are obtained. The calculated and experimental dependences of dislocation loop-satellite diameter on inclusion diameter are demonstrated. The preferences of the one or the other of considered mechanisms are discussed.

Structure Refinement of Aluminum Alloy 5083 under Severe Plastic Deformation: *Mark Yavorsky*¹; Vladimir Segal²; Phil Young²; Gopal Viswanathan¹; Vladimir Levit¹; Hamish Fraser¹; ¹Ohio State University; ²Engineered Performance Materials

Severe Plastic Deformation (SPD) combined with low temperature heat treatments is a common way of achievement required ratio of strength to ductility for very specific applications. Aluminum alloy 5083 (Al-Mg-Mn-Cr) has been deformed using equal channel angular extrusion (ECAE) and rolling under variety of thermo-mechanical conditions: in the temperature range of 77- 523 K, followed by annealing. Detailed structure investigation was provided using optical (OM), transmission (TEM) and scanning (SEM) electron microscopy, orientation imaging microscopy (OIM) including novel 3D characterization techniques. Tensile specimens were machined from deformed and heat treated material and tested after every step of the experimental thermo-mechanical procedure. Intimate mechanisms of nanostructure formation and final material properties are discussed in terms of conservative and non-conservative dislocation movement and their rearrangement as a balance of work hardening, dynamic and static recovery.

Study on Function of Modified Fly Ash in Production of Aluminum Foam: Wang Yong¹; Yao Guang-chun¹; Li Bing¹; ¹Northeastern University

The key of melt-foaming is to control cell size and bubble distributing uniformly in melt. In this work, fly ash was selected as reinforcement in melt-foaming. The most component are quartz and mullite was observed by XRD in the fly ash, therefore it's a kind of hardness ceramic particles. After 10 hours grinding, spherical particles increase and yield new surface that will improve their performance. Observing cell wall by SEM, we can see fly ash in the wall. These particles tend to increase molten aluminum viscosity, sustain the liquid within the film and delay the bubble of rupture. Through compression strength test, the effect of energy absorption of aluminum foam with similar aperture is in direct proportion to its density.

Superplasticity in Ultrafine-Grained Titanium: Observations and Properties Studies: *Irina Semenova*¹; Alexander Korshunov²; Vladimir Latysh³; Terry Lowe⁴; Ruslan Valiev¹; ¹Ufa State Aviation Technical University; ²All Russian Scientific Research Institute of Experimental Physics; ³Innovative Scientific and Technical Centre "Iskra"; ⁴Los Alamos National Laboratory

Elevated temperature tensile testing of ultrafine-grained (UFG) commercially pure titanium has shown superplastic deformation behavior, with elongations up to 300% at 500°C at a strain rate of 10-4 s-1. The microstructures that enable superplastic behavior were produced in Grade 4 titanium via a combination of equal-channel angular pressing (ECAP) and additional thermomechanical treatments. Room temperature tensile strength after severe plastic deformation processing and subsequent superplastic deformation were notably high with ultimate tensile strength as high as 1,240 MPa while retaining a ductility of 11%. The microstructure and mechanical tests of samples after superplastic deformation suggest that it is possible to further optimize equiaxed microstructures with grain boundaries capable of grain-boundary sliding and at the same time produce unique combinations of high ductility and strength at ambient temperature.

Synthesis and Behavior of Bulk Nanostructured Al 5083-Al₈₅Ni₁₀La₅ Composites: *Zhihui Zhang*¹; Bing Han¹; Yizhang Zhou¹; Enrique Lavernia¹; ¹University of California, Davis

Cryomilled Al 5083 was blended with Al₈₅Ni₁₀La₅ amorphous particles (10% and 20% in volume fraction) to explore the behavior of Al-based MMCs. The powder blends were subsequently degassed, cold isostatically pressed and extruded. The microstructure for the powders and bulk materials was examined using XRD, SEM and TEM. It was found that the Al₈₅Ni₁₀La₅ reinforcement presented a grain size of 100 ~ 200 nm and the Al 5083 matrix had a grain size around 200 nm in the fine-grained region interspersed by coarse-grained region with a grain size of 600 ~ 1500 nm. The mechanical properties of the Al 5083-Al₈₅Ni₁₀La₅ composites were investigated via compressive and tensile studies. The elevated temperature deformation behavior of the composites was also studied. The compressive strength of the as-extruded 10% and 20% Al₈₅Ni₁₀La₅ composites were determined to be 1025 MPa and 837 MPa, respectively.

The Effect of Severe Plastic Deformation on Structural-Phase State and Strengthening Mechanisms of Al-Mg-Li Alloy: *Evgeniy Naydenkin*¹; *Yury Kolobov*²; ¹Institute of Strength Physics and Materials Science; ²Centre of Nanostructured Materials and Nanotechnologies

In recent years ultra-fine grained (or nanostructured) metals and alloys (grain size <1µm) are being highly developed and investigated. In present paper the investigation of structure-phase state and strengthening mechanisms of commercial aluminum 1421 Al-Mg-Li alloy produced by equal-channel angular pressing has been carried out. It has been shown that severe plastic deformation leads to the formation of equiaxed ultra-fine grained (d~1µm) two-phase type structure with mainly high angle misorientations of grain boundaries. The evaluation of strength characteristics on the basis of analysis of structure-phase parameters found to be close to the values obtained during tensile tests. In the alloy after ECAP the disperse particles of Al(Sc, Zr) and AlLi phases make smaller contribution in strengthening because of their volume fraction decrease while the contribution related to the grain size reduction significantly increases in comparison with initial state.

The Investigation of Structure State Features Influence on the Regularities and Mechanisms of Plastic Deformation and Fracture of V-4%Ti-4%Cr System Alloys: *Ivan Ditenberg*¹; ¹Institute of Strength Physics and Material Science SB RAS

Transmission electron microscopy was used to examine the microstructure formed under severe deformations in V-4Ti-4Cr alloys rolled at room temperature. Microband nanostructured states and high-energy defect substructures have been detected that feature a high curvature of the crystal lattice, a high density of partial disclinations at the microband boundaries, and local internal stresses reaching E/30 (E being Young's modulus). It has been shown that important features of the microband structure are the prevailing reorientation of the microbands around type <110> directions and the high density of large-angle boundaries. It has been supposed that these features result from the plastic deformation and reorientation of the crystal lattice through mechanisms of local martensitic type reversible transformations (direct plus reverse transformations accompanied by a change of the reverse transformation system) in fields of high local stresses.

The Structure and Micro Hardness of Alloys Based Aluminum Produced by Rapid Quenching of a Melt: *N. Noskova*¹; *N. Vildanova*¹; *R. Churbaev*¹; ¹Institute of Metal Physics of UD RAS

The nanocrystalline (nanograin size 20 < d < 70 nm) alloys on Al-based: Al+1% Hf, Al+0.5% Ce, Al+0.12% Zr, Al+0.2% Sn, Al+0.2% Nb, Al+0.5% Re, Al+1% Hf+ 0.2% Nb+0.2% Sn and Al+30% Sn, Al+25% Sn+15% Pb, Al+5% Sn+35% Pb, and Al+0.5% Ce+0.5% Re+0.12% Zr (wt %), was produced by rapid quenching of a melt and severe plastic deformation (shear at a pressure of 5 GPa). The microhardness of nanocrystalline alloys is > 1.2 GPa. The deformation and failure of nanocrystalline alloys Al-(Mg, Hf, Ce, Zr, Sn, Re, Nb, Si, Pb) firstly was examined *in situ* in an electron microscope. The experimental results permitted determining physical parameters responsible for a high-strength state of alloys. It was shown that a high-strength state is realized if grains are not over 70 nm in size. A nanocrystalline material is deformed through a dislocation or combined (dislocation - rotational) mechanism. If nanograins are less than 30 nm in size the material is deformed only by rotational modes.

Unusual Mechanical Behaviour of Nanocrystalline Titanium Processed by High Pressure Torsion: *Rinat Islamgaliev*¹; *Lilija Kurmanaeva*¹; *Vil Kazykhanov*¹; *Larisa Schestakova*¹; *Ruslan Valiev*¹; ¹Ufa State Aviation Technical University

High pressure torsion (HPT) is a well established severe plastic deformation technique for producing nanostructured metallic materials. The present work introduces the new results obtained from recently developed HPT installation with the enhanced load of up to 200 tons. Using this new installation we have investigated the limitations in grain refinement of commercially pure titanium by HPT processing and found that there is the possibility of producing Ti samples with the diameter of 20 mm and a mean grain size as small as 50 nm. The given material demonstrates very high strength and essential ductility properties as well as superplasticity at elevated temperatures. The contribution of various microstructural parameters to strengthening of nanocrystalline titanium has been determined in accordance with the results of microstructural studies and tensile tests. Special attention has been paid to investigation of the influence of nanostructures on fatigue endurance of HPT samples.

Effect of Alloying on HPT Deformed Metals: *Martin Hafok*¹; *Reinhard Pippan*¹; ¹Erich Schmid Institute for Materials Science, Austrian Academy of Science

The variation of solute concentration of single phase materials affects the development of micro structure and the mechanical behaviour. Especially the structure size of high pressure torsion deformed metals obtained in the saturation region of the torque is influenced by the solute concentration. The effect of solute variation was examined by using brass due to the high solubility of zinc in copper and the resulting substitutional disorder. Scanning electron microscopy, transmission electron microscopy and atomic force microscopy were employed to characterise the development of microstructure in dependence on the zinc content. A significant decrease in structure size in comparison to a pure copper deformed by high pressure torsion was obtained. The decrease of microstructure size of the solid solution is accompanied with an increase of the torque in the saturation region.

Factors Influencing the ECA Pressing of Ti-6Al-4V Alloy Having Lamellar Microstructure: *Young Ko*¹; *Dong Shin*²; *Chong Lee*¹; ¹Pohang University of Science and Technology; ²Hanyang University

A study was made to investigate the factors influencing the formability on equal-channel angular-pressing (ECAP) of Ti-6Al-4V alloy, as a typical hard-to-work material, with a variation of forming (ram) speed. ECA pressings were carried out utilizing a set of die for isothermal condition for initial lamellar microstructure. In this study, the equation for effective strain rate during ECAP deformation was evaluated by considering the geometry of both die and sample, and its results were in good accord with that predicted by the finite-element method (FEM) analysis considering flow-softening behavior of present alloy. Based on this equation, strain rate less than 0.27 s⁻¹ was found to be the optimum condition for sound deformation whilst specimens showed the noticeable shear cracking with strain rate above 0.67 s⁻¹. In spite of optimum condition determined here, however, shallow shear segments were still found in a specimen. This was mainly attributed to the flow localization associated with flow-softening behavior of lamellar microstructure. Such behavior was dependent on the lamellar structure *per se*, which was in discussion on the relation and the ability to transmit slip across either colonial boundaries or α/β interfaces as a slip filter.

Microstructural Evolution in Copper Subjected to Severe Plastic Deformation: Experiments and Analysis: *Anuj Mishra*¹; *Bimal Kad*¹; *Morgana Martin*²; *Fabienne Gregori*³; *Naresh Thadhani*²; *Edward Kenik*⁴; *Marc Meyers*¹; ¹University of California; ²Georgia Institute of Technology; ³University of Paris; ⁴Oak Ridge National Laboratory

The evolution of microstructure and mechanical response of copper subjected to ECAP was investigated. The mechanical response is modeled by an equation containing two dislocation evolution terms: one for the cells/subgrain interiors and other for cell wall. Quasistatic compression and tensile testing, and dynamic tests using Hopkinson-bar and Taylor tests were carried out. The microstructures produced through adiabatic shear localization during high strain rate deformation and ECAP is compared. Calculations show that grains with size of 200 nm can rotate by ~30° during ECAP thereby generating and retaining a steady-state equiaxed structure. This is confirmed by a grain-boundary mobility calculation. Reverse Taylor tests were carried out on the



ECAP samples and the response was compared to predictions by Zerilli-Armstrong and Johnson-Cook constitutive equations. TEM analysis of the frontal surface of the Taylor impacted samples showed heavy recrystallization which is a result of the temperature rise during impact. This research is supported by the National Science Foundation under Grant CMS-0210173 (NIRT).

Microstructure and Microhardness of Copper Subjected to Ultra-High Strain Deformation: Azat Gimazov¹; Alexander Zhilyaev²; ¹Institute for Metals Superplasticity Problems; ²Centro Nacional de Investigaciones Metallúrgicas

An investigation was conducted to compare the microstructure and microhardness of pure copper subjected to ECAP (4 passes, route BC), HPT (P=6 GPa, N=5), machining and their combinations, such as machining of ECAP specimens, HPT of ECAP copper and HPT of machining chips. Microstructure, dislocation density and microhardness have been evaluated by x-ray, transmission and scanning electron microscopy. Influence of different processing routes is discussed in terms of accumulated strain and microstructure refinement.

Mechanical Response of Nanocrystalline Steel Obtained by Mechanical Milling: Rodolfo Rodriguez-Baracaldo¹; Josep Antoni Benito²; Jose Maria Cabrera²; Jose Manuel Prado³; ¹Universidad Nacional de Colombia; ²Universitat Politècnica de Catalunya; ³Centre Tecnològic de Manresa

The mechanical properties of 0.55 %C steel bulk specimens have been studied. Samples were obtained by warm static pressing of nanostructured iron powders severely deformed by mechanical milling. Specimens were consolidated at temperatures between 350-500°C at a relatively high pressure of 850 MPa. After the consolidation process, samples were near full density and the ferritic grain size was maintained in the nanometric range as well. A wide range of grain size (50 nm to 1 µm) was obtained by the combination of different compaction parameters and subsequent heat treatments. Hardness values of these samples were in good agreement with the Hall-Petch relation. The increase in hardness and compressive strength and the dramatic decrease of ductility were significant with decreasing grain sizes. Specimens with the lowest grain size (50 nm) showed a hardness of 8.33 GPa and compressive strength of 2500 MPa.

Low-Cycle Fatigue Behaviors of the As-Received and Deformed Magnesium Alloy, AZ31B Using Equal-Channel-Angular Pressing (ECAP): Liang Wu¹; Grigoreta Stoica¹; Douglas Fielden¹; Peter Liaw¹; ¹University of Tennessee

The cyclic-deformation behaviors of the as-received and deformed magnesium-alloy (AZ31B) samples using the Equal-Channel-Angular Pressing (ECAP) technology were investigated at fully reversed total constant strain amplitudes between 0.4% and 1.5% at room temperature. The fatigue-life data for both materials can be described by the laws of Manson-Coffin and Basquin. The fatigue results show that the low-cycle fatigue life of the AZ31B alloy can be enhanced through ECAP. The fatigue-property improvement is discussed in light of the grain-size refinement, enhanced ductility, and texture evolution. It is also noted that in contrast to the ECAP-deformed samples, the as-received samples exhibit a pronounced anisotropic cyclic deformation behavior. The relationship between the anisotropic cyclic deformation behavior, mechanical twinning, and texture was clarified using in-situ neutron diffraction. In addition, crack initiation and propagation modes are investigated, using scanning-electron microscopy (SEM) observations of the fracture surfaces of the fatigued specimens.

Nanomechanical Characterization of Individual Nano-/Microfibers: George Sunny¹; Pankaj Kaul¹; Vikas Prakash¹; Alexis Abramson¹; ¹Case Western Reserve University

The paper reports the development of a novel nanomechanical testing device that enables highly reliable tensile testing on individual micro-/nanowires. The device features independent measurement of both load and displacement in the specimen with nanonewton force and sub-nanometer displacement resolutions. Moreover, the device is well suited for in-situ testing of micro-/nanostructures within a SEM, which permits continuous high resolution imaging of the specimen during its nanomechanical straining. The device comprises of two main parts: (a) a three-plate capacitive transducer that doubles up as an actuator and a force sensor; and (b) nanomanipulator that facilitates transportation and

positioning of nanoscale structures with nanoprecision. In order to conduct the nanomechanical tests the ends of the specimen are attached to the probe tips of the nanomanipulator and the transducer using the EBID/IBID process. The working and capabilities of the device are illustrated by presenting results of nanomechanical tensile tests on electrospun polyaniline nanowires.

Atomic Modeling of the Influence of Lead Impurities on the Stability, Structure and Mechanical Properties of Three-Dimensional Nanostructured Aluminum: Yojna Purohit¹; Seonhee Jang¹; Douglas Irving¹; Clifford Padgett¹; Ronald Scattergood¹; Donald Brenner¹; ¹North Carolina State University

Motivated by recent experimental studies by Koch and co-workers, we have carried out extensive Monte Carlo and molecular dynamics simulations of the influence of lead impurities on the structure, stability and mechanical properties of three-dimensional nanostructured aluminum. Interatomic interactions in our simulations are described by the modified-embedded atom method with parameters fit to first principles results, and microstructures are generated using the Johnson-Mehl algorithm. The simulations predict that lead wets grain boundaries in aluminum and therefore trace amounts of lead can have a strong influence on the properties of this system. To quantify these properties, extensive simulations of grain stability, grain growth, grain boundary sliding and dislocation emission in strained nanocrystalline aluminum with different grain sizes and grain boundary structures have been carried out. Results from these simulations and their implications for stabilizing and controlling the mechanical properties of these alloys will be presented.

Deformation of Nanocrystalline Hexagonal Close-Packed Metals: Mechanisms and Cryogenic Effects: Guangping Zheng¹; ¹University of Hong Kong

Nanocrystalline metals with hexagonal close packed (HCP) structure exhibit some unusual deformation behaviors compared with their face centered cubic counterparts. In this work, deformation mechanisms of nanocrystalline HCP metals are investigated by molecular dynamics (MD) and ab-initio simulations. The generalized planar fault energies are used to characterize the deformation twinning and martensitic transformation in Co and Zr during the plastic deformation processes. The anomalous increments of the mechanical strengths of nanocrystalline Co, Zr and Mg at cryogenic temperature compared with those at room temperature are analyzed based on the atomistic stress accumulations and distributions in the grain boundaries. Among the nanocrystalline HCP metals studied by MD simulations, the enhanced cryogenic strength of cobalt is more significant and can be understood by the temperature effects on the emissions of partial dislocations. The temperature-dependent interfacial stresses of these nanocrystalline samples are quantitatively compared to elucidate the deformation mechanisms at cryogenic temperatures.

Plastic Strain-Induced Grain Refinement in the Nanometer Scale in a Mg Alloy: Y.-N. Shi¹; Haiqing Sun¹; ¹Institute of Metal Research, Chinese Academy of Sciences

By means of surface mechanical attrition treatment (SMAT), nanometer scaled grains of about 32±4nm were formed in the surface layer in a single phase AZ91D alloy. TEM investigation shows that the strain-induced grain refinement process in the single phase AZ91D alloy includes three steps. At the beginning twinning dominated the plastic deformation and divided the coarse grains into finer twin platelets. With the increasing of strain, double twins and stacking faults formed and a number of dislocation slip systems were activated. As results of the dislocation slip along these systems and of the cross slips, high density dislocation arrays formed, which further subdivided the twin platelets into subgrains with storage of high strain energy. As the further increase of strain, dynamic recrystallization (DRX) occurred within the high strain energy subgrains, which led to the formation of nanometer scaled grains in the surface layer of the AZ91D samples.

Towards Functional Nanomaterials: Synthesis, Characterization, and Applications: Nanowires and Nanotubes

Sponsored by: The Minerals, Metals and Materials Society, TMS Electronic, Magnetic, and Photonic Materials Division, TMS: Nanomaterials Committee
 Program Organizers: Zhiming Wang, University of Arkansas; Alexander Govorov, Ohio University; Andrey Rogach, Ludwig-Maximilians-Universität München

Tuesday PM Room: Oceanic 5
 February 27, 2007 Location: Dolphin Hotel

Session Chairs: Dapeng Yu, Peking University; Leigh Smith, University of Cincinnati

2:00 PM Invited

Highly Emissive Nanowires Grown from Colloidal CdTe Nanocrystals: John Donegan¹; Yury Rakovich¹; Yurii Gun'ko¹; Yury Volkov¹; Nikolai Gaponik²; Andrey Rogach³; ¹Trinity College Dublin; ²Technische Universitaet Dresden; ³Maximilians Universitaet Munchen

We report the assembly of CdTe nanocrystals into nanowires using an approach that attempts to capitalize on the self-assembling properties of naturally occurring processes. CdTe nanocrystals - building blocks for the nanowires - were synthesized in aqueous solution using thioglycolic acid as stabilizer. We present details on the CdTe nanowires formation and properties, which were found to grow in a standard physiological phosphate-buffered solution, including in-situ observation of growth with a confocal microscope, FLIM and TEM imaging. The choice of proper nanocrystals concentration allowed reasonably slow growth rates and thus a controllable formation of nanowires. Once formed in solution, nanowires showed a significant degree of structural rigidity and resistance to externally applied mechanical stress. Structural integrity of nanowires in standard buffer solutions and the stability of their luminescence properties make them attractive objects for future biological and/or biomedical experiments.

2:30 PM Invited

Nanochemistry of Silicon Nanowires: Ning-Bew Wong¹; Shuit-Tong Lee¹; ¹City University of Hong Kong

Using a new synthetic approach, oxide-assisted growth, we have prepared large quantity of high-purity silicon nanowires (SiNWs) of various morphologies in a controlled manner. SiNWs typically consist of a Si crystalline core clad with an amorphous Si oxide shell. When the SiNWs are removed of the oxide shell and terminated by hydrogen, they are exceptionally stable in air. We have determined the atomic structure and electronic properties of H-terminated SiNW by STM and STS, and demonstrated the effect of quantum confinement on bandgap. In contrast, the oxide-removed and H-terminated SiNWs are surprisingly reactive in an aqueous solution, reducing many metal ions quickly to neutral metal nanoparticles. We have demonstrated an application of SiNWs as a DNA sensor. SiNWs modified with Ag nanodots were used as sensors for detection of calf thymus DNA. Surface-enhanced Raman scattering has been employed for detection which reaches an ultrasensitive limit of 10–10 mg/ml.

3:00 PM Invited

Imaging the Electronic and Vibronic States of Single Semiconductor Nanowires: Leigh Smith¹; ¹University of Cincinnati

With the development of many new techniques for fabrication or synthesis of novel nanostructures, it has become more important than ever to understand the details of their electronic structure. However, such understanding is severely complicated by the fact that as structures become ever smaller, their surface to volume ratio increases by many orders of magnitude, and so the electronic states are often dominated by structural or surface imperfections. In this talk we discuss novel optical techniques for studying single semiconductor nanowires such as CdS, InP or GaAs/AlGaAs core-shell structures. Through slit-confocal spectroscopy we are able to image single nanowires with spectral, spatial and temporal resolution as a function of temperature in order to understand their intrinsic electronic states, the nature of surface defects, and the interaction of

excitonic spins in these structures. We will discuss the implications of this research for the development of novel semiconductor nanowire devices.

3:30 PM

Concept on Superconductivity from Quantum Confinement in Nanowires: J. Zheng-Johansson¹; ¹Institute of Fundamental Physics Research

In 1998 I developed at Bristol Univ a microscopic theory of He II (JXZJ, et al., Nova Sci., 2005, and other pubs.), which includes a superfluidity mechanism underlined by the concept "quantum confinement effect" (QCE). It shows that, an effectively null viscosity results as the accessible phonon excitation states of He II, having a normal viscosity in bulk, are suppressed due to discretization and thus spanning of gaps, when He II is confined in narrow channels. The theoretical predictions for critical velocity, viscosity, and other overall properties, are in satisfactory quantitative agreement with experimental data. It is tempting to test the QCE mechanism with the electron fluids in metals. In analogy, due to QCE in narrow, nano- to micron-scale wires, the collisions of conducting electrons with scatters will be suppressed. I present here a related theoretical evaluation, and relate the concept with today's nano materials and fabrications.

3:45 PM

Formation of Self-Organized Porous Oxide Nanotubes by Anodization in Fluoride Containing Solutions: Kouji Yasuda¹; Jan Macak²; Andrei Ghicov²; Saule Aldabergenova²; Patrik Schmuki²; ¹Kyoto University; ²University of Erlangen-Nuremberg

Self-organized nano porous systems produced by electrochemical processes such as porous alumina and porous Si have in the past decade attracted much interest due to remarkable potential applications. Our group has been investigating a formation of self-organized oxide nanotube layers on valve metals (Ti, Zr, Hf, Nb, W and Ta) by anodization. By anodizing metals in fluoride ion containing electrolytes, comparably thick layers consisting of oxide nanotubes with a diameter about 20-100 nm were synthesized. Oxide nanotubes grow as a result of a competition between an electrochemical oxide formation and chemical dissolution of oxide by fluoride ions. In this presentation, we report the recent results on a formation and applications of high-aspect-ratio and self-organized oxide nanotubes for several valve metals.

4:00 PM Break

4:10 PM Invited

Investigation on ZnO Nanowires: Dapeng Yu¹; ¹Peking University

Zinc oxide is of great interest due to their excellent optoelectronic, piezoelectric and semiconducting electrical properties, such as direct wide band-gap (3.37 eV) and large exciton binding energy (60 meV). ZnO nanowires are the ideal building blocks for nanometer-scale optoelectronic devices. Our group has long been working in synthesis of ZnO nanowires using physical evaporation method exploration of the physical properties of the nanowires. In this talk I will first give a brief review of the up-date progress in investigation of ZnO nanowires, then I will summarize the synthesis, microrstructure characterization, electronic and optical property studies of the ZnO nanowires in our group.

4:40 PM Invited

Cavity QED, Nanophotonics and Quantum Communication with Atomically Doped Carbon Nanotubes: Igor Bondarev¹; ¹North Carolina Central University

This talk reviews recent theoretical efforts towards understanding the near-field electrodynamic properties of carbon nanotubes doped with single atoms (ions). The research is motivated by the progress in the growth techniques of centimeter-long small-diameter single-walled nanotubes,¹ experiments on the encapsulation of single atoms into single-walled nanotubes,² and the need for the development of materials that may host quantum coherent states with long coherence lifetimes.³ A variety of quantum optics phenomena, such as spontaneous decay and van der Waals interactions,⁴ light absorption and entanglement of atomic states,⁵ will be discussed. ¹L.Zheng et al., Nature Materials 3, 673 (2004). ²G.-H.Jeong et al, Phys. Rev. B 68,075410(2003). ³T.Brandes, Phys. Rep. 408, 315 (2005). ⁴I.V.Bondarev and Ph.Lambin, Phys. Rev. B 70, 035407 (2004); *ibid.* 72, 035451 (2005); also in: Trends in nanotubes research (NovaScience, NY, 2006). ⁵I.V.Bondarev and B.Vlahovic, Phys. Rev. B 74, xxxxxx (2006); cond-mat/0605579.



5:10 PM

Tunability of Anodized Titania Nanotubes: Role of Stress and Current – Potential Fluctuations: *Ajay Karakoti*¹; H. Koeplin²; Jochen Schneider²; Ming Su¹; Sudipta Seal¹; ¹University of Central Florida; ²RWTH Aachen

Titania nanotubes have become one of the most lucrative materials gaining attention in various aspects of engineering disciplines. It finds widespread applications in photocatalysis, sensing, biomedical and solar cell research. Anodized titania nanotubes array have shown improved performances over the conventional hydrothermal nanotubes being regularly patterned and extending over a few micron lengths. Despite this, the mechanism of such regular array of nanotubes, being different from anodized alumina, still eludes the researchers. The present paper emphasizes on the role of stress in the evolution of titania nanotubes grown on Ti thin films deposited at various bias. Any fluctuations in current density and potential were determined using potentiostatic and galvanostatic control and related to the mechanism of such regular array of nanotubes.

5:25 PM

Fractal Structure of ZnO Columns: Abil Asvarov¹; *Aslan Abduev*¹; Akhmed Akhmedov¹; ¹Institute of Physics, DSC, RAS

The influence of the gas-phase clusterization of reagents on the structure of ZnO layers, deposited on the graphite cathode by electro-arc sputtering of ZnO ceramic anode at $P(\text{Ar}) = 1000$ Pa, has been investigated. SEM investigations have shown that ZnO layers has the evident columnar structure with the fractal sign of self-resemblance. The value of the fractal dimension amounted to 2.94. XRD analysis has revealed polycrystalline structure of the deposited ZnO without preferred orientation. The nature of formation of ZnO columns can be explained by formation of three-dimensional fractals from fractal clusters according to the model of “cluster-cluster” interactions. The absence of preferred orientation in ZnO columns can be explained by low value of a mobility of clusters and zero total dipole moment of ZnO cluster. Thus the presence of clusters in the flow of reagents results in the formation of the columnar structure in ZnO layers.

5:40 PM Invited

Carbon Nanotube-DNA Nanoarchitectures and Electronic Functionality: *Cengiz Ozkan*¹; ¹University of California

Biological molecules such as deoxyribonucleic acid (DNA) possess inherent recognition and self-assembly capabilities and are attractive templates for constructing functional hierarchical material structures as building blocks for nanoelectronics. Here we report the assembly and electronic functionality of nanoarchitectures based on conjugates of single-wall carbon nanotubes (SWNT) functionalized with carboxylic groups and single strand deoxyribonucleic acid (ssDNA) sequences possessing terminal amino groups hybridized together by adopting a straightforward synthetic route. Morphological and chemical-functional characterization of the nanoarchitectures are investigated using scanning (SEM) and transmission electron (TEM) microscopes, Energy Dispersive X-ray spectroscopy (EDX), Raman spectroscopy and Fourier transform infrared spectroscopy (FT-IR). Conductivity measurements (I-V characterization) of the nanoarchitectures demonstrate negative differential resistance (NDR) with the presence of SWNT-ssDNA interfaces, which indicate a biomimetic route to fabricate resonant tunneling diodes (RTD). I-V characterization on Platinum metallized SWNT-ssDNA nanoarchitectures indicate modulation of their electrical properties, with characters ranging from a resonant tunneling diode to a resistor depending on the amount of metallization. Electron transport through the nanoarchitectures has been analyzed via calculations using the density functional theory (DFT). Our studies illustrate the great promise of biomimetic assembly of functional nanosystems based on biotemplated materials and pave new avenues towards exciting future opportunities in nanoelectronics and nanobiotechnology.

Wide Band-Gap Semiconductor Nanostructures: Session IV

Sponsored by: The Minerals, Metals and Materials Society, TMS Electronic, Magnetic, and Photonic Materials Division, TMS: Electronic Materials Committee, TMS: Nanomaterials Committee, TMS: Thin Films and Interfaces Committee, TMS: Young Leaders Committee

Program Organizers: Ashutosh Tiwari, University of Utah; Haiyan Wang, Texas A&M; Minseo Park, Auburn University

Tuesday PM

Room: Oceanic 4

February 27, 2007

Location: Dolphin Hotel

Session Chair: Renato Camata, University of Alabama

2:00 PM Invited

Self- and Artificially-Assembled ZnO Multi-Dimensional Nanostructures with Multi-Functional Properties: *Sang-Woo Kim*¹; ¹Kumoh National Institute of Technology

Self-assembled single crystalline ZnO nanodots with low-dimensional quantum characteristics were successfully synthesized on thermally grown SiO_2 layers on Si. Atomic force microscopy studies also showed that the density and size of nanodots can be easily controlled by varying the growth conditions. In order to fabricate ZnO nanodots with controlled morphology and dimension, highly ordered one- and two-dimensional ZnO-nanodot arrays were realized on SiO_2/Si substrates patterned by focused ion beam. Free exciton emission from a position-controlled single ZnO nanodot was clearly observed at room temperature. In addition, exciton-related phenomena such as biexciton emission as well as stimulated emission due to exciton-exciton scattering have been observed in nanodots and nanowires. Electrical transport properties of a single nanowire and field-emission characteristics from vertically well-aligned nanowires will be also presented. ZnO nanowall networks grown on $\text{Si}_3\text{N}_4/\text{Si}$ and $\text{GaN}/\text{Al}_2\text{O}_3$ substrates showed effective chemical sensing properties.

2:35 PM Invited

First-Principles Study of Harmonic and Anharmonic Lattice Dynamics in SiC and ZnO: *Jianjun Dong*¹; Xiaoli Tang¹; ¹Auburn University

We will present our recent calculation results of harmonic phonon frequencies and 3rd order lattice anharmonicity in wide-band-gap semiconductors such as SiC and ZnO. The calculations are based on the ab initio density functional theory (DFT) within the local density approximation (LDA). Both 2nd order harmonic and 3rd order anharmonic interatomic interactions are evaluated using an efficient real-space super-cell algorithm. Group theoretical analysis is performed to reduce computational loads. We will discuss our theoretical results in comparison with available experimental measurements of Raman frequency shifts and temperature-dependent linewidths of Raman spectra.

3:10 PM

Synthesis and Characterization of Sol-Gel Derived Ag/ITO Nanocomposite Thin Films: *Boen Houng*¹; Cheng-Ju Huang¹; Bing-Yi Hou¹; ¹I-Shou University

Silver nanoparticles embedded in tin doped indium oxide (ITO) matrix thin films were prepared by a sol-gel process. The effect of Ag concentration and annealing temperature on the structure, electrical and optical properties were investigated. Delafossite structure of AgInO_2 was found at lower annealed temperatures in all compositions and then decomposed into ITO and Ag as annealed temperatures were increased. The interconnected network of large Ag phases provides effective conducting paths that reduced the electrical resistivity of the thin films. The optical transmissions of the films are greater than 80 % in visible wavelength and show an absorption band towards to longer wavelength at higher Ag concentrations.

3:35 PM Break

3:55 PM

Schottky-Type Visible-Blind Ultraviolet Photodetector Fabricated on Bulk GaN Substrate: *Yi Zhou*¹; Jia Zhu¹; An-Jen Cheng¹; Dake Wang¹; Claude Ahyi¹; Chin-Che Tin¹; John Williams¹; Minseo Park¹; N. Williams²; Andrew Hanser²; Edward Preble²; ¹Auburn University; ²Kyma Technologies, Inc.

We report on the fabrication and characterization of vertical Schottky-type ultraviolet photodetector based on bulk n- GaN substrate. Full backside ohmic

TUESDAY
PM

contact was realized by using Ti/Al, and subsequent annealing at 850°C. Nickel target alloyed with 7% Vanadium was used for a sputter deposition of the Schottky contacts. A reduction in the dark current and an increase in Schottky barrier height were achieved by using rapid thermal annealing of the Schottky contact. Dark current as low as 0.56 pA at -10V was achieved with Schottky contact of 150 μm in diameter annealed at 300°C. Spectral responsivity measurement was made using a 150W Xe Arc lamp and a monochromator. Optical power dependent photocurrent measurement was performed using a 325 nm line of HeCd laser. UV/Visible rejection ratio was defined as the responsivity ratio at 325nm and 442nm. The device showed an excellent UV/Visible contrast and it is ideally visible-blind.

4:20 PM

Ga:ZnO Films for Transparent Electrode Applications: Vikram Bhosle¹; Jagdish Narayan¹; ¹North Carolina State University

We report on the synthesis and processing, and structure – property correlations in gallium doped ZnO films grown on (0001) sapphire and glass substrates by pulsed laser deposition. Films with varying microstructure were grown on amorphous glass by changing the pulsed laser deposition parameters, namely temperature and oxygen partial pressure. The results corresponding to these films were compared with those from epitaxial single crystal films grown on (0001) sapphire. It is shown that resistivities and transmittance comparable to epitaxial Zn_{0.95}Ga_{0.05}O films ($\rho=1.4 \times 10^{-4} \Omega\text{-cm}$, %T>80) can be achieved in the nanocrystalline films ($\rho=1.8 \times 10^{-4} \Omega\text{-cm}$, %T>80) deposited on glass by carefully controlling the deposition parameters. We have investigated and modeled the conduction mechanisms (carrier generation and carrier transport) in the novel Ga:ZnO films through detailed structural characterization, chemical analysis, and electrical and optical property measurements. The device applications based on these highly conducting and transparent films as electrodes will also be discussed.

4:45 PM

Highly Reflective and Low Resistance Cu-Ag Alloy Ohmic Contacts on p-Type GaN: Jun Ho Son¹; Jeong Hoon Lee¹; Gwan ho Jung¹; Jong-Lam Lee¹; ¹Pohang University of Science and Technology

Vertical-structured GaN-based LEDs (VLEDs) have been exploited to improve light extraction efficiency and thermal stability. In VLEDs, reflectance is a key aspect because emitted light from active regions is reflected-up from reflective ohmic contacts on p-type GaN. In this paper, new metallization scheme with high-reflectance and low-resistance has been developed for high-power VLEDs. Excellent ohmic characteristics with a specific contact resistivity as low as $\sim 10^{-4} \Omega\text{cm}^2$ were obtained by annealing the Cu-Ag/Ru contact and the high reflectance of 88% was observed at the 460nm wavelength. Synchrotron radiation photoemission spectroscopy revealed that the oxidation annealing promoted the outdiffusion of Ga atoms to dissolve in the Ag, leaving Ga vacancies. Cu prevents Ag from agglomeration and oxidation during annealing. Ru acted as a diffusion barrier for excessive oxygen incorporation into the underlying Cu-Ag layers with the transformation into RuOx. Thus, suppression of the oxidation results in the good contact resistivity and high reflectance.

5:10 PM

Growth, Characterization and Magnetic Properties of FePt Thin Films and Nanostructures Integrated with Silicon: Gopinath Trichy¹; Jagdish Narayan¹; Honghui Zhou²; ¹North Carolina State University; ²Los Alamos National Laboratory

The FePt material system, owing to applications in the high-density recording media, has generated much research interest in recent years. We report here the synthesis of epitaxial FePt thin films and FePt nanostructures on Si (100) substrates by pulsed laser deposition. Growth on Si was achieved using TiN as a template. The TiN template was used to control the epitaxy and induce L10 ordering in the FePt thin film/nanostructures. X-ray diffraction results for both the thin films and nanostructures showed presence of L10 order and a strong growth orientation along the [001] direction. TEM (transmission electron microscopy) studies confirmed L10 ordering and showed the following epitaxial relationship; FePt(001)T<001>//TiN(100)<001>//Si(100)<001>. Magnetic measurements showed that the FePt thin films and nanostructures are predominantly perpendicularly magnetized and have high values of coercivity. Room temperature coercivity for the FePt thin film was $H_c = 2250 \text{ Oe}$ and for multilayered FePt nanostructures $H_c=1650 \text{ Oe}$.

5:35 PM

Magnetoresistance, Electrical Transport and Magnetic Studies on 2D Layered Manganite System $\text{La}_{1.2}\text{Ba}_{1.8}\text{Mn}_{2-x}\text{Ru}_{1-x}\text{O}_7$: Nori Sudhakar¹; R. S. Ningthoujam²; K. P. Rajeev³; N. S. Gajbhiye⁴; Jagdish Narayan¹; ¹North Carolina State University; ²Bhabha Atomic Research Centre; ³Indian Institute of Technology; ⁴Indian Institute of Technology Kanpur

Layered manganese oxides are the important manifestation of the well-known Ruddlesden-Popper homologous series $(\text{La,A})_{n+1}\text{Mn}_n\text{O}_{3n+1}$, with the n = 2 structure showing a variety of exotic magnetic phases owing to the complex interplay among the spin, charge, orbital degrees of freedom and reduced dimensionality. They undergo a large drop in electrical resistivity in presence of a few Tesla magnetic fields, a property that is of paramount importance for the development of magnetic memory and switching devices. Here we report some of the physical properties and establish the structure property relationship for $\text{La}_{1.2}\text{Ba}_{1.8}\text{Mn}_{2-x}\text{Ru}_{1-x}\text{O}_7$ system. The average crystallite size is found to be 25 nm. Ferromagnetic to paramagnetic (T_c) transitions above the room temperature is observed in all except the highest doped Ru sample ($x=1.0$). The large values of magnetoresistance for the undoped sample at 10 K are 55% and 60% at applied magnetic fields of 5 and 10 T respectively.



General Poster Session

Sponsored by: The Minerals, Metals and Materials Society
 Program Organizer: James Foley, Los Alamos National Laboratory

Mon PM-Wed PM Room: Northern Hemisphere Foyer
 February 26-28, 2007 Location: Dolphin Hotel

Al-Cu Joining: Influence of Various Surface Treatments of Al by Laser: Vamsi Balla¹; Amit Bandyopadhyay¹; ¹Washington State University

Al-Cu combination is incompatible because they have high affinity to each other at high temperatures and produce brittle, low strength and high electrical resistance intermetallics at the interface during fusion joining. This preliminary work explores the influence of various surface treatments in successfully modifying the Al surface for joining with Cu structures, using laser in Laser Engineered Net Shaping (LENSTM). Among the various surface treatments studied, heat treatment at 150°C, 1h resulted in sound interfacial bond between Al and Cu-38wt%Ni coating at 500W laser power – lowest power reported so far for Al laser processing. Other treatments such as anodising and 550°C, 1h before Ni coating revealed excessive intermetallics and large pores at the interface. Finally an attempt has been made to evaluate solderability/brazability of coated Al with Cu structures. It is concluded that by suitably modifying the surface characteristics, the metallurgical compatibility of Al and Cu can be ensured.

Deformation Behavior of 7075 Al Wrought Alloy in the Semi-Solid State: Young-Ok Yoon¹; Shae K. Kim¹; ¹Korea Institute of Industrial Technology

7075 Al wrought alloy with good mechanical properties has been used with tendency to obtain weight-saving in aerospace, shipbuilding and transport industries. However, it generally allows low extrusion speed and low extrudability index and also causes rather high extrusion pressure when extruded conventionally. Thixoextrusion, one of the thixoforming processes, has advantages of high productivity, reduction of the extrusion pressure, extension of the die life and cost saving due to low energy consumption compared with conventional extrusion processes. Especially, thixoextrusion process is expected to be very effective for hard-to-form materials with high strength. The aim of this study is to investigate the deformation behavior of 7075 Al wrought alloy for thixoextrusion through simple compression test in the semisolid state.

Development of Trivalent Chromium Plating Electrolyte and Plating Process for Automotive Parts: Beomsuck Han¹; ¹Korea Automotive Technology Institute

Every year, end of life vehicles generate between 8 and 9 million tonnes of waste in the Community. The European Commission adopted a Proposal for a Directive which aims at making vehicle dismantling and recycling more environmentally friendly, sets clear quantified targets for reuse, recycling and recovery of vehicles and their components. Hexavalent chromium is a main substance of regulated element. Trivalent chromium baths have numerous environmental and health advantages. We are developing a functional trivalent chromium plating bath using a chromium chloride (CrCl₃) as a replacement for commercial hexavalent chromium plating bath. We investigate a functional chromium plating process using a non-toxic trivalent chromium. We compare the chromium coatings fabricated with trivalent chromium plating process with a state of art hexavalent chromium plating process.

Effects of Alumina Additions on Sintering Behavior of Ce_{0.8}Sm_{0.2}O_{1.9} Ceramics Synthesized by Pechini Method: Joo-Sin Lee¹; Kwang-Hoon Choi¹; Dat Quach²; Vladimir Kodash²; Joanna Groza²; ¹Kyungshung University; ²University of California

Ceria-based ceramics are difficult to be densified below 1550°C. In order to lower the sintering temperature, other methods such as the use of fine powders and the use of additives should be exploited. The preparation of ultrafine powder has been studied by many investigators. Only limited reports, however, are available on the densification of ceria-based ceramics by using sintering additives. In the present study the effects of alumina additions on the sintering behavior of Ce_{0.8}Sm_{0.2}O_{1.9} ceramics was investigated by the use of powders synthesized by Pechini method. Both sintered density and grain size increased with increasing additive content up to 1 mol% for Al₂O₃ addition.

However, they decreased with further addition of the additive. We will discuss the effects of Al₂O₃ additions on the sintering behavior of Sm₂O₃-doped CeO₂, with particular emphasis being placed on the variation in the sintered density and microstructure.

Effects of CaO and Ca on Oxidation and Ignition Resistance of Pure Mg: Seong-Ho Ha¹; Jin Kyu Lee¹; Hyung-Ho Jo¹; Shae K. Kim¹; ¹Korea Institute of Industrial Technology

The applications of Mg alloys are increasing due to their good properties such as low density, good castability and high specific strength. However, molten Mg and Mg alloys are easily ignited and oxidized due to their high reactivity. Many researchers have performed studies to improve ignition and oxidation resistance of Mg through alloying to Mg alloys. It is well known that Ca, though its high cost, is used to improve ignition and oxidation resistance of Mg. However, Ca is difficult to handle due to its high reactivity. It has been attempted to improve ignition resistance of Mg alloys through CaO addition. The aim of this study is to investigate ignition and oxidation behaviors of CaO or Ca added pure Mg. Pure Mg was used instead of Mg alloys to minimize the effects of other elements.

Effects of MgO-Na₂O-P₂O₅ Doping on Flexural Properties of Beta-Tricalcium Phosphate (β-TCP) Bioceramics: Robert Fleming¹; Samar Kalita¹; ¹University of Central Florida

Biomedical engineering has been advanced by the discoveries of emerging biomaterials. β-TCP is an exciting material in this category. The possibility of tailoring its resorption rate, through doping shows promise of using it creating viable controlled strength-loss osteogenic bone-grafts. It has been shown that β-TCP doped with MgO-Na₂O-P₂O₅, can help control its resorption as well as enhance sintered density by 9%, hardness by 40% and compression strength by 38%. To further explore the benefits of these sintering additives, biaxial flex tests (ASTM F-394) were performed on uniaxially compacted MgO-Na₂O-P₂O₅ doped β-TCP structures. The results demonstrated as much as a 200% improvement in flexural strength over pure β-TCP. This is a surprising and fantastic improvement on the flexural strength over pure β-TCP. XRD analyses, performed on powdered sintered structures, showed no alteration in phase purity. Biodegradation and bioactivity were assessed in simulated body fluid. This presentation will present our findings.

Examination of Thiol Adsorption on Zn-Terminated and O-Terminated ZnO Substrates: Patrick Sadik¹; David Norton¹; ¹University of Florida

ZnO has been widely studied for a myriad of uses as a transparent semiconductor, as a blue/UV LED, and as a chemical sensor for both gas and liquid phase applications. The ability to grow ZnO high surface area phases including nanowires, nanorods, and nanobelts among other has greatly increased the prospects of achieving single molecule detection. For this reason the adsorption of dodecanethiol on both Zn-terminated and O-terminated ZnO substrates has been examined using RHEED and XPS measurements for temperature increments between 25°C and 500°C. We found that on both Zn-terminated and O-terminated ZnO substrates, dodecanethiol readily adheres to the surface at temperatures in excess of 400°C with the Zn surface having the greater thiol adsorption. On both surfaces the XPS analysis shows that the thiol (-SH) moiety seemed to be largely responsible for surface adsorption.

Fabrication and Reliability Evaluation of Au-Sn Flip Chip Solder Joint: Jeong-Won Yoon¹; Hyun-Suk Chun¹; Ja-Myeong Koo¹; Seung-Boo Jung¹; ¹Sungkyunkwan University

In recent years, the use of optoelectronic packages is increasing rapidly. In these packages, solder alloys are commonly employed for mounting active devices, such as laser diodes, on the substrate of the package. Solders for bonding applications in microelectronic/optoelectronic packages are classified as soft solders and hard solders. Especially, among hard solders, eutectic Au-20wt.% Sn is the preferred alloy because of its relatively low melting point, low elastic modulus, high thermal conductivity, and high strength compared with the other solders. In addition, the flip-chip technology is generally considered the ultimate first level connection because the highest density can be achieved and the path length is shortest so that optimal electrical characteristics are achieved. The objective of this research is to evaluate the interfacial reactions and mechanical reliability of the electroplated Au-Sn flip-chip solder bump. The results on the electroplating, reflowing and bump shear testing will be presented in more detail.

Fabrication of Fe Nanoparticles by Direct Electrochemical Reduction from Fe₂O₃ Nanoparticles: Won-Kyu Han¹; Jung Ho Baik¹; So Jin Kim¹; Chung Man Choi¹; Sung Goon Kang¹; ¹Hanyang University

In this report, Fe nano particles have been prepared by direct electrochemical reduction from Fe₂O₃ nano particles and the reduction mechanism was investigated. To investigate the reduction mechanism, Fe₂O₃ has been deposited on the AISI 430 by magnetron sputtering in various Ar/O₂ ratio and the cyclic voltammetry (CV) was performed in 0.5 M NaCl solution at 300 K. This result indicated that the oxygen from the Fe₂O₃ was ionized at -1.30 V (versus SCE) and reduced to Fe. The structure of the films were analyzed by XRD, SEM/EDS and XPS.

Laser Surface Modifications of Alumina Ceramic for Applications in Precision Grinding of Materials: Sandip Harimkar¹; Narendra Dahotre¹; ¹University of Tennessee

Laser Surface modification of the ceramics is a novel technique for achieving improved surface properties. The high cooling rates associated with the laser surface processing results in the formation of various novel phases and morphology. The present study deals with the tailoring the surface morphology of the alumina ceramic with a potential application in micro-scale material removal during surface grinding of materials. Thermal effects during laser surface processing are correlated with subsequent development of the microstructural features such as crystallographic and morphological textures, grain size, depth of melting etc. Also, results of microstructure development on the grinding performance are presented.

Metal Ion Doped Beta-Tricalcium Phosphate Bioceramic with Improved Properties: Alton Davenport¹; Samar Kalita¹; ¹University of Central Florida

Recent years have seen a quest for new bioresorbable biomaterials. Beta-tricalcium phosphate (β -TCP) with excellent biocompatibility is ideal for bone-grafting. However, β -TCP suffers from poor flexural strength, poor densification and rapid *in vivo* degradation. In our research, we improved densification and flexural strength of β -TCP by introducing small quantities of divalent metal ions coupled with material-specific sintering which also controlled its degradation rate *in vitro*. High purity metal ions, known to be prevalent in the bone mineral, were introduced into β -TCP powder via ball milling. Dense structures were prepared by uniaxial pressing with green density of 1.7 g/cc and sintered at 1250°C, in air. Results showed 5-12% increase in density, 50-120% increase in microhardness and 30-100% increase in biaxial flexural strength. XRD analysis confirmed no alteration in phase purity. Biodegradation study was performed in dynamic SBF. *In vitro* assay performed, using prostate cancer cells confirmed that these materials were non-toxic.

Microstructural Characteristics and Mechanical Properties of Thixoextruded 2024 Al Wrought Alloy: Dong-In Jang¹; Young-Ok Yoon¹; Shae K. Kim¹; Hyung-Ho Jo¹; ¹Korea Institute of Industrial Technology

The 2024 Al wrought alloy has been used for a wide range of applications such as automobile and aircraft. However, extrusion process for the 2024 Al wrought alloy was not easy due to its low extrudability. Thixoextrusion, one of the thixoforming processes, has advantages of high productivity, reduction of the extrusion pressure and cost saving due to low energy consumption compared with conventional extrusion processes. Especially, thixoextrusion process was expected to be very effective for hard-to-form materials with high strength. In this paper, effects of extrusion parameter, such as extrusion temperature, speed and die bearing length, on the microstructure and mechanical properties of 2024 Al wrought alloy were interested. The thixoextrusion was carried out at 607° and 631° with extrusion speeds of 10°/sec, 20°/sec and 30°/sec. The die bearing lengths were 7° and 15°. The results of thixoextrusion experiments were compared with conventional extrusion results.

Microstructural Evolution of 7075 Al Wrought Alloy for Thixoextrusion Process: Young-Ok Yoon¹; Dong-In Jang¹; Shae K. Kim¹; Hyung-Ho Jo¹; ¹Korea Institute of Industrial Technology

The study for thixoextrusion of 7075 Al wrought alloy was carried out with respect to reheating rate, isothermal holding temperature and time with an emphasis to the effect of homogenization on thixotropic microstructures during the partial remelting. The main emphasis of this study was to investigate feasibility of microstructural control in the low liquid fraction ($f_L < 0.3$) for the thixoextrusion of 7075 Al wrought alloy without additional pretreatment. The

results show that the liquid fraction and average grain size were almost uniform with respect to isothermal holding temperature and time. It is considered very useful for thixoextrusion in terms of process control such as billet temperature control and actual extrusion time. Microstructural control of 7075 Al wrought alloy both before and after homogenization could be possible and thixotropic microstructures were obtained in both specimens.

Notch Toughness of a Cu-Based Bulk Metallic Glass: Matthew Freels¹; Peter Liaw¹; Gongyao Wang¹; ¹University of Tennessee, Knoxville

Cu-based bulk-metallic glasses (BMGs) have received much interest of late due to their high strength and low cost compared to the widely studied Zr-based BMGs. Consequently, it is important that Cu-based BMG systems be further studied and developed. In this study, the fracture toughness of (Cu₆₀Zr₃₀Ti₁₀)₉₉Sn₁ BMG was examined using the three-point bending method. Notch toughness tests were performed on an MTS servohydraulic testing machine under constant displacement rates ranging from .1mm/min. Notch radii ranged from 150 μ m to 300 μ m. Notch depth was kept constant at .45W (2.15 mm). Load versus displacement was monitored during testing. Preliminary results indicate notch toughness values calculated from the maximum load at fracture range from 35 MPa \sqrt{m} up to 65MPa \sqrt{m} . Fracture surface characteristics, as well reasons for the large variability in the data will be explored.

On the Phase Diagram and Thermodynamics of the Al-Nd-Ni System: A Combined Approach of Experiments, CALPHAD and First-Principles Calculations: Michael Gao¹; Michael Widom¹; Gary Shiflet²; Marek Mihalkovic¹; ¹Carnegie Mellon University; ²University of Virginia

A novel approach that combines critical experiments, CALPHAD modeling and first principles (FP) calculations is used to study the Al-Nd-Ni ternary phase diagram and the underlying thermodynamics. Two new ternary compounds are experimentally identified, i.e. Al₁₉Nd₃Ni₅ and Al₅NdNi₂. Based on our FP calculations, they are suggested to be isostructural with Al₁₉Gd₃Ni₅ (Pearson symbol oC108) and Al₅CeNi₂ (oI16) respectively. Other compounds that are likely stable include Al₄NdNi, Al₃NdNi₂, Al₂NdNi, AlNdNi, AlNd₂Ni₂ and AlNd₃Ni₈, whose crystal structures are suggested with FP calculations. Several compounds exhibit compositional homogeneity range via Al/Ni substitution that are measured experimentally at 773 K: Al₂Nd (~3 at% Ni); Al₃NdNi₂ (46-52 at% Al); Al₅NdNi₂ (25-28 at% Al). Based on the present experimental data and FP calculations, the complete phase diagram and the thermodynamic descriptions are determined via CALPHAD modeling. Application to glass formation is discussed in light of present study.

Phase Equilibria Study and Thermodynamic Assessment of the Al-Ce-Co System Assisted by First-Principles Energy Calculations: Michael Gao¹; Necip Unlu²; Marek Mihalkovic¹; Michael Widom¹; Gary Shiflet²; ¹Carnegie Mellon University; ²University of Virginia

This study investigates the phase equilibria of the Al-rich Al-Ce-Co system using a range of experimental techniques including melt spinning, TEM, EPMA, XRD and DTA. The glass formation range in the Al-rich corner is determined, and a partial 773 K isotherm is constructed. Three stable ternary phases are confirmed, namely, Al₈CeCo₂, Al₄CeCo and AlCeCo, while a metastable phase, Al₅CeCo₂, was discovered. Also confirmed are our previous results [Metall. Mater. Trans. A 2005;36A:3269.] that a polymorphous transformation of α/β Al₃Ce exists in the Al-Ce binary system, and that the transformation between Al₁₁Ce₃oI28 and Al₄Ce.tI10 can't be polymorphous. The equilibrium and metastable phases identified by the present and earlier reported experiments are further studied by first-principles calculations. Based on new experimental data and FP calculations, the thermodynamics of the Al-Co-Ce system is optimized using the CALPHAD method. Model calculated phase equilibria and phase boundaries conform with the present experimental results.

Porous Titanium Electrodes for Microbial Fuel Cell (MFC) Applications: David Beeler¹; Leroy Long¹; Emily Henderson¹; Daniel Young¹; Raghavan Srinivasan¹; ¹Wright State University

Microbial fuel cells (MFC) work on the principle that during metabolism certain bacteria produce electrons which can be harnessed as a source of electrical energy. This paper presents the results of a study on the production and use of porous titanium electrodes in MFC. Electrodes were produced by powder metallurgy (PM) techniques using 20 micrometer CP titanium powder,



and powders of another material as place holders. Mixtures with different titanium to place holder material ratios were cold compacted use to produce green bodies from which the place holder material was etched out. The porous compact was then sintered to produce electrodes for the MFC. Results to be presented include characterization of the titanium electrodes in terms of microstructure, specific surface area, and permeability. Results from the use of the electrodes in MFC will also be presented.

Reaction of Co Phase in the WC-Co Coatings with Molten Zinc: Byeog-Geun Seong¹; Sung-Hee Kwon²; Kyoo-Young Kim³; *Kee-Ahn Lee*²; ¹Research Institute Science and Technology; ²Andong National University; ³POSTECH

The main objective of this study is to investigate the detailed reaction mechanism of Co phase with molten zinc. Pure Co, Co-W alloys specimens were used to understand role of the phase and alloying effect. These specimens were immersion tested in Zn bath. After immersion of Co in a pure molten zinc bath at 460°C to 520°C four kinds of Co-Zn intermetallic compound layers, β_1 , γ , γ_1 , and γ_2 were formed on the Co matrix. Rate controlling step for this reaction was diffusion through β_1 compound layer and the activation energy was calculated to be 214.9 kJ/mole. Co-10%W alloy showed no W alloying effect on the reaction rate in a molten zinc bath but the reaction rates increased as W contents increase to 20% and 30%. β_1 layer was not formed on Co-20%W alloy and no stable Co-Zn intermetallic compound layer was found on the Co-30% alloy.

Recovery of Pd(II) and Pt(IV) Ions by Introducing SCN⁻ Soft Ligand with Tannin Gel: *Yoshio Nakano*¹; Yeon Ho Kim¹; ¹Tokyo Institute of Technology

We have developed a new Pd(II) and Pt(IV) recovery process from wastes such as spent catalysts or scraps, which is simple and generates little secondary waste, using tannin gel particles synthesized from condensed-tannin, ubiquitous and inexpensive natural material. We have reported that in chloride solution, Pd(II) ionic species are adsorbed onto the tannin gel particles through inner-sphere redox reaction mechanism: two-electron transfer from tannin gel to chloro-palladium(II) complexes, accompanied by ligand substitution between chloro-palladium(II) complexes and hydroxyl groups of tannin gel. In the present investigation, The intermediate step (ligand substitution) plays an essential role in the Pd(II) and Pt(IV) adsorption, because the ligand substitution rate is increased by introducing a soft ligand (SCN⁻). Addition of SCN⁻ ion to chloride solution leads to the formation of chlorothiocyanocomplexes which is more favourable for the ligand substitution with tannin gel than chlorocomplexes because of the trans-effect.

Reprocessing of Silicon Carbide-Based Inert Matrix Fuels: *Soraya Benitez*¹; Ronald Baney¹; James Tulenko¹; ¹University of Florida

Silicon carbide (SiC) is one of the prime candidates for the fabrication of ceramic based inert matrix fuels (IMF) for the burning of plutonium and for the transmutation of long-lived actinides. However, reprocessing of SiC-based IMF to separate transuranic species for both spent and unspent nuclear fuel from the SiC matrix is not well defined. A potential reprocessing method under investigation is the use of alkali and alkali earth molten salt baths to dissolve the SiC matrix. SiC samples with and without ceria will be reprocessed using the molten salt method to determinate ease of separation, dissolution rates, and resulting compounds. Ceria is used as a surrogate for plutonium and for the transuranic species.

Stress Rupture Property of Inconel 718 Alloy: *Ji Soo Kim*¹; Chong Soo Lee¹; ¹Pohang University of Science and Technology

Stress rupture properties of base metal and weldment of Inconel 718 Alloy for aerospace applications were examined in the present study. The specimens were solution heat treated according to the specification of ASM 5596, i.e., heating to a temperature of 980°C, holding at the temperature for an hour and air cooled. Afterward, precipitation heat treatment was done by heating to 720°C for 8 hours, furnace cooled to 621°C, holding at 621°C for 8 hours and furnace cooled. The test temperatures were varied from 649°C to 760°C. With the increase of test temperature, stress rupture life was shortened at the same stress ratio. The weldment was more fragile than the base metal. Detailed microstructures and fracture surfaces after the rupture test were investigated by the optical microscope and SEM.

Study of Hot Deformation Behavior of Ti-6Al-4V Alloy with Widmanstätten Microstructure by Artificial Neural Networks: N. Reddy¹; *Chan Hee Park*¹;

¹Pohang University of Science and Technology

The present work demonstrates the use of an artificial neural networks (ANN) model in generating processing maps for hot working processes for Ti-6Al-4V alloy with widmanstätten microstructure. The flow stress data for ANN model training was obtained from continuous compression tests performed on a thermo-mechanical simulator over a wide range of temperatures (700-1100°C) with the strain rates of 0.0001-100 s⁻¹ and true strains of 0.1 to 0.6. It has been found that the flow stress values predicted by the ANN model agree closely with actual experimental values, thus indicating the possibility of using neural networks approach to tackle hot deformation problems. The specimen failures at various instances have been predicted and metallurgical explanations had been presented. The flow stress predicted at finer intervals of temperature and strain rate regions and subsequently processing maps were developed. The safe domains of hot working of alloy were identified and validated through microstructural investigations.

The Effect of Composition of Carbon Fibre on the Mechanical and Morphological Properties of PA6/Carbon Composite: *Albert Ude*¹; Husna Azhari¹; ¹National University of Malaysia Bangi

A study to investigate the mechanical property-morphology relationship of polyamide 6 reinforced carbon fibre composites has been carried out. The composites were prepared by melt mixing, in a composition of wt% PA6/wt%CF; 95/5, 90/10, 85/15, 80/20 respectively. The length of the fibre was 500µm. The mechanical properties were measured. These properties were correlated to the morphology. The mechanical properties suggest that carbon fiber has the potentials to reinforce polyamide 6; hence an increase in strength recorded, displaying that strength is a function of the volume of the reinforcement (fibre). Morphological study of the tensile fractured surface showed the mechanism of failure to be the dispersed domain pulling out of a continuous matrix, leaving voids in their alert. The size of the voids seems to correspond with the size of the fibrils, making the inference that the voids observed were space left by the pulled-out fibre distributed in different direction apparently reasonable.

X-Ray Absorption near Edge Structure Analysis of Chromium Oxynitride Thin Films: *Jun Inoue*¹; Tadachika Nakayama¹; Tsuneo Suzuki¹; Hisayuki Suematsu¹; Weihua Jiang¹; Koichi Niihara¹; ¹Nagaoka University of Technology

We have already reported the hardening in Cr(N,O) thin films by the increase in the oxygen content (x). X-ray absorption near edge structure (XANES) in the thin films was observed to clarify electronic structure change associated with the hardening. The Cr(N,O) thin films were prepared by PLD method. The beam line BL-12C of PF in High Energy Accelerator Research Organization was used for XANES measurements. It was found that the ionicity between metal and nonmetal atoms has increased by replacing nitrogen atoms in CrN by oxygen atoms, since the Cr-K edge peak shift to higher energy was observed with increasing x. Furthermore, the peak attributed to the electronic transition from 1s to band that formed by 3d of metal atom and 2p of nonmetal atoms decreased with x increases. It can be understood the reason for this result is that the total valence electron density increased gradually with increasing x.

In-Situ Chemical Oxidation of Soil Contaminated by Benzene, Lead and Cadmium: Marcia Bragato¹; *Jorge Tenorio*¹; ¹Escola Politecnica-Universidade de Sao Paulo

Soil contamination by oil and its derivatives is found at many sites in Sao Paulo, Brazil. In this research, the chemical oxidation was used as remediation method for soil contaminated simultaneously by benzene, lead and cadmium simulating in-situ conditions. Tests were carried out under laboratory conditions. In the oxidation tests the efficiency of Fenton's reagent (H₂O₂/Fe⁺²) on the benzene oxidation was performed. Under the imposed oxidizing conditions lead in the lecheate increased in TLCP tests. Using the Fenton's reagent the increase of lead concentration in the lecheate was 4 times greater under natural conditions. On the other hand, cadmium presented the opposite behavior, e.g., Cadmium concentration in the lecheate was decreased 50% for the oxidizing conditions.

Development and Validation of High Performance Thick Thermal Barrier Coating (TBC) for Application on Turbine Components: *Gabriele Rizzi*¹;A. Scrivani¹; ¹Turbocoating

This paper addresses the development of thick TBC (with thickness in the range of 1.5 - 2 mm), focusing attention on the microstructure and the porosity of the Ytria Partially Stabilised Zirconia (YPSZ) coating, in relation to its resistance to thermal cycling fatigue (TCF). TBC coatings have been produced by means of a NiCoCrAlY bond coat and Ytria Partially Stabilised Zirconia top coat, both sprayed by Air Plasma Spray. The obtained samples have been characterized from the metallographic point of view in order to determine the structure and the porosity of the coating. Finally the samples have been submitted to TCF test, according to the procedure of two important OEMs. The study enabled determination of a good microstructure of the TBC coating with high TCF resistance independent of the porosity of the coating itself.

Development of CVD Overaluminising Method on Different Conicrally Bond Coats Deposited by Low Pressure Plasma Spray (LPPS), High Velocity Oxygen Fuel (HVOF) and Air Plasma Spray (APS): *Gabriele Rizzi*¹;A. Scrivani¹; ¹Turbocoating

This paper addresses the study of Aluminium coatings deposited by CVD on CoNiCrAlY bond coats deposited by three thermal spray techniques. The different CoNiCrAlY coatings structure obtained by these three techniques (Low Pressure Plasma Spray or Vacuum Plasma Spray, High Velocity Oxygen Fuel and Air Plasma Spray) with different content of oxides and porosity could affect the deposition rate and quality of the Al coatings. The obtained samples have been characterized from the metallographic point of view (porosity, thickness and structure). Al coating thickness has been taken as parameter in order to define the Al coating deposition rate on the three different CoNiCrAlY coatings. Oxidation test has been performed in order to evaluate and compare the oxidation resistance of this three different coatings.

Self-Organized Periodic Array of Single Crystal Oxide Nano Islands: *L.**Zimmerman*¹; Michael Rauscher¹; S. Dregia¹; J. Lee¹; S. Akbar¹; ¹Ohio State University

We have deposited a gadolinium doped ceria thin film on an yttria-stabilized zirconia substrate using RF magnetron sputtering. Subsequent spalling of the thin film and a high temperature anneal combine to create a periodic array of single crystal islands with regular size, shape, and distance from their nearest neighbors. The features can be used as a template to transfer the pattern to other materials of interest, with the high strength of the material allowing for superior durability and fidelity of pattern transfer. In its current form, the nanostructure may find use in manipulation of single proteins and single molecules of DNA, as well as in nanoscale analytics. We predict the ability to establish long-range periodicity in the alignment of the islands creating a regular 2D network of nanochannels. These structures represent a tunable, self-assembling, low-cost, non-cleanroom means of producing nanoscale features suitable for nanofluidic channel fabrication and numerous other applications. In this work, we discuss the conditions necessary to create the novel nanostructure, and highlight the influence of annealing on the structure features. We have performed preliminary characterization of the system to determine its intrinsic usefulness for a range of optical, electronic, magnetic, and biological nanofluidic applications. We also discuss early efforts to create nanofluidic devices based on the pattern.



A

- Abbaschian, R85
 Abdel, E250
 Abd Elhamid, M94
 Abdelrahman, M143
 Abduev, A221
 Abdulla, A70
 Abe, H253
 Abe, T209
 Abedrabbo, S55
 Abelev, G142, 193
 Abolmaali, A249
 Abramson, A219
 Abreu, A232
 Abruña, H65
 Abu-Dheir, N262
 Abu-Farha, F93
 Abu Al-Rub, R261
 Abu Leil, T257
 AbuOmar, O120
 Acharya, A44, 266, 320
 Acharya, S291
 Acoff, V50, 225, 317
 Adam, G39, 255
 Adams, B44, 96, 97, 146, 147, 199, 260, 312
 Adams, J192
 Adams, T167
 Adapa, R347
 Adessio, F133
 Adebisi, O94
 Adedokun, S88
 Adharapurapu, R133, 233, 243, 339
 Afanasyev, K155
 Aga, R83, 235
 Agarwal, A223, 274, 275
 Ager, J125
 Aggarwal, G227
 Aghion, E194, 257
 Agnew, S19, 68, 75, 92, 93,
120, 144, 169, 170, 228, 279
 Agrawal, D354
 Agren, J239, 293
 Ahluwalia, R240, 249
 Ahluwalia, S331
 Ahmad, Z274
 Ahn, B215
 Ahn, I276
 Ahn, J34, 56, 137, 148, 334, 335, 346
 Ahn, S144, 145, 190, 292
 Ahrenkiel, R149
 Ahsan, M274
 Ahyi, C62, 221
 Ahzi, S96
 Aindow, M301
 Aissa, B115
 Ajayan, P64
 Ajayi, O351
 Ajdelsztajn, L214, 358
 Ajideh, H347
 Akahori, T306
 Akamatsu, S135, 188
 Akarca, S240
 Akbar, S162, 362
 Akhmedov, A221
 Akhtar, S81
 Akihiro, S107
 Akin, I234, 302
 Akinc, M321
 Akli, L307
 Akogwu, O22
 Alaradi, E123
 Alba Baena, N185
 Albers, R189
 Alcorn, T30, 31
 Aldabergenova, S220
 Alexander, B72
 Alexander, D90
 Alexandrescu, R63
 Alexandrov, I113
 Alford, F114
 Ali, A306
 Alihossieni, H279
 Allahverdi, K350
 Allard, L282
 Allen, C82, 83, 134, 187, 248, 298, 341, 342
 Allen, T49, 151, 314
 Allison, J91, 255, 288, 292, 307, 324
 Alman, D192, 193, 198
 Almasri, A261
 almazouzi, A263
 Almer, J121
 Alonso, E60
 Alpas, A240
 Altenhof, W240
 Alven, D57
 Alvi, M69
 Alyousif, O129
 Amancherla, S169
 Ambacher, O115
 Ambrová, M173
 Amirthalingam, M346
 An, K134, 200
 An, Q294
 Anand, L88
 Andelman, T115
 Anderoglu, O211
 Anderson, I66, 103, 142, 166, 264, 290
 Anderson, M93
 Anderson, P168
 Anderson, S248
 Anderson, T33, 55, 108, 353
 Ando, D93
 Ando, T250
 André, J341
 Andre, S174
 Andreas, D88
 Andrieux, J182
 Andrus, M197
 Ang, J131, 208
 Anger, G88
 Angerer, P18
 Aning, A302
 Ankem, S348
 Annamaneni, S187
 Anopuo, O350, 353
 Anselmi-Tamburini, U358
 Antille, J283
 Antipov, E283
 Antoun, B294
 Antrekowitsch, H138, 148
 Anyalebechi, P45, 46, 97, 148, 200
 Aoki, Y208
 Apel, M240
 Apisarov, A283, 329
 Appel, F169, 212
 Appel, J108, 150
 Aprigliano, L43
 Aquino, R129
 Arafah, D55, 108, 149
 Arai, M208
 Arai, Y85
 Arakawa, K355
 Arbegast, W82, 83, 134, 135, 137,
187, 248, 298, 299, 342
 Archbold, G30
 Ardakani, M85
 Ardell, A65
 Arenholz, E146
 Ares, A45, 289
 Argon, A73
 Arias, A215
 Arin, M234
 Arkhipov, G174
 Armstrong, L281
 Armstrong, R29, 79
 Arnaboldi, S217
 Arnaud, W38
 Arnold, W29
 Aron, A194, 257
 Arroyave, R28
 Arsenaute, S224
 Arsenlis, T207
 Artemev, A239
 Artemyev, M161
 Artyukhin, A22
 Artz, E22, 23, 71, 124,
175, 176, 233, 284, 330
 Arunkumar, S301
 Asahi, R252
 Asano, S87
 Asay, J132, 243, 244
 Ashby, M38
 Asp, K239
 Aspandiar, R34
 Assadi, H86
 Asta, M84, 89, 137
 Asvarov, A221
 Aswath, P125, 249, 285
 Ataoglu, S96
 Atar, E348
 Athreya, B32
 Atwell, D195
 Atwood, R270
 Atzmon, M73
 Aude, M17
 Ausland, G81
 Austin, R295
 Averbach, R201, 207
 Avila-Davila, E336
 Avraham, S257
 Awakura, Y334
 Awang, M298
 Aydin, S35
 Aydiner, C121
 Ayer, R248
 Azevedo, K216
 Azhari, H361
B
 Baars, D57
 Babu, S292
 Bach, F166
 Backman, D256
 Bacon, D48, 201, 203
 Badarinarayan, H92, 297
 Badillo, A188, 201
 Bae, D277
 Bae, G145

Bae, J	50, 333, 335	Baxter, G	322	Bhowmick, S	234
Bae, S	276	Baxter, J	125	Bhuiya, A	110
Baek, E	223	Baydogan, M	351	Bialiauskaya, V	250
Baer, D	275	Bayles, R	247	Bianhua, H	167
Baeslack, W	83	Beals, R	40, 41, 91, 92, 143, 144, 194, 195, 257, 258, 307, 309, 350, 352	Biava, D	192
Bagnall, S	156	Bearne, G	21, 70, 123, 124, 173, 174, 231, 232, 283, 329	Bica, D	63
Bahia, H	347	Beauchemin, S	238	Bice, S	70
Bahr, D	49, 64, 166, 325, 326	Beaudoin, A	29, 280	Biegalski, M	64
Bai, J	170	Bebelaar, D	157	Bieler, T	45, 57, 68, 228
Bai, M	110	Becherer, G	323	Biener, J	224
Bai, Y	73, 133, 295, 313	Becker, C	84	Bigot, J	245
Baik, J	360	Becker, J	244	Bijun, R	175, 232, 340
Baik, S	290	Beckermann, C	84, 86, 188	Bilgram, J	188
Baird, J	20	Becquart, C	48, 100, 150, 201, 202, 263, 314, 315, 316, 355	Billia, B	85, 188
Baizhen, C	99	Becze, L	34	Billinge, S	139
Bakajin, O	22	Beeler, D	360	Bilodeau, J	296
Baker, I	76, 343	Beer, A	353	Bin, Z	282
Baker, S	160	Behrani, V	269	Binci, M	199
Bakshi, S	275	Behrens, B	166	Bing, L	46, 217, 349
Balani, K	275	Behrens, C	245	Bingert, J	26, 57
Balk, T	160, 326	Beilstein, M	81	Biol, Y	172
Balla, V	193, 250, 268, 359	Beke, D	78	Birtcher, R	356
Ballato, J	55	Belak, J	80, 336	Biswas, K	264
Balogh, L	212	Bele, E	348	Björkas, C	150
Balooch, G	125	Bellaiche, L	114	Black, W	273
Bamberger, M	257, 308	Bellis, S	176	Blanchard, P	194
Bammann, D	261	Bellon, P	201, 207	Blandin, J	257, 288, 331
Ban, Y	258, 284, 340	Belova, I	78, 293	Blawert, C	257, 259, 350
Bandar, A	170	Belt, C	55, 56, 110, 157, 209, 269, 323	Bleda, E	19
Bandyopadhyay, A	193, 250, 268, 359	Beltran, E	280	Bless, S	80
Bandyopadhyay, P	268	Bement, M	102	Bletchly, P	122
Banerjee, R	18, 25, 126, 226, 234	Ben-Artzy, A	309	Bley, F	322
Baney, R	361	Ben-Hamu, G	195, 308	Bligh, R	171
Bang, W	144, 145, 149, 150, 196, 205	Benitez, S	361	Blue, C	39
Banovic, S	19, 140	Benito, J	219	Blumenthal, B	30
Bantounas, I	349	Benkahl, B	71	Blumenthal, W	244
Bao, Y	351	Bennett, M	254	Bobrovitchii, G	129, 290
Barabash, O	247, 262	Benson, D	295	Bocher, F	43
Barabash, R	80, 191, 253	Benson, M	180	Bocquet, J	202
Barajas, A	342	Bentley, J	96	Bodde, S	71
Baranov, A	161	Benzerga, A	68, 267, 312	Bodéa, S	85
Barashev, A	201, 203	Bera, S	178	Boehlert, C	17, 49, 226, 255, 308
Barbu, A	202, 263, 264	Berezin, A	329	Boehner, A	267
Barlat, F	253	Berger, C	94	Boettinger, W	181
Barnard, B	332	Berghmans, A	54	Bogdan, S	286
Barnett, M	93, 195, 353	Berglin, R	244	Bogdanov, Y	71
Barney, I	16	Bergman, L	163	Bogges, T	269
Barpanda, P	115, 164, 279	Bergmann, A	252	Bohlen, J	145, 258
Barrera, E	117	Bernard, D	53, 228	Boileau, J	279
Barresi, J	179	Berndt, G	296	Boin, U	259
Barrett, C	156, 269	Bertram, M	333	Bojar, Z	18, 66
Barron, M	180, 227	Beshay, Y	112	Bokerman, G	94
Barry, E	26, 121, 312	Bet, S	163	Boldsaikhan, E	134, 135
Bartolo, L	40	Bettge, D	226	Bolduc, S	237
Bartsch, A	293	Betzwar-Kotas, A	318	Bonade, R	48
Baruchel, J	85, 188	Bewerse, C	249, 300	Bondarenko, V	274
Basaran, B	299	Bewlay, B	169, 322	Bondarev, I	220
Baskes, M	19, 27, 67, 69, 132, 151, 316, 356	Beyerlein, I	80, 170, 228	Bonnier, M	21
Basoalto, H	156	Bhagat, R	90	Boom, R	259
Bass, M	55	Bhandari, Y	44, 130	Boone, S	345
Bassani, J	51	Bhanumurthy, K	131, 298	Booty, M	109
Bassani, P	217	Bharathula, A	126, 177	Borg, J	183
Bassim, N	80	Bhattacharya, S	172, 302	Borgenstam, A	240
Bassler, K	140	Bhattacharyya, D	320	Borlini, M	180
Batista, E	231	Bhide, R	349	Borzenko, M	283
Battaile, C	26, 77, 130, 181, 239, 291, 327, 335, 337	Bholoa, A	202	Bose, S	193, 250, 268
Battle, T	323	Bhosle, V	116, 163, 222	Bosselet, F	182
Batwal, A	95, 250			Boteler, J	80
Baumann, J	135			Bothara, M	236
				Bottin-Rousseau, S	135



- Bouchard, P74
 Bourke, M299
 Bourne, N243, 294, 295
 Bouville, M240, 249, 291
 Bouwhuis, B17, 254
 Bove, P108
 Bower, A228, 229
 Boyanov, B238
 Boyce, B160, 244
 Boyle, K68, 228
 Bradshaw, R235
 Brady, M41, 93, 131, 145, 197,
198, 259, 260, 310, 323, 353
 Braga, C231
 Braga, R21
 Bragato, M361
 Brahme, A69
 Branagan, D358
 Brandimarte, G339
 Brandstetter, S154
 Brannon, R338
 Brenner, D216, 219, 357, 358
 Brett, D90
 Brewer, J80
 Brewer, R333
 Briceno, M48
 Bright, M75, 323
 Bringa, E29, 184, 357
 Brinley, E149
 Brinson, C248, 299
 Brito, M260
 Brockdorf, K25
 Brody, H211
 Brooks, C178
 Brooks, G97, 185
 Brooks, J156
 Brow, R24, 74
 Brown, C290
 Brown, D30, 93, 121, 134,
169, 178, 207, 248, 249
 Brown, E183, 251
 Browning, N212
 Brueckner, K115
 Bruski, R74
 Bryant, G162
 Buchanan, R23, 73, 126, 177,
178, 235, 286, 331, 332
 Buchheit, T183
 Buczek, M256
 Budhani, R164
 Buffet, A85, 188
 Bugge, M71
 Buha, J308
 Bullard, S111
 Bulut, M116, 163
 Bunin, I239
 Bunker, C114
 Burford, D83, 298, 342
 Burkins, M196
 Burris, B347
 Burton, C121
 Bus, T101
 Busby, J48, 151, 263, 315
 Busch, R235, 236, 287
 Bush, J269
 Buta, D84
 Butler, J168
 Butu, M238
 Buzunov, V244
 Byczynski, G210
- C**
- Cabibbo, M352
 Cabrera, J219
 Caceres, C210, 352
 Caceres-Valencia, P129
 Cady, C133, 243, 251
 Cai, L170
 Cai, M254
 Cai, S20
 Cai, W161, 344
 Cai, Z335
 Calder, A201
 Calin, M216
 Calinas, R275
 Camacho, Á273
 Camacho, R16
 Camata, R116, 163, 164, 176, 221, 285, 330
 Camel, D332
 Campbell, C28, 78, 131, 182, 241, 293
 Campbell, G30, 278
 Campbell, J111, 158, 159, 210, 270, 324
 Campbell, P60, 347
 Canales, A210
 Cañas, R122
 Cannova, F341
 Cao, B28, 29
 Cao, D233
 Cao, F66
 Cao, G144, 310, 350
 Cao, H310
 Cao, J217
 Cao, W230, 281, 336
 Cao, X111, 186, 187, 238
 Cao, Z70, 129, 204, 276, 277
 Captain, J94
 Cardello, J176
 Cardoso, M210
 Cargill, G246
 Caris, J250, 251
 Carlberg, T179
 Carlson, D108
 Carlton, C224
 Caro, A150, 151, 154
 Caro, M150, 151
 Caron, P155, 208
 Carpenter, J75
 Carreon, H76
 Carrier, J341
 Carter, E29, 268
 Carter, J92, 144, 258, 300
 Caruso, L31
 Casem, D141, 304
 Castro-Colin, M303
 Castro-Román, M159
 Catalina, A86
 Caton, M107, 108
 Catoor, D251
 Caturla, M203, 314
 Cavin, O47
 Cazacu, O147, 243
 Ceccaroli, B65
 Celik, O138
 Cerezo, A76
 Cerreta, E29, 30, 79, 132, 133, 138, 183,
190, 243, 250, 294, 301, 338, 348
 Cetinel, S125
 Ceyhan, U280
 Cha, P169, 287
 Chabinyk, M215
- Chada, S50, 102, 104, 151, 153,
204, 205, 264, 265, 317, 318
 Chakraborti, D163
 Chakravarthy, S36
 Chaldyshev, V217
 Champagne, E115
 Chan, C22, 181
 Chan, K28, 97, 306
 Chan, L349
 Chan, P32
 Chandler, R75
 Chandra, D43, 348
 Chandrasekar, S113, 272
 Chang, A169
 Chang, C50, 105, 154, 297, 345, 353
 Chang, E319
 Chang, H73, 177
 Chang, J282
 Chang, L66, 319
 Chang, R49
 Chang, Y152, 196, 296, 310, 322, 332, 336
 Chang-Chien, P154
 Chan Gyung, P191
 Chanturiya, V239
 Chao, H170
 Charbonneau, C90
 Charit, I260, 315
 Chartrand, P283, 329
 Chatterjee, U241
 Chaubal, M171
 Chawla, N18, 50, 204
 Chelikowsky, J291
 Chellappa, R43
 Chembarisova, R113
 Chen, B213
 Chen, C51, 66, 104, 151, 152, 153, 204,
205, 206, 246, 265, 296, 318, 330, 345
 Chen, D223
 Chen, G178, 236, 321
 Chen, H51, 115, 319, 344
 Chen, I76
 Chen, J54, 70, 95, 108, 173, 232, 344
 Chen, K49, 101
 Chen, L28, 32, 64, 77, 119, 149, 181, 198, 246,
260, 290, 296, 297, 318, 342, 343, 344
 Chen, M152, 200, 288
 Chen, P22, 176, 204
 Chen, Q276, 281, 282
 Chen, R204, 308
 Chen, S50, 60, 76, 102, 104,
133, 153, 205, 232, 243,
246, 264, 265, 296, 297, 318, 342
 Chen, T238, 289, 317
 Chen, W60, 140, 141, 206, 294, 345
 Chen, X31
 Chen, Y38, 79, 186, 187, 298, 331
 Chen, Z50, 169, 326
 Cheney, J133, 243
 Cheng, A116, 221
 Cheng, C212, 349
 Cheng, J354
 Cheng, M227
 Cheng, S215
 Cheng, T342
 Cheng, X70
 Chenggui, M233, 296
 Cheong, S349
 Cheong, Y292
 Cherukuri, B254
 Chesonis, D179

Chhabildas, L.....	338	Clausen, B.....	30, 93, 134, 169, 178, 207, 228, 248, 299	Cutler, E.....	322
Chi, A.....	89	Clements, B.....	133	Czerwinski, F.....	91
Chi, D.....	291	Clifton, R.....	294	Czyryca, E.....	306, 339
Chiang, C.....	288	Clouet, E.....	105	D	
Chiang, F.....	97	Cluff, D.....	230	D'Abreu, J.....	98
Chiang, H.....	102	Cochran, J.....	118	d'Almeida, J.....	129, 181
Chiang, K.....	43	Cockcroft, S.....	136	D'Armas, H.....	340
Chiang, L.....	259	Cocke, D.....	35	D'Souza, N.....	85
Chiarbonello, M.....	180	Cockeram, B.....	57, 110, 315	Daehn, G.....	320
Chien, W.....	348	Cohea, B.....	122	Dahle, A.....	112, 179, 194, 237, 264, 265
Chimbli, S.....	135	Cole, B.....	354	Dahotre, N.....	360
Chintalapati, P.....	159	Cole, G.....	91, 143	Dai, C.....	183
Chiu, C.....	50, 265	Coleman, P.....	208	Dai, K.....	271
Chiu, S.....	152	Collieux, C.....	76	Dai, L.....	133
Cho, H.....	56, 137, 276, 328, 334	Colligan, K.....	82, 83, 341	Dai, S.....	175, 232, 340
Cho, J.....	319, 335	Collins, P.....	26, 121, 130, 229, 255, 306, 312	Dakshinamurthy, V.....	170
Cho, K.....	97, 334	Colon, J.....	286	Dalmijn, W.....	157
Cho, M.....	104	Colvin, J.....	295	Dalton, D.....	80
Cho, W.....	257	Compton, C.....	57	Damm, E.....	190
Cho, Y.....	273	Compton, W.....	113	Dan, X.....	330
Choate, W.....	276	Comstock, R.....	295	Dandekar, D.....	80
Choi, C.....	223, 360	Conner, B.....	73	Dando, N.....	21
Choi, H.....	62, 277	Conte, F.....	346	Danielewski, M.....	28, 241, 242
Choi, J.....	119, 146, 225	Contreras, S.....	328	Daniels, E.....	158
Choi, K.....	359	Converse, G.....	124, 234	Danks, D.....	37
Choi, W.....	16, 63, 117, 164, 165, 223, 274	Conway, P.....	119	Dantzig, J.....	32
Choi, Y.....	95, 224, 225, 320	Cooksey, M.....	173, 174, 232	Dao, M.....	58
Choo, D.....	144, 145	Coombe, V.....	324	Dargusch, M.....	112
Choo, H.....	23, 24, 73, 95, 126, 127, 134, 177, 180, 189, 200, 212, 213, 215, 235, 236, 286, 287, 302, 331, 358	Cooper, R.....	194	Darras, B.....	69
Chou, H.....	342	Copland, E.....	131	Das, A.....	195, 314, 324
Chou, K.....	304	Copley, J.....	89	Das, D.....	157
Chou, Y.....	145	Cordero, N.....	160	Das, K.....	241
Choudhuri, D.....	151, 153, 204	Cordill, M.....	160, 207	Das, S.....	55, 59, 69, 70, 110, 122, 123, 157, 172, 209, 230, 269, 270, 282, 323, 327
Chowdary, K.....	81	Corine, G.....	17	Dashwood, R.....	90, 192, 321
Chrissey, D.....	284	Cortes, V.....	180	da Silva, A.....	259
Christensen, M.....	28	Corwin, D.....	229	Dassylva-Raymond, V.....	134
Christodoulou, J.....	240, 292, 307	Corwin, E.....	134, 135	Datta, M.....	351
Christou, A.....	54, 108	Costanza, G.....	339	Datta Roy, A.....	165
Chrzan, D.....	52, 207, 327	Costello, A.....	299, 302	Dauskardt, R.....	125
Chu, H.....	319	Côté, J.....	81	Davenport, A.....	360
Chu, J.....	266, 287, 288	Cotten, W.....	329	David, S.....	134, 247, 262
Chu, M.....	288	Cotton, J.....	18	Davidson, C.....	237
Chuang, H.....	206	Coughlin, J.....	50	Davies, R.....	327, 328
Chuang, T.....	305	Coulombe, P.....	22	Davis, B.....	34, 35, 87, 137
Chuang, Y.....	152	Counter, J.....	281	Davis, C.....	247
Chuanrong, C.....	107	Courtenay, J.....	75	Davisson, T.....	238
Chui, A.....	173	Coventry, G.....	156	Daw, M.....	19, 207, 327
Chumbley, L.....	76, 290	Covert, L.....	108	Dawson, P.....	147, 199, 321
Chumbley, S.....	290	Covino, B.....	111	Dawson, R.....	349
Chumlyakov, Y.....	299	Cowan, K.....	18	Day, K.....	242
Chun, H.....	359	Cowen, C.....	255	Day, S.....	43
Chung, H.....	148	Cox, A.....	110	Dayananda, M.....	182, 242, 293
Chung, K.....	186, 247	Cox, B.....	91	Daymond, M.....	20, 120
Chung, S.....	259	Cox, I.....	98	deBoer, D.....	229
Chung Ho, W.....	202	Craviso, G.....	233	Decamps, B.....	106
Chunling, Z.....	61	Crenshaw, T.....	244	de Carvalho, E.....	180
Churbaev, R.....	218	Crepeau, P.....	111, 158, 210, 270, 324	de Castro Neto, E.....	340
Churi, N.....	262	Crimp, M.....	45	Decker, R.....	195
Chuzhoy, L.....	86	Crosby, C.....	346	Deem, N.....	323
Chwa, E.....	326	Cross, C.....	260	de Fontaine, D.....	89, 192
Çiftja, A.....	323	Croy, J.....	311	Degen, C.....	259
Cimalla, V.....	115	Csoke, B.....	56	DeGraef, M.....	25, 189, 327
Cimenoglu, H.....	138, 270, 348, 351	Cuenya, B.....	353	de Groot, J.....	75
Clark, B.....	48	Cui, B.....	99	Dehghani, K.....	279
Clark, C.....	345	Cui, J.....	31, 197, 238	Deibert, M.....	198
Clark, R.....	156	Cummins, S.....	86	de Jong, T.....	158
Clarke, A.....	190, 249	Currie, K.....	143	Delaire, O.....	78, 303
Clarke, K.....	190, 295	Curtin, W.....	51, 105		
		Curtis, C.....	300		



- del Campo, A.....23
 DeLorme, R.....196
 Delos-Reyes, M.....304
 Delzer, K.....244
 Demchak, M.....354
 Demeri, M.....253
 Demirkiran, H.....125
 Demkowicz, M.....326, 356
 Demopoulos, G.....34, 87, 90
 Deng, J.....267
 Deng, X.....338
 Den Hond, R.....171
 Denisov, V.....283
 Dennis, K.....166
 de Nora, V.....283
 Denton, M.....249
 Deo, C.....316
 Deppisch, C.....205
 Derlet, P.....106
 DeRushie, C.....292
 Desai, T.....234
 Desai, V.....268
 Deschamps, A.....322
 Deschamps, J.....136
 Deshpande, S.....292
 Deslippe, J.....207
 DeSouza, E.....23
 Detor, A.....212, 291
 Deuerling, J.....234
 Deutscher, R.....304
 Devincre, B.....206, 266
 De Vries, P.....128
 DeWeese, S.....69
 Dewit, R.....38
 De Yoro, J.....23
 DeYoung, D.....74, 127, 179, 237, 288, 333
 Dezellus, O.....182, 226
 Dharmaparakash, M.....64
 Dhere, N.....33
 Dias, C.....56
 Dick, R.....121
 Dickinson, J.....254
 Didier, R.....17
 Didier, T.....17
 Diercks, D.....18, 189
 Dieringa, H.....257, 352
 Dieumegard, D.....117
 DiGiacomo, S.....340
 Dilsizoglu, B.....88
 Dimas, P.....229
 Dimiduk, D.....26, 44, 130, 160, 225, 266, 320
 Dimos, D.....101
 Ding, F.....233
 Ding, W.....47, 195, 196, 309, 353
 Ding, Y.....97
 Dinh, L.....214
 Dinsdale, A.....104
 Dinwiddie, R.....143
 Di Sabatino, M.....166
 DiSalvo, F.....65
 Dispinar, D.....111
 Ditenberg, I.....215, 218
 Ditmire, T.....80
 Divakaran, P.....232
 Do, E.....33
 Dobatkin, S.....112
 Dobesberger, H.....63
 Dobra, G.....71, 238
 Dogan, B.....280
 Dogan, O.....57, 110, 111, 335
 Dogo, H.....150
 Doherty, R.....121, 241, 280, 282, 328
 Domain, C.....201, 202, 263, 315, 355
 Donegan, J.....220
 Dong, C.....87
 Dong, H.....39, 85, 305
 Dong, J.....47, 217, 221, 309, 353
 Dong, L.....57
 Dong, P.....311
 Dong, Y.....56
 Dong, Z.....172, 275, 283
 Donner, W.....89, 139, 191, 252, 303
 Donohue, A.....160
 Doraiswamy, A.....163, 284, 285
 Dorin, R.....304
 Dosch, H.....252
 dos Santos, J.....134, 259
 dos Santos, L.....290
 Doty, H.....25, 328
 Doucet, J.....122, 171, 229, 280
 Doucette, R.....224
 Dougherty, L.....30, 133, 138
 Dougherty, S.....165
 Douglas, J.....32
 Dowding, R.....113
 Downs, T.....248
 Doye, J.....291
 Doyle, F.....165
 Drautz, R.....27
 Dregia, S.....162, 362
 Drevermann, A.....65, 135
 Drevet, B.....332
 Dring, K.....90
 Drozd, D.....286
 Drukteinis, S.....330
 Du, N.....229
 Du, W.....287, 313
 Du, Y.....57
 Duda, A.....150
 Dudarev, S.....27, 52, 202
 Duerig, T.....249
 Dufour, G.....341
 Duh, J.....102, 104, 182, 266
 Dumitrache, F.....63
 Dumoulin, S.....68
 Dunand, D.....282
 Dundar, M.....70
 Dupas, N.....21
 DuPont, J.....182
 Dupont, V.....155, 211
 Dupuis, C.....127
 Durnford, A.....278
 Durst, K.....23, 267
 Dursun, A.....88
 Durut, L.....328
 Duszczyk, J.....310
 Dutrizac, J.....238
 Dutta, I.....317
 Dutton, R.....138, 190, 250, 301, 348
 Duval, H.....128
 Duvvuru, H.....69, 199
 Duygulu, O.....176
 Duz, V.....192
 Dvorak, J.....146
 Dwivedi, D.....328
 Dye, D.....321, 349
 Dymek, S.....173
- E**
 Eakins, D.....183, 295, 312
 Earthman, J.....177, 249, 275, 347
 Eastman, J.....64
 Easton, M.....179
 Eaton, B.....285
 Eberl, C.....208
 Ebrahimi, F.....156, 225, 358
 Eckert, C.....111
 Eckert, J.....113, 177, 178, 216
 Edmonds, D.....190
 Edwards, B.....287
 Edwards, D.....315
 Edwards, H.....171
 Edwards, L.....81
 Edwards, M.....229
 Egami, T.....126, 235
 Eggeler, G.....320
 Eick, I.....296
 Eiken, J.....32
 Eisinger, N.....17
 Ekenes, M.....333
 Ekpenu, S.....317
 El-Ashry, M.....117, 345
 El-Awady, J.....96
 El-Azab, A.....267, 320
 El-Bealy, M.....289
 El-Emary, H.....289
 Elbaccouch, M.....276
 Elbarawy, K.....250
 Elboujdaini, M.....292
 Elder, K.....181
 El Ghaoui, Y.....245
 Elias, C.....233
 Eliezer, A.....92, 309
 Eliezer, D.....195, 258, 308
 El Kadiri, H.....280
 Elkadiri, H.....312
 El Khakani, M.....115
 Elle, J.....178
 Ellendt, N.....37
 Elliott, A.....53
 ElMehtedi, M.....352
 Elmustafa, A.....135
 Elsener, A.....106
 Eltgroth, M.....234
 Elwazri, A.....144
 Emamian, A.....277, 347
 Emanetoglu, N.....55
 Embree, T.....34
 Emerson, D.....81
 Engberg, G.....228
 Engelberg, D.....129
 Engelhard, M.....100
 Engh, A.....323
 Engler-Pinto Jr, C.....292
 Enright, M.....97
 Eppich, B.....25
 Epstein, S.....333
 Erdélyi, Z.....78
 Erdemir, A.....351
 Erdmann, R.....324
 Ergun, N.....302
 Erie, J.....344
 Ertekin, E.....327
 Es-Said, O.....89
 Escobar de Obaldia, E.....270
 Escobedo B, J.....159
 Escuadro, A.....58

Eskin, D.....	75, 84, 237	Fernando, G.....	274	Fratzl, P.....	72, 175
Esmaeili, S.....	230	Ferranti, L.....	244	Fray, D.....	57, 90, 110
Espana, F.....	193	Ferrasse, S.....	114	Frazer, E.....	304
Espeland, O.....	245	Ferreira, A.....	21, 129	Frear, D.....	151, 317
Espinoza Orías, A.....	234	Ferreira, P.....	224, 275	Frederick, A.....	298
Essa, M.....	123	Ferri, E.....	185	Free, M.....	34, 35, 87, 137, 166, 303, 349
Essadiqi, E.....	68, 92, 144, 258	Ferron, C.....	87	Freels, M.....	24, 178, 360
Estrada-Mateos, B.....	35	Fertig, R.....	160	Freeman, A.....	51, 302
Estrin, Y.....	178, 272	Fiedler, T.....	78	Freney, T.....	298, 342
Eugene, Z.....	30	Field, A.....	240	Fréty, N.....	180, 182
Euh, K.....	118	Field, D.....	20, 149, 170, 228, 244	Frew, D.....	294
Evangelista, E.....	352	Field, F.....	60	Freyman, T.....	72
Evans, A.....	66, 184, 185, 294	Field, R.....	190, 243, 249	Fridy, J.....	121
Evans, J.....	179	Fielden, D.....	219	Friedman, L.....	273
Evers, F.....	337	Fields, R.....	38, 140, 304	Fries, S.....	65
Evteev, A.....	78	Figueiredo, F.....	81	Frischknecht, A.....	67
Ewing, R.....	100	Figueiredo, R.....	112	Froes, F.....	39, 90, 141, 192, 254, 305, 349
Eylon, D.....	254	Fikar, J.....	202	Frohberg, G.....	293
F					
Fafard, M.....	296	Filatov, A.....	283	Froideval, A.....	95
Fagan, R.....	223	Filliben, J.....	140	Frolov, A.....	329
Fahrman, M.....	107	Filoti, G.....	63	Fromm, B.....	97
Faivre, G.....	31, 83, 84, 135, 188	Fine, M.....	138, 282	Frommeyer, G.....	18, 306, 322
Fan, C.....	236	Finel, A.....	191	Fu, C.....	27, 96, 190, 202, 344, 356
Fan, G.....	23, 24, 73, 126, 177, 212, 235, 286, 287, 331	Finlayson, T.....	136, 210	Fu, E.....	215
Fan, X.....	112	Finnigan, P.....	256	Fu, H.....	114, 313
Fan, Y.....	335	Finstad, T.....	17	Fu, L.....	212
Fan, Z.....	86, 195, 239, 313, 314, 324	Fiory, A.....	54, 55, 109, 149	Fu, N.....	334
Fang, H.....	66	Firrao, D.....	180, 339	Fu, X.....	322
Fang, J.....	211, 319	Fischer, J.....	352	Fu, Y.....	166
Fang, X.....	324	Fischer, R.....	322	Fuchs, G.....	49, 107, 322
Fang, Y.....	354	Fischer, W.....	123	Fuentes, A.....	125
Fang, Z.....	118, 197, 224, 225, 276	Fisher, J.....	342	Fujiwara, S.....	349
Fantini, D.....	245	Fitzgerald, T.....	205	Fuller, C.....	341
Fardeau, S.....	71	Fitzner, K.....	209	Fuller, E.....	278
Farias, E.....	280	Fitzpatrick, M.....	210	Fuloria, D.....	228
Farias, S.....	22	Fjær, H.....	172, 237	Fultz, B.....	78, 303
Farid, M.....	232	Flandorfer, H.....	104, 105	Funato, M.....	162
Farkas, D.....	51, 105, 154, 155, 206, 260, 266, 271, 320, 337	Flaud, V.....	180	Funkhouser, C.....	168
Farmer, J.....	43	Fleck, C.....	258, 351	Fuoss, P.....	64
Farrar, C.....	102	Fleck, N.....	38	Fuqiang, A.....	224
Faruqi, M.....	300	Fleming, R.....	359	Furnish, M.....	338
Faulkner, R.....	203, 315	Flicker, J.....	16	Furuya, K.....	100
Faupel, F.....	293	Flinn, B.....	72	G	
Fechner, D.....	259	Florando, J.....	320	Gabb, T.....	52, 106, 107, 155, 156, 208, 268, 321
Fecht, H.....	235, 286, 306, 358	Flores, K.....	126, 156, 177, 187, 331	Gabbitas, B.....	255
Felderman, E.....	119	Floro, J.....	338	Gaboury, A.....	22
Feldman, A.....	354	Focht, E.....	339	Gadalla, M.....	300
Felicelli, S.....	46, 270, 280	Foecke, T.....	19, 140	Gadd, D.....	124
Fellner, P.....	173	Foiles, S.....	67, 84, 130, 338	Gagne, J.....	341
Feng, C.....	36, 247, 248	Foley, J.....	38, 359	Gaies, J.....	240
Feng, G.....	53	Follstaedt, D.....	130, 357	Gajbhiye, N.....	164, 222
Feng, Q.....	52, 106, 155, 156, 208, 268, 321	Foltz, J.....	300, 346	Galarraga, R.....	122
Feng, S.....	58, 59, 203	Fonda, R.....	247, 248	Galenko, P.....	86
Feng, Y.....	174	Fong, D.....	64	Gall, K.....	160, 161, 299
Feng, Z.....	134, 247, 262, 345	Fong, H.....	125	Gallardo, E.....	148
Fenske, G.....	351	Fong, J.....	140, 253	Gallino, I.....	236
Fenske, J.....	48	Foosnaes, T.....	30, 81, 340	Gallon, J.....	353
Fenton, J.....	93	Forrest, D.....	247	Galuszka-Muga, B.....	197
Fenwick, W.....	345	Forrest, M.....	184	Galvani, C.....	144
Feret, F.....	173	Forté, G.....	229	Gamweger, K.....	128
Ferguson, I.....	345	Fortin, S.....	229	Gan, J.....	151
Fergusson, L.....	230	Fourment, L.....	134	Gan, W.....	247, 248
Ferkel, H.....	58	Fox, S.....	141	Ganapathysubramanian, B.....	19, 99
Fernandez-Baca, J.....	46	Fragner, W.....	66	Gandy, D.....	247, 262
Fernandez Lisbona, D.....	31	Frank, I.....	30	Gang, X.....	61
		Frank, S.....	81	Gang, Z.....	186
		Franke, O.....	23, 267	Gang-chun, Y.....	46
		Frankl, B.....	82	Gangopadhyay, A.....	235
		Fraser, H.....	26, 77, 121, 130, 160, 199, 217, 226, 229, 234, 255, 306, 312		



- Gannon, P.....198
 Gansemer, T.....179
 Gao, B31, 238
 Gao, D256
 Gao, F104, 152, 314, 316
 Gao, H159
 Gao, J28, 214
 Gao, M26, 27, 227, 354, 360
 Gao, P239
 Gao, W351
 Gao, X60, 311
 Gao, Y23, 73, 98, 99, 103, 126, 177, 197, 207,
235, 251, 264, 286, 288, 313, 331, 337
 Gaponik, N.....61, 220
 García-García, O159
 García-Ramos, E.....35
 Garg, A107, 189
 Garimella, N.....131, 242, 260
 Garkida, A137
 Garlea, E95
 Garlick, R269
 Garmestani, H44, 70, 96, 97, 146,
199, 260, 310, 312, 330
 Garofalini, S.....18
 Garvin, J.....136
 Garza, K176
 Gascoin, F335
 Gaustad, G.....270
 Gauthier, C288, 341
 Gavrila, L63
 Gawde, P.....131
 Gay, H245
 Gayda, J.....107
 Gayden, X187, 298
 Gayle, F.....140
 Gebelin, J324
 Gebhardt, U.....252
 Gecim, K35
 Gell, M223
 Gella, V87
 Gelse, K.....23
 Gemein, R81
 Genau, A189
 Genc, A226
 Gendre, M.....245
 Gengwei, J.....355
 George, Y307
 Georgelin, M85, 136
 Gerberich, W.....154, 160, 207, 325
 Gerdemann, S.....192, 193, 254
 Gerger, A108
 Gerken, J147
 German, R.....19, 142
 Gerosa, R.....180
 Gertsberg, G.....194
 Gesing, A158
 Ghali, E292
 Gharghour, M.....309
 Gheewala, I100
 Gheorghe, I.....172
 Ghicov, A.....220
 Ghidini, A.....180
 Ghoniem, N.....96
 Ghosh, A.....195, 279
 Ghosh, D339
 Ghosh, K241
 Ghosh, S.....44, 96, 130, 170, 199
 Giannuzzi, L.....25, 26
 Gianola, D.....211
 Gibson, L.....72
 Gikling, H71
 Gila, B108
 Gill, A129
 Gill, D65
 Gilman, J.....267, 302
 Gimazov, A.....219
 Glade, S.....316
 Glavicic, M212
 Gleeson, B.....54, 131, 208, 259, 268
 Glicksman, M.....25, 26
 Glosli, J336
 Gloter, A.....76
 Glotzer, S40
 Gnaepel-Herold, T304
 Gnauk, J18
 Goddard, W227
 Godet, S.....92
 Goede, F245
 Goeken, M.....267
 Goesele, U.....246, 297
 Goettert, J.....285
 Gökken, M23
 Gokhale, A.....25, 44, 75, 128, 179,
238, 254, 277, 289, 309, 334
 Golchert, B.....56
 Goldenfeld, N.....32
 Goller, G.....234, 302
 Golmakani, H.....147, 301
 Golovashchenko, S122, 313
 Golovin, I276
 Golubov, S.....201, 316
 Gomes, J.....35
 Gómez, A.....34
 Gomez, G244
 Gomez, J200
 Gómez-Briceño, D263
 Goncalves, C137
 Gong, Y98, 115
 Gonzalez, A.....200
 Gonzalez, G.....180
 Gonzalez, J.....174, 227
 Gooch, W196
 Goodwin, P.....244
 Goorsky, M154
 Gopalan, V64
 Goranson, G193
 Gorantla, M.....345
 Gorantla, S25, 74
 Gordon, B.....167, 168
 Gordon, P52, 327
 Goren, T242
 Gornostyrev, Y51
 Gorny, A308
 Gorokhovskiy, V198
 Gösele, U246, 296
 Goswami, R.....17
 Goto, M.....252
 Gouda, K117
 Gough, N.....307
 Gourlay, C194, 264, 265
 Gouttebroze, S.....172
 Govender, J81
 Govier, B244
 Govorov, A.....60, 114, 161, 162, 220, 273
 Goyal, D331
 Grabis, J252
 Graczyk, D284
 Grady, D79, 132, 183
 Graeb, H.....75
 Graham, R.....79
 Graham, W183
 Granasy, L31
 Gránásy, L32
 Grant, B.....322
 Grant, G.....187, 298, 327, 328, 342
 Gravier, S288
 Gray, G29, 30, 79, 132, 133, 183,
243, 244, 251, 294, 295, 338
 Green, N.....278
 Greenfield, S340
 Greer, A.....104, 153, 177, 205, 265, 318
 Greer, J161, 215
 Gregori, F.....218
 Gregory, E.....100
 Gregory, J60
 Greif, R33
 Greiner, C23
 Grey, C26
 Griesche, A.....293
 Griffin, J159
 Griffin, R351
 Griffiths, J210, 352
 Griffiths, W112, 324
 Grimes, R356
 Grimm, T.....57
 Gripenberg, H.....75
 Gritsko, V329
 Groeber, M44, 130
 Groebner, J309
 Groening, O.....117
 Gröger, R.....51
 Grong, Ø172
 Gross, S145
 Groza, J99, 182, 251, 359
 Grummon, D300, 346
 Grundy, A336
 Grunschel, S294
 Grunspan, J123
 Gruss, D37
 Gschneidner, K.....207
 Gu, G292
 Gu, S171, 280
 Gu, Y42
 Guan, Y288
 Guang-Chun, Y349
 Guang-chun, Y46, 217
 Guangchun, Y.....119, 275, 345
 Guangfeng, L165
 Guanghui, L142
 Gudbrandsen, H30
 Guduru, R.....317
 Guenther, B226
 Guerdoux, S134
 Guerin, M.....187
 Guillot, J128
 Guimazov, A273
 Gulians, E114
 Gul Karaguler, N.....125
 Gulluoglu, A96
 Gun'ko, Y220
 Gunderov, D213, 215
 Gungor, M39, 90, 141, 192, 254, 305, 349
 Gungormus, M125
 Gunnarson, A.....254
 Gunyuz, M351
 Guo, D239
 Guo, F50, 102, 103, 110,
131, 151, 204, 264, 317
 Guo, J38, 262, 301
 Guo, X28, 100, 118

Guo, Y	258	Hao, Y	306	Hennig, R	77, 189	
Guo, Z	111, 145, 172, 194, 205, 231, 288	Haon, C	332	Henriksen, B	237	
Guorong, H	311	Hara, S	98	Henriksen, P	36	
Gupta, A	163	Harada, H	53, 54, 131, 156, 157, 208	Heong Ryeal, Y	138	
Gupta, G	94	Haraya, K	98	Her, E	319	
Gupta, H	72	Harder, D	72	Herbert, E	129	
Gupta, N	168	Hardie, G	283	Heringer, M	82	
Gupta, S	33, 163, 217, 345	Hardy, J	146	Herlach, D	86, 136	
Gupta, V	75, 111	Hariharan, S	164	Herling, D	187, 298, 342	
Gupta, Y	244	Hariharaputran, R	120	Hermans, M	346	
Gurov, A	213	Harimkar, S	360	Hernández-Mayoral, M	203, 263	
Guruprasad, P	68, 267	Harish, K	98	Herrera-Trejo, M	159	
Guruswamy, S	166, 276	Harjunmaa, A	355	Herrero, A	108	
Gusberti, V	124, 174	Harley, B	72	Heyrman, M	283	
Gusev, A	185, 329	Haro Rodriguez, S	328	Hezeltine, W	34	
Gustafsson, M	174	Harper, D	39	Hibbard, G	17, 254, 348	
Guthrie, R	288	Harrell, G	122	Hickman, Z	161	
Gutierrez, I	114	Harrell, J	164	Higashi, K	259	
Gutierrez-Mendez, M	336	Harringa, J	103, 264	Higuchi, K	306	
H					Hilgraf, P	22
Ha, S	258, 319, 359	Harrington, W	122	Hin, C	316	
Haarberg, G	30	Harris, K	53	Hines, J	64, 91, 166	
Haataja, M	131	Harris, S	279	Hioki, S	83	
Haberl, A	74	Harry, P	341	Hirai, M	161, 344	
Habermeier, H	252	Hart, G	26, 27	Hiralal, I	171	
Habingreither, R	300	Hart, J	179	Hirano, S	247	
Hackenberg, R	137, 249	Hartley, C	44	Hirasawa, S	297	
Hackett, M	95	Hartmann, H	86	Hirata, K	32, 33	
Haeni, J	64	Hartwig, J	85	Hiroshi, H	107	
Hafez Haghighat, S	202	Härtwig, J	188	Hisatsune, K	229	
Hafok, M	218	Hartwig, T	57	Hiskey, J	349	
Hagelstein, K	59	Hashikawa, T	87	Hitchcock, M	314	
Hagen, E	90	Hashimoto, N	66	Hixson, R	243	
Hagen, M	245	Haslam, J	43	Ho, C	50, 151, 153, 204	
Hagie, S	187	Hassan, A	300	Ho, K	84	
Hagiwara, R	304	Hathcock, D	292	Ho, P	246	
Haigang, D	142	Haupt, T	256	Ho, T	331	
Haiyan, Y	281	Hawkins, J	54	Hoagland, R	211, 215, 326, 356	
Haiyan, Z	47	Hawley, M	64	Hoang, T	148	
Hajra, J	291	Hawreliak, J	29	Hobbs, R	53	
Halley, J	291	Hayes, C	101	Hoc, T	206	
Hallstrom, S	293	Haynes, A	209	Hodge, A	22, 71, 124, 175, 176, 224, 233, 278, 284, 330	
Halsey, C	52	Hazel, B	209	Hodgson, P	125, 184	
Hamed, M	112, 300	He, H	338	Hoelzer, D	27, 96, 317	
Hamer, S	127, 237	He, J	87	Hoffelner, W	95	
Hamilton, C	173	He, K	190	Hofman, G	132	
Hammerberg, J	244	He, M	50, 317	Hogan, T	59	
Hammond, C	60	He, S	332	Hoglund, L	293	
Hamza, A	224	He, W	20	Hohsen, M	143	
Han, B	218, 272, 359	Hebert, R	25, 278	Holby, E	93	
Han, C	346	Hecht, U	135	Holleis, B	138	
Han, D	34	Hector, Jr., L	258	Holm, E	65, 67, 130	
Han, E	143, 308	Hector, L	105	Holmedal, B	68	
Han, G	56, 118, 137, 225, 334	Heguri, S	87	Holmes, D	307	
Han, H	91, 103, 154, 186, 233	Heidloff, A	54	Holroyd, J	146	
Han, K	98, 99, 290, 302	Heilmaier, M	118	Holt, J	22	
Han, L	310	Hein, M	115	Holt, R	20, 120	
Han, Q	46, 98, 143, 261, 262, 307, 313, 354	Heinisch, H	314	Homley, G	124	
Han, S	103, 252, 275	Heinze, J	59	Hon, M	18, 51, 206, 318	
Han, W	360	Hellmig, R	178	Hong, C	272	
Han, X	100	Hellstrom, E	26	Hong, K	26, 51	
Hanbicki, A	17	Helmick, D	310	Hong, S	83, 94	
Hanlon, A	86	Helminck, R	106	Hong, Y	121	
Hanrahan, R	42, 94	Hemker, K	44, 208, 211, 243, 312	Hono, K	352	
Hansen, E	120	Hemptenmacher, J	226	Hoon, K	138	
Hansen, N	121, 211	Henderson, E	360	Hopkins, M	124, 176	
Hanser, A	62, 221	Henderson, R	75	Horita, T	260	
Hao, H	102	Hendricks, T	276	Horita, Z	59, 271	



- Horstemeyer, M19, 20, 121, 169,
170, 256, 280, 309, 312
- Hort, N257, 259, 350, 352, 353
- Horton, J.....247
- Hosegawa, A38
- Ho Seop, S138
- Hoshino, S.....56
- Höskuldsson, G231
- Hosokawa, Y110
- Hotaling, N.....132
- Hou, B221
- Hou, G135
- Hou, M165, 202
- Houghton, B.....74
- Houng, B221
- House, J.....243
- Houston, D194
- Houze, J.....19
- Hovanec, C.....121, 241, 328
- Hovanski, Y.....39, 141
- Howard, S187, 248, 299, 302
- Hoyer, J23
- Hoyt, J31, 83, 84, 101, 135, 188, 337
- Hryn, J55, 110, 157, 209, 269, 284, 323
- Hsia, K159, 208, 268
- Hsiao, C.....50, 265
- Hsiao, H206
- Hsiao, L104
- Hsieh, G34
- Hsieh, H331
- Hsieh, K153
- Hsiung, L30, 72
- Hsu, C153, 297
- Hsu, E144, 323
- Hsu, F159
- Hsu, T102
- Hsu, Y152
- Hu, G311
- Hu, H143, 172, 281, 310
- Hu, J197, 354
- Hu, S27, 67, 69, 343
- Hu, X31, 186, 238
- Hu, Z126, 286
- Hua, D61
- Hua, F205, 317
- Hua, L355
- Huang, B332
- Huang, C206, 221, 324, 354
- Huang, E180, 189
- Huang, F208, 339
- Huang, H343
- Huang, J58, 59, 117
- Huang, K337
- Huang, L21
- Huang, M22
- Huang, P182
- Huang, S.....22
- Huang, T.....227
- Huang, X.....121, 137, 138, 211, 355
- Huang, Y153, 257, 290, 353
- Huang, Z32, 119
- Hubbard, C46, 95, 134, 200
- Hubbard, F333
- Hubbard, J.....253
- Hudanski, L.....117
- Hudson, L.....238
- Huey, B16
- Hufnagel, T288
- Hugron, I71
- Huh, J51
- Hui, X99, 236
- Hulbert, D358
- Hults, W137
- Hung, F181, 290
- Hung, L105
- Hunt, F92, 297
- Huo, Y281
- Husseini, N.....156
- Hutchins, C272
- Hutchinson, J.....294
- Hvidsten, R232
- Hvistendal, J.....237
- Hwan Cha, Y.....327
- Hwang, B74, 191, 213
- Hwang, D214
- Hwang, J25, 137, 138, 238,
289, 290, 328, 334, 355
- Hwang, R101
- Hyers, R86, 235, 255, 302, 307
- Hyland, M173
- I**
- Iadicola, M19
- Ibrahiem, M.....340
- Ibrahim, I250
- Ice, G80, 192, 229, 253
- Idzerda, Y146, 198
- Ienco, M180, 339
- Iffert, M231
- Ikeda, M255
- Ikemoto, Y.....32, 33
- Iliescu, D76
- Imai, H53, 157
- Imam, M.....39, 90, 141, 192, 254, 305, 349
- Inal, K92
- Inman, D90
- Inoue, A.....24, 74, 178, 286
- Inoue, J361
- Inoue, K.....209
- Inzunza, E296
- Ipser, H104, 105, 318
- Irons, G98
- Irving, D216, 219
- Isac, M288
- Isheim, D.....138
- Ishida, H289
- Ishida, K.....104, 204, 265
- Ishikawa, N88, 100
- Ishitsuka, M.....98
- Islam, Z139
- Islamgaliev, R218
- Ismail, A250
- Itapu, S298
- Ito, K32, 33, 246
- Itoh, Y306
- Ivanisenko, J358
- Ivanov, K.....213
- Ivanov, M213
- Ivanov, V283
- Iyer, A33
- Iyoda, M56
- Izumi, T54
- J**
- Jablonski, P145, 198, 335
- Jackman, J144
- Jackson, E80
- Jackson, J167, 225
- Jackson, M90, 321
- Jacobsen, L.....39, 141
- Jacot, A32
- Jagadish, C273
- Jahazi, M187
- Jain, A68, 92, 93
- Jain, M172
- Jain, P321
- Jakobsen, B267
- Jallu, K300
- James, A311
- James, M316
- Jana, S342
- Janardhan, G347
- Janes, J177
- Jang, B94
- Jang, D360
- Jang, G104, 250
- Jang, J49
- Jang, S55, 108, 216, 219
- Jang, Y252
- Jankowski, A78, 295
- Janssens, K.....18, 67, 119, 168, 227, 278, 327
- Janz, A309
- Jao, C153
- Jaques, A132
- Jaradeh, M179
- Jaramillo, D191
- Jaramillo, R.....46, 47, 262
- Jarmakani, H357
- Jarvis, D158
- Jasak, H307
- Jasthi, B248, 299
- Jata, K82, 134, 186, 247, 297, 341
- Jawahir, I70
- Jayaraman, T166, 276
- Jee, K204
- Jeedigunta, H.....274
- Jelinek, B.....19
- Jenkins, M151, 202
- Jensen, M173
- Jensen, N102
- Jeon, Y273
- Jeong, C335
- Jeong, J34
- Jeong, S337
- Jeong Hoon, K138
- Jha, G69
- Jha, M34, 87
- Jha, S107, 108, 350
- Ji, C296
- Ji, H144, 194
- Ji, L165
- Ji, S195, 324
- Jia, N213
- Jia, Z164
- Jian, L47
- Jiang, D50, 265, 272, 358
- Jiang, F127, 133, 243, 287, 331, 339
- Jiang, H57, 331
- Jiang, L92, 215, 242, 273
- Jiang, W23, 73, 100, 126, 177,
235, 237, 286, 288, 331, 361
- Jiang, Y246, 351
- Jianguo, W341
- Jianping, P341
- Jianzhong, C313
- Jiao, Z315
- Jie, L61, 185, 186
- Jihong, M296
- Jimack, P85

Jin, C	55, 109, 163	Kahler, D	54	Kawakita, H	209
Jin, H	326	Kai, W	331	Kawasaki, M	112
Jin, L	196, 231	Kainer, K	41, 145, 195, 257, 258, 259, 350, 352	Kaya, A	67, 176, 350
Jin, M	325	Kainuma, R	204, 265	Kaya, G	67
Jin, S	117, 175	Kakarlapudi, P	110	Kaya, R	176
Jin, X	61, 114	Kakkar, B	296	Kayal, S	284
Jin, Y	343, 344	Kalagara, S	298	Kayali, E	138, 270, 348, 351
Jing, J	98	Kalay, E	290	Kazakov, S	283
Jing, P	216	Kale, G	131	Kazakov, V	171
Jing, Y	341	Kalgraf, K	173	Kazuo, F	148
Jinhong, L	329	Kalidindi, S	69, 121, 199, 200, 280, 328	Kazykhanov, V	218
Jintakosol, T	17	Kalisvaart, P	197	Ke, F	73
Jo, H	196, 258, 328, 359, 360	Kalita, S	124, 176, 346, 359, 360	Keckes, L	113, 243
Jo, Y	103	Kalu, K	20	Keiser, D	131, 132
Joannopoulos, J	337	Kalu, P	47, 69	Keles, O	70
Jodoin, B	358	Kalya, P	135	Kelley, J	37
Jody, B	158	Kamaya, M	20	Kelly, R	229
Jog, J	223	Kamikawa, N	211	Kelly, S	127
Johannes, J	101	Kammer, D	189	Kellsall, G	349
Johannesson, B	210	Kampe, S	17, 168, 277, 278, 302	Kelson, I	154
Johansson, A	75	Kan, H	186, 284, 340	Kelton, K	24, 235
John, G	64	Kandukuri, S	83	Kendig, K	17, 65, 118, 167, 225, 226, 277
John, R	107, 350	Kane, R	124, 234	Kenik, E	218
Johnson, C	198, 260, 333	Kaneko, Y	83	Kennedy, M	326
Johnson, D	29, 77, 192	Kang, B	54, 62, 108	Kenny, S	19, 100, 202
Johnson, J	30, 81, 185, 244, 296, 340, 341	Kang, C	150, 205, 335	Keppens, V	286
Johnson, M	72, 86	Kang, D	145	Ker, M	319
Johnson, S	18, 66	Kang, H	50, 118, 194	Kessler, M	156
Johnson, W	23, 24, 54	Kang, J	172, 190, 227	Kessler, O	37
Jolly, M	159, 270, 278	Kang, K	191	Kettner, M	60
Joly, L	202	Kang, M	257	Khachaturyan, A	189
Jonas, J	92	Kang, S	16, 32, 50, 63, 102, 104, 117, 118, 151, 164, 186, 204, 223, 264, 274, 317, 319, 343, 344, 360	Khan, H	97
Jones, H	247	Kao, C	50, 105, 152, 204, 246, 296, 297	Khomami, B	287
Jones, J	92, 156, 292, 307, 348	Kaoumi, D	356	Khraisheh, M	69, 93, 262, 327
Jones, T	196, 277	Kapoor, R	285	Khramov, A	173, 329
Jones, W	108, 310, 352	Kapustka, N	187	Khurana, S	248
Jong Gu, B	191	Kar, A	163, 233	Kieft, R	74, 127, 179, 237, 288, 333
Jonker, B	17	Kar, S	63, 169	Kiggans, J	39
Joo, J	319	Karabelchtchikova, O	183, 290	Kilmametov, A	358
Joo, Y	104, 153, 205, 265, 318	Karaca, H	299	Kim, B	97, 204, 272, 273
Jordan, E	223	Karakoti, A	149, 221, 275	Kim, C	54, 149, 150, 186, 199, 205, 247, 252
Joshi, S	113, 216	Karaman, I	119, 193, 228, 272, 299, 300	Kim, D	73, 145, 148, 177, 186, 196, 257, 265, 307
Joung, J	63	Karanjai, M	23	Kim, H	58, 79, 126, 176, 272, 273, 285, 330, 335, 344
Joyce, J	140	Karczowski, K	18	Kim, I	144, 145
Józef, J	177, 235, 286	Kardokus, J	114	Kim, J	40, 64, 85, 94, 104, 128, 146, 148, 154, 169, 180, 186, 197, 204, 265, 300, 335, 361
Józwia, S	18	Kar Gupta, R	278	Kim, K	33, 153, 287, 361
Jozwik, P	66	Karma, A	32, 188	Kim, M	34, 204, 301
Ju, S	16	Karradge, M	322	Kim, N	70, 74, 145, 191
Juarez, J	180	Karthikeyan, J	269	Kim, S	16, 19, 70, 83, 138, 186, 188, 196, 221, 252, 258, 317, 328, 335, 345, 353, 359, 360
Juhas, M	342	Kaschner, G	170	Kim, T	333
Jun, B	63	Kashyap, B	23	Kim, W	145, 177, 188, 202, 257, 307, 353
Jun, H	248, 332	Kasper, N	252	Kim, Y	42, 73, 74, 132, 143, 178, 180, 213, 225, 266, 276, 287, 290, 292, 361
Jung, C	188	Kassner, M	215, 273, 304	Kimura, A	151
Jung, G	222	Katgerman, L	75, 84, 237, 310	Kimura, H	110, 210, 334
Jung, H	85, 143, 188, 319	Kato, C	81, 245	King, A	78, 79, 113
Jung, I	144, 145	Kato, H	24	King, B	324
Jung, S	50, 265, 266, 318, 319, 359	Katoh, Y	100, 101	Kinosz, M	111
Junxia, D	230	Katsman, A	308	Kioseoglou, G	17
Junzo, F	107	Katz, J	90	Kirchain, R	60, 270
Jurczyk, M	224	Kaufman, J	123, 230, 270	Kirchheim, R	211
Juretzko, F	231	Kaufman, M	18, 25, 126, 189, 226, 328	Kirishima, A	138
Jurisová, J	173	Kaufmann, H	194	Kirk, M	151, 202
Juslin, N	150	Kaul, P	219	Kirkland, S	69
Juul Jensen, D	20	Kawabata, K	353		
		Kawabata, T	142		
		Kawagishi, K	54, 131, 157, 208		
		Kawakami, M	142		
		Kawakami, Y	162		

K

Kacprzak, D	174
Kad, B	71, 218
Kadkhodabeigi, M	175



- Kishimoto, H260
 Kishimoto, N60
 Kisner, R46, 47, 262
 Kiss, L134, 237, 283
 Ki Sub, C138
 Kitamura, T337
 Kitashima, T54
 Kityk, I61
 Kjar, A122
 Klammer, G60
 Klarstrom, D180, 271
 Klaver, P27
 Klett, C171
 Klette, H17
 Klimenkov, M315
 Klingensmith, D264, 316
 Klinger, L283
 Klinov, D161
 Klose, F46
 Klueh, R66, 151
 Klug, K305
 Knap, J155
 Knapp, J357
 Knepper, R160
 Knezevic, M199, 200
 Knipling, K248, 282
 Knittel, K308
 Knott, S105, 318
 Knuteson, D54
 Ko, S294
 Ko, Y214, 218
 Kobayashi, T53, 208, 243
 Koch, C59, 272, 358
 Koch, K82, 191, 342
 Kocharian, A274
 Kockar, B300
 Kodash, V99, 182, 251, 359
 Koduri, S26, 121, 130, 229, 312
 Koenigsmann, Z53
 Koepflin, H221
 Koepffel, B146
 Koh, S63, 223, 274
 Koike, J33, 93
 Koike, M306
 Koizumi, Y53
 Kokawa, H247
 Kolesnikova, A160, 217
 Kolli, P138, 139
 Kolobov, Y213, 218
 Kon Bae, L138
 Kondo, M70
 Kondo, S100, 101
 Kondo, T55
 Kondoh, K353
 Kong, C272
 Kong, M216
 Konitzer, D52, 106, 155, 208, 268, 321
 Kontsevoi, O51, 302
 Koo, J318, 359
 Kooptarnond, K56
 Kopka, L91
 Koppitz, T145
 Kordes, M161
 Korinko, P167
 Kornev, I114
 Korshunov, A214, 216, 217
 Korzekwa, D30, 243
 Korznikova, E113, 213
 Koss, D306
 Kostorz, G191
 Kothari, D231
 Kotov, N161
 Kou, S144, 310
 Kouznetsov, D281
 Kovacevic, R249
 Kovarik, L320
 Kovrov, V329
 Koyama, K349
 Kozlov, A309
 Kracher, A103
 Krachler, R291
 Kraemer, S268
 Kraft, O58
 Krajewski, P92, 229, 282, 309
 Kral, M352
 Kramer, D275, 337
 Kramer, L39, 305
 Kramer, M36, 166, 236, 321, 332
 Krane, M40, 278, 314
 Krasnochtchekov, P201, 207
 Kraus, L95
 Krauss, G76
 Kräutlein, C128
 Kravchenko, T214
 Krcmar, M27, 190
 Kresch, M78, 303
 Kretz, R88
 Krishna Moorthy, S16
 Krishnamurthy, K135
 Krishnamurthy, R330
 Krishnan, S303
 Krishnan, V248, 299
 Krishnapisharody, K98
 Kristensen, W231
 Kriz, R260
 Kroupa, A104
 Krstulich, J209
 Kruzic, J287
 Kryukovskii, V173
 Krzysztof, M235
 Kubin, L206
 Kucharova, K58
 Kuchibhatla, S275
 Kueper, A166
 Kugler, G45
 Kuhn, T179
 Kulkarni, A337
 Kumah, D156
 Kumar, A50, 56, 64, 161, 224, 232, 274, 296, 344
 Kumar, C300
 Kumar, D95, 115, 163, 354
 Kumar, K133, 251, 321
 Kumar, M80, 133, 278, 295
 Kumar, P353
 Kumar, S81, 109, 354
 Kumar, T275
 Kumar, V87
 Kumbhar, N298
 Kuncser, V63
 Kunets, V273
 Kunrath, A354
 Kunter, R55, 110, 157, 209, 269, 323
 Kunz, R93
 Kuo, C280, 323
 Kuokkala, V80
 Kuramoto, S52, 325
 Kurath, P280
 Kuribayashi, K306
 Kurmanaeva, L218
 Kuroda, S209
 Kurokawa, H87
 Kurt, K88
 Kurtulus, M67
 Kurtz, R48, 314, 316
 Kusano, H184
 Kuskovsky, I115
 Kuzminova, Z283
 Kvande, H71
 Kvithyld, A36, 88
 Kwak, C345
 Kwak, H273
 Kwak, K50
 Kwayisi, R147, 261
 Kweon, S280
 Kwon, S180, 361
 Kwon, Y93, 282, 336
- ## L
- Laabs, F66
 LaCombe, J132
 Laé, E128
 Lahreche, H108
 Lai, B114
 Lai, L275
 Lai, Y102, 152, 204, 233, 284
 Laik, A131
 Laird, B84
 Lalonde, K232, 329
 Lamb, J348
 Lamb, S60
 Lambotte, G112
 Lambros, J29
 Lan, H305
 Lan, J355
 Lan, K290
 Landgraf, F280
 Landry, P171
 Langdon, T59, 112, 271
 Lange, G66
 Langelier, B230
 Langerman, M82, 187
 Larsen, J106, 107, 108, 350
 Larsen, S81
 Larson, B304
 Larsson, H240
 Lashley, J136, 137
 Lasseigne, A167, 225
 Lassila, D184, 320
 Latysh, V217
 Laube, B224
 Laughlin, J141
 Launey, M287
 Lavender, C39, 141
 Lavernia, E217, 218, 272, 358
 Lavery, N158
 Lavigne, O208
 Lavrentiev, M27, 52
 Lawn, B234
 Leach, A161
 Lebensohn, R30, 97, 147, 228, 243
 LeBlanc, M320
 Leboeuf, S127
 Le Bouar, Y191
 Le Brun, P127, 128
 Leckie, R268
 Lederich, R187, 235
 Lee, A151, 153, 204, 308, 317
 Lee, B33, 49, 67, 178

Lee, C	40, 83, 139, 153, 186, 190, 214, 218, 266, 319, 327, 361	Li, T	52, 187, 248	Liu, Q	261, 340
Lee, D	70, 74, 120	Li, W	31, 160, 275	Liu, S	31, 83, 84, 86, 135, 188, 288
Lee, E	70, 89	Li, X	87, 115, 149, 195, 208, 261, 262, 290, 334	Liu, T	102
Lee, G	273	Li, Y	17, 36, 52, 64, 69, 104, 125, 126, 127, 169, 184, 204	Liu, W	80, 233, 264, 286, 304
Lee, H	103, 104, 153, 154, 196, 203, 205, 216, 223, 265, 318	Li, Z	47, 69, 122, 309, 342	Liu, X	104, 227, 236, 259, 260, 286, 313
Lee, I	334	Lian, J	100	Liu, Y	70, 129, 167, 172, 184, 185, 201, 213, 231, 233, 277, 283, 284, 311, 328, 330, 332, 346, 353
Lee, J	34, 50, 63, 77, 87, 93, 95, 103, 145, 148, 161, 162, 196, 204, 222, 250, 257, 258, 266, 273, 282, 302, 307, 333, 359, 362	Lian, T	43	Liu, Z	28, 77, 145, 194, 236, 256, 309, 332, 343, 351
Lee, K	63, 273, 301, 317, 332, 361	Liang, B	273	Livescu, V	26, 138
Lee, M	147, 183, 236, 333, 357	Liang, C	167, 343	Livingston, R	303
Lee, N	264	Liang, J	165	Lix, S	124
Lee, P	53, 136, 228, 270, 322, 331, 357	Liang, R	99	Lizaur, M	55
Lee, S	32, 33, 74, 97, 104, 130, 154, 176, 191, 204, 213, 220, 266, 275, 294, 309	Liang, S	118, 152, 206	Llewellyn, E	121
Lee, T	50	Liang, T	186	Loeche, D	258
Lee, W	116, 186	Liang, W	96	Löffler, J	66, 177
Lee, Y	26, 28, 93, 117, 139, 223, 257, 282, 345	Liao, C	206	Logan, S	91
Legagneux, P	117	Liao, H	73	Logar, A	134, 135
Lei, M	28, 100	Liao, J	231	Lohmueller, A	194
Lei, Y	102, 103, 110	Liao, S	22	Loiseau, A	139
Leichtfried, G	118	Liao, X	271, 313	Lombard, J	122
Leisenberg, W	244	Liaw, P	21, 23, 24, 73, 74, 95, 126, 127, 128, 177, 178, 180, 189, 200, 212, 213, 215, 219, 235, 236, 271, 286, 287, 288, 302, 331, 332, 358, 360	London, B	341
Lekakh, S	148	Liberati, M	146	Long, G	252
Lekstrom, M	85	Lieberman, S	44, 254, 277	Long, L	360
Lemmon, J	197	Lienau, C	273, 274	Long, X	317
Leonhardt, T	57, 110	Lienert, T	82, 134, 186, 247, 297, 341	Long, Y	186
Leopold, J	177, 286	Lienert, U	267, 358	Long, Z	230
Lepselter, M	109	Lilleodden, E	160	Longanbach, S	308
Lepsleter, M	54	Lim, C	22, 71, 124, 175, 176, 233, 252, 275, 284, 330	Loomis, E	29
Lerch, B	133, 269	Lim, H	145, 257, 307	Lopes, F	129, 181
Le Roy, G	128	Lim, J	50, 319	Lopez, C	227
LeSar, R	18, 67, 80, 119, 168, 227, 278, 327	Lima, A	181	Lopez-Hirata, V	336
Letzig, D	145, 258	Lima, J	233	Lorentsen, O	90
Leu, L	33	Limpijumnong, S	337	Lorenzana, H	29
Leu, M	324	Lin, A	22, 176	Losert, W	188
Levashov, V	235	Lin, C	206, 266	Lossius, L	81
Levchenko, E	78	Lin, D	196	Loutfy, R	39, 141
Levendis, Y	137	Lin, H	355	Louzuine, D	24
Levesque, J	92	Lin, J	108	Low, K	300, 346
Levi, C	66, 268	Lin, K	265	Low, S	305
Levi, K	125	Lin, S	264, 297	Lowe, C	40
Levine, L	38, 140, 253, 254, 304	Lin, W	154	Lowe, T	215, 217
Levit, V	26, 121, 130, 217, 255, 306, 312	Lin, Y	102, 152, 154, 204, 266, 272, 319, 331	Lowrey, M	325
Levitas, V	120, 182, 299	Lindau, R	315	Lu, C	197
Lew, K	206	Lindley, T	349	Lu, F	249
Lewandowski, J	17, 65, 73, 74, 118, 167, 178, 225, 251, 277, 333	Lindsay, S	21, 70, 123, 124, 173, 174, 231, 232, 283, 329	Lu, G	31, 238
Lewis, D	28, 78, 104, 131, 153, 182, 205, 241, 242, 265, 293, 318	Ling, Y	336	Lu, H	91, 165, 174, 233
Li, B	137, 138, 238, 246, 259, 289, 290, 296, 313	Linhardt, R	64	Lu, J	59, 166, 224, 290, 342
Li, C	109, 176, 260, 275	Link, R	140	Lu, K	146, 271, 272
Li, D	72, 97, 199, 288, 310, 330	Liou, W	153	Lu, L	179, 237
Li, G	216	Lipin, V	171	Lu, M	153
Li, H	17, 99, 144, 145, 194, 230, 287, 313, 358	Lipko, S	276	Lu, X	186, 304
Li, J	24, 25, 52, 58, 61, 75, 106, 107, 118, 128, 140, 161, 178, 179, 189, 206, 233, 238, 246, 284, 287, 289, 292, 304, 312, 327, 334, 344, 349	Litton, D	208	Lu, Y	94, 169
Li, K	118	Liu, B	288, 324	Lu, Z	127, 203, 260, 315, 323, 332
Li, L	20, 56, 131, 322	Liu, C	18, 21, 27, 51, 58, 102, 112, 127, 152, 159, 206, 211, 213, 251, 260, 266, 271, 318, 319, 323, 325, 357	Lucas, M	78, 303
Li, M	177, 247, 280, 288, 324	Liu, F	73, 82, 180, 288	Lucente, A	236
Li, N	91, 143, 194, 215, 345	Liu, G	195, 271, 314, 324	Luckowski, S	192
Li, Q	99, 168, 237, 326	Liu, H	258	Ludtka, G	46, 47, 98, 261, 262, 313, 354
Li, R	313	Liu, J	19, 68, 87, 103, 120, 121, 169, 212, 228, 264, 279, 281, 343	Luecke, W	140
		Liu, L	133, 209	Lui, T	125, 181, 290, 342
		Liu, M	68	Lund, M	325
		Liu, P	103, 204, 264	Luo, A	40, 91, 92, 143, 144, 194, 195, 257, 258, 307, 308, 309, 350, 352
				Luo, H	123
				Luo, J	111
				Luo, S	294, 340
				Luo, T	167, 186, 346
				Luo, X	200
				Lupulescu, A	28, 78, 131, 182, 241, 242, 293



- Lussier, A146, 198
Luton, M52
Luyten, J128
Lynn, K316
Lyssenko, T192
- M**
- Ma, A45
Ma, D65, 127, 332
Ma, E24, 58, 113, 155, 216, 243, 357
Ma, H262
Ma, L305
Ma, N44, 168, 239
Ma, S30, 157, 294
Ma, W20
Ma, X223, 271
Ma, Y211
Macak, J220
Macht, M293
Mackiewicz-Ludtka, G46, 47, 262
MacSleynne, J25
Madan, A353, 354
Maeda, M110, 210, 334
Maehara, Y25
Magalhaes, R232
Mahajan, V354
Mahieu, P245
Mahmood, M296, 329
Mahmoudi, M330
Mahoney, M82, 134, 186, 247, 297, 341
Maier, H119, 193, 299
Maier, P259
Maier, V23
Maiti, S184, 339
Maitra, P36
Maity, P36
Maiwald, D244
Maj, M91
Major, J89
Majumdar, B279
Makhlouf, M158, 211
Makino, K265
Makov, G154
Maldonado, S328
Malerba, L150, 202, 203, 263
Malik, M112
Mall, S226
Mallick, P298, 351
Malone, R244
Maloto, F232
Maloy, S151, 316, 356
Maltais, B127
Manaktala, S71
Manchiraju, S96
Mandal, S135
Mandava, V347
Mangelinck-Noel, N85, 188
Manhaes, R335
Maniruzzaman, M183, 290
Manjeri, R249
Manley, M136, 137, 189, 248, 299
Mann, G352
Mann, M117
Manna, I178
Mannava, S129, 225
Manosa, L137
Mantina, M28
Mao, P302
Mao, S60, 61, 357
Mao, Y254
Mao, Z27
Mara, N326
Marceau, D296
Marcheselli, C278
Marciniak, M63
Marcinkoski, J41
Marcolongo, P179
Marcus, H16
Mariage, J328
Marian, J154, 155
Marino, K268
Marion, E21
Markham, J55
Markmaitree, T197
Marks, J21
Marquis, F37, 249, 300, 345, 346
Marrow, T129
Marsen, B354
Marsh, S142, 193
Marshall, G72
Marshall, S72
Marte, J277
Marthandam, V301
Martin, G27
Martin, M79, 218, 243
Martin, O71, 329
Martin, P141
Martin, R356
Martin, S231
Martinez, E328
Maruyama, M88
Maruyama, T55
Masamoral, R130
Mashl, S210
Mason-Flucke, J156
Mastorakos, I170
Masuda, C167, 226
Masuno, A85
Mataya, M190, 295
Materna-Morris, E315
Mates, S141, 304
Mathias, M94
Mathieu, N245
Mathison, L343
Matlakhov, A76
Matlakhova, L76
Matlock, D190, 295
Matson, D86
Matsukawa, Y267
Matsumoto, K131, 208
Matsumoto, T72
Matsumura, M116, 163
Matsunaga, T306
Matsuoka, S55
Matsuyama, A142
Mattapelli, S187
Matteis, P180, 339
Matteo, E72
Matz, L149
Maudlin, P57, 133
Mavromaras, A28
Maxey, E236
Mayandi, J17
Mayer, G72
Mayer, J297
Mayeur, J261
Maziasz, P260, 323
Mazur, Y273
McCabe, A171
McCabe, R243
McCallum, R166
McCauley, J338
McClellan, K43
McClintock, D317
McCluskey, M163
McColskey, D140
McCowan, C140
McCune, R91, 350, 351
McDaniels, R235
McDeavitt, S42
McDermid, J46
McDonald, J30
McDonald, S112, 179
McDowell, D106, 155, 199, 256, 261, 295
McElwee-White, L33
Mceuen, S248
McGee, E19
McGregor, K304
McIntosh, P122, 171, 229, 280
McLeod, T16
McMurray, S189
McNaney, J184
McNaney, J29
McNelly, T113, 216, 341
McPherson, R312
McVay, G42
Medlin, D82, 135, 299
Meek, T262
Meese, D76
Meghlaoui, A231
Meguerian, R46
Mehrer, H293
Mehta, V108, 150
Meier, M123, 245
Meldrum, H125
Melo-Maximo, V336
Mena, M118
Mencer, D35
Mendelev, M83, 84
Mendis, B44, 208
Meneghini, A271
Menezes, G129
Meng, D149
Menon, S181
Mente, P285
Mercer, H82
Merchant, N108
Merkle, J190
Merriman, C170
Merry, J83
Meskers, C259
Meslin, E263, 264
Metwally, H56
Meydanoglu, O270
Meyer, A293
Meyer, J93
Meyer, T111
Meyers, M22, 29, 71, 79, 124, 132, 175,
.....176, 183, 184, 218, 233, 243,
.....271, 284, 294, 295, 330, 338, 357
Meyyappan, M16
Meza García, E258
Miao, J108
Miao, S100
Miao-Yong, Z336
Michael, N54, 108, 149
Michal, S177, 235, 286
Middlemas, M118
Middleton, J312

Mihalkovic, M.....	360
Mikhail, Y.....	94
Mikula, A.....	318
Miles, M.....	134, 247
Miller, D.....	160
Miller, E.....	354
Miller, F.....	25, 74
Miller, J.....	142, 349
Miller, M.....	27, 52, 53, 66, 96, 120, 126, 151, 199, 263, 316, 321
Miller, W.....	91
Millett, J.....	294, 295
Mills, M.....	44, 51, 105, 106, 107, 154, 156, 199, 206, 207, 229, 266, 312, 320
Millwater, H.....	350
Milne, W.....	117
Minakshi, M.....	311
Mindivan, H.....	270, 348
Mingdao, W.....	47
Minguett, J.....	122
Minich, R.....	133
Minor, A.....	325
Minoux, E.....	117
Miodownik, M.....	130
Miodownik, P.....	205
Miotto, P.....	245
Miracle, D.....	25, 74, 226, 235, 236, 255, 332
Mirkovic, D.....	309
Mishin, Y.....	44, 78, 181
Mishra, A.....	218
Mishra, B.....	167, 225
Mishra, C.....	230
Mishra, R.....	25, 74, 82, 83, 92, 134, 135, 186, 187, 228, 235, 247, 275, 297, 298, 325, 341, 342
Misra, A.....	121, 211, 215, 326, 356
Misra, D.....	276, 285
Misra, M.....	125, 233, 354
Missalla, M.....	171
Missori, S.....	180
Mistretta, M.....	300
Mitchell, D.....	311
Mitsuishi, K.....	100
Mittal, V.....	93
Miura-Fujiwara, E.....	229
Miwa, K.....	25, 143
Miyabe, Y.....	204
Miyake, M.....	110, 210, 289, 334
Miyamura, T.....	33, 93
Mizutani, U.....	252
Mo, A.....	172
Moat, R.....	322
Moehwald, K.....	166
Mohajeri, N.....	94
Mohamed, F.....	214, 271, 275
Mohammed, A.....	296
Mohan, P.....	268
Mohandas, K.....	57
Mohanty, R.....	242
Moitra, A.....	19
Mokkapat, S.....	273
Moldovan, P.....	238
Mollah, M.....	35
Molodov, D.....	46, 47
Moloney, M.....	307
Monk, J.....	155, 337
Montanari, R.....	180, 339
Monteiro, S.....	56, 76, 129, 179, 180, 181, 289, 290, 334, 335
Montgomerie, D.....	35
Moody, N.....	37, 160, 249, 300, 325, 326, 345, 346
Mook, W.....	207, 325
Moon, D.....	247, 248
Moon, J.....	319
Moon, W.....	73, 266
Moore, E.....	253
Moran, J.....	240, 292
Morariu, M.....	63
Moras, A.....	21
Mordehai, D.....	154
Mordike, B.....	352
Moreno, H.....	35
Moreno C., H.....	35
Morgan, A.....	16
Morgan, D.....	26, 49, 93, 181, 244
Morgan, T.....	315
Mori, G.....	148
Mori, H.....	63, 355
Morisaku, K.....	87
Morishige, T.....	259
Morishita, M.....	289
Morita, K.....	289
Moriyama, M.....	246
Morjan, I.....	63
Morkovsky, P.....	35
Morosin, B.....	79
Morozov, A.....	214
Morphett, A.....	124
Morrall, J.....	241, 242
Morris, A.....	40
Morris, D.....	59, 114
Morris, J.....	26, 77, 83, 84, 127, 130, 136, 181, 189, 190, 235, 239, 248, 291, 299, 317, 325, 335, 337
Morris, Jr., J.....	52
Morris, R.....	33
Morse, D.....	23
Morsi, K.....	149
Mortarino, G.....	180
Mortensen, D.....	237
Mosher, D.....	224
Moskovich, N.....	309
Moskovitch, N.....	194, 257
Möslang, A.....	315
Moss, S.....	89, 140, 303
Mostafa, S.....	311
Mothé, A.....	56
Motta, A.....	356
Moura, R.....	124
Mourao, M.....	35
Mourer, D.....	229, 320
Moxnes, B.....	71
Moxson, V.....	192
Moy, P.....	140, 141, 254
Mubarok, Z.....	148
Muci Kuchler, K.....	187, 298
Mucino, V.....	298
Mucsi, G.....	56
Mudryk, Y.....	76
Mueller, W.....	351
Muga, L.....	197
Mughrabi, H.....	96
Muhktar, A.....	272
Mukai, T.....	162, 184, 196, 308, 352
Mukaida, M.....	98
Mukherjee, A.....	272, 326, 358
Mukhopadhyay, J.....	36
Mukhopadhyay, S.....	16
Muller, C.....	233
Müller, S.....	37
Mullis, A.....	85
Mumcu, G.....	343
Muñoz-Morris, M.....	59, 114
Munroe, P.....	272
Muppidi, T.....	89
Muradov, N.....	354
Muraguchi, M.....	247
Murakami, H.....	209
Murakami, M.....	32, 33, 246, 296
Murakumo, T.....	54
Murashkin, M.....	358
Murch, G.....	78, 293
Murphy, J.....	20
Murphy, K.....	157
Murphy, T.....	292
Murr, L.....	117, 132, 176, 183, 185
Murty, G.....	167
Murty, K.....	58, 59, 260, 315
Murugan, R.....	22
Murugesan, S.....	64
Muschinski, A.....	307
Musz, E.....	198
Muthubandara, N.....	78
Myers, S.....	285
Myrvold, E.....	124
N	
Nabarro, F.....	272
Nabiev, I.....	161
Nadella, R.....	237
Nadtochy, A.....	71
Naeth, O.....	223
Nafisi, S.....	179
Nag, A.....	285
Nag, S.....	226, 234
Nagai, T.....	334
Nagaraj, B.....	209
Nagasako, N.....	52
Nagem, N.....	231
Nagy, P.....	179
Nahshon, K.....	294
Naik, R.....	162
Nair, A.....	260
Naixiang, F.....	233, 296, 341
Nakai, M.....	306
Nakajima, H.....	63
Nakamura, R.....	63
Nakanishi, T.....	43
Nakano, Y.....	361
Nakayama, T.....	43, 361
Nalamasu, O.....	64
Namboothiri, S.....	173
Namilae, S.....	223, 251
Nan, H.....	350
Nancollas, G.....	23
Nandiraju, D.....	249
Nandy, T.....	156
Nanstad, R.....	190, 317
Napolitano, R.....	37, 85, 188, 249, 290, 300, 345, 346
Narayan, J.....	55, 62, 109, 116, 163, 222, 271
Narayan, R.....	163, 284, 285
Narayana, G.....	123
Narayanan, R.....	78
Narita, H.....	87
Naritsuka, S.....	55
Narukawa, Y.....	162
Nascimento, A.....	81
Nascimento, M.....	351



- Nashat, A193
 Natesan, K110
 Nath, A98
 Nathenson, D80
 Naumov, I114
 Nawaz, A139
 Naydenkin, E218
 Nayuta, M148
 Nazarboolland, A279
 Nazon, J180, 182
 Neale, K92
 Neelamegham, N36, 40, 88, 91, 92,
143, 144, 194, 195, 257,
258, 307, 309, 350, 352
 Neelgund, G64
 Neeraj, T207
 Neil, C170
 Neil, C170
 Nelson, B248
 Nelson, T134, 186, 247, 248, 341
 Nenseter, B245
 Neri, M324
 Nes, E68
 Ness, D53, 322
 Nestler, K145
 Neu, C146, 148, 188
 Neu, R147
 Neubauer, E18
 Neuber, D25
 Neuefeind, J332
 Neumann, D89, 303
 Neumann, T134
 Newberry, P214
 Newbery, A217
 Newey, M188
 Neyrey, K81
 Ng, B57
 Ng, G272
 Nguyen, D291
 Nguyen, K125
 Nguyen, T283
 Nguyen-Manh, D27, 52
 Nguyen-Thi, H85, 188
 Nicholson, D47, 192, 286
 Nie, J352
 Nie, Z189, 198
 Niederberger, C32
 Niedling, J333
 Nieh, T73
 Nigam, A164
 Niihara, K361
 Niinomi, M306
 Nikles, D164
 Ning, B208
 Ningileri, S69, 172, 230, 269
 Ningthoujam, R164, 222
 Nino, J100
 Nishimiya, Y167
 Nishimura, T265
 Nishizuka, K162
 Nix, W159
 Nixon, M243
 Niyomwas, S200
 Nobuhiro, I148
 Noda, T255
 Noebe, R189
 Nogaret, T48
 Nogita, K112, 179, 264, 265
 Nogueira, A35
 Nohira, T304
 Nolan, D143
 Noldin, J98
 Noori, A154
 Nordlund, K150
 Norfleet, D44
 Northwood, D310
 Norton, D33, 62, 344, 359
 Norton, M49
 Noskova, N218, 325
 Nossa, J273
 Notten, P197
 Novichkov, S55
 Nowell, M75, 121
 Noy, A22
 Nuhfer, N189
 Nunna, R238, 347
 Nutt, S215
 Nyberg, E352
 Nychka, J71, 72, 204
 Nyilas, K212
- O**
- O'Brien, C242
 O'Brien, K281
 O'Brien, S115
 O'Connell, S37
 Obata, T283
 Obbard, R76
 Oberebt, C82
 Oberembt, C298
 Oberson, P348
 Ochsner, A78
 Ode, M209
 Odeshi, A80
 Odette, G263, 264, 314, 316
 Odunuga, S207
 Oehring, M212
 Ogale, S146
 Ogata, S178, 287
 Ogata, Y304
 Ogawa, M255
 Oginuma, H353
 Oh, B175
 Oh, C138
 Oh, K150, 154, 186, 205, 319
 Oh, Y290
 Oh-ishi, K341
 Ohishi, K352
 Ohkubo, T308, 352
 Ohnaka, K306
 Ohnuma, I104, 204, 265
 Ohriner, E57
 Ohshima, K253
 Ohtsuka, H47
 Oja, M33
 Okabe, T25, 75, 90, 128, 141,
179, 238, 289, 306, 334
 Okamoto, K92, 186, 247, 297
 Oki, S259
 Oktay, G176
 Okuniewski, M316
 Oleinikov, V161
 Oliver, E95, 210
 Oliver, W129
 Olmsted, D67, 84, 105
 Olsen, E166, 247
 Olson, D167, 225
 Olson, G79, 200, 299
 Omotunde, A112
 Omran, A230
 Omura, N25, 143
 Onishi, T246
 Onodera, H209
 Opalka, S224
 Opeil, C136
 Oppedal, A20
 Orchard, H205
 Ordaz, G42
 Oren, E125
 Orme, C23
 Oro, D244
 Ortega, U174
 Ortiz, C314
 Ortiz, M155, 227
 Osborn, W197
 Osborne, M111
 Osborne, R91
 Osetskiy, Y48, 267
 Osetsky, Y201, 203, 355
 Oshida, Y233
 Osman, T40
 Osvaldo, F86
 Otaki, M88
 Ott, R236, 357
 Ou, K234, 330
 Ouellet, B124
 Ouimet, L91
 Ou Yang, F206
 Ovcharenko, A316
 Ovid'ko, I160
 Ovrelid, E166
 Owens, A295
 Owolabi, G80
 Øye, H81, 340
 Ozawa, T306
 Ozkan, C221
 Ozolins, V27, 89
 Ozsoy, I299
- P**
- Packer, S341
 Paclawski, K209
 Padgett, C216, 219
 Padilla, H29
 Padilla, R148
 Padture, N268
 Pal, S184
 Palacio, H86
 Palandage, K274
 Palanisamy, P300
 Palit, D17
 Palkowski, H45, 66
 Palmer, M40
 Pan, F344
 Pan, J60
 Pan, T259, 298
 Pan, X95, 242
 Pan, Y28, 42, 43, 94, 234, 330
 Panat, R176
 Pandey, A17, 65, 81, 118, 167, 225, 277, 285
 Pandey, R33
 Pangan, A154
 Panico, M299
 Pantleon, W20, 267
 Pao, C338
 Pao, P247
 Papadimitrakopoulos, F16
 Papillon, F49
 Papis, K66, 88

Pappas, N	47	Peterson, B	26, 94, 121, 229, 255, 312	Porto, S	124
Pareige, C	263	Peterson, E	35	Posada, M	247
Pareige, P	263, 264	Peterson, R	55, 110, 157, 209, 269, 323	Potesser, M	138
Parga, J	35	Peterson, V	303	Potirniche, G	312
Parida, S	275	Petralia, S	339	Pouchon, M	95
Parisi, A	86	Petrillo, J	41	Poulsen, H	267
Park, C	40, 51, 190, 361	Petrova, R	183	Pouly, P	128
Park, D	276	Petrovic, J	42	Powell, A	40, 97, 303, 307, 349
Park, E	73, 177, 319	Pew, J	134	Powell, B	91, 310
Park, G	102	Pfeif, E	133	Pownceby, M	185
Park, H	22	Pharr, G	129, 251	Pozuelo, M	65
Park, J	335	Phillips, N	66	Pradhan, D	90
Park, K	139, 214	Phillion, A	136	Prado, F	110
Park, M	50, 62, 115, 116, 162, 221	Phillips, D	162	Prado, J	219
Park, N	287	Phillips, E	229	Prajapati, B	109
Park, S	19, 70, 138, 145, 186, 204, 247, 345	Phillpot, S	100, 356	Prakash, V	74, 80, 133, 178, 219, 333, 339
Park, W	16, 144, 145, 346	Piatkowski, D	89	Prasad, J	172
Park, Y	64, 149	Piccardo, P	339	Prasad, R	123
Parker, D	112	Pickens, J	55, 110, 157, 209, 269, 323	Prasad, S	160
Parkison, A	42	Pierce, D	333	Prasanna Kumar, T	301
Parmar, B	255	Pierre, L	17	Prask, H	304
Parra, M	43	Pietrzyk, M	242	Prater, J	109, 116, 163
Parra Garcia, M	95, 340	Piffer, V	81, 245	Pratt, L	27
Parsa, M	37	Pike, L	180, 322	Preble, E	62, 221
Parsey, J	54, 108	Pilchak, A	342	Preston, D	120, 299
Parthasarathy, T	266, 320	Pilote, S	296	Presuel-Moreno, F	43
Pashkovski, E	125	Pinasco, M	180, 339	Preuss, M	20, 322
Pate, T	244	Ping, L	224	Price, D	89, 303
Patel, J	324	Pingin, V	174	Price, N	37
Patel, M	336	Pinkerton, A	322	Pritchard, P	193
Patil, S	268, 286, 287	Pinoy, L	34	Proffen, T	178, 236, 332
Patnaik, A	82, 83, 298	Pint, B	52, 106, 155, 208, 209, 260, 268, 321, 323	Prorok, B	343
Patterson, B	282	Pinto, E	124, 174	Proshkin, A	31
Patwardhan, D	199	Pinzhin, Y	215	Proudhon, H	280
Patz, T	284	Piotr, L	177	Proulx, G	124
Paul, J	212	Pippan, R	218	Proust, G	68, 170
Paul, R	158	Piskazhova, T	329	Provatas, N	181
Paulino, L	232	Pitchure, D	253, 254	Puech, S	331
Pavel, M	30	Pitek, F	268	Puga, C	35
Pavez, P	148	Planes, A	137	Pulikollu, R	16
Payton, E	229	Plapp, M	31, 83, 84, 86, 135, 188	Pun, G	78
Payzant, E	353	Plascencia, G	191, 227	Purohit, Y	216, 219
Peace, J	21	Platek, P	69	Purushotham, S	284
Pearton, S	54, 55, 62, 108, 164, 165, 344	Platt, D	92	Pusateri, J	323
Peaslee, K	148	Player, R	35	Pushparaj, V	64
Peauger, F	117	Plohr, J	133	Pusztai, T	31, 32
Pecharsky, V	76	Plunkett, B	147, 243	Puthucode, A	126
Pedersen, K	172	Pocheau, A	85, 136	Puzyrev, Y	192
Pedersen, T	173	Poirier, D	324	Pyshkin, S	55
Peelamedu, R	354	Politano, O	106		
Pei, Z	262	Pollcok, T	157	Q	
Pekguleryuz, M	40, 41, 91, 92, 143, 144, 194, 195, 257, 258, 307, 309, 350, 352	Pollock, T	30, 53, 66, 92, 108, 156, 294, 307, 310, 312, 352	Qi, F	261
Pellati, G	180	Polyakov, L	214	Qi, L	171
Pelletier, J	288, 332	Polyakov, P	31, 329	Qian, L	346
Peng, P	234	Pomerance, A	188	Qian, M	143
Peng, Z	311	Pomykala Jr., J	158	Qiao, B	230
Pensado, O	43	Poncsak, S	237, 283	Qiao, D	286, 287, 331, 332
Penumadu, D	200	Pongsaksawad, W	303	Qiao, L	28
Peralta, P	29, 43, 95, 250, 340	Ponnazhagan, S	285	Qichu, L	313
Perepezko, J	25, 32, 278, 321	Ponomareva, I	114	Qing, L	186
Perez, A	240, 292	Pons, A	188	Qingcai, L	57
Perez, E	132	Pontin, M	294	Qiu, G	286
Pérez-Prado, T	215, 273	Poole, W	280	Qiu, K	237
Perron, A	134	Poon, J	24	Qiu, R	23
Perruchoud, R	123, 245	Pope, D	38	Qiu, S	248
Perrut, M	135	Popescu, G	238	Qiu, T	351
Peter, W	39	Popov, I	308	Qiu, Z	31, 175, 186, 233, 258, 283, 284, 304, 340
Peters, P	226	Portella, P	226	Qu, X	246
Petersen, E	64				



- Quach, D99, 182, 359
 Quast, J226
 Querin, J187
 Quick, N163
 Quinta da Fonseca, J20
 Quintino, L134
- R**
- R-Raissi, A93
 Raab, G215, 216
 Raabe, D45, 228
 Raber, T197
 Rablbauer, R322
 Rachmat, R143
 Rack, P288
 Radhakrishnan, B68, 223, 251, 312
 Radiguet, B263, 264
 Radosavljevic, S334
 Radosavljevic-Mihajlovic, A334
 Rae, C53
 Rae, P183, 251
 Raetzke, K293
 Raghunathan, S321
 Rahbar, N22
 Rais-Rohani, M256
 Raissi, A276
 Raiszadeh, R112
 Raj, S269
 Raja, K354
 Rajan, K40, 256
 Rajeev, K222
 Rajendran, A169
 Rajulapati, K59
 Rakovich, Y220
 Ramachandran, S109, 116
 Ramakrishna, S22
 Rama Murty, G277
 Ramanujan, R114, 284
 Ramar, A48, 355
 Ramasamy, K94
 Ramaswami, J232
 Ramesh, K79, 113, 140, 183, 216, 243
 Ramirez, A143
 Ramirez, J86
 Ramírez, J328
 Rammohan, A73
 Rämö, J80
 Ramusat, C208
 Ranganathan, S23
 Rangel, J129, 290
 Rao, K90, 257
 Rao, S105, 266
 Rao, W239
 Rasch, B127
 Rasty, J312
 Rathz, T235, 302
 Ratvik, A30
 Rauscher, M162, 362
 Ravi, C77
 Ravichandran, G184
 Ravindra, N54, 55, 108, 109, 149, 150
 Rawal, S33
 Rawlins, H148
 Ray, R45
 Ray, T291
 Razavi, F252
 Read, C42, 341
 Ready, W16, 63
 Real, C227
- Rebak, R42, 43, 94
 Reddy, A342
 Reddy, M277
 Reddy, N40, 327, 347, 361
 Reddy, R90, 94, 174, 350
 Reddy, S293
 Redkin, A173, 283
 Reed, B295
 Reed, R52, 53, 106, 155, 208, 268, 321
 Reiche, P64
 Reichelson, J288
 Reid, D64
 Reimanis, I278
 Reinhard, G188
 Reinhart, W338
 Reinovsky, R244
 Reis, A271
 Reis, S24
 Reisen, U145
 Reiso, O216
 Reizine, F346
 Remington, B184
 Rimmel, J145
 Ren, B31, 71
 Ren, F54, 55, 62, 108, 344
 Ren, J212, 214
 Ren, R197
 Ren, W247
 Ren, X59
 Ren, Y189, 212, 358
 Reno, R253
 Rest, J356
 Reuter, M259
 Reutzel, S86
 Rex, S135
 Reynolds, A297
 Reynolds, B179
 Reynolds, W146
 Rezvanian, O169
 Rhee, H312
 Rhim, W24
 Riani, J34
 Rice, J135
 Richard, C71
 Richards, V148, 324
 Richardson, H161
 Richardson, I346
 Richardson, J236, 332
 Richter, A100
 Richter, M235
 Richter, R333
 Ricker, R305
 Rickman, J130
 Rideout, C279, 347, 348
 Ried, P91
 Rieken, J66
 Rigsbee, M58, 112, 159, 211,
213, 271, 325, 357
 Rijkeboer, A171
 Rijssenbeek, J197
 Rimoli, J227
 Rinaldi, A250
 Rinck, M22
 Rinderer, B288
 Rios, P25, 26
 Rioult, F321
 Ripley, E354
 Riseborough, P136
 Ritchie, R125, 272
 Ritchie, S279, 347
- Rittel, D184
 Ritter, C124, 231
 Ritter, G187
 Rivard, J39
 Riverin, J22
 Rivero, R109
 Riveros, G35
 Rivière, C128
 Rivolta, B180
 Rizzi, G362
 Rizzo, F190
 Roalstad, J302
 Robelin, C329
 Roberts, S317
 Robertson, C48
 Robertson, I29, 48, 203, 216, 355
 Robertson, J89, 139, 191, 252, 303
 Robertson, S272
 Robinson, A306
 Robles-Hernandez, F191
 Robson, A349
 Rocha, L346
 Rockett, C118
 Rodchanarowan, A349
 Rodney, D48
 Rodriguez, G244
 Rodriguez, J89
 Rodriguez, R129
 Rodriguez-Baracaldo, R219
 Roe, C140
 Roeder, R124, 233, 234
 Roesler, J223
 Rogach, A60, 114, 161, 220, 273
 Rogers, J235, 302
 Rohatgi, P168
 Rohrer, C40
 Rohrer, G44, 45, 49, 176, 349
 Roldan Cuenya, B311
 Rollett, A19, 27, 69, 96, 97,
130, 176, 227, 349, 354
 Rolseth, S30
 Romanov, A160, 217
 Rombach, G128
 Romero, R137
 Romero-Serrano, J35
 Rong, H311
 Rong, Y256
 Rosam, J85
 Roschger, P72
 Rosen, G309
 Rosenberg, R246
 Rosenberger, A97, 107, 350
 Rosenkilde, C90
 Rosenson, H309
 Ross, N24, 235
 Roters, F45, 228
 Rotger, J245
 Rouns, T121
 Rousculp, C244
 Roven, H68, 216
 Rowenhorst, D130
 Rowlson, M322
 Roy, A301
 Roy, D178
 Roy, I214, 271, 275
 Roy, R354
 Roy, S165
 Roy, W192
 Roybal, L150
 Roytburd, A239

Rozak, G	57, 110	Sarikaya, M.....	125, 175	Scrivani, A.....	362
Ru, G	246	Sarma, G	68, 223, 251, 312	Scully, J.....	43, 236
Ruano, O	215, 273	Sarosi, P	107, 312, 320	Seal, S	16, 64, 149, 221,
Rubinsztajn, M.....	197	Sarradin, J	180, 182	268, 269, 275, 286, 292
Ruden, T.....	257	Sasaki, H.....	210	Seale, G.....	92
Ruiz, M.....	148	Sasaki, J.....	344	Sears, J.....	39, 90, 224, 276, 302
Rupnowski, P.....	108, 150	Sasaki, T.....	352	Seccombe, D.....	354
Russ, S.....	226	Sastikumar, D.....	98	Seckiner, A.....	302
Russell, A.....	207	Sato, A.....	54, 131, 156, 157, 208	Sediako, D.....	309
Russell, K.....	263, 316	Sato, E.....	306	Seelaboyina, R.....	117
Russo Spena, P.....	180	Sato, H.....	252	Segal, V.....	217
Ruvalcaba, D.....	84	Sato, K.....	306	Segall, A.....	227
Rye, K.....	31, 124, 232	Sato, M.....	22, 71, 124, 175, 176, 233, 284, 330	Segatz, M.....	174
Ryu, H.....	132	Sato, N.....	138	Seick, C.....	278
Ryu, J.....	51	Sato, S.....	138	Seidman, D.....	27, 138, 139, 282
Ryu, T.....	118	Sato, T.....	352	Sekhar, J.....	142
S					
Saal, J.....	309	Sato, Y.....	247	Seki, Y.....	71
Sabau, A.....	311	Satyapal, S.....	42	Sekido, N.....	321
Saboohi, Y.....	175	Saucedo Muñoz, M.....	336	Sekimoto, H.....	334
Saboungi, M.....	303	Saunders, N.....	205	Sekine, T.....	243
Sacerdote-Peronnet, M.....	182, 226, 277	Sawafta, R.....	165	Selim, F.....	316
Sachdev, A.....	91, 92, 195, 308	Saxe, P.....	28	Semenova, I.....	217
Sadayappan, K.....	210	Saxena, A.....	137, 189	Semenova, O.....	291
Saddock, N.....	92, 310, 352	Saylor, D.....	31, 199	Semiatin, S.....	170, 212
Sadik, P.....	62, 359	Scattergood, R.....	58, 59, 216, 219	Senkov, O.....	24, 25, 128, 167, 235, 236, 332
Sadler, B.....	81	Scavino, G.....	180, 339	Senkova, S.....	167
Sadoway, D.....	40	Schaedler, T.....	268	Senn, J.....	92
Saeed, U.....	104, 318	Schaeublin, R.....	355	Seo, J.....	64, 180
Saegusa, K.....	349	Schafler, E.....	113, 213	Seo, S.....	103, 104, 345
Saengdeejing, A.....	309	Schafrik, R.....	52	Seok, H.....	287
Safarik, D.....	287	Scharrer, M.....	194	Seong, B.....	301, 361
Saha Podder, A.....	45	Schäublin, R.....	48, 202	Seong Yong, P.....	191
Sahin, D.....	125	Schelling, P.....	291	Sepehrband, P.....	230
Sahin, F.....	302	Schenk, T.....	188	Serebrinsky, S.....	227
Saigal, A.....	33	Scherello, A.....	138	Serefoглу, M.....	85
Saito, K.....	60, 262	Scheriau, S.....	325	Sergueeva, A.....	326, 358
Sakai, N.....	260	Schestakova, L.....	218	Serna-Vasquez, A.....	55, 110, 157, 209, 269, 323
Sakamoto, K.....	87	Schiff, A.....	353	Sertel, K.....	343
Sakashita, S.....	43	Schildknecht, A.....	258	Setman, D.....	113, 213
Sakidja, R.....	321	Schille, J.....	205	Setyawan, A.....	24
Salamo, G.....	114, 273	Schlesinger, M.....	55, 110, 157, 209, 269, 323	Severo, D.....	124, 174
Salas, W.....	185	Schlom, D.....	64	Sezer, S.....	96
Salazar, J.....	174	Schmetterer, C.....	104, 105	Shackelford, J.....	251
Salazar, M.....	244	Schmid-Fetzer, R.....	309, 310	Shade, P.....	44, 160
Salee, D.....	237	Schmuki, P.....	220	Shaghiev, M.....	167
Saleh, T.....	358	Schneibel, J.....	118, 119	Shahbazian Yassar, R.....	19, 20, 68, 120,
Salem, A.....	170, 212	Schneider, H.....	315	121, 169, 228, 279
Salman, U.....	191	Schneider, J.....	187, 221	Shaikh, A.....	108
Samanta, A.....	52, 58, 106, 161	Schoenung, J.....	214, 215, 272	Shamsuzzoha, M.....	164, 231
Samaras, M.....	95	Schönfeld, B.....	191	Shan, A.....	212, 214
Samuel, S.....	234	Schott, A.....	37	Shan, Z.....	325, 357
Sanchez-Araiza, M.....	159	Schroers, J.....	331	Shang, L.....	258
Sanderson, S.....	248	Schuh, C.....	79, 212, 291	Shang, S.....	236
Sandhu, R.....	154	Schuldenzucker, P.....	88	Shangguan, F.....	121
Sandoval, D.....	183	Schulson, E.....	251	Shangguan, Z.....	230
Sangiorgi, G.....	271	Schultz, J.....	168, 278, 302	Shankar, R.....	170
Sankaran, S.....	120	Schuster, B.....	113	Shankar, S.....	36, 111, 112, 127, 211
Sansoz, F.....	155, 211	Schvezov, C.....	45, 289	Shannon, C.....	116
Santella, M.....	259, 298	Schwaiger, R.....	72, 128	Shao, H.....	214
Santhaweesuk, C.....	32	Schwandt, C.....	90	Shao-Horn, Y.....	93
Santisteban, J.....	95	Schwartz, L.....	101	Shaoxian, M.....	233, 341
Santodonato, L.....	46	Schwartz, W.....	298	Shapiro, S.....	136
Santos, A.....	335	Schwarz, M.....	174	Sharma, B.....	298
Sanville, E.....	202	Schwarz, R.....	59, 287	Sharma, S.....	332
Sanyal, S.....	197	Schwendiman, K.....	226	Sharma, V.....	347
Sarasmak, K.....	337	Scorey, C.....	39	Shaw, J.....	346
Sarihan, V.....	317	Scott, A.....	101	Shaw, L.....	197, 271
		Scott, J.....	236	Shazly, M.....	133
		Scott, M.....	226	She, H.....	71
		Scrase, S.....	81	Sheikh-Ali, A.....	106



- Shen, C106, 107, 189, 312
 Shen, G144
 Shen, H172, 283
 Shen, J353
 Shen, P55
 Shen, T58, 59, 112, 203
 Shendye, S324
 Sheng, X330
 Shenoy, V120
 Shet, S109
 Shi, J94
 Shi, S28, 137, 355
 Shi, W41
 Shi, Y102, 103, 110, 176, 219
 Shi, Z31, 186, 233, 238, 283, 284, 340, 351
 Shibata, N32, 33
 Shiffler, D240, 292
 Shiflet, G24, 236, 360
 Shih, D104
 Shih, T102, 266
 Shih, W152
 Shijie, G313
 Shim, J202, 203, 216
 Shimada, K60
 Shimizu, F178, 287
 Shimizu, T255
 Shimpō, R56
 Shin, C202
 Shin, D139, 213, 214, 218
 Shin, K143, 257, 308
 Shin, S191
 Shinohara, G138
 Shioi, R334
 Shivashankar, S64
 Shollock, B85
 Shorokhov, E213
 Shtanov, V283
 Shubayev, V177
 Shuiping, Z329
 Shukla, A83
 Shukla, P43, 100
 Shurov, N173, 329
 Shutthanandan, S151
 Shutthanandan, V100
 Shyamala, M232
 Shyng, Y234
 Sickafus, K100, 203
 Siegel, D27
 Siegmund, A55, 110, 157, 209, 269, 323
 Siewert, T140
 Sigworth, G179
 Sík, C56
 Sillekens, W195
 Silva, A231
 Silva, G180
 Silva, M245
 Silva, P33
 Silvestri, A180
 Simakov, D283
 Simmel, F61
 Simmons, J206, 327
 Simoes, S275
 Simsek, E188
 Sinaga, D70
 Sindelar, R292
 Singer, H188
 Singer, I188
 Singer, R194
 Singh, A196, 308
 Singh, H44, 254
 Singh, M80
 Singh, N54, 108, 319
 Singh, P145, 260, 269, 311
 Singh, U36
 Singh, V285
 Singjai, P17
 Singleton, N123
 Sinha, S252, 303
 Sinha, V226
 Sinn, H303
 Sinnott, S356
 Sintay, S97
 Sirivolu, S238
 Sisson, R182, 183, 290
 Sitdikov, V113
 Sivaraj, D351
 Siwecki, T228
 Sklad, P143
 Sklenicka, V58
 Skornyakov, V71
 Skrotzki, B226
 Skury, A129, 290, 334, 335
 Skybakmoen, E30
 Slade, S258
 Slattery, D225
 Slocik, J162
 Slooff, F310
 Slutsker, J239
 Smialek, J156
 Smid, I18, 227
 Smith, A270
 Smith, C29, 179
 Smith, G76
 Smith, J136, 137, 264, 316
 Smith, L220
 Smith, R19, 100, 150, 198, 202, 315
 Smitherman, M82
 Smolyakov, A214, 216
 Smugersky, J64, 65, 166, 214
 Snead, L57, 100, 101, 315
 Snure, M62, 116
 Snyder, R175
 Soare, I63
 Sobey, T61
 Soboyejo, W22, 288
 Sofie, S198
 Sohn, H118, 224, 225
 Sohn, Y28, 41, 78, 93, 131,
132, 145, 182, 197, 198, 241,
242, 259, 260, 268, 293, 310, 353
 Soisson, F263
 Sokhanvaran, S37
 Sokolov, M57, 151, 317
 Sokolowski, P166
 Solanki, K170
 Solberg, I124
 Soldano, C64
 Solheim, A30
 Soliman, M45
 Solis, F168
 Soloveichik, G197
 Soloviev, V216
 Solzbacher, F62, 162
 Somekawa, H196, 308
 Son, J222
 Son, S250
 Son, Y139
 Song, B141, 294
 Song, H179, 212
 Song, J206, 305, 318
 Song, K301
 Song, M100
 Song, X131
 Song, Y323
 Song, Z338
 Sonnleitner, R66
 Sopori, B54, 108, 109, 149, 150
 Sordelet, D208, 236, 357
 Sorensen, C134, 248, 341
 Sorlie, M21, 30, 31, 70, 74, 81, 122,
123, 127, 171, 173, 174, 179,
185, 229, 231, 232, 237, 244, 280,
283, 288, 296, 329, 333, 340, 341
 Soto, K176
 Soubeyroux, J331
 Soucy, G281
 Souidi, A202
 Southworth, A151, 153, 204
 Spaepen, F160
 Spangenberg, J158
 Spanos, G17, 130
 Spätig, P48
 Speakman, S209
 Specht, E229, 253
 Specker, A37
 Speer, J190
 Spencer, K144
 Spigarelli, S352
 Spoljaric, D138
 Spowitz, J168, 225
 Sreekala, S131
 Sreekumar, K123
 Sreeranganathan, A44, 254, 277, 309
 Srinivasan, R254, 255, 312, 320, 360
 Srinivasan, S132, 189, 224
 Srisukhumbowornchai, N166, 276
 Srivastava, A114
 Srivastava, R285
 Srivastava, S322
 Srivilliputhur, S67, 151, 316, 356
 Srolovitz, D130, 291, 330, 338
 St-Georges, L134
 St. John, D324
 Stach, E325, 357
 Stacy, J209
 Stadermann, M22
 Stadler, S146
 Stagno, E180, 339
 Staley, J210
 Stam, M70
 Stan, M65, 356
 Standen, C299
 Stanescu, C71
 Stanica, C238
 Stavehaug, F327, 328
 Stavrides, A354
 Steel, K31
 Steele, R247
 Stefanakos, E224
 Stefanescu, D86
 Stefanovic, P181
 Steigerwalt, E93
 Steinbach, I32, 65, 240
 Steinbrecher, T72
 Stelling, O37
 Stephan, R115
 Stephens, E327, 328
 Stephens, G70
 Stephens, J251
 Stephens, R55, 110, 157, 209, 269, 323

Stevenson, J.....	145, 198, 260	Suri, P	232	Tata, M	339
Stewart, D	55, 110, 157, 209, 269, 323	Suryanarayana, C	58, 112, 159, 211, 213, 271, 325, 332, 357	Tatiparti, S	225
Stiles, D	240	Suzuki, R	83	Tavasci, A	180
Stipcich, M	137	Suzuki, A	92, 107, 310, 352	Taylor, J	210
StJohn, D	112, 237	Suzuki, M	55, 110, 157, 209, 269, 323	Taylor, M	70, 173, 174, 232
Stocks, G	192	Suzuki, T	53, 361	Taylor, P	200
Stocks, M	252	Svoboda, M	58	Tedenac, J	17, 180, 182, 335
Stoica, A	126, 332	Swadener, J	59	Tedstrom, R	207
Stoica, G	219	Swadner, J	58	Teintze, S	198
Stojakovic, D	121, 280	Swaminathan, S	113, 216, 341	Telang, A	228
Stojanovic, J	334	Swan-Wood, T	78	Temur, D	67
Stokes, D	140	Sweeney, D	255	Teng, J	86, 135
Stoldt, C	160	Swift, D	29, 294	Tenorio, J	137, 361
Stölken, J	133	Syed Asif, S	325	Tenório, J	34
Stoller, R	48, 201, 267, 316, 317	Szczepanski, C	348	Teo, K	16, 117
Stolting, K	20, 120	Szcztygiel, P	216	TerBush, J	92, 310, 352
Stolz, D	107			Terentyev, D	203
Stone, D	335			Terpstra, R	66
Storm, R	39	T		Terrones, L	181
Störmer, M	352	T-Raissi, A	94, 354	Ter Weer, P	171
Story, C	146	Tabereaux, A	231	Tessandori, J	56
Stoudt, M	38, 140, 253, 254, 304, 305	Tack, W	39, 305	Teter, D	243
Street, R	215	Tadisina, Z	33	Tewary, V	40
Streiffer, S	64	Tagantsev, A	64	Tewksbury, G	37
Streitz, F	336	Takahashi, H	48	Thadhani, N	29, 79, 132, 175, 183, 218, 243, 244, 294, 295, 312, 338
Strickler, J	224	Takahashi, K	88	Thanneeru, R	268
Stroeder, M	171	Takahashi, T	83	Theuer, K	244
Strothers, S	114	Takaku, Y	204, 265	Thevuthasan, S	100, 151, 275
Strouse, G	162	Takano, C	35	Thibault, M	127, 341
Stubbins, J	95, 151, 316	Takashi, I	148	Thiebaut, C	328
Stupp, S	175	Takashi, K	148	Thierry, B	17
Su, J	16	Takeda, O	90	Thirumalai, N	52
Su, M	221	Takeda, Y	60	Thiyagarajan, K	36
Subhash, G	74, 79, 184, 339	Takeguchi, M	100	Thoma, D	49, 101, 137, 249
Subramanian, K	50, 102, 151, 153, 204, 264, 317	Takemoto, T	152	Thomas, A	161
Subramanian, S	194	Takenaka, T	142	Thomas, D	171, 229
Suda, H	98	Takeshi, A	148	Thomas, G	42
Sudbrack, C	27	Takeuchi, T	252	Thompson, D	69
Sudha, C	347	Takigawa, Y	259	Thompson, G	33, 282
Sudhakar, N	55, 109, 116, 162, 164, 222	Talamantes, J	210	Thompson, W	167
Sudik, A	27	Taleff, E	80, 229, 282	Thomson, K	272
Sudo, M	283	Talekar, A	43	Thonstad, J	173
Sueishi, Y	48	Talia, J	342	Thornton, K	168, 336
Suematsu, H	361	Tallapragada, R	23	Thornton, T	60
Suery, M	257	Tamerler, C	125, 175	Thorp, C	171
Suganuma, K	104, 153, 205, 265, 318	Tamirisa, S	226, 254	Thuanboon, S	166, 276
Suh, D	138	Tamirisakandala, S	44, 226, 254, 255, 277	Thuinet, L	53, 270
Sui, Z	334	Tamura, K	87	Thunuguntla, R	33
Sukhanova, A	161	Tamura, T	25, 143	Thuret, J	108
Sulger, P	245	Tan, H	273	Tian, J	271
Sun, F	39	Tan, L	119	Tian, W	230, 281
Sun, G	178	Tan, T	77	Tian, Z	231, 284
Sun, H	219, 331	Tanaka, M	87, 100, 349	Tien, L	62
Sun, J	281	Tang, F	46, 200, 215	Tien, S	266
Sun, N	258, 282	Tang, L	285	Tikare, V	18, 67, 119, 168, 227, 278, 327
Sun, W	126	Tang, M	58, 59, 203, 266	Tilak, R	127, 237
Sun, X	114, 115	Tang, W	166	Tiley, J	226, 348
Sun, Y	84, 86, 326	Tang, X	221, 224	Till, R	150
Sun, Z	228, 322	Tang, Z	321	Tin, C	62, 221
Sundararaghavan, V	77, 146, 199	Tanishita, K	124, 125	Tin, S	52, 53, 106, 155, 208, 268, 321
Sundlof, B	293	Tanniru, M	225	Tippur, H	295
Sung, H	62, 144, 145	Tao, J	142	Tiryakioglu, M	111, 158, 210, 270, 324
Suni, J	282	Tao, L	165	Tischler, J	304
Sunkara, B	285	Tao, N	272	Tissington, C	40
Sunny, G	74, 80, 219, 301	Tapasa, K	203	Tiwari, A	16, 62, 63, 115, 116, 117, 162, 164, 221, 223, 274
Surampudi, L	276	Tarakanov, A	329	Tiwari, V	168
Suravarapu, R	187	Tarcy, G	124, 173	Tkac, M	81
Suresh, S	58	Tarnuzzer, R	286	Tkacheva, O	329



- Tkatcheva, O283
 Tochiyama, O138
 Todaka, Y344
 Todd, M102
 Toguyeni, G99
 Toji, A198
 Tokozakura, D63
 Tomas, B57
 Tomasino, T71
 Tomchik, C151
 Tome, C30, 68, 169, 170, 228
 Tomesani, L271
 Toneguzzo, F193
 Tonisch, K115
 Tonmayopas, D56
 Topping, T217
 Torbet, C156
 Tortorelli, P259
 Tosta, R296
 Totemeier, A42
 Tran, T251
 Trapani, M35
 Treadway, J249
 Treadwell, C262
 Treglio, R354
 Trelewicz, J212
 Tretyakov, Y174
 Trichy, G116, 222
 Trigwell, S94
 Trinkle, D52, 77, 105, 136, 189
 Trivedi, P244
 Trivedi, R86, 135
 Trolier-McKinstry, S64
 Trott, W338
 Truci, H81
 Trujillo, C30, 133, 183
 Trumble, K37, 113, 272
 Tryon, B66, 156
 Tryon, R33
 Tsai, C261
 Tsai, L339
 Tsai, R154
 Tsai, T318
 Tschopp, M106, 155
 Tseng, Y153
 Tsirlina, G283
 Tsuchiya, K344
 Tsujikawa, M259
 Tsujimoto, M153
 Tsukimoto, S32, 33, 246
 Tu, K206
 Tucker, G155
 Tucker, J49
 Tuggle, J306
 Tuissi, A217
 Tulenko, J100, 356, 361
 Turano, S16
 Turbini, L50, 102, 103, 151, 204, 264, 317
 Turchi, P89, 139, 191, 252, 303, 336
 Turchin, A75
 Turri, G55
 Tweedy, B83, 298, 342
 Tyumentsev, A215
 Tzeng, Y116
- U**
- Ubertalli, G180, 339
 Uberuaga, B356
 Uchic, M25, 26, 44, 130, 160, 177, 266, 320
 Uchida, Y32, 33
 Ucok, I39, 305, 349
 Uccuncuoglu, S350
 Uda, T334
 Udaykumar, H136
 Ude, A361
 Uecker, R64
 Ueda, M162
 Uehara, T198
 Ugarte-Domínguez, V35
 Uggowitz, P66, 88
 Ugurlu, O76, 290
 Uhlenwinkel, V37
 Ukai, S151
 Ulbricht, N81
 Um, N137, 334
 Umemoto, M344
 Umeno, Y337
 Ungar, T212
 Ungureanu, A70
 Unitt, M74
 Unlu, N360
 Unocic, R107, 312, 320
 Urban, A304
 Ürgen, M88
 Uttarwar, M285
 Uz, M110
 Uzer, G97
- V**
- Vaidyanathan, R248, 249, 299, 300, 332
 Vaillant, M286
 Vainik, R179
 Valdes, A128
 Valdez, J100, 203
 Valiev, R113, 215, 217, 218, 358
 Valone, S27, 79, 356
 van Dellen, S70
 Vanderspurt, T224
 Van der Ven, A28, 77, 130
 van der Walt, T81
 van de Walle, A77, 303
 van Duin, A227
 van Heerden, C81
 Vanheule, B34
 Van Hoof, T165
 Van Linden, J60, 157
 van Linden, J55, 110, 157, 209, 269, 323
 Vanmeensel, K234
 Van Petegem, S154
 VanSchoiack, L177
 Van Swygenhoven, H106, 154, 160
 Van Tyne, C190
 van Veldhuizen, M157
 Vargas Orihuela, J159
 Varma, S110
 Vasantha Kumar, R36
 Vasarni, V86
 Vasekar, P33
 Vasshaug, K30
 Vassiliev, S283
 Vasudevan, V129, 179, 225
 Vauzelle, T328
 Vaynman, S138
 Vecchio, K23, 29, 79, 132, 133,
183, 233, 243, 294, 338, 339
 Vedala, H165
 Vedani, M217
 Vedernikova, I214
 Vekas, L63
 Vendette, H21
 Venkatachalapathy, V269
 VenkataSuryaPrakash, S36
 Venkatesan, T146
 Venkatesh, A301
 Venkatesh, T278, 305
 Venkateswaran, S189
 Ventelon, L51
 Ventura, T265
 Verbeken, K34
 Verbrugge, M41
 Verhaege, M34
 VÉRITÉ, G356
 Verma, R68, 92, 144, 195, 258, 342
 Vermeulen, B156
 Vermeulen, P197
 Verweij, H310, 311, 343
 Veselkov, V71
 Vespa, G144
 Veysiere, P207
 Viala, J182, 226, 277
 Viano, D210
 Vickery, C187
 Vidal, E200
 Vidrich, G58, 353
 Viehland, D189
 Vieira, C56, 180, 289
 Vieira, M275
 Vigliante, A252
 Vilaça, P134
 Vild, C60
 Vildanova, N218
 Vilela, A174
 Vilela, H334
 Villegas, J271
 Vincent, A149, 292
 Vincent, E263
 Vincent, H341
 Viswanath, R337
 Viswanathan, A98
 Viswanathan, G26, 121, 130, 217, 229, 312
 Vitichus, B341
 Vitek, V51, 206
 Vittala Pai, D232
 Viviers, K81
 Vízdal, J104
 Vlcek, J89
 Vleugels, J234
 Vlieg, E89
 Vogel, S30
 Vogler, T183, 338
 Vogt, R214
 Vohra, Y176
 Voicu, I63
 Volakis, J343
 Volkert, C58, 160, 266
 Volkov, Y220
 Volland, A257
 Volokhov, I329
 Vondra, F143
 Von Kaenel, R283
 Voorhees, P189, 335, 336
 Vormelker, P292
 Voss, D158
 Voyiadjis, G260, 261
 Vrešt'ál, J104
 Vuoristo, T80
 Vyas, G94

W

Wadsworth, J.....	64	Wedde, G.....	36	Willms, R.....	251
Wagermaier, W.....	72	Wee, A.....	60	Wilson, T.....	178, 236
Wagner, B.....	54	Weerasooriya, T.....	38, 140, 141, 253, 304, 305	Wimmer, E.....	28
Wagner, G.....	132	Weertman, J.....	58	Win, Z.....	345
Wagner, L.....	195	Wegener, J.....	42	Windl, W.....	126
Wagoner, R.....	146, 147, 148, 186, 188, 247	Wei, C.....	152, 204	Winter, R.....	187, 244
Wagstaff, R.....	237, 238	Wei, D.....	256, 320	Winterton, J.....	165
Wahl, J.....	53	Wei, H.....	16	Winther, B.....	121
Walden, W.....	141	Wei, J.....	355	Wirth, G.....	48, 100, 101, 150, 201, 202, 203, 216, 263, 264, 314, 316, 355
Waldner, G.....	63	Wei, L.....	119, 123, 345	Withers, J.....	39, 141
Walford, G.....	143	Wei, Q.....	113	Withers, P.....	322
Walker, D.....	179	Wei, W.....	55, 109, 163	Witt, P.....	97
Wall, J.....	302	Wei, Y.....	88	Witte, F.....	176, 352
Wallace, R.....	232	Wei, Z.....	184	Witusiewicz, V.....	135
Wallenius, J.....	150	Weidenmann, K.....	258	Wng, Y.....	195
Walleser, J.....	103, 264	Weigend, F.....	337	Wochner, P.....	252
Walley, S.....	132, 183	Weil, K.....	39, 41, 93, 94, 141, 145, 146, 197, 198, 259, 310, 353	Wögerer, C.....	60, 63, 88
Walter, S.....	72	Weiland, H.....	20, 68, 282, 349	Wolf, A.....	22
Wan, Z.....	345	Weinberger, C.....	161	Wolf, B.....	100
Wang, B.....	99	Weiss, B.....	318	Wolf, D.....	212
Wang, C.....	84, 104, 297, 344	Weissmüller, J.....	275, 326, 337	Wolf, W.....	28
Wang, D.....	58, 62, 116, 221, 331	Welch, B.....	231	Wolverton, C.....	27, 28, 77
Wang, E.....	87	Welk, B.....	130, 229, 312	Wong, C.....	240, 349
Wang, G.....	73, 178, 189, 212, 239, 332, 335, 360	Wells, J.....	158, 338	Wong, K.....	203
Wang, H.....	58, 60, 62, 108, 112, 115, 159, 162, 211, 213, 221, 271, 276, 325, 357	Wen, C.....	125, 184	Wong, N.....	220
Wang, J.....	196, 212, 213, 215, 233, 270, 281, 284, 335	Wen, Y.....	181	Wong, S.....	297
Wang, K.....	182, 313, 327	Weng, L.....	213	Wong, W.....	215
Wang, L.....	36, 46, 280	Wenner, M.....	186	Woo, C.....	202
Wang, M.....	18, 51, 206, 214, 318	Wensley, C.....	302	Woo, W.....	134
Wang, N.....	98, 148, 149, 201	Werner, F.....	210	Wood, W.....	37
Wang, P.....	20, 121, 133, 250, 279, 280, 312	Wesolowski, R.....	49	Woodard, S.....	52, 106, 155, 208, 268, 321
Wang, Q.....	41, 210, 281	Westbrooke, E.....	156	Woodward, C.....	51, 105, 154, 181, 206, 225, 266, 320
Wang, S.....	102, 143, 345	Westerholt, K.....	252	Wright, I.....	209, 259, 311
Wang, T.....	77, 274, 337	Weygand, D.....	58	Wright, S.....	75, 121, 169
Wang, W.....	24, 73, 338	Wheeler, K.....	43	Wright, T.....	79, 243
Wang, X.....	46, 124, 126, 127, 134, 215, 228, 332	Wheeler, R.....	160	Wu, A.....	152
Wang, Y.....	22, 25, 28, 32, 44, 50, 74, 77, 99, 106, 107, 121, 168, 169, 174, 189, 195, 203, 212, 213, 229, 235, 236, 239, 241, 242, 265, 312, 326, 343, 356	Whelan, S.....	124	Wu, C.....	357
Wang, Z.....	31, 60, 80, 114, 161, 186, 220, 233, 238, 273, 284, 340	White, D.....	74, 75, 348	Wu, D.....	276
Wanko, E.....	145	White, H.....	183	Wu, E.....	330
Wanner, A.....	258	White, P.....	198	Wu, H.....	294
Wanner, T.....	278	Whiteman, G.....	244	Wu, J.....	87, 110, 335
Warczok, A.....	35	Whitis, D.....	229, 255, 256, 307	Wu, K.....	125
Ward, W.....	116	Whitten, M.....	94	Wu, L.....	219, 326, 346
Warnken, N.....	65	Widener, C.....	83, 298, 342	Wu, M.....	76
Warren, J.....	31, 32, 40, 181, 199	Widom, M.....	27, 360	Wu, R.....	224
Warren, O.....	325	Wierzbza, B.....	28, 242	Wu, S.....	318
Warrior, N.....	194	Wierzbecki, A.....	23	Wu, T.....	146
Waryoba, D.....	20, 69	Wiesner, J.....	179	Wu, W.....	170
Was, G.....	48, 94, 95, 100, 150, 201, 202, 263, 314, 315, 316, 355	Wiezorek, J.....	357	Wu, X.....	56, 95, 113, 155, 216, 357
Watanabe, M.....	75	Wiggins, L.....	293	Wu, Y.....	166, 209
Watanabe, T.....	100, 356	Wijaya, H.....	287	Wu, Z.....	28, 318
Watkins, T.....	47	Wilde, G.....	32	Wuelker, C.....	25
Watson, A.....	104	Wilgen, J.....	46, 47, 262	Wunderlich, R.....	286, 306
Watson, M.....	309	Wilhelm, C.....	89	Wunsch, C.....	284
Way, C.....	236	Wilkening, S.....	81		
Weaver, D.....	170	Wilker, J.....	285		
Weaver, M.....	208	Wilkins, J.....	189	X	
Webb, E.....	338	Wilkinson, D.....	38, 172	Xi, J.....	185
Webb, S.....	298	Wilks, G.....	168	Xia, G.....	94, 198, 260
Weber, M.....	316	Will, F.....	115	Xia, K.....	113, 216, 294
Weber, W.....	100	Willaime, F.....	51, 202, 356	Xia, S.....	215
		Williams, C.....	350	Xia, Z.....	98, 102, 103, 110, 264
		Williams, D.....	75	Xiang, L.....	186
		Williams, J.....	18, 50, 62, 116, 156, 164, 199, 221, 342	Xiang, Q.....	330
		Williams, N.....	62, 221	Xiangdong, Y.....	232
		Williams, P.....	181	Xiao, Y.....	259
		Williams, R.....	26, 34, 130	Xiao, Z.....	276
		Williams, S.....	156, 207	Xichang, S.....	99



- Xie, C350
 Xie, J64, 286
 Xie, M273
 Xie, X110
 Xie, Y185
 Xie, Z121
 Xin, Y302
 Xinzheng, L.....185
 Xiong, J125, 184, 313
 Xiong, S288, 324
 Xiong, X.....76
 Xiong, Y214, 260
 Xiquan, Q.....296
 XiYun, Y.....99
 Xu, C112
 Xu, D103, 262, 313, 316
 Xu, F120
 Xu, H247, 251, 262
 Xu, J31, 126, 231, 260, 283
 Xu, M236
 Xu, S151
 Xu, W21, 113, 216
 Xu, X59, 70, 73, 214, 217, 295, 350
 Xu, Y295
 Xu, Z238, 274, 289
 Xuanhui, Q.....224
 Xue, J281, 340
 Xueliang, D.....341
 Xueping, Z.....224
 Xueyi, G.....323
 Xuguang, G.....311
- Y**
- Yablinsky, C156
 Yadava, M.....187
 Yajima, M.....154
 Yalisove, S.....30, 294
 Yamaguchi, A.....209
 Yamaji, K260
 Yamamoto, T.....263, 264, 314
 Yamamoto, Y.....55, 260, 323
 Yamazaki, A344
 Yan, X185
 Yan, Y324
 Yan, Z343
 Yanada, I153
 Yang, B89
 Yang, C50, 104, 115, 125
 Yang, D276
 Yang, F204, 239, 287
 Yang, G46
 Yang, H214, 241, 331
 Yang, J27, 158, 188, 284, 296, 297
 Yang, K358
 Yang, L118, 126, 318, 332
 Yang, Q61, 165
 Yang, R306
 Yang, S50, 105, 258, 297, 304
 Yang, W.....172, 232, 283, 304, 322
 Yang, Y136, 169, 213, 288, 322, 336, 343
 Yang, Z41, 93, 94, 145, 197,
198, 239, 259, 260, 310, 353
 Yanli, J296
 Yannas, I.....72
 Yanqing, L.....185
 Yao, G17, 46, 70, 118, 123, 129,
144, 145, 167, 172, 184, 185,
194, 230, 231, 277, 283, 328, 346
 Yao, Z151, 202
- Yaowu, W233, 341
 Yapici, G119, 193, 228
 Yarrapareddy, E.....249
 Yashiki, T43
 Yasuda, K220, 304
 Yavari, A.....67, 261
 Yavorsky, M217, 306
 Yavuz, M223
 Ye, F236
 Ye, J207
 Ye, W61
 Ye, Y190, 236
 Yeh, A156
 Yen, Y153, 265
 YeXiang, L61
 Yexiang, L185
 Yi, J156, 292
 Yihan, L119, 345
 Yilmaz, S278
 Yim, C143
 Yin, D196, 213
 Yin, F335
 Yin, J281
 Yin, W69, 282
 Yin, Z276, 281
 Yokokawa, H.....42, 260
 Yokokawa, T53, 157
 Yokoyama, Y.....74, 178, 286, 332
 Yolton, C254, 305
 Yoneyama, T289
 Yong, W46, 217, 349
 Yong, Z186
 Yonggang, Z57
 Yoo, C190
 Yoo, J204
 Yoo, K34
 Yoon, E273
 Yoon, J50, 253, 319, 359
 Yoon, K27
 Yoon, S180, 353
 Yoon, Y196, 328, 359, 360
 Yorikado, Y153
 Yo Sep, Y191
 Yoshikawa, T.....289
 You, B143
 You, K34, 56, 137, 334
 Young, D131, 360
 Young, H345
 Young, P217
 Youssef, Y322
 Yu, C265
 Yu, D220
 Yu, F143
 Yu, H46, 123, 184, 207, 328
 Yu, J50, 85, 102, 151, 204, 223, 264, 317
 Yu, K39, 305
 Yu, L56
 Yu, S334
 Yu, Y103
 Yu, Z81, 228
 Yuan, B268
 Yuan, F178, 333, 339
 Yuan, Q276
 Yuan, W335
 Yuan, Z111
 Yucel, O35, 302
 Yue, S92, 144, 258
 Yue, W234
 Yuefeng, G107
 Yuezhang, D.....233, 296
- Yufeng, G142
 Yujin, C61
 Yun, Y204
 Yunaz, H70
 Yurkov, V329
- Z**
- Zabaras, N19, 77, 99, 119, 120, 146, 199
 Zabel, H.....252
 Zabinski, Jr., J162
 Zagrebenny, D.....314
 Zaidi, T345
 Zaikov, Y.....173, 283, 329
 Zaluzny, M274
 Zangiacomì, C.....232
 Zarandi, F.....92, 144
 Zarkevich, N77
 Zarouni, A231
 Zartoshtimanesh, S.....72
 Zayak, A136
 Zehetbauer, M113, 213
 Zeifert, B35
 Zeller, S18
 Zemanová, A104
 Zeng, K153
 Zeng, Q117, 343
 Zeng, X47, 92, 154, 195, 196, 211, 309, 353
 Zerilli, F29
 Zestrea, V99
 Zettler, R134, 259
 Zhai, Q46, 98, 99, 261, 262, 313, 354
 Zhai, X166
 Zhan, J87, 110, 201, 335
 Zhang, C87, 99, 110, 201, 310, 335
 Zhang, D213, 255, 272
 Zhang, F228
 Zhang, H54, 74, 77, 79, 126, 130, 289, 309
 Zhang, J71, 115, 131, 212, 285, 295, 304
 Zhang, K58
 Zhang, L36, 53, 76, 87, 128,
237, 256, 322, 323, 339, 343
 Zhang, M17, 42, 174
 Zhang, R42, 201, 225
 Zhang, S195
 Zhang, T236, 275
 Zhang, W162
 Zhang, X23, 41, 58, 112, 159, 211, 213,
215, 271, 275, 325, 326, 339, 357
 Zhang, Y37, 59, 100, 127, 209, 212, 295, 306
 Zhang, Z28, 217, 218, 286
 Zhao, J197, 241, 242
 Zhao, L239
 Zhao, M16
 Zhao, P313
 Zhao, W232
 Zhao, Y225, 271, 274
 Zheleva, T163
 Zheng, G219
 Zheng, H141
 Zheng, K353
 Zheng, L294
 Zheng, W240, 292
 Zheng, X280
 Zheng-Johansson, J220
 Zhgilev, I213
 Zhi, Z304
 Zhilyaev, A113, 216, 219, 273, 341
 Zhimeng, G165
 Zhipeng, C47

Zholnin, A	55
Zhong, H	230, 281
Zhong, J	33
Zhongliang, T	185
Zhou, H	222, 310
Zhou, J	71, 72
Zhou, L	271
Zhou, M	96, 337
Zhou, N	242
Zhou, O	63, 117
Zhou, Y	56, 62, 218, 221
Zhu, A	24
Zhu, C	76, 331
Zhu, F	353
Zhu, H	258
Zhu, J	38, 145, 198, 221, 310, 336
Zhu, L	34
Zhu, T	58, 106, 161, 327
Zhu, W	338
Zhu, X	100, 261, 292
Zhu, Y	58, 112, 159, 211, 213, 215, 271, 325, 357
Zhu, Z	126
Zhurkin, E	165
Zikry, M	169
Zimmerman, L	162, 362
Zimmerman, M	33
Zimprich, P	318
Zindel, J	91, 270
Zinkle, S	100, 316
Zok, F	294
Zöllmer, V	293
Zrnik, J	95, 112
Zu, G	17, 194, 230
Zúberová, Z	178
Zuniga, D	351
Zuo, L	189, 213
Zuo, R	275
Zuo, X	87

**Plan to join us in America's most authentic
and culturally rich city - rejuvenated!**

TMS2008

137th Annual Meeting & Exhibition



**March 9-13, 2008
Ernest Morial Convention Center
New Orleans, Louisiana
Details to come at www.tms.org/annualmeeting.html**



Linking Science and Technology for Global Solutions